Changing Facies

The 2020 Desert Symposium Field Guide and Proceedings

David M. Miller, editor

Desert Symposium, Inc. • April 2020

IN MEMORIAM

Mark A. Roeder

Mark Roeder, who passed away May 1, 2019, was a long-time member of MDQRC/Desert Symposium and Pacific Coast Archaeological Society. Mark grew up in San Diego, graduated from San Diego State University and lived in Orange County for more than 35 years. He worked as a "Free Agent" for different museums and for paleontological and cultural resource management companies. He helped establish the Cooper Center in Orange County, taught Junior Paleontology at the San Diego Museum of Natural History, and provided outreach programs for schools. He especially loved the discovery of new or rare fossils, and he has been recognized by fossils named in his honor: *Diopatrichnus roederensis* Kern, 1978, a trace fossil; *Macrotarsius roederi* Kelly, 1990, a primate.

Mark was coauthor on eleven archaeologic contributions and contributed to MDQRC/Desert Symposium with research on fish in the Mojave and Colorado Deserts, at Amboy, and at many localities in the Bouse Formation along the Colorado River. His first MDQRC paper was in 1985, followed by at least sixteen other contributions to Desert Symposium volumes.

Robert E. Reynolds Desert Symposium Student Research Award

This award to honor Bob Reynolds acknowledges Bob's decades of service to desert sciences, from directing large fossil excavations and exploring for minerals to mentoring numerous students and apprentices, as recognized by the Society of Vertebrate Paleontology with the 2019 Morris Skinner Prize. In addition, Bob has been central to holding the annual Desert Symposium for over 30 years, in many cases singlehandedly soliciting contributors, organizing the meeting, and running the field trip. Bob's leadership and service are honored with this award by promoting student research projects.

Information on applying for and donating to the award is available at http://desertsymposium.org. Donors will be identified in the annual volume published by the Desert Symposium. Desert Symposium Inc. is a non-profit 501(c)3 organization. Contributions are tax-deductible as allowed by law.

Reynolds Award 2020 donors

Anonymous	Hal Beesley	Valerie Castor
Tom Cluff	Chris Dalu	Thomas Davis
Timothy Elam	Pat Flanagan	Lowell Ford
Anna Garcia	Bruce Hamilton	John Harms
George Jefferson	Jeanne Johnstone	David Lynch
Norman Meek & Joy Barta		David Miller
Robert and Jennifer Reynolds	Mark Soden and	Francene Kaplan
Gregg Wilkerson	Michael Woodburne	Carole Ziegler

The 2020 award recipient:

Cali Tramnell of CSU Northridge
Basin analysis of the Eocene Goler Formation, Mojave Desert, California

Changing facies

David M. Miller, editor

2020 Desert Symposium Field Guide and Proceedings
April 2020

The April 2020 Desert Symposium annual meeting was cancelled because of restrictions on public gatherings to mitigate the spread of COVID-19. Some of the papers and abstracts in this publication may form the basis for presentations at the next Desert Symposium. —*the editor*

Front cover:

Red sandstone below pink tuff breccia, Red Rock Canyon State Park. *Xiaoming Wang photograph.*

Back cover:

Black Canyon Anticline. *Jennifer Reynolds photograph.*

Aerial view at China Lake following the Trona–Ridgequest earthquake sequence. *U.S. Geological Survey photograph.*

Title page:

Inside the Yellow Aster saloon and barber shop, Randsburg, ca. 1900. *California Historical Society.*

The Desert Symposium is a gathering of scientists and lay people interested in the natural and cultural history of arid lands. The meeting comprises scientific presentations followed by a field trip. The Desert Symposium and its field trip take place annually, usually in April. The Desert Symposium publishes a volume of papers and a field trip road log. Safety, courtesy, desert awareness and self-reliance are expected of all participants.

A color version of this and past volumes may be viewed at http://www.desertsymposium.org/History.html

Table of contents

Middle Miocene temperature and paleoenvironmental changes recorded in paleosol carbonates (Barstow Formation, Mud Hills, CA)
Katharina Methner, Katharine Loughney, Lydia Jork, Jens Fiebig, Catherine Badgley, and Andreas Mulch

A vascular flora of the Nopah Range, Inyo County, California
Carolyn Mills

Paleoecology of Columbian mammoths (*Mammuthus columbi*) in southern Nevada and California: how Terminal Pleistocene ecosystems shaped mammoths at the population level
Lauren E. Parry and Stephen M. Rowland

Taking the road less traveled: a comparison of desert tortoise road crossing at two study sites in the Sonoran Desert of California
Shellie R. Puffer, Jeffrey E. Lovich, Terence R. Arundel, Kirsten Ironside, Laura A. Tennant, Amanda L. Smith, Kathleen Brundige, and Michael Vamstad

Quantifying niche dynamics of Sahara mustard (*Brassica tournefortii)* to improve spatial predictions of areas at risk of invasion
Clarissa Rodriguez, Loralee Larios, and Janet Franklin

Evidence of Pleistocene marine incursions into the Salton Basin
Jenny E. Ross, Susan M. Kidwell, David L. Dettman, Jordon Bright, Rebecca J. Dorsey, and George T. Jefferson

Trace element scavenging at the sediment-poor water interface in surficial sediments of an arid region of southern Nevada, USA
Douglas B. Sims, Amanda C. Hudson, John E. Keller, Michael Strange, David Ferrari, Giavanna M. Fernandez, Juan Garcia-Hernandez, and Bailey D. Kesl

Lacustrine beds in the Chuckwalla Valley, southeastern California, and their likely facies relationship to the Chemehuevi Formation
W. Geoffrey Spaulding

What? There's water in the desert?
Carole Ziegler

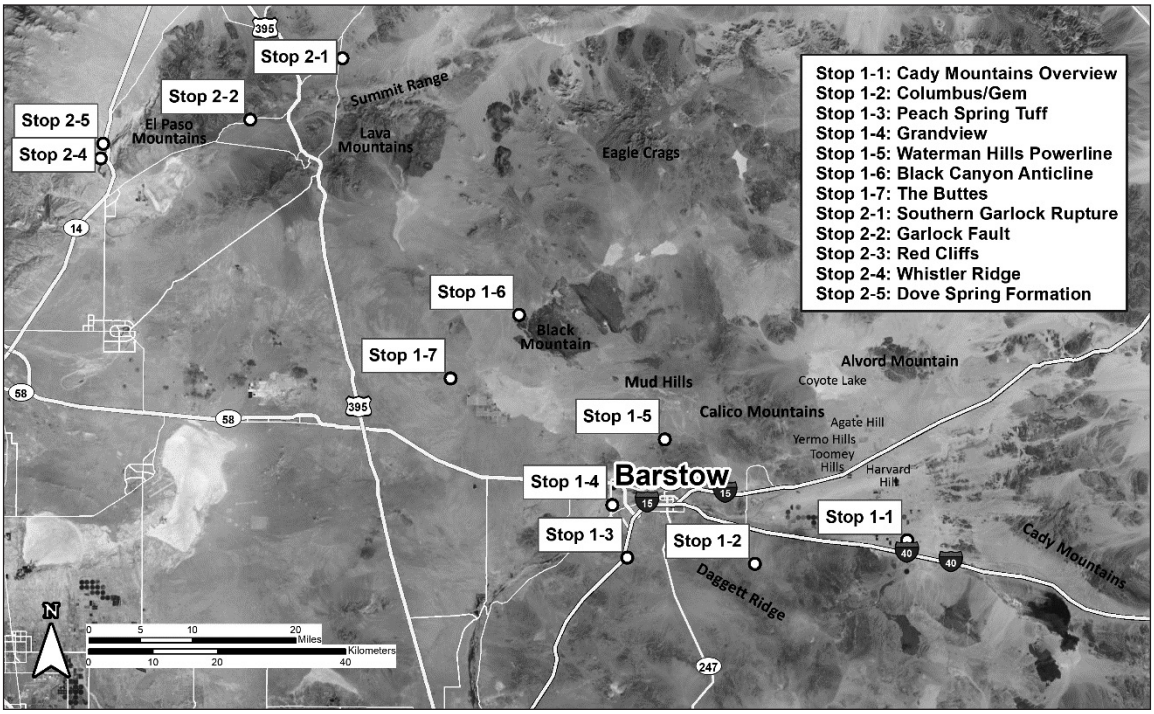

Figure 1. Overview map of all stops on Days 1 and 2 of the field trip.

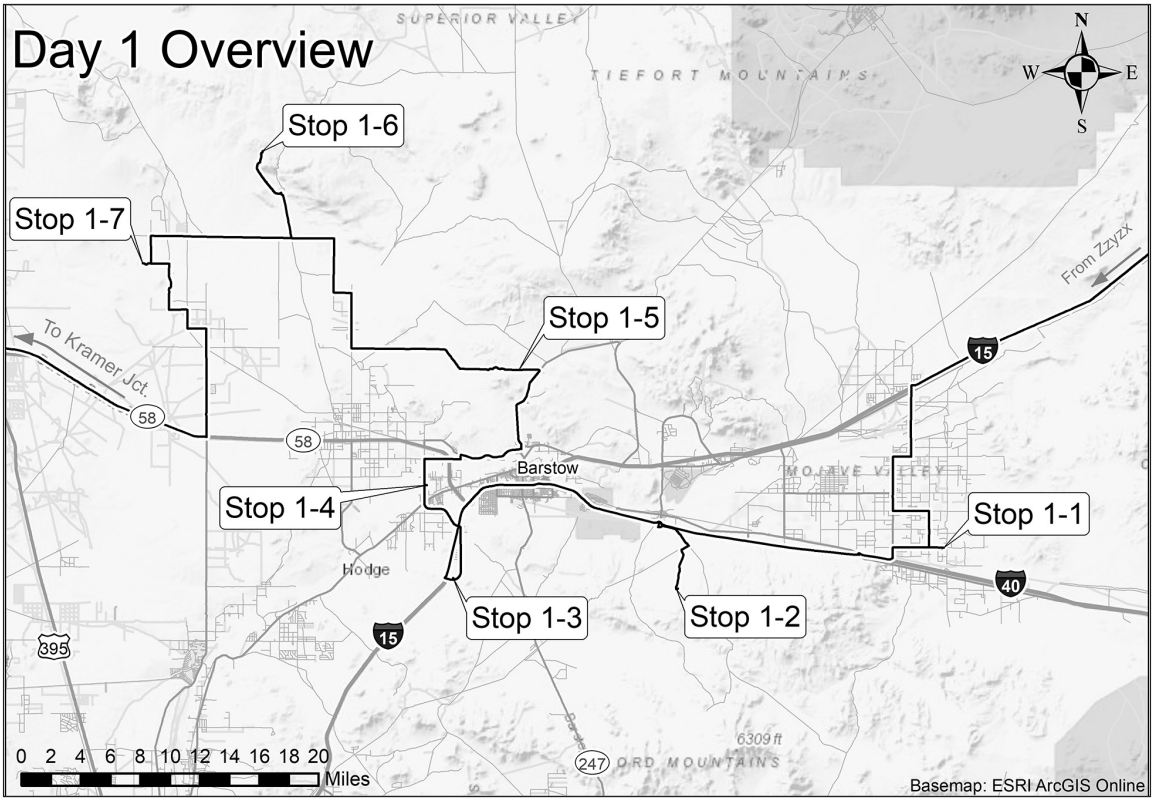

Figure 1-1. Overview map of Day 1 stops.

Changing facies: the road log

Katharine Loughney,[1] Robert E. Reynolds,[2] David Whistler,[3] and Gary T. Takeuchi[4]
[1]*Department of Ecology & Evolutionary Biology, University of Michigan, Ann Arbor, MI, 48109*
[2]*Redlands, CA. bob.reynolds220@gmail.com*
[3]*Curator Emeritus, Natural History Museum of Los Angeles County, 900 Exposition Blvd., Los Angeles, CA, 90007*
[4]*La Brea Tar Pits and Museum, 5801 Wilshire Blvd., Los Angeles, CA, 90036*

Convene at the Desert Studies Center. Make sure vehicles are packed with all your personal gear and a full tank of gas; we will not return to the Desert Studies Center. Bring water, snacks, and protection from sun and wind. We will camp overnight; be prepared with camping gear, food, and water. Directions to camp location are provided separately.

Field trip overview

This field trip emphasizes the change in sedimentary facies in the Mojave Desert region that took place through the Miocene (Fig. 1). From the Desert Studies Center, we will travel west to see Early and Middle Miocene deposits of the Barstow Formation and equivalent sediments in the central Mojave Desert. From the Barstow, California, area, we will head northwest across the Garlock Fault to see Middle Miocene deposits of the Dove Spring Formation and equivalent sediments.

Day 1: What we will see

On Day 1 we will visit outcrops that define the geographic extent of the Miocene Barstow Formation in the central Mojave Desert of southern California (Fig. 1-1). These outcrops exhibit distinctive facies that help us interpret the environments that formed in the basin through time and the movement of the basin depocenter. Radiometric dates on tuff layers or igneous rocks and magnetostratigraphy (MacFadden and others, 1990; Singleton and Gans, 2008; Miller and others, 2010) provide age constraints on the facies of the Barstow Formation and help correlations among outcrops.

The Barstow basin formed in the northwest-trending extensional Pickhandle trough that developed in relation to movement along the Waterman Hills detachment fault (Dibblee, 1968; Fillmore and Walker, 1990). The Pickhandle and Mud Hills formations were deposited during extension of the Pickhandle trough. These formations are characterized by volcaniclastic breccias, conglomerates, and lacustrine deposits that are typical of extensional facies (Fillmore and Walker, 1995; Ingersoll and others, 1996). The Barstow Formation unconformably overlies the Pickhandle and Mud Hills formations, and many authors (Glazner and others, 1989a, b; Dokka and Travis, 1990; Fillmore and Walker, 1990; Dokka and others, 1991; Ingersoll and others, 1996; Glazner and others, 2002; Anderson, 2017; Loughney and Badgley, 2017) interpret the Barstow Formation as post-extensional deposits. The breadth and margins of the Barstow basin are defined by outcrops which extend 35 miles from near Daggett, California, northwest to Black Canyon in the central Mojave Desert (Figs. 1, 1-1). Time-transgressive deposition started at about 20 Ma and continued past 13.4 Ma, a span of 7 Ma. Deposits of the lower Barstow Formation can be identified by the occurrence of several marker beds (Reynolds and others, 2010) that will be the focus of our stops on Day 1. The distribution of the marker beds provides evidence for the northwestward movement of the depocenter through time, the cause of which has not yet been explained. As the Barstow depocenter moved northwest over time, environments changed from lakes and alluvial fans to floodplains (Loughney and Badgley, 2017).

Marker beds (Reynolds and others, 2010) that assist with tracking the Barstow Formation are stratigraphically, from the lowest to highest, Massive Stromatolitic Limestone (MSL), Brown Platy Limestone (BPL), Insect Stromatolites (IS; Jenkins, 1986; Leggitt, 2000; Spencer, 2005) and Strontium-Borate (SrB) beds (Durrell, 1953; Dibblee, 1970). These marker beds formed in shallow-water nearshore environments of one or more saline-alkaline lakes (Durrell, 1953; Park, 1995). The MSL, BPL, and SrB beds are widespread near Barstow, California, and are often exposed in stratigraphic succession; the insect stromatolite horizon occurs sporadically in outcrop, but is always located between the BPL and the SrB layers (Fig. 1-2). The 18.8 Ma Peach Spring Tuff (PST) is an isochronic marker near the base of the section that helps constrain the age of the lower Barstow Formation (Hillhouse and others, 2010; Reynolds and others, 2010).

The Barstow Formation was formally described by Dibblee (1968) as follows:

> The Barstow Formation is here defined as that sequence of deformed, stream-laid conglomerates, sandstones, lacustrine clays, and several thin tuffs, which lies unconformably above granitic breccia and tuff of the Pickhandle Formation, unconformably below the flat-lying older alluvium of Pleistocene age, and which contains a mammalian fauna of…Miocene age. . . . The type locality of the Barstow Formation is here designated as the continuous section A-A measured and described by Durrell (1953…)

just west of Solomon Wash in the Mud Hills… the basal beds of the Barstow Formation… are included in Durrell's Section B-B in Ross Canyon…{where} the basal unit of the Barstow Formation is composed of 28 feet of dark algal limestone, …in angular discordance on…the Pickhandle Formation.

The formation is named for Barstow, California, and is applied to outcrops of Miocene sediments that are exposed in the nearby Daggett Ridge, Mud Hills, Calico Mountains, and Black Canyon (Figs. 1, 1-1). At Alvord Mountain, Cenozoic sediments of similar age are now excluded from the Barstow Formation, since they lack a stratigraphic section conforming to that designated by Dibblee (1968). The "Barstow Formation" at Alvord Mountain does contain a Barstovian

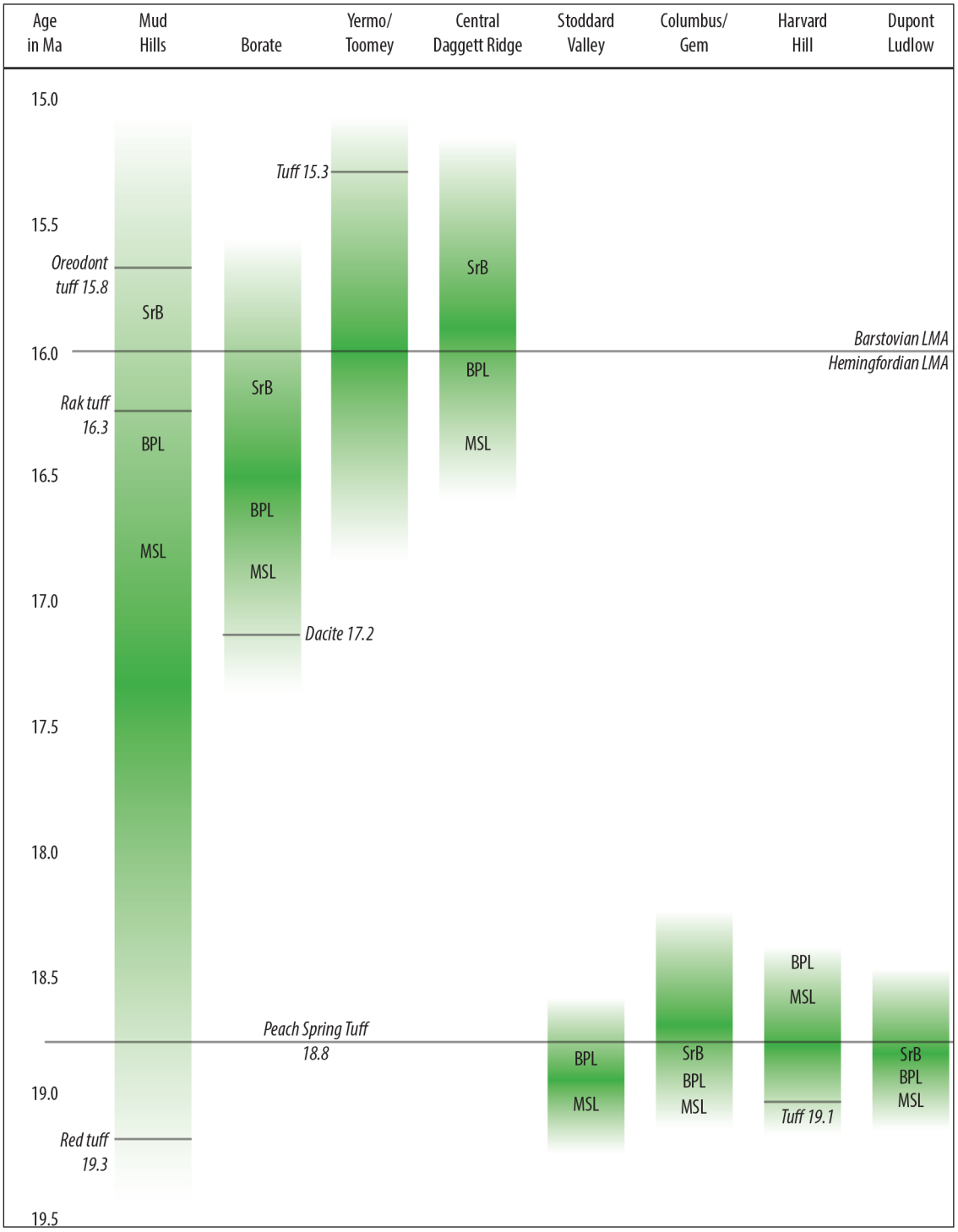

Figure 1-2. Chronostratigraphic correlation chart of Barstow Formation marker beds among outcrop areas near Barstow, California.

mammal fauna similar to that in the Mud Hills (Byers, 1960), but none of these marker beds have been recognized there. However, Byers (1960) describes two outcrops north-northwest and west of Alvord Mountain that contain the marker beds. Agate Hill (Byers, 1960, figs. 1, 3), south of Coyote Lake, contains the SrB layer, while hills immediately west of Main Base Fort Irwin expose the MSL, BPL and SrB layers (Byers, 1960; see saline minerals p. 65, and stratigraphic section p. 41; Reynolds and others, 2010, p. 155–156). The age and stratigraphic relationships of these marker beds to others in the Barstow, California, area are unresolved.

Due to the locations of exposures, available age estimates, and post-exhumation erosion, it is difficult to get a good picture of when and where the Barstow depocenter was at specific times during its time-transgressive filling of the Pickhandle trough. By tracing the marker beds and other facies of the Barstow Formation, it is possible to form a depositional history for the basin. We know that the Barstow basin filled first in the southeast, near the Columbus/Gem area, since the three marker beds underlie the PST there (Fig. 1-2). In west-central Daggett Ridge, the marker beds are present but the PST is missing. Based on the geographic position within the trough and the transgression of marker-bed deposition, we would expect the PST to occur between the marker beds at some stratigraphic position. Immediately east of the Lenwood Fault, at the Stoddard Cut-off road, the PST is overlain by the marker beds, a stratigraphic change from Columbus/Gem that was not accomplished by faulting (Dibblee, 1970). From Stop 1-3 north, the PST, where present, is overlain by the marker beds.

Lacustrine deposits are important for tracing the depositional history of the basin, as they are indicators of basin depocenters. The thickest lacustrine deposits in the Barstow Formation are those of the Calico Member in the Calico Mountains (Fig. 1). Radiometric dates on dacite domes constrain the age of these deposits between 19 and 17 Ma (Singleton and Gans, 2008). These beds were deposited in a saline-alkaline lake that shallowed over time (Park, 1995).

In the Toomey Hills (Fig. 1), 16 Ma lacustrine mudstones contain the spines of stickleback fish (Bell and Reynolds, 2010). Modern sticklebacks live in the Pacific Ocean and swim up rivers to breed. Their presence at Toomey suggests that there was a drainage connection that was able to bypass the Victorville Highland (Woodburne and Golz, 1972) and reach the Pacific Ocean. This through-flowing connection was available long enough to give populations of stickleback fish time to flourish in the Early Miocene lake environments near Toomey.

Lacustrine deposits in the eastern Mud Hills (Figs. 1, 1-1) are also important for understanding the history of the early Barstow Formation. Lacustrine facies in the eastern Mud Hills thicken eastward toward the Calico Mountains and are likely at least partly coeval with lacustrine deposits of the Calico Member (Loughney and Badgley, 2017). Tufa in Owl Canyon represents the MSL in the Mud Hills (Reynolds and others, 2010). An interesting comparison between southwest and northeast MSL facies in Owl Canyon was made by Cole and others (2005). They used U-Pb analyses to date tufa mounds and phytoherms (tufa precipitated around twigs and branches). Results from three dated localities are 15.39 ± 0.15 Ma and 15.30 ± 0.25 Ma at Owl Canyon Campground, and 16.25 ± 0.25 Ma on the northeast limb of the Barstow Syncline. Apparently, the MSL was actively forming over a period of nearly 1 million years in the Owl Canyon area. These dates indicate that lacustrine environments were younger in the Mud Hills area than in the Calico Mountains. Lacustrine deposits in Black Canyon (Figs. 1, 1-1) are not well dated but may be coeval with Barstow deposits in the Mud Hills, based on the occurrence of uncommon fossils of Barstovian mammals.

Evidence for fluctuations in lake level can be seen when examining the marker horizons in the Mud Hills. West of Rainbow Loop exit, gray, well-sorted nearshore lacustrine sands are sandwiched between two layers of phytoherms, part of the MSL. The layers of tufa tubes converge, and are inferred to represent a transgressive-regressive lake cycle.

After ~16 Ma, environments in the Mud Hills area of the Barstow basin transitioned from lacustrine to fluvial. Loughney and Badgley (2017) described six facies associations in the Mud Hills that encompass this change in depositional environments. Facies Associations 1 and 2 are alluvial-fan and lacustrine deposits that are primarily exposed in Owl Canyon and correspond to the Owl Conglomerate Member and the Calico Member in the Calico Mountains (Singleton and Gans, 2008). The overlying Facies Associations 3 and 4 represent a transition to fluvial environments in this part of the Barstow basin by ~16 Ma; these channel and floodplain deposits are exposed in the central Mud Hills. Facies Associations 5 and 6 are mudstone-dominated and contain layers with pedogenic features, including carbonate nodules and root casts. The deposits of Facies Association 5 represent poorly drained floodplains and wetlands, and the deposits of Facies Association 6 represent spring-fed wetlands that experienced periodic drying (Loughney and Badgley, 2017). The Robbins Quarry fossil concentration in the Upper Member of the Barstow Formation (Reynolds and Browne, 2015) is situated in mudstone with marl layers containing silicified roots. This locality likely formed in a wetland or poorly drained floodplain setting; such settings are generally interpreted to form in more basin-ward positions. Coarse-grained sandstones in the uppermost part of the Barstow Formation have been interpreted as alluvial-fan deposits by Woodburne and others (1990), indicating a position near the basin margin.

The major gaps in deposition and lack of widespread dated marker units in outlying outcrops of the Barstow Formation make it difficult to discern whether the

formation was originally deposited in one continuous trough or in multiple small basins. The evidence for through-going drainages with connection to the ocean in the Toomey Hills at ~16 Ma, tufa formation in the Mud Hills between 15.5 and 16.5 Ma, and the transition to fluvial environments in the Mud Hills after 16 Ma indicate that the depositional trough had open drainage during Barstow time. Small, possibly interconnecting depocenters may have occupied the trough as the depocenters moved northwestward through time.

Many questions still remain about the bounds of the Pickhandle trough and the physical constraints on the movement of the depocenter through time.

Abbreviations

Ar/Ar	Argon/Argon dating
BCA	Black Canyon Anticline
BLM	Bureau of Land Management
BPL	Brown Platy Limestone
BrSF	Bedrock Spring Formation
CCF	Cudahy Camp Formation
cm	centimeter
DSF	Dove Spring Formation
E	east
Hwy	Highway/State Route
I	Interstate
IS	Insect Stromatolites
K–Ar	potassium-argon dating
km	kilometer
LMA	Land Mammal Age
Ma	mega-annum (million years)
MP	mile post
m	meters
M	earthquake magnitude
mi	miles
mph	miles per hour
MSL	Massive Stromatolitic Limestone
N	north
No.	number
PST	Peach Spring Tuff
RRCSP	Red Rock Canyon State Park
S	south
SrB	Strontium-Borate
U. S.	United States
W	west
WHDF	Waterman Hills Detachment Fault

Convene at Zzyzx, CSU Desert Studies Center; proceed north to I-15.

0.0 (0.0) Re-set odometer to zero (0). Enter I-15 westbound.

5.9 (5.9) Pass Rasor Road interchange.

9.7 (3.8) Continue past the Basin Road interchange.

17.3 (7.6) Pass through faulted Miocene sediments in road cut (Miller and others, 2017, p. 29, MP 23.2)

18.6 (1.3) Pass Afton Road. View south to Manix Lake sediments (Reheis and others, this volume).

22.4 (3.8) Continue past the rest stop.

26.4 (4.0) Continue past Field Road and the anticlinally folded Plio-Pleistocene gravels.

30.5 (4.1) Pass under the Alvord Mountain Road overpass.

32.1 (1.6) Continue past the southeast arm of Lime Hill, with east-dipping Pliocene gravels that overlie Miocene sediments (Miller and others, 2011).

33.1 (1.0) EXIT at Harvard Road.

33.4 (0.3) Stop, then TURN LEFT (S) on Harvard Road.

34.5 (1.1) Stop at Yermo Road. Watch for traffic. Proceed south across the railroad tracks.

35.0 (0.5) Continue past Cherokee Road (pole line). Harvard Hill is to the right (SW). The pale green Peach Spring Tuff (PST) exposed on the north side of Harvard Hill is overlain by silicified limestone beds (MSL; Leslie and others, 2010; Buesch, this volume). The PST indicates that the Barstow basin was receiving water and lacustrine silts before 18.8 Ma, and that the MSL at Harvard Hill was deposited later than the MSL at Columbus/Gem (Stop 1-2). The marker facies at Columbus/Gem and Harvard Hill were both deposited earlier than the 16.7–16.9 MSL in the Mud Hills. It is difficult to correlate the Harvard Hill limestones because they change facies rapidly along strike (Leslie and others, 2010). Harvard Hill is one of the few places where basalt interfingers with the Barstow Formation (Leslie and others, 2010).

36.1 (1.1) Cross under power lines.

36.8 (0.7) Cross the Mojave River at River Bluff Ranch. On the terrace top, pass a road east to Camp Cady. "Camp Cady (1860–1871) was located on the Mojave Road which connected Los Angeles to Albuquerque. Non-Indian travel on this and the nearby Salt Lake Road was beset by Paiutes, Mohaves, and Chemehuevis defending their homeland. To protect both roads, Camp Cady was established by U.S. Dragoons in 1860. The main building was a stout mud redoubt. Improved camp structures were built ½ mile west in 1868. After peace was achieved, the military withdrew in 1871. The protection provided by Camp Cady enabled travelers, merchandise, and mail along both roads to boost California's economy and growth" (California Registered Historical Landmark No. 963; plaque placed by State Department of Parks and Recreation).

38.5 (1.7) SLOW. TURN RIGHT (W) on Riverside Road.

38.5 (1.0) Stop, TURN LEFT (S) on Newberry Road.

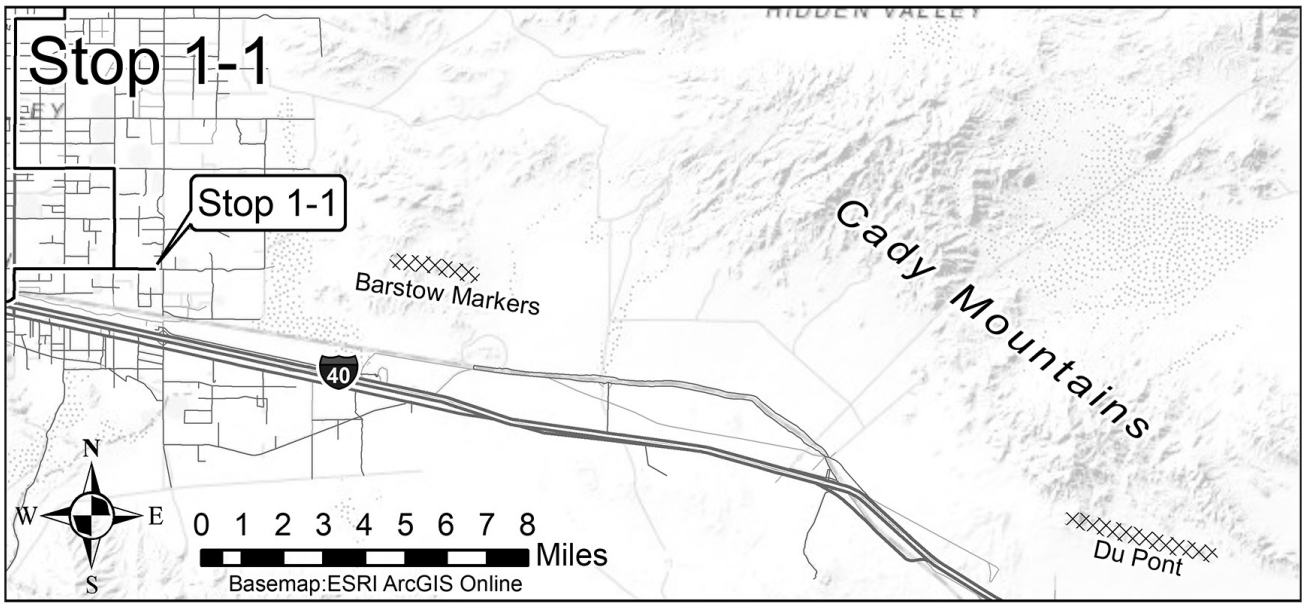

Figure 1-3. Detail of Stop 1-1 location and Barstow Formation marker beds (hachure marks) in the Cady Mountains.

40.5 (2.0) Pass Valley Center Road.

41.3 (0.8) Slow approaching Newberry Elementary School.

41.5 (0.2) TURN LEFT (E) on Silver Valley Rd.

42.5 (1.0) Pass Harvard Rd.

43.5 (1.0) TURN RIGHT (S) on Fremont Rd.

44.4 (0.9) Cross Cottonwood Road, jog left, then continue south.

45.4 (1.0) Fairview Road, stop, watch for traffic and TURN LEFT (E).

47.0 (1.6) **STOP 1-1**. View east toward the Cady Mountains with outcrops of Barstow Formation containing marker beds, and of the Hector Formation to the northeast (Fig. 1-3). Volcano house is to the east-northeast (on a conical hill that is not an actual volcano!). The Barstow Formation markers are in the near distance in the southwestern Cady Mountains (Reynolds and others, 2010; Reynolds, 2013; Miller and others, 2013, p. 23, stop 2-6). Northeast, across the Pisgah Fault, is the Hector Formation in the western Cady Mountains, the upper strata of which are coeval with the lower Barstow Formation (Woodburne, 1988). Farther east, Sleeping Beauty Mountain is on the skyline, and the eastern-most Barstow markers crop out on its southern flank in the Du Pont claims (Fig. 1-3; see Durrell, 1953; Reynolds and others, 2010). The Du Pont Markers are 30 miles east of Barstow Formation outcrops at Harvard Hill and Daggett Ridge. The steeply north-dipping Du Pont markers are bounded on the north by the South Cady Frontal Fault, and do not extend more than 700 feet south of that fault (Miller and others, 2013, p. 26, stop 2-10). Marker beds at Du Pont include nearshore deposits of the MSL, the BPL and the SrB horizon.

This sequence is overlain by the 18.8 Ma PST (Fig. 1-2; Durrell, 1953; Miller and others, 2013). The Du Pont PST has been rotated ~11.6° clockwise (No. 40 of Wells and Hillhouse, 1989). To the south on Pacific Mesa, the PST is rotated ~10.1° counterclockwise (No. 38 of Wells and Hillhouse, 1989). To the north at Baxter Wash in the Cady Mountains, the PST is rotated ~30.0° clockwise (Hillhouse and others, 2010). The differing degrees and directions of rotation suggest different histories for each PST block (Miller and others, 2013, p. 26, stop 2-10).

The Du Pont section, where the PST overlies the marker beds (Fig. 1-2; Reynolds and others, 2010), is similar to the Columbus/Gem section that we will see in Stop 1-2. These sections may have been deposited in an eastern arm of the Barstow basin, which has uncertain dimensions. These sections may also have been deposited near one another and later displaced, although faults that could have accomplished this movement have not been identified. RETRACE west on Fairview Road toward Newberry Road.

48.6 (1.6) Pass Fremont Road.

48.8 (0.2) Pavement starts.

49.5 (0.7) Harvard Road.

59.5 (1.0) Stop at Newberry Road. Watch for cross traffic. TURN LEFT (S).

60.0 (0.5) Cross railroad tracks.

60.1 (0.1) TURN RIGHT (W) onto Pioneer Avenue.

61.1 (1.0). Pass Mountain View and Element Specialties plant with evaporation ponds. As we approach the west end of Pioneer Avenue, we will be crossing the Calico Fault (Bortugno and Spittler, 1986).

62.1 (1.0) Stop. Watch for cross traffic. TURN LEFT on National Trails Highway.

62.2 (0.1) TURN RIGHT and enter I-40 westbound toward Daggett and Barstow.

68.0 (5.8) Continue past the Hidden Spring Road off ramp for the Barstow-Daggett Airport.

73.0 (5.0) EXIT at Daggett Road.

73.4 (0.4) Stop at Daggett Road (A Street) and TURN LEFT (S) toward Daggett Ridge.

73.7 (0.3) Stop at Camp Rock/ Pendleton Road on the south side of I-40 and TURN LEFT (E) on Camp Rock Road.

74.8 (1.1) BEAR RIGHT (S) on Camp Rock Road. Pavement ends.

75.7 (0.9) Continue past the first powerline road; wooden posts are on the right. Proceed to yellow metal posts on the south side of third powerline road.

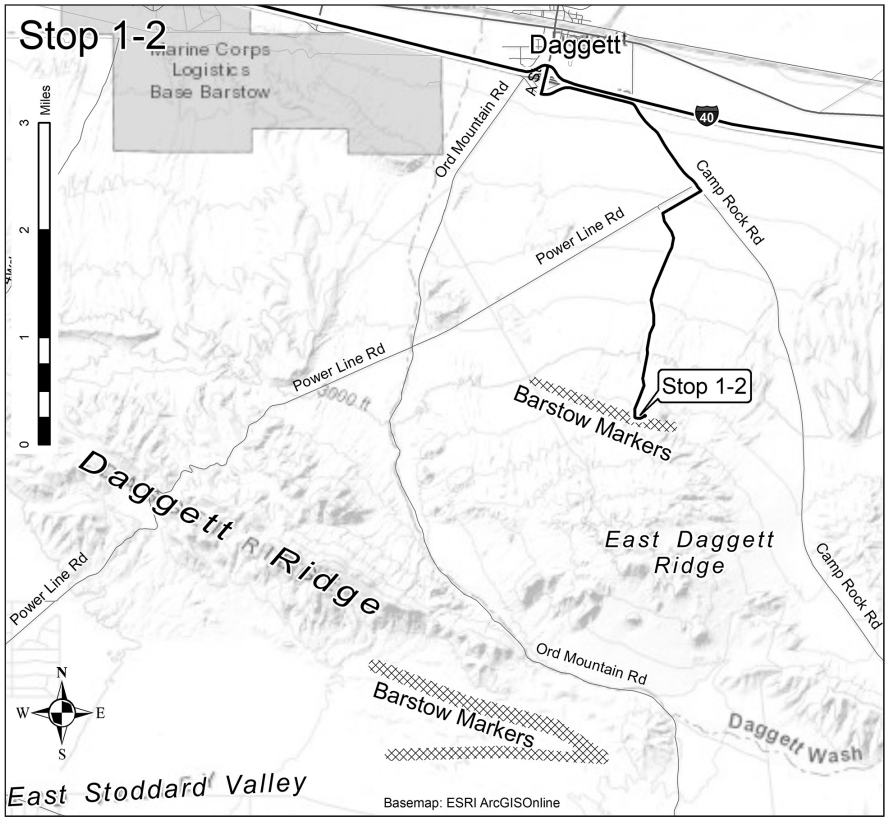

Figure 1-4. Detail of Stop 1-2 location and Barstow Formation marker beds (hachure marks) at Daggett Ridge.

75.9 (0.2) TURN RIGHT at yellow metal post on left. Proceed west-southwest along the powerline road (BLM 7350).

76.3 (0.4) TURN LEFT (S) just past Tower No. 449.2 (marked on its southeast leg).

77.9 (1.6) Continue south past a right turn (W) to the West Gem outcrops.

73.8 (0.4) Continue past a wash running left (SE).

74.0 (0.2) Cross over the pink PST and BEAR LEFT (E).

74.1 (0.1) PARK on drill pad.

STOP 1-2. Columbus/Gem Mine (Fig. 1-4). We are at the southeast end of Daggett Ridge, where the marker bed section of the Barstow Formation is locally overturned. The marker section is bounded on the east by a branch of the Camp Rock Fault and on the west by the Lenwood Fault. The lowest marker here is the MSL (uphill to south), exposed as interrupted lenses because its deposition was overwhelmed by an influx of near-shore granitic conglomerate. Immediately adjacent to our location and stratigraphically upsection from the MSL are the shallow nearshore facies of BPL and the SrB horizons, and farther upsection (downhill from where we stand) is the pink PST (Fig. 1-5). The position of the PST indicates that much of the Barstow Formation at Columbus/Gem was deposited prior to 18.8 Ma.

We have a view east toward Ludlow and west toward Barstow. Barstow Formation marker beds crop out from Ludlow, the Cady Mountains, Daggett Ridge (underfoot), the Yermo Hills, the Calico Mountains, and westward to the Mud Hills and beyond. Deposition of the base of the formation is oldest to the southeast and youngest to the northwest (Reynolds and others, 2010).

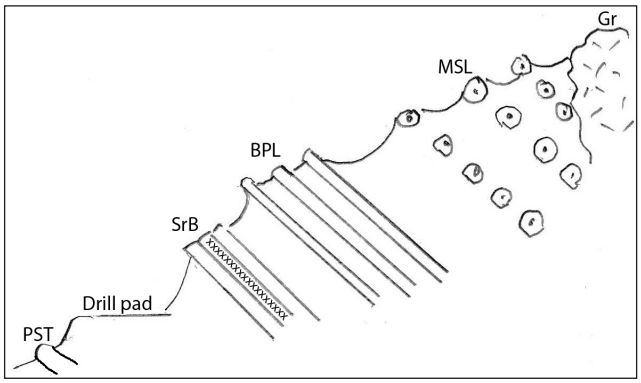

Figure 1-5. View east of the Barstow Formation marker bed stratigraphy at Columbus/Gem (Stop 1-2). PST, Peach Spring Tuff; SrB, strontium-borate beds; BPL, brown platy limestone; MSL, massive stromatolitic limestone; Gr, granite.

From Stop 1-2, the Barstow Formation extends south and west, covering almost 25 square miles of eastern Stoddard Valley. The MSL, BPL and PST were deposited in eastern Stoddard Valley. The only surface occurrence of the SrB horizon is here at northeastern Daggett Ridge (Fig. 1-2). Deposition in Stoddard Valley either ended soon after the PST was emplaced, or additional deposits were removed by erosion. Field observations (Reynolds and others, 2010) suggest that Daggett Ridge might have risen during deposition of the Barstow Formation and after deposition of the PST, causing indurated sheets of granitic debris to be shed southwestward and northeastward. The post-PST rising of Daggett Ridge may have halted the deposition of the Barstow Formation in Stoddard Valley, but allowed it to continue in the area northeast of Daggett Ridge.

Dokka and Travis (1990) presented a profile of Daggett Ridge suggesting compression between the Camp Rock and Lenwood faults caused the anticlinal fold of Daggett Ridge and overlying Barstow beds. However, the Barstow Formation at Columbus/Gem includes the basal granitic conglomerate overlying the MSL, which may have been derived from uplift at Daggett Ridge. This sequence indicates that uplift and debris shedding occurred prior to and during the deposition of the PST (Figs. 1-2, 1-5). A similar model for uplift can be seen at the northeastern end of Stoddard Valley. Further deformation of eastern Daggett Ridge between the Camp Rock and Lenwood faults occurred in the late Neogene (Dokka and Travis, 1990).

Several different models for extension that created the Pickhandle trough have been proposed (Glazner and others, 1989a, b; Dokka and Travis, 1990; Fillmore and Walker, 1990; Dokka and others, 1991; Ingersoll and others, 1996; Glazner and others, 2002; Anderson, 2017) but few discuss the time-transgressive nature of post-tectonic filling with fluvial and lacustrine sediments of the Barstow Formation (Dibblee, 1968). Fillmore and Walker (1990) proposed that there was a northeastern hanging wall that moved northeast over the footwall, opening a northwest-trending basin that was filled with syntectonic Pickhandle volcanics and clastics, followed by fluvial and lacustrine sediments of the Barstow Formation. Deposition of the diverse Barstow facies is discussed by Loughney and Badgley (2017) and Loughney and Hardy (this volume). The time transgressive nature of Barstow trough filling from southeast to northwest has been discussed by Reynolds and others (2010).

The Barstow Formation filled the Pickhandle trough, running 25 miles northwest from Daggett Ridge to the west end of the Mud Hills. Coarse clastic sediments are interpreted to delineate the margins of the trough. On the southwest side of the trough, coarse clastic facies include the granitic debris and glide sheets of red-weathered arkosic sandstone along Daggett Ridge (Stop 1-2) west to Ord Mountain Road and the San Bernardino Meridian, the Owl Conglomerate in the Red Division of the Mud Hills, coarse sediments associated with paleosols at Fossil and Truck Top Canyons, and the granitic fanglomerate facies of the Barstow Formation at Black Canyon Anticline (Stop 1-6). On the northeast side of the trough, debris is mostly volcaniclastic or volcanic and attributed to the older Pickhandle Formation. This coarse debris is seen in the northeastern reaches of Owl Canyon tributaries, the Pickhandle red sandstone along Copper City Road, and the volcaniclastic detritus north of Little Borate and Borate in the eastern Calico Mountains (Singleton and Gans, 2008).

Fine-grained facies, particularly lacustrine facies, indicate deposition toward the lowest part of the trough. Examples include sedimentary sections in the Toomey Hills, Lime Hill and the eastern section at Du Pont. In Owl Canyon in the Mud Hills, dating of the MSL indicates that it was forming from ~15.3 to 16.3 Ma (Cole and others, 2005) along the southwest and northeast portion of the basin. This would be expected during lacustrine deposition in an expanding trough in tandem with alluvial fans developing from rising highlands to the northeast and southwest.

RETRACE TO I-40 and Daggett overpass.

74.8 (0.7) Pass a left turn (W) to West Gem outcrops.

76.4 (1.6) Rejoin the powerline road and TURN RIGHT (E).

76.9 (0.5) Stop at Camp Rock Road. Watch for traffic. TURN LEFT (N) toward I-40.

78.0 (1.1) Turn left on paved Camp Rock Road.

79.0 (1.0) TURN RIGHT (N) on Daggett Road/A Street and cross over I-40.

79.3 (0.3) TURN LEFT (W) onto I-40 westbound toward Barstow.

81.8 (2.5) Pass Nebo Street.

83.9 (2.1) Pass the Marine Corps logistic base.

84.2 (0.3) Cross over National Trails Highway.

85.5 (1.3) Pass East Main Street exit.

86.8 (1.3) I-40 joins I-15. Carefully merge left.

87.2 (0.4) Pass Barstow Road and central Barstow.

89.1 (1.9) Pass L Street exit.

90.5 (1.4) Pass the exit right (N) for Hwy 58 to Bakersfield. Cross the trace of the Lenwood Fault (Bortugno and Spittler, 1986) just east of the road cuts. The Barstow Formation with marker beds is present to the north at Grandview (Stop 1-4).

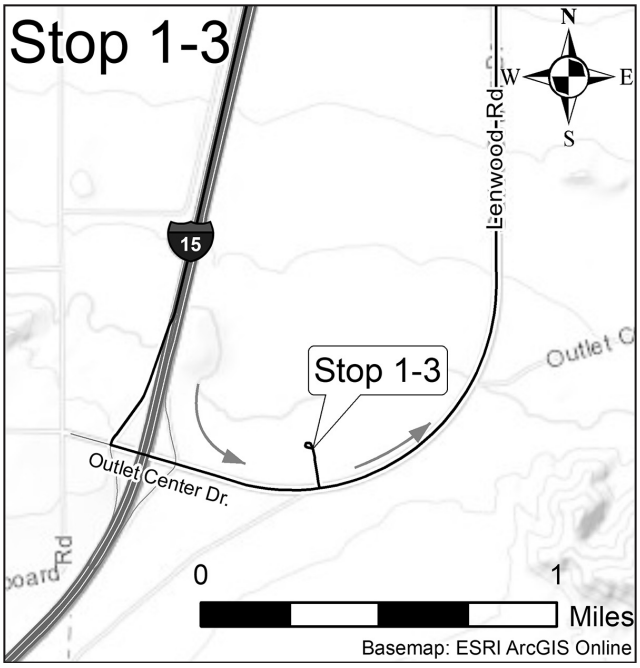

Figure 1-6. Detail of Stop 1-3 location off Outlet Center Drive.

92.1 (1.6) Pass the Lenwood off ramp. As we descend to the southwest we are crossing a splay of the Lenwood Fault (Bortugno and Spittler, 1986). Move to the right for upcoming exit.

95.1 (3.0) EXIT at Outlet Center Drive.

95.5 (0.4) Stop at south Outlet Center Drive. Watch for traffic, TURN LEFT (E). Road bears left (N) and is renamed Lenwood Road.

95.9 (0.4) Watch for oncoming traffic and turn left (N) across the pavement to a quarry in Peach Spring Tuff. Stay to the right on the dirt track, circle north, then west to the quarry.

96.1 (0.2) **STOP 1-3**. PARK on low hill south of the quarry. Examine Peach Spring Tuff (Fig. 1-6). The PST (see Hillhouse and others, 2010) crops out discontinuously from Outlet Center Drive eastward along the north flank of Daggett Ridge to the Stoddard Cutoff Road. Where crossed by branches of the Lenwood Fault, the sections of the PST (Dibblee, 1968, 1970) appear to be right-laterally offset a total of 2 miles, slightly more than the 1.6 miles of other estimates (Jachens and others, 2002; Hillhouse and others, 2010; Miller and others, 2010; Roche and others, 2016).

Return to paved Outlet Center Drive.

96.2 (0.1) Watch for cross traffic. TURN LEFT (E) onto Lenwood Road (Outlet Center Drive) and proceed northerly toward Outlet Center.

96.9 (0.7) Pass PST outcrops in low hills to the right (E).

98.7 (1.8) Slow while entering Outlet Center.

99.0 (0.3) Traffic signal at Mercantile Way.

99.1 (0.1) Traffic signal at Factory Merchants Road.

99.3 (0.2) Lenwood Road at Highpoint Road. Cross over I-15 and proceed north toward Lenwood.

99.6 (0.3) Traffic signal at Commerce Parkway. Fill up gas tanks here, as needed.

100.5 (0.9) Lenwood Road bears left and then right.

101.8 (1.3) Slow entering Lenwood.

102.0 (0.2) Stop at West Main Street (National Trails Highway). Proceed north on Lenwood Road across railroad tracks. Cross over one trace of the Lenwood Fault.

102.5 (0.5) Pass Jasper Street.

102.7 (0.2) Pass the northwest corner of Grandview mobile home park.

103.9 (0.3) TURN RIGHT on dirt track and drive east for 1/10 mile and park.

104.0 (0.1) PARK. **STOP 1-4**. The Barstow Formation at Grandview (Fig. 1-7) contains marker beds in shallow nearshore lacustrine siltstones dipping steeply north. From where we are parked, we can see a low ridge to the left (N) consisting of cemented granitic gravels (Reynolds and others, 2010, p. 154); the ridge ahead (E) is the MSL, and one to the right (SE) is the silicified BPL (Fig. 1-8). Out of sight to the south is a porphyritic sanidine dacite flow breccia that could potentially yield dates for this section. Branches of the Lenwood fault are mapped to the northeast and southwest of these Barstow Formation

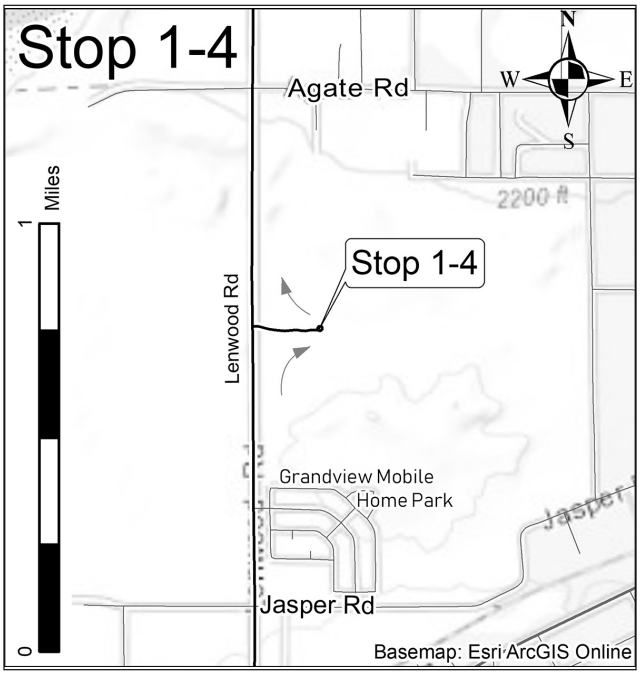

Figure 1-7. Detail of Stop 1-4 location at Grandview.

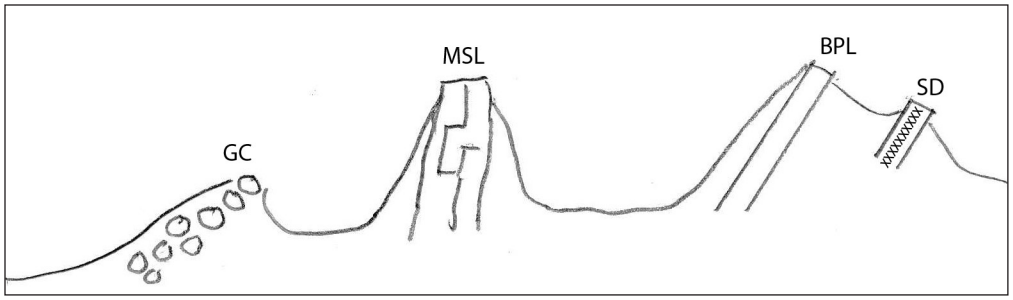

Figure 1-8. View east of the stratigraphic section at Grandview (Stop 1-4). GC, granite conglomerate; MSL, massive stromatolitic limestone; BPL, brown platy limestone; SD, sanidine dacite.

outcrops (Bortugno and Spittler, 1986). RETRACE to Lenwood Road.

104.1 (0.1). TURN RIGHT on Lenwood Road.

104.8 (0.8) Cross the Mojave River.

105.4 (0.6) Slow, TURN RIGHT (E) on Community Blvd.

106.4 (1.0) Pass the site of Hills Dairy.

106.7 (0.3) Pass under Hwy 58. Slow to 25 mph through the community on Community Blvd.

107.4 (0.7) SLOW: Community Blvd makes a sharp left (N).

107.7 (0.3) Stop, TURN RIGHT on Old Hwy 58. Dolomitic marble is being extracted from mines to the northeast at 11:00. Dolomite pods are within the Waterman gneiss.

108.3 (0.6) Old Hwy 58 bears east. Gneiss is on the north and yellow ochre limestone is to the south. In the western Calico Mountains and on the south limb of the Mud Hills syncline, ochre limestone occurs down section from the MSL. Perhaps other outcrops of ochre limestone are also early Miocene in age.

109.0 (0.7) Pass Waterman Street. Old Hwy 58 bears east.

109.4 (0.4) Pass Ramirez Road to the south.

110.1 (0.7) Terraces on left (N) mark the site of the Waterman Mill, which produced $1,611,429 in silver between May 1, 1881, and March 15, 1887, from the nearby Waterman silver mine (Vredenburgh and others, 1981).

111.1 (1.0) Stop at intersection of Old Hwy 58 and Old Irwin Road. TURN LEFT (N).

111.2 (0.1) Stop. Old Hwy 58 jogs to the right. PROCEED NORTH on Old Irwin Rd past a hill on the right of yellowish Barstow Formation limestone which occurs beneath Barstow markers elsewhere.

111.8 (0.6) Pass the north margin of Mountain View Cemetery.

113.5 (1.7) Slow to 40 mph entering curves through Waterman Hills. We have crossed the Harper Lake Fault (Bortugno and Spittler, 1986).

113.7 (0.2) Pass a road on the left (N) to the Waterman silver mine.

114.3 (0.6) Pass Bishop Road on the right (E).

115.0 (0.7) Pass a road on the left (W) to microwave towers and a good exposure of the Waterman Hills Detachment Fault (WHDF), where 19 Ma reddish porphyritic rhyolite sits above the mylonitized lower plate rocks (Glazner and others, 1989a, b).

116.0 (1.0) Slow, watch for traffic, and TURN LEFT onto the Waterman Hills powerline road, HL 7140. We will be following roads with BLM prefixes for each management polygon. These include HL = Harper Lake; BM = Black Mountain; FP = Fremont Peak. Bear right, then left, and proceed westerly to the fifth power pole.

116.1 (0.1) View northwest of low hills in foreground (1/2 mile) of Barstow Formation (Anderson and Onderdonk, 2018) supported by gray fine-grained sediments.

116.5 (0.4) Pass the third tower.

116.8 (0.3) Pass the fourth tower, No. 13-2.

117.8 (1.0) Pull into clearing around the fifth tower, No. 13-3.

118.9 (1.1) **STOP 1-5**. We are on the northeastern slope of the Waterman Hills, with exposures of the WHDF at the microwave station to the south (Fig. 1-9; Glazner and others, 1989a, b). The detachment fault consists of mylonitized Miocene granite in the lower plate (foot wall; 23–19 Ma; Fillmore and Walker, 1996) and a red rhyolite in the upper plate (hanging wall). Glazner and others (1989a, b) and Fillmore and Walker (1996) correlate the upper plate with volcanics of the Pickhandle Formation. The Pickhandle Formation was deposited in small hanging-wall basins related to extension along the detachment fault, beginning about 23.7 Ma and continuing until 18.9 Ma (Fillmore and Walker, 1996), although Anderson (2017) has questioned the presence of a detachment fault.

From this spot, we can look east to the Calico Mountains, Gypsum Basin, and Copper City Road and northwest to the Mud Hills (Reynolds and Miller, 2010; Miller and others, 2013). The marker sequence in the Barstow Formation is present at all of these localities. In the Mud Hills, the biostratigraphic divisions of the fossiliferous Barstow deposits were recognized by their distinct faunas and lithostratigraphy (Pagnac and others, 2013). Low in the Mud Hills we can see red conglomerate of Red

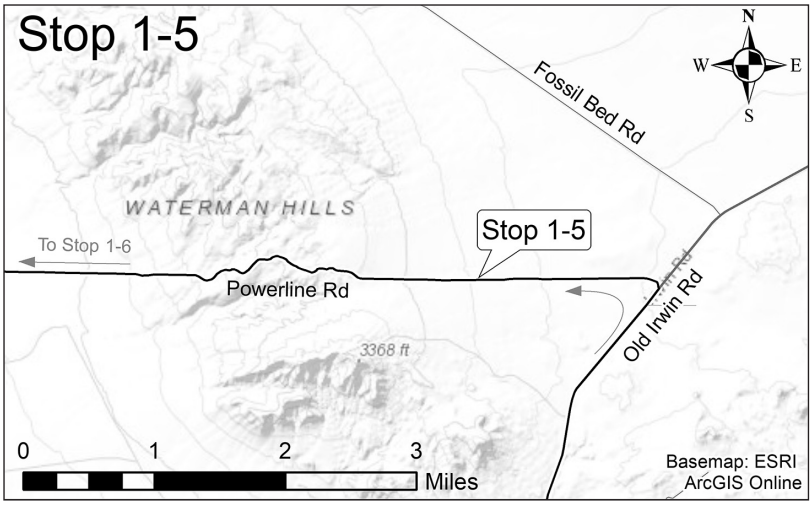

Figure 1-9. Detail of Stop 1-5 location on Powerline Road.

Division (19–17 Ma; Woodburne and Reynolds, 2010), gray shales of Rak Division (16.4–15.9 Ma; Woodburne and Reynolds, 2010), and the pale olive sandstones of the Green Hills with the white Skyline Tuff (>14.8 Ma; Pagnac, 2009) at the top of the section. The Upper Member is not visible from this spot. (For detailed description of the biostratigraphy and lithostratigraphy of the central Mud Hills see Pagnac, 2009; Woodburne and Reynolds, 2010.)

The Red Division sediments contain Red Division Quarry, the oldest faunal association in the Mud Hills. This late Hemingfordian LMA quarry is located just above the MSL that represents the first filling of the western Barstow Basin by lake sediments. Farther up section are the gray shales of Rak Division and other marker beds (BPL, IS, SrB).

Assuming that movement on the Waterman Detachment had ceased by 19 Ma (Fillmore and Walker, 1996; Ingersoll and others, 1996; Glazner and others 1989a, b), the Waterman Hills began to rise and shed clasts of the rhyolitic upper plate during the time of deposition of the Red Division (19–17 Ma). The rocks of the lower plate were exposed and shed clasts into the Red and Rak Division deposits, ending at about 16 Ma. The blue-gray color of sediments that we see in the Rak Division are caused by abundant metamorphic clasts that mark the unroofing of the mylonitized WHDF lower plate.

Loughney and Badgley (2017) offer a detailed description of Barstow Formation facies and depositional environments. Loughney and others (2020) discuss available moisture and changes in vegetation through the Middle Miocene Climatic Optimum (17–14 Ma), a major global warming interval in the Cenozoic.

Paleosols in the Barstow Formation of Mud Hills are relatively rare. In several places, red-colored sediments represent very weathered sediments derived from the unroofing of adjacent highlands rather than paleosols. Paleosols occur in the upper part of the Barstow Formation, exposed in the western Mud Hills (Fig. 1-10; Loughney and Badgley, 2017). These paleosols have carbonate nodules, slickensides, and other features indicative of repeated wetting and drying. They formed during climatic cooling following the Middle Miocene Climatic Optimum (Loughney and others, 2020).

In the west end of the Mud Hills, clasts of brown and purple dacite and quartz-rich flow-banded dacite, as well as lavender hornblende-biotite rhyodacite have been collected from arkosic sediments. These clasts suggest distinctive, localized sources (Dibblee, 1968, plate 1) from Pickhandle Formation outcrops to the east, indicating westward transport from across the Coolgardie Plain on the north side of the Pickhandle trough. This part of upper Barstow Formation stratigraphy raises questions:

Figure 1-10. Examples of paleosols in the upper Barstow Formation. Left, view northeast of paleosols at the mouth of Fossil Canyon, northern Mud Hills. Right, view north of paleosols in Truck Top Wash, northwestern Mud Hills.

Was the basin full, with sediments passing through to other basins? Did highlands on the pre-Miocene surface unload and erode, finally ceasing delivery of sediment? Did climate change decrease the rate of sediment delivery? Combined paleontological, sedimentological, and geochemical studies could address these possibilities. Continue westerly on the Waterman Hills powerline road.

120.6 (1.7) Continue straight as powerline road HL 7152 joins HL 7140 from the right.

121 (0.4) Cross the crest of the Waterman Hills and proceed downward into Water Valley and Harper Lake drainage. Bear right, avoiding tower stub roads.

122.7 (1.7) Cross HL 7134. Continue on HL 7140.

123.4 (0.7) HL 7140 bears right (NW).

123.6 (0.2) Pass HL 7142 running southwest.

124.7 (1.1) Road bears left (W) and is eventually renamed Homestead Road.

126.5 (1.8) Pass a road on the left (S) to eastern Mt. General and Hwy 58. An unusual Ag-Cu-Zn-V mineral locality is along this route to the south (Housley and Reynolds, 2002).

126.7 (0.2) Left (S) is the northernmost outcrop of the 1.9-mile-long Pedry quartz vein, running N 10°W from the mine at the north margin of Mt. General (Housley and Reynolds, 2002; Housley, 2009).

127.9 (1.2) Pass a road to the south.

128.3 (0.4) Cross northeast-trending Fossil Bed Road.

129.9 (1.6) Stop at paved Hinkley Road. Look for traffic. TURN RIGHT (N) onto Hinkley Road.

130.9 (1.0) Pavement on Hinkley Road ends.

132.3 (1.4) Pass northeast-trending road to Murphys Well.

132.9 (0.6) TURN LEFT toward Shadow Mountain Ranch.

133.2 (0.3) TURN RIGHT (N) at a sign for Shadow Mountain Ranch.

133.7 (0.5) Pass a right turn at the pole line to a residence and Hinkley Road.

134.1 (0.4) Pass a right turn toward Hinkley Road.

135.7 (1.6) Pass a gate on the left for Shadow Mountain Ranch.

136.2 (0.5) TURN LEFT on section line road HL 7159 and proceed west.

137.5 (1.3) Slow, TURN RIGHT (N) on Black Canyon Road (BM 6271).

139.9 (2.4) BEAR LEFT (W) at fork on Black Canyon Road (BM 6271)

140.1 (0.2) TURN SHARP LEFT (SW) toward Schweitzer Well on BM 6265.

140.2 (0.1) TURN RIGHT (NW) on BM 6251 on the trace of the Harper Lake Fault. Black Mountain to the northeast is covered with the 3.7 Ma Black Mountain basalt (Oskin and Iriondo, 2004).

141.2 (1.0) Pass through the open gate in fence line.

141.3 (0.1) Slow through curves across wash.

141.6 (0.3) Pass BLM cycle road 5388.

142.1 (0.5) Join "Anticline" Road (BM 6257). Proceed northerly past basalt.

142.3 (0.2) Drop into wash.

142.5 (0.2) Pass between ridges of Black Mountain basalt.

142.6 (0.1) BM 6260 cross roads.

142.9 (0.3) Stay right (E) at gray silt ridge of the Barstow Formation.

143.1 (0.2) Stay right at fork.

143.3 (0.2) TURN SHARP LEFT uphill onto loop road and PARK on terrace top just west of the main wash road.

STOP 1-6. Black Canyon Anticline (BCA). We are at a stratigraphic position in the Barstow Formation where lower gray and white lacustrine sediments give way to the upper tan, fluvial section of the Barstow Formation of the Gravel Hills (Fig. 1-11; Dibblee, 1968). The granitic fanglomerate clasts are mostly quartz monzonite with minor quartz diorite, diorite, aplite and pegmatite interpreted to be derived from the Fremont Peak area to the northwest (Dibblee, 1968). The terrace on which we are parked is Pleistocene arkose unconformably overlying Miocene sediments. Look east to see the angular unconformity. Miocene sediments are low in the foreground and are exposed on high slopes in all directions.

Location. This is the most northwesterly outcrop of lacustrine sediments of the Barstow Formation. The exposure is an east-plunging anticline west of Black Canyon. Black Mountain to the east is covered by the Pliocene Black Mountain basalt.

Stratigraphy. Immediately to the east, the core of the BCA contains gray Miocene lacustrine siltstones and white silty sandstones alternating with red sandstones. These beds may indicate distant unroofing of a deeply weathered granitic surface, which continued to rise and shed granitic debris into the Barstow trough. This lacustrine and fluvial sequence interfingers with the Miocene olivine "anticline basalt." This is overlain by a 4,500-foot thick coarse

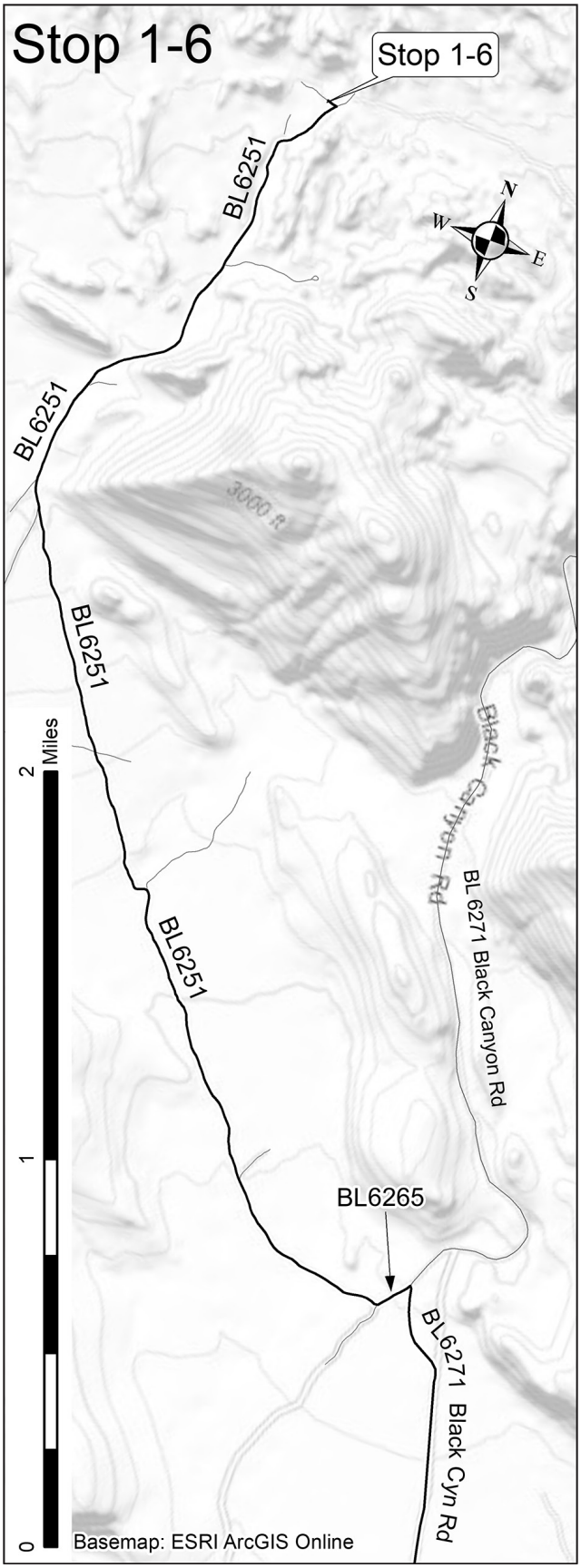

Figure 1-11. Detail of Stop 1-6 location in Black Canyon.

granitic sandstone and conglomerate. These granitic gravels are included in the Barstow Formation (Dibblee, 1968).

The gray lacustrine siltstones exposed in the BCA contain discontinuous lenses of the marker bed sequence (unpublished mapping, Reynolds, 2005): lenses of MSL, silicified BPL, and a dense carbonate layer that may be the SrB beds. Insect stromatolites at BCA have been studied in detail by Spencer (2005), who interpreted these stromatolites as having formed in clear, shallow water. The microfossil horizons occur in alternating carbonate, mudstone, and gypsiferous beds and reflect lacustrine transgressions and regressions. The ages of the BCA deposits are not well constrained. Dating BCA carbonates and basalt in the section might clarify the relationship to other outcrops of the Barstow Formation.

Structure. The Black Canyon Anticline is a tight fold that plunges easterly, toward Black Canyon, while the western portion of the axis trends west-southwest. Since the eastern portion of the axis trends east-southeast, there may have been drag along a right lateral fault mapped in Black Canyon (Dibblee, 1968). The Miocene olivine "anticline basalt" is included within this fold pattern. An anticlinal structure is mapped in Barstow Formation gravels one half mile south of the BCA on the east side of a north-striking unnamed fault in Black Canyon (Dibblee, 1968, plate 1) that suggests a small amount of post-Miocene right-lateral movement on the unnamed fault, which might be a branch of the northwest-striking Harper Lake Fault.

The nearshore, shallow-water siltstones continue upward into arkosic conglomerate of the Gravel Hills. Shallowly plunging anticlinal/synclinal fold pairs deform the section. Immediately east of Black Canyon and the BCA, Black Mountain is capped by the Black Mountain basalt, which appears as a shallow syncline unconformably overlying a thick section of Barstow Formation.

Age of sediments. The "anticline basalt" (new name) and white ashes are noted in the section (Dibblee, 1968) but none have been dated.

Fossil mammals in BCA sediments are rare. Those below the "anticline basalt" relate to the Green Hills Fauna of the medial Barstow Formation in the Mud Hills (Woodburne and others, 1990, fig. 6), calibrated at between 15.9–15.4 Ma. Those above the "anticline basalt" appear to correlate with the Barstow Fauna (ca. 14.8–13.4 Ma; First Division Fauna, Woodburne and others, 1990, fig. 6). These faunal relationships suggest that the BCA sediments correspond approximately to the Green Hills section of the Mud Hills. After lacustrine deposition ended in the western Mud Hills (13.4 Ma), paleosols formed, indicating slow basin filling. However, the Black Canyon portion of the trough appears to have filled rapidly with granitic conglomerates at that time. The Barstow Formation in the Black Canyon

area is overlain by the 3.7 Ma Black Mountain basalt (Oskin and Iriondo, 2004).

Summary. The fine-grained sediments of the Barstow Formation, from Columbus/Gem northwest to BCA, represent basins that were actively filling with wetland, lacustrine, and fluvial sediments (Ingersoll, 1996; Loughney and Badgley, 2017; Loughney and others, 2020). The Barstow Formation of the Black Canyon Anticline (Dibblee, 1968) poses additional questions:

1. Can ashes and basalts in the anticline be dated to allow comparison with the Barstow Formation in the Mud Hills (Durrell, 1953; Dibblee, 1968, Woodburne and others, 1990; Woodburne and Reynolds, 2010)?
2. The mammal fossils provide the best age range for BCA siltstones and mudstone deposition around 15.6 and 14 Ma. This is a rather young date for the deposition of the marker beds. Perhaps the recovery of more mammalian fossils and dating of the carbonates will resolve the apparent differences.
3. Will clasts in the granitic red sandstones confirm a source for sediments derived from the unroofing event that is different than Fremont Peak?

RETRACE southerly to south tip of gray silty ridge.

144.1 (0.8) Pass through basalt narrows.

144.3 (0.2) Road BM 6251 bears left (SSE) out of the wash.

144.5 (0.2) Stay left at fork as BM 6257 bears right.

145.0 (0.5) Pass BLM cycle road BM 5388 Continue on BM 6265.

145.2 (0.2) Slow. Drop into and cross the wash.

145.4 (0.2) Pass through open gate in fence line.

146.4 (1.0) TURN SHARP LEFT (NE) off BM 6261 at Schweitzer Well onto BM 6265. We are driving parallel to the trace of the Harper Lake Fault.

146.5 (0.1) TURN SHARP RIGHT (SE) on BM 6271 at the junction of Black Canyon Road.

149.0 (2.5) Slow at section line/utility road. TURN RIGHT (W) on HL 7159.

149.7 (0.7) Pass County Road 20776 heading north.

150.1 (0.4) Flood control structures for a dry lot subdivision from the 1970s are to the south.

151.4 (1.3) Pass more dry lot subdivision flood control structures.

151.8 (0.4) Cross HL 6257. Continue on FP 7159.

152.4 (0.6) Pass HL 6253 on the left.

153.3 (0.9) Pass a diagonal road on the right (N) leading to McDonald Well (Garcia and others, 2015).

153.7 (0.4) FP 6237 goes right (N) at a BLM kiosk.

154.5 (0.8) Slow for dips ahead.

154.9 (0.4) Cross section line road FP 6231.

155.5 (0.6) Pass a road to the north.

155.9 (0.4) Cross Hoffman Road, FP 6215, running south. Continue on FP 7159.

156.0 (0.1) Pass FP 6209 crossroads.

156.2 (0.2) Cross FP 5383.

156.9 (0.7) Slow. TURN LEFT (S) on FP 5605.

157.2 (0.3) Slow for the series of bumps in the rough road ahead.

157.4 (0.2) Caution—dip. Bear right.

157.6 (0.2) Pass through intersection with east-west section line road FP 5358.

158.1 (0.5) Slow. TURN RIGHT (W) onto unnumbered road through the Buttes.

158.3 (0.2) BEAR LEFT around the south side of a butte.

158.6 (0.3) PARK. **STOP 1-7.** The Buttes (Fig.1-12) are composed of a Miocene granodiorite with mylonitic foliation and metamorphism. Dokka and others (1994) "conclude that the M3 greenschist facies metamorphism and the Early Miocene rapid cooling event recorded in metamorphic core complex rocks are manifestations of incomplete rifting of the Mojave Extensional Belt. We further conclude that cooling of rocks of the Waterman Metamorphic Complex at ~20 Ma (Early Miocene) was the result of tectonic denudation, facilitated primarily by movements along the Mitchel and Harper Lake detachment faults and secondarily by upper plate normal faulting. Tectonic denudation is the overall vertical

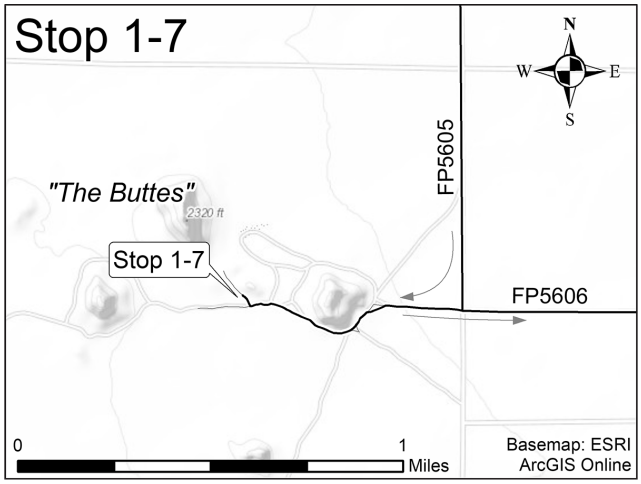

Figure 1-12. Detail of Stop 1-7 at the Buttes.

thinning of the lithosphere that occurs in conjunction with lateral extension" (p. 16–18). That is, the foliation in the granodiorite was caused by ductile deformation of the lower reaches of the WHDF. Cooling started ~23 Ma when the upper plate was removed, during Pickhandle deposition.

Walker and others (1995) write, "Results of U-Pb analyses on zircon from two pluton and two dike samples yield ages of 20 to 23 Ma. Synextensional basins formed by detachment faulting during the core complex development. Rocks in these basins compose the Jackhammer and Pickhandle formations and filled an elongate, NW trending trough more than 50 km long. The $^{40}Ar/^{39}Ar$ ages for tuff beds are as old as 23.8 ±-0.3 Ma near the base of the lower Pickhandle Formation and as young as 21.3 ±-0.5 Ma in the uppermost lower Pickhandle. Hence volcanism and plutonism are coeval" (p. 10477).

RETRACE east to section line road.

158.8 (0.2) BEAR RIGHT.

159.1 (0.3) BEAR RIGHT (S) and then TURN LEFT onto FP 5606 and proceed east.

160.1 (1.0) Slow. TURN RIGHT (S) on Hoffman Road, FP 6215.

160.6 (0.5) Pass FP 6200 on right.

160.7 (0.1) Hoffman Road bears left (SE) around a ridge with a rocky outcrop.

160.8 (0.1) Hoffman Road bears right.

161.3 (0.5) Hoffman Road, 6417, bears south at 6202 crossroads.

161.8 (0.5) Harper Lake solar mirror fields are on the left (E).

162.5 (0.7) Slow. TURN LEFT (E) on paved Hoffman Road.

163.4 (0.9) Jog to the right and prepare to turn right.

163.5 (0.1) TURN RIGHT (S) on Lockhart Ranch Road.

164.5 (1.0) Slow. TURN LEFT (E) on Lockhart Ranch Road.

165.5 (1.0) Stop. Look for oncoming traffic. TURN RIGHT (S) on Harper Lake Road. Cooling water from the solar generating fields is recycled into Harper Lake and supports wildlife (http://www.cawatchablewildlife.org/viewsite.php?site=87&display=q).

166.6 (1.1) Pass Santa Fe Street. Cross the trace of the Lockhart Fault.

170.0 (3.4) Slow to 25 mph for curves.

170.2 (0.2) Slow. Watch for oncoming trains. Carefully cross railroad tracks.

171.5 (1.3) Stop. Watch oncoming traffic. Cautiously TURN RIGHT (W) onto Hwy 58—*one car at a time.* Proceed along Hwy 58 to Kramer Junction.

177.9 (6.4) Pass through road cuts exposing paleosols.

181.6 (3.7) Pass over the railroad tracks.

184.4 (2.8) Exit at the Hwy 395 offramp at Kramer Junction.

184.8 (0.4) Stop at Hwy 395. Watch for traffic. TURN LEFT (S).

185.0 (0.2) Traffic signals at onramp to Hwy 58 east. Continue on Hwy 395.

185.1 (0.1) Traffic lights at Old Hwy 58. Fill gas tanks and obtain dinner and food for all day tomorrow before heading to your campsite. Drivers, refer to campsite handout for location.

End of Day 1

Day 2

Day 2: What we will see

Today, we will continue our exploration of the Miocene rocks of the Mojave region (Fig. 1), and we will see the vestiges of ore and mineral mining that sustained the area in 19th and 20th centuries. From Kramer Junction, we will drive north through the tungsten mining district of Atolia and the silver mines at Randsburg. On Trona Road (Stop 2-1) we will see fresh asphalt repairs of damage from the July 2019 Ridgecrest earthquakes.

We will continue north to the Garlock Fault, a major left-lateral strike-slip fault that forms the northern boundary of the Mojave tectonic block. On the north side of the Garlock Fault, west of the El Paso Mountains (Fig. 1), sedimentary and volcanic rocks of the Middle and later Miocene Ricardo Group are well exposed in Red Rock Canyon State Park. The Ricardo Group includes the Cudahy Camp and Dove Spring formations (Loomis, 1984; Loomis and Burbank, 1988). The Cudahy Camp Formation (17.9–15.0 Ma) is a predominantly volcanic and volcaniclastic unit unconformably overlain by the predominantly sedimentary Dove Spring Formation (12.5–8.0 Ma), which is well known for its rich mammalian faunal assemblages that span the Clarendonian and early Hemphillian land mammal ages (LMA; Whistler and others, 2009). These formations were deposited in an elongate, fault bounded trough, the El Paso Basin, that developed along the trace of the Garlock Fault. They and the El Paso Mountains have

subsequently been uplifted at least 5 km and tilted to the west by movement on the El Paso Fault, a normal fault that parallels the Garlock Fault (Fig. 2-3). The sedimentary facies of the Dove Spring Formation range from alluvial gravels, conglomerates and channel sandstones, lacustrine limestone, claystone and siltstone, as well as floodplain and overbank deposits (Whistler and others, 2009). Although pedogenic features are locally abundant, well-developed paleosols are uncommon.

On the southern side of the Garlock Fault, outcrops of sedimentary and volcanic units similar to those of the Ricardo Group help reconstructions of the Miocene depositional basins and their displacement by fault movement in the Miocene. Monastero and others (1997) proposed that volcanic rocks of the Eagle Crags volcanic field on the southern side of the Garlock Fault north of the Barstow Basin correlate with tuffs in the Cudahy Camp Formation, indicating 64 km of total offset since 17 Ma. Smith and others (2002) reconstructed the position of the Lava Mountains south of the El Paso Mountains between 10 and 12 Ma and interpreted that movement of the Garlock Fault initiated ~16.4 Ma.

Smith and others (2002) proposed correlations between rocks of the Ricardo Group and a complex succession of volcanic and volcaniclastic rocks in the Lava Mountains. One of these units, the Bedrock Spring Formation, contains a middle Hemphillian mammalian fauna. Whistler and others (2013) discussed these proposed correlations in more detail and concluded that the mammalian biostratigraphy is in conflict with their geochemical conclusions. More recently, Frankel and others (2008) proposed a correlation of volcanic rocks in the Summit Range on the south side of the Garlock Fault northwest of the Lava Mountains with volcanic rocks in the lower part of the Dove Spring Formation. These correlations suggest offset on the Garlock Fault of approximately 35 km in the last 10 Ma. They do not provide suggested correlations with any of the volcanic rocks in the Lava Mountains.

Day 2 begins a short distance north of the intersection of Hwy 395 and Hwy 58 at Kramer Junction (Fig. 2-1). Make sure that you arrive with a full tank of gas, drinks, water, and food for the day.

Proceed north on Hwy 395.

STOP at Kramer Junction (Hwy 395 and Hwy 58). Proceed north across intersection. Cross railroad tracks and under new Hwy 58 overpass, noting signals at both on/off ramps. After the second traffic signal, pull right into the open area and regroup. Reset your trip odometer.

0.0 (0.0) Regroup and proceed north on Hwy 395.

1.0 (1.0) Pass the FPL Energy solar generating field on the left (W).

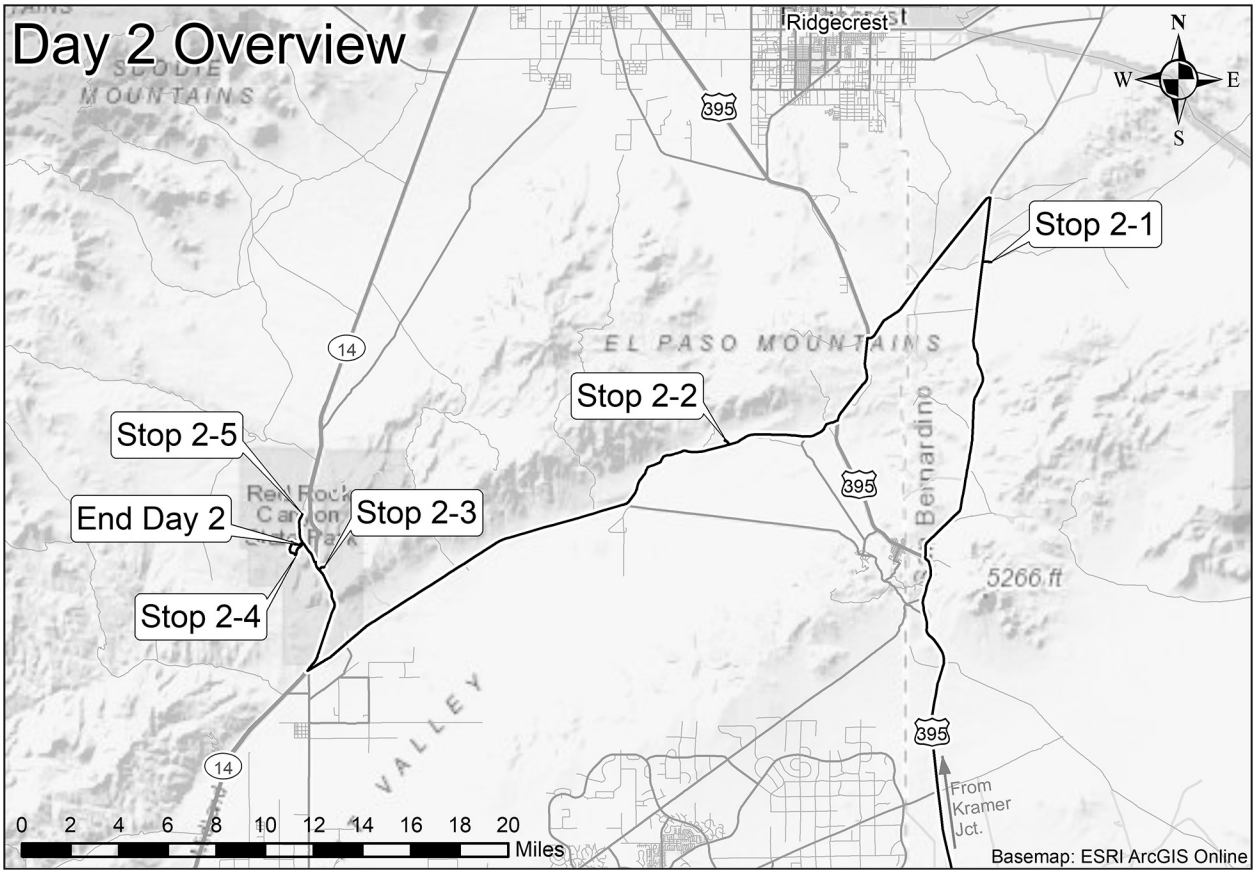

Figure 2-1. Overview map of Day 2 stops.

4.3 (3.3) Hwy 395 bears right.

5.5 (1.2) Pass the entrance to the former Kramer Detention Facility at Locust Road on the left (W). The domed structure at the hilltop remains in use by the Air Force and the Federal Aviation Administration.

6.4 (0.9) Pass a road on the right (E) to Harper Lake. The "Ball Dome" east of Hwy 395 is Edwards Nexrad Doppler radar station EYX serving Edwards Air Force Base.

13.5 (7.1) Pass Fremont Peak Road to right, leading east to the former siding of Fremont on the Randsburg Railroad (Myrick, 1991), which ran parallel to today's Hwy 395. This railroad was active from 1887 to 1933 (Myrick, 1991), serving rich mines in Randsburg and Johannesburg. A playa to the left (W) fills a depression along a branch of the Lockhart Fault (Jennings and others, 1962).

18.3 (4.8) Pass 20 Mule Team Parkway on the left, leading from the rail head at Mojave northeast past Cuddeback Dry Lake to Blackwater Well, Granite Well at Pilot Knob, through Panamint Valley, and down Wingate Wash to the Harmony Borax works in Death Valley (Faye, 1999).

20.6 (2.3) Hwy 395 bears right (N-NE).

22.2 (1.6) To the left and right are scheelite placer mines of the Atolia Tungsten District. Scheelite (calcium tungstate, $CaWO_4$) initially bedeviled dry placer gold miners. They were troubled by fragments of tungsten since it was heavy (specific gravity 6.0) and contaminated the gold concentrate. Scheelite was recognized as valuable in 1903. Separate claims purchased by Atkins and De Golia, with a contraction of names, became "Atolia." At the peak of tungsten production (1916 to 1918), the district netted nearly $10 million (Jessey and Reynolds, 2009).

22.4 (0.2) Enter the Atolia Mining District. The Paradox claims are on both sides of Hwy 395.

22.5 (0.1) Cross Hoffman Road, leading southeast past Fremont Peak to Harper Lake.

24.4 (1.9) Pass Randsburg Cutoff on left. View northwest of the 1990 Yellow Aster Mine dumps.

24.7 (0.3) Slow entering Red Mountain. The Kelly silver mine structures were to the west; the headframe has been removed. Initial samples from the mine assayed 300 ounces of silver with three ounces of gold per ton. It became California's largest silver deposit with over 20 million ounces produced between 1919 and 1942. The principal rocks underlying the Rand district are Mesozoic Rand Schist and Jurassic Atolia Quartz Monzonite. The Rand Schist is chiefly biotite schist with smaller amounts of amphibolite and quartzite. Most of the lode-gold deposits are in veins along faults, except at the Yellow Aster Mine where the gold occurs in a series of closely spaced veinlets (Jessey and Reynolds, 2009).

25.0 (0.3) Pass Osdick Road on the left.

25.5 (0.5) Pass Red Mountain Road on the left (W).

26.5 (1.0) Slow, watch for traffic. TURN RIGHT (N) on Trona Road.

27.8 (1.3) Proceed north on Trona Road.

28.5 (0.7) Trona Road bears left (N). Steam Wells Road runs easterly toward Black Water Wells (Kaldenberg, 2011). Some of the pumps on the wells that provided Johannesburg and Randsburg with water were operated by steam, an early use of geothermal power (Mendenhall, 1909; Reynolds and others, 1998). The steam wells are now fenced and in a wilderness area.

29.6 (1.1) Pass a left turn toward Summit Diggings.

30.5 (0.9) Pass a BLM road to the left.

31.3 (0.8) Pass Sadinia Road, a dirt track, on the left (W).

33.1 (1.8) Pass Savoy Road on the right.

33.4 (0.3) View left (W) of silty sediments (Dibblee, 1967).

33.6 (0.2) SLOW. Look for recent asphalt repair. Fresh asphalt marks the most southerly break on the faults associated with the 2019 Ridgecrest earthquakes of July 4 (6.4 M), July 5 (7.1 M), and associated foreshocks and aftershocks. The earthquakes caused up to $5 billion dollars of damage to structures on the Naval Weapons Air Station at China Lake (Reyes-Velarde, 2019).

> The major breaks of several feet were about a mile east of the intersection of Trona Rd. and 178, on 178. Breaks of several inches occurred along 178 west of the intersection with Trona Rd. Miles Wagner with SB County OES found additional breaks along 395 south of Ridgecrest. The Naval Weapons Air Station at China Lake had 12 foot horizontal and 11 foot vertical offsets near the epicenter. Minor damage to Trona Road north of the Spangler Hills; no damage to the road where the Garlock crosses it. Damage to the railroad tracks where the fault crossed it (Frank Jordon p. c. to Reynolds, July 29, 2019).

34.6 (1.0) Look for the Spangler Hills sign on the right, then cross the Garlock Fault. Argus Peak and Telescope Peak are to the NNE, Owens Peak is NW. The Spangler Hills are now a designated Open OHV area and have become crisscrossed with motorcycle routes. Camping is allowed here.

35.5 (0.9) Pass a dirt crossroads.

37.0 (1.5) Slow, TURN RIGHT (E) on Pinnacles Road (RM 143). Proceed east.

37.4 (0.4) **VIEW STOP 2-1.** Look ESE to outcrops 6 miles away on the south side of the Garlock Fault (Fig.

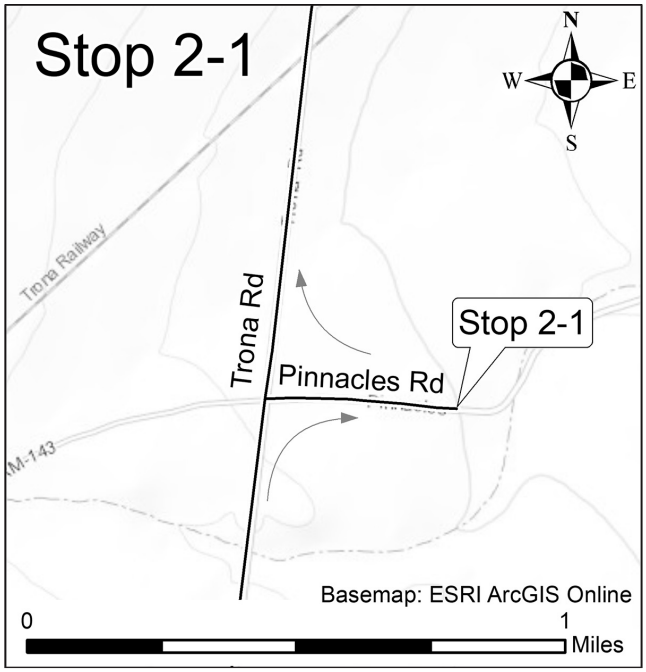

Figure 2-2. Detail of Stop 2-1 at Pinnacles Road.

2-2). Outcrops of the Bedrock Spring Formation contain fossil small mammals dated at 7.5–6 Ma (Hemphillian LMA), of similar age to fossils found in outcrops 30 miles west on the north side of the Garlock Fault, southwest of the Dove Spring Formation. The correlation of these sediments and faunas has been cited as evidence they were deposited in the same basin between 7–6 million years ago (Woodburne and Reynolds, 2010; Whistler and others, 2013), which conforms to the history of displacement along the Garlock Fault proposed by Monastero and others (1997) and Smith and others (2002). Retrace west to Trona Road.

37.7 (0.3) Stop at Trona Road. Watch for oncoming traffic. Turn right (N) on paved Trona Road and proceed north about two miles to Searles Station Cutoff Road. Railroad tracks ahead (N) were bent during the July 2019 Ridgecrest earthquakes.

38.2 (0.5) Caution when crossing railroad tracks.

38.4 (0.2) Pass Stevens Mine Road on right (E).

39.8 (1.4) Slow, watch traffic and turn left onto Searles Station Cutoff Road.

42.7 (2.9) Look for traffic while crossing railroad tracks.

44.7 (2.0) Slow while crossing two sets of railroad tracks. The road north leads to historic Garden City where water sources allowed vegetable gardens to be established.

46.1 (1.4) STOP at Hwy 395. Look carefully for fast cross traffic. TURN LEFT (S) onto Hwy 395.

47.6 (1.5) Slow on downhill stretch. We are crossing the Garlock Fault.

48.6 (1.0) Hwy 395 passes between hills. Slow for an upcoming right turn. Watch for traffic ahead and behind.

49.0 (0.4) Pull into the right lane and prepare for a right turn.

49.2 (0.2) TURN RIGHT (W) onto Garlock Road.

50.4 (1.2) Pass Goler Road on the left (S). The Goler Formation lies to the north, in the north-central portion of the El Paso Mountains (Fig. 1). The formation is a 2-mile (3-km) thick section of fluvial sediments capped by fossiliferous marine sediments (Cox and Edwards, 1984; Cox and Diggles, 1986; McDougall, 1987; Lofgren and McKenna, 2002; Albright and others, 2009; Lofgren, this volume). Intense prospecting for fossils has yielded a suite of small mammals that represent four Paleocene land mammal ages. The uppermost portions of the Goler Formation consist of fossiliferous marine sediments (Lofgren and others, 2020). This is the best section west of Wyoming and Colorado for studying Paleocene faunas (Albright and others, 2009). No fossils have been recovered from the lower members (1 and 2) of the Goler Formation, but if rates of deposition can be considered constant, lower strata project as Cretaceous in age (Cox, 1998). Clasts in the Goler Formation tell us that the Mojave Block to the south was elevated in the early Cenozoic (Cox, 1998).

52.6 (2.2) Pass Goler Gulch and the site of Goler on the right (N). SLOW for upcoming right turn. Watch for traffic from behind.

55.2 (2.6) Slow, watch for traffic from behind, and TURN RIGHT (NW) on Charlie Road (EP 146).

55.4 (0.2) Loop north on Charlie Road, then right (E) at the edge of the Garlock Fault scarp.

STOP 2-2. PARK above the playa on south side of the 70-foot-high scarp of the Garlock Fault (Fig. 2-3). This depression was offset left laterally from Goler Gulch, the next major drainage to the west. Cabins owned by the BLM are part of the Adopt-A-Cabin program. Recently, one cabin burned down, and the remaining cabin is in bad shape. Camping is allowed here.

Loop vehicles right (S) and RETRACE to the paved Garlock Road.

55.7 (0.3) Stop at Garlock Road. Look both directions for traffic. TURN RIGHT (W).

56.3 (0.6) The depression on the north side of the road is a left-laterally offset portion of Goler Gulch, the next drainage west (Reynolds and others, 1998). The cement foundation of an ore mill remains on the north scarp of the depression.

56.5 (0.2) Enter the Goler Gulch floodplain.

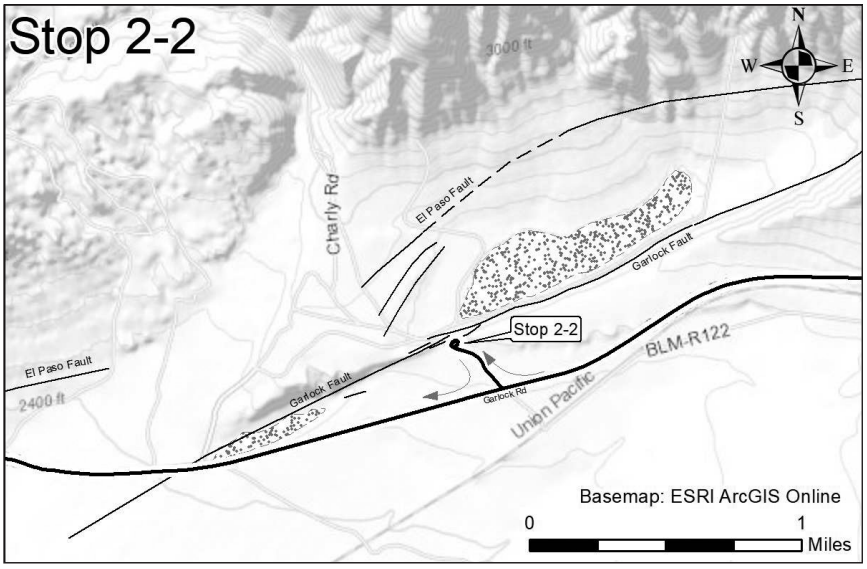

Figure 2-3. Detail of Stop 2-2 overlooking the Garlock and El Paso faults (dashed where approximate). Stippling highlights playas that formed in sags adjacent to the Garlock fault.

56.7 (0.2) Tamarisk trees mark the site of Cow Wells, where Eugene Garlock found water at 30 feet, and where the Yellow Aster mill was built in 1898. View west shows the El Paso Fault on the right, the Garlock Fault left, and a terrace in between.

57.0 (0.3) Slow. Garlock Road bears left (S) then right (W).

57.6 (0.6) Garlock Road bears left (S).

57.9 (0.3) Slow. Road bears right.

58.3 (0.4) Slow. Road bears left.

58.8 (0.5) The town site of Garlock is on the right (W). The town was a water source for western Mojave cattlemen and traders avoiding a trek through the El Paso Mountains to Ridgecrest. When gold was discovered in a nearby canyon in 1887, an arrastra was constructed to process the ore. In 1893 a nugget from Goler Canyon valued at approximately $2,000 caused a gold rush. In 1895, Eugene Garlock from Tehachapi constructed an eight stamp mill here (Hensher, 1998a). He later moved the mill to Cow Wells where more water was available (and because the town people couldn't stand the sound of the mill!), but the name Garlock stuck. Competing mills at Barstow and Randsburg caused the town to be abandoned by 1904 (Jessey and Reynolds, 2009).

All buildings that could be moved were hauled up the Red Rock Randsburg Road to Randsburg where they remain. The building made of railroad ties was the schoolhouse. There is a large arrastra in the SW corner of the fenced property. The pink building on the east side of the road was the bar and brothel.

After passing the Garlock town site, we are between the Garlock Fault (S) and the El Paso Fault (N) at base of the El Paso Mountains.

59.0 (0.2) Crossroads.

59.7 (0.7) Red Rock Randsburg Road on the left (S) joins Garlock Road and becomes the Red Rock Randsburg Road.

60.8 (1.1) Mesquite Canyon Road (EP 100), the major entrance to the road system of the El Paso Mountains, to Burro Schmidt's tunnel, and gold camps at Black Mountain and Bickel Camp.

64.7 (3.9) The western salty lobe of Koehn Playa is on the left (S). Koehn Playa is a graben between the Cantil Valley Fault on the south and the Garlock Fault on the north. The El Paso Fault is located farther north and cuts the southern granitic face of the western El Paso Mountains.

65.5 (0.8) Pass Saltdale Road leading south to salt evaporation ponds. The Consolidated Salt Company constructed a crushing and screening plant and narrow gauge railroad track onto the playa of Koehn Lake in 1914. The plant produced around 20,000 tons of salt annually (Hensher and others, 1998). The plant continued salt production until the late 1960s as a facility of the Morton Salt Company.

65.8 (0.3) Pass Last Chance Canyon Road.

66.9 (1.1) Cross north/south section line road.

67.2 (0.3) Crossroad leading left (S) to halite-rich sediments. The uplifted and exposed playa beds strike northwest and dip steeply northeast. The orientation of strata between two faults may suggest that the Garlock Fault moved left laterally more recently than the Cantil Valley Fault.

67.6 (0.4) Pass through crossroads. This is the site of Gypsite (S), named for the gypsite (gypsum and clay) mill operated by Charles Koehn in 1909. Gypsite is used for plaster and agricultural soil amendments (Hensher, 1998).

69.0 (1.4) Slow; cross Red Rock Canyon Wash.

69.8 (0.8) Pass Cantil Road on the left (S). The Ricardo branch of the Southern Pacific Railroad crossed here and stopped for water at the site now marked by tamarisk trees just visible inside Red Rock Canyon State Park.

70.6 (0.8) Slow; road bends right over the hill.

70.7 (0.1) Cross a major drainage.

71.2 (0.5) Pass Neuralia Road to California City on the left (S).

71.3 (0.1) Stop at Hwy 14 (Aerospace & Midland Trail). Watch for fast cross traffic. TURN RIGHT (N) on Hwy 14 toward Red Rock Canyon State Park. The Garlock Fault to the west may have a left-lateral slip rate of 7.6 mm/yr (95% confidence interval of 5.3–10.7 mm/yr), estimated using dendrochronologically calibrated radiocarbon dates (McGill, 2009).

72.0 (0.7) Hwy 14 crosses a major wash. View at 10:00 (NW) is toward a wedge of sediments that have always been mapped as part of the Dove Spring Formation but currently is referred to as "undifferentiated Ricardo Group." These sediments are totally fault bounded and separated from the DSF by the El Paso Fault. Kelly and Whistler (2014) and Whistler and others (2013) have suggested that these deposits are not part of the DSF but are an entirely separate formation containing an early Hemphillian fauna a little younger than that of the youngest faunas of the DSF. It has also been suggested that these deposits *might* be left-laterally offset from the outcrops of the Bedrock Spring Formation (BrSF) that lie easterly along the Garlock Fault (Stop 2-1; Fig. 2-2), a distance of approximately 30 miles in the last 6 million years. Testing these hypotheses will require detailed comparisons of the fossils in these deposits to those from the BrSF, but preliminary work (Whistler and others, 2013) suggest the BrSF mammalian assemblages are a bit younger.

72.8 (0.8) As you cross the El Paso Fault and enter the Red Rock Canyon gorge, you pass through Mesozoic granophyre forming the basement rocks of the southern El Paso Mountains. The winding gorge opens into an amphitheater of spectacular bluffs and cliffs composed of red channel conglomerates and sandstones capped by thick, pink lapilli tuff breccia that comprise the basal units of the upper Miocene DSF. Ahead, prepare to turn right into the Red Cliffs parking area for a short hike.

74.7 (1.9) Cross Red Rock Wash. Slow for upcoming right turn.

75.5 (0.8) Slow, TURN RIGHT into the Red Cliffs parking area. PARK. Restrooms available.

STOP 2-3. Red Cliffs parking area of Red Rock Canyon State Park (RRCSP; Fig. 2-4). Red and green color-banded sandstone beds are well exposed in the parking area. Here, these beds are capped by a thick pink tuff breccia seen to the west on exposures across Hwy 14. Follow the trail leading northwest out of the parking area. Once, a spring here watered the rare Red Rock Canyon monkeyflower which turned the ground purple, but the spring dried up 10 years ago following earthquakes in the area. Make the short hike (20 m elevation gain) up the trail to the top of a nearby hill. To the northeast, we overlook the Iron Canyon/Nightmare Gulch area where the lower part of the DSF crops out unconformably over Mesozoic basement exposed to the east. The extent of the pink tuff breccia can be seen along the cliffs to the west. Return to vehicles and RETRACE west to Hwy 14.

Stop. Watch for traffic. TURN RIGHT (N), move to left lane and proceed 0.3 miles to Abbott Drive, slowing for left turn.

75.8 (0.3) Watch for fast, oncoming traffic. TURN LEFT onto Abbott Drive and drive northwest to RRCSP visitor center and campground. Continue upsection through channel sandstones and several interbedded white vitric tuffs. Pass two basalt sequences just before reaching the Park headquarters. Zeolite minerals (analcime and stilbite) occur in basalt vesicles. We will spend this late morning and afternoon examining various sections of the DSF.

76.6 (0.8) TURN LEFT (SW) into Visitor Center parking area. Seasonal rainstorms can cause damage to roads and structures; recently, resculpting of berms has taken place to prevent further flood damage.

76.7 (0.1) PARK. **STOP 2-4.** Assemble at Red Rock Visitor Center (Fig. 2-5) for orientation and introduction to the DSF. Hikers—arrange carpooling to campsite 50. For the hike up Whistler Ridge, drive around the campsite loop to the trail parking area at Space #50. Hikers will need long-sleeved shirts, sun hats, sunscreen, and water.

Whistler Ridge hike:

OVERVIEW from basalt at the top of Whistler Ridge. The following description is with reference to facing east directly opposite the course of the trail up slope.

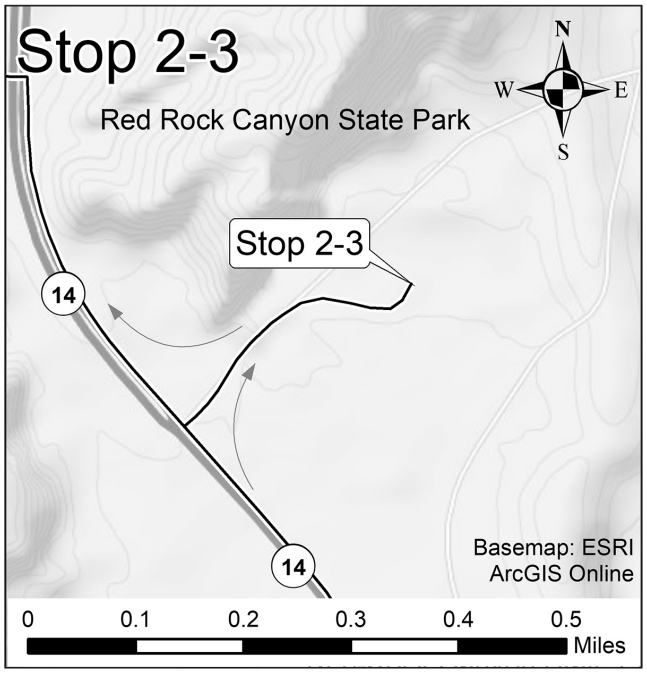

Figure 2-4. Detail of Stop 2-3 at Red Cliffs parking area in Red Rock Canyon State Park.

The high ridge at 12:00 is the southwestern end of the El Paso Mountains granophyre; the main gorge of Red Rock Canyon cuts this granophyre at 1:00. Beyond the gorge is Fremont Valley, bounded on the northwest by the El Paso and Garlock faults and on the southeast by the Rand Fault at the base of the Rand Mountains. The comparatively flat expanse of the western end of the Mojave Desert is visible beyond. In the middle distance between the granophyre and basalts is a prominent ridge and dip slope formed in pink tuff breccia in the lower part of the Dove Spring Formation (DSF). This tuff breccia caps many of the scenic cliffs in the lower part of Red Rock Canyon.

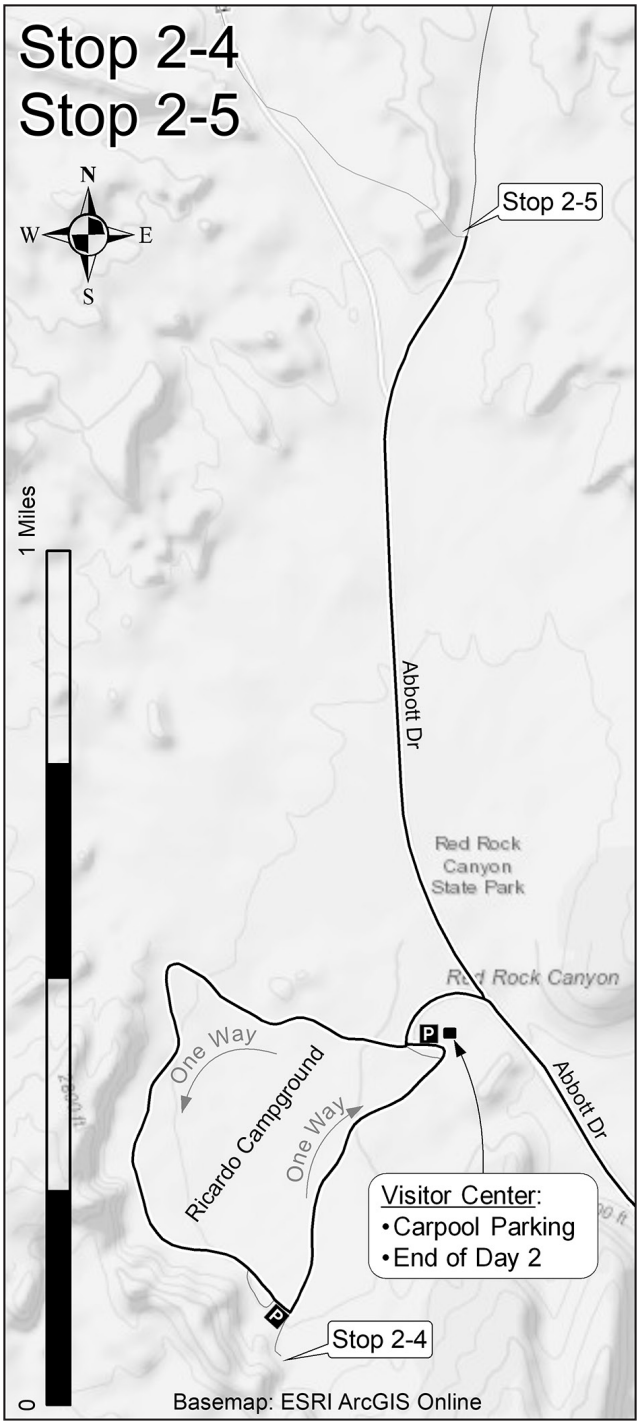

Figure 2-5. STOPS 2-4 and 2-5. Detail of Stops 2-4 and 2-5 in Red Rock Canyon State Park.

To the northeast, the high peak on the horizon at 10:00 is Black Mountain, the highest point in the El Paso Mountains. It is formed by the Black Mountain Basalt of Dibblee (1952), who referred it to a Quaternary age; it is now recognized as the uppermost unit within the middle Miocene Cudahy Camp Formation (CCF). Radiometric dates on this unit range from 17.9 ± 1.6 Ma to 15.1 ± 0.5 Ma (Cox and Diggles, 1986). Lighter colored tuffs and tuff breccias of the CCF are visible around the summit of Black Mountain. Although not obvious from this point, these tuff breccias are underlain by conglomerates and sandstones of the Paleocene Goler Formation.

Looking north at 9:00, the two prominent basalt-flow sequences are visible in the middle distance. We are standing on the upper basalt sequence. The uppermost flow in this sequence has been dated by Carl Swisher at Berkeley Geochron using K/Ar and $^{40}Ar/^{39}Ar$ at 10.5 ± 0.25 Ma (Whistler and Burbank, 1992).

In middle distance, down slope from the lower basalt, notice a prominent white ash. This is one of four ash beds between the pink tuff breccia and the lower basalt. In Last Chance Canyon, 8 km northeast from our location, this and an overlying ash each thicken to over 10 m where they were extensively mined between 1920 and 1940 by Old Dutch Cleanser company for use as an abrasive in the cleanser. A thinner ash a few meters below this bed (not visible) has been dated in Last Chance Canyon to the north by fission track methods at 11.8 ± 0.9 Ma (Burbank and Whistler, 1987).

In the middle distance at 8:30, the high point right (E) of highway is formed by localized boulder conglomerate in the upper part of the DSF. About 8 m below this conglomerate is a gray vitric tuff (mapped as DSF Ash number 16, counting from bottom of DSF; Whistler, 1969; Whistler and Burbank, 1992) that has been dated using K/Ar and $^{40}Ar/^{39}Ar$ at 8.5 ± 1.3 Ma (Whistler and Burbank, 1992). On the horizon behind this high point is the southern Sierra Nevada.

At 8:00 over the top of RRCSP headquarters is Dove Spring Wash that drains a large area between the Sierra Nevada and Red Rock Canyon. Dissected Quaternary bajadas extend toward our location from the Sierra Nevada. Uplift of the Sierra Nevada occurs along the Sierran Frontal Fault at the upper reach of the bajadas. The upper part of DSF is visible along Dove Spring Wash.

Look southwest down-trail at good exposures of middle and upper members of DSF in the middle distance. Cliffs at the back of the State Park campground are formed by resistant channel conglomerates. Note a remnant of the Quaternary bajada behind and a little left (S) of the cliffs.

At 5:00, the peak in the middle distance is formed by coarse-grained granite similar in composition to the Sierra Nevada batholith. The abrupt escarpment at the base of this hill was formed by Cliff Canyon Fault, the

southernmost segment of the Sierran Frontal Fault system. Remnants of Quaternary bajadas and dissected Neogene sediments are seen in the foreground. The latter are the southernmost exposures definitely assignable to the DSF. Although not obvious from this vantage point, the El Paso Fault crosses through this area and appears to terminate at the Cliff Canyon Fault.

Looking due south, the DSF is in the foreground, southern Fremont Valley in the middle distance, and the Tehachapi Mountains are on the right, while the flat Mojave Block stretches 129 km to the south with the San Gabriel Mountains on the far southern horizon. Soledad Mountain is the small peak rising out of the Mojave Block just a little left (E) of the front of the Tehachapi Mountains. This is an early and middle Miocene volcanic center south of Mojave (Vredenburgh, this volume; Wilkerson, this volume). It is a possible source for volcanics within the CCF. To the southeast, a small peak south of the Rand Mountains is Castle Butte, a volcanic outlier of the early and middle Miocene Tropico Group (Dibblee, 1967; Whistler, 1969). At California City near Castle Butte are two volcanic stocks also related to the volcanic rocks of the Tropico Group.

The DSF is a major source for late Miocene vertebrate fossil assemblages that have been under study since the early part of the last century, studies that continue today (Whistler and Takeuchi, 2019). The fossil faunas represent one of the most complete Clarendonian to early Hemphillian LMA successions in North America, thus providing key information for local and continent-wide correlations.

The Barstovian/Clarendonian LMA transition has not yet been documented by mammalian fossils in a single stratigraphic section, although the period of time can be inferred from several different California stratigraphic sections.

The Barstow Formation in the Mud Hills has produced fossils from near the position of the 13.4 ± 0.2 Ma Lapilli Sandstone (Woodburne and Reynolds, 2010). To the east, the West Cronese fauna is late Barstovian, and has produced fossils from 18 localities located at least 60 feet below a lapilli tuff dated at 12.6 ± 0.1 Ma (Swisher, 1992). The DSF in RRCSP contains a complete Clarendonian LMA section followed by a transition to the Hemphillian LMA (Fig. 2-6). This DSF section may be as old as 12.5 Ma (Whistler and others, 2009). The Iron Canyon Fauna is the lowest fauna in the DSF, and contains Clarendonian LMA vertebrate fossils, but no direct evidence of any Barstovian vertebrates. This suggests that the transition from Barstovian to Clarendonian LMAs may fall somewhere between 12.7 Ma and 12.5 Ma.

Loomis (1984) named the DSF and separated it from the Ricardo Formation (Merriam, 1914; Dibblee, 1952). Loomis recognized six members, but generally the more than 1800 m of fluviolacustrine sediments and volcanic and volcaniclastic rocks of the DSF can be broadly separated into five lithofacies, from the lowest:

(1) Fine-grained lacustrine deposits of clay, silt, reworked volcanic ash, fresh-water limestone, and bedded chert;

(2) Fluvial deposits of channel sandstone and channel conglomerates that weather reddish in color and regularly form prominent cliffs that are the source of the name "Red Rock Canyon";

(3) Overbank and floodplain siltstone deposits;

(4) Poorly sorted alluvial fan deposits; and

(5) Paleosol, caliche, and silicified hardpan deposits (silcretes).

Deposition in the lower members of the DSF resulted primarily from meandering, intermittent streams feeding into a semi-permanent lake in the center of a broad basin. The upper portions are coarser, representing alluvial fans that prograded into the filling basin. The uppermost DSF member (Unit 6 of Loomis, 1984) is a nearly flat-lying sedimentary sequence that lies disconformably on members 1–5 of the DSF.

An age range of 12.5 Ma to approximately 8 Ma for the DSF has been developed by direct radiometric dating of selected tuffs and basalts (Cox and Diggles, 1986; Whistler and Burbank, 1992; Frankel and others, 2008), tephrochronological correlations with well-dated Great Basin tuffs (Perkins and others, 1998, 2002; Whistler and others, 2009) and magnetostratigraphic correlations (Burbank and Whistler, 1987; Loomis and Burbank, 1988; Whistler and Burbank, 1992), although the latter have been questioned (see Whistler and others, 2009).

The DSF lies unconformably on the dominantly volcanic middle Miocene Cudahy Camp Formation (CCF), also named by Loomis (1984) for rocks of the lower Ricardo Formation of Dibblee (1952). The CCF was deposited from 19 to 15 Ma (Cox and Diggles, 1986; Loomis and Burbank, 1988; Monastero and others, 1997).

Monastero and others (1997) proposed a correlation of the CCF volcanics with nearly identical rocks in the Eagle Crags volcanic field on the south side of the Garlock Fault approximately 64 km east of the El Paso Mountains. This distance is probably a maximum for fault movement during and after the Miocene.

Smith and others (2002) proposed a correlation between the DSF and a complicated succession of volcanic and clastic rocks south of the Garlock Fault in the Lava Mountains that we passed earlier today, northeast of Johannesburg. They also presented a rather elegant reconstruction of the tectonics required to explain this correlation. Relationships between the rock units in the Lava Mountains are complicated, and mapping by several different groups (Smith, 1964; Smith and others, 2002) have yielded differing interpretations of the stratigraphic relationships. The only primarily clastic unit is the 1,700-m-thick Bedrock Spring Formation (BrSF), but there are no radiometric dates in these rocks; there are, however, two well developed 1 to 3-m-thick tuffs near the base that could be dated. Underlying the BrSF are units called "Older Tertiary volcanic rock"

and "Dacite of Summit Range" which have yielded dates of 10.73 Ma and 11.7 Ma, respectively. Overlying the BrSF is the "Andesite of Summit Diggins," dated at 10.34 Ma, and "Almond Mountain volcanic rocks," dated between 10.29 and 9.54 Ma. These dates above and below appear to leave little time for deposition of the 1,700 meters of mostly clastic BrSF. Superficially, these dates do fall within those recorded from the DSF and would support at least 40 km of offset on the Garlock Fault. However, the rocks of the clastic BrSF, lacking basalts, abundant vitric tuffs and silcrete paleosols, are considerably different in appearance than those of the DSF. The BrSF also contains a vertebrate fossil assemblage that has not been studied in detail, but taxa present support a middle Hemphillian LMA in the 7 to 6 Ma range (Whistler and others, 2013). Consequently, there

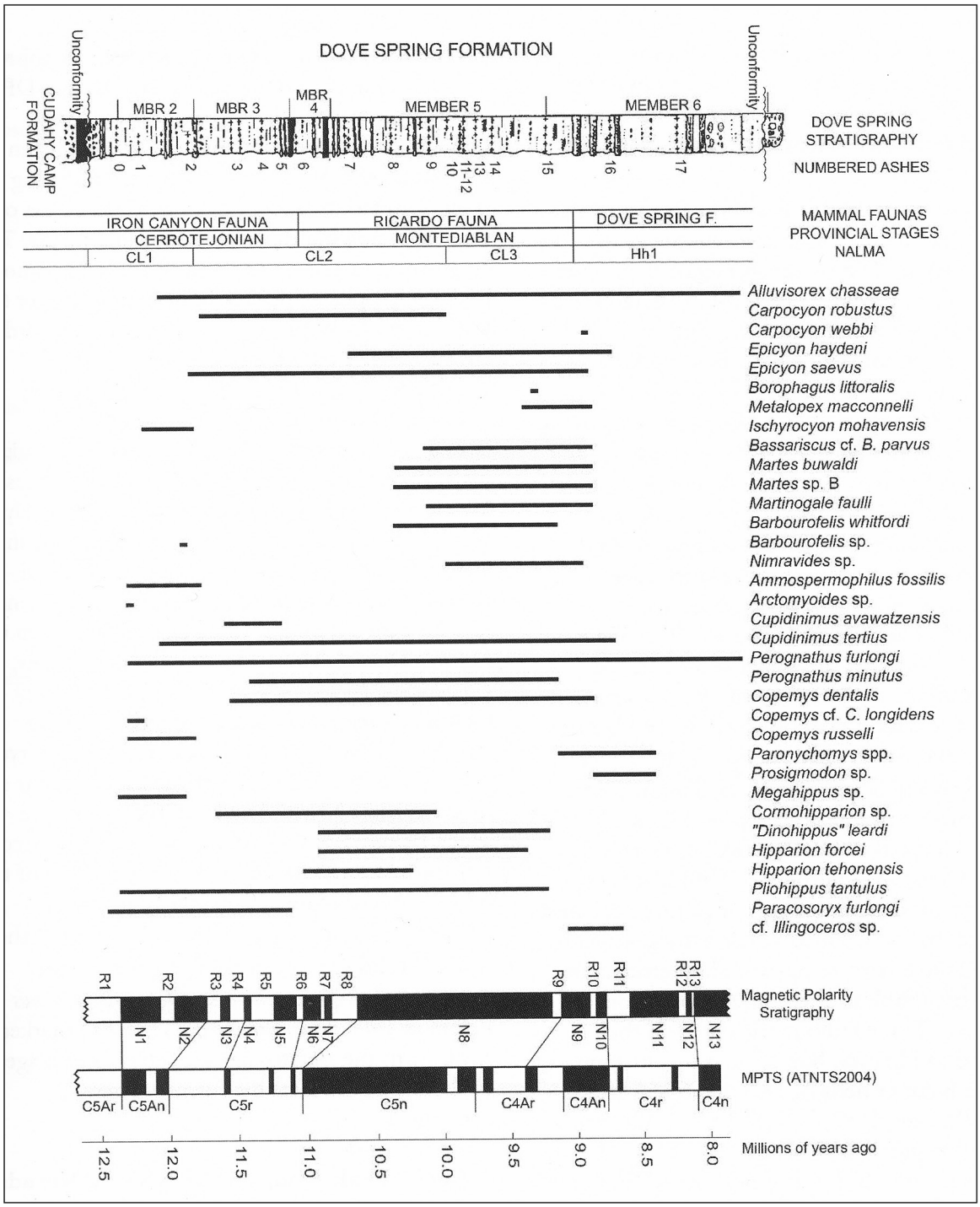

Figure 2-6. Selected vertebrate taxa with the greatest biostratigraphic significance within the Dove Spring Formation correlated to the magnetic polarity time scale (MPTS). See Whistler and others (2013), figure 6.

remains an unresolved conflict between radiometric ages recorded below and above the BrSF and the fossil mammal record.

Alternatively, Frankel and others (2008) proposed that volcanics in the Summit Range north of the Garlock Fault at the north end of the Koehn Valley are correlative with those in the lower part of the DSF. These Summit Range volcanics include a lapilli tuff breccia dated at 11.8 Ma that is similar to the thick pink lapilli tuff breccias in the lower part of the DSF, but paradoxically they contain no basalt flows. Frankel and others (2008) also argued that most of the vitric tuffs in the DSF were derived from this volcanic center, but many of these tuffs previously have been shown to be widespread with sources in the Great Basin and Yellowstone hotspot (Perkins and others, 1998; 2002). They also proposed that the very thick white tuffs (10+ m) in the DSF in upper Last Chance Canyon (source rock for the Old Dutch Cleanser mines) are a lateral extent of the lapilli tuffs in the Summit Range. On face value this appears to be a reasonable suggestion except that these tuffs are separated by 250 m of sediments from the lateral extent of the pink tuff breccia in Last Chance Canyon.

Both the CCF and DSF were deposited in the El Paso Basin, an elongate basin that developed along the trace of the Garlock Fault. Source areas across the Garlock Fault that have been proposed for both the CCF (Monastero and others, 1997) and the DSF (Smith and others, 2002; Frankel and others, 2008) support a total movement of approximately 64 km (39 mi) on the Garlock Fault since the middle Miocene.

Summary of the geology of the El Paso Basin:

Color of lithology

White: vitric tuffs
Gray: glassy volcanic ash
Tan to brown: overbank deposits and paleosols
Pink: lapilli tuff breccia
Red and green: weathered channel conglomerates and sandstones
Black: basalt

Age of geologic units

Goler Formation: 60 – 57 Ma
Cudahy Camp Formation (CCF): 18.1 – 15.1 Ma
Dove Spring Formation (DSF): 12.5 – 8 Ma
Basal DSF in Iron Canyon: 12.5 – 11.2 Ma
Bedrock Spring Formation (BrSF): 7.5 – 6 Ma (approximate, based on LMAs)

Return to Visitor Center. Plans for the afternoon include a local foot and vehicle tour to see uncommon DSF sedimentary soil structures. Arrange carpool in four-wheel drive vehicles to stops as long as time permits. Reset odometers to 0.0 at the Visitor Center.

0.0 (0.0) Depart Visitor Center.

0.2 (0.2) TURN NORTH on Abbott Drive (FWD recommended). Follow FT leaders 0.7 miles north and stay right at road fork.

0.3 (0.1) TURN LEFT, downhill, into wash and follow dirt road along the wash to Dove Spring.

1.0 (0.7) PARK. **STOP 2-5**. Park among gray hills with silcrete horizons resistant to erosion (Fig. 2-5). Examine silcretes for possible soil features.

Silicified root casts ranging from <5 to 25 cm long are common throughout the lithofacies of the DSF. Root casts range from horizontal networks of small (1–5 cm) roots to large (>10 cm) vertical roots. In the upper part of the formation, thin root-choked horizons coalesce into silcretes. Silcretes (and calcretes, the carbonate equivalent) typically form in environments where soil moisture evaporates quickly and close to the surface. For this reason, they are indicators of dry environments.

Other features that characterize paleosols (red color, color mottling, ped structure, slickensides, etc.) are rare or absent in the DSF. The absence of these features may be due to the overall low clay content in much of the formation. Clay particles are moved down through a soil profile by percolating precipitation or through animal burrowing. When clay concentrates in specific horizons, it can be further moved and concentrated as soil aggregates (peds) expand and contract during wetting and drying of the soil. Well-developed soils and paleosols typically have distinct blocky peds that form through many seasons of bio- and pedoturbation, as well as color mottling, carbonate nodules, and concentrations of clay along root traces, burrows, or ped edges.

The overall lack of well-developed paleosol features in the DSF may be due to the dominant sandy lithology through much of the formation (Loughney and Hardy, this volume). It is likely that after burial of the formation, silica leached from the numerous tuffs and sandstones replaced the organic remains of plant roots and helped preserve these structures as root casts. RETRACE along wash.

TURN RIGHT out of wash to pavement; TURN RIGHT.

1.0 (1.0) Return to RRCSP Visitor Center. The day has ended; review routes for travel home:

Hwy 14 runs north to Inyokern/Ridgecrest and meets Hwy 395 running north to Lone Pine and Bishop. Hwy 395 runs south to Kramer Junction. From Kramer Junction, Hwy 395 can be taken south to San Bernardino, Riverside, and Ontario.

Hwy 14 runs south to the town of Mojave, then south to Palmdale and Los Angeles.

Three miles north of Mojave, the new alignment of Hwy 58 runs west to Bakersfield and east to Kramer Junction and Barstow, where it connects with I-40 to Needles. At

Barstow, take I-15 to the Desert Studies Center near Baker and to Las Vegas.

Acknowledgements

Thanks to Tom Schweich and Bian Wang for preparing route maps and maps of the trip stops. Barstow BLM archaeologist Jim Shearer provided access on routes that provided access to road log stops. This manuscript was made better by review and comments from Jennifer Reynolds, David Miller, and Janet Westbrook.

References

Albright, L. B. III, Lofgren, D. L., and McKenna, M. C., 2009. Magnetostratigraphy, mammalian biostratigraphy, and refined age assessment of the Goler Formation (Paleocene), California. Museum of Northern Arizona Bull. 65:259–278.

Anderson, E. A., 2017. Major revisions of the timing, style, magnitude, and cause of Early Miocene extension in the Central Mojave metamorphic core complex and subsequent role of the Eastern California Shear Zone. California State University, Desert Studies Consortium, p. 60–70.

Bell, M. A., and R. E. Reynolds, 2010. Miocene and Late Pleistocene stickleback spines from the Mojave Desert, California. California State University, Desert Studies Consortium, p. 162–168.

Bortugno, C. J. and T. E. Spittler, 1986. Geologic map of California, San Bernardino Sheet: California Division of Mines and Geology, scale 1:250,000.

Burbank, D. W., and D. P. Whistler. 1987. Temporally constrained tectonic rotations derived from magnetostratigraphic data: Implications for the initiation of the Garlock Fault, California. Geology 15:1172–1175.

Burke, D. B., J. W. Hillhouse, E. H. McKee, S. T. Miller, and J. L. Morton, 1982. Cenozoic rocks in the Barstow Basin area of Southern California: stratigraphic relations, radiometric ages, and paleomagnetism. U.S. Geological Survey Bull. 1529-E, 16 p.

Byers, F. M., 1960. Geology of the Alvord Mountain quadrangle, San Bernardino County, California. U.S. Geological Survey Bull. 1089-A, 71 p.

Cox, B. F., 1998. Late Cretaceous and Early Paleogene tectonics and sedimentation near the Garlock fault, California—did Neogene strike-slip faulting exploit an older structural zone?: Redlands, San Bernardino County Museum Association Quarterly 45(1/2):45–54.

Cox, B. F., and L. F. Edwards, L.F., 1984. Possible marginal marine deposits in the Goler Formation (Paleocene), El Paso Mountains, California. Eos 65(45):1084.

Cox, Bret F., and M. F. Diggles, 1986. Geologic map of the El Paso Mountains Wilderness Study Area, Kern County, California. U.S. Geological Survey Misc. Field Studies MF-1827, 13 p.

Cox, B. F., J. W. Hillhouse, and L. A. Owen, 2003. Pliocene and Pleistocene evolution of the Mojave River, and associated tectonic development of the Transverse Ranges and Mojave Desert, based on borehole stratigraphy studies and mapping of landforms and sediments near Victorville, California, in Paleoenvironments and paleohydrology of the Mojave and southern Great Basin Deserts, Y. Enzel, S.G. Wells, and N. Lancaster (eds). Geol. Soc. of America Special Paper 368:1-42.

Dibblee, T.W., Jr. 1952. Geology of the Saltdale quadrangle, California. Calif. Div. Mines Bull. 160:7–43.

Dibblee, T.W. Jr., 1967, Areal geology of the western Mojave Desert, California: U.S. Geological Survey, Professional Paper 522, scale 1:125,000.

Dibblee, T. W. Jr., 1968. Geology of the Fremont Peak and Opal Mountain quadrangles, California. Calif. Div. Mines and Geology Bull. 188, 64 p.

Dibblee, T. W. Jr., 1970. Geologic map of the Daggett quadrangle, San Bernardino County, California. Calif. Div. Mines and Geology, Map I-592, scale 1:62,500.

Dokka, R. K. and C. J. Travis, 1990. Late Cenozoic strike-slip faulting in the Mojave Desert, California. Tectonics 9:311–340.

Dokka, R. K., D. J. Henry, T. M. Ross, A. K. Baksi, J. Lambert, C. J. Travis, S. M. Jones, C. Jacobson, M. M. McCurry, M. O. Woodburne, and J. P. Ford, 1991. Aspects of the Mesozoic and Cenozoic geologic evolution of the Mojave Desert. Geological Society of America, San Diego, Annual Meeting, field trip guidebook.

Dokka, R. K., D. J. Henry, G. F. Sella, J. F. Ford, D. F. MacConnell, C. McCabe, P. Neuffer, and R. Quinones, 1994. Critical events in the Late Mesozoic–Cenozoic geologic history of the Mojave Desert. SBCMA, Mojave Desert Quaternary Research Center Symposium.

Durrell, C., 1953. Geological investigations of strontium deposits in southern California. Calif. Div. Mines and Geology Special Report 32, 48 p.

Faye, T., 1999. Borax freighting routes in the Mojave Desert. Redlands, San Bernardino County Museum Quarterly 46(3):81–87.

Fillmore, R. P., and J. D. Walker, 1996. Evolution of a supradetachment extensional basin: the Lower Miocene Pickhandle basin, central Mojave Desert, California, in Reconstructing the history of Basin and Range extension using sedimentology and stratigraphy, K. D. Beratan (ed). Geol. Soc. of America Special Paper 303:107–126.

Frankel, Kurt L., A. F. Glazner, E. Kirby, F. C. Monastero, M. D. Strane, M. E. Oskin, J. P. Unruh, J. D. Walker, S. Anandakrisnan, J. M. Bartley, D. S. Coleman, J. F. Dolan, and R. E. Finkel, R. C., 2008. Active tectonics of the eastern California shear zone: Geol. Soc. of America Field Guide 11:43–84.

Garcia, A., J. R. Knott, A. D. Winkel, M. Howard, and A. Lopez, 2015. Old McDonald had a well… (McDonald Well 32S43E28K01), California State University, Desert Studies Consortium, p. 149–152.

Glazner, A. F., J. M. Bartley, and J. D. Walker, 1989a. Magnitude and significance of Miocene crustal extension in the central Mojave Desert, California. Geology 17(1):50–53.

Glazner, A. F., J. M. Bartley, and J. D. Walker, J. D., 1989b. The Waterman Hills detachment fault, central Mojave Desert,

California. SBCMA, Mojave Desert Quaternary Research Center Symposium, p. 52–60.

Glazner, A. F., J. D. Walker, J. M. Bartley, and J. M. Fletcher, 2002. Cenozoic evolution of the Mojave block of southern California. Geol. Soc. of America Memoir 195:19–41.

Hensher, A., 1998a. The history of early mining in the El Paso Mountains, in Finding fault in the Mojave, J. P. Calzia and R. E. Reynolds (eds.): California Desert Studies Center Research Symposium Field Trip Guide and Volume, p. 13–17.

Hensher, A., 1998b. Gypsite: A humble product from a humble camp, in Finding fault in the Mojave, J. P. Calzia and R. E. Reynolds (eds.): California Desert Studies Center Research Symposium Field Trip Guide and Volume, p. 18.

Hensher, A., L. M. Vredenburgh, and G. Wilkerson, 1998. The history of Saltdale, in Finding fault in the Mojave, J. P. Calzia and R. E. Reynolds (eds.): California Desert Studies Center Research Symposium Filed Trip Guide and Volume, p. 19–21.

Hillhouse, J. W., D. M. Miller, and B. D. Turrin, 2010. Correlation of the Miocene Peach Spring Tuff with the geomagnetic polarity time scale and new constraints on tectonic rotations in the Mojave Desert, California, Desert Symposium. California State University, Desert Studies Consortium, p. 105–121.

Housley, R. M., and R. E. Reynolds, 2002. Mineralogical survey of the Mount General area, in Between the basins: exploring the western Mojave and southern Basin and Range Province, R. E. Reynolds (ed.). California State University, Desert Studies Consortium, p. 61–63.

Housley, R. M., 2009. Mineralogical Survey of the Mount General Area, Barstow CA. https://www.mindat.org/article.php/803/Mineralogical+Survey+of+the+Mount+General+Area%2C+Barstow+CA+

Ingersoll, R. V., K. A. Devaney, J. K. Geslin and others 1996. The Mud Hills, Mojave Desert, California: Structure, stratigraphy, and sedimentology of a rapidly extended terrane. Geol. Soc. of America Special Papers 303:61–84.

Jachens, R. C., V. E. Langenheim, and J. C. Matti, 2002. Relationship of the 1999 Hector Mine and 1992 Landers fault ruptures to offsets on Neogene faults and distribution of Late Cenozoic basins in the Eastern California Shear Zone. Bull. Seismological Soc. of America 92(4):1592–1605.

Jefferson, G. T., M. Reheis, and D., Miller, 2020. A compilation of Lake Manix Basin geological and paleontological data and references. This volume.

Jenkins, J. E., 1986. Miocene Invertebrates from the Calico Mountains, San Bernardino County, California. San Bernardino County Museum Assoc. Quarterly, Winter 1986, p. 42.

Jennings, C. W., J. L. Burnett, and B. W. Troxel, 1962. Geologic map of California, Trona sheet: California Division of Mines and Geology, scale 1:250,000.

Jessey, D. R., and R. E. Reynolds. 2009. Landscape evolution at an active plate margin: a field trip to the Owens Valley. Day 1. Desert Studies Consortium, p. 7–59.

Kelly, T. S., and D. P. Whistler, 2014. New Late Miocene (Latest Clarendonian to Early Hemphillian) cricetid rodents from the upper part of the Dove Spring Formation, Mojave Desert, California. Paludicola 10(1):1-48.

Kaldenberg, R. L., 2011. The sounds of silence in the west Mojave: a summary of historic Blackwater Well and Steam Well and the folks who lived there. California State University, Desert Symposium, p. 71–84.

Leggitt, V. L., 2000. Three-dimensional microfossils from Rainbow Basin: Barstow Formation, Mojave Desert, California. Geol. Soc. of America Abstracts with Programs 32(7):A-15.

Leslie, S. R., D. M. Miller, J. L. Wooden, and J. A. Vazquez, 2010. Stratigraphy, age, and depositional setting of the Miocene Barstow Formation at Harvard Hill, central Mojave Desert, California. California State University, Desert Studies Consortium, p. 85–105.

Lofgren, D. L. and M. McKenna, 2002. The Goler Formation of California, in Between the Basins: exploring the western Mojave and southern Basin and Range Province, R. E. Reynolds (ed.). California State University, Desert Studies Consortium, p. 66–68.

Lofgren, D. L., H. Hutchison, R. Nydam, M. Paik, E. Lee, S. A. Butcher, and T. Kirkpatrick, 2020. A review of Paleogene vertebrates and invertebrates from the Goler Formation of California and their biostratigraphic and paleogeographic significance. This volume.

Loomis, D. P., 1984. Miocene stratigraphic and tectonic evolution of the El Paso Basin, CA. Unpublished Master's thesis, University of North Carolina, Chapel Hill, NC, 172 p.

Loomis, D. P. and D. W. Burbank, 1988, The stratigraphic evolution of the El Paso Basin, Southern California; implications for the Miocene development of the Garlock Fault and uplift of the Sierra Nevada. Geol. Soc. of America Bull. 100:12–28.

Loughney, K. M. and C. Badgley, 2017. Facies, environments and fossil preservation in the Barstow Formation, Mojave Desert, California. Palaios 32:396–412.

Loughney, K. M. and T. Smiley, 2019. The middle Miocene in southern California: Mammals, environments, and tectonics of the Barstow, Crowder, and Cajon Valley formations—Field Trip of the North American Paleontological Convention, June 22, 2019. Permalink https://escholarship.org/uc/item/521585s4 Journal PaleoBios, 36(0) ISSN 0031-0298 Publication Date 2019-06-20.

Loughney, K. M., M. T. Hren, S. Y. Smith, and J. L. Pappas, 2020. Vegetation and habitat change in southern California through the Middle Miocene Climatic Optimum: Paleoenvironmental records from the Barstow Formation, Mojave Desert, USA. Geol. Soc. of America Bull. 132(1-2):113–129.

McDougall, K., 1987. Foraminiferal biostratigraphy and paleoecology of marine deposits, Goler Formation, California, p. 43–67, in Basin analysis and paleontology of the Paleocene and Eocene Goler Formation, El Paso Mountains, California, B. F. Cox (ed.). SEPM Pacific Section.

McGill, S., 2009. Holocene slip rate and tectonic role of the western Garlock fault. California State University, Desert Studies Consortium, p. 165–171

Mendenhall, W., 1909. Some desert watering places in southeastern California and southwestern Nevada. U.S. Geological Survey Water-Supply Paper 224, 98 p.

Merriam, J. C., 1911. A collection of mammalian remains from the Tertiary beds on the Mohave Desert. University of California Dept. of Geol. Bull. 6:163–169, pl. 29.

Merriam, J. C., 1914. The occurrence of Tertiary mammalian remains in northeastern Nevada. California University Dept. of Geology Bull. 8(12):275–281.

Merriam, J. C., 1915. Extinct faunas of the Mohave Desert, their significance in a study of the origin and evolution of life in America. The Popular Science Monthly 86(3):245–264.

Merriam, J. C., 1919. Tertiary mammalian faunas of the Mohave Desert. University of California Dept. of Geol. Bull. 11:437–595.

Miller, D. M., S. R. Leslie, J. W. Hillhouse, J. L. Wooden, J. A. Vazquez, and R. E. Reynolds, 2010. Reconnaissance geochronology of tuffs in the Miocene Barstow Formation: implications for basin evolution and tectonics in the central Mojave Desert. California State University, Desert Studies Consortium, p. 70–84

Miller, D. M. M. C. Reheis, E. Wan, D. B. Wahl, and H. Olson, 2011. Pliocene and early Pleistocene paleogeography of the Coyote Lake and Alvord Mountain area, Mojave Desert, California. California State University, Desert Studies Consortium: p. 53–67.

Miller, D. M., R. E. Reynolds, G. A. Phelps, J. Honke, A. J. Cyr, D. C. Buesch, K. M. Schmidt, G. Losson, 2017. Active tectonics of the northern Mojave Desert: the 2017 Desert Symposium field trip road log. California State University, Desert Studies Consortium, p. 7–45.

Miller, D. M., P. Sadler, K. Schmidt, and R. E. Reynolds, 2013. Raising questions in the central Mojave: the field trip. California State University, Desert Studies Consortium, p. 5–30.

Monastero, F. C., A. E. Sabin, and J. D. Walker, 1997. Evidence for post-early Miocene initiation of movement on the Garlock fault from offset of the Cudahy Camp Formation, east-central California. Geology 25(3):247–250.

Myrick, D. F., 1991. Railroads of Nevada and eastern California, volume II: the southern roads. University of Nevada Press, p. 455–933.

Oskin, M., and A. Iriondo, 2004. Large-magnitude transient strain accumulation on the Blackwater fault, Eastern California shear zone. Geology 32:313–316. doi: 10.1130/G20223.1

Pagnac, D., 2009. Revised large mammal biostratigraphy and biochronology of the Barstow Formation (Middle Miocene), California. University of California Museum of Paleontology. PaleoBios 29(2):48–59.

Pagnac, D., Browne, I., and Smith, K., 2013. Stratigraphy and vertebrate paleontology of the middle Miocene Barstow Formation, San Bernardino County, California, in Field Guide of the 73rd Annual Meeting of the Society of Vertebrate Paleontology, Los Angeles, California, 29 October 2013, 26 p.

Park, L. E., 1995. Geochemical and paleoenvironmental analysis of lacustrine arthropod-bearing concentrations of the Barstow Formation, southern California. Palaios 10:44–57.

Reyes-Velarde, A., 2019. Ridgecrest earthquakes caused up to $5 billion in damage to China Lake naval base. Los Angeles Times, Aug. 14.

Reynolds, R. E., 2000. Marker units suggest correlation between the Calico Mountains and the Mud Hills, central Mojave Desert, California. San Bernardino County Museum Association Quarterly 47(2):1–10.

Reynolds, R. E., 2004. Widespread early Miocene marker beds unite the Barstow Formation of the central Mojave Desert. Inland Geological Society, p. 1–10.

Reynolds, R. E., 2013. Parapliohippus carrizoensis (Perissodactyla: Equidae) from early Miocene (Hemingfordian NALMA) Barstow Formation outcrops in the southwestern Cady Mountains, Mojave Desert, California, in Raising questions in the central Mojave, R.E. Reynolds (ed.). California State University, Desert Studies Consortium, p. 114–116.

Reynolds, R. E., and I. Browne, 2015. Robbins Quarry: Taphonomy and stratigraphic position in the Barstow Formation, Mojave Block, California. California State University, Desert Studies Consortium, p. 145–148.

Reynolds, R. E., J. P. Calzia, and B. Cox, 1998. Finding faults in the Mojave: Field trip guide. San Bernardino County Museum Association Quarterly 45(1,2).

Reynolds, R. E. and D. M. Miller, 2010. Overboard in the Mojave: the field guide. California State University, Desert Studies Consortium, p. 7–23.

Reynolds, R. E., D. M. Miller, M. O. Woodburne, and L. B. Albright, 2010. Extending the boundaries of the Barstow Formation in the central Mojave Desert. California State University, Desert Studies Consortium, p. 148–161.

Roche O., D. C. Buesch, and G. A. Valentine, 2016. Slow-moving and far-travelled dense pyroclastic flows during the Peach Spring super-eruption. Nature Commun. 7:10890.

Singleton, J. S., and P. B. Gans, 2008. Structural and stratigraphic evolution of the Calico Mountains: Implications for early Miocene extension and Neogene transpression in the central Mojave Desert, California. Geosphere 4(3):459–479. doi: 10.1130/GES00143.1.

Smith, E. I., A. Sánchez, D. L. Keenan, and F. C. Monastero, 2002. Stratigraphy and geochemistry of volcanic rocks in the Lava Mountains, California: Implications for the Miocene development of the Garlock fault, in Geologic evolution of the Mojave Desert and southwestern Basin and Range, A. F. Glazner, J. D. Walker, and J. M. Bartley (eds.). Geol. Soc. of America Memoir 195, p. 151–160.

Spencer, R., 2005. Paleoenvironmental and geochemical analysis of arthropod-bearing lacustrine deposits, Black Canyon, Barstow Formation, southern California. California State University, Desert Studies Consortium, p. 91.

Swisher, C. C., III, 1992. 40Ar/39Ar Dating and its application to the age calibration of the North American Land Mammal Ages. Unpublished Ph.D. dissertation, University of California, Berkeley, 239 p.

Vredenburgh, L. M., R. D. Hartill, and G. L. Shumway, 1981. Desert Fever. Living West Press: 324 p.

Walker, J. D., J. M. Fletcher, R. P. Fillmore, M. W. Martin, W. J. Taylor, A. F. Glazner, and J. M. Bartley, 1995, Connection between igneous activity and extension in the central Mojave metamorphic core complex: Journal of Geophysical Research 100(B6):10,477–10,495.

Whistler, D. P. 1969. Stratigraphy and small fossil vertebrates of the Ricardo Formation, Kern County, California. Unpublished Ph.D. dissertation, University of California, Berkeley, 269 p.

Whistler, D. P., and D. W. Burbank, 1992. Miocene biostratigraphy and biochronology of the Dove Spring Formation, Mojave Desert, California, and the characterization of the Clarendonian land mammal age (late Miocene) in California. Geol. Soc. of American Bull. 104:644–658.

Whistler, D. P., R. H. Tedford, G. T. Takeuchi, X. Wang, J. Z. Tseng, and M. P. Perkins, 2009. Revised Miocene biostratigraphy, biochronology of the Dove Spring Formation, Mojave Desert, California. Museum of Northern Arizona Bull. 65:331–362.

Whistler, W. P., G. T. Takeuchi, L. T. Groves, and X. Wang, 2013. Western Mojave Desert geology and vertebrate paleontology with special emphasis on the Dove Spring Formation. Field Trip Guidebook, Soc. Vert. Paleontology, 73rd Annual Meeting, Los Angeles, CA, 68 p.

Woodburne, M.O., 1988. Arikareean and Hemingfordian faunas of the Cady Mountains, Mojave Desert Province, California. Geol. Soc. of America Special Paper 325, p. 197–210.

Woodburne, M. O. and D. J. Golz. 1972. Stratigraphy of the Punchbowl Formation, Cajon Valley, southern California. University of California Publ. in Geological Sciences 92:1–57.

Woodburne, M. O., and R. E. Reynolds, 2010. The mammalian litho- and biochronology of the Mojave Desert Province. California State University, Desert Studies Consortium, p. 124–147.

Woodburne, M.O., R. H. Tedford, and C. C. Swisher, III. 1990. Lithostratigraphy, biostratigraphy and geochronology of the Barstow Formation, Mojave Desert, southern California. Geol. Soc. of America 102:459–477.

A compilation of Lake Manix basin geological and paleontological data and references

G. T. Jefferson,[1] M. Reheis,[2] and D. M. Miller[3]
[1]*Stout Research Center, California State Parks, Borrego Springs, CA 92004*
[2]*U.S. Geological Survey, Golden, CO*
[3]*U.S. Geological Survey, Retired, Menlo Park, CA*

Introduction

Lake Manix basin holds a Pleistocene sequence of sediments and fossils that together preserve a history of climate change during the past 500,000 years. This record is unique in the southwestern deserts for its span of time and because the sediments are well exposed in outcrop. Other nearby desert basins, such as Death Valley, China–Searles, and Tecopa, preserve sediment records that are either episodic in nature or can mainly be studied in cores. As a perennial source of water over many millennia, the Manix basin was also a magnet for terrestrial and aquatic life, and thus contains an exceptional fossil record. In addition, the area lies astride several active faults of the Eastern California Shear Zone. Because of these circumstances, the Manix basin has been a target of geologic mapping, paleoclimate, and paleontologic studies for many decades.

This report summarizes the chief findings from these studies. Tables and taxonomic lists are presented as they appeared in the cited publications. Abbreviations are as follows: cal = calendar year; ka = kilo (thousand) annum; kyr = kilo (thousand) years; masl = meters above sea level.

Lake Manix basin geologic history summary

The Manix basin in south-central California is one of a chain of interconnected basins crossed and linked by the modern Mojave River. The Mojave heads in the San Bernardino Mountains and in high-water years (Enzel and Wells, 1997) presently flows north and east to its terminus in Silver Lake playa north of Baker, California. During its evolution, the river has integrated several basins that were previously internally drained, including the Victorville, Harper, Manix, and Soda Lake basins (Cox et al., 2003; Enzel et al., 2003) (Figure 1). Sediments in the Manix basin contain a record of Mojave River discharge and lake fluctuations during the middle Pleistocene and most of the late Pleistocene, and also preserve abundant fossil remains (Jefferson, 2003, and references therein; Reheis et al., 2012, 2015). Prior to the arrival of the Mojave River from upstream, the Manix basin area was occupied by at least three separate endorheic basins: the Cady–Troy, Coyote Lake, and Afton basins, each floored by playas and surrounded by fringing alluvial fans. During the history of Lake Manix, these subbasins were separated at various times by low thresholds that influenced the depositional

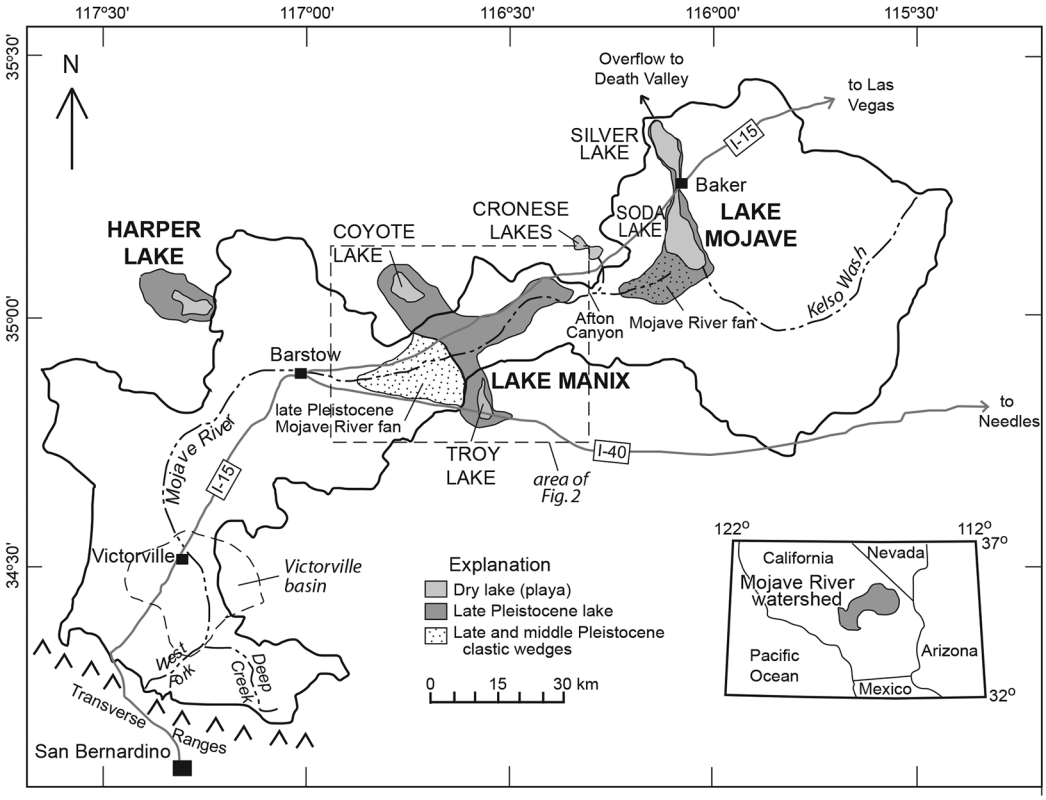

Figure 1. Map showing lake basins along the Mojave River corridor in Southern California (inset). Light gray, extent of modern playa surfaces. Dark gray, extent of late Pleistocene highstands of Harper Lake, Lake Manix, and Lake Mojave. Modified from Reheis and Redwine (2008) and Jefferson (2003).

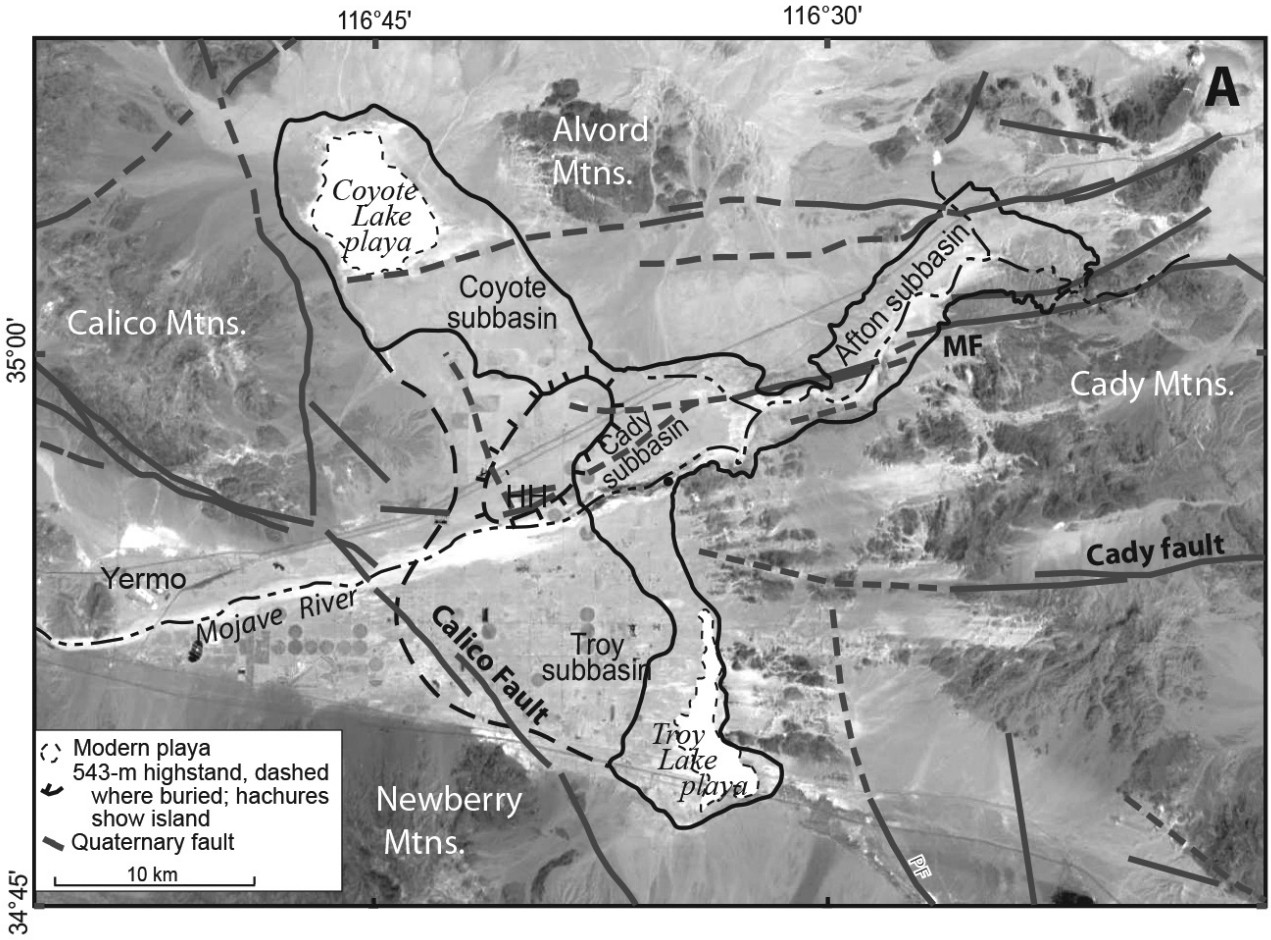

Figure 2. Aerial photograph of Manix nasin. Solid and dashed black lines are important Quaternary faults. Modified from figures 2 and 3 in Reheis et al. (2007). HH, Harvard Hill; MF, Manix fault.

sequences within them and the degree of dissection by the Mojave River (Figure 2).

Deposits of Pleistocene Lake Manix (the Manix Formation of Jefferson, 1968, 2003) have been studied for over a century. Buwalda (1914), for whom Buwalda Ridge is now named, first described the sediments in Manix Basin, and named them after a railroad siding approximately 30 km northeast of the town of Daggett. J.C. Merriam (1915) identified the associated vertebrate fossils. The stratigraphy, paleontology, and broad lake-level fluctuations were established by Ellsworth (1932; Blackwelder and Ellsworth, 1936), Jefferson (2003, and references therein), and Meek (1989a, 1989b, 1990, 2000). Reheis et al. (2012, 2014) obtained a sedimentary and paleoclimate record from a drill core taken near the confluence of Manix Wash with the Mojave River in the Cady subbasin and mapped the lacustrine deposits exposed along the Mojave River and its tributaries. Dudash (2006) and Miller et al. (2018) mapped the surficial geology and reconstructed the history of lake level fluctuations during the late Pleistocene in the Coyote subbasin. Reheis and Redwine (2008) addressed the late Pleistocene record of lake levels, overflow, and eventual incision of Afton Canyon.

Jefferson (1968, 1985, 2003) studied the stratigraphic sequence exposed near the confluence of the Mojave River and Manix Wash in the Cady subbasin and concluded that the Manix Formation there recorded five deep lake cycles proposed to correlate with marine isotope stages (MIS) 4, 6, 8, 12 and 14. Deposits that he interpreted as perennial-lake sediments and correlated with OIS 6 contain a tephra layer near the base that had an assigned age of 185 ka based on chemical correlation with a rhyolite in the southern Sierra Nevada; this tephra was also associated with a uranium-series age on bone of about 184 ka (summarized in Jefferson, 2003). Reheis et al. (2012) obtained an age of 184 ± 4 ka on the source rhyolite. Sediments representing a sequence of fluctuating lake levels were correlated with MIS 4 based on several uranium-series ages on bone ranging from 68 to 48 ka and several mostly infinite radiocarbon ages (Jefferson, 2003, p. 48). The youngest sediments at this site, coeval with MIS 3 and 2, were interpreted as interbedded fluvial and lacustrine deposits formed as the Mojave River delta prograded eastward.

Studies prior to 2007 interpreted the stratigraphic sequence in the Afton subbasin to represent two main lake phases, although Meek (1990) suggested there were older

lake deposits. The younger lake is mainly represented by nearshore sand and gravel, and the older lake by generally deeper-water deposits. An earlier lake formed when the Cady subbasin spilled across a threshold at Buwalda Ridge into the Afton area early in MIS 6 (Reheis et al., 2007, 2012). Meek (1989a, 1990, 1999, 2000, 2004) dated beach deposits of the younger lake phase in the Afton subbasin and in the Coyote Lake and Troy Lake subbasins. Reheis and Redwine (2008) revised the late Pleistocene history of Lake Manix and the record of downstream integration by the Mojave River using exposed stratigraphy, radiocarbon ages, and soils. They showed that Lake Manix reached a highstand of 547–558 masl (meters above sea level) at least twice prior to its previously known 543-m highstands; soil properties suggested an age of at least 35 to 50 ka. Beach deposits, locally with preserved barrier morphology, document the older highstands in both the Afton and Cady subbasins (Reheis et al., 2014). During two or more of these older highstands, the lake filled the Coyote subbasin (Reheis et al., 2015) and also spilled east over a threshold on the north rim of Afton Canyon to the Soda Lake basin. However, significant incision of the canyon did not begin until about 25 ka. Such timing is consistent with interpretations of Wells et al. (2003) that episodic flooding of the downstream Lake Mojave basin may have begun as early as 26.5 cal ka.

Dudash (2006) and Miller et al. (2018) mapped the surficial geology and reconstructed the history of lake level fluctuations during the late Pleistocene in the Coyote subbasin, with special focus on episodes when the Mojave River directly fed a lake after incision of Afton Canyon and headward erosion by the river. During this time, ~24.5 to 14 ka, the river's course alternated between northward flow to Coyote subbasin and northeastward flow to Lake Mojave.

Lake Manix basin palaeontology summary

Fossils recovered from exposures of the fluvial and lacustrine sediments of the Manix Formation (Tables 8, 9, 10) (Jefferson 2003) are now known to encompass the late lrvingtonian through late Rancholabrean North American Land Mammal Ages, approximately from over 350 to less than 20 kyr. The relative abundance and paleoecological character of the organisms recovered from the deposits permits a limited but significant reconstruction of Manix basin paleohabitats during the middle and late Pleistocene. Shortly after Buwalda's (1914) publication on the lacustrine deposits at Manix, J.C. Merriam (1915) described the first vertebrate fossils from the site. The extensive fossil avifauna from Lake Manix was first described by H. Howard (1955, also see Jefferson 1985b).

The Lake Manix fossil assemblage (termed the Camp Cady local fauna, Jefferson 1968) includes extinct and extralocal extant forms that reflect ecological conditions dramatically different from the present xeric environment of the central Mojave Desert. Inferences based on the ecology of extant taxa that are closely related to the extinct forms allow paleoenvironmental reconstructions of the local lacustrine and terrestrial paleohabitats. Most of the fossil molluscan taxa represent extant animals that live in an assortment of fluvial, lacustrine, or paralimnic habitats. Some are extralocal, preferring cooler waters. However, others presently inhabit perennial waters in the Mojave Desert region. Although now rare, all lower vertebrate taxa, fish and turtle, are known from the Mojave River drainage system.

The fossil avians (Table 9, Howard 1955, Jefferson 1985b) clearly suggest the presence of a variety of mildly saline or freshwater lake and lake margin environments. Judging from the food preferences, food procurement methods and nesting habits of extant bird species represented in the Manix avifauna, open water, sandy beach flats, and extensive reedy marshlands were the dominant lacustrine habitats in Lake Manix (Jefferson 1985b, 2003). The seasonally extralocal pattern of the migratory forms in the assemblage suggests an overall cooler or more equable climate. Extant migratory waterfowl present in the Manix avifauna presently use the North American Pacific Flyway.

A substantial portion of the extinct and extralocal fossil vertebrates were ecologically tied directly to the lacustrine and paralimnic environments of Lake Manix. These include essentially all lower vertebrate and avian species (Table 8). Mammalian browsers or browser-grazers (75% NISP, number of identified specimens, Table 10) that take advantage of seasonally available forage were the dominate large herbivores at Lake Manix and in the central Mojave Desert region during late Pleistocene time. Regional terrestrial vegetation patterns, reconstructed in part from packrat midden data (Spaulding et al. 1984, Spaulding 1990), permit inferences about the local paleoflora. The alluvial slopes and low hills surrounding Lake Manix probably supported a juniper–sage brushland, and the nearby mountains most likely were covered with a pinyon–juniper woodland (Spaulding 1980, 1990; Jefferson 1987, 1991a). Local valley bottoms probably supported patchy semi-desert grasslands and desert scrub. These floristic associations are consistent with the inferred browsing habits of the majority of the larger mammalian taxa (Tables 8, 10) (Jefferson 1987, 1991a, 2003).

Radiometric dates tables

Table 1. Radiometric and absolute dates from Lake Manix Basin (extracted from Table 1 in Jefferson 2003).

Age yr BP	Location	Material	Method	Laboratory	Reference
11,810 ± 100	Coyote Lake basin	*Anodonta* shell	^{14}C	UCLA 2609C	Meek, 1990
12,900 ± 120	Coyote Lake basin	*Anodonta* shell	^{14}C	UCLA 2606	Meek, 1990
13,560 ± 145	Coyote Lake basin	*Anodonta* shell	^{14}C	UCLA 2609B	Meek, 1990
13,800 ± 600	Coyote Lake basin	*Anodonta* shell	^{14}C	La Jolla 958	Hubbs et al., 1965
14,230 ± 1,325*	Afton basin	*Anodonta* shell	^{14}C	UCLA 2601	Meek, 1989, 1990
15,025 ± 230	Troy Lake basin	*Anodonta* shell	^{14}C	UCLA 2605	Meek, 1990
15,125 ± 270	Coyote Lake basin	*Anodonta* shell	^{14}C	UCLA 2608	Meek, 1990
16,750 ± 1,000	central Manix basin	oncoid stromatolite	^{14}C	UCLA 1079	Berger and Libby, 1967
17,950 ± 1,500	Coyote Lake basin	*Anodonta* shell	^{14}C	UCLA 6203	Meek, 1990
18,150 ± 400	Afton basin	*Anodonta* shell	^{14}C	UCLA 2607	Meek, 1990
19,100 ± 250	Manix basin D	*Anodonta* shell	^{14}C	QC 1467	R. Pardi, pers. comm., 1983; Jefferson, 1985a
19,300 ± 400	Afton basin	oncoid stromatolite	^{14}C	UCLA 121	Fergusson and Libby, 1962
19,500 ± 500	Afton basin	oncoid stromatolite	^{14}C	La Jolla 269	Hubbs et al., 1962
19,700 ± 260	central Manix basin	oncoid stromatolite	^{14}C	UCLA 2600B	Meek, 1990
20,500 ± ?	Afton basin	*Anodonta* shell	^{14}C	Yale	Stuiver, 1969; Bassett and Jefferson, 1971
20,980 ± 345	central Manix basin	oncoid stromatolite	^{14}C	UCLA 2602	Meek, 1990
21,300 ± 1,710	Afton basin	*Anodonta* shell	^{14}C		Meek, 1999
23,090 ± 445	central Manix basin	*Anodonta* shell	^{14}C	UCLA 2600A	Meek, 1990
28,960 ± 2,490	Afton basin	*Anodonta* shell	^{14}C	UCLA 2601C	Meek, 1999
29,310 ± 310	Afton basin	*Anodonta* shell	^{14}C	CAMS 1856	Meek, 1999
30,650 ± 890	Afton basin	*Anodonta* shell	^{14}C	UCLA 2604	Meek, 1990
30,950 ± 1,000	Afton basin	oncoid stromatolite	^{14}C	La Jolla 895	Hubbs et al., 1965
35 + (infinite)	Manix basin D	*Anodonta* shell	^{14}C	UCLA	R. Berger, pers. comm., 1982; Jefferson, 1985a
47 + (infinite)**	Manix basin D	*Anodonta* shell	^{14}C	Yale	Stuiver, 1969; Bassett and Jefferson, 1971
47,700 ± 2.0	Manix basin D	*Mammuthus* bone	U/Th	USGS 81-48	J. Bischoff, pers. comm. 1982, 1983: Jefferson, 1985a
51,200 ± 2.5	Manix basin D	*Hemiauchenia* bone	U/Th	USGS 81-49	J. Bischoff, pers. comm. 1982, 1983: Jefferson, 1985a
60,300 ± ?	Manix basin D	Mammalia bone	U/Th	USGS	Budinger, 1992
68,000 ± 4.0	Manix basin C	*Camelops* bone	U/Th	USGS 81-51	J. Bischoff, pers. comm., 1982, 1983; Jefferson, 1985a
74,000 ± ?	Manix basin D	*Anodonta* shell	U/Th	USGS	Budinger, 1992
80,000 ± ?	Afton basin	oncoid stromatolite	U/Th		Meek, 2000
183,800 ± 12.0	Manix basin C	*Camelops* bone	U/Th	USGS 81-30	J. Bischoff, pers. comm., 1982, 1983; Jefferson, 1985a
185,000 ± 15.0	Manix basin C	tephra	chemical		Bacon and Duffield, 1981; Izett, 1981
350 + (infinite)	Manix basin B	*Equus* bone	U/Th	USGS 80-51	Bischoff, pers. comm., 1982, 1983; Jefferson, 1985a

Notes: Ages are uncorrected. Manix Formation Members (B through D) are designated where known. Meek (1990) provides corrected ^{14}C ages for analyses from Manix basin and a discussion of the reliability of both *Anodonta* and oncoid stromatolite tufa determinations.

* This age has been revised, UCLA 2601C (Meek 1999).

** The previously reported age of 49 + ka for this sample (Jefferson, 1985a) is an error.

Table 2. Radiocarbon ages from outcrop samples near core site (extracted from Table 1 in Reheis et al. 2012).

Sample no.	Lab. no. (WW- prefix)	UTM zone	Easting	Northing	Height above unit D-C contact (m)	^{14}C age	^{14}C error (1 δ)	Calibrated age	Cal. lower bound (2δ)	Cal. upper bound (2δ)
M09NS-998	7376	11S	540717	3868778	8.5	25600	90	30438	30227	30719
M06NS-2405	6062	11S	540751	3868790	8.0	26300	160	30983	30646	31212
M03NS-1767	4564	11S	540726	3868771	7.0	29070	170	33741	33195	34486
M05NS-1965	5356	11S	539542	3868485	5.0	32060	190	36587	35699	36988
M05NS-2984	5518	11S	540625	3869416	3.7	32160	240	36663	35717	37367
M06NS-1865	5849	11S	540615	3869575	1.2	34950	460	40014	38888	41064
M06NS-941	5716	11S	539291	3870382	0.4	40030	610	43984	42994	44920

All measurements made on *Anodonta californiensis* shells. Samples arranged in depth order above stratigraphic contact of fluvial-deltaic deposits (unit D of Jefferson, 2003) over lacustrine / mudflat deposits (unit C; muds, generally gray or gray-green in color). Radiocarbon ages adjusted using estimated δ^{13}C value of -4‰ (average of measurements on *Anodonta* shells of similar age from Manix basin) and subtracting 140 yr for estimated old carbon (Miller et al., 2009). Calibration performed using Calib v. 6.0 (http://calib.qub.ac.uk/calib/) accessed April 2010.

Table 3. $^{40}Ar/^{39}Ar$ data for Long Canyon rhyolite sample (source of Manix tephra) (extracted from Table 2 in Reheis et al. 2012).

Long Canyon 1 Sanidine IRR275-07 J = 0.000398817

Run #	$^{40}Ar^{*}$ (mol/g)	% $^{40}Ar^{*}$	$^{40}Ar/^{39}Ar$	$^{37}Ar/^{39}Ar$	$^{36}Ar/^{39}Ar$	K/Ca	Cl/K	Age (Ma)
A	1.8060E-15	84.74	0.32404	0.00757	0.00017	69.29	0.00014	0.1976 ± 0.0059
B	1.8623E-15	90.92	0.30002	0.01126	0.00010	46.61	0.00010	0.1963 ± 0.0061
C	1.6582E-15	40.55	0.62816	0.00400	0.00127	131.33	0.00006	0.1833 ± 0.0067
D	2.0985E-15	54.41	0.47206	0.00369	0.00073	142.28	0.00012	0.1848 ± 0.0063
E	2.2228E-15	92.93	0.27152	0.00877	0.00007	59.86	0.00008	0.1815 ± 0.0047
F	2.3559E-15	79.48	0.29992	0.00922	0.00021	56.91	0.00017	0.1715 ± 0.0046
				Weighted Mean Age (Ma)		(MSWD = 3.39)		0.1841 ± 0.0042
				Total gas age (Ma)				0.1846 ± 0.0025

Table 4. Radiometric ages on samples from study area (extracted from Table 1 in Reheis and Redwine, 2008).

Site no.	Lab no.*	Figure	Material dated	^{14}C age	±1σ	Calendar age§	±1σ	Notes on location and stratigraphy
M04-23	WW4771	5	*Anodonta* shells	21,780	70	26,230	90	Sampled in nearshore sands overlying weak Bt horizon formed on lacustrine mud; below 543 m shoreline.
M04-32A/B	WW4772	2A	*Anodonta* shells	20,810	60	24,960	130	Well-bedded sands containing broken *Anodonta* shells in individual layers; apparently eolian sand sheets reworked from late Pleistocene lake deposits.
M04-74	WW5279	2A	*Anodonta* shells	28,170	120	32,860	130	~2 m below surface of railroad cut in second unit down.
M04-75	WW5357	4, 5	*Anodonta* shells	22,470	70	26,960	110	Within Manix fault zone; uppermost lake sediments, about 2 m below surface.
M05-07	WW5339	5	*Anodonta* shells	32,690	210	37,650	610	North of Manix fault; uppermost limit of probable lake sediment in well-sorted sand about 05 m below distinct paleosol; above 543 m shoreline.
M05-19I	WW5340	2B, 4	*Anodonta* shells	34,680	260	40,080	480	Sampled ~80 cm below surface beneath uppermost buried soil; soil overlain by younger beach gravel.
M05-20	WW5628	2B, 4	*Anodonta* shells	49,800	2000	n/a	n/a	Just above basal tufa of green mud unit; minimum limiting age
M05-21	WW5629	2B, 4	*Anodonta* shells	31,900	200	36,820	130	Sampled just below uppermost paleosol in muddy sand; in same stratigraphic position as M05-19I.
M05-22H	WW5341	3, 4	*Anodonta* shells	27,000	120	31,920	120	Top of beach ridge in youngest preserved lake unit; whole fragmented shells in growth position.
M05-23C	WW5342	3, 4	*Anodonta* shells	40,120	500	44,340	360	Shells are from base of oldest definite lake unit in measured section. Minimum limiting age.
M05-25J	WW5630	3, 4	*Anodonta* shells	45,500	1200	n/a	n/a	Shells are from top of oldest of three lake units in measured section. Minimum limiting age.
M05-26F	WW5631	3, 4	*Anodonta* shells	39,900	600	44,160	500	Shells are from top of oldest of three lake units in measured section and just below "interlacustral gravel" of Meek (1990). Minimum limiting age.
M05-26G	WW5632	3, 4	Gastropod shells	29,600	200	34,800	270	Gastropod shells and fish bones just below weak paleosol; top of middle lake unit, which overlies "interlacustral gravel" of Meek (1990).
M05-28B	WW5343	2B, 4	*Anodonta* shells	26,030	100	31,150	100	Uppermost lake unit above youngest paleosol.
M05-62	WW5633	3	*Anodonta* shells	28,440	160	33,090	180	Whole in situ shells 60 cm above a thickly tufa-coated bed.
JR04D-1	WW4924	2B, 4	*Anodonta* shells	25,420	120	30,660	110	Foreslope of beach barrier, adjacent to site M04-29B.
JR04D-68 248-255	WW5384	3, 10	Ostracodes	27,020	310	31,940	260	Bedded sand containing ostracode coquina; "slack-water" deposits, 248–255 cm below surface.
JR04D-68 331-338	WW5385	3, 10	Ostracodes	30,540	410	35,490	380	Laminated sand and clay; "slack-water" deposits, 331–338 cm below surface.
JR04D-68B 385-395	WW4909	3, 10	Ostracodes	28,020	160	32,740	150	Massive green clay with secondary gypsum and carbonate nodules; "slack-water" deposits, 385–395 cm below surface; Calgon used to disperse.
JR04D-68A 425-435	WW4908	3, 10	Ostracodes	30,180	210	35,200	140	Green silty clay with clay platelets; "slack-water" deposits, 425–435 cm below surface; Calgon used to disperse.
JR04D-68B 385-395	WW5077	3, 10	Ostracodes	29,280	320	34,340	560	Massive green clay with secondary gypsum and carbonate nodules; "slack-water" deposits, 385–395 cm below surface; only distilled water used.
JR04D-68A 425-435	WW5076	3, 10	Ostracodes	31,500	420	36,470	420	Green silty clay with clay platelets; "slack-water" deposits, 425–435 cm below surface; only distilled water used.
SL-830-Lb‡	WW4872	n/a	Ostracodes	18,040	70	21,510	110	Lake clays in USGS Soda-1 core, Soda Lake, 25.3 m depth.
SL-860-Lb‡	WW4873	n/a	Ostracodes	18,780	60	22,380	40	Lake clays in USGS Soda-1 core, Soda Lake, 25.3 m depth.

*Samples were pretreated at the ^{14}C laboratory of the U.S. Geological Survey (USGS) in Reston, Virginia (WW designation).

†^{14}C ages were determined at the Center for Accelerator Mass Spectrometry (CAMS), Lawrence Livermore National Laboratory, Livermore, California, and at National Science Foundation–Arizona Accelerator Mass Spectrometry facility in Tucson, Arizona. Quoted age is in radiocarbon years (B.P.) using Libby half-life of 5568 yr.

§Ages were calibrated using program available at http://www.radiocarbon.ldeo.columbia.edu/research/radcarbcal.htm (Fairbanks et al., 2005). Calibration was performed assuming no reservoir correction (see discussion in Methods); "n/a" indicates radiocarbon age is beyond current calibration limit of method.

‡Exact core location unknown; reported by Muessig et al. (1960) as NE/4 sec 1, T 12 N, R 8 E.

Table 5. Radiocarbon ages and site information for samples from Afton and Cady subbasins of Lake Manix (extracted from Table 1 in Reheis et al. 2014).

Station	Lab number[1]	Altitude (m)[3]	Samples	$\delta^{13}C$[4]	Age[5]	1 s.d.	Description
M04-23	WW4771	536	*Anodonta* valves	n.d.	21780	70	In-situ whole shells in nearshore sand overlying mud and silt beds; capped by weak buried soil; overlain by dune sand. South of Mojave River
M04-32A/B	WW4772	**557.8**	*Anodonta* fragments	n.d.	20810	60	Well bedded dune sand containing shell fragments in individual layers. North of North Afton beach ridge
M04-74	WW5279	**535**	*Anodonta* valves	n.d.	28170	120	Measured section M09-6 in railroad cut west of Dunn siding. 4 units within map unit Ql8. Abundant shells in S-dipping foreset sand beds above buried soil; 2.6 m above base of outcrop
M04-75	WW5357	**542**	*Anodonta* valves	n.d.	22470	70	Two lake units; upper unit contains shells 1.25 m below surface; overlies lower unit capped by debris flow and mottled red and white buried soil. West end of Buwalda Ridge
M05-07	WW5339	549	*Anodonta* fragment	n.d.	32690	210	Uppermost limit of probable lake sediment, unit Ql7?; well sorted sand about 0.5 m below distinct buried soil. West end of Buwalda Ridge
M05-19I	WW5340	**520.4**	*Anodonta* fragments	n.d.	34680	260	Measured section in upper Dunn wash at pipeline crossing. Upper 3 lake units within map unit Ql8, lowest 4th unit Ql7. Sampled shell in second unit from top, 80 cm below surface
M05-20A	WW5628	**527.5**	*Anodonta*, whole shell	n.d.	49800	2000	Shells are from just above oncoid tufa-coated clasts at base of unit Ql7, upper Dunn wash
M05-21	WW5629	**535.4**	*Anodonta* fragments	n.d.	31900	200	Shells from 40 cm below surface in second Ql8 unit from top; upper Dunn wash
M05-22H	WW5341	**539.4**	*Anodonta* valve	n.d.	27000	120	Measured section on east side of North Afton beach ridge; shells sampled at very top in unit Ql8.
M05-23C	WW5342	515	*Anodonta*, whole shell	n.d.	40120	500	Measured section on east side of North Afton beach ridge. Shells from 1 m above oncoid tufa-coated clasts at base of unit Ql7
M05-25J	WW5630	539	*Anodonta* valves, weathered	n.d.	45490	1200	Measured section on east side of North Afton beach ridge. Shells from 2.8 m above oncoid tufa-coated clasts at base of unit Ql7
M05-26F	WW5631	**521.7**	*Anodonta*, whole shell	n.d.	40000	600	Measured section on west side of North Afton beach ridge. Tufa-coated shells from 9.2 m above oncoid tufa-coated clasts at base of unit Ql7 and 25 cm below Bwk soil formed in unit Qia7
M05-26G	WW5632	**532.3**	*Anodonta* fragments	n.d.	29630	190	Measured section on west side of North Afton beach ridge. Sands containing shells, fish bones, and snails within unit Ql8, 9.1 m above unit Qia7
M05-28B	WW5343	**533.0**	*Anodonta* valves	n.d.	26030	100	Shells lie in greenish lagoonal sediment of unit Ql8, just above tufa-coated clasts on weak buried soil west of pipeline crossing in upper Dunn wash
M05-62	WW5633	**533.8**	*Anodonta*, whole shell	n.d.	28440	160	Large, abundant shells in beach sand and gravel of unit Ql8 1 m above unit Qia7, on west side of North Afton beach ridge
M05-62A	WW7485	**533.2**	*Anodonta* fragments	-3.7	31840	270	Shell fragment in beach gravel 45 cm above base of unit Ql8, on west side of North Afton beach ridge
M05-62A-2	WW7851	**533.2**	*Anodonta* fragments	-3.7			Re-analysis of sample M05-62A
M05-62C	WW7486	**534.0**	*Anodonta*, whole shell	-4.9	26620	150	Whole shell in beach gravel 1.4 m above base of unit Ql8; just below green mud bed; west side of North Afton beach ridge
M06-35A	WW5882	**526.0**	*Anodonta* valves	n.d.	47430	930	Abundant shells in horizontally bedded beach sand just above oncoid tufa-coated clasts at base of unit Ql7; east side of North Afton beach ridge
M06-62D	WW5885	**538.6**	*Anodonta* valve	n.d.	21310	50	Shells in-situ 30 cm below surface of beach gravel, 0.7 m thick; overlies Bwk on dune (?)sand; west side of North Afton beach ridge
M06-89	WW5886	**536.3**	*Anodonta*, whole shell	n.d.	23130	70	Measured section M09-6 in railroad cut west of Dunn siding. 4 units within map unit Ql8. Shell is from uppermost unit, 0.75 m below surface, above buried soil
M06-116A	WW6070	**533.1**	*Anodonta*, whole shell	-1.9	21140	70	Whole shell in beach sand and gravel, 50 cm above beach cobbles within unit Ql8; west side of North Afton beach ridge
M06-116B	WW6070	**533.6**	*Anodonta* valve	-4.9	20510	70	Whole shell in beach sand, 1 m above beach cobbles within unit Ql8; west side of North Afton beach ridge
M07-29	WW6343	**522.6**	*Anodonta* valve	-7.0	36040	400	Measured section M07-62. Shell in younger of two subunits of Ql8 near top of railroad cut west of Dunn siding

continues

Table 5 continued

Station	Lab number[1]	Altitude (m)[3]	Samples	$\delta^{13}C$[4]	Age[5]	1 s.d.	Description
M07-36a	WW6344	**533.0**	*Anodonta*, whole shell	-2.8	27070	140	Shells in muddy sand and gravel of upper unit Ql8; overlie thin debris flow and grade up into lacustrine sand and beach gravel forming a spit
M07-131	WW6346	**537.2**	*Anodonta*, whole shell	-5.3	26860	140	Whole shell in beach sand and gravel of unit Ql8, about 60 cm above unit Qia7; south side of Mojave River
M07-151A2	WW6345	**539.5**	*Anodonta* valves	-3.6	21580	70	Shells in beach sand and gravel of unit Ql8, 75 cm below surface; lie on tufa-coated gravel that caps weak soil formed on older Ql8 sand, in turn unconformably on soil formed on tilted unit Qalg. Upper Manix Wash
M08-58	WW6986	**542.4**	*Anodonta* fragments	-4.1	21450	70	Shell fragments in gravel bed 1 m below surface of beach ridge. Beach gravel of unit Ql8, 2.5 m thick, overlies unit Qia7. South of Mojave River
M08-60c-1	WW6987	**531.3**	*Anodonta* valves	-5.0	31510	230	Measured section on west side of Buwalda Ridge. Five subunits of Ql8 separated by tufa-coated clasts or weak soils overlie truncated soil formed on unit Ql7. Shell layer lies 75 cm above base in 4th unit from top
M08-60c-2	WW6988	**531.8**	*Anodonta* valves	-4.2	24400	130	Measured section on west side of Buwalda Ridge. Five subunits of Ql8 separated by tufa-coated clasts or weak soils. Shell layer lies 1.35 m above base, in third unit from top
M08-60c-3	WW7616	**532.0**	*Anodonta* fragments	-3.8	34970	450	Measured section on west side of Buwalda Ridge. Five subunits of Ql8 separated by tufa-coated clasts or weak soils. Shell layer 1.55 m above base in 2nd unit from top
M08-60c-3 resample	WW8113	**532.0**	*Anodonta* valves	-5.2	33320	210	Measured section on west side of Buwalda Ridge. Five subunits of Ql8 separated by tufa-coated clasts or weak soils. Shell layer 1.55 m above base in 2nd unit from top. Resampled to check age
M08-60c-4	WW8114	**533.0**	*Anodonta* fragments	-5.2	32710	190	Measured section on west side of Buwalda Ridge. Five subunits of Ql8 separated by tufa-coated clasts or weak soils. Shell layer 3 m above base in uppermost unit
M08-76A	WW7109	**524.0**	*Anodonta* valve	-5.9	26790	230	Shell layer in greenish sand 3 m above tufa-coated clasts marking base of unit Ql8. Overlies green gypsiferous sand and silt of unit Ql7. Likely separated from outcrop of M08-76B by fault. South of Mojave River
M08-76B	WW7110	**529.0**	*Anodonta* fragments	-1.8	21980	120	Shell fragments in tan beach sand, 3.5 m below surface of unit Ql8. Poor outcrop. Likely separated by fault from outcrop of M08-76A. South of Mojave River
M08-108	WW7201	**535.7**	*Anodonta* valves	-4.7	28230	190	Shells in beach gravel and sand of unit Ql8. To east, unit overlies buried soil formed on gravel capping unit Ql7. Exposed in ditch on N side of railroad service road, upper Manix Wash
M08-124	WW7202	**532.7**	*Anodonta* valves	-5.3	29090	190	Shells in ripple-laminated beach sand, 40 cm thick, overlain by 3 cm brown mud. Three subunits of Ql8 present; sample is from 2nd unit below top. West side of Buwalda Ridge
M08-124A	WW8116	**532.7**	*Anodonta* valves	-2.6	29610	130	Shells in thin bedded fine sand, 75 cm thick, coarsens at base; forms 3rd unit from top, and underlain by buried soil formed on green mud of unit Ql7. West side of Buwalda Ridge
M08-124C	WW8117	**532.7**	*Anodonta* valves	-6.6	27430	130	Shells at base of interbedded sand and pebble gravel, 3 m thick; forms uppermost unit. West side of Buwalda Ridge
M08-141	WW7108	**531.5**	*Anodonta* fragments	-2.6	34600	570	Shell fragments in beach sand and gravel of unit Ql8. As much as 1.2 m thick locally; overlies unit Ql7, both units apparently faulted. West side of Buwalda Ridge
M08-172	WW7496	**536.7**	*Anodonta*, whole shell	-3.7	23120	100	Measured section M08-172 in unit Ql8 south of Mojave River. Shell layer 1.0 m above base of uppermost unit, 1.7 m thick, which rests on a weak buried soil and is capped by ~2.5 m poorly sorted pebbly sand (eolian?)
M08-172A	WW8041	**533.5**	*Anodonta* valves, weathered	-6.7	27920	190	Measured section M08-172 south of Mojave River. Weathered shells in buried soil formed on green sand and silt of unit Ql8, overlying thickly tufa-coated boulders of unit Qvg. Three subunits present; shells are in third from top
M08-172C	WW8042	**534.9**	*Anodonta*, whole shell	-4.4	24400	120	Measured section M08-172 south of Mojave River. Shell layer in silt and sand 1.5 m thick, capped by weak buried soil. Sample lies 0.9 m above base of second unit from top and above sample M08-172A

continues

Table 5 continued

Station	Lab number[1]	Altitude (m)[3]	Samples	$\delta^{13}C$[4]	Age[5]	1 s.d.	Description
M08-172D	WW8043	**536.7**	*Anodonta* valves	-3.0	23200	100	Measured section M08-172 south of Mojave River. Shell layer 1.0 m above base of uppermost unit, 1.7 m thick, which rests on a weak buried soil and is capped by ~2.5 m poorly sorted pebbly sand (eolian?). Resampled to confirm stratigraphic position and age
M09-5	WW7492	**531.3**	*Anodonta* valve	-5.2	35980	450	Measured section M09-5 in upper Manix Wash. Shell layer in beach sand of unit Ql8, 20 cm above base of 2nd subunit from top; 1.4 m above base of Ql8
M09-5 (re-analysis)	WW7852	**531.3**	*Anodonta* valve	-5.2	35130	400	Measured section M09-5 in upper Manix Wash. Shell layer in beach sand of unit Ql8, 20 cm above base of 2nd subunit from top; 1.4 m above base of Ql8
M09-6A	WW7617	**533.0**	*Anodonta* valve	-5.7	39280	770	Measured section M09-6 at railroad cut west of Dunn siding. 4 units within map unit Ql8. Sample is from 1.6 m above base of outcrop
M09-6B	WW7491	**534.4**	*Anodonta* fragments	-3.1	27810	170	Measured section M09-6 at railroad cut west of Dunn siding. 4 units within map unit Ql8. Sample is from 3.05 m above base of outcrop
M10-3A	WW8115	522	*Valvata utahensis*	-6.2	36410	300	Fine silty sand in unit Ql8 contains abundant snails. Overlies buried soil formed on older subunit. Probably overlies soil on top of M07-29 unit, or is equivalent to that unit; lies across from measured section M07-62 at railroad cut west of Dunn siding
J06-15	WW7112	**529.9**	*Anodonta* valves, weathered	-2.9	33410	490	Measured section M09-5 in upper Manix Wash. Weathered shells in greenish fine sand of unit Ql8, 20 cm above stone line marking contact with unit Ql7, in 4th subunit from top
J06-16	WW7113	**530.6**	*Anodonta* valves, weathered	-3.9	34410	580	Measured section M09-5 in upper Manix Wash. Shell layer lies in ripple-bedded fine sand of unit Ql8, 12 cm above base of 2nd subunit from top; 1.7 m above base of unit Ql8
J06-17	WW5850	**532.5**	*Anodonta* valves	n.d.	31910	330	Measured section M09-5 in upper Manix Wash. Shell layer lies in medium sand of unit Ql8 at top of outcrop, 60 cm above base of 1st subunit; 3.05 m above base of unit Ql8
JR04CM-87	WW8004	**537.7**	*Limnocythere bradburyi*	n.d.	33120	710	Reworked ostracodes in fluvial sand of unit Qif, 3.5 m below surface; overlain by several fan deposits with buried soils; north rim of Afton Canyon
JR04D-1	WW4924	**541.0**	*Anodonta* valves	n.d.	25450	120	Shell layer at base of 50-cm-thick beach sand and gravel of unit Ql8; overlies buried soil. Occupies foreshore of beach ridge in upper Dunn Wash
JR04D-68 248-255	WW5384	*476*	Ostracodes	n.d.	27020	310	Bedded sand containing ostracode coquina; slack-water deposits, unit Qysl, 248-255 cm below surface
JR04D-68 331-338	WW5385	*476*	Ostracodes	n.d.	30540	410	Laminated sand and clay; slack-water deposits, unit Qysl, 331-338 cm below surface
JR04D-68B 385-395	WW4909	*476*	Ostracodes	n.d.	28020	160	Massive green clay with secondary gypsum and carbonate nodules; slack-water deposits, unit Qysl, 385-395 cm below surface. Calgon used to disperse
JR04D-68A 425-435	WW4908	*476*	Ostracodes	n.d.	30180	210	Green silty clay with clay platelets; slack-water deposits, unit Qysl, 425-435 cm below surface. Calgon used to disperse
JR04D-68B 385-395	WW5077	*476*	Ostracodes	n.d.	29280	320	Massive green clay with secondary gypsum and carbonate nodules; slack-water deposits, unit Qysl, 385-395 cm below surface; only distilled water used
JR04D-68A 425-435	WW5076	*476*	Ostracodes	n.d.	31500	420	Green silty clay with clay platelets; slack-water deposits, unit Qysl, 425-435 cm below surface; only distilled water used
JR06D-206A	WW5879	*536.3*	*Anodonta* valve	n.d.	21830	60	Measured section JR06D-206 in unit Ql8, south of Mojave River. 5 subunits of unit Ql8 overlie tufa-coated clasts on buried soil formed on unit Qia7, overlying green mud of unit Ql7. Shell layer is in beach gravel and sand of uppermost subunit, 0.5 m below surface
JR06D-206B	WW5880	*535.3*	*Anodonta*, whole shell	n.d.	20940	60	Measured section JR06D-206 in unit Ql8, south of Mojave River. 5 subunits of unit Ql8. Shell layer is in beach sand at base of uppermost subunit, 1.5 m below surface
JR06D-206C1	WW5881	*534.1*	*Anodonta*, whole shell	n.d.	26620	90	Measured section JR06D-206 in unit Ql8, south of Mojave River. 5 subunits of unit Ql8. Shell layer is in sand, 4th subunit from top, 2.5 m below surface

continues

Table 5 continued

Station	Lab number[1]	Altitude (m)[3]	Samples	$\delta^{13}C$[4]	Age[5]	1 s.d.	Description
JR06D-206E	WW7483	*535.1*	*Anodonta* valve	-4.9	23140	100	Measured section JR06D-206 in unit Ql8, south of Mojave River. 5 subunits of unit Ql8. Shell layer is at top of 3rd subunit from top, 1.6 m below surface
JR06D-206F	WW7484	*535.3*	*Anodonta*, whole shell	-3.0	21780	80	Measured section JR06D-206 in unit Ql8, south of Mojave River. 5 subunits of unit Ql8. Whole shell in growth position in beach sand at base of uppermost subunit, 1.5 m below surface. Re-collected to check age of sample JR06D-206B

[1] Samples were pretreated at the ^{14}C laboratory of the U.S. Geological Survey in Reston, Virginia (WW designation)
[2] All locations given in UTM units, WGS84 coordinates.
[3] Bold font indicates differentially corrected GPS data; altitudes in normal font estimated from topographic map and handheld GPS; italic font indicates altitudes from NASA ATM-III LIDAR data acquired September, 2004, funded by the U.S. Army Corps of Engineers, WRAP program R. Lichvar & D. Finnegan.
[4] $\delta^{13}C$ measured on all samples beginning in 2007
[5] ^{14}C ages were determined at the Center for Accelerator Mass Spectrometry (CAMS), Lawrence Livermore National Laboratory, Livermore, Californa, and at National Science Foundation–Arizona Accelerator Mass Spectrometry facility in Tucson, Arizona. Quoted age is in radiocarbon years (B.P.) using Libby half-life of 5568 yr. ^{14}C age reflects correction for $\delta^{13}C$ values if measured

Table 6. Locations, correlations, age ranges, and geochemical compositions of Manix Basin tephra layers (extracted from Table 2 in Reheis et al. 2015; see that table for oxide data).

Station	Easting[1]	Northing	Map unit	Tephra correlation	Tephra age (Ma)	Notes
M07-101A	545398	3871673	Tbrg	Tuffs of Mesquite Springs	3.35 - 3.10	Lower of two tephra beds in highest S-facing part of east end Buwalda Ridge. Separated by 2 m of section. Lenticular and interbedded with fan gravel up to boulder size
M07-101B	545398	3871673	Tbrg	Tuffs of Mesquite Springs	3.35 - 3.10	Upper of two tephra beds in highest S-facing part of east end Buwalda Ridge. Separated by 2 m of section. Lenticular and interbedded with fan gravel up to boulder size
M07-128	544564	3870904	Qmr	Tuffs of Blind Spring Valley	2.219 ±0.006 - 2.135 ±0.02	Tephra, medium-sand-sized pumice with biotite; airfall near base; in playa and lacustrine-fluvial deposits of Mojave River formation (informal)
M07-145	557766	3878699	Tcg	Ishi Tuff, correlated age	2.50	Tephra with carbonate cement at top of Cave Mtn. fanglomerate; reworked, fluvially bedded; overlain by fan gravel and fan-delta deposits of Ql7
M07-159B	552769	3879358	Ql6	Manix Basin tephra	0.184 ± 0.04	Between forks of Dunn Wash. Unit Ql6 contains tephra about 2 m above Qia fan gravel with fluvial bedding; tephra is overlain by ~1.2 m lake sand, silt, and reworked chunks of lake mud, capped by lag gravel
M08-164	542667	3868988	Qmr	Huckleberry Ridge ash bed	2.063 ±0.007	18-cm tephra in Mojave River formation. Sediments dip 12°SW. Cut by fault striking 70°, vertical, down to S by 2.5 m
M08-164A	542667	3868988	Qmr	Tuffs of Blind Spring Valley	2.219 ±0.006 - 2.135 ±0.02	Burrowed white lens, 0-3 cm thick, diatomite or altered tephra, 3.9 m below sample M08-164 on footwall of fault
M08-164B	542667	3868988	Qmr	Tuffs of Emigrant Pass, correlated age	<2.063, >1.96	Lenticular, 0-3 cm thick, 1.1 m above sample M08-164 on hanging wall of fault
M10-90	544673	3871144	Qmr	Huckleberry Ridge ash bed	2.063 ±0.007	~3 m above tephra M07-128 at sharp fold in Qmr. Thin cemented lens capping escarpment above playa-lake facies. Above this ash, deposits are coarser-grained, redder and more arkosic with paleosols; mapped as unit Qalg
M10-94	542763	3870995	Qmr	Similar to Bishop Tuff, and youngest set of tuffs of Upper Glass Mountain	0.759 ±0.0002 *or* 1.13 ±019 - 0.87 ±0.02	Tuffaceous marker bed at contact with reddish upper Qmr and lower more playa-like Qmr, N side river. Located near section with paleomagnetic data of Pluhar and others (1991), which suggests tephra lies within the Matayuma Reversed Chron (youngest tephra of Upper Glass Mountain); however, microprobe data suggest slightly closer resemblance to Bishop ash

Table 7. Radiocarbon Results for Coyote Lake Area, California (extracted from Miller et al. 2018).

											IntCal 13 calibration (2σ)			
Sample ID	Lab ID	Site	Material	UTM† E	UTM N	$\delta^{13}C$	^{14}C Age	adjusted age	1σ error	Dated on	lower	upper	mode	altitude (m)
EX1-Lvl 3	WW10253	D	*Anodonta*	522293	3874981	-2.60	12360	12220	25	03/10/15	14005	14225	14110	536.4
M09SM-640	WW7375	E	*Anodonta*	524179	3876257	-2.40	12425	12285	30	9/22/2009	14055	14405	14170	532.1
EX1-Lvl 6	WW10255	D	*Anodonta*	522293	3874981	-2.20	12455	12315	30	03/10/15	14085	14510	14210	536.1
EX1-Lvl 5	WW10254	D	*Anodonta*	522293	3874981	-4.80	12460	12320	25	03/10/15	14095	14500	14210	536.2
M03SM-1686	WW4563	D	*Anodonta*	522319	3874948	-4	13115	12975	40	12/16/2003	15305	15720	15510	536.3
M05SM-2464	WW5354	C	*Anodonta*	522443	3874733	-4	13780	13640	35	8/9/2005	16255	16645	16420	538.4
Coyote Wash 1	WW6538*	C	*Anodonta*	522418	3874785	-2.00	13900	13760	75	3/3/2008	16340	16930	16580	537.6
M14SM-2910	WW10256	D	*Anodonta*	522309	3875009	-3.20	14280	14140	35	03/10/15	17040	17415	17190	535.2
M08SM-882	WW7432	H	*Anodonta*	525216	3877757	-5.25	14285	14145	45	9/15/2009	17030	17430	17210	525.5
M05SM-2462	WW5353	B	*Anodonta*	522475	3874610	-4	14305	14165	35	8/9/2005	17080	17435	17240	537.4
SDCL06-1762	WW5714	L	*Anodonta*	528656	3878986	-4	14850	14710	80	7/19/2006	17660	18120	17920	534.2
SD04CL-1337	WW5144	A	*Anodonta*	522747	3874086	-4	15070	14930	40	2/7/2005	17965	18310	18140	539.1
M05SM-2474	WW5355	K	*Anodonta*	528459	3878999	-4	15555	15415	40	8/9/2005	18570	18790	18690	529.8
SD04CL-1381A	WW5146	J	*Anodonta*	528542	3877714	-4	15675	15535	40	2/7/2005	18680	18900	18790	535.2
SD04CL-1380A	WW5145	I	*Anodonta*	528440	3877482	-4	15775	15635	40	2/7/2005	18770	18980	18870	535.8
M05SM-2418A	WW5351	A	*Anodonta*	522748	3874088	-4	15795	15655	40	8/9/2005	18785	19005	18890	538.6
SD04CL-1381B	WW5147	J	*Anodonta*	528542	3877714	-4	15875	15735	40	2/7/2005	18860	19120	18950	535.0
M07SM-1939	WW6148	F	*Anodonta*	524235	3876908	-2.69	16000	15860	40	5/31/2007	18955	19270	19100	524.4
M05SM-2418B	WW5352	A	*Anodonta*	522748	3874088	-4	16140	16000	40	8/9/2005	19145	19505	19280	538.1
M06SM-22	WW5711	A	*Anodonta*	522749	3874082	-4	16160	16020	80	7/19/2006	19080	19565	19350	537.8
M07SM-1944	WW6149	G	*Anodonta*	524541	3877163	-2.49	16390	16250	45	5/31/2007	19460	19825	19600	524.6
SDCL06-1761	WW5713	L	*Anodonta*	528615	3878986	-4	16670	16530	90	7/19/2006	19650	20190	19960	533.9
M03SM-1664	WW4562	K	*Anodonta*	528449	3878975	-4	19630	19490	70	12/16/2003	23160	23725	23510	529.0
SD05CL-1381C	WW5519	J	*Anodonta*	528544	3877718	-4	19640	19500	60	12/20/2005	23200	23730	23510	534.4
SDCL06-1757	WW5712	J	*Anodonta*	528541	3877714	-4	22450	22310	170	7/19/2006	26135	27075	26520	533.5
M16SM-3207	Beta453799	M	*Anodonta*	527275	3877954	-5.90	25650	25510	100	12/29/2016	29275	30015	29580	529.0

• WW samples were processed at the ^{14}C laboratory of the U. S. Geological Survey in Reston, Virginia; Beta samples processed by Beta Analytic.

• WW sample ^{14}C ages were determined at the Center for Accelerator Mass Spectrometry (CAMS), Lawrence Livermore National Laboratory, Livermore, California. [* processed at NSF-Arizona Accelerator Mass Spectrometry facility in Tucson, Arizona]

• The quoted age is in radiocarbon years (BP) using the Libby half life of 5568 years, and is given in years before 1950 by convention.

• Values reported for $\delta^{13}C$, when given without decimal places, are the assumed values according to Stuiver and Polach (1977) and adjusted by methods described in text. Values with two decimal places were measured on the material dated.

† UTM data for zone 11, NAD 83

Table 8. Camp Cady paleofauna taxonomic list (extracted from Table 2 in Jefferson 2003).

Order	Taxonomic identification	Common name
Crustacea		
	Limnocythere bradburyi	ostracode, water flea
	L. ceriotuberosa	ostracode, water flea
	L. platyforma	ostracode, water flea
	L. robusta	ostracode, water flea
	Heterocypris sp.	ostracode, water flea
Pelecypoda		
	Anodonta californiensis	freshwater clam
	Pisidium compressum	freshwater clam
Gastropoda		
	Valvata humeralis	freshwater snail
	Fossaria modicella	freshwater snail
	Planorbella ammon	freshwater snail
	P. subcrenata	freshwater snail
	Planorbella sp. ? *P. tenuis*	freshwater snail
	Carinifex newberryi	freshwater snail
	Gyraulus vermicularis	freshwater snail
	Gyraulus sp.	freshwater snail
	Vorticifex effusa	freshwater snail
Osteichthyes		
	Gila bicolor mojavensis	tui (Mojave) chub
	Gasterosteus aculeatus	threespine stickleback
Reptilia		
	Clemmys marmorata	western pond turtle
Aves		
	Gavia sp. cf. *G. arctica*	Arctic loon
	Podiceps sp. cf. *P. nigricollis*	eared grebe
	Aechmophorus occidentalis	western grebe
	Pelecanus sp. aff. *P. erythrorhynchos*	American white pelican
	Phalacrocorax auritus	double-crested cormorant
	Phalacrocorax macropus	large-footed cormorant †
	Ciconia maltha	stork †
	Phoenicopterus minutus	small flamingo †
	Phoenicopterus copei	Cope's flamingo †
	Cygnus sp. cf. *C. columbianus*	tundra swan
	Branta Canadensis	Canada goose
Aves (cont.)		
	Anas sp. cf. A. crecca	green-winged teal
	Anas sp. cf. *A. platyrhynchos*	mallard
	Aythya sp.	greater scaup or canvasback
	Mergus sp. cf. *M. merganser*	common merganser
	Oxyura jamaicensis	ruddy duck
	Haliaeetus leucophalus	bald eagle
	Aquila chrysaetos	golden eagle
	Fulica americana cf. *F. a. minor*	small American coot †
	Grus sp.	crane
	cf. *Actitis* sp.	sandpiper
	Phalaropodinae	phalarope subfamily
	Larus sp. cf. *L. oregonus*	Oregon gull †
	Larus sp.	gull (large-size)
	Bubo virginianus	great horned owl
MammaIia		
	Megalonyx sp.	ground sloth (medium-size) †
	Nothrotheriops sp. cf. *N. shastensis*	Shasta ground sloth (small-size) †
	Paramylodon sp.	ground sloth (large-size) †
	Mammuthus sp.	mammoth †
	Lepus sp.	jack rabbit
	Cricetidae	mice
	Canis sp. cf. *C. dirus*	dire wolf †
	C. latrans	coyote
	Arctodus sp.	short-faced bear †
	cf. *Ursus* sp.	black bear
	Felis (*Puma*) sp.	mountain lion
	Homotherium sp. cf. *H. crenatidens*	scimitar-tooth cat, robust †
	Homotherium sp. cf. *H. serum*	scimitar-tooth cat, gracile †
	Equus conversidens	horse (small-size) †
	Equus sp.	horse (large-size) †
	Camelops sp. cf. *C. hesternus*	yesterday's camel †
	Camelops sp. aff. *C. minidokae*	Minidoka camel †
	Hemiauchenia macrocephala	llama †
	Antilocapridae	prong bucks
	Ovis canadensis	mountain sheep
	Bison sp. cf. *B. antiquus*	antique bison †

Note: Data are in part from Jefferson (1985a, 1987). † extinct taxon

Table 9. Relative abundance of avian taxa from Lake Manix paleofauna (extracted from Table 3 in Jefferson 2003).

Taxon	NISP	%NISP
Gavia sp. cf. *G. arctica*	1	0.7
Podiceps sp. cf. *P. nigricollis*	4	2.8
Aechmophorus occidentalis	41	29.5
Pelecanus sp. aff. *P. erythrorhynchos*	12	8.6
Phalacrocorax auritus	15	10.8
Phalacrocorax macropus _	2	1.4
Ciconia maltha _	6	4.3
Phoenicopterus minutus _	14	10.1
Phoenicopterus copei _	4	2.8
Cygnus sp. cf. *C. columbianus*	3	2.1
Branta canadensis	11	7.9
Anas sp. cf. *A. crecca*	1	0.7
Anas sp. cf. *A. platyrhynchos*	2	1.4
Aythya sp.	4	2.8
Mergus sp. cf. *M. merganser*	2	1.4
Oxyura jamaicensis	3	2.1
Haliaeetus leucocephalus	2	1.4
Aquila chrysaetos	2	1.4
Fulica americana cf. *F. a. minor*	1	0.7
Grus sp.	1	0.7
cf. *Actitis* sp.	1	0.7
Phalaropodinae	1	0.7
Larus sp. cf. *L. oregonus* _	3	2.1
Larus sp.	2	1.4
Bubo virginianus	1	0.7

Note: Total number of identified specimens is 139, and total % NISP is 99.5. Data are in part from Jefferson (1985b, 1987).
NISP = number of identified specimens
% NISP = number of specimens identified for each taxon divided by the total number of specimens
_ = extinct taxon

Table 10. Relative abundance of mammalian taxa from the Manix Formation (extracted from Table 4 in Jefferson 2003).

Taxon	NISP	%NISP
Megalonyx sp. _	1	0.1
Nothrotheriops sp. cf. *N. shastensis* _	2	0.3
Paramylodon sp. _	1	0.1
Mammuthus sp. _	37	5.2
Lepus sp.	11	1.6
Cricetidae	1	0.1
Canis sp. cf. *C. dirus* _	5	0.7
Canis latrans	5	0.7
Arctodus sp. _	1	0.1
cf. *Ursus* sp.	1	0.1
Felis (*Puma*) sp.	3	0.4
Homotherium sp. cf. *H. crenatidens* _	1	0.1
Homotherium sp. cf. *H. serum* _	2	0.3
Equus conversidens _	52*	7.4
Equus sp. (large-size) _	67*	9.5
Camelops sp. cf. *C. hesternus* _	371	54.7
Camelops sp. aff. *C. minidokae*	5	0.7
Hemiauchenia macrocephala _	117	16.6
Antilocapara sp.	2	0.3
Ovis canadensis	17	2.5
Bison sp. cf. *B. antiquus* _	1	0.1

Note: Total number of identified specimens is 703, and total % NISP is 101.5. Data are in part from Jefferson (1985a, 1987).
NISP = number of identified specimens
% NISP = number of specimens identified for each taxon divided by the total number of identified specimens
* = may represent more than one species

Combined Lake Manix bibliography

Awramik, S.M., Bucheim, H.P., Leggitt, L., and Woo, K.S., 2000, Oncoids of the late Pleistocene Manix Formation, Mojave Desert region, California. *in* Reynolds, R.E., and Reynolds, J., eds., Empty Basins, Vanished Lakes: San Bernardino County Museum Association Quarterly 47(2):25–31.

Bacon, C.R., and Duffield, W.A., 1981, Late Cenozoic rhyolites from the Kern Plateau, southern Sierra Nevada, California. American Journal of Science 281:1–34.

Bassett, A.M., and Jefferson, G.T., 1971, Radiocarbon dates of Manix Lake, central Mojave Desert, California. Geological Society of America Abstracts to Meetings 3(2):79.

Bassett, A.M., and Kupfer, D.H., 1964, A geologic reconnaissance in the southeastern Mojave Desert. California Division of Mines and Geology Special Report 83:1-43.

Beyers, F.M., Jr., 1960, Geology of the Alvord Mountain quadrangle, San Bernardino County, California. U.S. Geological Survey Bulletin 1089-A:1-71.

Binning, J.D., Brown, R.S., Meek, N., and Weil, E.B., 1985, Intermountain Power Project (IPP): The Cultural Resources Studies of the Ground Electrode Facility at Coyote Lake, San Bernardino County, California: Westminster, California, Prepared for City of Los Angeles, Department of Water and Power by Applied Conservation Technology, Inc. 188 p.

Blackwelder, E., 1954, Pleistocene lakes and drainage in the Mojave region, southern California. *in* Jahns, R.H., ed., Geology of Southern California: California Division of Mines and Geology, Bulletin 170:35–40.

Blackwelder, E., and Ellsworth, E.W., 1936, Pleistocene lakes of the Afton basin, California. American Journal of Science 5th Series 31:453–463.

Blanc, R.P., and Cleveland, G.B., 1961a, Pleistocene lakes of southeastern California, Part I. California Division of Mines and Geology, Mineral Information Service 14(4):1–8.

Blanc, R.P., and Cleveland, G.B., 1961b, Pleistocene lakes of southeastern California, Part II. California Division of Mines and Geology, Mineral Information Service 14(5):72–82.

Brown, W.J., and Rosen, R.M., 1995, Was there a Pliocene-Pleistocene fluvial lacustrine connection between Death Valley and the Colorado River? Quaternary Research 43:286–296.

Brown, W.J., Wells, S.G., Enzel, Y., Anderson, R.Y., and McFadden, L.D., 1990, The late Quaternary history of pluvial Lake Mojave: Silver Lake and Soda Lake basins, California. *in* Reynolds, R.E., S.G. Wells, and R.H. Brady III, eds., At the End of the Mojave: Quaternary studies in the eastern Mojave Desert, Redlands, California, Special Publication of the San Bernardino County Museum Association, 1990 Mojave Desert Quaternary Research Center Symposium pp. 55–72.

Budinger, F.E., Jr., 1992, Targeting early man sites in the western United States: an assessment of the Manix type section, central Mojave Desert, California. Master of Arts Thesis, Special Major, California State University, San Bernardino 229 p.

Buwalda, J.P., 1914, Pleistocene beds at Manix in the eastern Mojave Desert region. Bulletin Department of Geology, Berkeley, University of California 7(24):443–464.

Chidester, D.H., 1965, A short history of Camp Cady. Senior Thesis, Department of History, La Verne College, La Vern, California 28p.

Cox, B.F., and Tinsley, J.C., III, 1999, Origin of the late Pliocene and Pleistocene Mojave River between Cajon Pass and Barstow, California. *in* Reynolds, R.E., and Reynolds, J., eds., Tracks Along the Mojave: San Bernardino County Museum Association Quarterly 46(3):49–54.

Cox, B.F., Hillhouse, J.W., and Owen, L.A., 2003, Pliocene and Pleistocene evolution of the Mojave River, and associated tectonic development of the Transverse Ranges and Mojave Desert, based on borehole stratigraphy studies and mapping of landforms and sediments near Victorville, California, *in* Enzel, Y., Wells, S.G., and Lancaster, N., eds., Paleoenvironments and Paleohydrology of the Mojave and Southern Great Basin Deserts: Geological Society of America Special Paper 368:1–42, https://doi.org/10.1130/0-8137-2368-X.1.

Cyr, A.J., Miller, D.M., and Mahan, S.A., 2015, Paleodischarge of the Mojave River, southwestern United States, investigated with single-pebble measurements of 10Be: Geosphere 11(4):1158–1171, https://doi.org/10.1130/GES01134.1.

Dockter, R.D., 1980, Geophysical and Lithologic Data from Test Well CO-2, Coyote Dry Lake, San Bernardino County, California: U.S. Geological Survey Open-File Report 80-873, 1 plate.

Downs, T., Howard, H., Clements, T., and Smith, G.I., 1959, Quaternary animals from Schuiling Cave in the Mojave Desert, California. Los Angeles County Museum of Natural History, Contributions in Science 29:21.

Dudash, S.L. 2006, Preliminary surficial geologic map of a Calico Mountains piedmont and part of Coyote Lake, Mojave Desert, San Bernardino County, California: U.S. Geological Survey Open-File Report 2006–1090, 44 p., scale 1:24,000.

Ellsworth, E.W., 1933, Physiographic history of the Afton Basin of the Mojave Desert. Des Moines, Iowa, Pan-American Geologist, May 1933 59(4):308–309.

Enzel, Y., Wells, S.G., and Lancaster, N., 2003, Late Pleistocene lakes along the Mojave River, southeast California, *in* Enzel, Y., Wells, S.G., and Lancaster, N., eds., Paleoenvironments and Paleohydrology of the Mojave and Southern Great Basin Deserts: Geological Society of America Special Paper 368, p. 61–77, https://doi.org/10.1130/0-8137-2368-X.61.

Fergusson, G.J., and Libby, W.F., 1962, UCLA radiocarbon dates, I: Radiocarbon 4:109–114.

Garcia, A.L., Knott, J.R., Bright, J., and Mahan, S.A., 2014, Geochronology and paleoenvironment of pluvial Harper Lake, Mojave Desert, California: Quaternary Research 81:305–317, https://doi.org/10.1016/j.yqres.2013.10.008.

Groat, C.G., 1967, Geology and hydrology of the Troy Playa area, San Bernardino County, California. Master of Science Thesis, University of Rochester, New York 133 p.

Hagar, D.J., 1966, Geomorphology of Coyote Valley, San Bernardino County, California. Doctoral Dissertation, Department Geology, University of Massachusetts Amherst 210 p.

Hale, G.R., 1985, Mid-Pleistocene overflow of Death Valley toward the Colorado River, *in* Hale, G.R., ed., Quaternary Lakes of the Eastern Mojave Desert, California. Friends of the Pleistocene Pacific Cell Annual Field Trip Guidebook pp. 36–81.

Hamilton, P., 1976, A Geophysical Study of the Manix Fault; its Tectonic Relationship to the Western Mohave Desert, San Bernardino County, California, Master of Science. Thesis, Los Angeles, California, California State University 101 p.

Hastorf, C.A., and Tinsley, J.C., 1981, Maps and index of radiocarbon-dated samples from southern California. U.S. Geological Survey Miscellaneous Field Studies Map MF-1294, scale 1:500,000.

Hooke, R.L., 1999, Lake Manly(?) shorelines in the eastern Mojave Desert, California. Quaternary Research 52:328–336.

Howard, H.H., 1955, Fossil birds from Manix Lake, California. U.S. Geological Survey Professional Paper 264-J:199–205.

Hubbs, C.L., Bein, G.S., and Suess, H.E., 1962, La Jolla natural radiocarbon measurements, II: Radiocarbon 4:204–238.

Hubbs, C.L., Bein, G.S., and Suess, H.E., 1965, La Jolla natural radiocarbon measurements, IV. Radiocarbon 7:66–117.

Izett, G.A., 1981, Volcanic ash beds: Recorders of upper Cenozoic silic pyroclastic volcanism in the western United States. Journal of Geophysical Research 68(B11):10,200–10,222.

Jefferson, G.T., 1968, The Camp Cady local fauna from Pleistocene Lake Manix, California. Master of Arts Thesis, Department of Geology, Riverside, University of California 106 p.

Jefferson, G.T., 1983, A fragment of human skull from Schuiling Cave, Mojave Desert, California. Southern California Academy of Sciences Bulletin 82(2):98–102.

Jefferson, G.T., 1985a, Stratigraphy and geologic history of the Pleistocene Lake Manix Formation, central Mojave Desert, California. *in* Reynolds, R.E., ed., Cajon Pass to Manix Lake: Geological Investigations Along Interstate 15, Redlands, California, San Bernardino County Museum Association Special Publication pp. 157–169.

Jefferson, G.T., 1985b, Review of the late Pleistocene avifauna from Lake Manix, central Mojave Desert, California: Natural History Museum Los Angeles County Contribution in Science 362:1-13.

Jefferson, G.T., 1986, Fossil vertebrates from late Pleistocene sedimentary deposits in the San Bernardino and Little San Bernardino Mountains region. *in* Kooser, M., and Reynolds, R.E., eds., Geology Around the Margins of the Eastern San Bernardino Mountains: Redlands, California, Publications of the Inland Geological Society 1:77–80.

Jefferson, G.T., 1987, The Camp Cady local fauna: paleoenvironment of the Lake Manix Basin. San Bernardino County Museum Association Quarterly 34(3-4):3–35.

Jefferson, G.T., 1988, Late Pleistocene large mammalian herbivores: Implications for big game hunters in southern California. Southern California Academy of Sciences Bulletin 87(3):89–103.

Jefferson, G.T., 1989, Late Pleistocene and earliest Holocene fossil localities and vertebrate taxa from the western Mojave Desert. *in* Reynolds, R.E., ed., The west-central Mojave Desert. Quaternary Studies Between Kramer and Afton Canyon: Redlands, California, Mojave Desert Quaternary Research Center, San Bernardino County Museum Association Special Publication pp. 27–40.

Jefferson, G.T., 1990, Rancholabrean Age vertebrates from the eastern Mojave Desert, California. *in* Reynolds, R.E., Wells, S.G., and Bandy III, R.H., eds., At the End of the Mojave: Quaternary studies in the Eastern Mojave Desert, Special Publication of the San Bernardino County Museum Association, 1990 Mojave Desert Quaternary Research Center Symposium pp. 109–115.

Jefferson, G.T., 1991a, The Camp Cady local fauna: Stratigraphy and paleontology of the Lake Manix basin. *in* Reynolds, R.E., Woodburne, M.O., and Whistler, P. eds., Inland Southern California, The last 70 million years, San Bernardino County Museum Association Quarterly 38(3,4):93–99.

Jefferson, G.T., 1991b, Rancholabrean Age vertebrates from the southeastern Mojave Desert, California. *in* Reynolds, R.E., ed., Crossing the Borders: Quaternary Studies in Eastern California and Southwestern Nevada. Redlands, California, Mojave Desert Quaternary Research Center, San Bernardino County Museum Association Special Publication pp. 27–40.

Jefferson, G.T., 1991c, A catalog of late Quaternary vertebrates from California: Part two, mammals. Natural History Museum of Los Angeles County Technical Reports 7:129 .

Jefferson, G.T., 1994, Stratigraphy and Pliocene-Pleistocene history of the Lake Manix basin. *in* McGill, S.F., and Ross, T.M., eds., Geological Investigations of an Active Margin: Geological Society of America Guidebook, 27th Annual Meeting, San Bernardino, California pp. 175–177.

Jefferson, G.T., 1999, Age and stratigraphy of Lake Manix basin. *in* Reynolds, R.E., and Reynolds, J., eds., Tracks Along the Mojave: San Bernardino County Museum Association Quarterly 46(3):109–112.

Jefferson, G.T., 2003, Stratigraphy and paleontology of the middle to late Pleistocene Manix Formation, and paleoenvironments of the central Mojave River, southern California. *in* Enzel, Y., Wells, S.G., and Lancaster, N., eds., Paleoenvironments and paleohydrology of the Mojave and Southern Great Basin Deserts: Boulder, Colorado, Geological Society of America Special Paper 368:43-60.

Jefferson, G.T., and Steinmetz, J.J., 1986, Ostracode biostratigraphy and paleoecology of the late Pleistocene Manix Formation. Current Research in the Pleistocene 3:55–56.

Keaton, J.R., and Keaton, R.T., 1977, Manix fault zone, San Bernardino County, California. California Division Mines and Geology, California Geology 30(8):177–186.

Kenny, M.D., and Weldon, R.J., 1999, Timing and magnitude of mid to late Quaternary uplift of the western San Bernardino and northeastern San Gabriel Mountains, southern California. *in* Reynolds, R.E., and Reynolds, J., eds., Tracks Along the Mojave, San Bernardino County Museum Association Quarterly 46(3):33–46.

Kirby, M.E., Heusser, L., Scholz, C., Ramezan, R., Anderson, M.A., Markle, B., Rhodes, E., Glover, K.C., Fantozzi, J., Hiner, C., Price, B., and Rangel, H., 2018, A late Wisconsin (32–10k cal a BP) history of pluvials, droughts, and vegetation in the Pacific Southwest United States (Lake Elsinore, CA), Journal of Quaternary Science 33:238–254, https://doi.org/10.1002/jqs.3018.

Mahan, S.A., Miller, D.M., Menges, C.M., and Yount, J.C., 2007, Late Quaternary stratigraphy and luminescence geochronology of the northeastern Mojave Desert: Quaternary International 166:61–78, https://doi.org/10.1016/j.quaint.2006.12.010.

Martinson, D.G., Pisias, N.P., Hays, J.D., Imbrie, J., Moore, T.C., Jr., and Shackelton, J.N., 1987, Age dating and the orbital theory of the ice ages: Development of a high-resolution 0–300,000-year chronology. Quaternary Research 27:1–29.

McCulloh, T.H., 1965, Geologic Map of the Nebo and Yermo Quadrangles, San Bernardino County, California: U.S. Geological Survey Open-File Report 65-107, scale 1:24,000.

McDonald, H.G., Jefferson, G.T., and Force, C., 1996, Pleistocene distribution of the ground sloth *Nothrotheriops shastensis* (Xenarthra, Megalonychidae). *in* Reynolds, R.E., and Reynolds, J., eds., The 1996 Desert Symposium, Abstracts of Papers Submitted to the Meetings, San Bernardino County Museum Association Quarterly 43(2):151–152.

McGill, S.F., Murray, B.C., Maher, K.A., Lieske, J.H., Jr., and Rowan, L.R., 1988, Quaternary history of the Manix fault, Lake Manix basin, Mojave Desert, California. San Bernardino County Museum Association Quarterly 35(3, 4):3–20.

Meek, N., 1989, Geomorphic and hydrologic implications of the rapid incision of Afton Canyon, Mojave Desert, California. Geology 17:7–10.

Meek, N., 1990, Late Quaternary Geochronology and geomorphology of the Manix basin, San Bernardino County, California. Doctoral Dissertation, Department of Geography, University of California, Los Angeles 212 p.

Meek, N., 1994, The stratigraphy and geomorphology of Coyote basin, central Mojave Desert, California. San Bernardino County Museum Quarterly 41(3):5–13.

Meek, N., 1999, New discoveries about the late Wisconsin history of the Mojave River system. *in* Reynolds, R.E., and

Reynolds, J., eds., Tracks Along the Mojave: San Bernardino County Museum Association Quarterly 46(3):113–118.

Meek, N., 2000, The late Wisconsin history of the Afton Canyon area. *in* Reynolds, R.E., and Reynolds, J., eds., Empty basins, vanished lakes: San Bernardino County Museum Association Quarterly 47(2):33–34.

Meek, N., 2004, Mojave River history from an upstream perspective. *in* Reynolds, R. E., ed., Breaking Up, 2004 Desert Symposium Field Trip and Abstracts. Fullerton, California, California State University, Desert Studies Consortium pp. 41-49.

Meek, N., and Battles, D.A., 1991, Displacement along the Manix fault. California Division Mines and Geology, California Geology 44(2):33–38.

Meek, N., and Douglass, J., 2001, Lake overflow: An alternative hypothesis for Grand Canyon incision and development of the Colorado River, *in* Young, R.A., and Spamer, E.E., eds., Colorado River, Origin and Evolution: Grand Canyon Association Monograph 12:199–204.

Meisling, K.E., and Weldon, R.J., 1989, Late Cenozoic tectonics of the northwestern San Bernardino Mountains, southern California. Geological Society of America Bulletin 101:106–128.

Merriam, J.C., 1915, Extinct faunas of the Mojave Desert, their significance in a study of the origin and evolution of life in America. Popular Science Monthly, March 1915 pp. 245–264.

Miller, D.M., Dudash, S.L., Green, H.L., Lidke, D.J., Amoroso, L., Phelps, G.A., and Schmidt, K.M., 2007, A new Quaternary view of northern Mojave Desert tectonics suggests changing fault patterns during the late Pleistocene, *in* Miller, D.M.,, and Valin, Z.C., eds., Geomorphology and Tectonics at the Intersection of Silurian and Death Valleys, Southern California: U.S. Geological Survey Open-File Report 2007-1424:157–171.

Miller, D. M., Dudash, S.L., and McGeehin, J.P., 2009, Chronology of pluvial Lake Coyote, California, and implications for 25 to 10-ka Mojave River paleohydrology. PACLIM 2009 Abstracts.

Miller, D.M., Dudash, S.L., and McGeehin, J.P., 2018, Paleoclimate record for Lake Coyote, California, and the Last Glacial Maximum and deglacial paleohydrology (25 to 14 cal ka) of the Mojave River, in Starratt, S.W., and Rosen, M.R., eds., From Saline to Freshwater: The Diversity of Western Lakes in Space and Time: Geological Society of America Special Paper 536, p. 1–20, https://doi.org/10.1130/2018.2536(12).

Miller, D. M., Reheis, M. C., Wan, E., Wahl, D. B., and Olson, H., 2011, Pliocene and early Pleistocene paleogeography of the Coyote Lake and Alvord Mountain area, Mojave Desert, California. *in* Reynolds, R. E., ed., The Incredible Shrinking Pliocene, California State University, Desert Studies Symposium, April 2011 pp. 53-67.

Miller, D.M., Schmidt, K.M., Mahan, S.A., McGeehin, J.P., Owen, L.A., Barron, J.A., Lehmkuhl, F., and Lohrer, R., 2010, Holocene landscape response to seasonality of storms in the Mojave Desert: Quaternary International 215:45–61, https://doi.org/10.1016/j.quaint.2009.10.001

Miller, D. M., and Yount, J. L., 2002, Late Cenozoic tectonic evolution of the north-central Mojave Desert inferred from fault history and physiographic evolution of the Fort Irwin area, California. Geological Society of America Memoir 195:173-197.

Miller, R.R., 1948, The cyprinodont fishes of the Death Valley system of eastern California and southwestern Nevada: Miscellaneous Publications of the Museum of Zoology, University of Michigan 68:1-155.

Morley, J.J., and Hayes, J.D., 1981, Toward a high-resolution, global deep-sea chronology for the last 750,000 yr. Earth and Planetary Science Letters 53:279–295.

Murray, B.C., and Nagy, E.A., 1990, The relationship of the Manix Formation to the "Mojave River Formation". Mojave Desert Quaternary Research Center Symposium, San Bernardino County Museum Association Quarterly 37(2):1-32.

Nagy, E.A., and Murray, B.C., 1991, Stratigraphy and intrabasin correlation of the Mojave River Formation, central Mojave Desert, California. San Bernardino County Museum Association Quarterly 38(2):5–30.

Nagy, E. A., and Murray, B., 1996, Plio-Pleistocene deposits adjacent to the Manix fault: implications for the history of the Mojave River and transverse Ranges uplift. Sedimentary Geology 103(1-2):9-21.

Owen, L.A., Bright, J., Finkel, R.C., Jaiswal, M.K., Kaufman, D.S., Mahan, S., Radtke, U., Schneider, J.S., Sharp, W., Singhvi, A.K., and Warren, C.N., 2007, Numerical dating of a late Quaternary spit-shoreline complex at the northern end of Silver Lake playa, Mojave Desert, California: A comparison of the applicability of radiocarbon, luminescence, terrestrial cosmogenic nuclide, electron spin resonance, U-series and amino acid racemization methods: Quaternary International 166:87–110, https://doi.org/10.1016/j.quaint.2007.01.001.

Pluhar, C.J., Kirschvink, J.L., and Adams, R.W., 1991, Magnetostratigraphy and clockwise rotation of the Pliocene-Pleistocene Mojave River Formation, central Mojave Desert, California. San Bernardino County Museum Association Quarterly 38(2):31–42.

Reheis, M.C., Adams, K.D., Oviatt, C.G., and Bacon, S.N., 2014, Pluvial lakes in the Great Basin of the western United States—A View from the Outcrop: Quaternary Science Reviews 97:1-25.

Reheis, M. C., Bright, J., Lund, S. P., Miller, D. M., Skipp, G., and Fleck, R. J., 2012, A half-million-year record of paleoclimate from the Lake Manix core, Mojave Desert, California. Palaeogeography, Palaeoclimatology, Palaeoecology 365-366:11-37.

Reheis, M. C., and Miller, D. M., 2010, Environments of nearshore lacustrine deposition in the Pleistocene Lake Manix basin, south-central California. in Reynolds, R. E., and Miller, D. M., eds., Overboard in the Mojave,l 20 Million Years of Lakes and Wetlands: Abstracts of Proceedings, 2010 Desert Symposium, Zzyzx, California pp. 24-37.

Reheis, M. C., Miller, D. M., and Redwine, J. L., 2007, Quaternary stratigraphy, drainage-basin development, and geomorphology of the Lake Manix basin, Mojave Desert. U.S. Geological Survey Open-File Report 2007-1281:1-31.

Reheis, M. C., and Redwine, J. L., 2008, Lake Manix shorelines and Afton Canyon terraces: Implications for incision of Afton Canyon. in Reheis, M.C., Hershler, R., and Miller, D. M., eds., Late Cenozoic Drainage History of the Southwestern Great Basin and Lower Colorado River Region: Geologic and biotic perspectives, Geological Society of America Special Paper 439:227-260.

Reheis, M. C., Redwine, J. R., Wan, E., McGeehin, J. P., and VanSistine, D. P., 2014, Surficial geology and stratigraphy of Pleistocene Lake Manix, San Bernardino County, California. U.S. Geological Survey, Scientific Investigations Map 3312, scale 1:15,000.

Reheis, M.C., D. Miller, J.P. McGeehin, J.R. Redwine, C.G. Oviatt, and J. Bright, 2015, Directly dated MIS3 lake-level record from Lake Manix, Mojave Desert, California, USA. Quaternary Research 83:187-203.

Reimer, P.J., Bard, E., Bayliss, A., Beck, J.W., Blackwell, P.G., Ramsey, C.B., Buck, C.E., Cheng, H., Edwards, R.L., Friedrich, M., Grootes, P.M., Guilderson, T.P., Hafl idason, H., Hajdas, I., Hatter, C., Heaton, T.J., Hoffmann, D.L., Hogg, A.G., Hughen, K.A., Kaiser, K.F., Kromer, B., Manning, S.W., Niu, M., Reimer, R.W., Richards, D.A., Scott, E.M., Southon, J.R., Staff, R.A., Turney, C.S.M., and van der Plicht, J., 2013, INTCAL13 and MARINE13 radiocarbon age calibration curves, 0–50,000 years cal BP: Radiocarbon 55:1869–1887, https://doi.org/10.2458/azu_js_rc.55.16947.

Reynolds, R.E., and G.T. Jefferson, 2010, A brief comparison of central Mojave Desert lakes: Miocene Barstow Formation and Pleistocene Lake Manix. in by Reynolds, R.E., and Miller, D., eds., Overboard in the Mojave 20 Million Years of Lakes and Wetlands, The 2010 Desert Symposium, , Desert Studies Consortium California State University, Fullerton pp. 66-69.

Reynolds, R.E., and Reynolds, R.L., 1985, Late Pleistocene faunas from Daggett and Yermo, San Bernardino County, California. *in* Reynolds, R.E., ed., Cajon Pass to Manix Lake: Geological investigations Along Interstate 15, San Bernardino County Museum Association Special Publication pp. 175–191.

Roeder, M.A., 1985, Late Wisconsin records of *Gasterosteus aculeatus* (Threespine Stickle-back) and *Gila bicolor mojavensis* (Mojave Tui Chub) from unnamed Mojave River sediments near Daggett, San Bernardino County, California. *in* Reynolds, R.E., ed., Cajon Pass to Manix Lake: Geological investigations along Interstate 15, San Bernardino County Museum Special Publication pp. 171–174.

Rosen, M.R., 1989, Sedimentological, geochemical and hydrological evolution of an intercontinental closed-basin playa (Bristol Dry Lake): a model for playa development and its implications for paleoclimate. Doctoral Dissertation, University of Texas 266 p.

Scott, E., 1996, The small horse from Valley Wells, San Bernardino County, California. *in* Reynolds, R.E., and Reynolds, J., eds., Punctuated Chaos in the Northeastern Mojave Desert, San Bernardino County Museum Association Quarterly 43(1, 2):85–89.

Scott, E., 1997, A review of *Equus conversidens* in southern California, with a report on a second, previously unrecognized species of Pleistocene small horse from the Mojave Desert. Journal of Vertebrate Paleontology 17(3):75A.

Scott, E., 1998, *Equus scotti* from southern California. Journal of Vertebrate Paleontology, Abstracts of Papers 18(3):76A.

Scott, E., 1999, The *Equus* (*Plesippus*)–*Equus scotti* transition in western North America. Journal of Vertebrate Paleontology, Abstracts of Papers 19(3):74A.

Scott, E., 2000, Fossil horses at Fort Irwin, the paleontology of Bitter Springs Playa. Environmental Division of the Directorate of Public Works, Fort Irwin, California, Natural and Cultural Resources Series 2:1-15.

Sarna-Wojcicki, A.M., Bowman, H.R., Meyer, C.E., Russell, P.C., Asaro, F., Michael, H., Rowe, J.J., Jr., Baedecker, P.A., and McCoy, G., 1980, Chemical analyses, correlations, and ages of late Cenozoic tephra units of east-central and southern California. U.S. Geological Survey Open-File Report 80-231:1-52.

Sarna-Wojcicki, A.M., Bowman, H.R., Meyer, C.E., Russell, P.C., Woodard, M.J., McCoy, G., Rowe, J.J., Jr., Baedecker, P.A., Asaro, F., and Michael, H., 1984, Chemical analyses, correlations, and ages of upper Pliocene and Pleistocene ash layers of east-central and southern California. U.S. Geological Survey Professional Paper 1293:1-40.

Seiple, E., 1994, Lake Manix. California Division Mines and Geology, California Geology, March/April 47(2)50–57.

Snyder, C.T., Hardman, G., and Zdenek, F.Z., 1964, Pleistocene lakes in the Great Basin: U.S. Geological Survey Miscellaneous Geological Investigations Map I-416 scale 1:1,000,000.

Spaulding, W.G., 1990, Vegetational and climate development of the Mojave Desert: the last glacial maximum to the present. *in* Betancourt, J.L., T.R. Van Devender, and P.S. Martin, eds., Packrat Middens: The Last 40,000 Years of Biotic Change, University of Arizona Press, Tucson, Arizona pp. 166–199.

Spaulding, W.G., Leopold, E.B., and Van Devender, T.R., 1984, Late Wisconsin paleoecology of the American southwest. *in* Spaulding, C.P., ed., Late-Quaternary Environments of the United States, Volume 1: The late Pleistocene, University of Minnesota Press, Minneapolis pp. 259–293.

Steinmetz, J.J., 1987, Ostracodes from the late Pleistocene Manix Formation, San Bernardino County, California. *in* Reynolds, J., ed., Quaternary History of the Mojave Desert, San Bernardino County Museum Association Quarterly 34(3-4):46–47.

Steinmetz, J.J., 1988, Biostratigraphy and paleoecology of limnic ostracodes from the late Pleistocene Manix Formation. Masters Thesis, Department of Biological Sciences, California State Polytechnic University, Pomona 64 p.

Stuiver, M., 1969, Yale natural radiocarbon measurements, IX. Radiocarbon 11(2):545–658.

Stuiver, M., and Polach, H.A., 1977, Discussion: Reporting of 14C data: Radiocarbon 19:355–363, https://doi.org/10.1017/S0033822200003672.

Thompson, D.G., 1929, The Mojave Desert Region, California; Geographic, Geologic, Hydrographic Reconnaissance: U.S. Geological Survey Water Supply Paper 578, 759 p.

Taylor, D.W., 1967, Late Pleistocene molluscan shells from the Tule Springs area. *in* Wormington, H.M., and Ellis, D., Pleistocene Studies in Southern Nevada, Nevada State Museum Anthropological Papers 13:395–399.

Weldon, R.J., II, 1982, Pleistocene drainage and displaced shorelines around Manix Lake. *in* Cooper, J.D., ed., Geologic Excursions in the California Desert: Geological Society of America, Cordilleran Section Guidebook pp. 77–81.

Weldon, R.J., II, 1985, Implications of the age and distribution of late Cenozoic stratigraphy in Cajon Pass, southern California. *in* Reynolds, R.E., ed., Cajon Pass to Manix Lake: Geological Investigations Along Interstate 15, Redlands, California, San Bernardino County Museum Association Special Publication pp.59–68.

Wells, S.G., and Enzel, Y., 1994, Fluvial geomorphology of the Mojave River in the Afton Canyon area, eastern California—implications for the geomorphic evolution of Afton Canyon. *in* McGill, S.F., and Ross, T.M., eds., Geological Investigations of an Active Margin: Geological Society of America, Cordilleran Section Guidebook pp. 177–182.

Wells, S.G., Brown, W.J., Enzel, Y., Anderson, R.Y., and McFadden, L.D., 2003, Late Quaternary geology and paleohydrology of pluvial Lake Mojave, southern California, *in* Enzel, Y., Wells, S.G., and Lancaster, N., eds., Paleoenvironments and Paleohydrology of the Mojave and Southern Great Basin Deserts: Geological Society of America Special Paper 368:79–114, https://doi.org/10.1130/0-8137-2368-X.79.

Wells, S.G., Anderson, R.Y., McFadden, L.D., Brown, W.J., Enzel, Y., and Miossec, J., 1989, Late Quaternary paleohydrology of the eastern Mojave River drainage, southern California: quantitative assessment of the late Quaternary hydrologic cycle in large arid watersheds. New Mexico Water Resources Research Institute, Technical Completion Report, Project 14–08–0001-G1312, no.242, 253 p.

Winters, H.H., 1954, The Pleistocene fauna of the Manix Beds in the Mojave Desert, California. Masters Thesis, Department of Geology, California Institute of Technology, Pasadena, California 58p.

Review of the Barstow Formation and the Barstovian North American Land Mammal Age

Michael O. Woodburne
Department of Geological Sciences, University of California, Riverside, CA 92527, mikew@npgcable.com

ABSTRACT—A review of the Barstow Formation and its designation as the basis for the Barstovian North American Land Mammal Age (NALMA) focuses on the stratigraphic coherence of the formation, the lack of important hiatuses, its isotopic ages, magnetostratigraphic framework, and small and large mammal biochronology. This recognizes the revision of the original Barstovian NALMA to include an early Barstovian interval, its coherence with underlying strata of late Hemingfordian age, and a late Barstovian interval that equates with the original Barstovian designation. Under current chronology, the Barstovian NALMA is of middle Miocene age.

Introduction

To paraphrase from Galusha et al (1966) and Schweich (2010), fossil mammals from beds now known as the Barstow Formation were first discovered by a placer miner, H.S. Mourning sometime prior to 1911. Berkeley student John R. Suman brought some of Mourning's material to U.C. Berkeley professor John C. Merriam, as indicated in his preliminary report (Merriam, 1911). In the spring of 1911 Merriam also sent a field party led by Charles L. Baker to collect more specimens and make geological observations. Their work was recorded in Merriam (1911) as being in the uppermost part of the Tertiary sequence, Merriam's "fossiliferous tuff member." Field work in 1913 by John C. Buwalda and H.S. Mourning focused on sequences stratigraphically below the 1911 sequence, including the 'resistant breccia member' of Baker (1911). A hiatus in collecting ended in 1921 when Annie M. Alexander and Louise Kellogg, both long-term volunteer field workers on behalf of the University of California, returned to the Barstow beds to continue work in the upper part of the section. Also at this time, a long-term team from the Frick Laboratory of the American Museum of Natural History led by Joseph Rak (1923-1929), Jack Wilson (1930-1939), and Ted Galusha (1950-1952) pursued field studies in the Mud Hills and adjacent areas. This early work was followed in the 1960's and 1970's by R.H. Tedford (Univ. California Riverside) and Raymond M. Alf (Webb Schools, Claremont, CA) [See also History of Study in Woodburne et al. (1990)].

As reviewed by Dibblee (1968), the Barstow Formation of the Mud Hills, north of Barstow, CA. (Figure 1) was coined by Merriam (1915, 1919) to encompass the sequence of strata that was then known to contain fossil mammals. The formation was redefined by Dibblee (1968). It was further mapped and analyzed by Steinen (1966), as a student of R.H. Tedford. A hiatus in Barstow

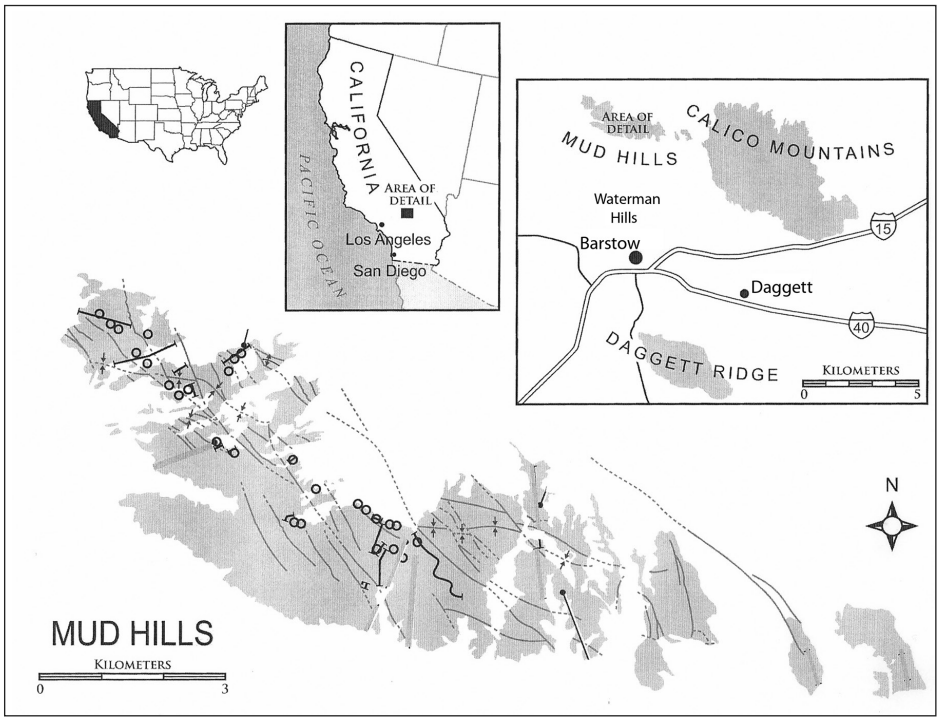

Figure 1. Map showing the location of the Mud Hills that contain the Barstow Formation. The Calico Mountains and Daggett Ridge also contain beds of the Barstow Formation. The Waterman Hills experienced early and middle Miocene uplift along a detachment fault, with erosion contributing to elements of the Owl Conglomerate of the Barstow Formation in the Mud Hills. Based on Loughney and Badgley (2017; Fig. 1), with various circles and lines reflecting their sites. The north and south limbs of the Barstow syncline are reflected by its axis.

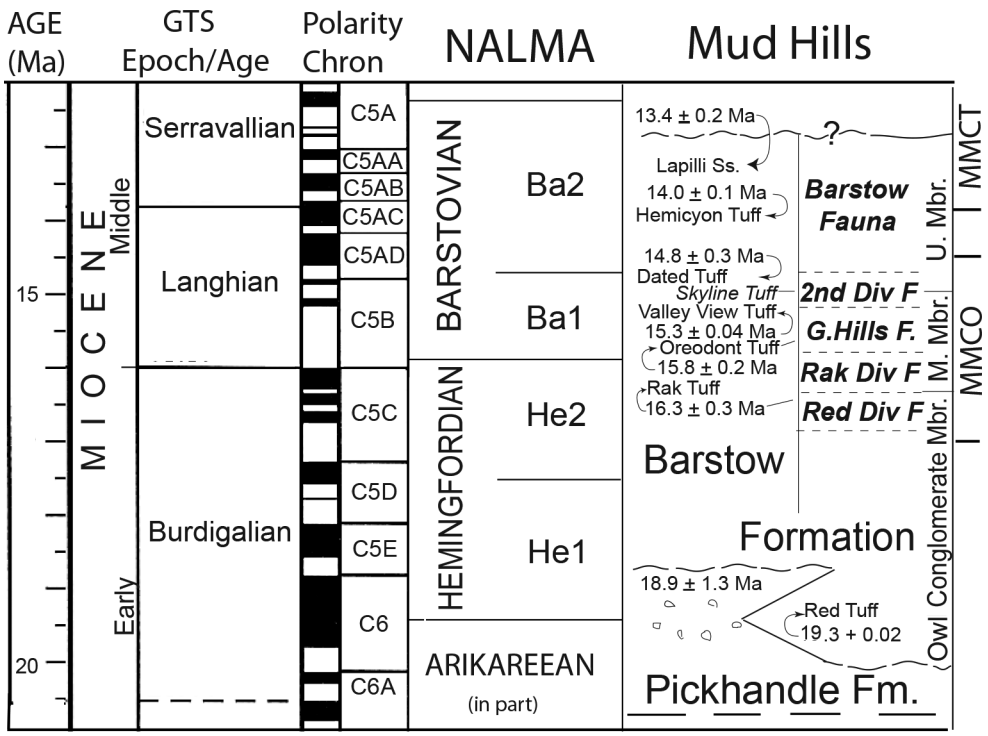

Figure 2. Chart showing the age of the Barstow Formation, early (Ba1) and late (Ba2) divisions of the Barstovian NALMA, and stratigraphic position of dated tuff beds. The Barstow Formation basally overlies and interfingers with the Pickhandle Formation. MMCO = Middle Miocene Climatic Optimum; MMCT = Middle Miocene Climatic Transition, after Loughney et al. (2019). Red Div. F. = Red Division Fauna; Rak Div. F. = Rak Division Fauna; G. Hills F. = Green Hills Fauna; 2nd Div. F. = Second Division Fauna. After Woodburne (2015; Fig. 2); note that some ages for tuffs have been revised since 2015 (Fig. 3).

stratigraphic studies was followed by Lindsay (1972) who presented the first biostratigraphic investigation of Barstow small mammals (mainly rodents).

The Barstovian North American Land Mammal Age (NALMA) was named by Wood et al. (1941) specifically for the fossiliferous tuff member and its fauna and was considered to be of late Miocene age. The present study emphasizes the development of the Barstovian Land Mammal Age and the continued role of the Barstow Formation in providing valuable perspective on the tectonics and environmental reconstruction of the Mojave Desert region.

Stratigraphy

As discussed in Woodburne et al. (1990; Woodburne, 2015) the Barstow Formation in the Mud Hills is on the order of 1,800 m thick, ranges in isotopic age from about 19.3–13.3 Ma in the Mud Hills-Calico Mts, and contains fossil mammals of late Hemingfordian through Barstovian age. Its base in part interfingers with and unconformably overlies the subjacent Pickhandle Formation (Figure 2) of early Miocene age (ca 24-19 Ma; Woodburne, 2015; appendix). As discussed therein, the Pickhandle Formation is a largely pyroclastic unit that reflects extensional tectonics of the region which was essentially completed by the time of Barstow Formation deposition (Miller et al., 2010). Tuffaceous beds compared with the Peach Spring Tuff, ca 18.7 Ma in age, have been documented in the Harvard Hills, 8 mi. east of the Calico Mountains (Figure 1) by Leslie et al. (2010). The Peach Spring Tuff also crops out in association with the Barstow Formation at Daggett Ridge (Figure 1) and adjacent Stoddard Valley (Hillhouse et al., 2010) and suggests that the formation filled the area from there northeastward to the Calico Mountains (Singleton and Gans, 2008).

The Barstow Formation is composed of a sequence of fluviatile and lacustrine sediments, including beds of water-lain and air-fall tuffs considered (Miller et al., 2010) to have developed in NW–SE trending basins. The concept of multiple basins is supported by the northwest migration of time transgressive marker facies (Reynolds and others, 2010). Deposition began with conglomeratic sandstones along the western and southwestern margins in the Mud Hills (Loughney and Badgley (2017). The timing of coarse deposition continues after the late phases of extension of the Waterman Detachment Fault to the southwest (Waterman Hills, Figure 1). More central basin sediments include a variety of fluviatile to lacustrine deposits with significant air-fall tuffs amenable to radioisotopic dating, as also recognized in Dibblee (1968), Woodburne et al. (1990) and MacFadden et al. (1990).

The lower part of the Barstow Formation in the Mud Hills is known as the Owl Conglomerate Member, best exposed on the southern limb of the Barstow Syncline (Figure 2). As discussed in Woodburne et al. (1990), the unit is about 190 m. thick (Loughney and Badgley, 2017), and consists of vivid red-brown and maroon to pale brown and yellow coarse-grained beds of coarse-grained sandstone, breccia, and sparse tuffs with metamorphic clasts considered (Woodburne et al., 1990) to have been derived from the Waterman Hills to the south. The unit interfingers westward with yellow- to orange-brown fanglomerate units that signal the above-mentioned association with and post-dating activity on the

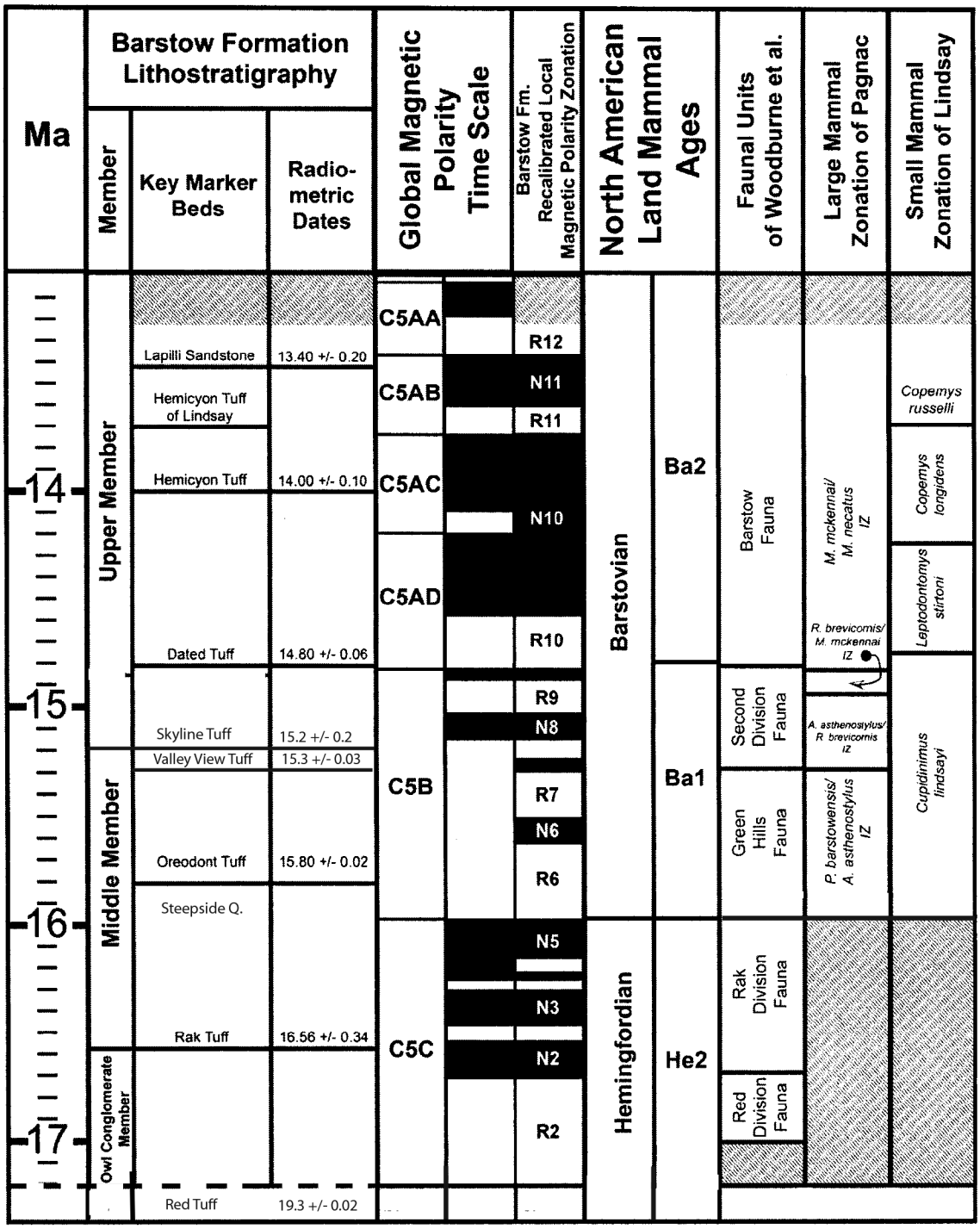

Figure 3. Lithostratigraphic, biostratigraphic, magnetostratigraphic, and geochronologic units of the Barstow Formation, after Pagnac et al. (2013; Fig. 4).

Waterman Detachment Fault. The Red Tuff at the base of the section (Figure 2) is dated at 19.3 ± 0.02 Ma, and the Rak Tuff at the top of the Red Division is dated at 16.56 ± 0.34 Ma (Figure 3).

Continuing upward stratigraphically, the Middle Member of the Barstow Formation is conformably above the Owl Conglomerate Member, and is about 570 m. thick on the north limb of the Barstow Syncline, and 470 m. on the south limb (Woodburne et al., 1990), reaching a total of about 730 m in places (Loughney and Badgley (2017). The upper limit of the member is defined by the base of the Skyline Tuff, recently dated at 15.2 ± 0.2 Ma (D.M. Miller, pers. commun. 8/11/2016). A local unconformity between the Middle and Lower members in the Rainbow Loop area, does not affect the overall continuity of these units (Woodburne et al., 1990; 468R). The sequence begins with a dark gray algal limestone, followed by a variety of epiclastic and lacustrine deposits (Loughney and Badgley,

2017), ending with beds of gray sandstone, gray-green claystone, and minor calcareous and bentonitic beds. As noted in Woodburne et al. (1990) and Pagnac (2009), the Oreodont Tuff near the middle of the unit is dated at 15.8 ± 0.02 Ma (MacFadden et al., 1990), with the Valley View Tuff about 170 m. stratigraphically higher dated at 15.3 ± 0.03 Ma (Figure 3).

The Upper Member of the Barstow Formation begins with the Skyline Tuff and is essentially equivalent to the Fossiliferous Tuff Member of Baker (1911) and the First Division of the Frick Laboratory. The unit is at least 160 m. thick (Woodburne et al., 1990) and incorporates the mudstone-dominated units FA5 and FA6 of Loughney and Badgley (2017). To the west, these units interfinger with about 200 m. of beds of orange to orange-red coarse-grained arkosic sandstone and conglomeratic sandstone. In addition to the basal Skyline Tuff, the Upper Member contains the Dated Tuff (14.8 ± 0.06 Ma), the Hemicyon Tuff (14.0 ± 0.1 Ma) and the Lapilli Sandstone (13.4 ± 0.2 Ma) near the top of the section (Figure 3).

Biostratigraphy

Previous workers such as Baker (1911) and Merriam (1915, 1919) recognized that Barstow fossil mammals were distributed in the Upper Fossiliferous Tuff Member of the deposits, but the first detailed biostratigraphy of this part of the Barstow Formation was presented by Lindsay (1972). The stratigraphically oldest of four assemblage zones (*Cupidinimus lindsayi* Assemblage Zone) begins in the middle part of the formation, at Steepside Quarry, about 35 m stratigraphically below the Oreodont Tuff (Figure 3). The uppermost unit (*Copemys russelli* Assemblage Zone) ends at the top of the Barstow Formation, about 30 m above the Lapilli Sandstone (Woodburne et al., 1990: 473R). Pagnac (2009) discusses an updated biostratigraphy of the Barstow Formation, and portrays large mammal records of the same interval in four interval-zones (Figure 3), as also discussed in Pagnac et al. (2013).

Biochronology

Biochronologic interpretation essentially began in 1915 when Merriam (1915; 1919) began to compare the mammal faunas of the Mojave Desert with those from other areas in North America and assigned the Barstow Formation an upper Miocene age. As noted by Simpson (1933), the Barstow Fauna was of late Miocene age, which was affirmed by the Wood Committee inaugurating the Barstovian Provincial Age (now, North American Land Mammal Age, or NALMA) in 1941. Lindsay (1972) provided a correlation of the Barstovian rodent faunas to others of comparable age in North America and considered the Fossiliferous Tuff member of Baker (1911) to yield the type mammalian fauna of the Barstovian NALMA as defined by Wood et al. (1941). Following the above, Tedford et al. (1987; 2004) used the Fossiliferous Tuff member as the main stratotype of the Barstovian, but also recognized that faunas from stratigraphically lower parts of the formation contained mammals of Barstovian, rather than Hemingfordian aspect and used those of the Green Hills and Second Division to represent the early Barstovian. Thus, the Barstovian of Wood et al. (1941) became what is now portrayed as late Barstovian (Ba2), whereas the early Barstovian is codified as Ba1.

Tedford et al. (2004) defined the beginning of the early Barstovian (Ba1) on the first appearance of the hemicyonine *Plithocyon* and the presence of the proboscidean *Zygolophodon*. The *Plithocyon* definition of the Barstovian was confirmed in Pagnac (2009) following a detailed analysis of large mammal biostratigraphy, although proboscideans were deleted. Pagnac (2009) also introduced the *Plithocyon barstowensis/Aelurodon asthenostylus* and *Aelurodon asthenostylus/Ramoceros brevicornis* interval zones for the early Barstovian. The late Barstovian (Ba2) of Tedford et al. (2004) was defined as the first appearance of gomphotheriid proboscideans. This was revised by Pagnac (2009) to reflect the first appearance of the antilocaprid *Ramoceros*, noting that the diachronous record of gomphotheriid proboscideans prevents them from defining the beginning of Ba2. Pagnac (2009) also introduced the *Ramoceros brevirostris/ Megahippus mckennai* and *Megahippus mckennai/ Merycodus necatus* interval zones for Ba2 (Figure 2). This paper accepts the revision of the Barstovian NALMA of Pagnac (2009) See also Pagnac et al. (2013).

Chronology

The first radioisotopic age data to be recovered from the Barstow Formation was presented by Evernden et al. (1964). This study reported a ^{40}K-^{40}Ar biotite age of 15.1 Ma for a unit that became designated as the Dated Tuff. MacFadden et al. (1990) provided a new Dated Tuff age of 14.8 ± 0.15 Ma based on the ^{40}K-^{40}Ar method, and a $^{40}Ar/^{39}Ar$ age of 14.8 ± 0.06 Ma. Cole et al. (2005) utilized U-Pb methods to obtain isotopic ages on tufas that are compatible with stratigraphically adjacent K-Ar and $^{40}Ar/^{39}$ ages and demonstrate the utility of the method.

As noted above, the Skyline Tuff has been dated recently at 15.2 ± 0.2 Ma, stratigraphically about 10 m. below the Dated Tuff (14.8 ± 0.06 Ma). Other dated units (Figs. 2, 3) indicate that the Barstow Formation in the Mud Hills is as old as 19.3 Ma and as young as 13.4 Ma (Woodburne et al., 1990; MacFadden et al, 1990).

The paleomagnetic analysis and correlation to the time scale follows that of Pagnac et al. (2013), as shown in Figure 3.

Discussion

The Barstow Formation is now an almost exceptional example of a North American Land Mammal Age in terms of its stratigraphic continuity that results in its detailed mammal record, the isotopic and magnetostratigraphic coverage, with the lower boundary well defined and recorded. A limitation that needs to

be diminished is the fact that the mammalian faunas of the Barstow Formation and the Great Basin have an endemic aspect relative to those of the Great Plains and other locations in North America (Tedford et al., 2004). Nevertheless, taxonomic elements of the Barstow Formation are distributed between the other areas, and detailed correlations are accomplished.

Loughney et al. (2019) combine isotopic analyses of carbon and hydrogen of *n*-alkanes and bulk soil organic matter of the Barstow Formation with analyses of phytoliths (plant silica) and diatoms to reconstruct its vegetation composition, habitat structure and moisture dynamics during the Middle Miocene Climatic Optimum (MMCO; 17-14.5 Ma; Figure 2). Terrestrial plants preserved in the formation prior to the time of the MMCO record an interval of drying that began continued past the Middle Miocene Climatic Transition (MMCT), about 13.8 Ma (to about 12.5 Ma; Figure 2). This overall drying was punctuated by an interval of increased moisture at the peak of the MMCO. The phytolith assemblages were dominated by riparian forests during the MMCO, with grass assemblages being important elements subsequently, as a reflection of a shift to drier and more open-canopy habitats. The establishment of dry, wooded grassland habitats in the Barstow Formation corresponds with the onset of the MMCT, cooling sea-surface temperatures of the Pacific Ocean. The data indicate that moist, closed-canopy habitats formed in southern California during climate warming. These were followed by savannas formed during climactic cooling and the shift to regimes of increased aridity and seasonal precipitation. Macroflora fossils support the results of microfloral analysis (Reynolds and Schweich, 2015).

The MMCO coincided with the heights of Great Basin Neogene tectonism (extension), which impacted changes due to environmental activity. Among other aspects, the environments supported a highly diverse mammalian fauna during the Miocene, with a major contribution made from the Barstow Formation, which is one of the faunal sequences that span the MMCO.

In summary, the detailed stratigraphic record of the Barstow Formation provides an importantly complete and coherent framework for the establishment of a detailed large and small mammal chronostratigraphic record and an informative reconstruction of the climatic and ecologic setting in which it was preserved. The middle Miocene Barstovian NALMA is a highly valuable reflection of this information.

References

Badgley, C., Smiley, T.M., and Loughney, K. 2015. Miocene mammal diversity of the Mojave region in the context of Great Basin mammal history, *in* Reynolds, R.E., ed., Mojave Miocene. The 2015 Desert Consortium. California State University Fullerton:34-43.

Baker, C.L. 1911. Notes on the later Cenozoic history of the Mohave Desert Region in southeastern California. Univ. Calif. Publ., Bull. Dept. Geol. 6: 333-383.

Cole, J.M., Rasbury, E.T., Hanson G.N., Montañez, I.P., and Pedone, V.A. 2005. Using U-Pb ages of Miocene tufa for correlation in a terrestrial succession, Barstow Formation, California. Geol. Soc. America Bulletin 117 (3/4):276-287.

Dibblee, J.W., Jr. 1968. Geology of the Fremont Peak and Opal Mountain Quadrangles, California. Calif. Div. Mines and Geology Bulletin 88:64p.

Evernden, J.F., Savage, D.E., Curtis, G.H., and James, G.T. 1964. Potassium-argon dates and the Cenozoic mammalian chronology of North America. Amer. Jour. Sci. 262:145-198.

Galusha, T., Skinner, M., Taylor, B., and Tedford, R. 1966. Preliminary analysis of the Lithostratigraphy and Biostratigraphy of the Barstow Formation in the Mud Hills, San Bernardino County, California. Stout Research Center Archive, Colorado Desert District, Department of Parks and Recreation, Borrego Springs, California 8p.

Hillhouse, J.W., Miller, D.M., and Turrin, B.D. 2010. Correlation of the Miocene Peach Springs Tuff with the geomagnetic polarity time scale and new constraints on tectonic rotations in the Mojave Desert, California, *in*. R.E. Reynolds and D.M. Miller, eds., Overboard in the Mojave. 20 million years of lakes and wetlands. Abstracts and proceedings: the 2010 Desert Symposium. Desert Studies Consortium, California State University, Fullerton: 105-212.

Leslie, S.R., Miller, D.M., Wooden, J.I., and Vazquez, J.A. 2010. Stratigraphy, age, and depositional setting of the Miocene Barstow Formation at Harvard Hill, central Mojave Desert, California, *in* Reynolds, R.E., and Miller, D.M., eds., Overboard in the Mojave. 20 million years of lakes and wetlands. The 2010 Desert Consortium. California State University Fullerton: 85-104.

Lindsay, E.H. 1972. Small mammal fossils from the Barstow Formation, California. Calif. Univ. Publ. Geol. Sci. 93: 104p.

Lofgren, D., Holiday, A., and Stoddard, R. 2016. Review of small mustelids from the Barstow Formation of California, *in* Reynolds, R.E., ed., Going LOCO. The 2016 Desert Symposium and Field Guide. California State University Desert Studies Consortium: 295-302.

Loughney, K.M. 2016. Environments in the Barstow Formation in the Mud Hills, southeastern California, *in* Reynolds, R.E., ed., ECSZ Does It: Revisiting the Eastern California Shear Zone. The 2017 Desert Consortium. California State University Fullerton: 237-240.

Loughney, K.M. and Badgley, C. 2017. Facies, environments and fossil preservation in the Barstow Formation, Mojave Desert, California. Palaios 32:396-412.

Loughney, K.M., Hren, M.T., Smith, S.Y., and Pappas, J.I. 2019. Vegetation and habitat change in southern California through the Middle Miocene Climatic Optimum: Paleoenvironmental records from the Barstow Formation, Mojave Desert, USA. Geological Society of America Bulletin 132, no. 1/2:113-129.

MacFadden, B.J., Swisher, C.C., III, Opdyke, N.D., and Woodburne, M.O. 1990a. Paleomagnetism, geochronology, and possible tectonic rotation of the middle Miocene Barstow

Formation, Mojave Desert, southern California. Geol. Soc. Amer. Bull. 102:478-493.

Merriam, J.C. 1911. A collection of mammalian remains rom Tertiary beds on the Mohave Desert. Univ. Calif. Publ., Bull. Dept. Geol. 6 (7):167-169.

Merriam, J.C. 1915. Extinct faunas of the Mohave Desert, their significance in a study of the origin and evolution of life in America. Pop. Sci. Monthly 86:245-264.

Merriam, J.C. 1919. Tertiary mammalian faunas of the Mohave Desert. Univ. Calif. Publ., Bull. Dept. Geol. 11(5): 437a-e, 438-595.

Miller, D.M., Leslie, S.R., Hillhouse, J.W., Wooden, J.L., Vasquez, J.A. and Reynolds, R.E. 2010. Reconnaissance geochronology of tuffs in the Miocene Barstow Formation: Implications for basin evolution and tectonics in the central Mojave desert, *in* Reynolds, R.E., and Miller, D.M., eds., Overboard in the Mojave. 20 million years of lakes and wetlands. The 2010 Desert Consortium. California State University Fullerton: 70-84.

Miller, D.M. 2016. The late Cenozoic Eastern California Shear Zone after 25 years of study, *in* Reynolds, R.E., ed., ECSZ Does It: Revisiting the Eastern California Shear Zone. The 2016 Desert Consortium. California State University Fullerton: 45-54.

Pagnac, D.C. 2009. Revised large mammal biostratigraphy and biochronology of the Barstow Formation (Middle Miocene), California. PaleoBios 29(2): 48-59.

Pagnac, D.C., Browne, I., and Smith, K. 2013. Stratigraphy and vertebrate paleontology of the middle Miocene Barstow Formation. San Bernardino County, California; 73rd annual Meeting of the Society of Vertebrate Paleontology, Los Angeles, CA.

Reynolds, Robert E., David M. Miller, M. O. Woodburne, and L. B. Albright, 2010. Extending the boundaries of the Barstow Formation in the central Mojave Desert; 2010 Desert Symposium Volume, California State University, Desert Studies Consortium. p. 148-161.

Reynolds, R.E., and Schweich, T. 2015. Additions to the floras of the Barstow Formation in the Mud Hills, California. In, R.E. Reynolds, ed., Mojave Miocene. The 2015 Desert Symposium Field Guide and Proceedings, California State University Desert Studies Consortium, p. 119-129.

Schweich, T. 2010. John C. Merriam and the Barstow Syncline, *in* Reynolds, R.E., and Miller, D.M., eds., Overboard in the Mojave. 20 million years of lakes and wetlands. The 2010 Desert Consortium. California State University Fullerton: 122-123.

Simpson, G.G. 1933. Glossary and correlation charts of North American Tertiary mammal-bearing formations. American Museum Natural History Bulletin 67:79-121.

Singleton, J.S., and Gans, P.B. 2008. Structural and stratigraphic evolution of the Calico Mountains: Implications for early Miocene extension and Neogene transpression in the central Mojave Desert, California. Geosphere 4(3):459-479.

Steinen, R.P. 1966. Stratigraphy of the middle and upper Miocene Barstow Formation, San Bernardino County, California (M.S. Thesis): Riverside, California; University of California, Riverside, 150p.

Tedford, R.H., Galusha, T., Skinner, M.F., Taylor, B.E., Fields, R.W., Macdonald, J.R., Rensberger, J.M., Webb, S.D., and Whistler, D.P. 1987. Faunal succession and biochronology of the Arikareean through Hemphillian interval (late Oligocene through earliest Pliocene epochs), North America, *in* Woodburne, M.O., ed., Cenozoic mammals: Geochronology and biostratigraphy. Berkeley, California, University of California Press, p. 153-210.

Tedford, R.H., Albright, L.B., III, Barnosky, A.D., Ferrusquia-Villafranca, I., Hunt, R.M., Jr., Storer, J.E., Swisher, C.C., III, Voorhies, M.R., Webb, S.D., and Whistler, D.P. 2004. Mammalian Biochronology of the Arikareean through Hemphillian interval (Late Oligocene through early Pliocene epochs), *in* Woodburne, M.O., ed., Late Cretaceous and Cenozoic Mammals of North America: Biostratigraphy and Geochronology. Columbia University Press, p. 169-23.

Wood, H.E., 1941. Nomenclature and correlation of the North American continental Tertiary. Geol. Soc. America Bull. 52: 1-48.

Woodburne, M.O. 1996. Precision and resolution in mammalian chronostratigraphy: Principles, practices, examples. Jour. Vertebrate Paleontology 16(3): 531-555.

Woodburne, M.O. 2006. Mammal ages. Stratigraphy 3(4): 229-261.

Woodburne, M.O. 2016. The Eastern California Shear Zone, Mojave Desert, California, *in* Reynolds, R.E., ed., ECSZ Does It: Revisiting the Eastern California Shear Zone. The 2016 Desert Consortium. California State University Fullerton: 55-59.

Woodburne, M.O., Tedford, R.H., and Swisher, C.C., III. 1990. Lithostratigraphy, biostratigraphy, and geochronology of the Barstow Formation, Mojave Desert, southern California. Geol. Soc. Amer. Bull. 102: 459-477.

Two fossil accumulations in the Upper Barstow Formation, Mud Hills, Mojave Desert, CA

Robert E. Reynolds
Redlands, CA, bob.reynolds220@gmail.com

ABSTRACT—Bones of fossil mammals at two accumulations, Robbins Fossil Quarry (RFQ) and Truck Top Quarry (TTQ), are found in wetland and alluvial deposits of the upper member of the Barstow Formation in the Mud Hills, central Mojave Desert. These bone concentrations date from or are younger than 13.8 Ma and are considered to be from the Middle Miocene Climatic Transition. After a catastrophic incident, skeletal remains at RFQ were deposited in a shallow lake or pond. The skeletal elements recovered from TTQ were deposited on a slowly accumulating surface where bones were eventually recovered from paleosols. Differing amounts of taxa, especially rodents, suggest that multiple habitats were locally available toward the end of the Barstovian Land Mammal Age.

Introduction and geographic relationships

This paper compares faunas from Truck Top Quarry (TTQ) and Robbins Fossil Quarry (RFQ), both in the Upper Member of the Barstow Formation in the northwestern Mud Hills (Table 1).

The Barstow Formation fills a northwest-trending trough in the northwestern Mud Hills (Miller and others, 2010). RFQ is located on the northeastern margin of the trough, one-third mile southwest of the margin of the quartz monzonite basement rocks exposed in the Coolgardie Highland. The Coolgardie Highland was shedding clasts into the Miocene Barstow Formation sediments and is shedding clasts southwestward into drainages cutting the Miocene sediments today. Two miles west of RFQ, TTQ is located on the western margin of the trough one and one-half miles west of the Coolgardie Highland. The area is crossed by the northwest-trending Fossil Canyon Fault (Dibblee, 1968, pl. 3).

Age and chronostratigraphy

Both localities appear to be within the Middle Miocene Climatic Transition (post-14 Ma, Loughney and Badgley, 2017; Loughney and others, 2019). Fossil horse bone from RFQ has been directly dated by U-Pb methods at 13.8 Ma (James Edmonds, Stonybrook, p. c. to Woodburne, Reynolds, Sept. 2017). TTQ is in a paleosol within a thick fluvial sediment that overlies wetland mudstone and undated volcanic tuffs. Since TTQ produces the late Barstovian Land Mammal Age (LMA) horse (*Megahippus mckennai*), antelope (*Merycodus*) and canid (*Cynarctus*, lg.) the age of the accumulation may be as young as the Lapilli Tuff (13.4 Ma).

Taphonomy

The RFQ concentration is situated in mudstone that contains silicified roots and root clusters that suggest palm islands (Reynolds and Browne, 2015; Loughney and others, 2019). Reynolds and Browne (2015) propose a nuée ardente as the cause of death for RFQ large mammals. Skeletal remains were then redeposited by downslope sheet flood transport, predation, trampling, and burial at a wetland margin or poorly drained floodplain.

In contrast, the TTQ fossils concentrated on a relatively stable surface with developing soil. Indications of the soil-forming processes include carbonate kernels and carbonate rinds around bones. Basin-filling fluvial sediments and tan paleosols are upsection from ash-rich gray mudstones interpreted as wetland deposits.

One interpretation for the accumulation of small mammal remains is predation. By this interpretation, accumulation of rodent bones was initially by raptors (hawk and owl) dropping bones or digestive pellets of bones and hair at the base of their perches. Trees are known to have been present at RFQ. Fossil root complexes indicating palm tree islands were present along strike from RFQ, and samples taken around their bases proved rich in rodent mandibles and bone. Another interpretation for fossil accumulation is movement by flowing water. Owl pellets can easily float in shallow moving water until reaching a damming structure where they are concentrated (Reynolds, pers. obsv., 1982, along Mojave River overbank). The concentration and parallel orientation of long bones at RFQ (Reynolds and Browne, 2015) suggest movement by water to and at the final resting position. Rodent carcasses and owl pellets may have collected against such a bone "log" jam. At both localities, rodent remains may also have been concentrated by surface sheet flooding.

Taxa by locality

Robbins Fossil Quarry taxa. RFQ produced two horse taxa (*Scaphohippus intermontanus* and *S. sumani*), one rhinoceros (*Peraceras* sp), antelope (*Merycodus* sp.), and a large camel (*Aepycamelus* sp.). It also yielded an

insectivore (*Paradomnina* cf. *relictus*), canids (*Aelurodon* sp., *Paratomarctus* sp., *Cynarctus* sp., *Leptocyon* sp.) and felids (*Nimravides* sp., *Pseudaelurus* sp.) along with abundant specimens of three deer mouse species (*Copemys* sp.) and one species of pocket mouse (*Perognathus minutus*). Two species of ancestral kangaroo rats (*Cupidinimus* spp.) are present and gophers (Geomyiidae: *Mojavemys* spp.) are scarce (Browne, 2002).

Truck Top Quarry taxa. TTQ produced two horse species (*Scaphohippus intermontanus* and the Anchitheriine horse *Megahippus*), antelope (*Merycodus* sp.), and large camel (*Aepycamelus* sp.) but just one carnivore, a canid (*Cynarctus* sp. lg.). TTQ has no cricetid rodents. Two pocket mice (*Perognathus* sp.) are known from this time period and both appear at TTQ. Two species of ancestral kangaroo rats (*Cupidinimus* spp.) are present and one (*C. halli*) is abundant. Gophers (*Mojavemys* spp.) are abundant.

Locality similarities. Both localities have a horse (*Scaphohippus intermontanus*), antelope (*Merycodus* sp.), and large camel (*Aepycamelus* sp.). Only one carnivore is present at both, the canid *Cynarctus* sp. The small rabbit (*Hypolagus* sp.) is present at both localities. Both quarries contain ground squirrels (*Miospermophilus* sp.) in about equal abundance, and each has a single record of chipmunk (*Tamias* sp.). The pocket mouse (*Perognathus minutus*) is at both quarries, as are two kangaroo rats (*Cupidinimus halli; Cupidinimus lindsayi*). One of the gophers (*Mojavemys lophatus*) was recovered from both localities.

Locality differences. The late Barstovian horse (*Scaphohippus sumani*) and the rhinoceros (*Peraceras*) are present only at RFQ. The large late Barstovian Anchitheriine horse (*Megahippus mckenn*ai) is present only at TTQ. Insectivores, mustelids, canids and felids (Table 1) were found in accumulations at RFQ, while only one large canid (*Cynarctus*) was present at TTQ.

The greatest contrast between taxa at the two localities is between the small mammals, especially the rodents. RFQ produced 32 specimens of the three cricetid species (*Copemys* spp.) but TTQ has no cricetids. Two pocket mice species (*Perognathus* spp.) are present at TTQ while only one (*P. minutus*) is at RFQ. Although two species of ancestral kangaroo rats (*Cupidinimus* spp.) are present in each quarry, the large kangaroo rat (*C. halli*) is five times more abundant at TTQ. The gophers (Geomyidae: *Mojavemys* spp.) are scarce at RFQ but abundant at TTQ.

Habitat preferences

General habitat preferences of extant rodents are presented by Engles (1965). Modern (contemporary) counterparts of the Miocene small mammals can be used to infer habitat preferences of their ancient relatives. For instance, the Cricetidae (deer mice: *Copemys* sp.) today prefer a brushy, sometimes rocky understory for foraging and surface nest building.

Table 1. Taxa by locality

Taxon	RFQ*	TTQ*
LARGE HERBIVORES		
Megahippus sp.		1
Scaphohippus intermontanus	4	2
Scaphohippus sumani	5	
Peraceras sp.	1	
Merycodus sp.	6	1
Aepycamelus sp.	3	1
INSECTIVORE		
Paradomnina cf. *relictus*	1	
CARNIVORES		
Mustelidae indeterminate	2	
Aelurodon asthenostylus	1	
Paratomarctus temerarius	1	
Cynarctus galushai	4	1
Leptocyon sp.	2	
Nimravides sp.	2	
Pseudaelurus intrepidus	1	
RABBITS and RODENTS		
Hypolagus parviplicatus	2	1
Miospermophilus sp.	1	2
Tamias ateles	1	1
Copemys barstowensis	1	
Copemys longidens	8	
Copemys cf. *tenuis*	4	
Perognathus minutus	1	1
Perognathus furlongi		1
Cupidinimus halli	2	10
Cupidinimus lindsayi	1	2
Mojavemys lophatus	1	3
Mojavemys alexandrae		1

*Minimum number of individuals. RFQ: Robbins Fossil Quarry. TTQ: Truck Top Quarry.

Heteromyidae such as pocket mice and kangaroo rats (*Perognathus* spp., *Cupidinimus* spp.) are found in a xeric environment with a substrate of rocky or sandy soils that support grasslands or xerophilous plants. Gophers (Geomyiidae: *Mojavemys* spp.) prefer friable soils with enough moisture to support edible plants and their roots: grasses, shrubs, seedlings, and trees.

Barstow Formation habitats. The model presented by Reynolds and Browne (2015) speculates that after death, taxa near RFQ washed down slope from the Coolgardie Highland to a wetland margin. The rodent taxa from RFQ suggest that there were areas of brushy, sometimes rocky understory for foraging and nest building by cricetids upslope from the final bone concentration. Fossil roots suggest that palm trees were present where raptors might have roosted.

The rodents from TTQ suggest a slowly accumulating, stable surface of a grassland or parkland habitat frequented by heteromyids and geomyids. Horses and antelopes present indicate that grassland habitat that was close or at a distance. Rhinoceros, anchitheriine horse (*Megahippus*) (MacFadden, 1992), and camels suggest browsing in a savannah parkland of mixed grasses, brush and copses of trees. Again, these could have been distant habitats. *Cynarctus* was one of the omnivorous 'coyotes'

(Wang and Tedford, 2008) of the time, perhaps denning and hunting across open grassland.

Summary

At 14 Ma, the Middle Miocene Climatic Optimum was fading on the west coast and across the continent (Zachos and others, 2001) and the transition to an equitable climate of the Middle Miocene Climatic Transition (MCT) with seasonal precipitation had started (Loughney and others, 2019). Bone accumulations at Robbins Fossil Quarry and Truck Top Quarry are younger than 14 Ma, and probably within the transition to the MCT. Wetland siltstone and mudstone of the Barstow Formation accumulated within a northwest trending trough situated southwest of the granitic Coolgardie Highland and northeast of low alluvial slopes with developing soil horizons.

The fossil mammals suggest that on the northeastern margin of the trough (RFQ), there were occasional grasslands between areas of brushy, sometimes rocky understory of open canopy parkland. Riparian plants including palms were present near wetland margins.

North of the exhumed Waterman Hills, the western margin of the trough (TTQ) consisted of low-angle alluvial slopes with slowly developing soil horizons (paleosols) that prograded over central basin wetlands. Fossil mammals suggest that the surfaces of the slopes supported a grassland or parkland habitat with a nearby mix of wooded grasslands where brush and copses of trees were interspersed with grasslands.

Acknowledgements

This research was carried out under permit CA-16-06P. Access to the field localities was provided by several Barstow BLM archaeologists over the years, most recently by James Shearer. Specimens are housed at the San Bernardino County Museum. Many museum volunteers worked at both fossil concentrations over the past 50 years, including Quintin Lake, Mark Roeder, Tom Howe, Mike Moore, Steve Mains, Peg Howe, and Sugar White. Recent access to SBCM collections was provided by curators Ian Gilbert and Crystal Cortez. Careful review by Katherine Loughney helped clarify some of the concepts presented herein.

References cited

Browne, I. D., 2002. Late Barstovian mammalian fauna of Robbin's Quarry (Barstow Formation, San Bernardino County, California). Unpublished Master's Thesis. Geological Sciences, University of California, Riverside, 111 p.

Dibblee, T. W. Jr., 1968. Geology of the Fremont Peak and Opal Mountain quadrangles, California. Calif. Div. Mines and Geology, Bull. 188, 64 p.

Engles, L. G., 1965. Mammals of the Pacific States: California, Oregon, Washington. Stanford University Press, Stanford, CA. 506 p.

Loughney, K. M. and C. Badgley, 2017. Facies, environments and fossil preservation in the Barstow Formation, Mojave Desert, California. Palaios, 32: 396-412. http://dx.doi.org/10.2110/palo.2017.008

Loughney, K. M., M. T. Hren, S. Y. Smith, and J. L. Pappas, 2019. Vegetation and habitat change in southern California through the Middle Miocene Climatic Optimum. Paleoenvironmental records from the Barstow Formation, Mojave Desert, USA. Geological Society of America Bulletin: 17 p. https://doi.org/10.1130/B35061.1

MacFadden, B. J., 1992. Fossil horses: systematics, paleobiology, and evolution of the family Equidae. Cambridge University Press, 369 p.

Miller, D. M., S. R. Leslie, J. W. Hillhouse, J. L. Wooden, J. A. Vazquez, and R. E. Reynolds, 2010. Reconnaissance geochronology of tuffs in the Miocene Barstow Formation: implications for basin evolution and tectonics in the central Mojave Desert. California State University, Desert Studies Consortium: 70-84.

Pagnac, D., 2009. Revised large mammal biostratigraphy and biochronology of the Barstow Formation (Middle Miocene), California. University of California Museum of Paleontology, PaleoBios 29(2):48-59.

Reynolds, R. E., and I. Browne, 2015. Robbins Quarry: Taphonomy and stratigraphic position in the Barstow Formation, Mojave Block, California. California State University, Desert Studies Consortium: 145-148.

Wang, Xiaoming and R. H. Tedford, 2008. Dogs: their fossil relatives and evolutionary history. Columbia University Press, 219 p.

Zachos, J.C., Pagani, M., Sloan, L.C., Thomas, E., and Billups, K., 2001, Trends, rhythms, and aberrations in global climate 65 Ma to present: Science, v. 292, p. 686–693, https://doi.org/10.1126/science.1059412.

Fossil-bearing facies of extensional basins: Examples from the Miocene Barstow and Dove Spring formations, Mojave region, California

Katharine Loughney[1] and Fabian Hardy[2]
[1]*University of Michigan Department of Ecology & Evolutionary Biology, 1105 North University Ave., Ann Arbor, MI 48109*
[2]*University of Michigan Department of Earth & Environmental Sciences, 1100 North University Ave., Ann Arbor, MI 48109*

ABSTRACT—The Barstow and Dove Spring formations are two of the most paleontologically important Miocene sedimentary sequences of the Mojave Desert region of California, and they preserve large and small mammals throughout their stratigraphic extent. The facies settings of fossil localities, however, differ between the formations, indicating that depositional environments were broadly different in the Barstow and Dove Spring formations. We summarize the lithology and facies of the two formations and discuss the influence of tectonics and climate on the deposition of fossiliferous strata.

Introduction

Extensional-basin systems are important settings for Neogene fossil localities in western North America. Many fossiliferous formations occur in the Basin and Range physiographic province of Utah, Nevada, Arizona, New Mexico, and California, and provide important records of mammal evolution during intervals of heightened tectonic activity and climate change in the Miocene (Woodburne et al., 2004). The Basin and Range physiographic province extends over much of western North America and formed through widespread extension beginning ~35 Ma (McQuarrie and Wernicke, 2005). This extension created numerous sedimentary basins that preserve the Neogene sedimentary and fossil records of the region.

The northern Basin and Range, southern Basin and Range, and Mojave region are tectonically distinct, reflecting differences in bedrock geology, extensional history, and underlying mantle properties (Parsons, 2006). During the Late Oligocene to Early Miocene, high-magnitude extension along low-angle detachment faults exposed metamorphic core complexes throughout the northern, central, and southern Basin and Range. After ~13 Ma, extension mainly occurred along high-angle normal faults in the northern and southern Basin and Range (Parsons, 2006). In the Mojave region, tectonic deformation continued through strike-slip faulting that initiated after ~11 Ma (McQuarrie and Wernicke, 2005).

The tectonic regimes of these subregions affected the timing and style of sedimentation in individual basins. Individual basin history has an important effect on the environments and facies that form during deposition, which can affect the preservation of fossils. Even formations with similar mammalian faunal assemblages may have different facies contexts for fossil localities. Here, we compare the facies settings of mammal-fossil localities in two formations of the Mojave region with distinctive basin histories. The Barstow Formation and the Dove Spring Formation of California each have well-known Miocene mammalian assemblages that span the Hemingfordian, Barstovian, and Clarendonian North American Land Mammal Ages. These formations differ in terms of lithostratigraphy and the facies settings for fossil preservation, which may be related to differences in tectonic history, climate, or the depositional environments present during deposition.

Barstow Formation

The Barstow Formation crops out in the central Mojave Desert in California (Fig. 1). Northeast-directed extension in this area occurred between ~23 and 19

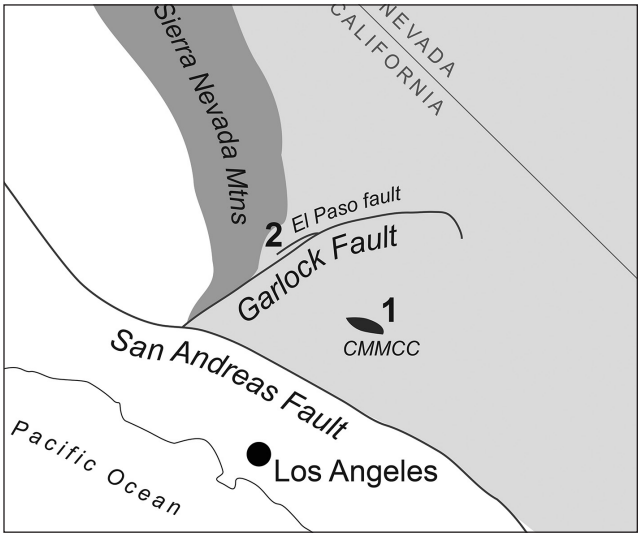

Figure 1. Map showing locations of the Barstow (1) and Dove Spring (2) formations in southern California. Light gray indicates the Mojave Desert region of the Basin and Range physiographic province; CMMCC = central Mojave metamorphic core complex.

Ma in association with exposure of the central Mojave metamorphic core complex and the Waterman Hills detachment fault (Glazner et al., 2002). The Early Miocene Jackhammer, Pickhandle, and Mud Hills formations include over 400 m of coarse volcaniclastic breccias, conglomerates, and mudstones that represent landslide, alluvial fan, and lacustrine deposits that formed during active extension (Fillmore and Walker, 1996; Ingersoll et al., 1996). The Pickhandle and Mud Hills formations are generally non-fossiliferous, although Garrison and Reynolds (2015) reported rare plants and snails from one locality in the Pickhandle Formation.

The Barstow Formation unconformably overlies the Pickhandle and Mud Hills formations in the Calico Mountains and Mud Hills. The Barstow Formation is divided into four members, the Calico, Owl Conglomerate, Middle, and Upper members (Fig. 2; Singleton and Gans, 2008; Woodburne et al., 1990), all deposited after extension had ended in the central Mojave region. Radiometric dating of prominent tuff layers and magnetostratigraphy constrain the age of the formation

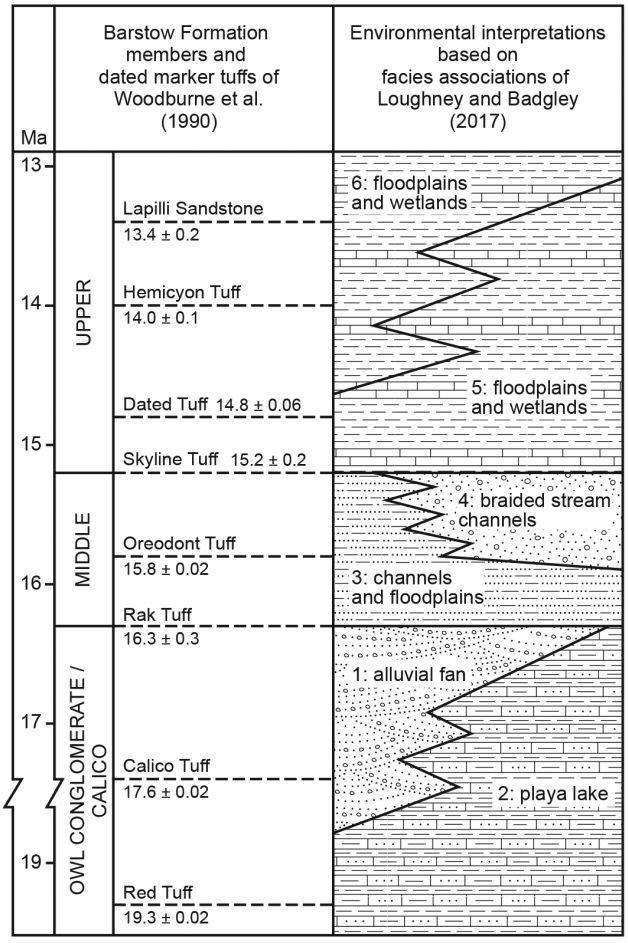

Figure 2. Generalized stratigraphic section of the Barstow Formation in the Calico Mountains and Mud Hills, showing facies associations and environmental interpretations from Loughney and Badgley (2017). Ages of dated tuff layers from MacFadden et al. (1990) and Miller et al. (2013). Modified from Loughney (2017).

between 19 and 17 Ma in the Calico Mountains and between ~19 and 13 Ma in the Mud Hills (MacFadden et al., 1990; Singleton and Gans, 2008). In the Calico Mountains, the Calico Member of the Barstow Formation is characterized by a thick section of alternating, thin beds of mudstone, sandstone, and marl. These beds are interpreted as forming in a shallow saline-alkaline lake, and upwards-increasing amounts of gypsum indicate that the lake experienced increased drying over time (Park, 1995). These sediments produce an exceptionally well-preserved arthropod assemblage that includes fairy shrimp, damsel fly larvae, and midges (Park and Downing, 2001).

The lacustrine deposits in the Calico Mountains may be partly coeval with deposits of the lower Barstow Formation in the Mud Hills. Thin-bedded mudstone, sandstone, and marl are well exposed in Owl Canyon and may represent a westward extension of the lacustrine environments represented by the Calico Member (Loughney and Badgley, 2017). In the Owl Conglomerate Member in the Mud Hills, lacustrine deposits interfinger with sandstone and conglomerate that represent channel deposits of alluvial fans. Vertebrate body fossils in the lower Barstow Formation are relatively rare, and the few localities that occur in the alluvial fan deposits contribute to the Hemingfordian mammal faunas of the formation (Lindsay, 1995; Woodburne et al., 1990). Lacustrine deposits in the Mud Hills do not preserve vertebrate material, but several mammal trackways occur in these sediments (Alf, 1966).

The deposits of the Middle Member of the Barstow Formation mark a shift in depositional environments from lacustrine and alluvial fan dominated to fluvial dominated (Fig. 2; Loughney and Badgley, 2017). Siltstones and sandstones interbedded with mudstone and marl represent channel, near-channel floodplain, and abandoned-channel deposits. The presence of marl layers, color mottling, and redox concentrations around root traces indicate that water tables were high and moisture was abundant in these floodplain environments (Loughney et al., 2020). Numerous mammal-fossil localities of Barstovian age and 42 large-mammal species occur in these deposits. The thickness and prominence of sandstone layers increase upwards through this part of the formation into laterally extensive stacked sandstone beds (Fig. 3). These layers represent channel deposits of a braided-stream system, with few fine-grained overbank deposits (Loughney and Badgley, 2017). Vertebrate localities also occur in this sandstone-dominated succession, and 28 large-mammal species occur in this facies.

The Upper Member of the Barstow Formation is dominated by mudstone, siltstone, and sandstone. Fossil localities are common in drab-colored tuffaceous mudstone interbedded with root-cast-bearing marl layers. These beds were deposited in ponded floodplains and wetlands (Fig. 2) that were sites where mammals

Figure 3. The Middle Member of the Barstow Formation in the Mud Hills, California. Interbedded sandstones and mudstones (right) represent proximal-channel floodplain deposits that give way upsection to stacked sandstone (left) representing channel beds at the top of the Middle Member.

congregated (Loughney and Badgley, 2017). In the uppermost part of the formation, siltstone beds alternate with algal and brecciated marl layers and drab-colored mudstone. Pedogenic features are moderately to well developed in this part of the formation, indicating that sediment-accumulation rates were low and landscape surfaces were relatively stable (Loughney and Badgley, 2017). Brecciated marls form from periodic subaerial exposure, and the presence of carbonate nodules and slickensides indicate that these deposits experienced repeated wetting and drying. These deposits represent ephemeral wetlands and well-drained floodplains. Many fossil localities occur in these facies, and 38 species of large mammals are known from these sediments (Loughney and Badgley, 2017).

Dove Spring Formation

Approximately 90 km northwest of the Barstow Formation (Fig. 1), the El Paso Basin is located at the intersection of two distinct tectonic settings: the Walker Lane belt and the Eastern California Shear Zone, which are separated by the Garlock Fault (Andrew et al., 2014; Dixon and Xie, 2018; Loomis and Burbank, 1988). The Garlock Fault extends eastward from the San Andreas Fault and separates the strike-slip and compressive Eastern California Shear Zone to the south from the dextral strike-slip and extensional Walker Lane belt to the north. This fault system accommodates dextral shear movement in the Mojave region that initiated between 11 and 10 Ma (Golombek and Brown, 1988; Loomis and Burbank, 1988). The El Paso Basin is structurally similar to the Basin and Range north of the Garlock Fault, with a history of tilting followed by extension (Loomis and Burbank, 1988).

The sedimentary fill of the El Paso Basin consists of the Paleocene Goler Formation, the Early Miocene Cudahy Camp Formation, and the Middle to Late Miocene Dove Spring Formation, with the latter two formations collectively known as the Ricardo Group (Loomis and Burbank, 1988). The Cudahy Camp Formation is a series of andesite-rich volcaniclastic conglomerates and tuff, as well as exposures of the Black Mountain Basalt (Loomis and Burbank, 1988). Based on K-Ar dates of the Black Mountain Basalt and a pair of andesite flows, the Cudahy Camp Formation was deposited between approximately 18 and 15 Ma (Loomis and Burbank, 1988).

The Dove Spring Formation was deposited above the Cudahy Camp Formation from 12.5 to 8.0 Ma. The age of the Dove Spring Formation is based on magnetostratigraphy, and the presence of at least 18 ash layers within the section allows for tephrochronological correlations throughout the Great Basin (Whistler et al., 2009). Radiometric dates have been measured for seven of the ash layers. Loomis and Burbank (1988) interpreted the 1800 m Dove Spring Formation as a continuous series of fluvial sediments, divided into six members and containing three major volcanic components (a tuff breccia and two basalt flows). The Dove Spring Formation is dominated by sandstone, but has significant variation in grain size and sedimentary structures at the meter-scale (Fig. 4).

Member 1 was deposited by 12.5 Ma and consists of coarse, matrix-supported conglomerates with abundant volcanic clasts from a source outside the basin (Loomis and Burbank, 1988; Whistler et al., 2009). Based on composition, the source for these volcanic clasts is interpreted to be the El Paso Mountains. Members 2 and 3 are composed primarily of sandstones that fine upward and are interspersed with pyroclastic and basaltic sediments from vents interpreted to have been located west of El Paso Basin (Loomis and Burbank, 1988; Whistler et al., 2013). Sediments generally coarsen upward from Member 4 through Member 6, deposited between 11.0 and 10.0 Ma. Compositional changes in sandstone lithology and conglomerate clasts at the top of Member 6 suggest a shift to a Sierra Nevada sediment source (Loomis and Burbank, 1988; Whistler et al., 2009).

Member 5 notably contains the most fossil localities in the Dove Spring Formation (Fig. 5), which suggests

Figure 4: The Dove Spring Formation is characterized by extensive sandstone deposits that give Red Rock Canyon State Park its name.

that sediments deposited between 10.5 and 9.5 Ma had the highest potential to preserve mammal remains. The base of this interval contains numerous crossbedded sandstones interspersed with siltstones, potentially representing a mix of overbank and channel-fill deposits. Disarticulated vertebrate fossils are prevalent in the lower portion of Member 5 and become less common as the crossbedded sandstones give way to massive sandstones that coarsen upward.

The massive sandstones of Member 5 are cyclic, alternating between resistant, cliff-forming layers and less-resistant, slope-forming layers over 30 to 45 m-thick intervals. Large complexes of silicified root casts are common in this interval, features consistent with well-drained paleosols developed in a setting with a declining sediment-accumulation rate (Tabor and Myers, 2015). Movement along the El Paso fault and basin rotation initiated midway through deposition of Member 5, and the increased thickness of sandstones through Member 6 may reflect erosion of the Sierra Nevada and alluvial fan progradation (Loomis and Burbank, 1988).

Fossiliferous facies in the Barstow and Dove Spring formations

The lithology of the Barstow and Dove Spring formations in their type areas are broadly different. Despite each preserving rich fossil mammal assemblages, the fossil-bearing deposits of these formations have significant differences in terms of lithological

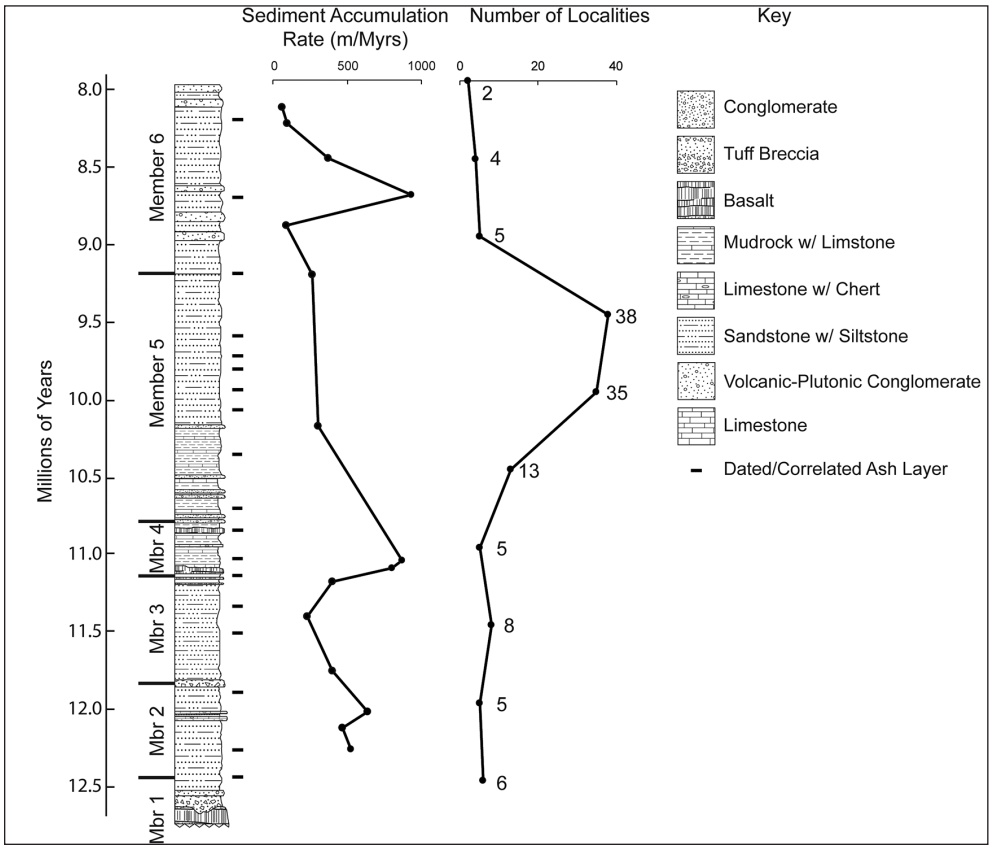

Figure 5: Composite stratigraphic column, modified from Whistler et al. (2009), with newly calculated sediment-accumulation rates (SAR) and number of fossil localities in half-million-year time bins. SAR declines between 11.0 and 9.0 Ma, coinciding with basin rotation and extension along the El Paso fault. The 11.0 to 9.0 Ma interval is also associated with the highest frequency of fossil localities, peaking at 9.5 Ma. Ash dates and tephra correlations are provided in Whistler et al. (2009).

and facies characteristics. The Barstow Formation is overall finer-grained than the Dove Spring Formation, indicating the preservation of lower-energy depositional settings throughout much of its depositional history, compared to the higher-energy settings represented in the Dove Spring Formation. The oldest portions of both the Barstow and Dove Spring formations contain the least fossiliferous strata. The conglomerates and laterally extensive fine-grained lacustrine sediments of the lower Barstow Formation preserve few mammal fossils, although arthropods are well preserved in the Calico Member (Park, 1995). Conversely, the lower Dove Spring Formation is dominated by medium- to coarse-grained sandstones, and lacustrine deposits are uncommon and geographically limited.

The middle portions of both formations are more similar. In the Barstow Formation, many fossil localities occur in the proximal-channel floodplain facies and channel-dominated strata of the Middle Member (Figs. 2, 3). In both the Barstow and Dove Spring formations, sandstones are more prominent upsection, forming stacked beds indicative of channel deposits of braided-stream systems (Miall, 1977, Loughney and Badgley, 2017). Fossils in the Dove Spring Formation are most common from this stage of basin development, and are primarily recovered from overbank and floodplain deposits (Whistler et al., 2009)

In the Dove Spring Formation, the interval deposited between 10.5 and 9.5 Ma is associated with the highest species richness, based on occurrences of at least 56 species of large mammals. Ungulates (including horses, antilocaprids, camels, and oreodonts) are well-represented by multiple species. Singletons and rare taxa such as carnivores are most common in Member 5, which supports the hypothesis that this interval coincided with enhanced fossil preservation. Curiously, horses disappeared from the fossil record of the Dove Spring Formation by 9.0 Ma, while other groups persisted (Fig. 6). The last appearance of horses by this time could be due to ecosystem changes that led to their extirpation or local extinction. Continuing studies of paleoenvironments and ungulate paleoecology will aid analyses of changing faunal richness in the Dove Spring Formation through time.

Both formations exhibit greater pedogenic development toward the top of their sections, although the expression of pedogenic features differs between the upper Barstow and Dove Spring formations. Paleosols in the upper Barstow Formation are developed in fine-grained ephemeral-wetland and floodplain deposits and contain numerous fossil localities. In the upper Dove Spring Formation, pedogenic features are expressed as abundant silicified root casts in massive, coarse-grained sandstones. Fossils occur less frequently in the upper Dove Spring Formation, and the poor preservation potential may be related to the abundance of silica in its sediments as well as the potential predominance of high-energy depositional environments.

Discussion

The Barstow and Dove Spring formations represent sedimentary sequences deposited during different phases of Miocene tectonic activity in the Mojave region. These formations have the highest mammal-species richness in the Mojave region, and these records are important for understanding faunal geographic relationships within the Great Basin at this time (Badgley et al., 2015). Despite preserving similar numbers of mammal species, the lithological and facies characteristics of the Barstow and Dove Spring formations differ over their extents. Key differences in the geography and tectonic history of these depositional basins and the climate setting during which they formed may contribute to their differing facies composition.

Tectonic setting and basin history may be important factors contributing to the development of different facies within the Barstow and Dove Spring formations. The Barstow Formation in the central Mojave Desert (Fig. 1)

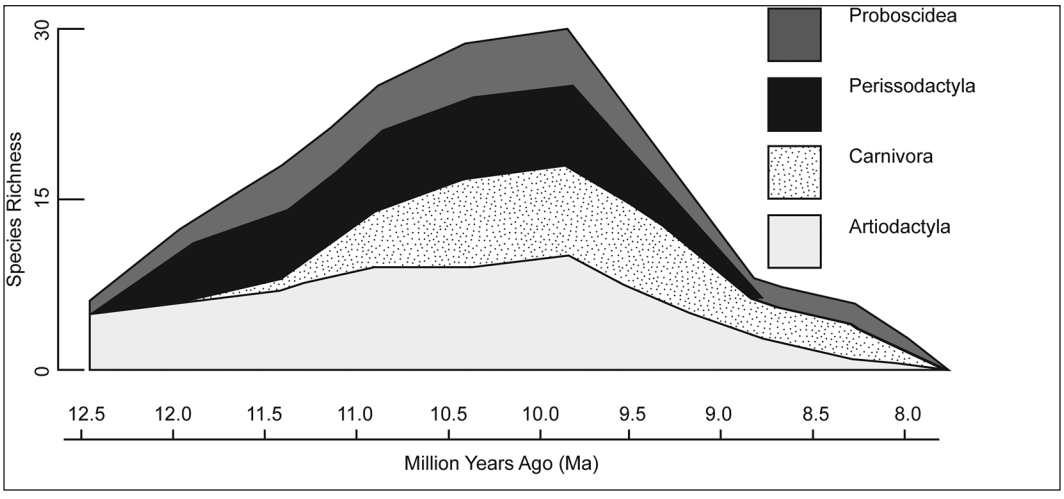

Figure 6: Species richness of major orders in the Dove Spring Formation. The rapid disappearance of perissodactyls (~9.0 Ma) prior to other species suggests a potential change in environmental conditions. The abundance of rare taxa such as carnivores during the same interval suggests that taphonomic conditions captured a reasonable sample of large mammals.

is part of the Mojave tectonic block. The Early Miocene development of the central Mojave metamorphic core complex and associated extension along the Waterman Hills detachment fault was the major tectonic event that created depositional basins in the central Mojave region (Fillmore and Walker, 1996; Glazner et al., 2002). The magnitude of extension is debated (Anderson, 2017), but the Barstow Formation represents the post-extensional deposits into the extended basin (Fillmore and Walker, 1996). Loughney and Badgley (2017) interpreted decreasing subsidence and accommodation rates in the post-extensional basin as important controls on the development of the major facies of the Barstow Formation. The overall fining-upward characteristics of the Barstow Formation and the change from alluvial fan to floodplain-dominated environments reflects the transition from a closed-drainage to open-drainage basin with decreasing accommodation.

In contrast, the tectonic history of the El Paso Basin is more complicated than that of the Barstow Formation. The western boundary of the El Paso Basin is the Sierra Nevada frontal fault system, and the east-west trending El Paso fault is located at its southern margin (Loomis and Burbank, 1988). Movement along the El Paso fault at ~10 Ma contributed to syndepositional counterclockwise rotation of the basin and its lateral displacement up to 64 km to the west (Loomis and Burbank, 1988; Smith et al., 2002). This period of deformation coincides with a sediment-accumulation rate that remained nearly constant for approximately 1.5 million years. This indicates steady basin growth as deposition occurred, generating new habitats for mammals that were preserved between 11.0 and 9.5 Ma. Basin rotation was followed by west-northwest tilting and extension that deformed strata beginning at 9 Ma (Loomis and Burbank, 1988).

Climate change through the Middle Miocene is another important factor in facies and environmental development in the Barstow and El Paso basins. Significant climatic transitions in the Miocene included the Middle Miocene Climatic Optimum (MMCO), a global warming episode between 17 and 14 Ma, and the subsequent Middle Miocene Climatic Transition (MMCT; <14 Ma), a climatic cooling trend that continued through the end of the Miocene (Zachos et al., 2001). The Barstow Formation (19.3 to 13.0 Ma) was deposited during the MMCO and beginning of the MMCT, whereas the Dove Spring Formation (12.5 to 8.0 Ma) was deposited through the MMCT.

Leading up to the MMCO in the Barstow Basin, conditions may have been relatively dry and trending toward increasing aridity, as indicated by increasing gypsum and enrichment of δ18O values from the saline-alkaline lacustrine deposits in the Calico Mountains (Park, 1995; Park and Downing, 2000). During the MMCO, depleted deuterium (D) isotopic values and other paleoenvironmental indicators from the Barstow Formation indicate that conditions in the Barstow Basin were wet in the Mud Hills. These data correspond with interpretations of summer-dominant precipitation patterns in western North America based on paleofloral compositions from the Barstow Formation and other Middle Miocene formations (Axelrod, 1939; O'Connor, 1982). By the time of deposition of the uppermost portion of the Barstow Formation, enriched δ13C and δD values from sedimentary proxies indicate drier conditions in the basin during the MMCT (Loughney et al., 2020). Drying conditions associated with global cooling coincided with a shift to winter-dominant precipitation regimes in western North America (Lyle et al., 2008).

The Dove Spring Formation was deposited entirely during the MMCT, and may have been subject to increasingly seasonal precipitation patterns. Horton and Chamberlain (2006) reported enriched δ18O from carbonates and smectite clays from the El Paso Basin, which they interpreted as resulting from increased evaporation of surface waters combined with a shift in airmass pathways from western to southern sources. Values of δ18O from serially sampled mammal teeth also display a strong intratooth seasonal signal, although changes in magnitude have not yet been examined through the section (Bowman et al., 2017).

The changing species composition of the Dove Spring Formation (Fig. 6) may also reflect a change in moisture during its deposition. The abundance of large-mammal species (such as horses and antilocaprids) adapted for cursorial movement in open grassland habitats increases through the section until a peak in species richness midway through Member 5 (Fig. 6). Horses subsequently disappear from the record in Member 6 (Illius, 1997; Whistler et al., 2009). C_3 vegetation dominated the Late Miocene Dove Spring grasslands (Bowman et al., 2017; Liddy et al., 2018), consistent with the modern vegetation composition and winter-dominant precipitation regime of California (Lyle et al., 2008). Increasingly seasonal climate in the Late Miocene may have caused changes in habitat or vegetation that could have contributed to the disappearance of horses from the Dove Spring Formation after 9 Ma. Further study of paleoclimate of the Dove Spring Formation will allow us to examine the effects of climate on mammalian distribution and paleoecology.

Summary

The Barstow and Dove Spring formations are Miocene sedimentary sequences from the Mojave region of California that preserve well-known fossil-mammal assemblages. Although these formations share some aspects of geography, age, and paleontology, they are also distinct in many ways. The two formations differ lithologically, and consequently, the facies characteristics of fossiliferous strata differ as well. In the Barstow Formation, mammal fossils occur primarily in fine-grained deposits representing proximal-floodplain and wetland settings. In the Dove Spring Formation, mammal

fossils occur in medium-grained sandstone representing near-channel fluvial settings.

Differences in basin history and climate likely contributed to the development of facies within both formations. The Barstow Formation was deposited following active extension under declining rates of subsidence and accommodation. The Dove Spring Formation was deposited through prolonged episodes of basin translation, rotation, and extension. The environments of the Barstow Formation may have had greater moisture availability than those of the Dove Spring Formation, particularly during the Middle Miocene Climatic Optimum. Cooling climate during the Middle Miocene Climatic Transition coincided with drying in the upper Barstow Formation; this cool, dry climate regime persisted through deposition of the Dove Spring Formation. Mammal diversity in the Barstow and El Paso basins remained high during intervals of tectonic and climatic change, indicating that environments in these basins were attractive habitats for mammals, despite their differences.

Acknowledgments

We thank Catherine Badgley, Xiaoming Wang, Rachel Thorpe, Anna Harkness, Tara Smiley, Bian Wang, Ethan VanValkenberg, and Wesley Johnston for their assistance in the field. We thank David Miller for providing helpful comments and suggestions on the manuscript.

References

Alf, R. M., 1966, Mammal trackways from the Barstow Formation, California: Bulletin of the Southern California Academy of Sciences, v. 65, no. 4, p. 258–264.

Anderson, R. E., 2017, Major revisions of the timing, style, magnitude, and cause of Early Miocene extension in the Central Mojave metamorphic core complex and subsequent role of the Eastern California Shear Zone, *in* Reynolds, R.E., ed., ECSZ Does It: Revisiting the Eastern California Shear Zone, The 2017 Desert Symposium Field Guide and Proceedings: Zzyzx, California, California State University Desert Studies Consortium, p. 60–70.

Andrew, J. E., Walker, J. D., and Monastero, F. C., 2014, Evolution of the central Garlock fault zone, California: A major sinistral fault embedded in a dextral plate margin: Geological Society of America Bulletin, v. 127, no. 1/2, p. 227–249.

Axelrod, D. I., 1939, A Miocene Flora from the Western Border of the Mohave Desert: Washington, D.C., Carnegie Institution of Washington, v. 516, 129 p.

Badgley, C., Smiley, T. M., and Loughney, K. M., 2015, Miocene mammal diversity of the Mojave region in the context of Great Basin mammal history, *in* Reynolds, R. E., ed., Mojave Miocene: The 2015 Desert Symposium Field Guide and Proceedings: Zzyzx, California, California State University Desert Studies Consortium, p. 34–43.

Bowman, C. N., Wang, Y., Wang, X., Takeuchi, G. T., Faull, M., Whistler, D. P., and Kish, S., 2017, Pieces of the puzzle: Lack of significant C_4 in the late Miocene of southern California: Palaeogeography, Palaeoclimatology; Palaeoecology, v. 475, p. 70–79.

Dixon, T. H., and Xie, S., 2018, A kinematic model for the evolution of the Eastern California Shear Zone Zone and Garlock Fault, Mojave Desert, California: Earth and Planetary Science Letters, v. 494, p. 60–68.

Fillmore, R. P., and Walker, J. D., 1996, Evolution of a supradetachment extensional basin: The lower Miocene Pickhandle basin, central Mojave Desert, California, *in* Beratan, K. K., ed., Reconstructing the History of Basin and Range Extension Using Sedimentology and Stratigraphy: Geological Society of America Special Paper 303, p. 107–126.

Garrison, J., and Reynolds, R.E., 2015, A fresh look at the Pickhandle Formation: Pyroclastic flows and fossiliferous lacustrine sediments, *in* Reynolds, R.E., ed., Mojave Miocene: The 2015 Desert Symposium Field Guide and Proceedings: Zzyzx, California, California State University Desert Studies Consortium, p. 59–62.

Glazner, A. F., Walker, J. D., Bartley, J. M., and Fletcher, J. M., 2002, Cenozoic evolution of the Mojave block of southern California: Geological Society of America Memoirs, v. 195, p. 19–41.

Golombek, M. P., and Brown, L. L., 1988, Clockwise rotation of the western Mojave Desert: Geology, v. 16, p. 126–130.

Horton, T. W., and Chamberlain, C. P., 2006, Stable isotopic evidence for Neogene surface downdrop in the central Basin and Range Province: Geological Society of America Bulletin, v. 118, no. 3–4, p. 475–490.

Illius, A. W., 1997, Physiological adaptation in savanna ungulates: Proceedings of the Nutrition Society, v. 56, p. 1041–1048.

Ingersoll, R. V., Devaney, K. A., Geslin, J. K., Cavazza, W., Diamond, D. S., Heins, W. A., Jagiello, K. J., Marsaglia, K. M., Paylor, E. D., II, and Short, P. F., 1996, The Mud Hills, Mojave Desert, California: Structure, stratigraphy, and sedimentology of a rapidly extended terrane, *in* Beratan, K. K., ed., Reconstructing the History of Basin and Range Extension Using Sedimentology and Stratigraphy: Geological Society of America Special Paper 303, p. 61–84.

Liddy, H. M., Feakins, S. J., Corsetti, F. A., Sage, R., Dengler, N., Whistler, D. P., Takeuchi, G. T., Faull, M., and Wang, X., 2018, Photosynthetic pathway of grass fossils from the upper Miocene Dove Spring Formation, Mojave Desert, California: Palaeogeography, Palaeoclimatology; Palaeoecology, v. 490, p. 131–140.

Lindsay, E. H., 1995, *Copemys* and the Barstovian/Hemingfordian Boundary: Journal of Vertebrate Paleontology, v. 15, no. 2, p. 357–365.

Loomis, D. P., and Burbank, D. W., 1988, The stratigraphic evolution of the El Paso basin, southern California: Implications for the Miocene development of the Garlock fault and uplift of the Sierra Nevada: Geological Society of America Bulletin, v. 100, p. 12–28.

Loughney, K.M., 2017, Environments of the Barstow Formation in the Mud Hills, southeastern California, in, Reynolds, R.E., ed., ECSZ Does It: The 2017 Desert Symposium Field Guide and Proceedings, California State University Desert Consortium, Zzyzx, p. 235-238.

Loughney, K. M., and Badgley, C., 2017, Facies, environments, and fossil preservation in the Barstow Formation, Mojave Desert, California: PALAIOS, v. 32, no. 6, p. 396–412.

Loughney, K. M., Hren, M. T., Smith, S. Y., and Pappas, J. L., 2020, Vegetation and habitat change in southern California through the Middle Miocene Climatic Optimum: Paleoenvironmental records from the Barstow Formation, Mojave Desert, USA: Geological Society of America Bulletin, v. 132, no. 1–2, p. 113–129.

Lyle, M., Barron, J., Bralower, T. J., Huber, M., Olivarez Lyle, A., Ravelo, A. C., Rea, D. K., and Wilson, P. A., 2008, Pacific Ocean and Cenozoic evolution of climate: Reviews of Geophysics, v. 46, no. 2, p. 1–47.

MacFadden, B. J., Swisher, C. C., III, Opdyke, N. D., and Woodburne, M. O., 1990, Paleomagnetism, geochronology, and possible tectonic rotation of the middle Miocene Barstow Formation, Mojave Desert, southern California: GSA Bulletin, v. 102, no. 4, p. 478–493.

McQuarrie, N., and Wernicke, B. P., 2005, An animated tectonic reconstruction of southwestern North America since 36 Ma: Geosphere, v. 1, no. 3, p. 147–172.

Miall, A. D., 1977, A review of the braided-river depositional environment: Earth-Science Reviews, v. 13, p. 1-62.

O'Connor, S. K., 1982, Palynology of Barstow Formation (Miocene), Rainbow Basin, southern California [abs]: AAPG Bulletin, v. 66, no. 10, p. 1696–1697.

Park, L. E., 1995, Geochemical and paleoenvironmental analysis of lacustrine arthropod-bearing concretions of the Barstow Formation, southern California: PALAIOS, v. 10, no. 1, p. 44–57.

Park, L. E., and Downing, K. F., 2001, Paleoecology of an exceptionally preserved arthropod fauna from lake deposits of the Miocene Barstow Formation, southern California, USA: PALAIOS, v. 16, no. 2, p. 175–184.

Parsons, T., 2006, The Basin and Range Province, *in* Olsen, K.H., ed., Continental Rifts: Evolution, Structure, Tectonics: Developments in Geotectonics, v. 25, p. 277–326.

Singleton, J. S., and Gans, P. B., 2008, Structural and stratigraphic evolution of the Calico Mountains: Implications for early Miocene extension and Neogene transpression in the central Mojave Desert, California: Geosphere, v. 4, no. 3, p. 459–479.

Smith, E. I., Sánchez, A., Keenan, D. L., and Monastero, F. C., 2002, Stratigraphy and geochemistry of volcanic rocks in the Lava Mountains, California: Implications for the Miocene development of the Garlock fault, *in* Glazner, A. F., Walker, J. D., and Bartley, J. M., eds., Geologic Evolution of the Mojave Desert and Southwestern Basin and Range: Geological Socieyt of America Memoir 195, p. 151–160.

Tabor, N. J., and Myers, T. S., 2015, Paleosols as indicators of paleoenvironment and paleoclimate: Annual Review of Earth and Planetary Sciences, v. 43, no. 1, p. 333–361.

Whistler, D. P., Takeuchi, G. T., Groves, L. T., and Wang, X., 2013, Western Mojave Desert geology and vertebrate paleontology with special emphasis on the Dove Spring Formation, Society of Vertebrate Paleontology Annual Meeting, Field Trip Guidebook, 76 p.

Whistler, D. P., Tedford, R. H., Takeuchi, G. T., Wang, X., Tseng, Z. J., and Perkins, M. E., 2009, Revised Miocene biostratigraphy and biochronology of the Dove Spring Formation, Mojave Desert, California: Museum of Northern Arizona Bulletin, v. 65, p. 32.

Woodburne, M. O., Tedford, R. H., and Swisher, C. C., III, 1990, Lithostratigraphy, biostratigraphy, and geochronology of the Barstow Formation, Mojave Desert, southern California: Geological Society of America Bulletin, v. 102, p. 459–477.

Zachos, J. C., Pagani, M., Sloan, L. C., Thomas, E., and Billups, K., 2001, Trends, rhythms, and aberrations in global climate 65 Ma to present: Science, v. 292, p. 686–693.

Correlations along a 140 km transect in the westernmost Peach Spring Tuff, and tracing changing facies through depositional environments

David C. Buesch
350 N. Akron Rd., Moffett Field, CA, 94035, dbuesch@usgs.gov

ABSTRACT—Tephrochronology is the correlation of tephra beds and tuffs by various means, and it is an important tool in refining stratigraphic and structural interpretations. The 18.78 Ma Peach Spring Tuff (PST) is a large-volume ignimbrite that was deposited across a ~200 km x 360 km area of southeastern California, northwestern Arizona, and southern Nevada. The PST is a valuable stratigraphic marker in several stratigraphic sequences in this area. In this study, the field characteristics, mineral abundance, and feldspar composition of eight ignimbrite locations are examined along a 140 km swath across the northwestern extent of the PST in the Mojave Desert. Five of the ignimbrites have geochronologic or paleomagnetic data and are PST. Three ignimbrites do not have supporting geochronologic and/or paleomagnetic data, but one has physical stratigraphy, mineral abundances and properties, and feldspar compositions that indicate it is PST; however, two have enough similarities to be possible PST. In 53 regionally dispersed locations of the PST, including the three possible PST ignimbrites in this study, the overlying and underlying sedimentary deposits are described in order to determine the depositional changes, if any, resulting from the geologically instantaneous deposition of the ignimbrite. Of the 53 locations, 37 locations allow interpretation of the pre- and post-PST depositional environments. Of the 37, 25 have finer grained and thinner beds above the PST compared to below, indicating that the deposition of the ignimbrite resulted in (1) disruption and change in local stream gradients and sediment supply, (2) a long period of time for depositional systems to propagate to and regenerate at a location, or (3) a lack of re-establishment of the pre-PST environments. However, 12 have no significant difference pre- and -post PST beds, so there apparently was minimal disruption to the depositional system.

Introduction

Sedimentation, depositional environments, and sedimentary facies vary across basins, and one method to help identify laterally equivalent facies is where fallout tephra deposits or pyroclastic flow deposits (ignimbrites) are deposited in a short period of time (possibly only days). Tephrochronology is the correlation of tephra deposits using glass morphology or composition, or mineral abundances or mineral composition (Sarna-Wojcicki and Davis, 1991). Tephrostratigraphy is correlation of tuffs by physical and chemical characteristics. Tephrochronology and tephrostratigraphy are especially powerful where associated with geochronologic data. In the area of southeastern California, southern Nevada, and western Arizona, during the Miocene there were many sedimentary basins resulting a variety of structural and tectonic settings (Sherrod and Nielson, 1993). The Peach Spring Tuff (PST), originally described by Young and Brennan (1974) and redefined by Billingsley and others (1999), was deposited across ~200 km x 360 km area (Glazner and others, 1986; Buesch, 1991; Fig. 1). The 18.78±0.02 Ma PST erupted from the Silver Creek Caldera that was subsequently disrupted and separated across the Colorado River Extensional Corridor (Ferguson and others, 2013; Fig. 1), and the super eruption produced ~650 km^3 of outflow ignimbrite (Buesch, 1991) and an estimated ~650 km^3 of intra-caldera ignimbrite (Ferguson and others, 2013). Correlation of the PST is based on tephrostratigraphic data (stratigraphic characteristics and mineral abundances and composition; Gusa and others, 1987; Buesch, 1993; Buesch, 2015), paleomagnetic data (Hillhouse and Wells, 1991; Hillhouse and others, 2010), and $^{40}Ar/^{39}Ar$ and U/Pb geochronology (Ferguson and others, 2013; Miller and others, 2010). This broad distribution of the PST makes it an important tephrostratigraphic marker for stratigraphic and structural evolution in this area (Glazner and others, 1986; Fig. 1).

This paper describes three main topics. First is to summarize physical characteristics and feldspar mineral compositions of the Peach Spring Tuff

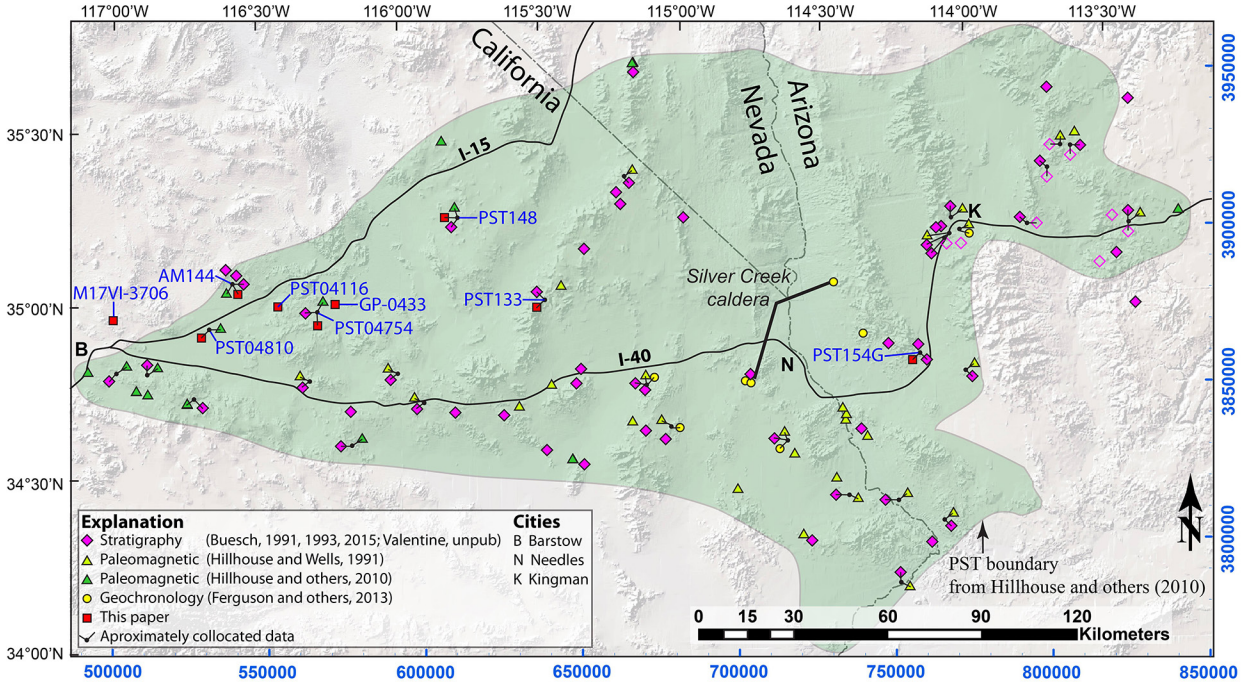

Figure 1. Mapped distribution of the Peach Spring Tuff in southeast California, southern Nevada, and northwest Arizona. The Silver Creek caldera is the source of the Peach Spring Tuff, and two sides of the caldera were separated across the Colorado River External Corridor (Ferguson and others, 2013). Eight locations of the Peach Spring Tuff, or possible correlatives of the ignimbrite, are shown in an approximately west-trending, 140 km long swath in the northwest part of the PST distribution area.

(PST) for tephrostratigraphic purposes. Second is the tephrostratigraphic correlation of ignimbrites in eight locations in the northwestern part of the PST distribution. Five locations are known to be PST based on geochonologic or paleomagnetic methods. The other three have not been studied previously with tephrostratigraphic methods; one is consistent with being PST, and two are possible PST. Third is to document and interpret the sedimentary facies in the rocks below and above the PST. A regional study of pre- and post-PST sedimentary facies included 47 locations (Buesch, 1991), and this paper includes an additional six locations.

Peach Spring Tuff stratigraphy

Exposures of the PST outflow sheet are 0-140 m thick and formed onlap deposits on highlands and as valley-fill deposits (Buesch and Valentine, 1986; Buesch, 1991). Thickness of the PST varies locally depending on the basins traversed by the PST parental pyroclastic flow (or pyroclastic density current, PDC), but there is a regional decrease in thickness toward the distal edges. For instance, recently identified exposures of the PST in the northwest Spanish Canyon area near Alvord Mountain, California, are ~1 m thick (Buesch, 2014). Highland and valley-fill deposits help define Miocene valleys, or at least one side of a valley. Most PST exposures are valley-fill deposits, but the geometry of the valley is difficult to determine except from stratigraphic facies of the subjacent and superjacent deposits.

Physical stratigraphy

The PST ignimbrite has a well-formed vitroclastic texture of fine- to coarse-grained ash matrix, consisting of glass shards with crystal, pumice, and lithic clasts, that supports larger crystal fragments (sanidine and plagioclase grains up to 3 mm, hornblende grains up to 2 mm, and biotite up to 1 mm) with lapilli to bomb size pumice and lithic clasts. Crystals (and fragments thereof) are typically 8-20 percent of the rock, most notably sanidine > plagioclase ± quartz, <2 percent hornblende ≥ biotite ± clinopyroxene, and trace amounts of apatite, allanite, perrierite (or chevkinite), and pyrrhotite (Buesch, 1993). In the Kingman, Arizona, area there are stratigraphic variations with (1) largest sanidine:plagioclase ratios (of abundance based on point counting or grain counts) and lowest hornblende:biotite ratios near the base, (2) pleochroism in hornblende and biotite, and (3) clinopyroxene occurs high in the section (Buesch, 1987). These stratigraphic relations can be traced laterally, and partially mantle topographic highlands such as cinder cones and bedrock highlands. This general stratigraphy also occurs throughout the PST distribution, except in more distal sections the mineral assemblages and properties that are higher in the section in Kingman are closer to the base. Lithic clasts (or accidental clasts) can be derived from magma chamber or conduit wall rocks or incorporated from the ground surface into the parental PDC as locally derived lithic clasts (Buesch, 1992b; Roche and others, 2016).

Post-depositional processes formed many of the fairly distinctive field characteristic of the PST. The ignimbrite

was deposited from a hot PDC, and in the PST exposed in Kingman, Arizona, the depositional temperature was 664 to 780 °C (Riehle, 2015). The ignimbrite typically has a compaction (welding) profile with moderately to densely compacted rock in deposits >15 m thick, and in many sections the densely compacted rock forms 30-50 percent of the section and moderately compacted rock 30-40 percent. In 3-4 m thick deposits, a maximum of partially compacted ignimbrite can form. Noncompacted to partially compacted ignimbrite (and locally moderately and densely compacted rock) are typically vitric, but the original glass can be altered to zeolite or clay minerals (typically by interaction with groundwater). Locally, densely compacted ignimbrite developed lithophysae while the rock was still glass (and later crystallized). Where moderately to densely compacted (and some partially compacted), the glass crystallized during cooling and formed fine- to very fine-grained equigranular groundmass (in Kingman, at 47 m in a 75-m thick section grains are 1-3 μm with dispersed grains 4-6 μm), and the vitroclastic texture can be preserved by axiolitic texture where grains grew from the shard wall inward. Locally, glass was corroded by hot vapor. During the cooling of the ignimbrite, minerals (sublimates) were deposited from the vapor and partially lithified the upper partially compacted rock. In the western exposures, deposits as thin as 4-7 m are partially compacted and have at least some (incipient) crystallization.

Timing of deposition of the PST relative to pre- and post- sedimentary rocks can be broadly inferred. Locally, the PST was deposited on sedimentary rocks with a poorly developed paleosol, indicating deposition on a stable geomorphic surface. The top of an ignimbrite such as the PST is noncompacted and vitric, and the preservation of this part of the ignimbrite provides evidence for no erosion before subsequent sedimentation. Below the top there is a downward gradational increase in compaction to partially to densely compacted ignimbrite, and noncompacted and partially compacted vitric rocks are more readily eroded whereas moderately to densely compacted vitric rocks are resistant to erosion (Table 1). At some depth below the top, typically there is a contact between vitric and crystallized, or vitric and vapor-phase lithified rock. In the PST, the upper contact of (1) moderately to partially compacted ignimbrite, or (2) crystallized or vapor-phase lithified to vitric partially compacted ignimbrite, can be sharp and 3-10 m below the depositional top of the ignimbrite, with a good example in the southeastern Black Mountains, Arizona (location PST154G in Fig. 1; Fig. 2 in Buesch, 1991). Where vitric and noncompacted rock near the top of the deposit is preserved, subsequent sedimentation probably occurred shortly after deposition of the PST. If sediment was deposited on crystallized or moderately to partially compacted PST, the noncompacted and vitric material was eroded, and it is difficult to constrain the elapsed time before sediment deposition.

Mineral composition stratigraphy

Mineral compositions influence the physical and optical properties of the minerals, but also provides detailed and quantified data for understanding the stratigraphy of the PST. This section describes how composition was measured using electron microprobe (EMP) and scanning electron microscope (SEM) techniques, and general interpretations of the PST stratigraphy.

Micro-analytical methods

The locations of points analyzed by EMP and SEM techniques are based on a variety of textural settings in a thin section including phenocrysts in pumice clasts, grains with attached glass, phenocrysts or grains in lithic clasts, crystal clots, and grain fragments with no textural context (that is, broken edges only). Composition of some crystal clots and broken grains are the same as those of phenocrysts in pumice clast and grains with attached glass, and support definition of magmatic compositions from the PST parental magma chamber compared to other compositions of "accidental" grains.

Mineral composition data in this paper are from three generations of collecting: (1) 1989-1990 on an Electron microprobe (EMP) at Los Alamos National Laboratory (Buesch, 1992a, unpublished Ph. Ph.D. dissertation; Buesch, 1993), (2) 2015 on an EMP at the U.S. Geological Survey (USGS) in Menlo Park (Buesch, 2015), and (3) on a scanning electron microscope (SEM) at the USGS in Menlo Park (this paper). EMP and SEM data collection differ, but as demonstrated in this paper, are reliably comparable. EMP data are quantitative wavelength dispersive spectrometry (WDS) where specific elements (ultimately reported as weight percent oxides) are specifically measured, and reliably report feldspar orthoclase (OR), albite (AB), or anorthite (AN) endmember values to 0.2 percent. The 1990 analyses used a beam diameter of 5 μm, with count times of 20 seconds for Si, Al, Ca, Ba, Na, and K, and 90, 60, and 30 seconds for Fe, Mg, and Sr, respectively. The 2015 analyses used a beam diameter of 5 μm, and the detectors (that had different designs from those used in 1990) were not as flexible in count times per element, so all were counted for 20 seconds. To compare the two generations of data, a sample from 1990 was reanalyzed and 75 points were relocated based on visual positioning of annotated photomicrographs, and the difference (1990 value minus 2015 value) was calculated. Of 31 points in 16 plagioclase grains, the average difference in AN was 0.01 with a standard deviation of 1.44, and OR was 0.36 with a standard deviation of 0.79. Of 44 points in 17 sanidine grains, the average difference in AN was -0.11 with a standard deviation of 0.38, and OR was 0.94 with a standard deviation of 2.05.

SEM data, which are considered more semi-quantitative than EMP data, are based on curve-fitting algorithms of backscatter emissions (BSE), and oxide percentages less than 1 or 2 percent have an increased

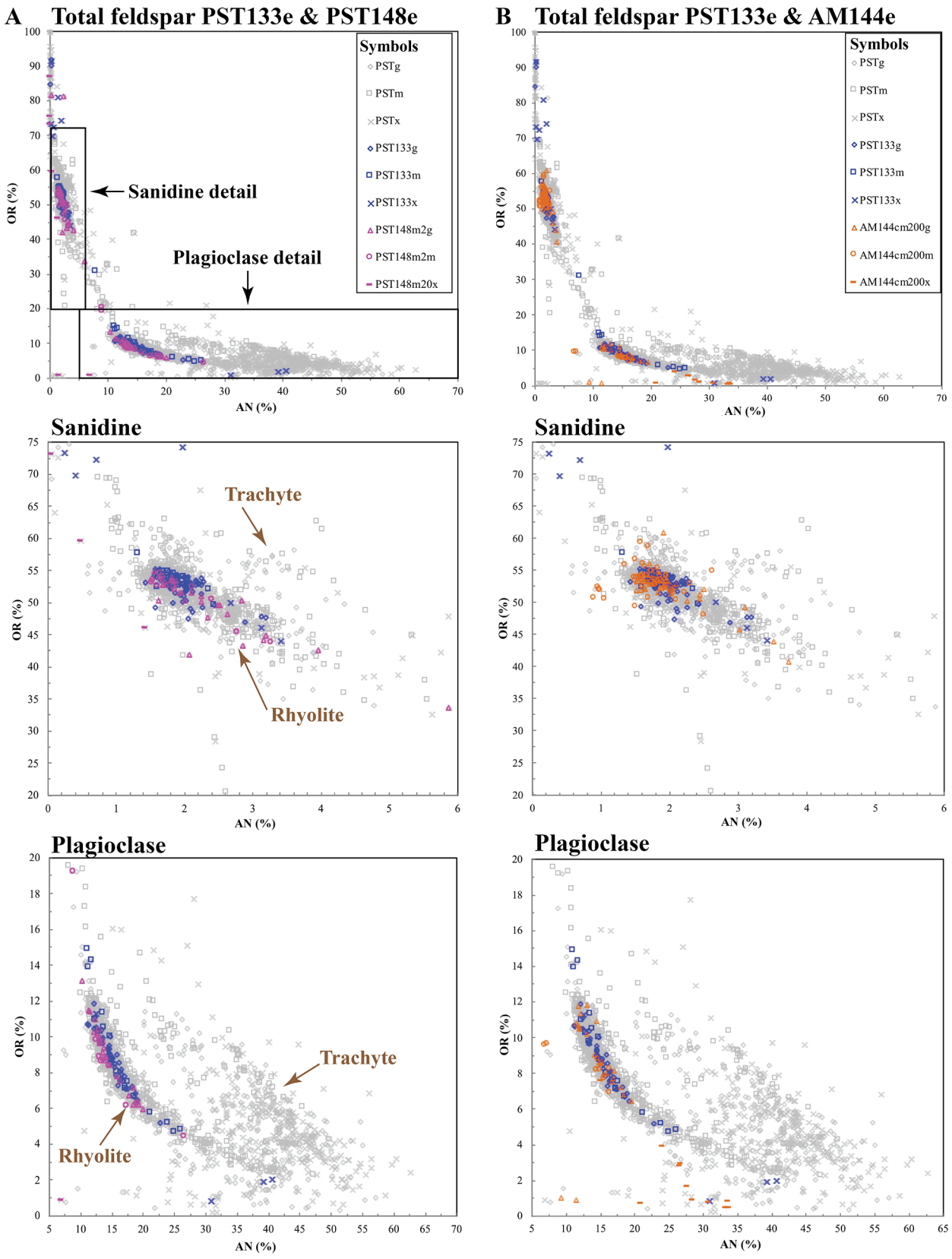

Figure 2. Graphs of electron microprobe determined OR versus AN endmembers in feldspars for the Peach Spring Tuff from the Providence Mountains, Granite Springs, and Spanish Canyon. (A) Total Peach Spring Tuff (PST), Providence Mountains (PST133D), and Granite Springs (PST148). (B) Total Peach Spring Tuff (PST), Providence Mountains (PST133D), and southeastern Spanish Canyon area (AM144). (A and B) Three graphs of total feldspar analyses with details for sanidine and plagioclase. Textural classifications of grains include "g" as non-diagnostic fragments, "m" as magmatic grains with attached glass, in pumice, or as mantled feldspar or crystal clots, and "x" as grains in xenoliths.

amount of uncertainty. The typical sample area was about 5x5 µm (some rectangular areas had similar total areas), with count times of 10 seconds. To assess the accuracy of the SEM data compared to EMP data, a thin section (AM144cm200) from the 2015 study was analyzed using the previously used method of relocation of specific points along, and collection from other crystal fragments to compare the general distribution of the values. For 53 specific point comparisons, the SEM values were subtracted from the EMP values. Of 13 points in 7 plagioclase grains, the average difference in AN was 0.3 with a standard deviation of 0.4, and OR was -0.1 with a standard deviation of 0.4. Of 40 points in 17 sanidine grains, the average difference in AN was -0.3 with a standard deviation of 0.3, and OR was 0.5 with a standard deviation of 1.5.

Mineral composition stratigraphy in the Peach Spring Tuff

The regional, local, and stratigraphic variations in crystal fragments, and their composition, can be used for correlation of PST deposits, and enable inferences of the eruption history of, transportation in, and deposition from the parent PDC. Electron microprobe values for minerals including feldspar, hornblende, biotite, pyroxene, magnetite, and ilmenite, and glass compositions from the PST are distinct from other tuffs in southeastern California and western Arizona (Buesch, 1993). PST feldspar composition in sanidine and plagioclase forms two diffused but defined trends that are consistent with rhyolite and trachyte magma, and there are some grains that are transitional between rhyolite and trachyte (Buesch, 1992a, unpublished Ph. Ph.D. dissertation; Buesch, 1993). For comparison with the locations described in this paper, in the Kingman area, Arizona, the compositionally zoned PST has an average sanidine composition is 53.5±5.2 OR and 1.8±0.8 AN, and average plagioclase is 8.2±8.4 OR and 16.72±10.6 AN (Buesch, 1993).

Correlation of ignimbrites in eight locations

Eight locations of ignimbrite, five with known exposures of the PST and three possible PST, were studied along a 140-km-long swath in the northwest exposures of the PST (Fig. 1). The correlations of the ignimbrites are based on physical stratigraphy, mineral type and abundance, and feldspar composition.

Peach Spring Tuff

1. Providence Mountains

The PST exposed in the northeastern Providence Mountains (PST 133 in Fig. 1) is up to 70-m thick and was mapped as part of the study of the Woods Mountains volcanic center (McCurry, 1985). The southern exposures of the PST in the Providence Mountains are up to 60-m thick (Stone and others, 2017). Wells and Hillhouse (1989) and Hillhouse and Wells (1991) used paleomagnetic properties to correlate exposures of the stratigraphically lowest ignimbrite to the PST. The physical stratigraphy of the PST includes the typical compaction and crystallization profiles, the mineral abundances and pleochroism of biotite are consistent with the typical ranges in the PST, and there is only a possible trace of small oxidized hornblende (Buesch, 1993; Stone and others, 2017). EMP mineral composition was determined on samples 30 cm and 29 m above the base in a 35-m thick section (Buesch, 1992, unpublished Ph. Ph.D. dissertation). Regionally, PST feldspars have compositions consistent with rhyolite and trachyite magmas, as portrayed by the two arcuate trends in binary plots of OR versus AN endmembers (Buesch, 1992a, unpublished Ph. Ph.D. dissertation; Buesch, 1993), and data from PST133 (30 cm and 28 m) samples are consistent with only the rhyolite trend (Fig. 2A).

2. Granite Spring

The Granite Spring locality is located on the west side of Cima Dome (PST148 in Fig. 1), and the 3-15 m thick exposure of the PST was confirmed as PST using paleomagnetic properties (Hillhouse and Wells, 1991) and sanidine single-crystal $^{40}Ar/^{39}Ar$ ages (Hillhouse and others, 2010). The ignimbrite has well-preserved vitroclastic texture, is partially compacted, partially crystallized, and the upper noncompacted part was eroded away (Table 1). Mineral abundances and pleochroism of hornblende and biotite are consistent with the typical ranges in the PST (Buesch, 1993). Feldspar mineral composition is comparable to that from the Providence Mountains (PST133), and replicates the rhyolite compositional trend (Fig. 2A).

3. Spanish Canyon area (Alvord Mountain area)

The PST is part of the 24-123 m thick Spanish Canyon Formation in the Alvord Mountain area and was mapped by Byers (1960) with refined stratigraphic descriptions by Buesch (2014) (AM144 Fig. 1). Hillhouse and others (2010) confirmed that the paleomagnetic properties of the partially compacted and crystallized ignimbrite in the southeast exposure near sample AM144 were those of the PST.

Exposures of the PST can be traced ~11 km around the Spanish Canyon anticline where it thins from 7.0 m in the southeast to 1.5 m in the northwest. The north-northwest thinning of the PST probably represents part of the distal edge of the ignimbrite as the parental PDC flowed across (and up) a very broad, long, shallow-gradient valley with low relief across the basin floor. In all exposures, the vitroclastic texture is well preserved, but in the 7-m thick section in the southeast the glass in the core was crystallized, in the 3-5 m thick sections in the east the glass was altered to zeolite or clay minerals (either during cooling by auto-devitrification, or well after cooling by interaction with groundwater), and in the 1.5-m thick

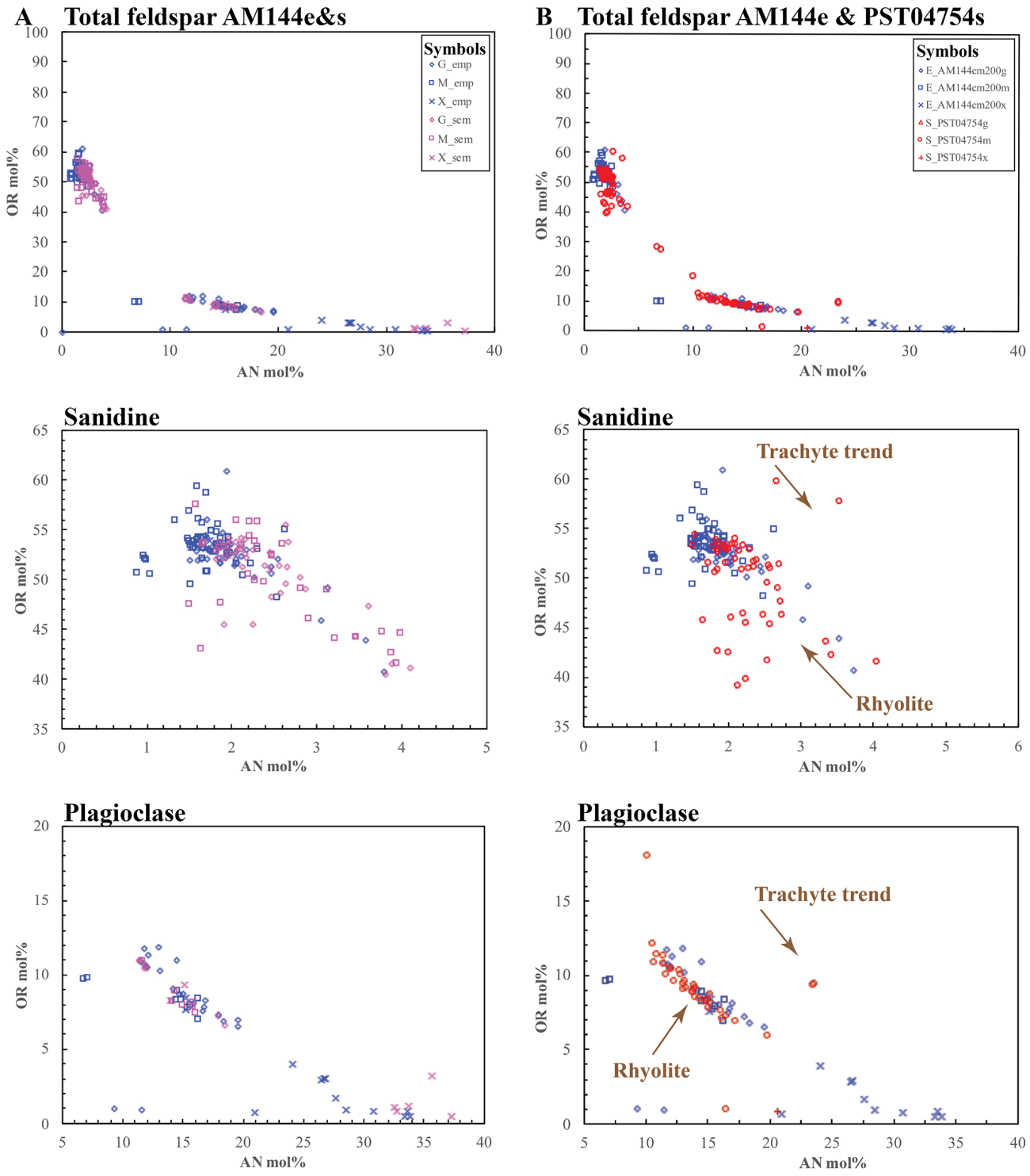

Figure 3. Graphs of electron microprobe (EMP) and scanning electron microscope (SEM) determined OR versus AN endmembers in feldspars for the Peach Spring Tuff from Spanish Canyon and southeast Baxter Wash. (A) AM144 EMP and SEM. (B) AM144 EMP and PST04754 SEM in southeast Baxter Wash. Analytical method EMP as "emp" or "E", SEM as "sem" or "S". Textural classifications of grains include "g" as non-diagnostic fragments, "m" as magmatic grains with attached glass, in pumice, or as mantled feldspar or crystal clots, and "x" as grains in xenoliths.

section in the northwest the glass altered to clay minerals (also from interaction with groundwater). Mineral abundances and pleochroism of hornblende and biotite are consistent with typical ranges in the PST (Buesch, 1993). EMP data from AM144 (sample AM144cm200) are almost identical to EMP data from PST133 (Fig. 2B). Comparison of EMP and SEM data from AM144 was summarized at the end of the "Peach Spring Tuff Stratigraphy", and are displayed in Fig. 3A.

4. Southeast Baxter Wash, northeast Cady Mountains

The eastward draining Baxter Wash in the northern Cady Mountains (PST04754 in Fig. 1) has numerous exposures of the PST. Miller (1980) mapped the southeast part of Baxter Wash where the PST is interstratified with the Hector Formation. Paleomagnetic characteristics and zircon geochronologic age confirms the PST in this section (Hillhouse and others, 2010; Miller and others, 2010). The PST forms an erosionally resistant ledge of partially compacted and crystallized ignimbrite, and where >7 m thick, it can be moderately compacted and crystallized. In this approximately 500x500 m area, the PST ledge can be traced through variations in thickness from 4-12 m. The lower noncompacted and vitric ignimbrite is covered by talus; however, it is probably 1-2 m thick based on the exposures in the Spanish Canyon area. The upper part of the ignimbrite is typically covered by colluvium, and the overlying post-PST fine- to course-grained sandstone was deposited on partially compacted and crystallized PST, so the noncompacted ignimbrite was probably eroded away (Table 1). Mineral abundances and pleochroism of hornblende and biotite are consistent with typical ranges in the PST (Buesch, 1993). For sample PST04754, SEM measured sanidine and plagioclase compositions cluster along the rhyolite trend with one plagioclase and two sanidine grains along the trachytic trend (Fig. 3B).

5. Mesquite Hills

On the west end of the Mesquite Hills (GP-0433 in Fig. 1), a 5-10 m thick ignimbrite is interstratified with poorly exposed and undifferentiated sedimentary and volcanic rocks (Geoff Phelps, USGS, written commun, 2020, with the sample GP-M16-0443 shortened to GP-0443). This area is only ~4.5 km northeast of the PST04754 site in southeastern Baxter Wash location where the PST is exposed, so there is the potential of similar sections. No paleomagnetic or geochronologic data are available for this ignimbrite.

The ignimbrite is a pale red to pinkish gray, lithic bearing, slightly pumiceous, crystal vitric ignimbrite with vitroclastic textures (poorly preserved in hand specimen, but well preserved in thin section), and is partially compacted and crystallized. Mineral abundances and pleochroism of hornblende and biotite are consistent with the typical ranges in the PST (Buesch, 1993). SEM measured sanidine and plagioclase compositions cluster along the rhyolite trend with a few grains of plagioclase that are consistent with being transitional to the trachyte trend (Fig. 4A). Partially compacted and crystallization textures, mineral characteristics, and feldspar compositions are all consistent with the ignimbrite being the Peach Spring Tuff.

6. Harvard Hill

Harvard Hill (PST04810 in Fig. 1) has exposures of the PST based on detail mapping, physical stratigraphy, mineral assemblage, paleomagnetic properties, and zircon geochronology (Leslie and others, 2010; Hillhouse and others, 2010, and Miller and others, 2010). The base of the PST is not exposed, but the ignimbrite is at least 7 m thick; an unreliable thickness of 17 m was measured in a partly covered and structurally complex area (Leslie and others, 2010; Miller and others, 2010). Leslie and others (2010) described the ignimbrite as celadonite-altered (a clay mineral), light lime green color, nonwelded, and mostly massive except near its upper contact where it is locally thin-bedded, silicified, and a paler green. The tuff contains pumice clasts and conspicuous megascopic phenocrysts (actually crystal fragments as clasts) of sanidine, plagioclase, biotite, and sphene in an altered, fine-grained matrix, and lithics are small and inconspicuous (Leslie and others, 2010).

At the locations examined for this study, the ignimbrite is at least 7 m thick, and the general features described by Leslie and others (2010) were mostly confirmed, with addition of several details about the mineral assemblage and feldspar composition. In most of the ignimbrite, rather than "massive", there is a poorly developed alignment of crystal fragments that impart an internal fabric (a foliation) that parallels the top of the deposit, and probably developed during deposition of the laterally flowing PDC. In the sample (PST04810) collected ~5 m below the top of the deposit, the vitroclastic texture might have a slightly better development of the foliation resulting from minor amounts of compaction (near the transition of noncompacted to partially compacted). The contact with the superjacent limestone is planar across exposures (and projected between exposures) with no identifiable rills, incisions, nor paleosol development. These relations indicate the deposition of the limestone was very shortly after deposition of the PST. Mineral abundances and pleochroism of hornblende and biotite are consistent with the typical ranges in the PST (Buesch, 1993; Leslie and others, 2010). The SEM measured sanidine and plagioclase compositions cluster along the rhyolite trend with a few grains of plagioclase that are consistent with being transitional to (or in) the trachyte trend (Fig. 4B).

Because the base of the PST is not exposed, and the PST is >7 m thick (and especially if it is much thicker than 7 m) with mostly noncompacted to almost partially compacted texture, Leslie and others (2010) proposed that the PST was deposited in a lake (and possibly even a deep

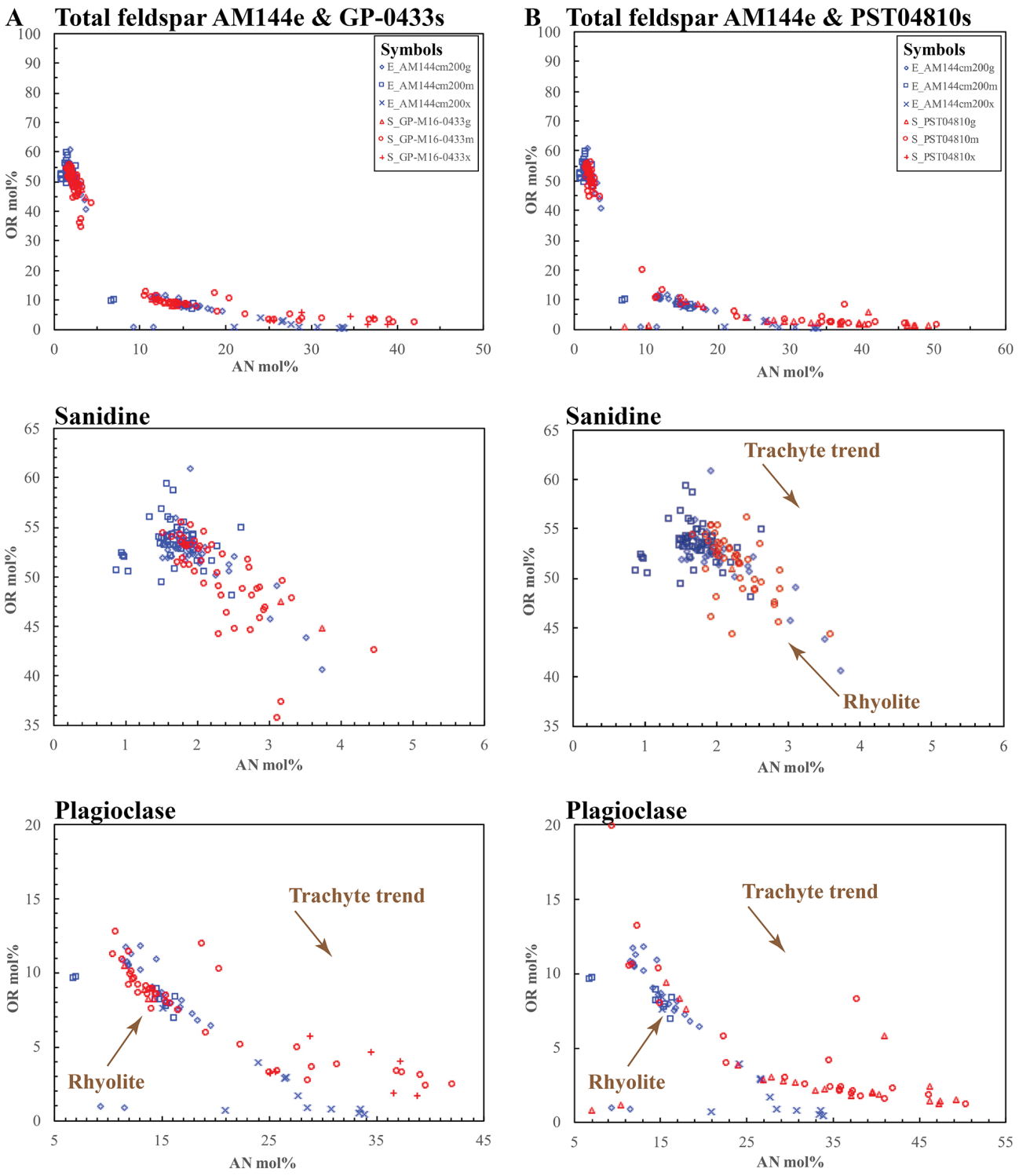

Figure 4. Graphs of electron microprobe (EMP) and scanning electron microscope (SEM) determined OR versus AN endmembers in feldspars for the Peach Spring Tuff from Spanish Canyon, Mesquite Wash, and Harvard Hill. (A) AM144 EMP and GP-0433 SEM in Mesquite Hills. (B) AM144 EMP and PST4810 SEM in Harvard Hill. Analytical method EMP as "E", SEM as "S". Textural classifications of grains include "g" as non-diagnostic fragments, "m" as magmatic grains with attached glass, in pumice, or as mantled feldspar or crystal clots, and "x" as grains in xenoliths.

lake). Interactions of a hot PDC with a body of water can be very complicated and what happens depends on many factors. These factors include (1) volume and density of the PDC that encounters a water body, (2) the size and geometry of the water body (volume, surface area, depth, slope of the bottom of the water body), (3) the ratio of PDC and water volumes, and rate of delivery of the PDC to the water, (4) the geometry of the interface between the PDC and the water body, not just the shoreline angle, but irregularities of the lobe and cleft boundaries of the PDC, and (5) the temperature differential between the PDC and the water body. These conditions can enable the PDC to flow across the water, or transition through the water interface where the PDC remains largely intact, or the PDC could mix with the water and explosively fragment. Leslie and others (2010) might be right, but, based on my observations, there does not appear to be enough data at Harvard Hill to support their interpretation of a hot PDC interacting with standing water.

As an alternative, it is true that the PST exposed at Harvard Hill contrasts with the 7-m thick PST exposed in southeast Spanish Canyon area (sample AM144 about 16 km northeast of Harvard Hill) where the ignimbrite of similar thickness is partially compacted and crystallized. However, 2-3 km north of that in eastern Spanish Canyon are 3-5 m thick PST exposures of noncompacted to partially compacted ignimbrite that were altered to green zeolite or clay and were deposited in a middle to lower fan depositional environment (Buesch, 2014, 2015). So, there appears to be a critical thickness of 5-7 m where compaction and crystallization becomes more effective in these relatively thin deposits of the PST, and maybe there was no need for the PST to be deposited in a lake.

Possible Peach Spring Tuff

Two locations have ignimbrites that share some physical attributes and feldspar compositions with the PST, but there are differences, so these are considered *possible* PST.

7. Northwest Baxter Wash, northern Cady Mountains

In the northern Cady Mountains, in the northwest part of Baxter Wash (PST04116 in Fig. 1), there are numerous faults and structural blocks containing cliff- and mesa-forming ignimbrite in the Hector Formation (Moseley, 1978). This ignimbrite was correlated to the similar-looking ignimbrite ~8 km to the east in the southeastern Baxter Wash (Moseley, 1978) where it was later identified as the PST (Hillhouse and others, 2010; Miller and others, 2010; see sample site PST04754). The ignimbrite is at least 14.3-m thick (the top is not exposed), the lowermost 3 m is non-welded and very poorly indurated, and the deposit thins slightly to the northwest (Moseley, 1978).

At location PST04116 in the northwest part of the exposures, the deposit is a 3-4 m thick, slightly pumiceous, crystal vitric ignimbrite with partially to well-preserved vitroclastic textures of bubble-wall glass shards and pumice clasts that are partially to moderately compacted. The lower and upper noncompacted parts of the ignimbrite are not exposed; however, nearby, the lower noncompacted to partially compacted ignimbrite is ~2 m thick, and the upper noncompacted ignimbrite appears to have been eroded away. In the center, vitroclastic texture is faintly preserved, but partially obscured by a very fine-grained (~2 µm) equigranular crystallized groundmass with distributed 4-8 µm diameter grains. Compared to the center of the deposit, near the top (thin section T) there are well-preserved vitroclastic textures, and ~5 times more and 5-10 times larger crystal fragments, so the ignimbrite is texturally graded. The upper sample includes crystal fragments with ~8 percent (<2 mm) sanidine, <0.5 percent (< 0.25 mm) biotite with yellow to red brown pleochroism, no hornblende, and trace (<0.5 mm) sphene, magnetite, and apatite, but chevkinite was not observed. Crystal clots are <1 percent (up to 1.0 mm). No plagioclase was identified in either thin section, but individual grains or crystal clots (feldspar, sphene, magnetite, and zircons) with what might have been plagioclase that has been altered or recrystallized to fine-grained aggregates are common. There are ~1 percent small lithic clasts.

SEM measured sanidine compositions at PST04116T have a very tight cluster of ~53 percent OR that overlaps the PST rhyolite trend, numerous grains of high-OR (65-98 percent) sanidine, and only three analyses of plagioclase in a single broken grain with no textural context (Fig. 5A). In the PST04116T sample, sanidine clusters at 53.1±1.6 percent OR and 2.1±0.5 percent AN, and this compares to PST ignimbrite samples in Kingman, Arizona, that average 53.5±5.2 percent OR and 1.8±0.8 percent AN (Buesch, 1993). The high-OR sanidine occur with attached glass, as mantled sanidine or in crystal clots (some with as low as ~53 percent OR sanidine), rock fragments (initially identified as xenoliths), or broken grains with no textural context. Using the associations of grains with attached glass or in pumice clasts with other similar compositions in different textural contexts, these grains might have formed in a related magma chamber.

These high-OR sanidine analyses and grains are a bit problematic for interpreting whether or not they are related to the PST magma. In the 1990 PST feldspar database (Buesch, 1992a, unpublished Ph. Ph.D. dissertation; Buesch, 1993), 106 analyses are 65-98 percent OR, 68 of which are in grains either identified as being in xenoliths or grains with no textural context; however, 38 are in grains with attached glass or in pumice clasts, and 22 of these are from the Fort Rock Creek unit on the Colorado Plateau (Buesch, 1993). More recently, two of these high-OR grains in pumice clasts are in a pre-PST tuff in the Spanish Canyon Formation. So, these infrequent and spatially diverse high-OR sanidine grains are not unique in either time or space. They might be an overlooked part of the feldspar composition of the PST that was tapped and then transported in and deposited as compositionally distinct cargo from the PST parental PDC. Alternatively, they might be crystals or rock

fragments from one deposit incorporated as "accidental" crystals or lithic clasts into the PST parental PDC. This accidental crystal and lack of a unique interpretation might result from the limited major and minor element composition of sanidine.

Compared to the typical PST where both sanidine and plagioclase have diffused but defined variations in compositions, in sample PST04116T there are no plagioclase grains, sanidine compositions that are near the average 53.1 percent OR have about 30 percent the variability compared to the PST in Kingman, and have numerous high-OR values, making these data somewhat different (Buesch, 1992a, unpublished Ph. Ph.D. dissertation; Buesch, 1993). Identification of analyzed points in all samples from the 1990, 2015, and current studies used the same approach of selecting representative grains of various sizes and points at various textural positions (Buesch, 1992a, unpublished Ph. Ph.D. dissertation; Buesch, 1993; Buesch, 2015). Even with this texturally specific method of selecting points to analyze, and the inherent quasi-randomness in which points are chosen, it is interesting that if minimal variation near 53 percent OR and high-OR sanidines are from the PST magma chamber, then this sample contains just these two compositional subsets.

Based on field relations of the ignimbrite and similarity of the stratigraphic sections in the northwest (PST04116) and southeast (PST04754) areas of Baxter Wash, one could correlate the ignimbrites. Additionally, the average 53.1 percent OR sanidine compositions in PST04116 closely matches the 53.5 percent OR in Kingman, Arizona, and the typical PST (Buesch, 1992a, unpublished Ph. Ph.D. dissertation; Buesch, 1993; Buesch, 2015). However, in contrast to the typical PST, and nearby PST deposits at southeast Baxter Wash (PST04754), Spanish Canyon area (AM144), and Harvard Hill (PST04810), ignimbrite at PST04116 has a different groundmass crystallized texture for such a thin deposit, lack of plagioclase, a very narrow range in ~53 percent OR sanidine, an abundance of high-OR sanidine, a few small biotite grains, and no hornblende (nor chevkinite). If the ignimbrite at PST04116 is the PST, then in many of these detailed properties it would be different from the typical PST, and this would have interesting implications for the magma chamber conditions and the processes in the parental PDC. There are tantalizing overlaps in the ignimbrite at PST04116 with the PST, but there are differences, and none of which is uniquely conclusive. Further investigations are warranted, but for now this ignimbrite is considered to be a *possible* correlative to the PST.

8. Mitchel Range

The stratigraphic and structural setting of the middle Miocene in the Mitchel Range was interpreted as being part of an extensional and metamorphic complex (Glazner et al 2002), and several of the stratigraphic and structural relations have been reinterpreted (Andersen, 2017; Andersen and Onderdonk, 2018; Fig. 1). A 2-m thick light pinkish brown ignimbrite was tentatively identified as the PST (Andersen, 2017; Andersen and Onderdonk, 2018). There are no geochronologic nor paleomagnetic data on the ignimbrite at M17VI-3706b (Fig. 1), but it has been examined in detail to evaluate the correlation to the PST.

The 2-m thick ignimbrite is slightly compacted to (barely) partially compacted, and a thin section (M17VI-3706b) from 1 m above the base has the vitroclastic texture preserved, but partially obscured, by a very fine-grained equigranular crystallization with distributed 0.05 mm diameter grains. This type of compaction and crystallization is not very common in such thin ignimbrites of the Mojave Desert. Crystal fragments include ~8 percent sanidine (up to 1.5 mm), no plagioclase, <0.5 percent biotite (with a few grains up to 0.4 mm) with yellow to reddish brown or dark brown pleochroism (typically oxidized), no hornblende, and trace amounts of sphene, magnetite, zircon, apatite, but chevkinite was not observed.

SEM measured sanidine compositions have an average of 52.5±8.5 percent (1σ of 2.7) OR and 2.6±0.9 percent (1σ of 0.7) AN that are along the PST rhyolite trend with a few grains of sanidine that are consistent with being transitional to (or in) the trachyte trend, and no plagioclase grains were analyzed (although searched for) (Fig. 5B). Numerous grains of high-endmember OR (75-99 percent OR) occur with attached glass, in crystal clots (some of which include ~53 percent OR sanidine), or rock fragments (initially identified as xenoliths), or broken grains with no textural context. The compositions and textural context of these high-OR grains are very similar to those in the sample (PST04116) from northwest Baxter Wash, and as in that sample, the petrogenetic interpretation of these analyses and grains are not unique.

Similar to the ignimbrite at PST04116, the ignimbrite at M17VI-3706b is thin (2 m) and has a an unusually distinct crystallization texture for a thin deposit, and there are numerous high-OR sanidine grains, no plagioclase, a few small biotite grains, and no hornblende (nor chevkinite) making this ignimbrite a bit problematic for correlations to the PST. However, in M17VI-3706, partial development of a compaction profile in a thin deposit, the average (52.6) percent and range of OR in sanidine (exclusive of high-OR grains), and especially the sanidine grains transitional to (or in) the trachyte trend are consistent with the typical PST. As with the ignimbrite at PST04116, there are tantalizing overlaps in the ignimbrite at M17VI-3706 with the PST, but there are differences, and none of which is uniquely conclusive. Further investigations are warranted, but for now this ignimbrite is considered to be a *possible* correlative to the PST.

Stratigraphic facies above and below the Peach Spring Tuff

The large-volume PST was deposited across variable topography with many (apparently) internally drained

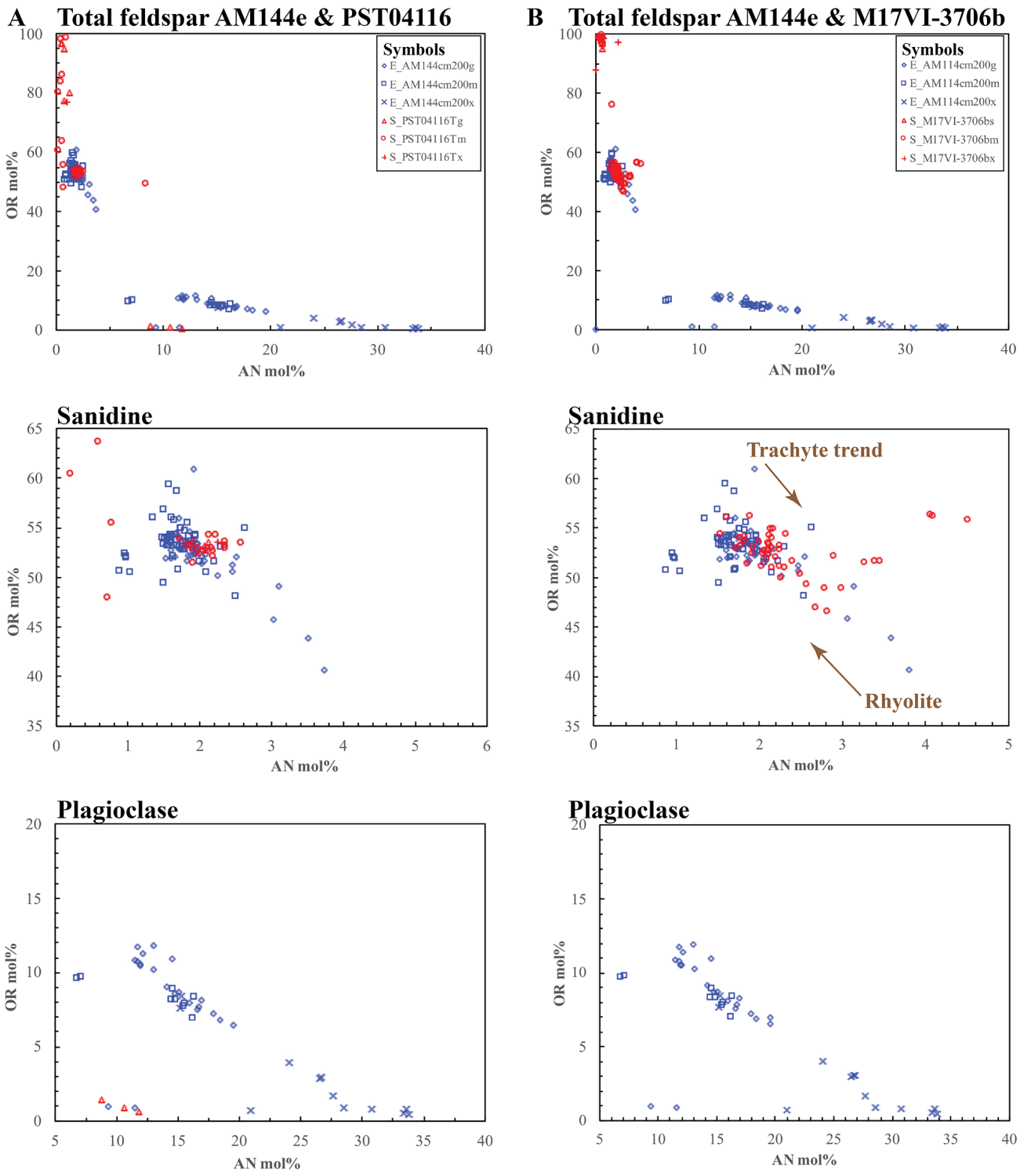

Figure 5. Graphs of electron microprobe (EMP) and scanning electron microscope (SEM) determined OR versus AN endmembers in feldspars for the Peach Spring Tuff from Spanish Canyon, northwest Baxter Wash, and Mitchell Range. (A) AM144 and PST4116 in northwest Baxter Wash. (B) AM144 and M17VI-3706b in the Mitchell Range. Analytical method EMP as "E", SEM as "S". Textural classifications of grains include "g" as non-diagnostic fragments, "m" as magmatic grains with attached glass, in pumice, or as mantled feldspar or crystal clots, and "x" as grains in xenoliths.

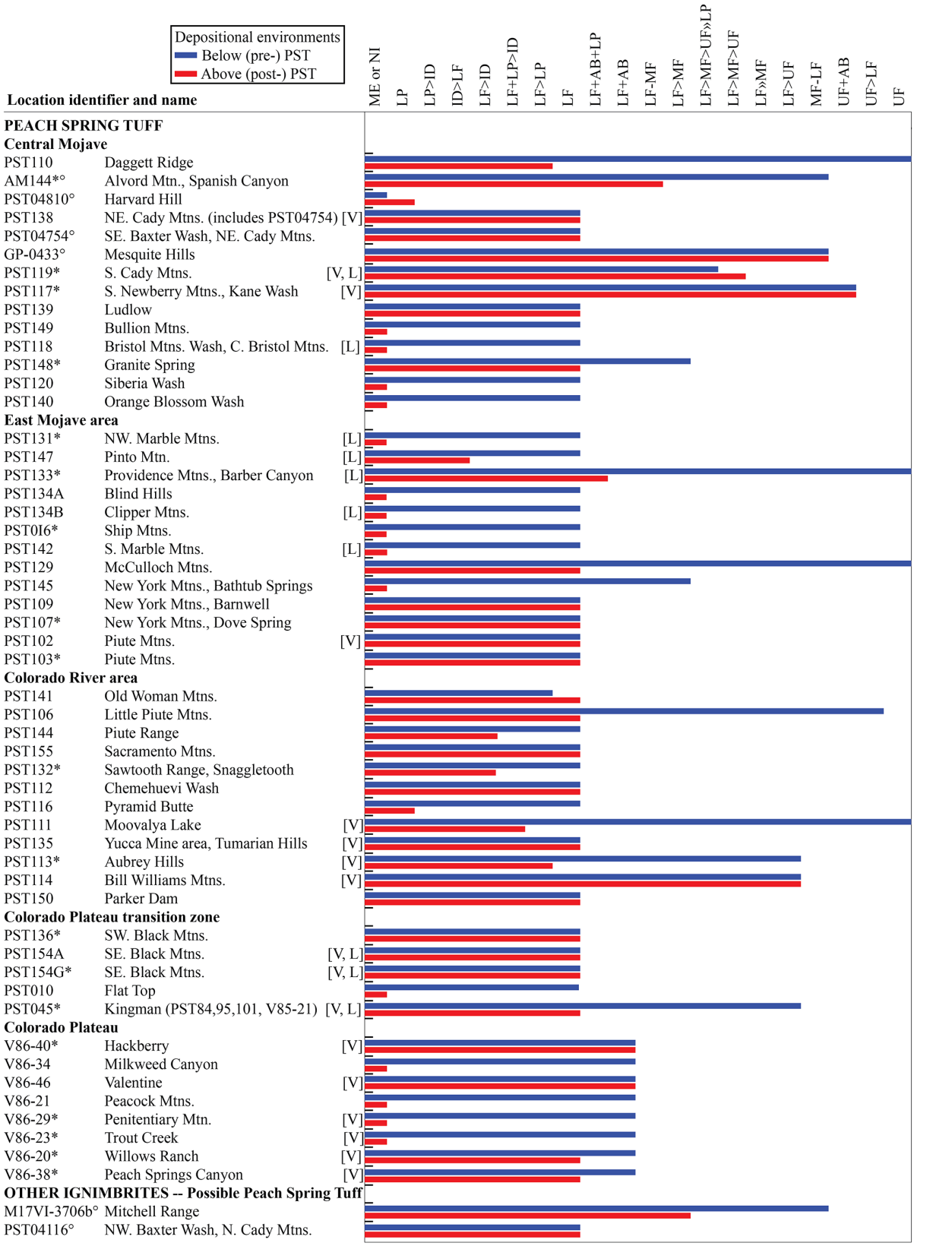

Figure 6. Graph comparing depositional environments of sedimentary rocks below and above PST and possible PST ignimbrites. Locations in a paleovalley or part of paleovalley are indicated by [V], and those with onlap onlap facies of the PST are indicated by [L]. ME = mesa forming exposure, NI = no information (not exposed), ID = isolated depression, LP = lacustrine/playa, LF =- lower (distal) alluvial fan. AB =axial braided stream or regional trunk braided stream, MF = middle alluvial fan, UF = upper (proximal) alluvial fan. The order of facies in this figure (left to right) represents the amount of energy in the system for transportation and deposition.

basins. Deposition of the PST in internally drained basins resulted in the dominance of local processes on post-PST sedimentation that were highly dependent on the basin geometry.

This paper recounts the stratigraphy described by Buesch (1991) and includes five locations of the PST (or *possible* PST) not described in 1991. Both this and the previous study focus on the stratigraphic interval within 20 m above and below the PST, although a few locations only include <10 m sections. There are extensive areas of early Miocene rocks exposed in the study area, there are only limited exposures (1 to 100 krn^2) of rocks that were deposited very close in time to the PST, and these locations are typically 5 to 50 km apart. Thus, only relatively small parts of the depositional system are represented at many locations. The emphasis in this paper is on the vertical changes between the pre- and post-PST sections (or those below and above the PST, respectively) with respect to the relative proportion of 1) gravel- versus sand-dominant deposits, 2) debris-flow- and sheetflow-versus channelized-braided-stream deposits, and 3) steep-sided, meter-deep versus sloping-sided, decimeter-deep channels. Buesch (1991) described the components of lithofacies, the architectural elements and hierarchy of bedding contacts, and characteristics of depositional environments.

The PST was deposited by volcanological processes completely independent of the alluvial, fluvial, or lacustrine processes active in the basin at the time of PST deposition. In this sense, the PST disrupted the depositional systems in the basin, but after the PST was deposited, the depositional systems were re-established. Comparing the rocks, and associated facies and depositional systems, in the sedimentary rocks below and above the PST (pre- and post-PST) represents the impact of PST deposition. Table 1 includes the summary grain size or relative abundance in grain sizes of deposits, and the associated depositional environment, of the rocks below and above (pre- and post-) PST. Table 1 also summarizes the comparison of grain sizes (and the associated depositional environments) from deposits below and above the PST relative to whether there is an upward fining and thinning of grain sizes and bed thicknesses.

Regional stratigraphic summary

In all 47 areas of PST exposures (Buesch, 1991) and 6 additional areas described in this paper (Table 1), the PST was deposited on sedimentary rocks; however, in some exposures the PST formed local onlap deposits across pre-PST Miocene volcanic rocks or Mesozoic and older granitoid and metamorphic rocks. The pre- and post-PST deposits consist of several facies that formed in numerous depositional environments. For the pre-PST rocks, 28 are distal (lower) alluvial fan with has localized lacustrine or playa deposits at one location. Eight locations are distal (lower) alluvial fan and [or] axial braided stream; six are distal (lower) to middle alluvial fan; three are middle to distal (lower) fan; one is proximal (upper) fan and [or] axial braided stream; and five are proximal (upper) fan (Fig. 6). The base of the PST is not exposed at one location, so there is no information on the pre-PST stratigraphy. Because 15 locations are capped by a mesa formed by the PST, there is no information regarding whether there was any sediment deposited on the PST. This lack of information at these 16 locations means that comparisons of facies in the below and above the PST sections can only be done for 37 sections (Fig. 6). In 25 locations, there are finer grained and thinner beds above the PST compared to below, and the facies and depositional systems in which they formed shifted to lower amounts of energy in the transportation and deposition systems. In 12 locations, there are no changes in the grain size and thickness of beds in the deposits below to above the PST, thus no changes in facies and depositional systems.

Stratigraphy below and above the eight ignimbrites

Eight locations of ignimbrite, five with known exposures of the PST and three possible PST, were studied along a 140-km-long swath in the northwest exposures of the PST. The stratigraphy and stratigraphic settings of the sedimentary sections below and above the PST (and possible PST) are described.

1. Providence Mountains

The PST, which is up to 70-m thick, and sedimentary rocks below and above the PST that are exposed in the northeastern Providence Mountains (PST 133 in Fig. 1) were mapped as part of the study of the Woods Mountains volcanic center (McCurry, 1985). The PST has highland facies where it onlapped Paleoproterozoic gneiss or Jurassic plutonic rocks (Stone and others, 2017). The valley-fill facies in the PST was deposited across fluvial arkosic sandstone and conglomerate and poorly sorted carbonate conglomerate (McCurry, 1985; Buesch, 1991: Reynolds and others, 1995). The contact between the upper noncompacted PST and sedimentary rock above the PST was traced across several kilometers and indicates minimal time between deposition. The sedimentary sequence above the PST grades upward from alluvial fan facies, to axial braided streams that are laterally equivalent to limestone beds formed in a lacustrine environment (McCurry, 1985; Buesch, 1991: Reynolds and others, 1995). Comparing the grain sizes and bedding characteristics of the depositional environments in the sedimentary rocks below and above the PST, there is an upward fining and thinning trend (Table 1, Fig. 6).

2. Granite Spring

Granite Spring is located on the west side of Cima Dome (PST148 in Fig. 1), and the exposure of the PST is 3-15 m thick. Variations in thickness of the PST indicate it was deposited in a broad swale developed on sandstone and pebbly sandstone in a lower to possibly middle alluvial fan

Table 1. Locations of Peach Spring Tuff and two other ignimbrites with depositional environments of sedimentary rocks below and above (pre- and post-) Peach Spring Tuff.

Field No.[1]	Location (Figure 1)	UTM E. (m)[2]	UTM N. (m)[2]	Thick (m) L2max[3]	Thick (m) L2min[3]	Paleo-topog[4]	Thickness Factor[5]	Top of PST[6]	Pre-PST Environ[7]	Pre-PST Grain size[8]	Fining Thinning[e]	Post-PST Environ[7]	Post-PST Grain size[8]
PEACH SPRINGS TUFF													
Central Mojave													
PST110	Daggett Ridge	500720	3852000	23	0		23.0	NW	UF	G≥S	Y	LF>LP	S>F+M
AM144*°	Alvord Mtn., Spanish Canyon	539153	3880682	10	1		10.0	NW	MF-LF	S>G>P	Y	LF>MF	S>P>F>M
PST04810°	Harvard Hill	530042	3866894	7	5		1.4	NW	NI	NK	NI	LP	C>M>F
PST138	NE. Cady Mtns. (includes PST04754)	565000	3871600	12	2	V	6.0	NW±PW	LF	S≥P	Y	LF	S>F+M
PST04754°	SE. Baxter Wash, NE. Cady Mtns.	564962	3871878	12	4		3.0	PW±NW	LF	S≥P	Y	LF	S>F
GP-0433°	Mesquite Hills	568505	3874579	10	5		2.0	PW	MF-LF	P>G>S	N	MF-LF	P>G>S
PST119*	S. Cady Mtns.	562680	3849600	60	5	V, L	12.0	PW	LF>MF>UF»LP	S+P>G»F	Y	LF≥MF≥UF	S>G
PST117*	S. Newberry Mtns., Kane Wash	525800	3843660	30	0	V	30.0	NW	UF+AB	G+S	N	UF+AB	G+S
PST139	Ludlow	575850	3840000	6				PW	LF	S≥P	N	LF	S≥P
PST149	Bullion Mtns.	576000	3828800	20				PW	LF	S≥P≥G≥F	NI	ME	NK
PST118	Bristol Mtns. Wash, Central Bristol Mtns.	590900	3852000	35	9	L	3.9	PW	LF	S+G	NI	ME	NK
PST148*	Granite Spring	610000	3901620	15	3		5.0	PW	LF>MF	S+P	Y	LF	S
PST120	Siberia Wash	599200	3842880	25	11		2.3	PW	LF	S+G	NI	ME	NK
PST140	Orange Blossom Wash	609300	3839600	16				PW	LF	S+P≥G	NI	ME	NK
East Mojave area													
PST131*	NW. Marble Mtns.	624750	3838880	33	6	L	5.5	PW	LF	S+P	NI	ME	NK
PST147	Pinto Mtn.	650020	3892300	22	10	L	2.2	PW	LF	S≥P	Y	ID≥LF	C+M+S
PST133*	Providence Mms., Barber Canyon	637400	3875800	35	2	L	17.5	NW	UF	G≥S	Y	LF+AB+LP	S+F+M>G
PST134A	Blind Hills	649400	3853680					PW	LF	S	NI	ME	NK
PST134B	Clipper Mtns.	647900	3849000	30	2	L	15.0	PW	LF	S	NI	ME	NK
PST0I6*	Ship Mtns.	650380	3823180	35	6		5.8	PW	LF	S+P	NI	ME	NK
PST142	S. Marble Mtns.	638550	3827750	30	5	L	6.0	PW	LF	S≥G	NI	ME	NK
PST129	McCulloch Mtns.	666000	3948800	2	0			NW	UF	G+S	Y	LF	S
PST145	New York Mtns., Bathtub Springs	660420	3910220					PW	LF>MF	S+P	NI	ME	NK
PST109	New York Mtns., Barnwell	661800	3906500	30	12		2.5	PW	LF	S+P	N	LF	S+P
PST107*	New York Mtns., Dove Spring	662700	3915100	22	8		2.8	PW	LF	S+P	N	LF	S+P
PST102	Piute Mtns.	669880	3846900	220	20	V	11.0	PW	LF	S+P	N	LF	S+P
PST103*	do.	670700	3848350										
Colorado River area													
PST141	Old Woman Mtns.	670200	3834020	20	5		4.0	NW≥PW	LF≥LP	S+P>G≥F+M	N	LF	S+P+G
PST106	Little Piute Mtns.	676480	3831160	55	6		9.2	PW	UF>LF	G+S	Y	LF	S+G
PST144	Piute Range	682100	3902450	30	3		10.0	PW	LF	S≥G	Y	LF>ID	S>C
PST155	Sacramento Mtns.	703500	3852000	85		E		PW	LF	S+P	N	LF	S+P
PST132*	Sawtooth Range, Snaggletooth	715100	3830900	140	35		4.0	PW	LF	S+F	Y	LP>ID	F+C
PST112	Chemehuevi Wash	734860	3813260	50	10		5.0	PW	LF	S+P	N	LF	S+P
PST116	Pyramid Butte	723300	3798800	25	12		2.1	PW	LF	S+P	N	LP	S+P
PST111	Moovalya Lake	752020	3785400	12	3	V	4.0	PW≥NW	UF	P+G>S	Y	LF+LP>ID	S+F+M+C
PST135	Yucca Mine area, Tumarian Hills	738900	3834650	200	20	V	10.0	PW>NW	LF	S+P>G	Y	LF	S≥G
PST113*	Aubrey Hills	751250	3811650	60	10	V	6.0	PW	LF>UF	S+P+G	Y	LF>LP	S≥P≥F+M
PST114	Bill Williams Mtns.	765700	3805400	30	4	V	7.5	NW>PW	LF>UF	S+P>G	Y	LF>UF	S>P>G

Field No.[1]	Location (Figure 1)	UTM E. (m)[2]	UTM N. (m)[2]	Thick (m) L2max[3]	Thick (m) L2min[3]	Paleo-topog[4]	Thickness Factor[5]	Top of PST[6]	Pre-PST Environ[7]	Pre-PST Grain size[8]	Fining Thinning[9]	Post-PST Environ[7]	Post-PST Grain size[8]
PST150	Parker Dam	761600	3798480	6	0	E	6.0	PW>NW	LF	S+P>G	N	LF	S+P>G
Colorado Plateau transition zone													
PST136*	SW. Black Mtns.	747600	3861080	100	20		5.0	PW	LF	S+P	N	LF	S+P
PST154A	SE. Black Mtns.	757080	3861740	100	4	V, L	25.0	NW>PW	LF	S+P	Y	LF	S»G
PST154G*	do.	757800	3858800	100				NW	LF	S+P	Y	LF	S»G
PST010	Flat Top	772500	3853000	16	10	E	1.6	PW	LF	S+P	NI	ME	NK
PST045*	Kingman	764220	3899200	100	5	V, L	20.0	PW>NW	LF»UF	S+P>G	Y	LF	S+P»G
PST084*	do.	767540	3902080										
PST095*	do.	765500	3895700										
PST101*	do.	766100	3895600										
V85-21	do.	762800	3898800										
Colorado Plateau													
V86-40*	Hackberry	253100	3916650	24	4	V	6.0	PW	LF+AB	S+P	Y	LF+AB	S
V86-34	Milkweed Canyon	254600	3942100	12	0			PW	LF+AB	S+P>G	NI	ME	NK
V86-46	Valentine	260800	3923100	24	6	V	4.0	PW	LF+AB	S+P>G	Y	LF+AB	S+P
V86-21	Peacock Mtns.	245800	3898600	15	8		1.9	PW	LF+AB	S+P	NI	ME	NK
V86-29*	Penitentiary Mtn.	273800	3888100	22	5	V	4.4	PW	LF+AB	S>P	NI	ME	NK
V86-23*	Trout Creek	278900	3871900	22	0	V		PW	LF+AB	S+P>G	NI	ME	B
V86-20*	Willows Ranch	277500	3897500	12	3	V	4.0	PW	LF+AB	S+P>G	Y	LF	S+P
V86-38*	Peach Springs Canyon	280300	3937000	16	8	V	2.0	PW	LF+AB	S>G	Y	LF	S
OTHER IGNIMBRITES -- Possible Peach Spring Tuff													
M17VI-3706b°	Mitchell Range	500197	3869208	2	0		2.0	PW	MF-LF	S>G>P	Y	LF>MF	S-P>G
PST04116°	NW. Baxter Wash, N. Cady Mtns.	557423	3873762	4	2			PW	LF	S≥P	Y	LF	S>F+M

[1] Detailed electron microprobe data (*). Reconnaissance electron microprobe data (+). Scanning electron microscope (°)

[2] UTM = Universal Transverse Mercator. Central Mojave to Colorado Plateau transition zone are UTM Zone 11. Colorado Plateau locations are UTM Zone 12. Grid coordinates to the nearest 20 m.

[3] Maximum and minimum thickness of ignimbrite (L2) (m). Data from east of Kingman (AZ) are from Valentine (per. commun.) and unpublished mapping by Buesch. Other data from Buesch (unpublished

[4] Paleovalley fill (V), onlapping or topographic high (L), post-PST erosion (E).

[5] "Thickness Factor" is the maximum thickness divided by the minimum thickness. This value is a qualitative (scalor) of the minimum relief filled by the ignimbrite.

[6] Zone or compaction (welding) at the top or the PST. NW = nonwelded or co-ignimbrite fallout. PW = partially welded (in 1991 data the rocks are typically vapor-phase mineralized or partially to moderately compacted and crystallized). NE = Not well enough exposed.

[7] UF = proximal (upper) fan, MF = middle fan, LF = distal (lower) fan. AB = axial braided stream or regional trunk braided stream, LP = lacustrine/playa, ID = isolated depression, ME = mesa forming exposure, NI = no information (not exposed).

[8] Grain size or the most abundant beds. G = gravel (cobble-boulder conglomerate), P = pebbly sandstone. S = sandstone, F = fine to medium sandstone, M = mudstone, C = carbonate, B = basalt flow, NK = not known (no deposit).

[9] Fining or thining of the grain size and associated facies and depositional environments. Y = section has a fining- and thinning-upward trend, N = no fining- and thinning-upward trend. NI = no information, mesa-forming exposures or overlain by basalt.

(LF>MF in Fig. 6). The sedimentary rocks above the PST are sandstone that were deposited in a lower alluvial fan. Based on grain size and bedding characteristics from below to above the PST, there was slight fining and thinning change and therefore a slight change in depositional environments (Table 1, Fig. 6).

3. Spanish Canyon area (Alvord Mountain area)

The 1-10 m thick PST is part of the 24-123 m thick Spanish Canyon Formation in the Alvord Mountain area (Byers, 1960; Buesch, 2014; AM144 Fig. 1). The PST was deposited on sandstone, local conglomerate, and tuffaceous sandstone, and bedding characteristics are indicative of middle to lower fan depositional environments. Sedimentary sequences above the PST are arkosic sandstone (and a distinct lack of tuffaceous deposits), and the bedding characteristics in sandstone, local pebbly sandstone, and fine-grained sandstone to mudstone are indicative of lower fan, minor middle fan, and localized possible playa depositional environments. So, there was slight fining and thinning change in grain sizes and bedding characteristics and depositional environments from below to above the PST (Table 1, Fig. 6). The reduction in grain size and bedding characteristics might be influenced by the widely deposited, but relatively thin, PST across a relatively low-relief basin, and the resulting time for alluvial fans to propagate across the basin. However, the more fundamental change from mostly tuffaceous to arkosic sediment supply might have resulted from (1) the fortuitous termination shortly before deposition of the PST of the local volcanism that produced the tuffaceous material, and (2) the effectiveness of different parts of the basin headwaters (for sediment provenance and supply) to develop integrated steam networks to propagate alluvial fans across the low-relief basin.

4. Southeast Baxter Wash, northeast Cady Mountains

The eastward draining Baxter Wash in the northern Cady Mountains contains a 4-12 m thick PST interstratified with the Hector Formation (Miller, 1980; PST04754 in Fig. 1). The sedimentary rocks below the PST are mostly volcaniclastic with an upward fining grain size from pebbly sandstone and small-cobble conglomerate with channel fill structures and cross bedding to sandstone in more tabular bedsets. The sandstone above the PST was deposited on partially compacted and crystallized PST, so the noncompacted ignimbrite was probably eroded away. The sandstone above the PST is fine to medium grained sandstone and grades upward to pebbly sandstone and farther up section to increased amounts of conglomerate. Although sections below and above the PST were deposited in the distal (lower) alluvial fan facies, comparing the overall trends in grain size and bedding characteristics from below to above the PST there appears to be a slight upward fining and thinning trend (Table 1, Fig. 6). In the generalized stratigraphic section by Miller (1980, Fig. 4), the fining and thinning trend in the rocks below the PST and the sandstone that grades upward to an increase in conglomerate are consistent with the descriptions above, and they might simply be the cyclic migration of the depositional facies and only partially influenced by the deposition of ~12 m of ignimbrite.

5. Mesquite Hills

On the west end of the Mesquite Hills (GP-0433 in Fig. 1), the 5-10 m thick PST is interstratified with poorly exposed and undifferentiated sedimentary and volcanic rocks (Geoff Phelps, USGS, written commun. 2020). This area is ~4.5 km northeast of the PST04754 site in southeastern Baxter Wash, so there is the potential of similar sections. Because exposures of the sedimentary rocks below and above PST are poor, only general characteristics can be estimated, but both sequences appear to be sandstone, conglomerate, volcaniclastic sandstone, so there is no apparent upward fining or thinning trend (Table 1, Fig. 6).

6. Harvard Hill

Harvard Hill (PST04810 in Fig. 1) has a 40-50 m thick conformable section with no exposures of rocks below the PST, and at least 7 m of PST (Leslie and others, 2010). The sedimentary rocks above the PST consists of (1) thin- to upwardly thick-bedded limestone with variable silicification and locally interbedded with tuffaceous lacustrine sandstone, (2) massive silicified limestone with stromatolites, (3) well-sorted alluvial sandstone to pebble conglomerate interbedded with lacustrine sandstone and siltstone, and (4) fossiliferous platy limestone, (Leslie and others, 2010). These rock and facies associations represent variously developed lacustrine environments with variations of input of detrital materials that grade upward to alluvial environments, and then revert to lacustrine environments. Some of these trends might represent progradation and lateral migration of detrital sediments into sediment-deprived lacustrine environments. Because there are no rocks below the PST exposures, a below and above the PST comparison of sedimentary facies cannot be made (Table 1, Fig. 6).

Possible Peach Spring Tuff

These next two locations have ignimbrites that are considered possible PST.

7. Northwest Baxter Wash, northern Cady Mountains

In the northern Cady Mountains, in the northwest part of Baxter Wash (PST04116 in Fig. 1), the *possible* PST ignimbrite is at least 14.3-m thick (the top is not exposed) and thins to the west (Moseley, 1978). The ignimbrite locally overlies an up to 5-m thick white tuff in a section of distal alluvial fan sandstone and thin beds of lacustrine sandstone (Moseley, 1978; Miller and others, 2010). The post-ignimbrite sedimentary rocks are tuffaceous lacustrine sandstone, siltstone, and mudstone (Moseley, 1978). Based on the differences in sedimentary rocks below and above the possible PST ignimbrite, there is an

upward thinning and fining trend that reflects the change from more alluvial fan deposition below to lacustrine depositional environments above (Table 1, Fig. 6).

8. Mitchel Range

The *possible* PST ignimbrite is ~2 m thick and interstratified with the Pickhandle Formation that consists of brown siliciclastic and volcaniclastic sandstone, conglomerate, and breccia, and locally lava flows (Andersen, 2017; Andersen and Onderdonk, 2018). The top of the ignimbrite is slightly compacted and lithified, so the noncompacted top might have been eroded prior to deposition of the overlying sandstone. The sedimentary section above the ignimbrite contains conglomerate with cobbles and boulders of PST that are more compacted and crystallized (densely welded) than the local exposures, indicating the clasts are exotic to the area, and Andersen (2017) proposed the conglomerates were derived from the east. There is a slight fining and thinning trend from the sedimentary sequences below to above the *possible* PST ignimbrite (Table 1, Fig. 6).

Conclusions

There are five conclusions regarding use of fallout tephra and (or) ignimbrites in understanding changes in sedimentary basin facies.

1. The PST is an important 18.8 Ma tephrostratigraphic marker because it was deposited across a broad area and has a relatively unique mineral assemblage, feldspar composition, compaction profiles, vitric crystallization development or alteration facies that allow correlation.
2. There is a good correlation of feldspar composition determined by EMP and SEM on the same analytical points that enables the judicious use of either technique for tephrochronology.
3. Six of the established PST locations examined in this study have a good correlation of stratigraphic properties and, especially, feldspar compositions.
4. Two ignimbrites, in the northwest Baxter Wash of the Cady Mountains and Mitchel Range areas, have some of the field relations and average sanidine OR compositions consistent with being the PST. However, mineral abundance, details in composition, and groundmass crystallization in such thin deposits differ from typical PST. Although these ignimbrites are *possible* PST, additional study is warranted to understand these variations in the context of tephrostratigraphic correlations.
5. The PST was deposited in a wide variety of basins and depositional environments with numerous facies within these basins. Most environments include variations in distal-alluvial-fan facies and lacustrine facies, and fewer in the middle and proximal alluvial fan facies. Where comparisons are made between depositional environments below and above the PST, 67 percent have finer grained sediments and/or thinner beds above than below, and 33 percent have no significant change. These changes might result from the local changes in the depositional system resulting from the deposition of the PST and the re-establishment of post-depositional system. However, in some locations, such as in the southeast Baxter Wash area of the northern Cady Mountains, the PST might have simply been deposited during a period of spatial shifting of the locations of finer and coarser lower fan environments. Future evaluations might examine the depostional environment more closely and compare changes to thickness of the tuff.

References

Andersen, E., 2017, Major revisions of the timing, style, magnitude, and cause of Early Miocene extension in the Central Mojave metamorphic core complex and subsequent role of the Eastern California Shear Zone; in Reynolds, R.E., eds., "ECSZ Does It", Desert Studies Consortium California State University, Fullerton, p. 60-70.

Andersen, E., and Onderdonk, N., 2018, Guide to an informal field trip to the southeast part of the Central Mojave Metamorphic Core Complex; in Miller, D.M, eds., "Against the Current", Desert Studies Consortium California State University, Fullerton, p. 35-43.

Billingsley, G.H., Wenrich, K.J., Huntoon, P.W., and Young, R.A., 1999, Breccia-pipe and geologic map of the southwestern part of the Hualapai Indian Reservation and vicinity, Arizona: U.S. Geological Survey Miscellaneous Investigations Series, Map I–2554, scale 1:48,000, 50 p.

Buesch, D.C., 1987, Stratification in Layer 2 deposits in the Peach Springs Tuff, Arizona: Response to topography and lateral variations: International Union of Geodesy and Geophysics, XIX General Assembly, Vancouver, Canada, August 9-22, Abstract Volume 2, p. 394

Buesch, D.C., 1991, Changes in the depositional environments resulting from emplacement of a large-volume ignimbrite: in Fisher, R.V. and Smith, G.A., eds., Sedimentation in Volcanic Settings: Society of Economic Paleontologists and Mineralogists (Society for Sedimentary Geology) Special Publication No. 45, p. 139-153.

Buesch, D.C., 1992a, Field and geochemical investigations of the Peach Spring Tuff, southeastern California, western Arizona, and southern Nevada: Santa Barbara, University of California, Ph.D. dissertation, 196 p.

Buesch, D.C., 1992b, Incorporation and Redistribution of Locally Derived Lithic Fragments Within a Pyroclastic Flow: Geological Society of America Bulletin, v. 104, n.9, 1178-1192.

Buesch, D.C., 1993, Feldspar Geochemistry of Four Miocene Ignimbrites in Southeastern California and Western Arizona: in Sherrod, D.R., and Nielson, J.E., Tertiary Stratigraphy of Highly Extended Terranes, California, Arizona, and Nevada: U.S. Geological Bulletin 2053, p. 55-85.

Buesch, D.C., 2014, Interstratified arkosic and volcanic rocks of the Miocene Spanish Canyon Formation, Alvord Mountain area, California— descriptions and interpretations: in

Reynolds, R.E., ed, "Not a Drop Left to Drink", California State University Desert Studies Consortium, p. 190-203.

Buesch, D.C., 2015, Regional and local correlations of feldspar geochemistry of the Peach Spring Tuff, Alvord Mountain, California: in Reynolds, R.E., ed, "Mojave Miocene", California State University Desert Studies Consortium, p. 44-50.

Buesch, D.C., and Valentine, G.A., 1986, Peach Springs Tuff and volcanic stratigraphy of the southern Cerbat Mountains, Kingman, Arizona, in Cenozoic stratigraphy, structure and mineralization in the Mojave Desert: in Cenozoic stratigraphy, structure and mineralization in the Mojave Desert: Geo- logical Society of America, Cordilleran Section, 82d, Los Angeles, Calif., March 1986, Guidebook and Volume, Field Trips 5 and 6, p. 7-14.

Byers, F. M., 1960, Geology of the Alvord Mountain Quadrangle, San Bernardino County, California: U.S. Geological Survey Bulletin 1089-A, 71 p.

Ferguson, C.A., McIntosh, W.C., and Calvin F. Miller, C.F., 2013, Silver Creek caldera—The tectonically dismembered source of the Peach Spring Tuff: Geology, v. 41, p. 3-6. doi:10.1130/G33551.1.

Glazner, A.F., Walker, J.D., Bartley, J.M., and Fletcher, J.M., 2002. Cenozoic evolution of the Mojave block of southern California: in Glazner, A.F., Walker, J.D., and Bartley, J.M., Geologic evolution of the Mojave Desert and southwestern Basin and Range: Geological Society of America Memoir 195, p. 19-41.

Glazner, A.F., Nielson, J.E., Howard, K.A., and Miller, D.M., 1986, Correlation of the Peach Springs Tuff, a large-volume Miocene ignimbrite sheet in California and Arizona: Geology, v. 14, no. 10, p. 840-843.

Gusa, Sharon, Nielson, J.E., and Howard, K.A., 1987, Heavy-mineral suites confirm the wide extent of the Peach Springs Tuff in California and Arizona, U.S.A.: Journal of Volcanology and Geothermal Research, v. 33, no. 4, p. 343-347.

Hillhouse, J.W., Miller, D.M., and Turrin, B.D., 2010, Correlation of the Miocene Peach Springs Tuff with the Geomagnetic Polarity Time Scale and New Constraints on Tectonic Rotations in the Mojave Desert, California: in Reynolds, R.E and Miller, D.M, eds., "Overboard in the Mojave", Desert Studies Consortium California State University, Fullerton, p. 105-121.

Hillhouse, J.W, and Wells, R.E., 1991, Magnetic fabric and source area of the lower Miocene Peach Springs Tuff in California, Nevada, and Arizona: Journal of Geophysical Research, v. 96, no. B7, p. 12,443-12,460.

Leslie, S.R., D. M. Miller, J. L. Wooden, and J. A. Vazquez, 2010, Stratigraphy, age, and depositional setting of the Miocene Barstow Formation at Harvard Hill, central Mojave Desert, California: in in Reynolds, R.E and Miller, D.M, eds., "Overboard in the Mojave", Desert Studies Consortium California State University, Fullerton, p. 85-104.

McCurry, M., 1985, The petrology of the Woods Mountains Volcanic Center, San Bernardino County, California: Los Angeles, University of California, Ph.D. dissertation, 403 p.

Miller, D. M., S. R. Leslie, J. W. Hillhouse, J. L. Wooden, J. A. Vazquez, and R. E. Reynolds, 2010, Reconnaissance geochronology of tuffs in the Miocene Barstow Formation; implications for basin evolution and tectonics in the central Mojave Desert: in in Reynolds, R.E and Miller, D.M, eds., "Overboard in the Mojave", Desert Studies Consortium California State University, Fullerton, p. 70-84.

Miller, S.T., 1980, Geology and mammalian biostratigraphy of a part of the northern Cady Mountains, Mojave Desert, California: U. S. Geological Survey Open-File Report 80-878, 126 p. doi:10.3133/ofr80878

Moseley, C.G., 1978, "The geology of a portion of the northern Cady Mountains, Mojave Desert." Master's Thesis, University of California, Riverside, 131pp.

Reynolds, R.E., Miller, David, Nielson, J.E., McCurry, Michael, 1995, Field Trip Guide: Ancient Surf aces of the East Mojave Desert, in Reynolds, R.E., and Reynolds, J., eds., Ancient surfaces of the east Mojave Desert: San Bernardino County Museum Association Quarterly, v. 42, no. 3, p. 5-26.

Riehle, J.R., 2015, Relations between thermal history and secondary structures of ignimbrites exclusive of rheomorphism: Geosphere; June 2015; v. 11; no. 3; p. 572–605. doi:10.1130/GES01089.1

Roche, O. Buesch, D.C., and Valentine, G.A., 2016, Slow-moving far-travelled dense pyroclastic flows during the Peach Spring super-eruption: Nature Communications, 7:10890, 8 p. doi:10.1038/ncomms10890

Sarna-Wojcicki, A.M., and Davis, J.O., 1991, Quaternary tephrochronology: in Morrison, R.B., ed., Quaternary nonglacial geology; conterminous U.S.: Geological Society of America, The Geology of North American Geology, v. K-2, p. 93-116.

Sherrod, D.R., and Nielson, J.E., eds., 1993, Tertiary stratigraphy of highly extended terranes, California, Arizona, and Nevada; proceedings of a workshop held at the Desert Research Center, Soda Springs (Zzyzx) California, February 9-12, 1990, U.S. Geological Survey Bulletin 2053, 250p.

Stone, Paul, Miller, D.M., Stevens, C.H., Rosario, Jose, Vazquez, J.A., Wan, Elmira, Priest, S.S., and Valin, Z.C., 2017, Geologic map of the Providence Mountains in parts of the Fountain Peak and adjacent 7.5′ quadrangles, San Bernardino County, California: U.S. Geological Survey Scientific Investigations Map 3376, 52 p., doi:10.3133/sim3376

Wells, R.E., and Hillhouse, J.W., 1989, Paleomagnetism and tectonic rotation of the lower Miocene Peach Springs Tuff: Colorado Plateau, Arizona, to Barstow, California: Geological Society of America Bulletin, v. 101, p. 846-863.

Young, R.A., and Brennan, W.J., 1974, Peach Springs Tuff—Its bearing on structural evolution of the Colorado Plateau and development of Cenozoic drainage in Mohave County, Arizona: Geological Society of America Bulletin, v. 85, no. 1, p. 83–90.

Ridgecrest–Trona fault complex and earthquake sequence

Frank Jordan,[1] Miles Wagner,[2] and Searles Valley Working Group[3]
[1] *San Bernardino County Engineering Geologist, frank.jordan@lus.sbcounty.gov*
[2] *San Bernardino County Emergency Services Officer*
[3] *Searles Valley Working Group, Appendix 1*

San Bernardino County Fire, Office of Emergency Services (OES) staff, in partnership with Land Use Services and volunteers of the Searles Valley Working Group, is conducting continuing surveys and monitoring of active faulting and lateral spreading associated with the 2019 Ridgecrest–Trona fault complex and earthquake sequence in the Searles, Salt Wells, and Indian Wells valleys. The Ridgecrest–Trona fault complex and earthquake sequence started on July 4 and 5, 2019, when two large earthquakes struck the extreme northwest corner of San Bernardino County (Southern California Earthquake Data Center [SCEDC], 2019). The M_W 6.4 foreshock occurred along a northeast-striking fault mapped by the California Geological Survey (CGS) (Bryant, 2005) and the U.S. Geological Survey (USGS and CGS, 2006-2017) as the Little Lake Fault. The next day, an M_W 7.1 earthquake ruptured a previously unmapped northwest-striking fault that offset playa sediments in China Lake and Paxton Ranch Playa (Figure 1, Ponti *et al.*, 2020). Damage to the Naval Air Weapons Station–China Lake (NAWS–CL) and in the community of Trona–Argus was particularly severe (Geotechnical Extreme Events Reconnaissance Association [GEER], 2019a, 2019b). The use of interferometry satellite imagery made available from the Advanced Rapid Imaging and Analysis (ARIA) team at the National Aeronautical and Space Administration's Jet Propulsion Laboratory (NASA JPL) and Interferometric Synthetic Aperture Radar (InSAR) imagery made available from the University of California, San Diego (UCSD) Institute of Interplanetary Geophysics and Planetary Physics (IGPP) to preliminarily

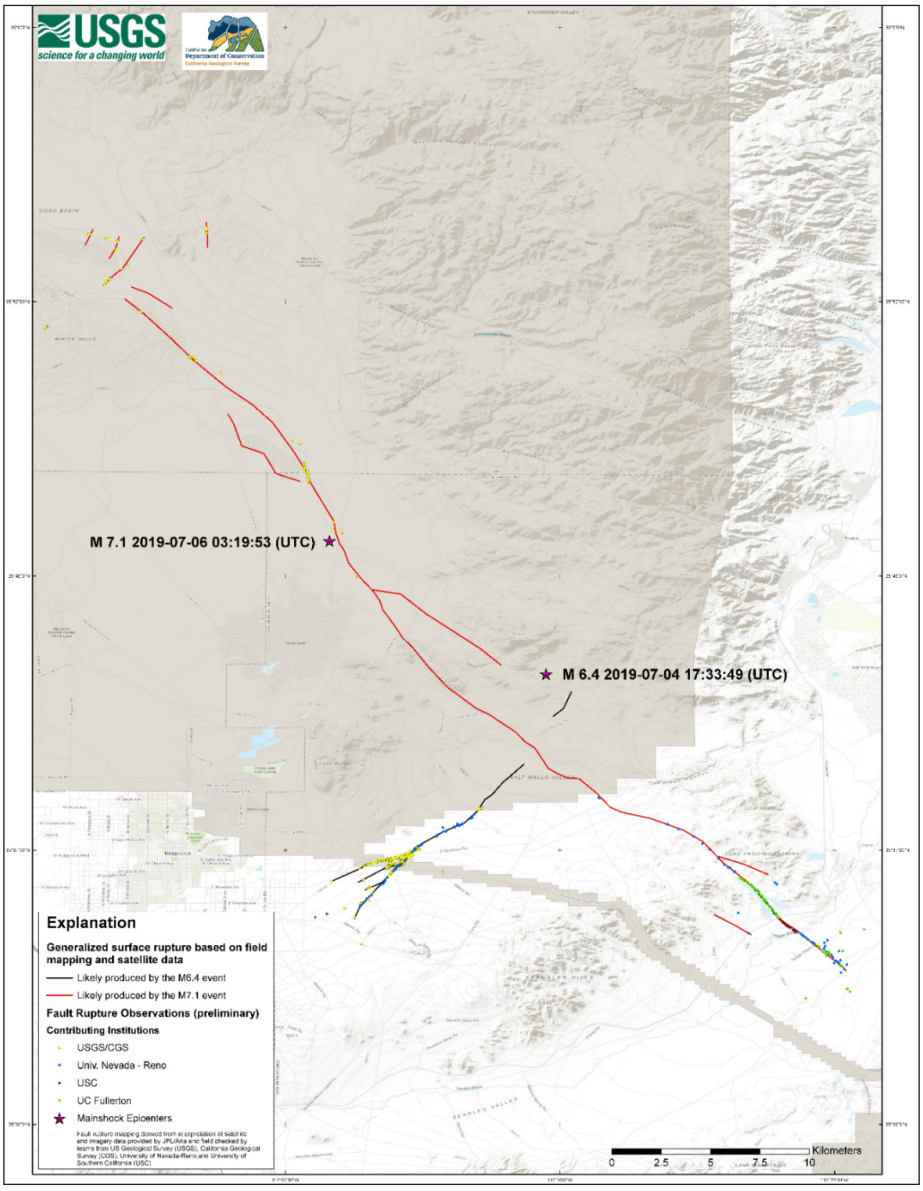

Figure 1. Salt Wells Valley and Paxton Ranch mapped fault ruptures (Ponti *et al.*, 2020; Pridmore and Thomas, 2020). The NW-striking Paxton Ranch fault is shown as the red line; the NE-striking Salt Wells Valley fault is shown as the blue line on this map. The shaded area represents the boundaries of the Naval Air Weapons Station–China Lake (NAWS-CL). Fainter lines are county boundaries.

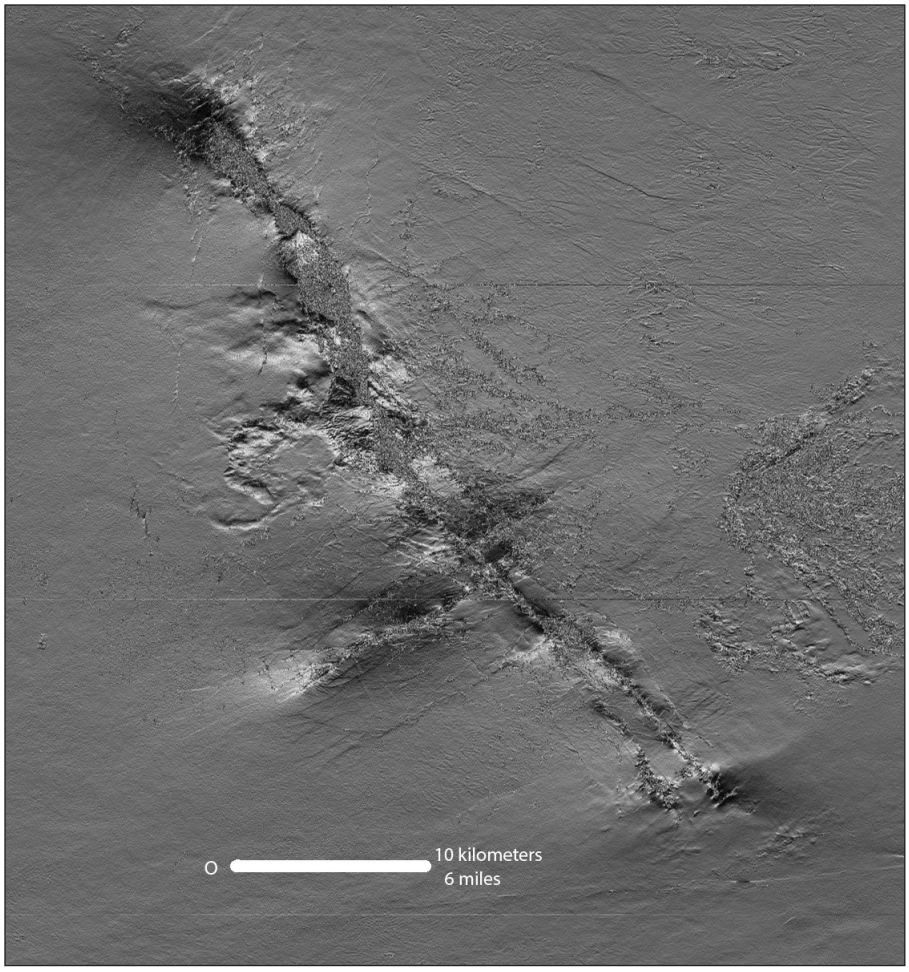

Figure 2. InSAR Range Phase Gradient Map (Xu, 2019). Note the double fault in the south, not mapped in Figure 1.

identify suspected surface fault ruptures and suspected liquefaction-affected areas has been borne out by localized field mapping to verify the correlation between the two mapping methods (Figure 2, Xu, 2019).

The existing Little Lake Fault is mapped by CGS within a series of discontinuous Alquist–Priolo Earthquake Fault Zones (A-P EFZs or A-P Zones) in the western Indian Wells Valley. Additional discontinuous branches of the Little Lake Fault Zone and associated A-P Zones are mapped in the eastern portion of Indian Wells and Salt Wells Valleys by CGS. CGS includes faults defined as "active" or "potentially active" within A-P EFZs. Active faults are those that display evidence for offset during Holocene time (last 11,000 years). Potentially active faults display evidence for movement during Pleistocene time (last 2.6 million years) (Parrish, 2018). The County preferred to recognize the surface ruptures of the Ridgecrest–Trona fault complex as separate fault zones independent of the mapped Little Lake Fault Zone. The County initially recognized the new faults as the northeast-striking Salt Wells Valley Fault Zone and the northwest-striking China Lake Fault Zone (Wagner and Jordan, 2019). The China Lake Fault had also been informally referred to as the Paxton Ranch Fault (Jordan, 2020a, in press). Subsequent to these publications, CGS officially named the faults the NE-striking Salt Wells Valley and the NW-striking Paxton Ranch Fault Zones (Pridmore and Thomas, 2020).

Detailed mapping of surface ruptures in the eastern Searles Valley by the volunteers of the Searles Valley Working Group confirmed the presence of northeast-striking faults in the Trona, Argus, Panorama Point, and Windy Acres areas. The County informally refers to these faults as the Trona and Aguirre Ranch Faults in the eastern Searles Valley, as well as several previously unmapped splays of the Salt Wells Valley Fault Zone in the Windy Acres area. An additional, suspected northeast-striking fault may rupture the surface of Searles Lake just north of the U.S. Bureau of Land Management's Pinnacles Natural Area in the southeast portion of the Searles Valley. We have informally referred to this fault as the Searles Valley Fault Zone.

A west-northwest-striking fault identified by deformed and uplifted pavement along Trona Road at West End has been mapped as the "Miles" Fault. North-striking fault ruptures mapped in the western Searles Valley, are informally referred to as the West Searles Valley Fault Zone, branches 1, 2 and 3.

Evidence for primary fault ruptures within the fault complex were observed in the Trona and western Searles Valley areas based on review of stacked phase gradient radar imagery made available by the Institute of Geophysics and Planetary Physics (Xu, 2019). Fault ruptures were preliminarily identified as linear tonal deformations on the radar imagery. Ground truthing identified en échelon ground fractures in zones up to 1.5 kilometers (1 mile) in length trending generally perpendicular to topographic contours. Apparent senses of rupture are left-oblique along northeast-striking faults and right-oblique along northwest-striking faults. The ruptures display up to 3.8 centimeters (1½ inches) of horizontal and vertical offsets. The faults display ground lurching and shattered slopes from strong ground shaking, and, locally, continued creep movement consistent with primary faulting. Creeping faults have deformed paved roadways. Mapping of these fault

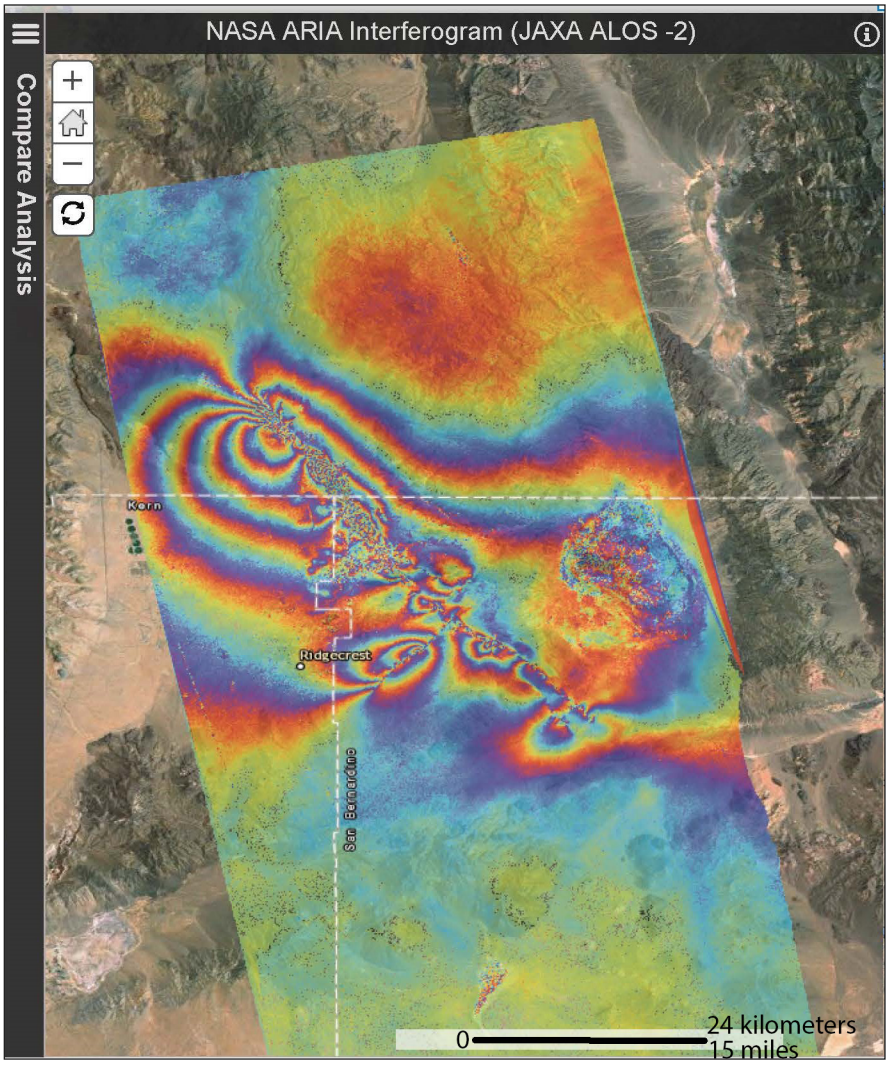

Figure 3. Interferometric overlay map showing lateral displacements and deformation of Searles Lake (Yun *et al.*, ARIA Team, NASA-JPL, 2019). The image shows relative movement between pre-earthquake (April 8, 2018) and post-earthquake (July 8, 2019) movement and/or rotation along flatter faults, perhaps pre-existing detachment faults underlying the southern Basin and Range Province. The post-quake imagery was acquired on July 8, 2019 and compared with April 8, 2018 data from the same region. Each color cycle represents 12 centimeters (4.8 inches) of ground displacement either toward or away from the satellite. The linear features that cut the color fringes in the southeast indicate likely locations of surface rupture caused by the earthquakes while the "noisy" areas in the northwest and east may indicate locations where the ground surface was disturbed by liquefaction:

ruptures will result in new A-P EFZs and/or County Fault Hazard Zones.

The strong ground shaking resulted in measured ground motions of over 0.5g. Geologic effects displayed at China Lake and Trona suggest actual ground motions exceeding 1g. Damage in the Trona–Argus area of the County was particularly severe, considering the distance of these communities to the earthquake epicenters and rupture zones. Damage in downtown Trona has been linked to faulting preliminarily identified as the Trona and Aguirre Ranch Faults.

Liquefaction-induced lateral spreads moved towards Searles Lake in areas underlain by lakebed sediments and shallow groundwater. Liquefaction fractures have been mapped generally parallel to the current playa margin. Liquefaction fractures are mostly restricted to a zone parallel to and within 300 meters (1,000 feet) of the existing Searles Lake margin. Sand boils were observed on the playa and along the playa margin in Trona. Interferometric imagery showed the entirety of Searles Lake as having shaken severely during the quakes and that the playa surface subsided, or seismically settled, several millimeters vertically (Figure 3, Xu, 2019). This permanent deformation was not observed on the interferogram at China Lake, which is located at the epicenter of the M7.1 earthquake. Deformation at Searles Lake is attributed to hot solution mining practiced by Searles Valley Minerals Corporation, shallow groundwater, and subterranean cavities developed over seven decades of mining operations at the lake. Mapping of liquefaction features in the County is expected to aid in the development of new County Liquefaction Hazard Zones. These zones will be added to the County's Hazard Mitigation Plan.

As of the date of this writing, more than 50,000 aftershocks (greater than M0.5) have been recorded by the California Institute of Technology. Analyses of the aftershock sequence have noted the relatively shallow source depths of these quakes. Depth evaluations have also recognized the existence of several planar alignments of microquakes (Wagner and Jordan, 2020, in press). The shallowest of these alignments are recognized at a depth of 8 kilometers (5 miles) and are relatively parallel to the existing ground surface, while deeper alignments, below a depth of about 10 km (6¼ mi) are inclined at shallow angles to the east. These planar alignments may represent tectonic movement and/or rotation along flatter faults, perhaps pre-existing detachment faults underlying the southern Basin and Range Province.

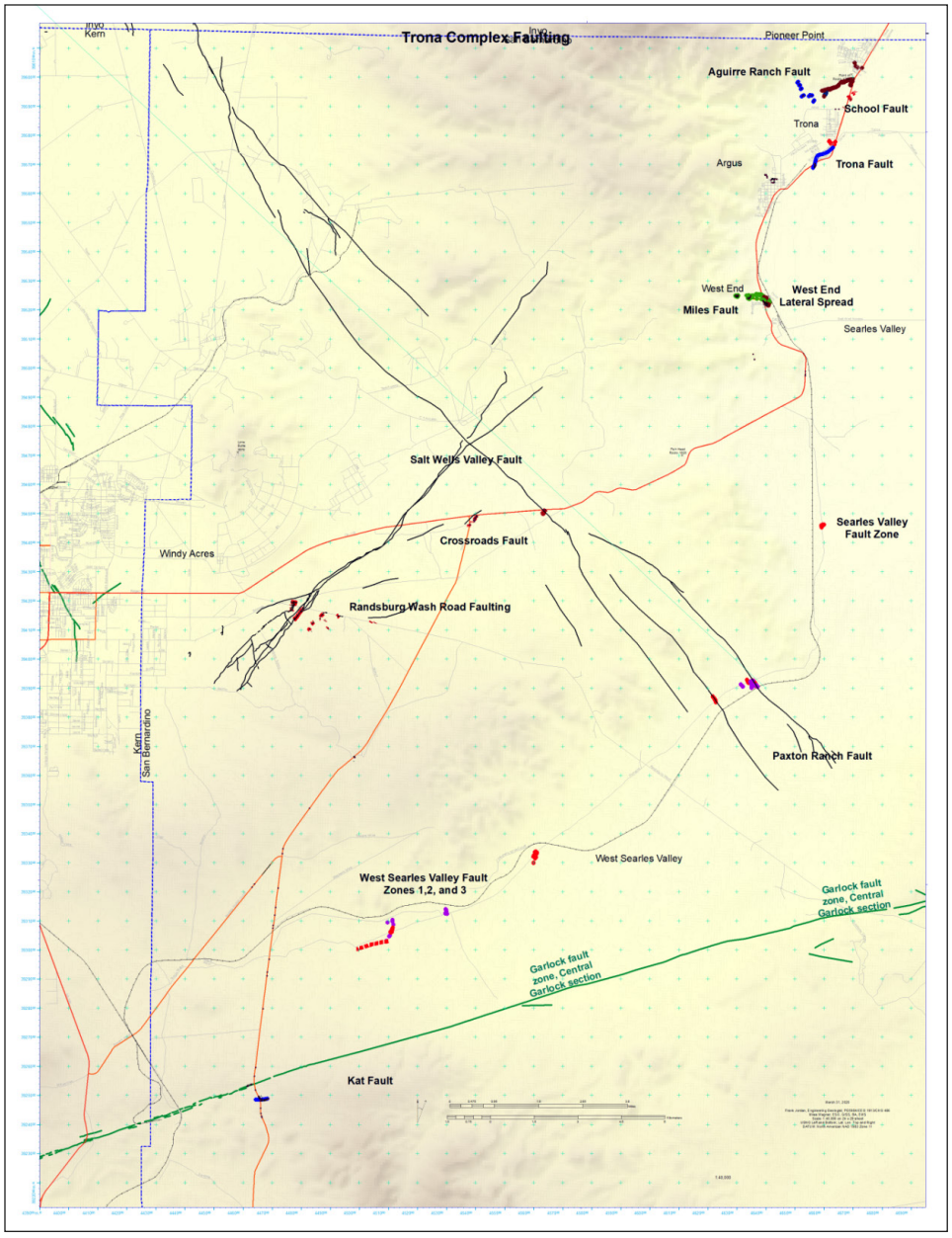

Figure 4. Map showing locations and names of faults mapped in San Bernardino County by the Searles Valley Working Group in 2019–2020 (Wagner, 2020).

Miles Wagner, Emergency Services Officer, and Frank Jordan, County Geologist, recognized the need for detailed mapping of the Trona area fault ruptures and formed the nucleus of the geologic mapping crew. Volunteers were invited to accompany the survey crew and contributed to the data acquisition and data analyses. The volunteers were informally organized into the Searles Valley Working Group. Members of the group participated in the surveys on an "as available" basis. The surveys documented the locations, lengths, orientations, offsets, sense of motions, and damage patterns using geographical positioning systems (GPS) devices and/or smart phone applications (apps).

Creeping motions and widely distributed fracture/fault zones were observed throughout the northern Searles Valley area. Sand boils and lateral spreading fractures resulting from liquefaction were mapped and photodocumented in the immediate vicinity of the Searles Lake margin. These patterns were roughly aligned with damaged and destroyed properties, damaged road surfaces, and broken underground utilities.

Using a combination of known fault lines, inferred possible fault locations, information provided by aerial and satellite reconnaissance, and field reports, an area survey was conducted. Locations for the surveys were chosen after studying the interferogram and stacked phase gradient InSAR maps.

The first faulting observed was on Trona Road in the West End area on the Saturday after the M7.1 event. A noticeable vertical tenting raised the road approximately 10 centimeters (4 inches), creating a definite traffic hazard. This fault is directly north of the County Public Works Yard at West End with mapping showing the fault displacement continuing under the yard's parking lot. This fault was not shown on any USGS or CGS preliminary map.

Additional area surveys were conducted in the Argus, Trona, Pioneer Point and Windy Acres communities in the Searles Valley and Salt Wells Valley areas. Fractures were observed in all communities. Many buildings beyond NAWS-CL were damaged or destroyed (Figure 5), roads, water storage and transmission /distribution systems damaged or destroyed, electrical infrastructure heavily damaged, natural gas transmission and distribution pipes damaged, and waste water systems broken and destroyed (Wagner, 2020, in press).

Windshield surveys included video recordings of all streets in an affected community, marking of damages and fractures with handheld GPS units, and extensive still photography. Field mapping of fracture and fault ruptures

Figure 5. Tensional wall fractures and ruptured roof at Esparza Restaurant (Jordan, 2019).

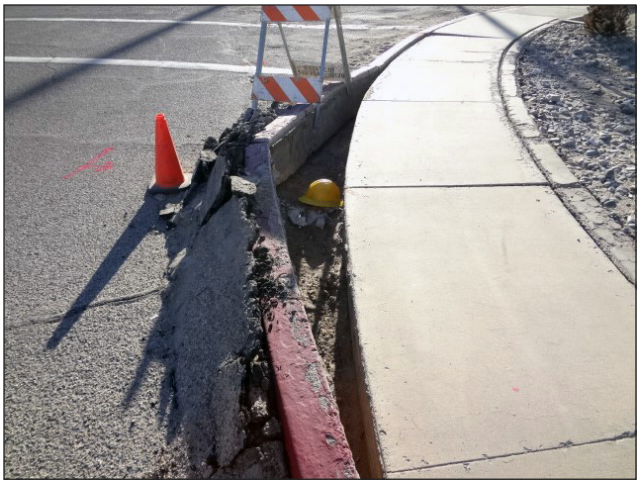

Figure 6. Shoved curb and tented asphalt pavement at the intersection of Main Street and Center Street in downtown Trona (Jordan, 2019).

Figure 7. Spalled sidewalk concrete and shoved and shattered concrete curb at the intersection of Main Street and Searles Street in downtown Trona (Jordan, 2019).

Figure 8. Shoved concrete sidewalk slab and tented tiles and grout in front of Esparza Restaurant along Main Street in downtown Trona. Tape measure extended 33 centimeters (13 inches) (Jordan, 2019).

Figure 9. Lateral spread fissures and fractures at Trona Rest Area (Jordan, 2019).

Figure 10. Sand boils adjacent to rest room facilities at Trona Rest Area (Jordan, 2019).

started with the August 3, 2019 survey. Field mapping was conducted using handheld Garmin 64 GPS units, supplemented by photo-documentation.

The following are summaries of the nine individual surveys conducted to date.

July 10, 2019 survey

This survey focused on downtown Trona. Damage occurred to almost all the downtown commercial structures and was photo-documented as part of the survey. Concrete sidewalks displayed shoving of concrete curbs and asphalt pavement due to compression from lateral displacements on planar slip surfaces (Figure 6). Asphalt pavement was tented and tilted on edge adjacent to displaced curbs. One sidewalk in front of the town museum showed evidence of spalling, apparently from rapidly applied lateral compression (Figure 7). The sidewalk in front of the red-tagged Esparza restaurant also displayed evidence of compression and shoving (Figure 8).

At least ten commercial and government structures were red tagged as unenterable after the quakes. Lateral spread fissures (Figure 9) and several sand boils (Figure 10) disrupted facilities at the local commuter rest area located at the east edge of downtown and the west margin of Searles Lake (Jordan, 2020b, in press). A buried water pipeline running along Trona Road in front of this rest area was broken, locally flooding the rest area. A buried natural gas pipeline was broken across the road from the rest area. Electric utility poles along the east edge of the rest area expressed evidence for having swung around their embedments in a manner described as "joysticking" (Figure 11).

Searles Lake is operated as a solution extraction mine by the Searles Valley Minerals Corporation (SVM). Damage was observed to cinder block walls and old smokestacks at the facility. We later learned that the entire operation was knocked offline due to red tagged conditions within several of SVM's structures, loss of power generation, and loss of steam boilers. Red tagging of the facilities was conducted not by representatives of the County, but by representatives of the company's insurance company. The rails of the Trona Railroad were coach whipped by surface offset where the Paxton Ranch Fault crossed under the tracks in the western Searles Valley. Settlement of roadbed ballast by over one meter (several feet) was observed just east of Argus. The rails and underlying ballast were later replaced. The plant required extensive repairs and did not restart for over a month. Several injection wells on the lake collapsed into hollowed out subsurface voids due to the shaking. Due to the lack of power and steam generation, the lake sediments experienced a significant cooling, further impacting the productivity of the mine.

Figure 11. Joysticked utility pole adjacent to Searles Lake (Jordan, 2019).

Chimneys were toppled at several residences in Trona. Churches within Trona were also shaken violently, with several displaying open fractures of their walls and yards. Classrooms and walkways at Trona High School were damaged by tensional fracturing. The freshwater pipeline to the town was severed by offset of both the Salt Wells Valley and Paxton Ranch Faults adjacent to Highway 178. Sections of the pipeline required replacement. The water tank feeding this pipeline was damaged by elephant's foot spreading of the wall of the tank but remained in service. A buried natural gas transmission pipeline running adjacent to the water line was bent by the ground offset but did not rupture due to its inherent flexibility. The bent section was later replaced.

Although not a part of this survey, reports indicated that several commercial, residential, and mobile homes in Ridgecrest received damage from the shaking. A portion of the roof at the city's movie theater collapsed. A fire destroyed a garage. At least two mobile homes slipped off their support pedestals and at least one other broke free of its earthquake tie-down restraints. Damage reports indicated extreme damage to U.S. Navy facilities on the China Lake base. The commissary and a large hanger were severely damaged. News and television reports indicated that up to $5 billion dollars would be needed to repair the facilities.

August 3, 2019 survey

The survey was conducted in the western Searles Valley east of Trona Road. Shortly after starting east on Pinnacle Road the first fracture zone was discovered. This zone was several miles west of any expected displacements. After mapping, this area was tentatively named Searles Valley Fault Zone 1. The mapped portion of the zone is approximately 75 meters (250 feet) wide, 150 meters (500 feet) long, trends N 20 E, and has vertical displacement up to 3 cm (a little over an inch).

Continuing east, two additional unexpected fracture zones were discovered. These zones were named Searles Valley Fault Zones 2 and 3, respectively. Fault displacement similar to zone 1 was observed in these zones. The two zones were also mapped and photographed. Each zone is approximately 75 meters (250

feet) wide, 180 meters (600 feet) long, trending N 20 E, with vertical displacements up to 3 cm (slightly over an inch).

East of the Randsburg Wash Road, still on Pinnacle Road, the survey located the southern end of the Paxton Ranch Fault Zone crossing the road. Field surveys of this area revealed three areas of faulting not previously mapped. The survey team also walked, mapped and photographed fault features in the known surface rupture zones of the Paxton Ranch Fault Zone. The zone is approximately 90 meters (300 feet) wide, over 1,050 meters (3,500 feet) long, trends N 20 W, and has vertical displacement up to 3 cm (about an inch).

North of Pinnacle Point, on the southern reaches of Searles Lake, a fifth zone of faulting and possible lateral movement (low angle landslide) was found. This feature was mapped and photographed. The zone is approximately 210 meters (700 feet) wide, 365 meters (1,200 feet) long, trends N 50 E, and has vertical displacement up to 15 cm (6 inches). Due to the presence of unexpected faulting and the complexity of the fault breaks, the day's survey ended with only one third of the planned mapping having been completed.

August 28, 2019 survey

This survey also focused on downtown Trona. Damage to the Searles Valley Minerals office and surroundings was photodocumented. Concrete sidewalks still displayed shoving of concrete curbs and asphalt pavement, although repairs had been completed to sidewalk and curbing at various intersections.

August 31, 2019 survey

Another survey of the western Searles Valley was conducted on August 31. Searles Valley Fault Zones 1, 2, and 3 were re-checked with additional fractures/faults found on the north and south ends of Zones 1 and 2. No additional surface ruptures were found at Fault Zone 3.

Figure 12. Paxton Ranch Fault rupture looking NW from Trona railroad (Jordan, 2019).

The areas checked near the zones were greatly expanded as compared with the August 3rd survey. An older fault scarp, probably associated with the Garlock Fault, was located and mapped along the south end of West Searles Valley Fault Zone 1. Fault Zone 1 was extended on both ends. The mapped zone is approximately 90 meters (300 feet) wide, 1.2 kilometers (4,000 feet) long, trends N 20 E, and has vertical displacement up to 3 cm (over an inch).

Mapping of the Paxton Ranch Fault Zone during this survey revealed three areas of extensive new surface ruptures not previously observed during the August 3 survey. Two of the trends were generally parallel to the original observations of August 3 but were at different locations. The third zone of surface ruptures north of the railroad tracks had been previously mapped during the August 3 survey However, additional mapping along this trend southeast of the previous survey found the fault both bracketing and penetrating a relatively large tufa deposit immediately north of the tracks. Seven distinct surface ruptures were mapped at this location, with individual tensional offsets up to 30 centimeters (1 foot) in width and right-lateral offsets up to 5 centimeters (2 inches) in length. These fault displacements were extensively mapped and photographed (Figure 12). The Paxton Ranch Fault Zone at this location was modified to approximately 450 meters (1,500 feet) wide and 1.5 kilometers (1 mile) long, with vertical displacements up to 10 cm (4 inches). The railroad tracks at this location had been bent and contorted by the fault offset, although by the date of this survey, both the steel tracks and the gravel ballast had been replaced.

The final stop of the day was at the "Miles From Anywhere Fault" crossing of Trona Road at West End, first measured on July 6, 2019. County Public Works had removed the tented pavement, regraded the roadway and repaved the road during the week of July 8–12, 2019. The road was smoothed and flattened upon completion. On August 30 a notable tenting of the pavement had occurred, although the asphalt road surface had not yet cracked. A survey of the area on the east side of the road showed additional cracking of the ground surface, with the fault traces trending N 45 W. On the west side of Trona Road, the fault trace trends N 85 W to the west edge of an abandoned borrow pit. Additional fracturing was not found west of the area and the survey was called off due to failing light. The "Miles" Fault Zone is approximately 45 meters (150 feet) wide, 365 meters (1,200 feet) long, trends N 50 W, and has vertical displacements up to 3 cm (about an inch).

October 5, 2019 survey

The next survey was conducted on Saturday, October 5, 2019. This survey covered areas northeast of Red Mountain and south of the Garlock Fault, the area north of Searles Valley on Trona Road to SR 178, the SR 178 area where both the Salt Wells Valley Fault and the Paxton

Ranch Fault cross the highway, and the Pioneer Point area of Trona.

Recent faulting was found in the Pioneer Point Area and in the Salt Wells Valley Fault Zone and the Paxton Ranch Fault Zone where the faults cross SR 187. The Salt Wells Valley Fault Zone rupture was indicated on the CGS maps as detected by instruments immediately after the M 6.4 earthquake, but not verified by field truthing. Our field investigation showed a fairly extensive rupture zone about 1.5 kilometers (1 mile) east of the faulting detected by satellite imagery. This fault was informally identified as the Crossroads Fault. The fault was mapped crossing both SR 178 and Trona Road, just south of their intersection. The ground-truthed fault trend roughly parallels the remotely imaged fault, about N 45 E. The Crossroads Fault continues to develop an upward tenting of the asphalt pavement where the fault crosses SR 178, typical of vertical uplift. This tenting and uplift of the pavement is evidence of continued post-seismic creep along the fault.

Field work in the Pioneer Point area found three areas of ground surface ruptures. The first area was located south of Pioneer Point, near the intersection of Athol Street and Telescope Avenue. The southern terminus of these ruptures is located north of Trona Cemetery. This zone of surface rupture was observed trending N 45 E for about 400 meters (0.25 mile). An extensive area of faulting was found on both sides of Trona Road. There were no residential structures in this area, with this fault crossing vacant land. This fault was informally named the Cemetery Fault. The fault may extend southwest into portions of the Trona business district to the southwest.

A second zone of surface ruptures was found just south of the Cemetery Fault, trending N 30 E. Damage to portions of the sewer lateral from Pioneer Point to the sewer treatment system may have been caused by movement of this rupture zone. This zone was informally named the School Fracture Zone, as the south end trends toward Trona High School. This zone requires further investigation, as it may be caused by faulting, lateral spreading/low angle landsliding, or a combination of the two types of movement.

The third and most extensive area of faulting begins at the Pile of Rocks area of Pioneer Point and extends west-southwest along the base of the Argus Mountains. While mapping the Cemetery Fault, a local resident invited the team to observe surface breaks trending through the southern edge of his property. This zone was mapped for about 1 ¼ kilometers (¾ mile) by two teams. This series of faults has many en échelon surface ruptures, all with about 1 to 5 mm (up to 1/5 inch) of vertical offset and an unmeasured amount of horizontal offset (Figure 13). This fault zone is informally named the Aguirre Ranch Fault, after the ranch property where it was first recognized. The overall trend of the Aguirre Ranch Fault is N 70 E.

October 19, 2019 survey

This survey focused on three areas. The team surveyed the West End area to determine the extent of the "Miles" Fault, the Trona area west of Point of Rocks–Pioneer Point, and the Argus area.

The "Miles" Fault survey recognized both low angle landsliding (lateral spread) and faulting. The area surveyed extended from the margin of the playa west 1¼ kilometers (3/4 mile) up canyon to the end of traversable terrain. Areas of lurch shattering were found along with faulting. Up canyon, large boulders had rolled down into the canyon, bouncing while rolling down slope. Some impressive impact craters were left by these boulders. The segment of the "Miles" Fault crossing Trona Road continues to develop an upward tenting feature typical of vertical uplift. This tenting and uplift of the pavement is evidence of continued post-seismic creep along the fault. To the east of Trona Road, en échelon ruptures of the fault were mapped in a vacant lot adjacent to 1st Street and crossing the intersection of 1st Street and A Street (Figure 14). The fault continues within an abandoned

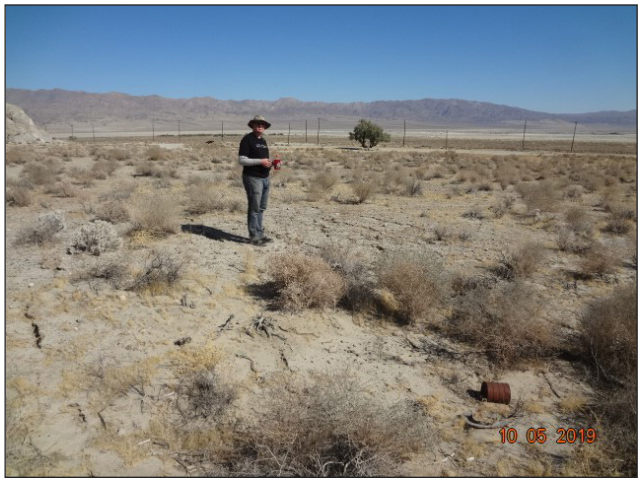

Figure 13. Northeast-striking surface ruptures of the "Aguirre Ranch" Fault visible around the feet of Dylan Terry SW of Point of Rocks (Jordan, 2019).

Figure 14. "Miles" Fault east of Trona Road (Jordan, 2019).

housing tract, uplifting a wooden fence and passing beneath a red-tagged garage and residence. Evidence of randomly oriented surface ruptures, characteristic of lateral spreading (or low angle landsliding), was also observed adjacent to the margin of the playa. This lateral spread/landslide was mapped southeast of the previously mentioned residence and garage, and also affects the County Public Works Yard for South Trona.

Our survey of the Argus area proved inconclusive, as many of the observable surface ruptures had been eliminated through reconstruction and grading. Additional fieldwork is needed.

The survey re-examined the Aguirre Ranch Fault along the toe of the Argus Mountains. This survey managed to extend the fault about 2.5 kilometers (1.5 miles) to the west-southwest of Pile of Rocks. Most of the observed movement along this fault is vertical and occurs over several parallel faults within the fault zone. The zone was mapped trending N 70 E to N 75 E, and is about 75 to 120 meters (250 to 400 feet) in width for most of the observed fault. Near the west end of the zone, a branch of the fault veers off, trending south-southwest towards the Searles Valley Minerals coal pile. The interferogram produced by NASA-JPL suggested that the ground surface moved downward in this area. Although not accessible for field measurement, it is suspected the strong ground shaking from the earthquakes caused seismic settlement of the unconsolidated material in the SVM coal pile. The location and trend of the Aguirre Ranch Fault are similar to the Salt Wells Valley Fault to the southwest. Although no surface fault rupture has been portrayed on NAWS-CL base within the Argus Range, geomorphology recognized by the team during review of imagery available from Google Earth suggests that the Aguirre Ranch Fault may represent a northeast extension and/or continuation of the Salt Wells Valley Fault Zone into Searles Valley.

December 14, 2019 survey

Several rain events in the Trona and Searles Valley areas apparently camouflaged the surface ruptures and faults with a thin veneer of transported sediment. While several ruptures were found and mapped during this survey, the area of interest near the County Landfill/Transfer Station west of the SVM plant had apparently experienced thunderstorms in the time since the previous survey. Mapping of surface ruptures was deemed unproductive.

The survey did include observation of the UNAVCO GPS station mounted on an outcrop representing a portion of the Independence Dike "swarm" material, along a ridge southwest of West End. This station was measured to have moved about 50 centimeters to the southeast at the time of the M7.1 main shock.

Reconnaissance mapping of the west end of the Salt Wells Valley Fault rupture, where the fault crossed Randsburg Wash Road, found that rainfall and runoff had not buried this portion of the fault and determined that the surface rupture was in a mappable condition. It was decided to return at a later date to focus on mapping the ground surface ruptures associated with this fault and try to determine the impact of this fault on the Windy Acres community.

January 3, 2020 survey

Field mapping concentrated on the west and southwest-striking portions of the Salt Wells Valley Fault at its crossing with Randsburg Wash Road. Students of Dr. Kerry Cato's GEO 391 field mapping class mapped strands of the fault north of the road. The mapping found that the surface ruptures were discontinuous, en *é*chelon breaks similar to those found along several other faults. The mapping effort by the class members also documented that the main trace of the Salt Wells Valley Fault was expressed by surface ruptures along the southern toe of a low, uplifted ridge of Pleistocene-age alluvium. The elevation difference between the alluvial fan south of the ridge and the ridge itself indicates a minimum of at least 6 meters (20 feet) of vertical displacement across this portion of the fault during late Pleistocene-Holocene time. Numerous antecedent drainages were found to traverse this ridge from south to north. The larger drainages displayed evidence of up to 85 meters (280 feet) of left-lateral offset along the fault trace, also during late Pleistocene–Holocene time. Both these features attest to the antiquity and continued movement of the fault.

February 1, 2020 survey

Field mapping concentrated on the west- and southwest-striking portions of the Salt Wells Valley Fault at its crossing with Randsburg Wash Road (Figure 15). Detailed mapping of the discontinuous, en échelon nature of the surface breaks was documented. The northwesternmost fault strand separated Holocene-age alluvium, inclined at a shallow angle to the north, from the low, east-trending ridge of older alluvial materials and rock outcrops. Further evidence was gathered documenting that the north to northeast-trending drainages traversed the ridge

Figure 15. Salt Wells Valley Fault rupture north of Randsburg Wash Road (Jordan, 2020).

from south to north, and displayed evidence of left-lateral offset along the strike of the fault. The incision of the drainages through the ridge validates the antecedent nature of the drainages and verify that the alluvial fan and its drainage pattern predated uplift of the ridge. Mapping of the left-lateral offset of the drainages affirmed that the drainages had either subsequently, or simultaneously, been left-laterally offset by movement along the fault. Mapping of surface ruptures south of Randsburg Wash Road did confirm faulting at locations predicted by the InSAR imagery. Although previously listed as only detected by review of remotely sensed imagery, the mapping verified the presence of at least two additional strands of the Salt Wells Valley Fault east of the currently mapped locations.

Summary

Using InSAR and interferometric imagery to preliminarily identify fault and liquefaction areas has been substantiated by localized field mapping that verified the correlation between the mapping methods. Additional field studies must be completed to accurately develop a mitigation strategy for the Trona area. This may include development of State Alquist–Priolo EFZs, County Fault Hazard Zones, County Liquefaction Hazard Zones; or areas in need of a prescriptive geotechnical report prior to issuance of a building permit. Current building codes should be reviewed with respect to any proposed development in the Trona and Windy Acres areas to determine if any modifications or changes to the codes are warranted.

References

Bryant, W.A. (compiler), 2005, Digital database of Quaternary and Younger Faults from the Fault Activity Map of California, version 2.0: California Geological Survey website: http://www.consrv.ca.gov/CGS/information/publications/Pages/QuaternaryFaults_ver2.aspx.

Geotechnical Extreme Events Reconnaissance Association (GEER), 2019a, Preliminary Report on Engineering and Geological Effects of the July 2019 Ridgecrest Earthquake Sequence: Geotechnical Extreme Event Reconnaissance Association, version 1, 69 p.

Geotechnical Extreme Events Reconnaissance Association (GEER), 2019b, Preliminary Report on Engineering and Geological Effects of the July 2019 Ridgecrest Earthquake Sequence: Geotechnical Extreme Event Reconnaissance Association, version 2, 77 p.

Jordan, Frank, in press (2020a), abstract, Ridgecrest-Trona Earthquake and Fault Complex, San Bernardino County: 2020 National Earthquake Conference & 72nd Earthquake Engineering Research Institute Annual Meeting.

Jordan, Frank, in press (2020b), abstract, Ridgecrest-Trona Earthquake Complex, Liquefaction and Lateral Spreading, San Bernardino County: 2020 National Earthquake Conference & 72nd Earthquake Engineering Research Institute Annual Meeting.

Parrish, J.G., 2018, Earthquake Fault Zones, A Guide for Government Agencies, Property Owners / Developers, and Geoscience Practitioners for Accessing Fault Rupture Hazards in California: California Geological Survey, Special Publication SP 42, 93 p.

Pridmore, C.L. and Thomas, K, 2020, California Earthquake Clearinghouse, July 4th and 5th 2019 Ridgecrest Earthquake Sequence: 2020 National Earthquake Conference & 72nd Earthquake Engineering Research Institute Annual Meeting.

Southern California Earthquake Data Center (SCEDC), July 5, 2019, Recent Earthquakes in California and Nevada: https://scedc.caltech.edu/recent/Maps/118-36.html

U.S. Geological Survey and California Geological Survey, 2006-2017, Quaternary fault and fold database for the United States, accessed July 10, 2019, at: https://www.usgs.gov/natural-hazards/earthquake-hazards/faults.

Ponti, D.J., Blair, J.L., and 74 others. (2020). Documentation of surface fault rupture and ground deformation features produced by the Ridgecrest M6.4 and M7.1 earthquake sequence of July 4 and 5, 2019, Seismol Res Lett (in press).

U.S. National Aeronautics and Space Administration (NASA) , 2019, NASA ARIA wrapped interferogram produced using JAXA ALOS-2, from imagery taken on July 8, 2019, https://maps.disasters.nasa.gov/arcgis/apps/MinimalGallery/index.html?appid=7ac57cc4586241d2991d89f6e621afab#viewer=e880bcfe1428433cbb9b4517f756e397

Wagner, Miles, in press (2020), San Bernardino County Emergency Response to July 4th–5th Ridgecrest–Trona Earthquake Complex: 2020 National Earthquake Conference & 72nd Earthquake Engineering Research Institute Annual Meeting.

Wagner, Miles, and Jordan, Frank, 2019, Trona-Ridgecrest Earthquakes, The San Bernardino County Perspective, Association of Environmental and Engineering Geologists – Inland Empire Chapter August Meeting, presented on August 17, 2019.

Wagner, Miles, and Jordan, Frank, in press (2020), abstract, Trona Post-Earthquake Geologic Fault Investigation, Pacific Section, American Association of Petroleum Geologists, Annual Convention.

Xu, Xiaohua, 2019, InSAR range phase gradient map of the Ridgecrest fault ruptures, University of California, San Diego, Institute of Geophysics and Planetary Physics.

Yun, S-H., Owen, S, Hua, H., Agram, P., Bekaert, D., and the ARIA Team, 2019, Interferogram of the Ridgecrest Earthquake Sequence developed using synthetic aperture radar (SAR) data from the ALOS-2 satellite to produce a map showing surface displacement from the earthquakes. Produced by the Advanced Rapid Imaging and Analysis (ARIA) team at the National Aeronautical and Space Administration's Jet Propulsion Laboratory.

Appendix 1: Searles Valley Working Group

Madison Andrews, California State University, San Bernardino

Jessie Bagby, Colorado River Basin Regional Water Quality Control Board

Suzanne Baltzer, California State University, Los Angeles

Alicia Borchman, Lahontan Regional Water Quality Control Board

Karin Burger

Dr. Kerry Cato, California State University, San Bernardino

Kevin Clark

Joe Cota, Earth Resources

Shanna Delgado,

Mark Doerschlag, Aragon Geotechnical

Ian Espinoza, California Department of Water Resources

Brian Ferwerda, US Bureau of Land Management

Jeffrey Fitzsimmons, Lahontan Regional Water Quality Control Board

Silvia Flores, Lahontan Regional Water Quality Control Board

Darryl Forrester

Anna Garcia, Mojave Water Agency

Greg Johnson, Los Angeles County Department of Public Works

Kristin Koehler

Rob Markoff, LOR Geotechnical

Emmons McKinney, University of California, Los Angeles; Cal Poly Pomona

Alondra Navarro, California State University, San Bernardino

Alice Orton

Jennifer Pareda, California State University, San Bernardino

Gamaliel Pelayo, California State University, San Bernardino

David Perry, Wood PLC

Tracy Roberts, California State University, San Bernardino

Donn Schwartzkopf, Terra Geosciences

Robert Skinner, Fontana Unified School District

Mark Spykerman, Earth Systems, Southwest

Dylan Terry, California State University, San Bernardino

Jesus Ulloa, California State University, San Bernardino

Kathryn VonSydow, California State University, San Bernardino

Daniel Wetterhus, Chaffey Community College

Review of Paleogene vertebrates and invertebrates from the Goler Formation of California and their biostratigraphic and paleogeographic significance

Donald Lofgren,[1] Howard Hutchison,[2] Randall Nydam,[3] Michael Paik,[4] Elizabeth Lee,[4] S. Alejandra Butcher,[4] and Thea Kirkpatrick[4]

[1]*Raymond M. Alf Museum of Paleontology, Claremont, CA 91711*
[2]*Museum of Paleontology, University of California, Berkeley, CA 94720*
[3]*Midwestern University, Glendale, AZ 85308*
[4]*The Webb Schools, Claremont, CA 91711*

ABSTRACT—The Goler Formation is the only Paleocene rock unit in North America west of the Rocky Mountains that has yielded a diverse assemblage of vertebrates. Exposed in the El Paso Mountains in the northern Mojave Desert, the formation is composed of 4,000 m of strata subdivided into four members that represent nonmarine sediments capped by marine strata. Members 1-2 have not yielded fossil remains of any type, and the sparse fauna from Member 3 composed of only three partial turtles and a fish skeleton have limited utility in determining the age of the formation. Strata representing Member 4a-4b have yielded numerous specimens of vertebrates, primarily mammals, turtles, lizards, and crocodilians, as well as a partial avian humerus, a ray tooth, and a few gastropod shells. New taxa based on specimens from these strata include three new genera and seven new species of mammals and two new genera and species of turtles. Based primarily on its mammalian assemblage, Member 4a-4b is middle Tiffanian (late Paleocene) when compared to Paleocene mammal assemblages in the Western Interior, an age supported by magnetostratigraphic correlation of Member 4a-4b to Chron 26r. Based on the age of overlying Member 4 strata, Member 3 is middle Tiffanian (late Paleocene) or older. The late Paleocene or early Eocene Member 4d marine section contains cocoliths, planktic and benthic foraminifera, marine mollusks, shark teeth and a terrestrial mammal tooth, and probably represents a near shore marine facies of a river delta. Marine section paleomagnetic samples are of reversed polarity that probably correlate to either Chron 25r or Chron 24r. The non-marine fauna of the Goler Formation exhibits significant endemism as more than 45% of mammalian taxa are not found elsewhere and only five mammal taxa can be confidently referred to species from the Western Interior. Turtles reflect similar endemism and the remains of gars, a common fish in Paleocene strata from the Western Interior have yet to be found in Goler strata. The high degree of endemism reflected in the vertebrate fauna of the Goler Formation strongly suggests geographic isolation, which led to the formation of a unique west coast faunal province in what is now southern California during the late Paleocene.

Introduction

The Goler Formation is composed of about 4000 meters of mostly nonmarine sediments (Cox and Diggles, 1986) that crop out within the El Paso Mountains in the northern Mojave Desert (Figure 1). The formation is divided into four members (numbered 1-4), with Member 4 consisting of four informal units, listed in ascending stratigraphic order as 4a, 4b, 4c and 4d (Cox 1982, 1987) with 4d containing marine sediments (Cox and Edwards, 1984; Cox and Diggles, 1986). Member 1-3 consist of locally derived fluvial and debris-flow deposits that accumulated mostly on alluvial plains and fans on a southward sloping piedmont while the majority of Member 4 strata consist of distally derived fluvial deposits that accumulated in the axial region of the Goler Basin south of the piedmont slope until an eastward transgression of the Pacific Ocean eventually invaded it (Cox, 1982; Cox and Diggles, 1986; Cox, 1987).

The age of the Goler Formation is based mostly on vertebrate and invertebrate fossils recovered since 1950, although Members 1-2 and 4c have yet to yield fossils of any type. The earliest reports of Goler fossils were leaf impressions recovered from mudstones now mapped as Member 3 that were thought to indicate an Eocene age (Fairbanks, 1896; Axelrod, 1949). In 1952, R. Tedford and M. McKenna found a crocodilian tooth in Member 4, higher in the formation than where the "Eocene" plant fossils were recovered and McKenna returned to the site in 1954 and found a mammal jaw of Paleocene age (McKenna, 1955). Subsequent discoveries of mammal

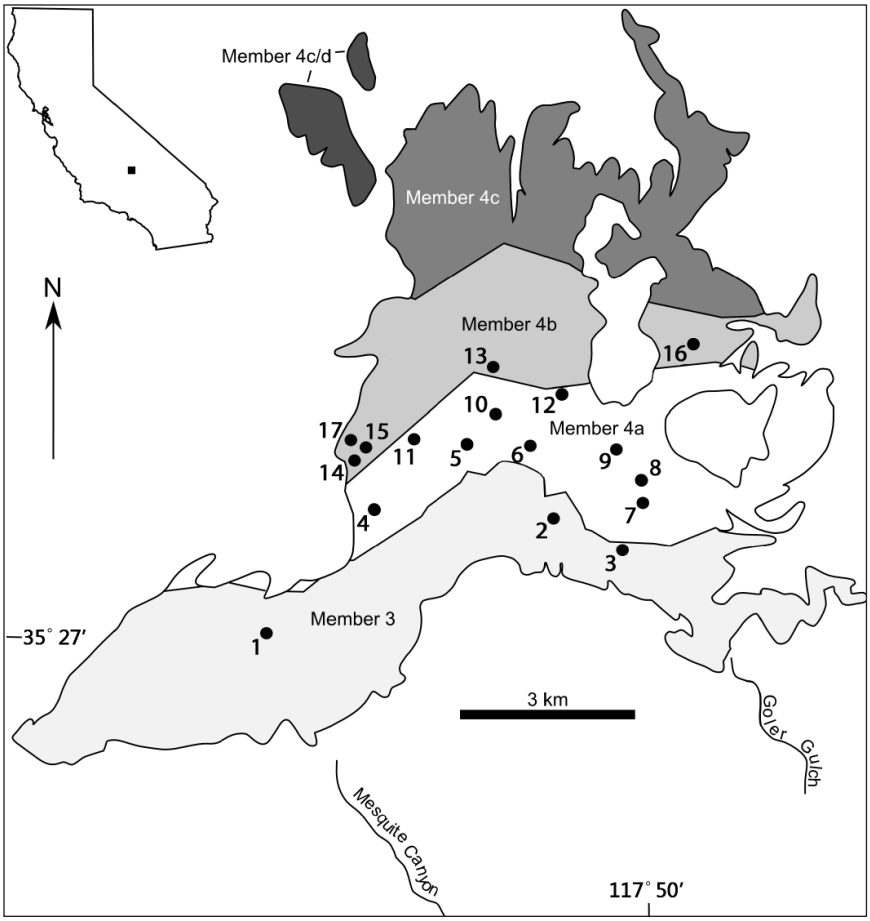

Figure 1. Map of California with the location of the study area shaded and outcrop map of Member 3 and Member 4 of the Goler Formation (adapted from Cox, 1982; Cox and Diggles, 1986) showing location of non-mammalian vertebrate sites in Table 1.

teeth and jaws in Member 4a and 4b confirmed the Paleocene age which was further refined based on the similarity of the Goler mammals to Torrejonian (middle Paleocene) mammals from the Rocky Mountain states (McKenna, 1960; West, 1970; McKenna et al., 1987). About the same time, late Paleocene or early Eocene foraminifera, marine mollusks, and cocoliths were recovered above the mammal sites in strata mapped as Member 4d (Cox and Edwards, 1984; Cox and Diggles, 1986; McDougall, 1987; Squires et al. 1988; Reid and Cox, 1989).

A renewed phase of collecting in Member 4a and Member 4b began in the early 1990s and resulted in the recovery of a numerous specimens of vertebrates, primarily mammals, turtles, lizards, and crocodilians, as well as a partial avian humerus and a ray tooth (Lofgren et al., 2002, 2008, 2009, 2014, 2018; McKenna and Lofgren, 2003; McKenna et al., 2008; Nydam and Lofgren, 2008; Stidham et al., 2014; Williamson and Lofgren, 2014). The eutherian mammalian assemblage from Member 4a and Member 4b indicates that these strata are middle Tiffanian (late Paleocene) (Lofgren et al., 2014) rather than Torrejonian (middle Paleocene). Also, a nonmarine mammal tooth, shark teeth and additional marine mollusks were recovered from previously unknown sites in Member 4d (Lofgren et al., 2010).

The Goler Formation is the only Paleocene rock unit in North America west of the Rocky Mountains that has yielded a diverse assemblage of vertebrates and we review the entire vertebrate and invertebrate fauna of the Goler Formation for the first time.

Abbreviations, materials, and methods

RAM: Raymond M. Alf Museum of Paleontology, Claremont, California; **UCMP**: University of California Museum of Paleontology, Berkeley, California. The RAM and UCMP record each vertebrate locality by using a V followed by numbers (e.g. V98012 or UCMP 5250) and specimens are each given a unique number following RAM or UCMP (e.g. RAM 9044 or UCMP 81603). RAM localities in the text will be referred to only by number (e.g. V98012), while UCMP localities will carry the UCMP designation to avoid confusion. Screen-washing of approximately 12 tons of sediment at RAM localities V98012 and V94014 yielded over 200 specimens identifiable to taxon; all others were found as surface float. Images of many mammal specimens listed here were provided in McKenna et al. (1987), West (1970), McKenna and Lofgren (2003), McKenna et al. (2008), Lofgren et al. (2014, 2018), and Williamson and Lofgren (2014). Published images for non-mammalian taxa listed here are noted in the text. Site numbers in Figure 1 refer to localities and non-mammalian taxa identified from them listed in Table 1. Similarly, Figure 4 numbers refer to localities and mammalian taxa identified from them listed in Table 2.

Member 3

The first vertebrate fossils reported from the Goler Formation were a mammal tooth and a partial turtle carapace found in 1950 by R. Tedford and R. Schultz from sediments (#1 in Figure 1) mapped as Member 3 by Cox (1982, 1987). These specimens were given to C. Stock at the California Institute of Technology so they could be studied, but soon thereafter, Stock died unexpectedly and apparently the fossils were discarded (McKenna et al. 1987; Lofgren et al., 2009). This was a great loss because intense prospecting of outcrops of Member 3 over the last six decades has not yielded additional mammalian

Figure 2. Macrobaenid carapace (RAM 14538) as found in 2010 in Member 3.

specimens. However, three partial turtle shells and a partial skeleton of a fish were recovered. A concretion containing the dorsal and pelvic fins of a bass-shaped osteichthyan (UCMP 81603, UMCP V5250) was found in 1952, about one km east of the Tedford-Schultz site and was tentatively identified as a beryciform or peciform (spiny-rayed fishes) (McKenna et al., 1987; Table 1). If UCMP 81603 does indeed represent a beryciform (extant beryciforms are marine), it suggests a marginal marine environment might have been preserved in Member 3 (McKenna et al., 1987).

In 1996, M. McKenna found turtle shell fragments about .5 km south of the Tedford-Schultz site and these specimens housed at the UCMP have yet to be studied. Just over a decade later, two partial shells were found a few km east of the Tedford and Schultz site. RAM 14538 (Figure 2) is a nearly complete carapace of a macrobaenid from V201001 (#3 in Figure 1) and RAM 9958 is a fragmentary carapace from V200916 (#2 in Figure 1) that has not been identified to taxon. Extensive prospecting of Member 3 over the last two decades did not yield additional vertebrate specimens, a testament to the rarity of fossils in Member 3. The few known specimens from Member 3 have limited utility in determining the age of these strata; based on the age of overlying Member 4 strata, Member 3 is middle Tiffanian (late Paleocene) or older (Albright et al., 2009; Lofgren at al., 2014).

Member 4a and Member 4b

Locating fossils in Member 4a and Member 4b is difficult, but concentrated efforts over the last three decades yielded a surprisingly diverse assemblage of vertebrates and a small number of gastropod shells (Lofgren et al., 2014, 2018, and references therein). The fauna from these strata (Figure 1, Table 1) includes:

Gastropods: The few gastropods recovered represent a single nonmarine taxon, but they lack anatomical details, so could only be confidently identified as representing the Order Stylommatophora (McKenna et al., 1987).

Birds: A proximal humerus of *Lithornis* (RAM 15530) was found at V200001 (#5) in 2013 and it represents the oldest Cenozoic bird from the west coast of North America (Stidham et al., 2014, fig. 2); lithornithids were ground dwellers that foraged with their slender bills.

Table 1. Types of vertebrates (excluding mammals) recovered from RAM and UCMP sites in the Goler Formation with turtles broken into four groups. Sites organized by member and listed left to right 1-17 based on approximate ascending stratigraphic order; (1) UCMP V5250; (2) RAM V200916; (3) RAM V201001; (4) RAM V200509, V200510, V200803; (5) RAM V200001; (6) RAM V200602; (7) RAM V200302; (8) RAM V200603, V200203; (9) RAM V200304, 200303;(10) UCMP V81035; (11) RAM V200048; (12) RAM V94014, UCMP V5252, V67158, V5870, V99042; (13) UCMP V6516; (14) RAM V201301; (15) RAM V201302; (16) RAM V94015, V98012; (17) UCMP V5251.

	Member 3			Member 4a									Member 4b				
Taxon	**1**	**2**	**3**	**4**	**5**	**6**	**7**	**8**	**9**	**10**	**11**	**12**	**13**	**14**	**15**	**16**	**17**
Trionychid	-	-	-	-	-	X	-	X	-	-	X	X	X	-	-	-	X
Macrobaenid	-	-	X	-	-	-	X	-	-	X	-	X	-	-	-	-	-
Baenid	-	-	-	-	-	-	-	-	-	-	-	-	X	-	-	-	-
Turtle indet.	-	X	-	X	X	-	-	-	X	-	-	X	-	X	X	X	-
Crocodylia	-	-	-	X	X	-	-	-	-	-	-	X	-	-	-	X	-
Lacertilia	-	-	-	X	-	-	-	-	X	-	-	X	-	-	-	X	-
Fish	X	-	-	-	-	-	-	-	-	-	-	-	-	-	-	-	-
Ray teeth	-	-	-	-	-	-	-	-	-	-	-	-	-	-	-	X	-
Lithornis		-	-	-	X	-	-	-	-	-	-	-	-	-	-	-	-

Rays: The single ray tooth (RAM 7180, V98012, #16) has a flat rombic crown with paired roots and resembles the anterior teeth of *Hypolophodon*. Ray teeth are commonly found in marginal marine and nonmarine fluvial deposits of Paleocene age.

Crocodilians: Teeth, osteoderms, and a skull fragment were recovered from four sites (#4, #5, #12, #16) and are similar in morphology to the Paleogene alligator *Allognathosuchus*. These specimens are a skull fragment (RAM 9173) from V200803, teeth (RAM 18279, 6985, 6982) and osteoderms (RAM 6983, 18280) from V94014, a single tooth from V98012 (RAM 1823) and UCMP V67158 (UCMP 55402), and three teeth (RAM 18278, 9724, 9723) from V200001.

Lizards: Osteoderms were commonly recovered from screen-washing at V98012 (#16) and there are two main morphotypes: (1) non-keeled, imbricating osteoderms with shallow pits/grooves (RAM 10018, 10022, 10030-31, 10033-36) that are most similar to the anguid *Proxestops* (but might also represent *Odaxosaurus*), a frontal fragment with ornamentation (RAM 10028) also represents this taxon; (2) keeled, imbricating osteoderms with prominent rugose ornamentation (RAM 10019-10021, 10023-24) similar to the anguid *Exostinus* (Nydam and Lofgren, 2008). Six lizard jaws are also recovered from V98012 and they represent anguids (RAM 7187, 7182), xantusiids (RAM 7183, 7186), a scincomorphan (RAM 7181) and an indeterminate taxon (RAM 7188). A second scincomorphan (RAM 7213) was found at V200203 (Nydam and Lofgren, 2008). Unstudied specimens are a jaw (RAM 7190) from V94014 and a jaw (RAM 9702) and osteoderm (RAM 9705) from V200510. Anguids are alligator lizards, scincomorphans are relatives of skinks (leaf litter dwellers) and xantusiids are relatives of night lizards (rock/tree bark dwellers) (Nydam and Lofgren, 2008; Lofgren et al. 2009). These Goler Formation specimens represent the western-most Paleocene lizards in North America (Nydam and Lofgren, 2008).

Turtles: Shell fragments are commonly found in Member 4a and Member 4b strata. In addition to these fragmentary remains, partial shells, skulls, and postcranial material have also been recovered. These specimens represent three families, Baenidae, Macrobaenidae and Trionychidae. Baenids are known from two specimens, a hypoplastron fragment (UCMP 131765, UCMP V6516, #13) and a skull (UCMP 179519, UCMP V99042, #12) which is the holotype of *Goleremys mckennai* (Hutchison, 2004). UCMP 179519 is the first specifically identifiable record of a baenid from the Pacific slope of North America (Hutchison, 2004). Baenids are river turtles found in Cretaceous to late Eocene strata.

Figure 3. Trionychid carapace (RAM 9967) from Member 4a.

There are a few specimens of macrobaenids, the most complete a partial plastron and carapace with postcranial elements (RAM 7214, V200302, #7). In 1952, a tibia of *Trionyx* (UCMP 55403) was found at UCMP V5251 (#17) and is now identified as a probable marcobaenid. Similarly, a phalange of a large unspecialized eucryptodire (UCMP 55401; McKenna et al. 1987, fig. 2) from UCMP V5252 (#12) is now tentatively identified as a macrobaenid metatarsal. Other specimens are more fragmentary and include two peripherals (UCMP 124941, UCMP V81035, #10; McKenna et al., 1987, fig. 1), bridge peripherals (UCMP 131764, UCMP V5870, #12) (McKenna et al., 1987), and shell fragments (RAM 15956, V94014 and RAM 15959, V94015). Macrobaenids are nonmarine turtles that range in age from Late Cretaceous to late Paleocene in North America and are unknown elsewhere on the Pacific slope.

Trionychids are the most common turtle in the Goler Formation and most of their occurrences are shell fragments: RAM 15951, V200602 (#6); RAM 6989, RAM 6992, RAM 6994 RAM 6999, RAM 7001, RAM 9360, RAM 15952, RAM 6995, RAM 9966, RAM 15953, V94014; RAM 6978, RAM V20001; UCMP 81605, UCMP 149164, UCMP 149165, UCMP V5252; UCMP 81609, UCMP V5870 (#12); UCMP 69580, UCMP V6516 (#13). A skull (RAM 7004) of an undescribed new genus of trionychid was found in 2000 at V200048 (#11). Also, a partial carapace (RAM 9967; Figure 3) from V200603 (#8) with thirteen costals and five neurals represents a new species (probably the same one as the skull RAM 7004).

Other records of turtles from the Member 4a and Member 4b are shell fragments that can't be referred to a specific group. These specimens are: RAM 9968, V200916;

RAM 15957, V200509; RAM 6979, RAM 6980, RAM 7206, V200001; RAM 15954, V200304, RAM 6988, RAM 6990, RAM 6991, RAM 6993, RAM 6996, RAM 7000, RAM 7002, RAM 15955, V94014; RAM 16018, RAM 16019, V201301; RAM 16020, V201302; UCMP 81606, UCMP V5252 (turtle indeterminate in Table 1).

Mammals: The record of mammals in the Goler Formation is represented by multituberculate, metatherian, and eutherian specimens that consist almost entirely of dental remains. Initial efforts in the 1950s to 1980s to recover fossils yielded a sparse mammalian assemblage (McKenna, 1955, 1960; McKenna et al., 1987). A renewed phase of collecting in the 1990s resulted in recovery of a few hundred mammalian specimens (Figure 4, Table 2) (Lofgren et al., 2014, 2018, and references therein).

Multituberculates: The early sample of three incisors (McKenna, 1960; McKenna et al., 1987) was augmented by 33 additional teeth listed below that include a new genus and species, *Golercosmodon mylesi* (Lofgren et al., 2018). Two skulls to be described later utilizing μCT technology represent *Neoliotomus*? (RAM 9663, V200014) and a new species of *Parectypodus* (RAM 9048, V200001) (Lofgren et al., 2018).

—*Neoliotomus conventus*: UCMP 49490, incisor fragment, UCMP 55399, incisor root, UCMP V5870 (#6 in Figure 4); RAM 7237, P4 fragment, V98012, (#7); RAM 7204, questionable referral p4, V200001 (#3). RAM 7237 exhibits the diagnostic P4 morphology of *Neoliotomus conventus* and confirms the presence of this rare taxon in California (Lofgren et al., 2018).

—*Golercosmodon mylesi* (new genus and species): RAM 6968, P4 (holotype), RAM 6965, P4 and RAM 9656 partial P4, V98012 (#7); RAM 9685, P4, V200510 (#2). The P4s of *Golercosmodon mylesi* differ from other microcosmodontids in the development of the labial cusp row and the number of medial row cusps (Lofgren et al., 2018). cf. *Golercosmodon mylesi*: these isolated molars are a tentative referral; RAM 7232, RAM 6969, RAM 6970, RAM 6971, RAM 6434, RAM 9999, RAM 9988, RAM 7230, RAM 6483, RAM 6731, RAM 6975, RAM 7235, RAM 6463, RAM 9993, RAM 9971, RAM 9995, RAM 6967, RAM 9990, RAM 9974, RAM 9975, RAM 9972, V98012 (#7); RAM 6980, RAM 9676, V200510 (#2); RAM 6447, RAM 6422, V94014 (#6); RAM 9722, V200001 (#3).

—Microcosmodontid genus indeterminate: This heavily worn P4 (RAM 9987, V98012, #7) is not *G. mylesi*, so it represents a second microcosmodontid species in the Goler Formation.

Multituberculates from Member 4a and Member 4b increase the known taxonomic diversity of microcosmodontids and confirm the previously proposed geographic range extension of *Neoliotomus* and microcosmodontids to the west coast of North America (McKenna, 1960; McKenna et al., 1987) during the late Paleocene (Lofgren et al., 2018).

Metatherians: Specimens listed below include seven teeth that represent *Golerdelphys stocki*, a new genus and species of herpetotheriid, and a maxilla and two partial teeth identified as *Peradectes* (Table 2) (Williamson and Lofgren, 2014).

—*Peradectes* sp.: RAM 12403 maxilla with M1, M3-4, V200001 (#3); RAM 6476 partial M1 and RAM 9989 molar trigonid, V98012 (#7). These specimens are too fragmentary to be identified to species but are similar to peradectids from the Western Interior (Williamson and Lofgren, 2014).

—*Golerdelphys stocki* (new genus and species): RAM 6432 right M2

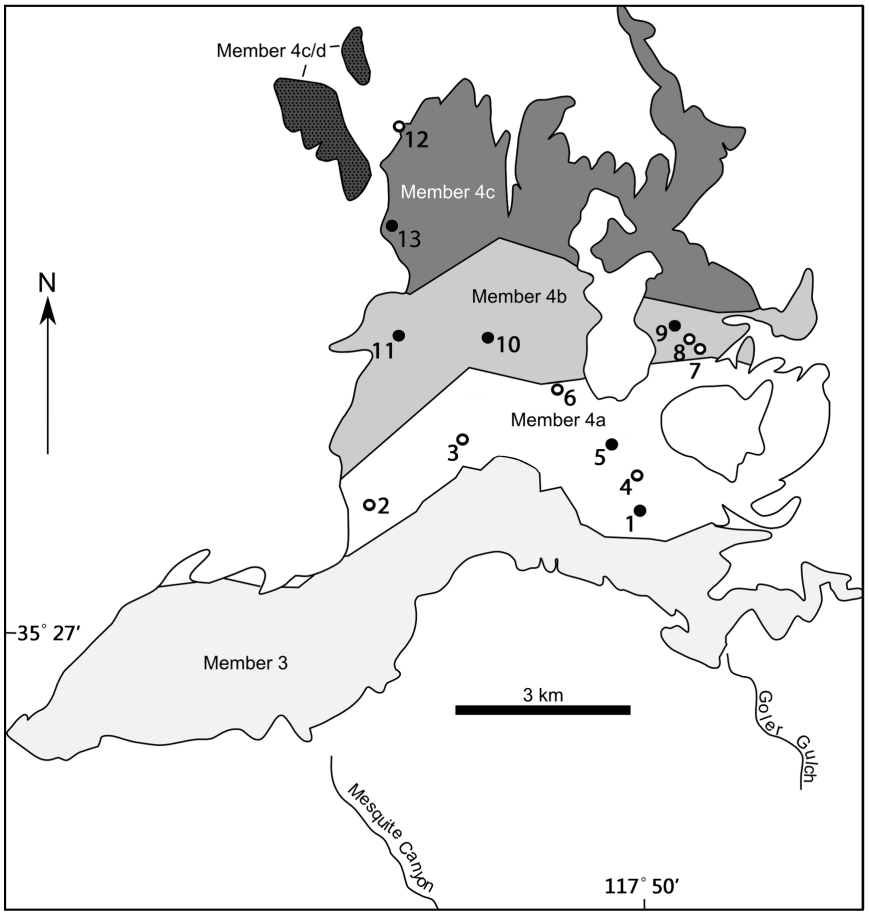

Figure 4. Outcrop map of Members 3 and 4 of the Goler Formation (adapted from Cox, 1982; Cox and Diggles, 1986) showing location of mammalian and invertebrate sites in Table 2 (except #13 which is the Squires Mollusk Site). Open circles are sites that underwent paleomagnetic analysis (results presented in Albright et al., 2009).

Table 2. Eutherians, metatherians, and multituberculates (* new taxon) from RAM localities in the Goler Formation with sites organized by member and listed 1-12 in approximate ascending stratigraphic order; 1) V201014, V201122; 2) V200508, V200510, V200706, V200802, V200804; 3) V200001, V201346, V201481; 4) V200603, V200612 V201211, V201757; 5) V200303, V200304, V200702; 6) V91014, V94133, UCMP 5251, 5870; 7) V98012; 8) V200202; 9) V200704; 10) V200613, UCMP V65170; 11) V200120; 12) V200307, I200306, I200305.

	Member 4a						Member 4b					4d
Taxon	1	2	3	4	5	6	7	8	9	10	11	12
Neoliotomus conventus	—	—	X	—	—	X	X	—	—	—	—	—
*Golercosmodon mylesi**	—	X	X	—	—	X	X	—	—	—	—	—
Peradectes sp.	—	—	X	—	—	—	X	—	—	—	—	—
*Golerdelphys stocki**	—	—	—	—	—	—	X	—	—	—	—	—
Taeniodonta	—	—	—	X	—	—	—	—	—	—	—	—
Bessoecetor septentrionalis	—	X	—	—	—	—	—	—	—	—	—	—
Protictis paralus	—	—	X	—	—	—	—	—	—	—	—	—
Protictis cf. *P. agastor*	—	—	X	—	—	—	—	—	—	—	—	—
Paromomys depressidens	—	—	—	—	—	X	—	—	—	—	—	—
Ignacius frugivorus	—	—	—	—	—	—	X	—	—	—	—	—
*Nannodectes lynasi**	—	X	—	—	—	—	X	X	—	—	—	—
Thryptacodon sp.	—	X	—	—	—	—	—	—	—	—	—	—
*Mimotricentes tedfordi**	X	X	X	—	—	—	—	—	—	—	—	—
Lambertocyon cf. *L. gingerichi*	—	—	X	X	—	—	—	—	—	—	—	—
Arctocyondidae?	—	—	—	—	—	—	—	—	—	X	—	—
*Protoselene ashtoni**	—	—	—	—	X	—	—	—	—	—	—	—
*Promioclaenus walshi**	—	X	X	—	—	—	—	—	—	—	—	—
Phenacodus cf. *P. bisonensis*	X	X	X	X	X	—	X	—	X	—	—	—
Phenacodus cf. *P. matthewi*	—	—	X	—	—	—	—	—	—	—	—	—
Phenacodus cf. *P. grangeri*	—	—	X	—	—	X	—	—	—	—	—	—
Phenacodus cf. *P. vortmani*	—	—	—	—	—	—	—	—	—	—	—	X
*Goleroconus alfi**	—	—	—	—	—	X	—	—	—	—	X	—
Dissacus sp.	—	—	—	—	—	X	—	—	—	—	—	—

(holotype), RAM 6404 molar talonid, RAM 6471 molar trigonid, RAM 6699 m2 or m3, RAM 6470 partial M3, V98012 (#7). These specimens represent the only known herpetotheriid from the late Paleocene of North America (Williamson and Lofgren, 2014).

Eutherians: This sample consists of over eighty specimens, representing seventeen species, including five new taxa; *Nannodectes lynasi*, *Promioclaenus walshi*, *Protoselene ashtoni*, *Goleroconus alfi*, *Mimotricentes tedfordi*. These and the other eutherian taxa (Table 2) were described by McKenna and Lofgren (2003), McKenna et al. (2008), and Lofgren et al. (2014).

—*Bessoecetor septentrionalis*: RAM 9099, dentary with m2-3, V200510 (#2). This pantolestid is well known from the Rocky Mountain states.

—*Protictis paralus*: RAM 6927, dentary with c, p1-2, p4-m1, and *Protictis* cf. *P. agastor*: RAM 7246, dentary with partial m1, both from V200001 (#3). These specimens constitute the oldest known mammalian carnivores from the west coast of North America.

—Taeniodont: RAM 15328 is a canine fragment from V200612 (#4) and represents the only known taeniodont from California.

—*Paromomys depressidens*: RAM 6426, P4, V94014 (#6), and Ignacius frugivorus: RAM 6433, m3, V98012 (#7). These primate-like species are well-known from the Rocky Mountain states.

—*Nannodectes lynasi*: RAM 9044 (holotype), dentary with p3-m3, RAM 9668, maxilla fragment with C, P4-M1, RAM 9669, skull fragment with broken I1, P4, M1-2 and associated p3, V200510 (#2); RAM 9429, dentary with p3-m3, V200706 (#2); RAM 10029, dentary with p4-m3, V200804 (#2); six m3s (RAM 6960, RAM 6963, RAM 6700, RAM 6961, RAM 6934, RAM 6963), m2 (RAM 6446), mx (RAM 6935), mx trigonid (RAM 6946), M3 (RAM 6957), M2 (RAM 6962), P3 (RAM 6931), 2 I1s (RAM 6431, RAM 6929) from V98012 (#7); RAM 7193, dentary with p4-m1, broken m2, V200202 (#8); RAM 6925, m3, V94014 (#6). These specimens represent a new species of plesiadapid primate only known from the Goler Formation.

—*Thryptacodon* sp: RAM 9041, m1, V200510 (#2). RAM 9041 is the only oxyclaenid from the Goler Formation.

—*Mimotricentes tedfordi*: RAM 6908 (holotype), maxilla with P4-M3, V94133 (#6); RAM 15622, dentary with p4 talonid and m1-2, V201014 (#1); RAM 6928, dentary with m3 talonid, RAM 15333, M2, V200001 (#3); RAM 9670, dentary with p4-m1, V200510 (#2); *Lambertocyon* cf. *L. gingerichi*: RAM 9040, M1 and RAM 9043, p3 fragment, V200001 (#3); RAM 19622, M1, V2006012 (4); ?Arctocyonidae: RAM 9660, px or PX, V200613 (#10). Most of these arctocyonid specimens represent *Mimotricentes tedfordi*, which is only known from the Goler Formation. The three specimens of *Lambertocyon* cf. *L. gingerichi* may represent a new species of *Lambertocyon* as RAM 9040 has a large mesostyle and RAM 19622 has a distinct metaconule and an incomplete posterior cingulum, unlike *Lambertocyon gingerichi*. But

more complete specimens are needed before a new species of *Lambertocyon* can be erected.

—*Protoselene ashtoni*: RAM 9047 (holotype), dentary with p4-m1, V200702 (#5); and *Promioclaenus walshi*: RAM 9098 (holotype), dentaries with left m1-3 and right m2-3, V200510 (#2); RAM 6724, dentary with m2 and talonid of m1, RAM 6926, maxilla fragment with M2-3 (referral questionable), V200001 (#3). These specimens represent two new species of hyposodontid condylarths only known from the Goler Formation and they significantly increase the known diversity of hyopsodontids in North America.

—*Phenacodus* cf. *P. bisonensis*: UCMP 69122, dentaries with right m2 and left p4-m2, UCMP V65710; RAM 9659, M1 from V98012 (#7); RAM 6722, M1, RAM 7205, dP4, RAM 7245, maxilla with dP3-4, RAM 7208, dP4, RAM 9725, dP4, RAM 6721, damaged m2, RAM 6723, dentary with m2-3, RAM 18562, m3, V200001 (#3); RAM 7248, maxilla with P4–M1 and damaged M2, V200304 (#5); RAM 9019, m3, V200508 (#2); RAM 9022, dentary with dp4-m1, RAM 9672, maxilla with P3-4, RAM 18564 p4, RAM 18617, M3, RAM 18569, M3, V200510 (#2); RAM 9025, m1, RAM 9021, M2, RAM 9046, dentary with m1-3, RAM 18563, m2, V200603 (#4); RAM 9020, M2 and M3; RAM 9024, dentary with m2-3, RAM 9023, dentary with p3-m3, RAM 20874 DP3-DP4 and M1, V200612 (#4); RAM 9045, dp4, V200704 (#9); RAM 10290, dentary with m1-2, RAM 10291, m3, RAM 10292 left dentary with c–m3 and right dentary with i1-2, and c-m1, V200802 (#2); RAM 15000 maxilla with dP4-M2, V201122 (#1); RAM 15620, m1 or m2, V2012011 (#4); RAM 18567 M1 or M2, RAM 18565, P3, RAM 18568 P4, RAM 18566, left p2-3 and right p2 and p4, RAM locality V201014 (#1); RAM 20875, M1, V2017057 (#4). This mid-sized phenacodontid is the most common mammal recovered from the Goler Formation. *Phenacodus* cf. *P. bisonensis* resembles *Phenacodus bisonensis* in most ways, but a few minor differences in the upper molars and the size of the dentition indicate the Goler sample is not *Phenacodus bisonensis* (Lofgren et al., 2014). Twelve additional specimens were found between 2014 and 2018 and these fossils inspired a re-analysis of the entire Goler sample of *Phenacodus* cf. *P. bisonensis*. However, the Goler sample still does not exhibit the consistent diagnostic features needed to erect a new species of phenacodontid.

—*Phenacodus* cf. *P. matthewi*: RAM 7210, dentary with p4, V200001 (#3). RAM 7201 is very similar to the smallest species of *Phenacodus*, *P. matthewi*, but has a smaller p4 paraconid (Lofgren et al., 2014). Additional specimens of this small phencodontid are needed to determine if a new species is present.

—*Phenacodus* cf. *P. grangeri*: RAM 7172, left m3, RAM locality V94014 (#6); RAM 18570 m1 or m2, V201481 (#3); RAM 18571, canine, left and right p4, and m1, V201346 (#3). Referral of these large specimens to *Phenacodus* cf. *P. grangeri* is tentative because *P. grangeri* is difficult to distinguish from *P. intermedius* (Thewissen, 1990).

—*Goleroconus alfi* (new genus and species): RAM 7171 (holotype), dentary with p4-m2 and part of m3, V200120 (#11); RAM 6506, m2, RAM 6417, p3, UCMP 131790, m2, UCMP 44761, dentary with m3, UCMP 49487, m3, V94014 (#6) (equals UCMP V5252). Specimens referred to *Goleroconus alfi* are only known from the Goler Formation and include the first mammal (UCMP 44761) identified from the formation (McKenna, 1955). A suitable holotype (RAM 7171) for this new periptychid was not found until 2001 (McKenna et al., 2008).

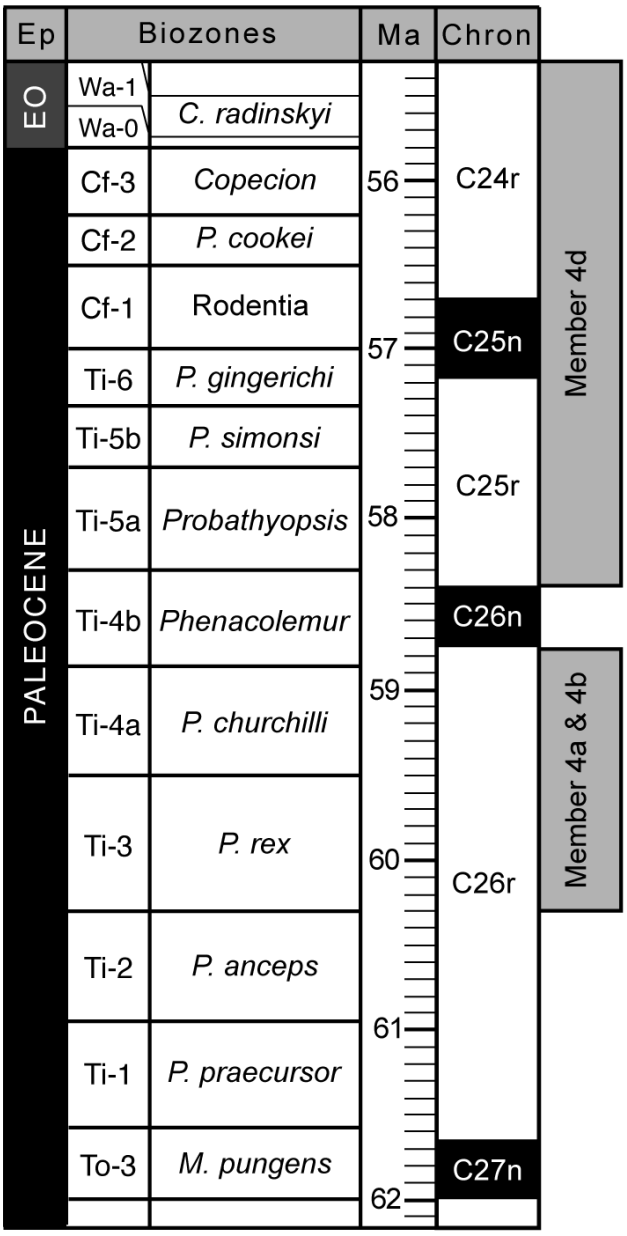

Figure 5. Biochronology and geochronology of the late Paleocene and early Eocene after Secord et al. (2006, fig. 3). Correlation of Member 4a and Member 4b based on mammalian biochronology and magnetostratigraphy and correlation of Member 4d based on vertebrate and invertebrate biostratigraphy and magnetostratigraphy (Albright et al., 2009; Lofgren et al., 2010, 2014, and references therein).

—*Dissacus* sp: RAM 6507, talonid of m1 or m2, V94014 (#6). Mesonychids are rare mammals that may be related to ancestors of whales and RAM 6507 is the oldest mesonychid known from the west coast of North America.

The stratigraphic interval that represents Member 4a and the lower part of Member 4b is about 500 m thick and cannot be subdivided into discrete biostratigraphic units based on mammalian biochronology, so mammals from this interval are referred to as the Goler Assemblage (Lofgren et al., 2014). The Goler Assemblage was compared to Tiffanian assemblages from the Western Interior and indicate a middle Tiffanian (late Paleocene) age for this part of the Goler Formation (Figure 5) (Lofgren et al., 2014, 2018). The middle Tiffanian age is supported by magnetostratigraphic correlation of Member 4a and Member 4b to C26r (Albright et al., 2009; Lofgren et al., 2014).

Member 4D

In the 1980's, an interval of marine sediments was discovered in the uppermost part of the Goler Formation in Member 4d (Cox and Edwards 1984; Cox and Diggles, 1986; Cox 1987). Initial collections of marine invertebrates from Member 4d indicated that these strata (northwest of #12) were late Paleocene (CP8) based on cocoliths (Reid and Cox, 1989) and early Eocene (P8 and ?P9) based on foraminifera (McDougall, 1987). Another small outcrop of Member 4d (#13) yielded fifty-one specimens of late Paleocene–early Eocene mollusks (Squires et al., 1988).

In 2003, RAM crews identified an additional section of fossil-bearing marine strata (#12) situated roughly between the previously identified marine outcrops and three sites (V200305, V200306, V200307) from this newly discovered section yielded abundant and well-preserved marine invertebrates along with shark teeth and the tooth of a terrestrial mammal (Lofgren et al., 2004, 2010). These RAM localities are within a series of cobble-pebble conglomerate and sandstone lenses where gastropods and shark teeth are rare and whole valves and shell fragments of oysters are common. Surprisingly, a tooth of the terrestrial mammal was found at V200307. Also, oysters and other mollusks with original shell material are present at V200305. Specimens listed below from the three RAM marine sites were briefly described by Lofgren et al. (2010).

Pelecypoda: Six taxa were identified and all were previously described by Squires et al. (1988) from site #13, but these RAM specimens are more numerous and complete.

—*Acutostrea idriaensis*: This oyster is the most common mollusk and over 100 whole and fragmentary valves were recovered from V200306 and V200307 (#12).

—*Barbatia biloba*: One specimen (RAM 9633) was collected at V200306 (#12).

—*Corbula* aff. *C. dickersoni:* Eight specimens were recovered, seven from V200305 (RAM 9567, 9593-94, 9563, 9610-11, 9576) and one from V200306 (RAM 9626).

—*Ledina duttonae*: One specimen (RAM 9627) was found at V200306.

—*Nemocardium linteum*: Twelve specimens were recovered from V200305 (RAM 9573, 9614, 9565, 9582, 9585, 12248-12254).

—*Thracia* aff. *T. condoni*: Five specimens were identified, three from V200305 (RAM 9601, 9615, 9586) and two from V200306 (RAM 9619, 9625).

Gastropoda: In contrast to pelecypods, only two (*Calyptraea diegoana, Turritella buwaldana*) of the eight gastropod species recovered from the RAM marine sites were previously described by Squires et al. (1988), but the six new records remain unidentified to taxon. Three specimens of *Calyptraea diegoana* were recovered from V200305 (RAM 9584, 9599, 9613), as well as 27 specimens of *Turritella buwaldana* including complete shells; V200305 yielded 22 and V200306/V200307 five. The six additional gastropod morphotypes are from V200305 except three specimens of morphotype A from V200306. These morphotypes (A-F) are: A) RAM 9621-22 (V200306) and RAM 9600 (V200305); B) RAM 9592 resembles *Admete*; C) RAM 9591 has seven whorls and well-defined costa; D) RAM 9616 resembles *Gyrodes*; E) RAM 9602 has strong ribbing and costae; F) RAM 9604 has four whorls.

Chrondrichthyes: Sharks are represented by isolated striated teeth (RAM 7256, 7255, 7254) from V200307 which are similar in morphology to those of *Striatolamia*, a shark widespread in late Paleocene and Eocene strata in North America.

Mammals: A p4 of *Phenacodus* cf. *P. vortmani* (RAM 7253) was found at V200307. If RAM 7253 does represent *Phenacodus vortmani*, its occurrence would indicate a late Paleocene or early Eocene age (Thewissen, 1990; Secord et al., 2006; Secord, 2008).

The RAM marine localities (#12) extended the known area of the marine transgression that deposited a large part of Member 4d. The older known marine sequence consists of sandstones and conglomerates with marine mollusks, overlain by a marine siltstone unit with planktic and benthic forminifera (indicating water depths of 50–150 m) which was interpreted to represent a braided river delta (Cox, 1987; McDougall, 1987). The RAM marine section probably represents a more proximal delta facies because the well-preserved mollusks, shark teeth and a nonmarine mammal tooth (both nonmarine and marine vertebrates and marine invertebrates) suggest a near shore marine facies where nonmarine fossils were deposited in a delta lobe with oysters and other marine invertebrates (Lofgren et al., 2010).

Strata at the RAM marine section was sampled for paleomagnetic analysis and all samples were of reversed polarity (Albright et al., 2009). Correlation to Chron 25r or Chron 24r (Figure 5) is the most plausible based on the correlation of Member 4a and Member 4b strata to Chron 26r (Albright et al., 2009; Lofgren et al., 2014) and the late Paleocene to early Eocene age of Member 4d based on

invertebrates (McDougall, 1987; Squires et al., 1988; Reid and Cox, 1989).

Paleobiogeography and prospectus

The non-marine fauna of the Goler Formation exhibits significant endemism as more than 45% of mammalian taxa (ten of twenty-one) are not found in middle Tiffanian faunas from the Rocky Mountain states. Endemic taxa are the metatherian, *Golerdelphys stocki* (Williamson and Lofgren, 2014), the multituberculate *Golercosmodon mylesi* (Lofgren at al., 2018) and eutherians *Goleroconus alfi*, *Nannodectes lynasi*, *Mimotricentes tedfordi*, *Protoselene ashtoni*, and *Promioclaenus walshi* (McKenna and Lofgren, 2003; McKenna et al., 2008; Lofgren et al., 2014). In addition, *Phenacodus* cf. *P. bisonensis*, *Lambertocyon* cf. *L. gingerichi*, and *Phenacodus* cf. *P. matthewi* are represented in the Goler Assemblage by specimens that have significant character differences compared to their respective species from the Western Interior and likely represent new species that require more complete specimens for confirmation. Also, only five Goler mammalian taxa can be confidently referred to species from the Western Interior of North America (i.e. *Neoliotomus conventus*, *Bessoecetor septentrionalis*, *Protictis paralus*, *Ignacius frugivorus*, *Paromomys depressidens*), a strong indication of endemism.

Turtles from Member 4a and Member 4b also reflect significant endemism (Hutchison, 2004) and the remains of gars, a type of fish commonly found in Paleocene strata in the Rocky Mountain states, have yet to be found in the Goler Formation (Lofgren et al., 2008). This degree of vertebrate endemism strongly suggests that the Goler Basin was geographically isolated from Paleocene sedimentary basins of the Western Interior and this isolation provided excellent opportunity for the formation of a unique west coast faunal province in what is now southern California during the late Paleocene.

There is much yet to accomplish with respect to Goler Formation paleontology. Very little prospecting of finer grained strata of Member 2 with the potential to yield vertebrates or invertebrates has occurred. Also, the extensive outcrops of Member 3 still could yield additional vertebrate specimens which could provide a more precise age determination for these strata. Finally, detailed analysis of invertebrates from the RAM marine sites in Member 4d would be productive as the original study of these specimens was cursory (Lofgren et al., 2010) and many more specimens have been collected since 2010.

Outcrops of the Goler Formation extend for many kilometers north–south and east–west, and prospecting this very broad geographic area would likely yield unexpected results. Plant fossils are extremely rare, but there is potential to discover identifiable specimens because sedimentary facies that commonly preserve floral material are common in Member 3 and Member 4. By the 1980s, the Goler Formation had developed a reputation of being too sparsely fossiliferous to be worthy of further prospecting. That all changed in the last three decades when numerous specimens were recovered representing new taxa and some incredibly rare fossils were found (i.e. mammal and turtle skulls). Thus, more treasures await the meticulous researcher.

Acknowledgments

We thank the late M. McKenna for inspiration; members of The Webb Schools Community for field assistance; M. Stokes for preparation of specimens; the Bureau of Land Management of California for permits (especially D. Storm); M. Woodburne for reviewing the manuscript, G. Santos, L. Gerken, and F. Hu for assistance with figures and tables; and the David B. Jones Foundation, the Mary Stuart Rogers Foundation, and the Malcolm C. McKenna Goler Research Endowment for financial support.

Literature cited

Albright, L. B, III, Lofgren, D. L., and M. C. McKenna. 2009. Magnetostratigraphy, mammalian biostratigraphy, and refined age assessment of the Goler Formation (Paleocene), California. p. 259-277, in L. B. Albright III (ed.), Papers on Geology, Paleontology, and Biostratigraphy in Honor of Michael O. Woodburne, Museum of Northern Arizona Bulletin 65.

Axelrod, D. I. 1949. Eocene and Oligocene Formations in the Western Great Basin. Geological of Society Bulletin 60:1935-6.

Cox, B. F. 1982. Stratigraphy, sedimentology, and structure of the Goler Formation (Paleocene), El Paso Mountains, California: Implications for Paleogene tectonism on the Garlock Fault Zone. Ph.D. dissertation, University of California, Riverside, 248 p.

Cox, B. F. 1987. Stratigraphy, depositional environments, and paleotectonics of the Paleocene and Eocene Goler Formation, El Paso Mountains, California, geologic summary and road log; pp. 1-30 in Cox, B.F. (ed.), Basin Analysis and Paleontology of the Paleocene and Eocene Goler Formation, El Paso Mountains, California. SEPM (Society for Sedimentary Geology) Pacific Section Publication 57.

Cox, B. F., and L. F. Edwards. 1984. Possible marginal-marine deposits in the Goler Formation (Paleocene), El Paso Mountains, California. Eos 65:1084.

Cox, B. F., and M. F. Diggles. 1986. Geologic Map of the El Paso Mountains Wilderness Study Area, Kern County, California. United States Geological Survey Miscellaneous Field Studies Map, MF-1827, scale 1:24,000.

Fairbanks, H. W. 1896. Notes on the Geology of Eastern California. American Geologist 17:63-74.

Hutchison, J. H. 2004. A new Eubaenine, *Goleremys mckennai*, gen et sp. n., (Baenidae, Testudines) from the Paleocene of California. Bulletin of the Carnegie Museum of Natural History 36:91-96.

Lofgren, D. L., M. C. McKenna, S. L. Walsh, J. H. Hutchison, R. L. Nydam, and J. G. Honey. 2002. New records of Paleocene vertebrates from the Goler Formation of California. Journal of Vertebrate Paleontology 22 (supplement to 3):80A.

Lofgren, D. L., M. C. McKenna, R. Nydam, and T. Hinkle. 2004. A phenacodont from Paleocene-Eocene marine beds

of the uppermost Goler Formation of California. Journal of Vertebrate Paleontology 24:84A.

Lofgren, D. L., J. G. Honey, M. C. McKenna, R. L. Zondervan, and E. E. Smith. 2008. Paleocene primates from the Goler Formation of California. p. 11-28, in Wang, X., and L. G. Barnes (eds.), Geology and Vertebrate Paleontology in Western and Southern North America, Contributions in Honor of David P. Whistler. Science Series 41, Natural History Museum of Los Angeles County.

Lofgren, D. L., R. Nydam, J. Honey, B. Albright, C. McGee, and S. Manning. 2009. The Goler Club: How One Man's Passion Opened a Rare Window into California's Geologic Past. p.148-158, in Landscape Evolution at an Active Plate Margin, eds. R. Reynolds and D. Jessey, Field Guide and Proceedings from 2009 Desert Symposium Proceedings, California State University Desert Studies Consortium.

Lofgren, D. L., B. A. Silver, T. A. Hinkle, and F. Ali-Khan. 2010. New marine sites from Member 4D of the Goler Formation of California. p. 232-240, in: R.E. Reynolds and D.M. Miller (eds.). Overboard in the Mojave: 20 Million Years of Lakes and Wetlands. Desert Studies Consortium, California State University.

Lofgren, D., M. McKenna, J. Honey, R. Nydam, C. Wheaton, B. Yokote, L. Henn, W. Hanlon, S. Manning, and C. McGee. 2014. New records of eutherian mammals from the Goler Formation (Tiffanian, Paleocene) of California and their biostratigraphic and paleobiogeographic implications. American Museum Novitates 3797:1-57.

Lofgren, D. L., R. L. Nydam, M. Gaumer, E. Kong, and M. C. McKenna. 2018. New records of multituberculate mammals from the Goler Formation (Tiffanian, Paleocene) of California. Paludicola 11:149-163.

McDougall, K. 1987. Foraminiferal biostratigraphy and paleoecology of marine deposits, Goler Formation, California; pp. 43-67 in Cox, B.F. (ed.), Basin Analysis and Paleontology of the Paleocene and Eocene Goler Formation, El Paso Mountains, California. SEPM (Society for Sedimentary Geology) Pacific Section Publication 57.

McKenna, M. C. 1955. Paleocene mammal, Goler Formation, Mojave Desert, California. Bulletin of the American Association of Petroleum Geologists 39:512-515.

McKenna, M. C. 1960. A continental Paleocene vertebrate fauna from California. American Museum Novitates 2024:1-20.

McKenna, M. C., J. G. Honey and D. L. Lofgren. 2008. *Goleroconus alfi*, a new small periptychid (Mammalia, Eparctocyona) from the late Paleocene of California. p. 29-42, in Wang, X., and L. G. Barnes (eds.), Geology and Vertebrate Paleontology in Western and Southern North America, Contributions in Honor of David P. Whistler. Science Series 41, Natural History Museum of Los Angeles County.

McKenna, M. C., J. H. Hutchison, and J. H. Hartman. 1987. Paleocene vertebrates and nonmarine mollusca from the Goler Formation, California. p. 31-42 in Cox, B.F. (ed.), Basin Analysis and Paleontology of the Paleocene and Eocene Goler Formation, El Paso Mountains, California. SEPM (Society for Sedimentary Geology) Pacific Section Publication 57.

McKenna, M. C. and D. L. Lofgren. 2003. *Mimotricentes tedfordi*, a new Arctocyonid from the Late Paleocene of California: Bulletin of the American Museum of Natural History 279:632-643.

Nydam, R. L., and D. L. Lofgren. 2008. Preliminary report on lizards from the Goler Formation (Paleocene) of California. Journal of Vertebrate Paleontology 28:121A.

Reid, S. A., and B. F. Cox. 1989. Early Eocene uplift of the southernmost San Joaquin Basin, California. American Association of Petroleum Geologists Bulletin 73:549-550.

Secord, R. 2008. The Tiffanian land mammal age (middle and late Paleocene) in the northern Bighorn Basin, Wyoming. University of Michigan Papers on Paleontology 35:1-192.

Secord, R., P. D. Gingerich, M. E. Smith, W. C. Clyde, P. Wilf, and B. S. Singer. 2006. Geochronology and mammalian biostratigraphy of middle and upper Paleocene continental strata, Bighorn Basin, Wyoming. American Journal of Science 306:211-245.

Squires, R. L., B. F. Cox, and C. L. Powell, III. 1988. Late Paleocene or Early Eocene mollusks from the uppermost part of the Goler Formation, California. p. 183-187 in M. V. Filewicz and R. L. Squires (eds.), Paleogene Stratigraphy, West Cost of North America, Society of Economic Paleontologists and Mineralogists Pacific Section 58.

Stidham, T. A., D. L. Lofgren, A. A. Farke, M. Paik, and R. Choi. 2014. A lithornithid (Aves: Palaeognathae) from the Paleocene (Tiffanian) of southern California. PaleoBios 31:1-7.

Thewissen, J. G. M. 1990. Evolution of Paleocene and Eocene Phenacodontidae (Mammalia, Condylarthra). University of Michigan Papers on Paleontology 29:1-107.

West, R. M. 1970. *Tetraclaenodon puercensis* (Mammalia: Phenacodontidae), Goler Formation, Paleocene of California, and distribution of the genus. Journal of Paleontology 44:851-857.

Williamson T. E. and D. L. Lofgren. 2014. Late Paleocene (Tiffanian) metatherians from the Goler Formation, California. Journal of Vertebrate Paleontology 34:477-482.

Dynamics of a western Joshua tree (*Yucca brevifolia*) population, Red Rock Canyon State Park, California

James W. Cornett
JWC Ecological Consultants, 3745 Bogert Trail, Palm Springs, California 92264, jwcornett@aol.com

Introduction

In the last two decades of the twentieth century, there was a developing consensus among atmospheric scientists that Earth's climate was warming (Broecker, 1987; Plantico, et al., 1990; Houghton et al., 1992). It is well known that a change in climate has profound effects on the distribution and survival of plants including species with broad ecological significance (Daubenmire, 1956; Booth, 1990; Stephenson, 1990).

The western Joshua tree, *Yucca brevifolia*, is one such species (Figure 1). Many authors consider the tree an icon of the Mojave Desert (Foster, 1987; Jaeger, 1961; Larson, 1977). It may be classified as a keystone plant as well since over vast areas it often provides the sole source of food, water and shelter for a host of animal species (Cornett, 2018; Esque at al., 2003; Jaeger, 1961; Miller and Stebbins, 1964; Smith et al., 2009; Zweifel and Lowe, 1966). Because of the Joshua tree's significance and the widespread recognition of a warming climate in the early 1990s, I created a one-hectare study site to monitor changes in the establishment, vigor and survival of the Joshua tree. The study site was in Red Rock Canyon State Park, California (Figure 2). The Park is in the southern half of the species' distribution and near the lower-elevational limit of *Y. brevifolia* (Baldwin et al., 2012). I conjectured impacts of a warming climate on Joshua trees would be detected earliest at a location having such characteristics.

Figure 1. Joshua tree, *Yucca brevifolia*, Red Rock Canyon State Park study site. Photograph taken of tree #317 in 1995. Absence of dead leaf rosettes on tree or ground resulted in a vigor score of 1.00. By 2016, #317 had lost 18 leaf rosettes and vigor score dropped to 0.72.

Methods

The study site location was selected because of the high density of Joshua trees, with contingents of both adult and juvenile plants. The site was on an east-facing bajada with a slight (4.5%) grade. Site elevation was 805 m. The hectare was square with the following corner coordinates: northwest 35°22'33.8"N, 117°59'43.2"W; northeast 35°22'33.9"N, 117°59'39.5"W; southwest 35°22'30.5"N, 117°59'42.5"W; southeast 35°22'30.8"N, 117°59'38.6"W. Low hills of the El Paso Range were located 0.2 km to the southwest. Surface and subsurface soil to a depth of 1.5 m was a mix of sand and silt with occasional pebbles and cobbles. A 7-m-wide wash cut through the site from west to east. Perennial plant species recorded within site boundaries and listed in decreasing order of coverage were: Mormon tea (*Ephedra nevadensis*), four-winged saltbush (*Atriplex canescens*), Joshua tree (*Yucca brevifolia*), cheesebush (*Ambrosia salsola*), bur-sage (*Ambrosia dumosa*), desert matchweed (*Gutierrezia microcephala*), wash rabbit brush (*Chrysothamnus paniculatus*), indigo bush (*Psorothamnus arborescens*), creosote bush (*Larrea tridentata*), spiny hop-sage (*Grayia spinosa*), bladdersage (*Salazaria mexicana*), golden cholla (*Cylindropuntia echinocarpa*), bladder pod (*Isomeris arborea*), Mojave aster (*Xylorhiza tortifolia*), desert senna (*Senna armata*), linear-leaved goldenbush (*Ericameria linearifolia*), cottonthorn (*Tetradymia axillaris*), blue sage (*Salvia dorrii*), winter fat (*Krascheninnikovia lanata*), Anderson boxthorn (*Lycium andersonii*), apricot mallow (*Sphaeralcea ambigua*), California buckwheat (*Eriogonum*

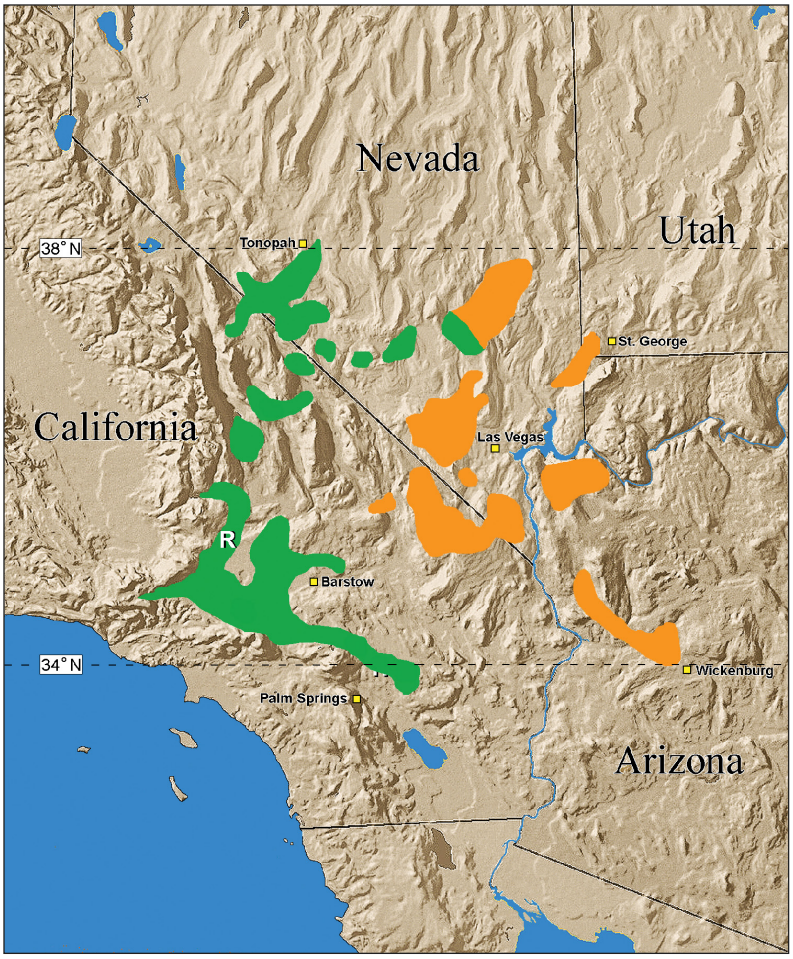

Figure 2. Location of Red Rock Canyon State Park Joshua tree study site (R). Site lies in southern half of *Yucca brevifolia* distribution. Green indicates range of western Joshua tree (*Y. brevifolia*). Orange indicates distribution of eastern Joshua tree (*Y. jaegeriana*).

fasciculatum), beaver-tail cactus (*Opuntia basilaris*), and desert trumpet (*Eriogonum inflatum*). There was no evidence of plant life being affected by historical wildfires or livestock grazing.

The study site was marked with permanent steel stakes driven into the four corners. Trees were identified with numbered aluminum tags wired loosely around trunks so that trunk expansion was not inhibited. Data sets were collected by me, T. Johnson, and V. Rohrback. We counted trees and number of living and dead leaf rosettes in April from 1995 through 2016. A tree with one or more green terminal leaf rosettes was considered living. A tree with no green leaf rosettes was considered dead. Trees that had not yet flowered were recorded as juveniles and usually less than 1 meter in height. Trees that had flowered were recorded as adults and always more than 1 meter in height. Test excavations indicated that new *Y. brevifolia* sprouts less than 3 m from a mature tree, or beneath its crown, were likely rhizome sprouts of that tree and were, therefore, not counted as a separate plant.

Tree vigor, used as a measure of vitality and possible indicator of survival duration, was determined by counting the number of living leaf rosettes of trees more than one meter in height and dividing that number by the total number of living and dead rosettes. Both dead rosettes affixed to a tree and fallen rosettes on the ground were counted. Using this method of analysis, a tree which had all green terminal rosettes and no dead rosettes had a quotient of 1 and was considered to have maximum vigor. A tree in which leaf rosettes were dying more rapidly than new rosettes were being produced was considered to be in decline and had a vigor quotient of less than 1. A dead tree had a quotient of 0.

The site and surrounding areas were severely impacted by a flood in the late afternoon of 3 September 1997. More than 100 mm of rain fell in less than two hours. Based on a review of historical records, the flood was thought to be the most severe in recorded history (park ranger Mark Faull, personal communication). Fifteen trees within the study site were uprooted and carried away by floodwaters. Data in Figure 3 includes trees lost in flood. The only long-term climate data summarized and available (and used in this study) were for the entire California desert region and compiled by the National Oceanic and Atmospheric Administration, National Centers for Environmental Information (NOAA, 2020a).

Tree death was recorded as resulting from one of three factors: flood, herbivory, or drought. Flood mortality is described above, and the 1997 event was the only flood during the study. Death by herbivory was concluded when a tree was gone but its tag still present on the ground. In practice, this only applied to trees < 0.3 m in height. Leaf herbivory on trees > 1m was common but never considered a sole cause of mortality. A tree of any size that died and showed little or no evidence of browsing was assumed to have expired as a result of drought.

Results

Tree density declined from 54 trees in 1995 to 29 trees in 2016, a 46% decrease over the 21-year study period (Figure 3). Declines were recorded for both small trees (< 1m) and larger trees (> 1m) but the rate of decline was greatest for small trees. This demonstrates a statistical movement towards a population of older and larger trees and a decline of young recruits into the population.

Though the loss of 9 small and 6 large trees in the flood of 1997 exaggerated the trends described above, it did not change them. In the unlikely occurrence that all 15 of the flood-killed trees would have survived into 2016, overall numbers of large and small trees would still have decreased from 54 to 44 and there would have been a shift towards an older population.

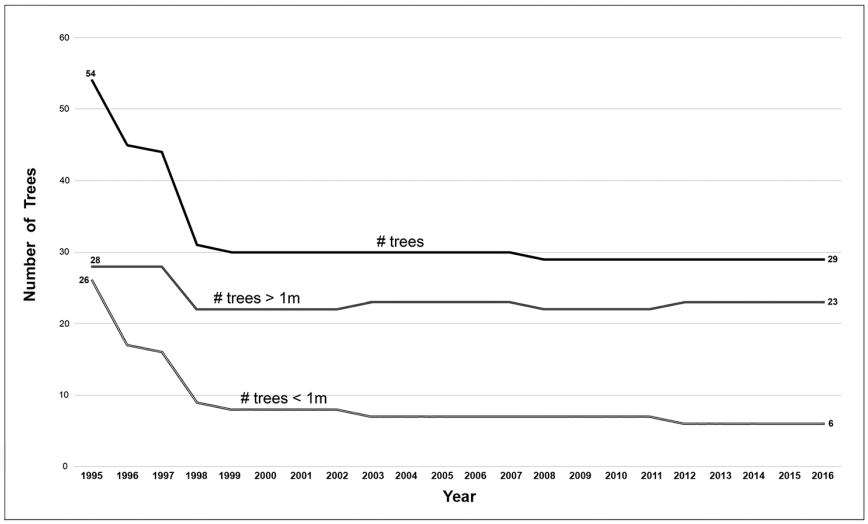

Figure 3. Changes in density of Joshua trees within a 1-hectare study site located in Red Rock Canyon State Park, California. Tree numbers declined and shifted from a shorter/younger (<1m) to taller/older (>1m) population.

Tree vigor declined from 0.97 in 1995 to 0.63 in 2016. This suggests surviving trees were more stressed at the end of the study than at the beginning. They were shedding leaf rosettes faster and replacing them less often by 2016.

From 1995 through 2016 the mean temperature rose 0.7^0 C in the California desert region compared with the 21-year period before the study (Table 1). Regional precipitation decreased from a mean of 177 mm per year in the 21 years before the study to 143 mm per year during the study period.

Discussion

The Joshua tree population within the study site appeared robust at the inception of the study in 1995. Tree density was high, young recruits represented 48% of the Red Rock population and the vigor quotient was 0.96 with only 2 of the 28 adult trees having shed leaf rosettes. However, by 2016, total numbers, percentage of young trees, and tree vigor had all declined. Negative values in the two former categories are phenomena associated with declining populations (Barbour et al., 1987).

Most of the decline occurred in the first three years of the study and resulted from herbivore attacks on small Joshuas in 1995–96 and the flood in 1997 (Figure 3). The heavy rains and flood on 3 September 1997 dropped 113 mm of precipitation in the immediate area, washed away 15 large and small Joshua trees from the study site, and saturated surface soils (NOAA, 2020b). One might argue the flood was an important, perhaps primary, cause of the decline of Joshua trees within the study site. However, the decline in the number of small Joshua trees and vigor of large trees occurred both before and after the flood. The flood may have exacerbated the downward trends but does not appear to have been the cause. In addition, the heavy rainfall might have been expected to initiate a pulse of Joshua tree germination and growth on the study site but there were no measurements indicating this occurred (Noy-Meir, 1973).

In the absence of other detectable factors such as insect infestations, disease, frost damage, vandalism, or fire, it seems most likely the declines described in this paper are the result of a warming and drying of the climate and attendant secondary impacts. The study period experienced both warmer temperatures and a decline in precipitation from 1995 through 2016. A rise in temperature of 0.7^0 C and a decrease of 34 mm in annual precipitation may not appear significant but, as mentioned previously, the study site was located near the distributional limit and climatic tolerances of *Y. brevifolia*. Severe weather events, such as the Red Rock flood of 1997, may be a secondary effect of a warming climate (Karl et al., 2008). As mentioned previously, there is evidence that the intense thunderstorm and flood may have been the most severe in recorded history. Herbivory was a contributing factor in the decline of Joshua trees on the study site. Rodent and lagomorph browsing on Joshua tree leaves and stems has been shown to be positively associated with an increase in aridity. Moisture-seeking animals often turn to Joshua trees as a source of water during times of drought (Cornett, 2016; Esque et al., 2015). The intensity of the attack may be an indirect impact of increasing aridity in the region.

The one-hectare study site represents a tiny fraction of the total area of the Park supporting Joshua trees. Did the decline of Joshua trees on the study site represent what is occurring throughout the Park? A visual inspection of the region in 2016 suggested these declines were

Table 1. Mean annual precipitation (mm) and mean annual temperature (^{0}C) for California desert region (1973-1994, inclusive) and 21-year study period (1995-2016). Precipitation declined and temperature increased during study period compared with previous 21-year period. Climate data from NOAA, National Centers for Environmental Information (2020).

Time Period	$\bar{x}$ Precipitation	Annual Temperature
1973-1994	177	18.2
1995-2016	143	18.9
Decrease/Increase	-34	+0.7

widespread with juvenile trees being uncommon and adult trees typically with numerous shed leaf rosettes and fallen branches. If the rate of decline in numbers continues, a decline of 46% every 21 years, Joshua trees will be extirpated from the study site before the year 2140 and possibly in the Park as well. The data suggest the additional stress of an increase in temperature and decrease in water availability has resulted in the Red Rock population reaching a tipping point where it may no longer be self-sustaining.

These field findings and possible future population trend agree with a computer modeling study conducted by Kenneth Cole at al. (2011). Cole predicted "future elimination of Joshua tree throughout most of the southern portions of the tree's current range" (Cole at al., 2011:148) and suggested southern and low-elevation populations were unsustainable under projected climate regimes.

Acknowledgements

Mark Faull, John Crossman, and Jean Scott of California State Parks Department provided important park information and assisted with the establishment of the study site. The Joshua Tree National Park Association and Garden Club of the Desert provided financial support throughout the entire 21-year study period. Tom Johnson and Victor Rohrback assisted with data collection. Mark Borchart, David Miller, an anonymous reviewer, and my wife, Terry Cornett, made many helpful suggestions on early drafts of the manuscript. I thank each of these individuals and organizations for their assistance and support.

Literature cited

Baldwin, B. G., D. H. Goldman, D. J. Keil, R. Patterson, T. J. Rosatti and D. H. Wilken, editors. 2012. *The Jepson manual: vascular plants of California*, second edition, University of California Press, Berkeley, California.

Barbour, M. G., J. H. Burk and W. D. Pitts. 1987. *Terrestrial plant ecology*. Benjamin-Cummings Publishing Company, Menlo Park, California.

Booth, T. H. 1990. Mapping regions climatically suitable for particular tree species at the global scale. Forest Ecology Management 36:47–60.

Broecker, W. S. 1987. Unpleasant surprises in the greenhouse? Nature 328:9 July 1987, 123-126.

Cole, K.L., K. Ironside, J. Eischeid, G. Garfin, P. B. Duffy and C. Toney. 2011. Past and ongoing shifts in Joshua tree distribution support future modeled range contraction. Ecological Adaptations 21(1):137-149.

Cornett, J. W. 2016. Long-term population dynamics of the Joshua tree (*Yucca brevifolia*) at Saddleback Butte State Park, Los Angeles County, California. California State University Desert Studies Center 2016 Desert Symposium Field Guide and Proceedings, April 2016:211-217.

Cornett, J. W. 2018. *The Joshua Tree* (second edition). Nature Trails Press, Palm Springs, California.

Daubenmire R 1956 Climate as a determinant of vegetation distribution in eastern Washington and northern Idaho. Ecological Monographs 26:131–154.

Esque, T. C., D. F. Haines, L. A. DeFalco, J. E. Rodgers, K. A. Goodwin and S. J. Scoles. 2003. Mortality of adult Joshua trees (Yucca brevifolia) due to small mammal herbivory at Joshua Tree National Park, California. Report TA#J8R07020011, Great Basin Coop. Eco. Studies Unit, National Park Service.

Esque, T. C., P. A. Medica, D. F. Shryock, L. A. DeFalco, R. H. Webb and R. B. Hunter. 2015. Direct and indirect effects of environmental variability on growth and survivorship of pre-reproductive Joshua trees, *Yucca brevifolia* Englem. (Agavaceae). American Journal of Botany 102(1): 85–91.

Foster, L. 1987. *Adventuring in the California Desert*. Sierra Club Books, San Francisco, California.

Houghton, J. T., B. A. Callander and S. K. Varney. 1992. Climate Change 1992, the supplementary report to the IPCC scientific assessment. Cambridge University Press, United Kingdom.

Jaeger, E. C. 1961. *Desert Wildlife*. Stanford University Press, Stanford, California.

Karl, T. R., G. A. Meehl, C. D. Miller, S. J. Hassol, A. M. Waple and W. L. Murray (editors). 2008. Weather and Climate Extremes in a Changing Climate, Regions of Focus: North

America, Hawaii, Caribbean, and U.S. Pacific Islands. Department of Commerce, NOAA's National Climatic Data Center, Washington, D.C., USA, 164 pp.

Larson, P. 1977. *The Deserts of the Southwest*. Sierra Club Books, San Francisco, California.

Miller, A. H. and R. C. Stebbins. 1964. *The Lives of Desert Animals in Joshua Tree National Monument*. University of California Press, Berkeley, California.

NOAA, 2020a. Climate at a glance at www.ncdc.noaa.gov/cag/time-series/us.

NOAA, 2020b. Storm database at www.ncdc.noaa.gov/stormevents/eventdetails.jsp?id=5617428

Noy-Meir, I. 1973. Desert ecosystems: environment and producers. Annual Review of ecology and systematics. 4:25-51.

Plantico, M.S., T.R. Karl, G. Kukia and J. Gavin, 1990. Is recent climate change across the United States related to rising levels of anthropogenic greenhouse gases? Journal of Geophysical Research 95:16,617-16,637.

Smith, C. I., C. S. Drummond, W. Godsoe, J. B. Yoder and O. Pellmyr. 2009. Host specificity and reproductive success of yucca moths (*Tegeticula* spp. Lepidoptera: Prodoxidae) mirror patterns of gene flow between host plant varieties of the Joshua tree (*Yucca brevifolia*: Agavaceae). Molecular Ecology 18:5218-5229.

Stephenson, N. L. 1990. Climatic control of vegetation distribution: the role of the water balance. American Naturalist 135:649–670.

Zweifel, R. G. and C. H. Lowe. 1966. The ecology of a population of *Xantusia vigilis*, the desert night lizard. American Museum Novitates 2247:1-57.

Geology of the Mojave Mining District and surrounding areas, Kern County California

Gregg Wilkerson
yosoygeologo@gmail.com

Location

The Mojave district of Troxel and Morton (1962, p. 43) was described as:

> "…. in southeastern Kern County. [It] comprises 70 square miles centered about 8 miles southwest of the town of Mojave. Five prominences separated by alluvia ted areas contain all the mines of the district but comprise only a small proportion of the total area. Of these prominences Soledad Mountain, 5 miles south of Mojave, is the most important both in productivity and in the number of deposits. Tropico Hill and Middle Butte, 6 miles south and 4 miles west respectively from Soledad Mountain, are next in overall importance. Willow Springs Mountain, 6 miles southwest of Soledad Mountain, and the western part of the Rosamond Hills-which are between Tropico Hill and Soledad Mountain-are less well endowed with known mineral wealth".

The Mojave District as defined by Troxel and Morton (1962) is reproduced in Figure 1. A photograph of Soledad Mountain from Troxel and Morton (1962) is reproduced in Figure 2. This study considers a larger area than the Mojave Mining District, as shown on Figure 3. This larger area includes the Garlock Fault to the northwest, a right-lateral fault between the Garlock Fault and Rosamond to the southwest, a northwest to southeast striking fault along the northeastern edge of hills southwest of Twin Buttes to the northeast, the median through Rogers Lake to the southeast, and Rosemond Lake to the south. This area covers 619 square miles. It includes 138 mines, prospects and occurrences in the USGS MRDS database (2011). I have subdivided this area into seven mine groups. The mine groups are also illustrated in Figure 3. Of these, the following are within the boundaries of the Mojave District of Troxel and Morton (1962):

- Elephant Butte – Standard Hill
- Middle Butte – Cactus Queen
- Soledad Mountain
- Rosamond Hills
- Willow Springs Butte – Milwaukee – Tropico

Mine groups outside of the Mojave District of Troxel and Morton (1962) are:

- South of Oak Creek Canyon

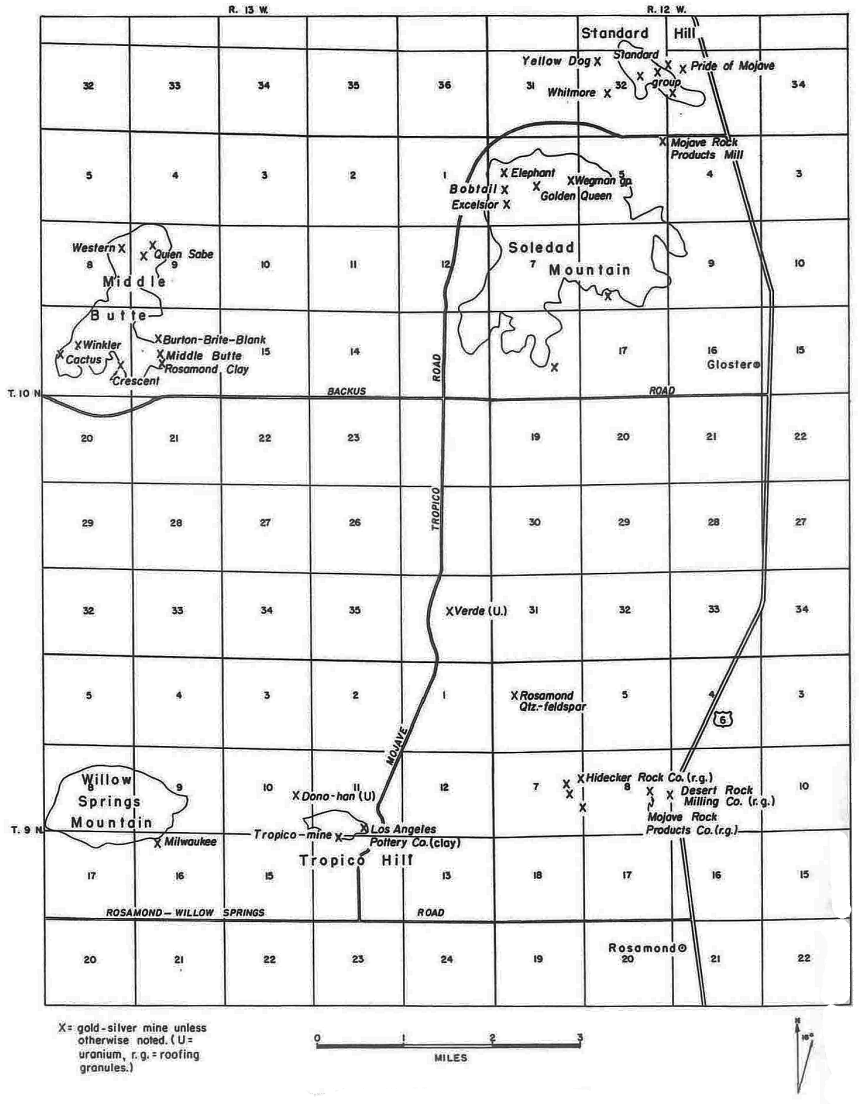

Figure 1. Mojave District from Troxel and Morton, 1962, p. 42.

Figure 2. Photograph of Soledad Mountain. From Troxel and Morton, 1962, p. 44.

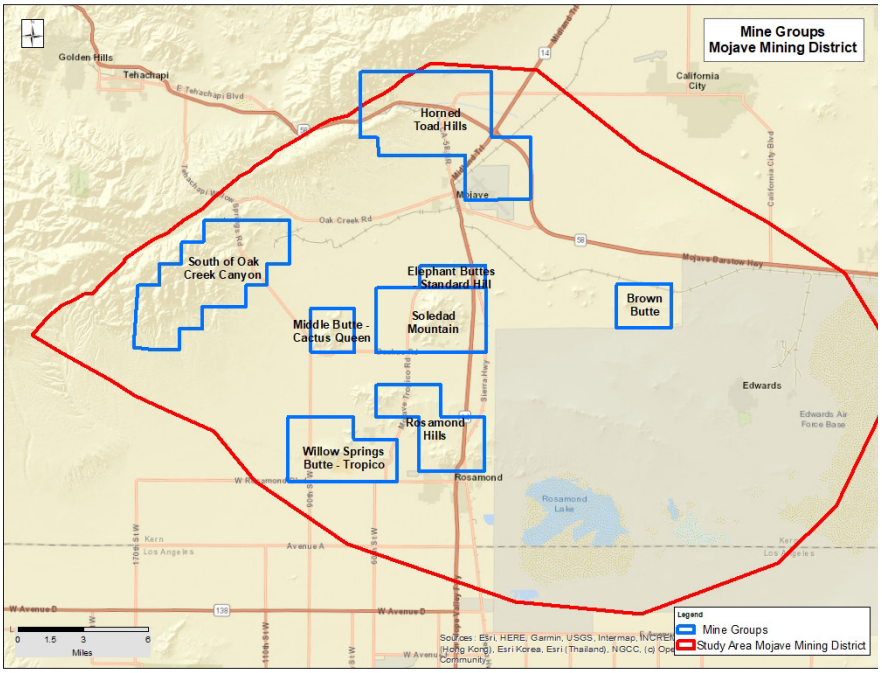

Figure 3. Locations of mine groups in greater Mojave district area.

- Horned Toad Hills
- Brown Butte-Bissel–Simons

Figure 4 is a topographic map for the study area.

Development history

Figure 5 is a mine map of the study area. Table 1 is an alphabetical listing of mines in the study area available online at http://www.greggwilkerson.com/mojave-mining-district.html.

Clay

A clay prospect (#70 Unknown Clay Deposit No. 2) was listed among the mines of the Horned Toad Hills Group in 1958 (Troxel and Morton, 1962, p. 80). It developed a 30-foot thick bed of greenish-gray bentonite.

The Los Angeles Clay deposit (Snow White) in the Willow Springs Butte-Tropico Group had greenish-gray clay derived from altered volcanic rocks. It was first described by Aubury (1906, p. 212). Aubery states that the clay from this mine "has been shipped during the past 15 years to the factory in Los Angeles" (e.g. 1891).

The Webb Clay deposit in the Willow Springs Butte-Tropico Group was developed by a 50-foot tunnel and first described by Dietrich (1928, p. 90).

Gold

The exploration and development history for the gold mines in the Mojave Mining District is described by Vredenburgh (this volume) for the Elephant Hill-Standard, Soledad, Rosamond Hills, Willow Springs Butte-Tropico and Middle Butte-Cactus mine groups.

Limestone

The limestone deposits in the South of Oak Creek Canyon Group were first developed at the California Portland Cement Company in December 1955 (Troxel and Morton, 1962, p. 214).

Magnesite

In circa 1909, the Bissel Magnesite Clay mine in the Brown Butte Group was discovered. It has swelling bentonite and sedimentary magnesite beds. It was leased to the Rex Plaster Company 1914–1916 and mined by the International Magnesite Company in 1917 and 1918. Through 1923 it had a total production of 15,757 tons. It was owned by the Southern Pacific Company in 1961 (Troxel and Morton, 1962, p. 76 and 237).

Sand and gravel

Most of the sand and gravel quarries in the Mojave District are spatially related to the Southern Pacific Railroad or to highways (Cal Trans pits).

Stone

The Desert Rock Milling Company operated stone quarries in the Rosamond Hills Group starting in 1950. Their mill was expanded in 1955. It produced three colors of granules: "desert rose", "surf green", and "bronze."

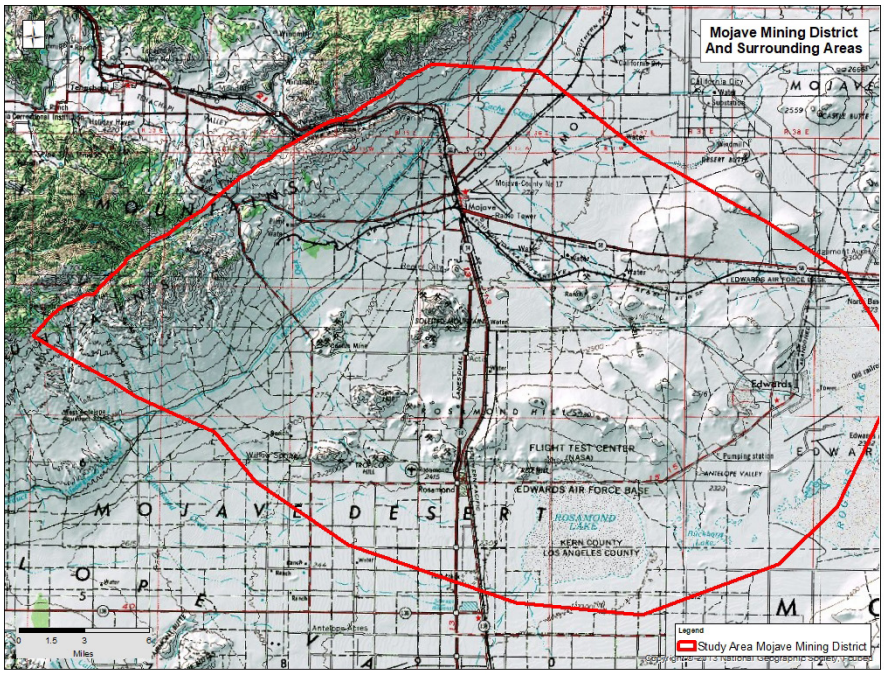

Figure 4. Topographic map with locations of mines.

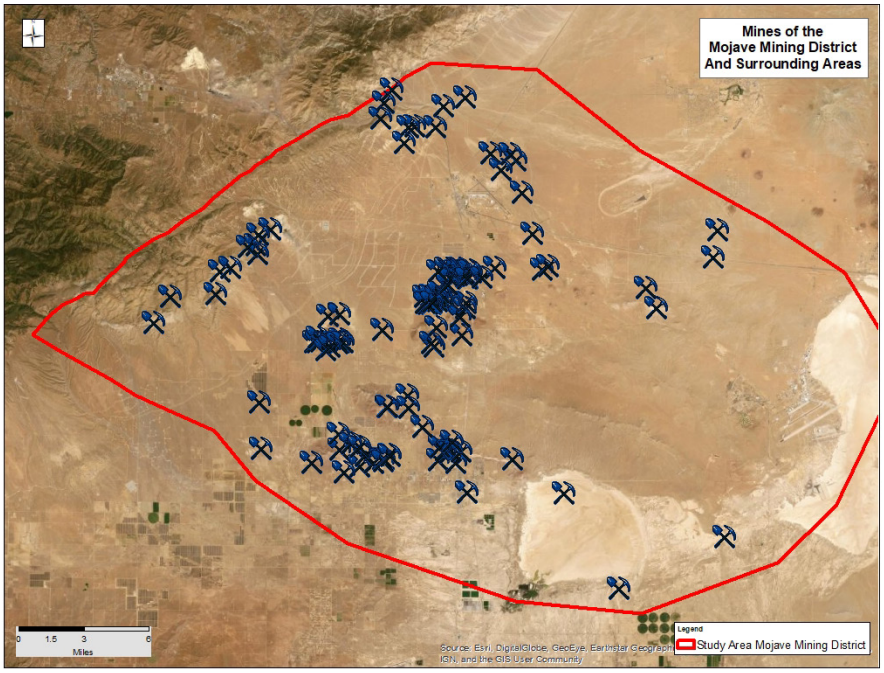

Figure. 5. Mines of the Mojave District area. Aerial image in background.

Mill M-8 on the southeastern side of Rosamond Hills processed these materials (Troxel and Morton, 1962, p. 271).

A stone quarry named "Section 12-24" in the South of Oak Creek Canyon Group produced materials used in the manufacturing of cement, presumably in 1950 (Troxel and Morton, 1962, p. 271)

The Hansen Dg Pit and Broken Stone #4 pits in the Horned Toad Hills Group are listed in California Division of Mines and Geology Special Publication 103.

Tungsten

There are three tungsten deposits in the South of Oak Canyon Group at the Leona Mill and-Esperanza Mine. The area was under claim to Tilo Lopez in 1958 (Troxel and Morton, 1962, p. 315; MRDS, 2011).

Uranium

Several uranium occurrences were discovered in the Mojave Mining District by Geiger counter surveys following World War II.

In the Horned Toad Group, uranium was found at the Emerald Queen prospect (Southern Pacific, 1987, p. 63; Walker and others, 1956, p. 11).

In the Middle Buttes-Cactus Group, "anomalous radioactivity amounting to 15 times background count" was found in association with gold ores at the Bluett and Quien Sabe No 314 Prospects. The Quien Sabe gold mine was located by William S. Allen in 1937 (Troxel and Morton, 1962, p. 180, 338; Walker and others, 1956, p. 9, 10, 17).

In the Soledad Mountain Group, the Mamie prospect, near the Double Eagle gold mine, had "anomalous radioactivity along shear zone in rhyolite" (Troxel and Morton, 1962, p. 340; Southern Pacific, 1987, p. 62).

There are four uranium prospects near the Stillwell property No. 675 in the Rosamond Hills Group (Troxel and Morton, 1961, p. 341; Southern Pacific, 1964, p. 62, 63). These are the Rosamond Uranium Prospect (Nelson, 1957, p. 14; Walker, 1953,p. 8; Walker and others, 1956, p. 11, 15), Stillwell Property (Troxel and Morton, 1962, p. 341; Walker and others, 1956, p. 11, 31), Verdi Development Company Anomaly No. 3 (Barrett and Magleby, 1954, p. 9; Nelson, 1957, p. 7-9; Troxel and others, 1957, p. 675, 677; Walker and others, 1956, p. 11, 15) and Kitty Kat Prospect (MRDS, 2011).

Geology

The following description of the Mojave District is given by Troxel and Morton (1962 p. 44-45):

"The gold and silver are in veins along faults in Tertiary rhyolitic volcanic rocks. The oldest rock in the district is a medium-grained quartz monzonite of Mesozoic age. It is exposed in the low areas peripheral to resistant masses of younger intrusive rock and in parts of the northwestern Rosamond Hills. Intrusive into the quartz monzonite are small pegmatite and aplite dikes also of Mesozoic age. Overlying the Mesozoic rocks are Mio-Pliocene nonmarine sedimentary and pyroclastic rocks of the Tropico group (Dibblee, 1958, p. 136) which, in the Rosamond Hills, are homoclinal in structure and strike west-northwest, and dip moderately south-southwest (Roberts, 1951). These rocks also crop out in parts of the other prominences in the area. Later Tertiary rhyolitic volcanic rocks have been intruded into both the quartz monzonite and the Tropico group. These volcanic rocks are resistant and are the most abundant rock exposed in the mountainous and hilly portions of the district except in the Rosamond Hills."

"The gold-silver deposits of the Mojave district are in epithermal fissure veins that occupy faults and shear zones. In general, the veins are confined to the rhyolitic volcanic rocks, although some of them have been traced downward into quartz monzonite. The principal ore minerals are cerargyrite, argentite, and free gold, but pyrargyrite, proustite, tetrahedrite, stromeyerite, native silver, and electum also have been found (Schmitt, 1940, unpublished report). The most common gangue minerals are quartz, pyrite, arsenopyrite, and hydrous iron oxides. Locally abundant in some deposits are chalcopyrite, galena, and stibnite. At Middle Butte the most common gangue is a kaolinite-alunite-quartz mixture".

"Quartz and feldspar are mined periodically from a pegmatite dike in the Rosamond Hills and are used as exposed aggregate and in ceramics. Pink, yellow, green, and lavender volcanic rocks in the Rosamond Hills are mined, crushed, and bagged for use as roofing granules. Clay suitable for use in manufacture of pottery has been mined from the northeast flanks of Tropico Hill. Small amounts of weathered volcanic rock are collected

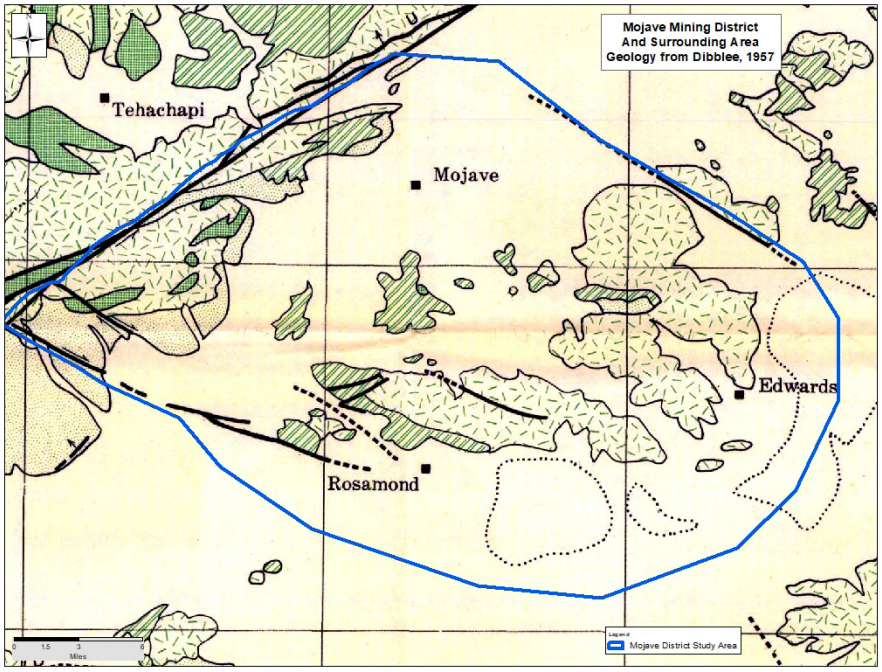

Figure 6. Geology map from Dibblee (1963a). Hachure pattern for granitic rocks, lined pattern for Miocene rocks, shaded pattern in the Tehachapi area for metamorphic rocks. Dotted lines enclose playas

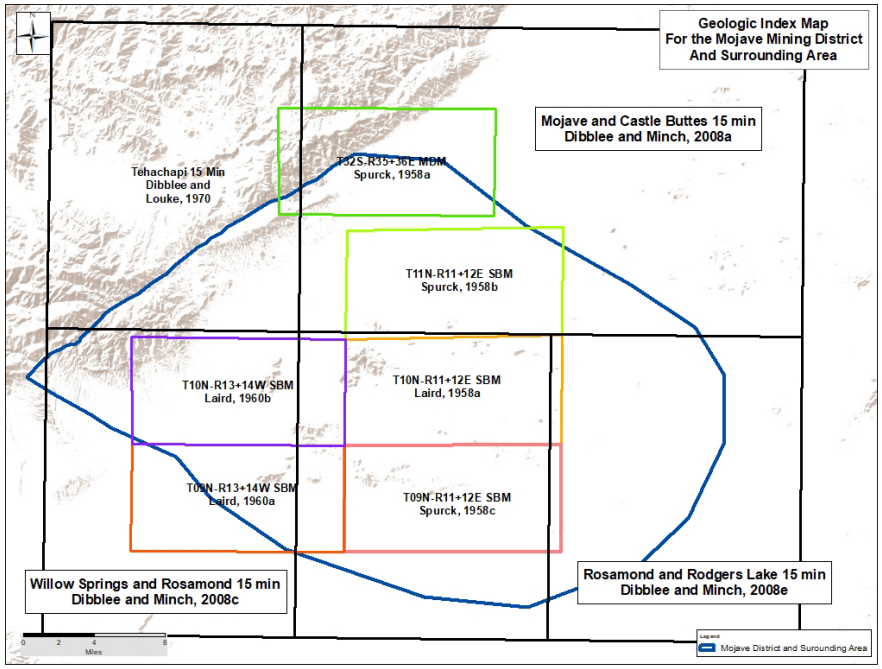

Figure 7. Locations and references for detailed geologic maps.

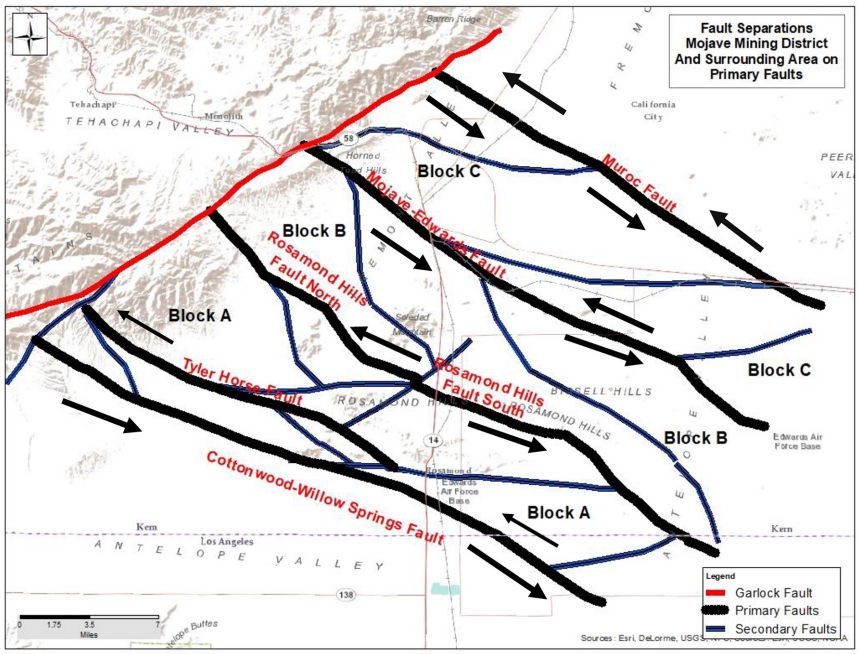

Figure 8. Primary and secondary faults generalized from maps in Figs. 6 and 7. Many secondary faults are hypothetical. Arrows show inferred separations on faults

from the east side of Middle Butte and sold as field stone".

"Two uranium localities in the district have been explored: the Rosamond prospect and other nearby sources in an area 3 miles northeast of Tropico Hill were explored in 1955-56; and the Donohan mine, half a mile. Northwest of Tropico Hill, was still under development in 1959. Both properties remained prospects in early 1959".

Figure 6 is a generalized geologic map of the study area from Dibblee (1957). Figure 7 is a geologic index map for the study area.

Structure

The geologic mapping by Dibblee (1957, 1958, 1963a, 1963b), Dibblee and Louke, 1970, Dibblee and Minch (2008a, 2008b), Spurck (1958a, 1958b, 1958c) and Laird (1950a, 1950b, 1960a, 1960b), suggest a possible set of primary faults that strike N70oW. This set of primary faults is nearly parallel to the orientation of the San Andreas Fault 17 miles to the southwest and is presumed to be right-lateral. Shear on the primary faults gave rise to a secondary set of faults (Figure 8). These secondary faults present as a "Lazy S" curve between the primary faults. The ore deposits apparently are localized by these secondary faults which developed low-pressure areas at the apex of the "Lazy S" curves between the primary faults. The tectonically created low pressure zones at the apex of the secondary faults resulted in enhanced permeability, ore fluid migration and ore deposition. Burnett and Brady (1990) suggested that the area was a resurgent caldera. A geologic mosaic of the study area is available on line at http://www.greggwilkerson.com/mojave-mining-district.html.

Mineralogy

Although in this district gold is the chief mineral in value, silver is predominant by a 5:1 ratio and is an important by-product of the gold ore. Cerargyrite (AgCl) and argentite (Ag_2S) are the most common silver minerals in these veins, but some ores also contain pyrargyrite (Ag,SbS_3), native silver, stromeyerite ($(Ag,Cu)_2S$), electrum, and argentian tetrahedrite ($(Cu,Fe)_{12}Sb,S_{13}$) (Troxel and Morton, 1962, p. 280). The USGS classified some mines in the district (Soledad) as being epithermal veins (Sado type, Model 151). The age of mineralization is 16.1 m.y at Soladad Mountain (see Gardner, 1954, Perez, 1978, Bruff, 1998a, 1998b, Ennis and Hertel, 2012).

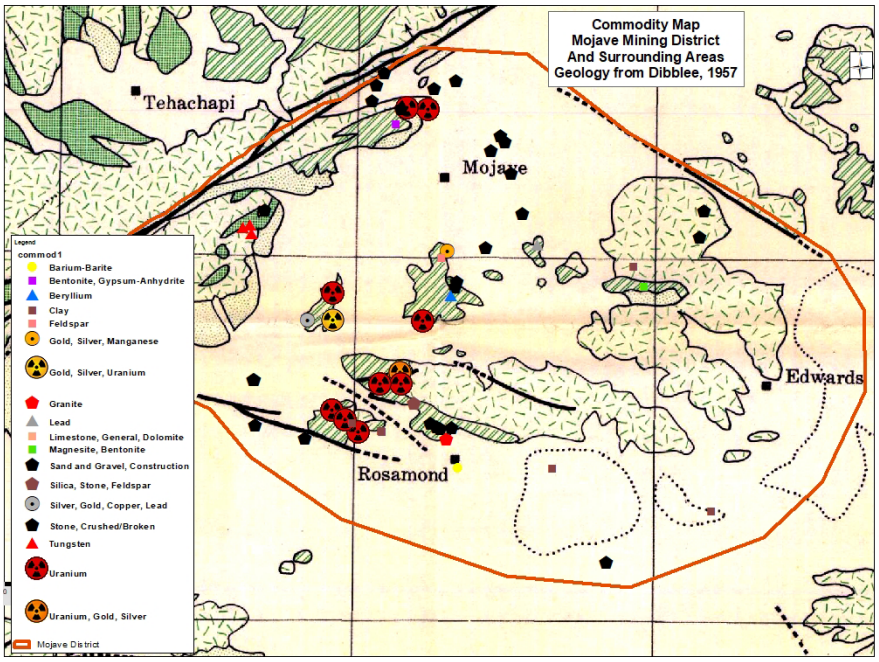

Figure 9. Commodity types in the Mojave District area.

Table 2. Commodities and mines of the Mojave District area.

COMMODITY	NUMBER OF MINES	PRIMARY MINES
Barium-Barite	1	Rosamond Mill
Bentonite	2	Tehachapi Clay Mine
		Unnamed Clay Deposit Prospect
Beryllium	1	Pharlap Claims Prospect
Clay	5	Antelope Materials Co. Mine
		Los Angeles Mine
		Riley Clay Deposit Mine
		Simons Brick Co. Mine
		Tropico Pit Mine
Feldspar	1	Rosamond Feldspar Occurrence
Gemstone	1	Cameron Siding Occurrence
Gold	71	Bluebird
		Bobtail Mine
		Burton-Brite-Blank Mine
		Cactus Gold Mine
		Desert Queen
		Echo
		Elephant Eagle
		Elephant Group
		Excelsior
		Exposed Treasure Mine
		Exposed Treasure Mine
		Four Star
		Golden Queen Mine
		Gum Tree Mine
		Hoegee Mine
		Ladd Mine
		Last Chance Mine
		Lida
		Marie Celesle
		Middle Butte Mine
		Milwaukee Mine
		Mojave Mining and Milling Co.
		Pride of Mojave Mine
		Queen Esther
		Quien Sabe
		Rosamond-Mojave
		Sailor Boy Mine
		Soledad Mountain Project
		Standard Hill Mine
		Standard Group
		Tropico
		Tropico Mines
		Victory
		Wegman Group
		Whitmore Mine
		Yellow Dog Extension
		Yellow Dog Mine
		Yellow Rover Mine
		Zoledad East
Granite	1	Pious Quarry
Lead	1	Ladd
Limestone	6	California Portland Cement Co.
		Monolith Limestone Quarry
		Monolith Portland Cement Co.
Magnesite	1	Snowball Deposit
Sand and Gravel		Borrow Pit
		Caltrans #101
		Miller - Mojave Pit
		Mojave Pit
		Mojave Pit
		Rosamond Sand Pits
		Sand and Gravel #2
		Sand and Gravel #5
		Sanborn Sand and Gravel
		Soledad Sand and Gravel
		Willow Springs Pit
Silica	2	Rosamond Mine
		Silver Queen Mine
Silver, Gold	4	Cactus Queen Mine
		Monarch Mine
		Soledad Mountain Deposit
		Middle Buttes (Cactus) Deposit
Sodium	1	Cameron Lake
Stone	12	Broken Stone #2
		Broken Stone #5
		Broken Stone #1
		Decomposed Granite Pit
		Desert Rock Milling Co. Quarry
		Hansen Dg Pit
		Hidecker Rock Co. Mill & Quarries
		Mojave Rock Products
		Mojave Rock Products
		Section 13-24 Quarry Mojave
		Portland Cement Co
Tungsten	3	Esperanza
		Esperanza Prospect
		Leona Tungsten Mine
Uranium	11	Goldenrod Prospect
		Stillwell Property

Alteration

The fissure vein deposits in Elephant Butte, Soledad Mountain, Rosamond Hills, Middle Butte, and Willow Springs Butte all exhibit pervasive low grade pyritic alteration. The quartz veins, up to 20 feet wide, have low sulfide concentrations. These sulfide haloes impart a distinctive red-brown color to these topographic features.

Mine and commodity summary

Figure 9 is a commodity map for the study area. Table 2 is a listing of mines in the study area by commodity.

Table 3. Reports for mine groups of the Mojave District area.

MINE GROUP	URL LINK
Elephant Butte – Standard Hill	https://www.academia.edu/41884470/Elephant_Butte_-_Standard_Hill_Group_Mojave_Mining_District_Kern_County_California
Middle Butte – Cactus Queen	https://www.academia.edu/41869931/Middle_Butte_Cactus_Queen_Mine_Group_Mojave_Mining_District_Kern_County_California
Soledad Mountain	https://www.academia.edu/41883267/Soledad_Mountain_Group_Mojave_Mining_District_Kern_County_California
Rosamond Hills	https://www.academia.edu/41875747/Rosamond_Hills_Group_Mojave_Mining_District_Kern_County_California
Willow Springs Butte – Milwaukee – Tropico	https://www.academia.edu/41875706/Willow_Springs_Mountain_Tropico_Group_Mojave_Mining_District_Kern_County_California
South of Oak Creek Canyon	https://www.academia.edu/41875670/South_of_Oak_Creek_Canyon_Group_Mojave_Mining_District_Kern_County_California
Horned Toad Hills	https://www.academia.edu/41869884/Horned_Toad_Hill_Group_Mojave_Mining_District_Kern_County_California
Brown Butte-Bissel – Simons	https://www.academia.edu/41869820/Brown_Butte_Mine_Group_Mojave_Mining_District_Kern_County_California

Mine groups

Reports for the seven mine groups, and for every producer or past producing mine within them, are found at the links given in Table 3. These reports have larger versions of all maps in this summary.

References and bibliography

Aubury, L. E., 1906, The structural and industrial materials of California: California Mining Bureau. Bulletin. 38, p. 69-72, 100, 128,212-2I3, 273, 274-275, 284, 355, 374-378.

Bateson, Charles E. W., 1907, The Mojave District of California, Transactions of the American Institute of Mining Engineers, Volume XXXVII, p. 160-177.

Bonham, H.F. Jr, James Cooksiey and Max Schafer, 1959 Aerial Economic Geology of T.06N, R.13&14E, SBM. Summary described in, Southern Pacific Company, 1987, Minerals for Industry, Southern California Volume III, Summary of Geological Survey 1951-1961, Data in support of Special Publication 95, California Division of Mines and Geology, unpublished map.

Bruff, S.R., 1998a (April), Summary of Corrections Made to GQM LLC Drill Hole Database, unpublished report by Humboldt Mining Services for Golden Queen Mining Company, 12 p.

Bruff, S.R., 1998b (July), Cross section polygonal resource estimate, Soledad Mountain Project, unpublished report by Humboldt Mining Services for Golden Queen Mining Company,70 p.

Burnett, John L. and James Brady, 1990. Cactus Gold Mine, California Geology, Volume 43, No. 4, April 1990 Edition, California Division of Mines and Geology, p. 5-88.

Collier, J.T., 1958, Aerial Economic Geology of T.10N, R.07&08E, SBM. Summary described in Southern Pacific Company, 1987, Minerals for Industry, Southern California Volume III, Summary of Geological Survey 1951-1961, Data in support of Special Publication 95, California Division of Mines and Geology, unpublished map.

Coonrad, Warren L., 1958, Aerial Economic Geology of T.11N, R.07&08E, SBM. Summary described in Southern Pacific Company, 1987, Minerals for Industry, Southern California Volume III, Summary of Geological Survey 1951-1961, Data in support of Special Publication 95, California Division of Mines and Geology, unpublished map.

Coonrad, Warren L., 1959a, Aerial Economic Geology of T.07N, R.11&12E, SBM. Summary described in Southern Pacific Company, 1987, Minerals for Industry, Southern California Volume III, Summary of Geological Survey 1951-1961, Data in support of Special Publication 95, California Division of Mines and Geology, unpublished map.

Coonrad, Warren L., 1959b, Aerial Economic Geology of T.08N, R.07&08E, SBM. . Summary described in, Southern Pacific Company, 1987, Minerals for Industry, Southern California Volume III, Summary of Geological Survey 1951-1961, Data in support of Special Publication 95, California Division of Mines and Geology, unpublished map.

Coonrad, Warren L., 1959c, Aerial Economic Geology of T.10N, R.11&12E, SBM. Summary described in Southern Pacific Company, 1987, Minerals for Industry, Southern California Volume III, Summary of Geological Survey 1951-1961, Data in support of Special Publication 95, California Division of Mines and Geology Unpublished map.

Coonrad, Warren L., 1959d, Aerial Economic Geology of T.11N, R.09&10E, SBM. Summary described in, Southern Pacific Company, 1987, Minerals for Industry, Southern California Volume III, Summary of Geological Survey 1951-1961, Data in support of Special Publication 95, California Division of Mines and Geology, unpublished map.

Coonrad, Warren L. and E.A. Damehy, 1959, Aerial Economic Geology of T.09N, R.07&08E, SBM. Summary described in Southern Pacific Company, 1987, Minerals for Industry, Southern California Volume III, Summary of Geological Survey 1951-1961, Dasta in support of Special Publication 95, California Division of Mines and Geology, unpublished map.

Danehy, E.A. and M.C. Garner, 1961, Aerial Economic Geology of T.11S, R.13&14E, SBM. Summary described in, Southern Pacific Company, 1987, Minerals for Industry, Southern California Volume III, Summary of Geological Survey 1951-1961, Data in support of Special Publication 95, California Division of Mines and Geology, unpublished map.

De Kalb, Courtenay, 1907, Geology of the Exposed Treasure lode, Mojave, California: Am. Inst. Min. Met. Eng. Bull. 13, p. 15-24; Cited by Troxel and Morton, 1962, p. 349.

De Kalb, Courtenay, 1908, Geology of the Exposed Treasure lode, Mojave, California, Trans 38, p. 310-319. Cited by Troxel and Morton, 1962, p. 349.

Dietrich, W.F.T., 1928, The clay resources and the ceramic industry of California: California Min. Bur. Bull. 99, p. 88-90.

Dibblee, T.W., 1957, Simplified geologic map of the western Mojave Desert, California: U.S. Geological Survey, Open-File Report OF-57-39, scale 1:250,000

Dibblee, T. W. Jr., 1958, Tertiary stratigraphic units of western Mojave Desert, California: Am. Assoc. Petroleum Geologists Bull., vol. 42, no. 1, p. 135-144. See p. 136.

Dibblee, T.W., 1959, Geology of the Rogers Lake quadrangle, California: U.S. Geological Survey, Open-File Report OF-59-29, scale 1:48,000.

Dibblee, T.W., 1960, Geology of the Rogers Lake and Kramer quadrangles, California: U.S. Geological Survey, Bulletin 1089-B, scale 1:62,500.

Dibblee, T.W., 1963a, Generalized Geology of the Mojave Desert Region: U.S. Geological Survey, Bulletin 1089, Plate 7; scale 1:500,000.

Dibblee, T.W., 1963b, Geology of the Willow Springs and Rosamond quadrangles, California: U.S. Geological Survey, Bulletin 1089-C, scale 1:62,500.

Dibblee, Thomas W., Jr., 1967, Areal geology of the western Mojave Desert, California: U.S. Geological Survey Professional Paper 522, 153 p.

Dibblee, Thomas W. Jr., and Gladys P. Louke, 1970, Geologic Map of the Tehachapi Quadrangle, Kern County, California: U.S. Geological Survey, Miscellaneous Geologic Investigations, Map I-607. Scale 1:62,500.

Dibblee, T.W. and Minch, J.A., 2008a, Geologic Map of the Mojave and Castle Butte 15 Minute Quadrangles, Kern County, California, Dibblee Geological Fountation Map DF 401. Scale 1:62,500.

Dibblee, T.W., and Minch, J.A., 2008b, Geologic map of the Neenach & Willow Springs 15 minute quadrangles, Kern & Los Angeles Counties, California: Dibblee Geological Foundation, Dibblee Foundation Map DF-383, scale 1:62,500.

Dibblee, T.W., and Minch, J.A., 2008c, Geologic map of the Rosamond and Rodgers Lake 15 minute quadrangles, Kern & Los Angeles Counties, California: Dibblee Geological Foundation, Dibblee Foundation Map DF-384, scale 1:62,500.

Dibblee, T.W., and Minch, J.A., 2008d, Geologic map of the Tehachapi and Cummings 15 minute quadrangles, Kern & Los Angeles Counties, California: Dibblee Geological Foundation, Dibblee Foundation Map DF-397, scale 1:62,500.

Dibblee, T.W., and Minch, J.A., 2008e, Geologic map of the Rosamond & Rogers Lake 15 minute quadrangles, Kern & Los Angeles Counties, California: Dibblee Geological Foundation, Dibblee Foundation Map DF-384, scale 1:62,500.

Dietrich, W. F.t T., 1928, The clay resources and the ceramic industry of California: California Min. Bur. Bull. 99, p. 88-90.

Ennis, S., and Hertel, M., 2012, Soledad Mountain Project NI 43-101 Technical Report, report by Norwest-AMEC to Golden Queen Mining Company, 235 p.

Eric, John H., 1948, Copper Deposits in California: California Division of Mines, Bulletin 144, Table No. 16, p. 255.

Gamble, James, 1959a, Aerial Economic Geology of T.06N, R.09&10E, SBM., Summary described in Southern Pacific Company, 1987, Minerals for Industry, Southern California Volume III, Summary of Geological Survey 1951-1961, Data in support of Special Publication 95, California Division of Mines and Geology, unpublished map.

Gamble, James, 1959b, Aerial Economic Geology of T.07N, R.09&10E, SBM. Summary described in, Southern Pacific Company, 1987, Minerals for Industry, Southern California Volume III, Summary of Geological Survey 1951-1961, Data in support of Special Publication 95, California Division of Mines and Geology, unpublished map.

Gamble, James, 1959c, Aerial Economic Geology of T.08N, R.11&12E, SBM . Summary described in Southern Pacific Company, 1987, Minerals for Industry, Southern California Volume III, Summary of Geological Survey 1951-1961, Data in support of Special Publication 95, California Division of Mines and Geology, Southern Pacific Corporation, Copyright © Southern Pacific Company, 1964, unpublished map.

Gamble, James, 1959d, Aerial Economic Geology of T.09N, R.11&12E, SBM. . Summary described in, Southern Pacific Company, 1987, Minerals for Industry, Southern California Volume III, Summary of Geological Survey 1951-1961, Data in support of Special Publication 95, California Division of Mines and Geology, unpublished map.

Gamble, James and E.A. Danehy 1959, Aerial Economic Geology of T.10N, R.01&02E, SBM. Summary described in, Southern Pacific Company, 1987, Minerals for Industry, Southern California Volume III, Summary of Geological Survey 1951-1961, Data in support of Special Publication 95, California Division of Mines and Geology, unpublished map.

Gardner, D.L., 1954, Gold and silver mining districts in the Mojave Desert region of southern California, in Jahns, R.H., ed., Geology of southern California, California Division of Mines Bulletin 170, p. 5-20.

Jennings, Charles W. and Rudolph Strand, 1969, Los Angeles Sheet, Geologic Map of California, California Division of Mines and Geology. Sixth printing, 1991, 1:250,000.

Jennings, Charles W., John L. Burnett and Bennie W. Troxel, 1962, Geologic Map of California, Olaf P. Jenkins Edition, Trona Sheet, California Division of Mines and Geology, 1:750,000.

Jordan, J.T., 1941, Geology of the Cactus mines, Rosamond, Kern County, California: Pasadena, California Institute of Technology, M.S. thesis.

Julihn. C. E., and Horton, F. W., 1937, Mineral industries survey of the United States. California, Kern County, Mojave district. The Golden Queen and other mines of the Mojave district, California: U. S. Bur. Mines Information Circular 6931, 42 p. See p. 4-5.

Laird, Raymond, 1958a, Aerial Economic Geology of T.10N, R.11&12W, SBM. Summary described in, Southern Pacific Company, 1987, Minerals for Industry, Southern California Volume III, Summary of Geological Survey 1951-1961, Data in support of Special Publication 95, California Division of Mines and Geology, unpublished map.

Laird, Raymond, 1959a, Aerial Economic Geology of T.06N, R.11&12W, SBM. Summary described in, Southern Pacific Company, 1987, Minerals for Industry, Southern California Volume III, Summary of Geological Survey 1951-1961, Data in support of Special Publication 95, California Division of Mines and Geology, unpublished map.

Laird, Raymond, 1959b, Aerial Economic Geology of T.08N, R.09&10E, SBM. Summary described in Southern Pacific Company, 1987, Minerals for Industry, Southern California Volume III, Summary of Geological Survey 1951-1961, Data in support of Special Publication 95, California Division of Mines and Geology, unpublished map.

Laird, Raymond, 1959c, Aerial Economic Geology of T.09N, R.09&10W, SBM. Summary described in Southern Pacific Company, 1987, Minerals for Industry, Southern California Volume III, Summary of Geological Survey 1951-1961, Data in support of Special Publication 95, California Division of Mines and Geology, unpublished map.

Laird, Raymond, 1959d, Aerial Economic Geology of T.09N, R.09&10W, SBM. Summary described in Southern Pacific Company, 1987, Minerals for Industry, Southern California Volume III, Summary of Geological Survey 1951-1961, Data in support of Special Publication 95, California Division of Mines and Geology, unpublished map.

Laird, Raymond, 1960a, Aerial Economic Geology of T.09N, R.13&14W, SBM. Summary described in, Southern Pacific Company, 1987, Minerals for Industry, Southern California Volume III, Summary of Geological Survey 1951-1961, Data in support of Special Publication 95, California Division of Mines and Geology, unpublished map.

Laird, Raymond, 1960b, Aerial Economic Geology of T.10N, R.13&14W, SBM. Summary described in, Southern Pacific Company, 1987, Minerals for Industry, Southern California Volume III, Summary of Geological Survey 1951-1961, Data in support of Special Publication 95, California Division of Mines and Geology, unpublished map.

Maynard, R.G., 1947, Geology of the Tropico mine. Rosamond, California: Los Angeles, University of California, M.A. thesis.

MRDS, 2011, Mineral Resource Data System, U.S. Geological Survey.

Nelson, H. E., 1957, Uranium occurrences in the Mojave mining district, Kern County, California: U. S. Atomic Energy Comm. RME 2058, 26 p.

Osterling, William A., 1958, Aerial Economic Geology of T.06S, R.09&10E, SBM. Summary described in, Southern Pacific Company, 1987, Minerals for Industry, Southern California Volume III, Summary of Geological Survey 1951-1961, Data in support of Special Publication 95, California Division of Mines and Geology.

Perez, H.R., 1978, Geology and geochemical exploration of the gold-silver deposits at Soledad Mountain, Mojave, Kern County, California, unpublished MSc thesis, University of California-Los Angeles, 146 p.

Roberts, W. B, 1951, Geology of a part of the Rosamond Hills area, Kern County, California: Unpublished MS thesis, California Institute of Technology, Division of Geologic Science, Pasadena, California., 39 p.

Rogers, Thomas H., 1967, Geologic Map of California, Olaf P. Jenkins Edition, San Bernardino Sheet, California Division of Mines and Geology, 1:250,000.

Schmitt, Harrison, 1940, unpublished report of the Cactus Queen mine, Kern County.

Smith, Alexander, 1947, The geochemistry and paragenesis of the ores of the Cactus mine. Kern County, California: Pasadena, California Institute of Technology, Ph.D. dissertation.

Smith, Arthur R., 1964, Geologic Map of California, Olaf P. Jenkins Edition, San Bernardino Sheet, California Division of Mines and Geology, 1:250,000.

Southern Pacific Company, 1987, Minerals for Industry, Southern California Volume III, Summary of Geological Survey 1951-1961, in Special Publication 95, Volume 3 California Division of Mines and Geology.

Shafer, M., and A. Cunningham, 1958, Aerial Economic Geology of T.05N, R.11&12E, SBM. Summary described in, Southern Pacific Company, 1987, Minerals for Industry, Southern California Volume III, Summary of Geological Survey 1951-1961, Data in support of Special Publication 95, California Division of Mines and Geology, unpublished map.

Spurck, F.D., 1958a, Aerial Economic Geology of T.32S, R.35&36E, MDM. Summary described in Southern Pacific Company, 1987, Minerals for Industry, Southern California Volume III, Summary of Geological Survey 1951-1961, Data in support of Special Publication 95, California Division of Mines and Geology, unpublished map.

Spurck, F.D., 1958b, Aerial Economic Geology of T.11N, R.11&12E, SBM. Summary described in, Southern Pacific Company, 1987, Minerals for Industry, Southern California Volume III, Summary of Geological Survey 1951-1961, Data in support of Special Publication 95, California Division of Mines and Geology.

Spurck, F.D., 1958c, Aerial Economic Geology of T.09N, R.11&12E, SBM. Summary described in, Southern Pacific Company, 1987, Minerals for Industry, Southern California Volume III, Summary of Geological Survey 1951-1961, Data in support of Special Publication 95, California Division of Mines and Geology, unpublished map.

Spurck, W.H., 1960, Aerial Economic Geology of T.10N, R.17&18E SBM. Summary described in, Southern Pacific Railroad, Minerals for Industry, , Southern California Volume III, Summary of Geological Survey 1951-1961, Data in support of Special Publication 95, California Division of Mines and Geology, unpublished map.

Stejer, F. A., 1958, Aerial Economic Geology of T.11N, R.11&12E, SBM. Summary described in Southern Pacific Company, 1987, Minerals for Industry, Southern California Volume III, Summary of Geological Survey 1951-1961, Data in support of Special Publication 95, California Division of Mines and Geology, , unpublished map.

Tischler, M.S. and W.H. Spurck, 1960, Aerial Economic Geology of T.11N, R.15&16E, SBM. Summary described in Southern Pacific Company, 1987, supporting data for Minerals for Industry, Southern California Volume III, Summary of Geological Survey 1951-1961, Special Publication 95, California Division of Mines and Geology, unpublished map.

Tischler, M.S., H.F. Bonham, Jr. and W.H. Spurck, 1960, Aerial Economic Geology of T.11N, R.17&18E, SBM. Summary described in, Southern Pacific Company, 1987, Minerals for Industry, Southern California Volume III, Summary of Geological Survey 1951-1961, Data in support of Special Publication 95, California Division of Mines and Geology, unpublished map.

Troxel, B.W. and P.K. Morton, 1962, Mines and Mineral Resources of Kern County, County Report No. 1, California Division of Mines and Geology.

Troxel, B. W., Stinson, M. C., and Chesterman, C. W., 1957, Uranium: California Div. Mines Bull. 176, p. 669-687.

Tucker, W.B. and R.J. Sampson, 1935, Mining Activity at Soledad Mountain and Middle Buttes – Mojave Mining District, Kern County: California Journal of Mines and Geology, p. 474-475.

Tucker, W.B. and R.J. Sampson, 1940, Current Mining Activity in Southern California: California Journal of Mines and Geology, Quarterly Chapter of State Mineralogist's Report XXXVI, p. 35-36.

Walker, G. W., 1953, Rosamond uranium prospect, Kern County, California: California Div. Mines Special Report 37, 8 p.

Walker. G. W., Lovering, T. G., and Stephens, H. G., 1956, Radioactive deposits in California: California Div. Mines Special Report. 49, 38 p.

Walker, J.D., Berry, A.K., Davis, P.J., Andrew, J.E., and Mitsdarfer, J.M., 2002, Geologic map of northern Mojave Desert and southwestern Basin and Range, California: Geological Society of America, Memoir 195, scale 1:250,000.

The Mojave Mining District: a brief history of gold mining

Larry M. Vredenburgh
lvredenb@gmail.com

Introduction

Soledad Mountain, which rises almost 1,400 feet above from the surrounding, mostly flat, western Mojave Desert, has been a sentinel for explorers, travelers and prospectors who have passed by this solitary mountain on their way to somewhere else, yet not realizing they were passing by a literal mountain of gold.

Kern County has been blessed with immense mineral riches essentially lying on the surface. In the Taft area oil has been flowing to the surface in seeps and springs since the Pleistocene Epoch (since about 2 million years ago). The world's largest borax mine, located at Boron, California, was discovered in 1913 by John Suckow, at a depth of 40 feet while drilling for water on his homestead claim. There are so many other examples of riches found at the surface: the Big Blue Mine at Kernville, gold in the El Paso Range and Randsburg, silver at the Kelly Rand mine, and tungsten at Atolia to name just a few.

On the northeast side of Soledad Mountain, literally in its shadow, tiny Standard Hill rises a mere 450 feet above the desert. But it was here, originally named Bowers Hill, that a rich surface exposure of gold-bearing rock was first found in 1894. Soon gold was also discovered on Soledad Mountain, Middle Butte and Tropico Hill (also see Wilkerson, this volume). These hills fit within a 12.3-mile diameter circle. After initial mining activity until about 1914, the mining district saw a revival from about 1933 until 1942, and sporadically from the mid-1980s until present time.

1894 – 1914

Standard Hill

Gold was first discovered in the Mojave Mining District in 1894 after George Bowers stepped off the train in Mojave to get a bite to eat while the locomotive stopped for water. He noticed Indians selling quartz crystals, bought some and inquired where they came from. Bowers returned on a subsequent trip and discovered gold just south of town. Bowers wasn't just some raggedy prospector. Born in 1833 in Pennsylvania, by 1870 he was living in Grass Valley, where the census taker listed him as a quartz miner. In the San Francisco city directory two decades later, his occupation is listed as Mining.

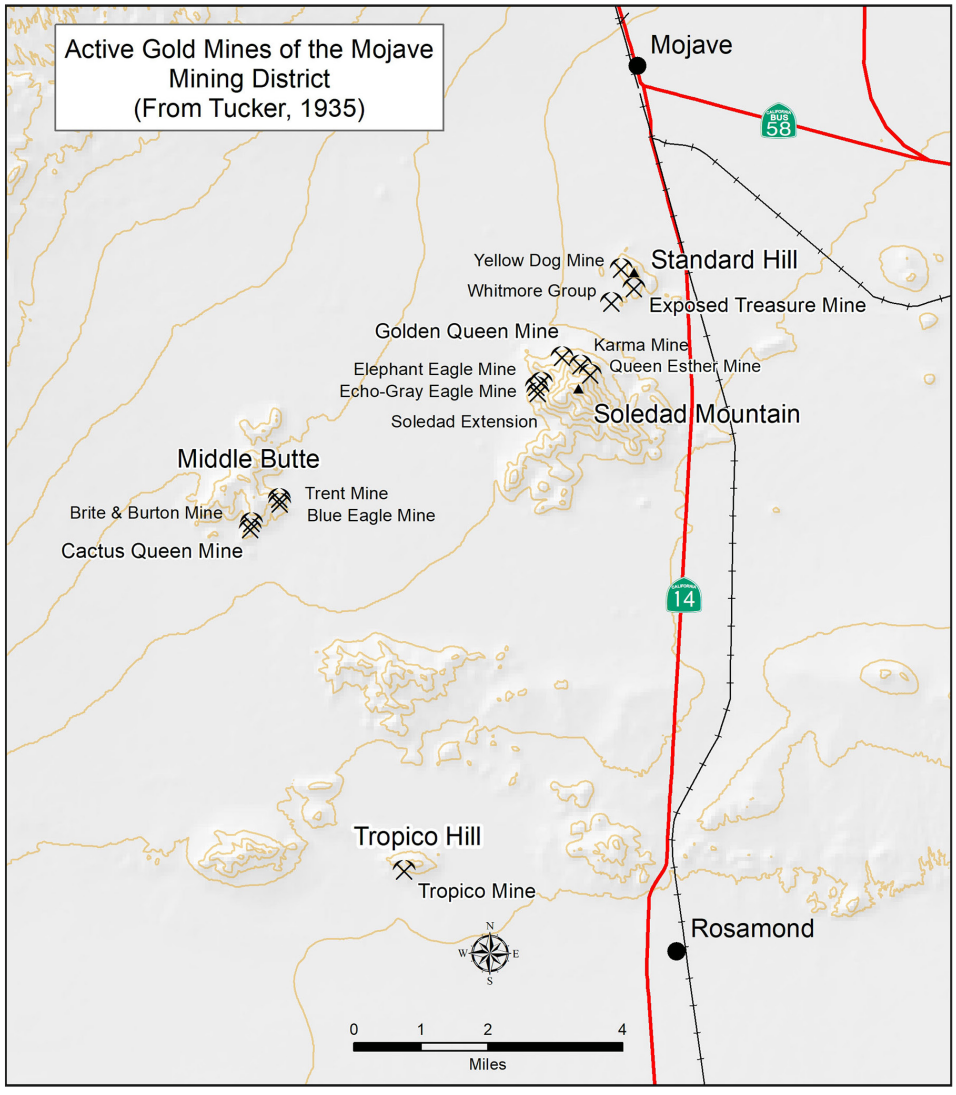

The Exposed Treasure Mine in the early 1900s, Standard Hill, Mojave Mining District. Photo by C. C. Pierce.

The date of his discovery is recorded as March 8, 1894. A few days later the Bakersfield *Daily Californian* reported that "George E. Bowers and C. Bowers each located quartz claims at a point about four miles south of Mojave." Another account stated that Bowers located 6 claims in 1894. Bowers found a gold-rich surface outcrop on what is now known as Standard Hill, half a mile west of the Southern Pacific Railroad. His first "mining" consisted of gathering up about 40 tons of loose gold-bearing surface rock which he shipped to a mill by railcar at a profit. Bowers quickly set to work sinking shafts. The mine that was developed from this find was named the Exposed Treasure.

Soon the area was swarming with prospectors, several of whom were rewarded with "many valuable finds in low grade gold bearing ore. . ." Because of this increase in mining activity, a Mojave Mining District was established on November 29, 1896, with H. E. Coleman the elected recorder.

After attempting to interest investors in the property, Bowers sold his claims to K. A. Calkins and C. N. Davidson in June 1898. During 1901 a 20-stamp mill was erected at the Exposed Treasure and an 18-mile long water line was laid from Oak Creek.

In 1912 Mojave Consolidated Gold Mines Company purchased all of the mines on Standard Hill and operated them until 1915. It is estimated that about 105,000 ounces of gold were produced from the Exposed Treasure Mine from 1894 until 1915.

In 1921 a spectacular discovery was made at the Yellow Dog Mine, on Standard Hill. Percy Wegman, son of E. H. Wegman, owner of the Queen Esther and Karma mines located on Soledad Mountain, found several pieces of gold rich "float" rock on a wagon road a hundred feet from an existing mine shaft. However, the ore body which was discovered proved to be small. In 1921 Standard Mining and Milling Company operated the mines from 1921 until 1928.

Soledad Mountain

Mining began on the north slope of Soledad Mountain at the Queen Esther, Karma, Echo, Elephant, and Gray Eagle mines by 1897. In 1902 a 10-stamp mill (later enlarged to 20-stamps) was erected at the Echo Mine. At the Queen Esther, a roller mill with 75 tons of daily capacity was erected in 1903; the mill capacity was increased to 150 tons the following year.

The Karma Mine, between 1897 and 1904, shipped ore averaging 50 ounces of silver and .5 ounce of gold per ton to the smelter. These shipments yielded $287,000. In 1904 a 20-stamp mill was erected to treat ore from the Karma Mine.

Between 1894 and 1909 the Queen Esther produced about 62,500 ounces the Karma 37,500 ounces of gold.

The Tropico Mine and the Burton brothers

Shortly after Bowers' 1894 discovery, more rich gold ore was discovered on the south end of the district. Beginning in the 1870s clay was mined by Dr. L. A. Crandall from

the north side of what is now known as Tropico Hill. Eventually, Ezra Hamilton, owner of a manufactured fire clay pipe company in Los Angeles, began buying clay from Crandall, and in 1882 he purchased the quarry. Years later, in the early 1890s, Hamilton decided to pan some of the clay and found specks of gold. He soon hooked up his team and, with his son Truman, headed out to find the source of the gold. But it wasn't easy. It took two years of prospecting whenever he could get away, before he discovered the source of the gold. Finally, in 1896 Hamilton made a rich strike at the crest of a hill. Then he and his son began staking out claims and started sinking a prospect shaft. His first shipment of 21 tons netted them $4,600 from which they purchased mining machinery. In 1898 he purchased a two-stamp mill. Hamilton sold one of his claims in 1900 for an astounding $100,000. Soon afterward Hamilton built a 5-stamp mill to process ore from the Lida and Fairview claims. Under Hamilton's management the mine produced $260,000 (about 13,000 ounces) of gold from a narrow vein that carried 1 to 5 ounces of gold per ton.

The mine changed hands several times until it was acquired in 1909 by Tropico Mining and Milling Company. Several of the stockholders of this company were from a small community known as Tropico located near Glendale, California.

In 1910 Clifford Burton, who eventually came to own the Tropico mine, began working for the company. In 1900, at the age of 12, Clifford's family moved from England to a ranch 5 miles west of Lancaster, California. When Clifford was 18, he set out with Mike O'Mara, an old prospector who was passing through the Antelope Valley on his way to Death Valley. At Ballarat Clifford met Mel Stanford. The two of them began prospecting together, and before the end of the year they discovered the Gold Bug mine high in the Slate Range. After selling the mine for $2,000 he took courses in assaying and other mining subjects. He had this and other mining experience under his belt prior to beginning work for the Tropico Mining Company. In June 1914, a short time after he began working for the company, he was promoted to superintendent. At this time, he hired his brother Cecil. After serving during World War I Clifford returned to find the mine shut down. At first, he was granted permission to reprocess tailings; then, in 1920, he worked the mine under a lease. Slowly the two brothers purchased the mine's stock and by 1928 Clifford and Cecil formed the Burton Brothers Corporation for the purpose of operating the Tropico Mine and the Burton Brothers Custom Mill.

Under their ownership they expanded the mill and extended drifts westward toward the Kid claim where they encountered the largest ore bodies found at the mine. This mine, as nearly all gold mines in the country, were closed down in 1942. After the war the mine was operated on a small scale until 1956. During the life of the mine, between six and eight million dollars was produced.

The 1930s

Soledad Mountain

In the 1930s the Mojave Mining District experienced a significant revival that U. S. Bureau of Mines mining engineers C. E. Julihn and F. W. Horton attributed in no small part to Clifford and Cecil Burton.

They described the Burton Brothers, in their 1937 report on mining in the district as,

> hard-rock miners themselves, who had labored and sacrificed to become owners of Tropico mine, mill, and general supply store. With faith in the district, they were persistent grubstakers of worthy prospectors, as well as outstanding good citizens of the little hamlet of Rosamond in the Mohave Desert.
>
> It was they who, at the onset of the great depression, leased the Exposed Treasure and other old properties, subleased small parcels of the ground to miners out of employment, grubstaked them, and milled at Tropico whatever small lots of ore the mines produced. As a result, there were ultimately 50 to 60 groups of leasers in the district making a living through deliveries of ore to the Tropico mill. These small leasing operations produced $180,000 worth of ore. A leaser looking for a new place to work found the now famous horn shaped piece of rich gold float that led to discovery of the Golden Queen vein, to his suddenly becoming a millionaire, and to revival of mining in a big way throughout the moribund Mojave district.

During the early 1930s numerous leasers were working the old mines of the district. George Holmes was one of these leasers. He was born in 1903 and was 26 when he began mining in 1929 near the Elephant Eagle Mine on the northwest side of Soledad Mountain. Though born in Michigan he grew up in Grass Valley. He began working in the mines at 16. He had worked at the North Star Mine in Grass Valley for three years, and in other mines in Nevada and California. In addition, he took some geology courses at the University of Southern California but lacked finances to complete his courses. Though he had done well on his lease on Soledad Mountain, he held out hope to find another outcrop to work.

On Sunday morning September 17, 1933, while scouting high up on the northwest side of the mountain he encountered Bruce Minard, another leaser who also was looking for a better prospect to work. Later that day, Holmes broke a horn shaped piece from a large loose boulder. The fresh fracture surface showed free gold. (Later, when assayed, the sample yielded a phenomenal 45 ounces of gold and 377 ounces of silver per ton.) The new partners immediately set out to find the source of the rich gold sample. After a few days they found what

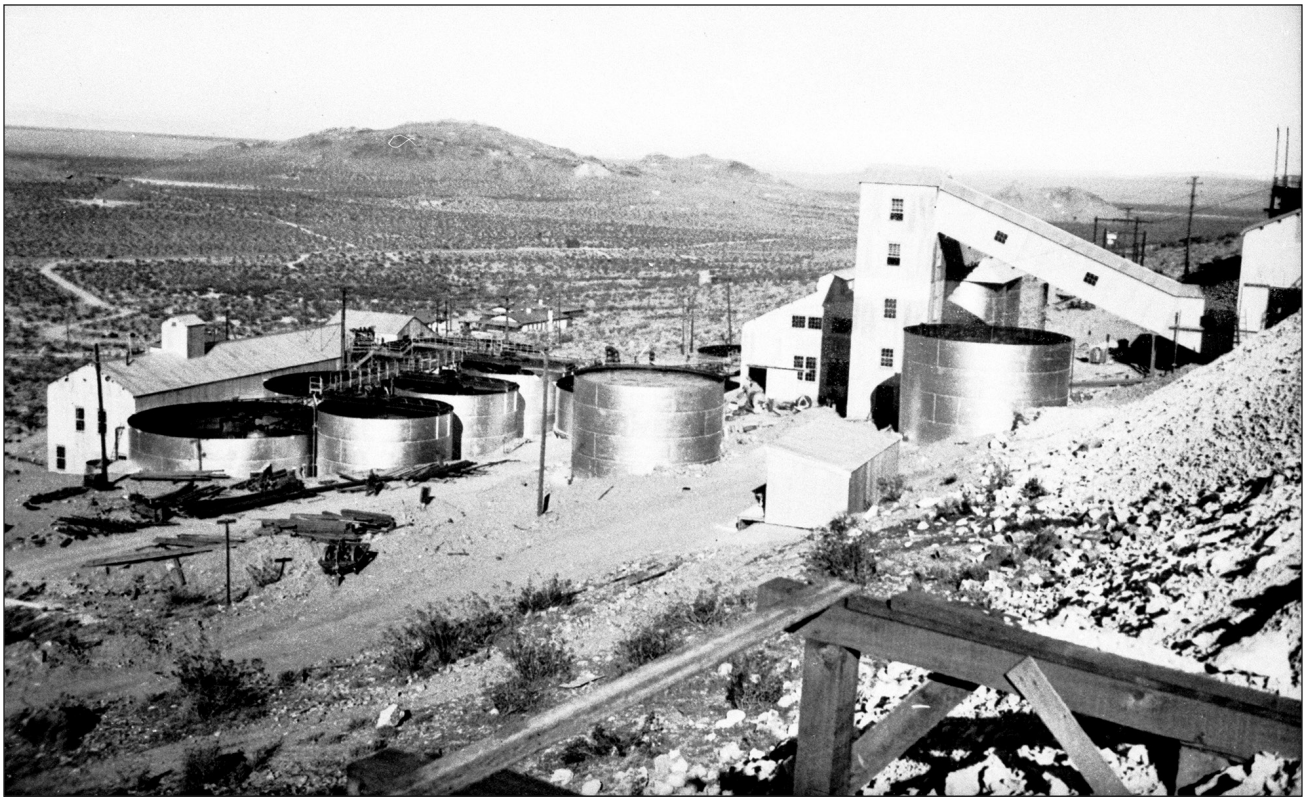

"Golden Queen Mining Co. New 300-ton mill and cyanide plant. Photo by W. W. Bradley." California Geological Survey photo, Tucker, 1935, p. 477.

they believed was the source, and after checking, they determined the ground was unclaimed. The claim that they recorded included Holmes and Minard's names as well as Minard's friend W. E. Dew and George's father Marvin.

They named their claim the Silver Queen. To prove this was more than an isolated find, trenching and digging prospect pits was required. According to one account, Minard and Dew were "not impressed with initial results and sold their interests to Cy Townsend, an ex-Justice of the Peace, for $1,500." But Holmes and a small crew persisted and the first 30 sacks of ore were dug out with a pick and shovel, and carried down the mountain on their backs. They also began sinking two incline shafts. Over the next year, as work progressed, about 4,000 tons of ore was shipped which yielded $20 (about .57 ounces) per ton, or about $80,000 with gold at $35 per ounce.

Months later, in January 1935, Holmes and his father sold the property to a syndicate headed by the Gold Fields American Development Company for $3,170,000, plus they retained a royalty interest.

After purchasing the mine, which the Gold Fields Company renamed as the Golden Queen, they conducted extensive exploration, and by October 1935 erected a mill with a 300-ton per day capacity. The Golden Queen Mine eventually expanded to include the Karma, Queen Esther, Echo, and Gray Eagle properties. Between 1936 and 1942 about 500,000 tons were processed yielding about 171,000 ounces of gold. This mine was shut down by the government in 1942.

As was the case in the 1890s following the original discovery by George Bowers, soon prospectors were again scouring the hills in the Mojave Mining District.

Middle Butte

At Middle Butte, on the west side of the district, several discoveries were made. The most significant was the Cactus Mine in the fall of 1934. Soon after this discovery the property was purchased by Clifford Burton, who leased and later sold it to Cactus Mines Company. From 1935 until 1942 more than 230,000 tons was produced which yielded .35 ounces of gold and 10 ounces of silver per ton.

Standard Hill

Mining from 1928 until 1940 on Standard Hill was mostly done by lessees who shipped ore to the Tropico mill. In 1940 Standard Hill Mines purchased the property and mined it until 1942. Total historic production was estimated at about 150,000 ounces of gold and 500,000 ounces of silver. Up to 85 percent of this total is credited to the Exposed Treasure vein.

1980s and Beyond

Middle Butte

In 1979 the Cactus mine was acquired by CoCa Mines of Denver Colorado. Commercial production started August 1986. Active mining ceased in 1992. Heap leaching of stockpiled ore continued until 1996. Total production during this period was about 400,000 ounces of gold and 3,000,000 ounces of silver. Subsequent exploratory drilling discovered an additional gold resource beneath the Shumake Pit. The new resource may contain as much as 600,000 ounces of gold.

Standard Hill

In 1983 Billiton Minerals USA, a subsidiary of Shell Mining, began an exploration sampling and drilling program on Standard Hill. Construction began at the mine March 1987, and mining in May. The first pour of precious metal occurred July 21, 1987. The average grade of the ore was .08 ounces per ton. Production continued through 1994.

Soledad Mountain

In the 1980s Golden Queen Mining Company began exploring the potential of reactivating the mine on Soledad Mountain. The proposal was approved by Kern County and the Bureau of Mines in 1997. A modified Environmental Impact Report was approved in 2010. At that time, it was estimated the mine would be active for 12 years, that 51.2 million tons would be heap leached, and up to 225 million tons of overburden mined. It was projected that gold and silver production would be 1,067,000 oz of gold and 12,039,000 oz of silver over a period of 15 years. The first pour of gold occurred in March 2016. As of January 2020, the mine was still going strong.

References

A note on references: I consulted numerous newspaper and mining periodical articles for the preparation of this paper. The list is too long to document here. However, I can provide them on request.

Burnett, J. L. and J. Brady, 1990, Cactus Gold Mine, Kern County, California. California Division of Mines and Geology: California Geology April p. 85 – 88.

Burton, A. E. G, D. B. Settle and G. A. Settle, 1999, Gold fever and forty years of K. A. H. S. digging for Antelope Valley history. Kern Antelope Historical Society, Rosamond, California, 89 p.

Crowder, F., 1937, Mojave – perennial frontier. Westways Magazine. June. p. 22-25.

Julihn, C. E. and F. W. Horton, 1937, Mineral Industries Survey of the United States, California, Kern County, Mojave District, the Golden Queen and other mines of the Mojave District, California. U. S. Bureau of Mines Information Circular 6931, p. 42.

Kegley, Howard, 1936, Treasure vaults of the Mojave Desert. The Union Oil Bulletin. July-August. p. 14-17

Kern County Planning Department, 2010, Draft SEIR - Volume 1, Chapters 1-10. https://www.kerncounty.com/planning/pdfs/eirs/SoledadMtn/SoledadMtn_vol1_ch1-10.pdf

Koehler, Brett, 1999, Mineral land Classification of Southeastern Kern County, California. California Geological Survey, OFR 99-15

Miller R. D., and P. J. Miller, 1992, Mines of the Mojave, La Siesta Press p. 13 – 17.

Panhorst, T., 1989, Overview of the Standard Hill gold mine, Mojave California, in The California Desert mineral Symposium Compendium U. S. Bureau of Land Management, California State Office, Sacramento California. P. 195 – 200.

Settle, G. A., 1964, Tropico, Red Hill with a glamorous history of gold. 16 p.

Settle, G. A., 1983, The antelopes left and the Settle-ers came. Kern Antelope Historical Society, Rosamond, California, p. 70 – 99.

Settle, G. A. and J. Burgess, 1965, Bears – borax and gold. Kern Antelope Historical Society, Rosamond, California, 52 p.

Settle, G. A. and J. Burgess, 1967, Along the rails from Lancaster to Mojave. Kern Antelope Historical Society, Rosamond, California, 84 p.

Settle, G. A. and Dorene Settle, editors, 1991, Antelope Valley Pioneers. Kern Antelope Historical Society, Rosamond, California, 98 p.

Settle, G. A. and C. Hansen, 1996, Mojave, a rich history of rails, mines & flight. Kern Antelope Historical Society, Rosamond, California, 124 p.

Troxel, B. W. and P. K. Morton, 1962, Mines and mineral resources of Kern County, California. California Division of Mines and Geology, County Report 1, 170 p.

Tucker, W. B., 1935, Mining activity at Soledad Mountain and Middle Buttes – Mojave Mining District, Kern County. California Division of Mines Report v. 31, p 465-485.

Tucker, W. B., R.J. Sampson, and G.B. Oakeshott, 1949, Mineral Resources Kern County, Golden Queen Mining Company. California Journal of Mines and Geology, v. 45, p. 220-223.

Wilkerson, 2020, this volume.

WZI Inc., 1996 Soledad Mountain Project Conditional Use Permit Application. Environmental Information Surface Mining Reclamation Plan and Plan of Operations. Vol IV, 556 p.

Investigating the use of a positive Europium anomaly and marine Y/Ho ratios as potential fingerprints for Gulf of California hydrochemistry with implications for the origin of southern Bouse Formation carbonate (Arizona and California, USA)

Jordon Bright
School of Earth and Sustainability, Northern Arizona University, Flagstaff, AZ, 86011

ABSTRACT—I have assembled a non-exhaustive compilation of rare earth element (REE) and Yttrium (Y) data from continental, estuarine, marine, and geothermal waters, from lacustrine and marine carbonates, from recent sediments from the Gulf of California, and from 17 carbonate samples (modern to late Miocene) from along the lower Colorado River corridor. The compilation is a work in progress to evaluate the usefulness of REE and Y data in addressing research questions related to the evolution of the upper Gulf of California, the Salton Trough, and the lower Colorado River corridor.

A subset of geothermal waters associated with sea-floor rifting environments and geothermal springs in the Salton Trough and Gulf of California yield strongly positive chondrite-normalized Eu anomalies whereas most continental, estuarine, and marine waters yield REE profiles with negative or no Eu anomaly. Geothermal waters in the Salton Trough yield Y/Ho values mostly > 60 whereas a Y/Ho value of about 40 separates marine water (> 40) from continental water (< 40), although some continental springs yield Y/Ho values > 40. Estuarine Y/Ho values range from ~25 to > 40 and show a positive correlation with salinity.

Modern biologic carbonate and carbonate-bearing sediments from the Gulf of California predictably yield a positive Eu anomaly, reflecting geothermally influenced waters in the region. Marine carbonates yield dilute REE profiles lacking positive Eu anomalies and yield Y/Ho values > 40, reflecting their marine water source. Nearshore, carbonate-rich marine sediments yield shale-like REE profiles lacking a positive Eu anomaly and Y/Ho values ranging from about 35 to 60. Carbonates along the lower Colorado River corridor yield REE profiles similar to a shale standard, indicating the possible influence of silicate REEs. None of the lower Colorado River carbonates, including the late Miocene and early Pliocene southern Bouse Formation, yields a positive Eu anomaly or a Y/Ho value > 40. The lack of a positive Europium anomaly and Y/Ho values < 40 in southern Bouse Formation carbonates support deposition in a continental rather than a marine environment. REEs and Y may be useful diagnostic indicators for distinguishing marine and continental depositional environments in the Salton Trough and lower Colorado River corridor.

Introduction

The Gulf of California (GoC) (Fig. 1) is a marine-flooded transtensional rift system delineating the boundary between the North American and Pacific plates and is a southern extension of the San Andreas Fault system (González-Fernández et al., 2005). Latest Miocene marine flooding of the uppermost GoC basins (Bennett et al., 2015; Umhoefer et al., 2018) slightly preceded the evulsion of the early Colorado River out of the western Grand Canyon (Spencer et al., 2001; Faulds et al., 2016) and the subsequent development of the lower Colorado River corridor (Pearthree and House, 2014; Crow et al., 2019). The southern Bouse Formation (SBF) (Metzger, 1968), exposed in Blythe basin (Fig. 1), has been the subject of a decades-long debate regarding the extent of marine flooding during the development of the upper GoC, the integration of the lower Colorado River corridor, and in particular, the evolution of Blythe basin (Fig. 1).

The origin of the SBF is controversial, with current interpretations favoring either a lacustrine (e.g., Bright et al., 2018a,b) or a marine (Dorsey et al., 2018) depositional environment. The argument for a lacustrine origin is

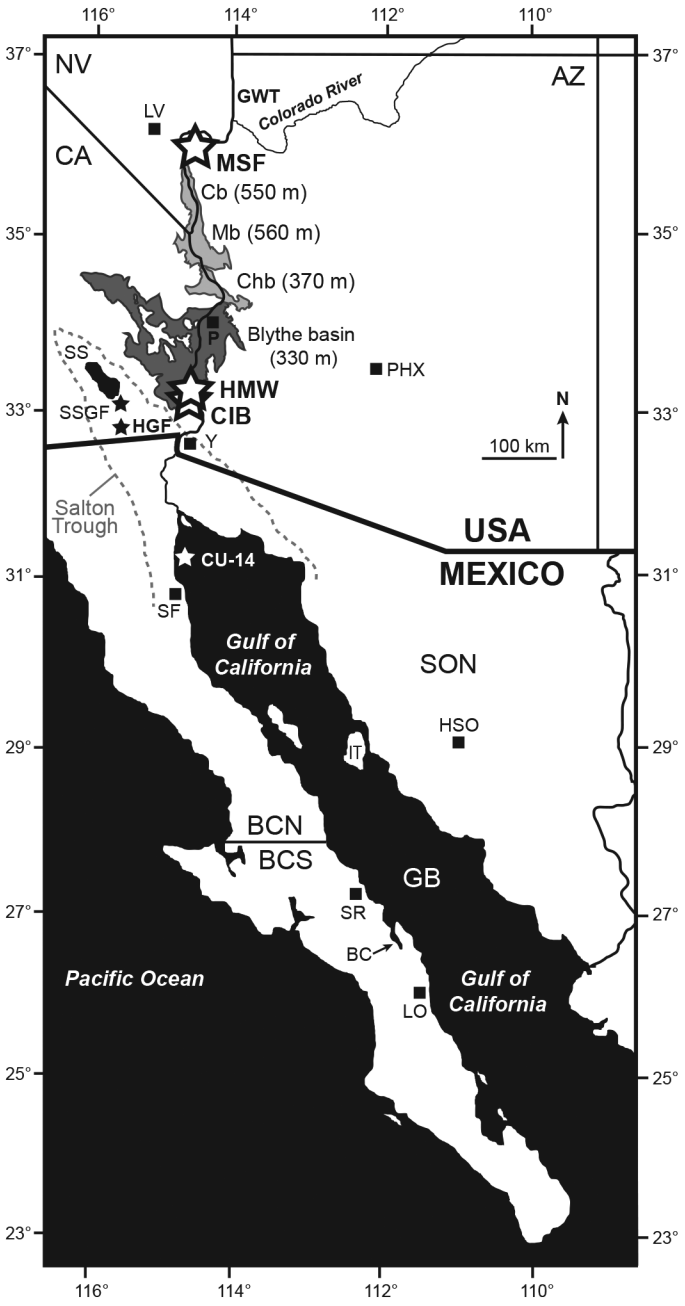

Figure 1. Map showing the location of the Blythe basin (southern Bouse Formation) in relation to the Colorado River, Cottonwood (Cb), Mohave, Mb) and Chemehuevi (Cb) basins (northern Bouse Formation), Grand Wash Trough (GWT), Salton Sea (SS), the Salton Trough, Guaymas Basin (GB), and Isla Tibúron (IT). White stars with black outline - JB19 samples from near Lake Mead (MSF), Hart Mine Wash (HMW), Cibola Wash (CIB). Small solid black stars – location of the Salton Sea and Heber Geothermal Fields (SSGF and HGF, respectively). Solid white star – location of core CU-14. Black squares – cities of Las Vegas (LV), Parker (P), Phoenix (PHX), Yuma (Y), Hermosillo (HSO), San Felipe (SF), Santa Rosalia (SR), and Loreto (LO). Location of Bahía Concepcíon (BC) is noted. The US states of Arizona (AZ), Nevada (NV), California (CA), and the Mexican states of Sonora (SON), Baja California Norte (BCN), and Baja California Sur (BCS) are labeled.

convincingly reinforced by exclusively continental strontium isotope ratios ($^{87}Sr/^{86}Sr$) in a variety of SBF materials (Spencer and Patchett, 1997; Roskowski et al., 2010; Crossey et al., 2015; Bright et al., 2018a). Proponents of a marine origin advocate that upstream water sources with high strontium concentrations and high $^{87}Sr/^{86}Sr$ ratios (e.g., Hualapai Limestone near the Grand Wash Trough; Fig. 1) potentially masked a marine $^{87}Sr/^{86}Sr$ signal in the SBF (Crossey et al., 2015). To date, SBF carbonate has not been analyzed for geochemical indicators that are specifically leveraged towards detecting a marine influence. This paper highlights the potential utility of using rare earth and trace element analysis to address ongoing questions about the evolution of the Salton Trough, the early GoC, and the lower Colorado River corridor (i.e., Blythe basin).

Background

Current models suggest that initial GoC extension began ~12 Ma and a second phase of extension that resulted in large-scale basin opening and marine flooding was initiated by ~8 Ma (Sutherland et al., 2012; Umhoefer et al., 2018). The uppermost basins of the GoC (north of Isla Tiburón; Fig. 1) were likely flooded by seawater ca. 6.5 Ma to 6.3 Ma (Bennett et al., 2015; Umhoefer et al., 2018). Continental rupture and the onset of seafloor spreading occurred first in Guaymas basin (Fig. 1) at roughly 6 Ma (Lizarralde et al., 2007), but seafloor spreading probably did not start until after 3 Ma in the southern GoC basins (Lonsdale, 1989) and until after 2 Ma in the uppermost basins (González-Fernández et al., 2005; Martín-Barajas et al., 2013). Several contested studies, primarily paleontological in nature, suggest that early GoC seawater spilled into Blythe basin (Fig. 1) sometime before 6 Ma, forming a tidal marine embayment that persisted until about 5.3 Ma (Smith, 1970; McDougall and Miranda-Martinez, 2014; Miranda-Martinez et al., 2017; O'Connell et al., 2017; Dorsey et al., 2018). This potential marine embayment is speculated to have deposited the SBF prior to the entry of the ancestral Colorado River into Blythe basin (McDougall and Miranda-Martinez, 2014; Dorsey et al., 2018). A depauperate marine flora and fauna (Smith, 1970; Bright et al., 2018b) and sedimentological features interpreted as tidal in origin (O'Connell et al., 2017) support the hypothesis that the SBF is a marine deposit.

Within ~1 myr of the latest stages of upper GoC flooding, the ancestral Colorado River exited the western Grand Canyon near Grand Wash Trough (Fig. 1) sometime between 6 Ma and 4.5 Ma, based on coarse age constraints provided by basalts that underlie and overlie exotic Colorado River gravel there (Spencer et al., 2001; Faulds et al., 2016). The early river then integrated a path towards the

early GoC through a process of filling-and-spilling to form mildly brackish lakes along a series of (initially) topographically closed basins between Grand Wash Trough and Chemehuevi basin (Fig. 1) (Pearthree and House, 2014). The early river reached Blythe basin shortly after 5 Ma, based on a < 5.24 Ma age constraint for first arriving Colorado River water in Cottonwood basin (Crow et al., 2019) (Fig. 1) and the presence of the 4.9 Ma Lawlor Tuff (Sarna-Wojcicki et al., 2011) that occurs at multiple locations in Blythe basin in topographically high exposures (~300 masl) of SBF carbonate (Sarna-Wojcicki et al., 2011; Miller et al., 2014). The Lawlor Tuff occurs in either SBF basal carbonate or in a slightly younger deposit, that are either overlain by or are coeval with fine-grained Colorado River-derived siliciclastic sediments (the Interbedded Unit of Metzger, 1968), respectively (Dorsey et al., 2018; Gootee et al., 2019). Contested interpretations suggest that SBF carbonate represents a mildly brackish, clear-water lacustrine environment derived from ponded ancestral Colorado River water (Spencer and Patchett, 1997; Bright et al., 2018b). Numerous sedimentological, paleontological, and geochemical studies have revealed overwhelming similarities between the SBF and the uncontested lacustrine northern Bouse Formation that is exposed in Chemehuevi basin (Fig. 1) and basins farther north (Spencer and Patchett, 1997; Poulson and John, 2003; Roskowski et al., 2010; Spencer et al., 2013; Crossey et al., 2015; Reynolds et al., 2016; Bright et al., 2016, 2018a, 2018b; Gootee et al., 2019).

Debate over the origin of the SBF features a *Marine Only* model (McDougall and Miranda-Martínez, 2014; Miranda-Martínez et al., 2017; Dorsey et al., 2018), a *Lacustrine Only* model (Spencer and Patchett, 1997; Roskowski et al., 2010; Bright et al., 2016, 2018a,b), and an intriguing lacustrine-dominated but perhaps *Marine-Influenced* hybrid model (Crossey et al., 2015; Bright et al., 2018a,b). Earlier estuarine models (e.g., Smith, 1970) have largely fallen out of favor for several reasons. The most recent marine-oriented interpretations suggest that SBF basal carbonate was deposited over a span of ~ 700,000 years *prior to* the arrival of the ancestral Colorado River (McDougall and Miranda Martínez, 2014; Miranda-Martínez et al., 2017; Dorsey et al., 2018), which eliminates the primary source of river discharge for a Blythe basin estuary (Bright et al., 2018a). Numerous other studies have consistently failed to find convincing geochemical evidence for a north-south mixing gradient that would lend support to an estuarine model (Spencer and Patchett, 1997; Roskowski et al., 2010; Crossey et al., 2015; Bright et al., 2018a). Furthermore, a survey of modern North American estuary sediments reveals consistently low calcium carbonate contents ($CaCO_3$ < 20% and routinely <10%, typically as shelly debris), with the exception of some bays and estuaries around Florida (Folger, 1972). If Blythe basin was an estuarine environment during the latest Miocene and earliest Pliocene, then the high carbonate content ($CaCO_3$ = 66 ± 21%, n = 23; Bright, unpublished data) and meters-thick outcrops of marl and limestone that typify the SBF's basal carbonate unit (Metzger, 1968; Homan, 2014) is highly unusual. Later discussion of the SBF will include a comparison with a modern carbonate-producing Florida estuary (Florida Bay).

Exclusively continental $^{87}Sr/^{86}Sr$ ratios in SBF carbonate lends considerable interpretational leverage to the Lacustrine Only model for the SBF (Spencer and Patchett, 1997; Roskowski et al., 2010; Crossey et al., 2015; Bright et al., 2018a). The $^{87}Sr/^{86}Sr$ ratios may be biased towards continental water sources with high strontium concentrations, however (Crossey et al., 2015). Analyzing SBF carbonate for a geochemical indicator specifically leveraged towards detecting the influence of the early GoC is an important priority. The combination of rare earth element chemistry coupled with the marine environment of the GoC may provide several such indicators.

Rare earth elements comprise the lanthanide series of the periodic table (sequentially La, Ce, Pr, Nd, Pm, Sm, Eu, Gd, Tb, Dy, Ho, Er, Tm, Yb, Lu), having atomic numbers ranging between 57 and 71. Occasionally, the metal Yttrium (Y) has been included in rare earth studies because although it is not a lanthanide element, it behaves similarly to Holmium (Ho) and its valence and ionic radius places it between Dysprosium (Dy) and Ho in a REE profile (Bau et al., 1995). Rare earth elements are rare in nature and typically do not form their own minerals (Möller, 2000). However, they are enriched in calcium-based minerals or they can substitute for other major elements in non-calcium-based minerals (Möller, 2000). Most REEs behave chemically similarly, but Europium (Eu) and the ratio of Y/Ho have characteristics that are of interest to this paper.

Europium has a large ionic radius that limits its incorporation into minerals (Möller, 2000), but it is common in feldspars, such as plagioclase, and it is more soluble at high temperatures (>250° C) compared to other REEs (Möller, 2000). Europium (particularly Eu^{2+}) is excluded from mineral phases during weak alteration of seafloor basalts, leading to strong aqueous Eu anomalies in the residual solutions that are particularly useful for fingerprinting geothermal fluids (Fig. 2A-D) (Michard, 1989; Klinkhammer et al., 1994; Bau and Dulski, 1999; Möller, 2000; Wood and Shannon, 2003). Carbonates that form in geothermal environments may possess a strongly positive Eu anomaly as well (Fig. 2E) (Bau et al., 2010; Zeng et al., 2019). In contrast, marine, estuarine, and non-geothermal continental water sources typically lack positive Eu anomalies (Fig. 2F-J). Europium's peculiar availability and solubility characteristics leads to predictably low Eu concentrations ([Eu]) in non-geothermal surface and groundwater and high concentrations in geothermal fluids; concentrations that are separated by orders of magnitude (Möller, 2000). A compilation of 201 surface and non-geothermal groundwater analyses yield

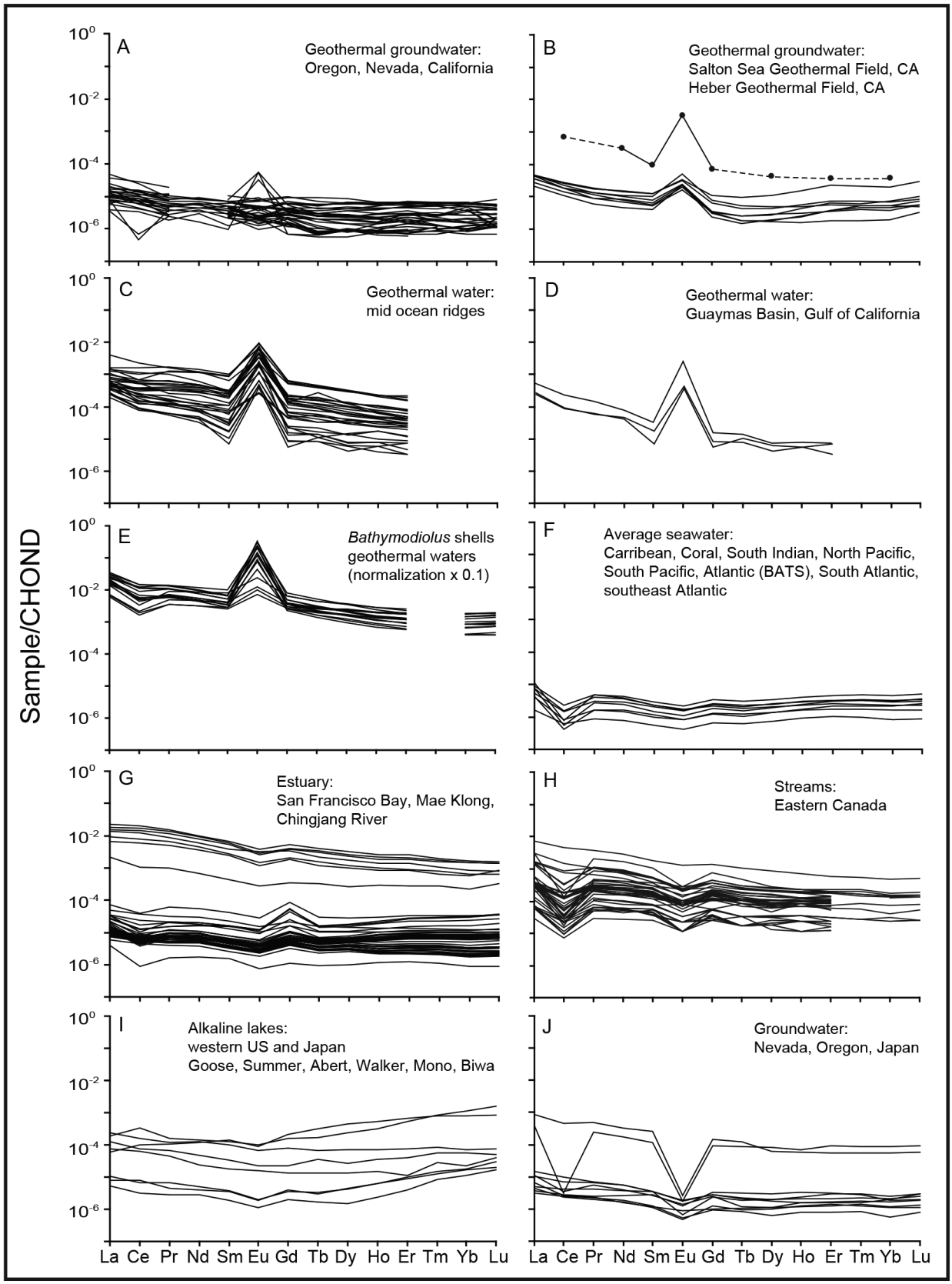

Figure 2. Compilation of chondrite-normalized REE profiles from a variety of natural waters and geothermal mussel shells. See text for discussion. Sources used are highlighted by an (*) in the References. Additional details are available upon request. Compilation features filtered water samples whenever possible. The data have not been screened.

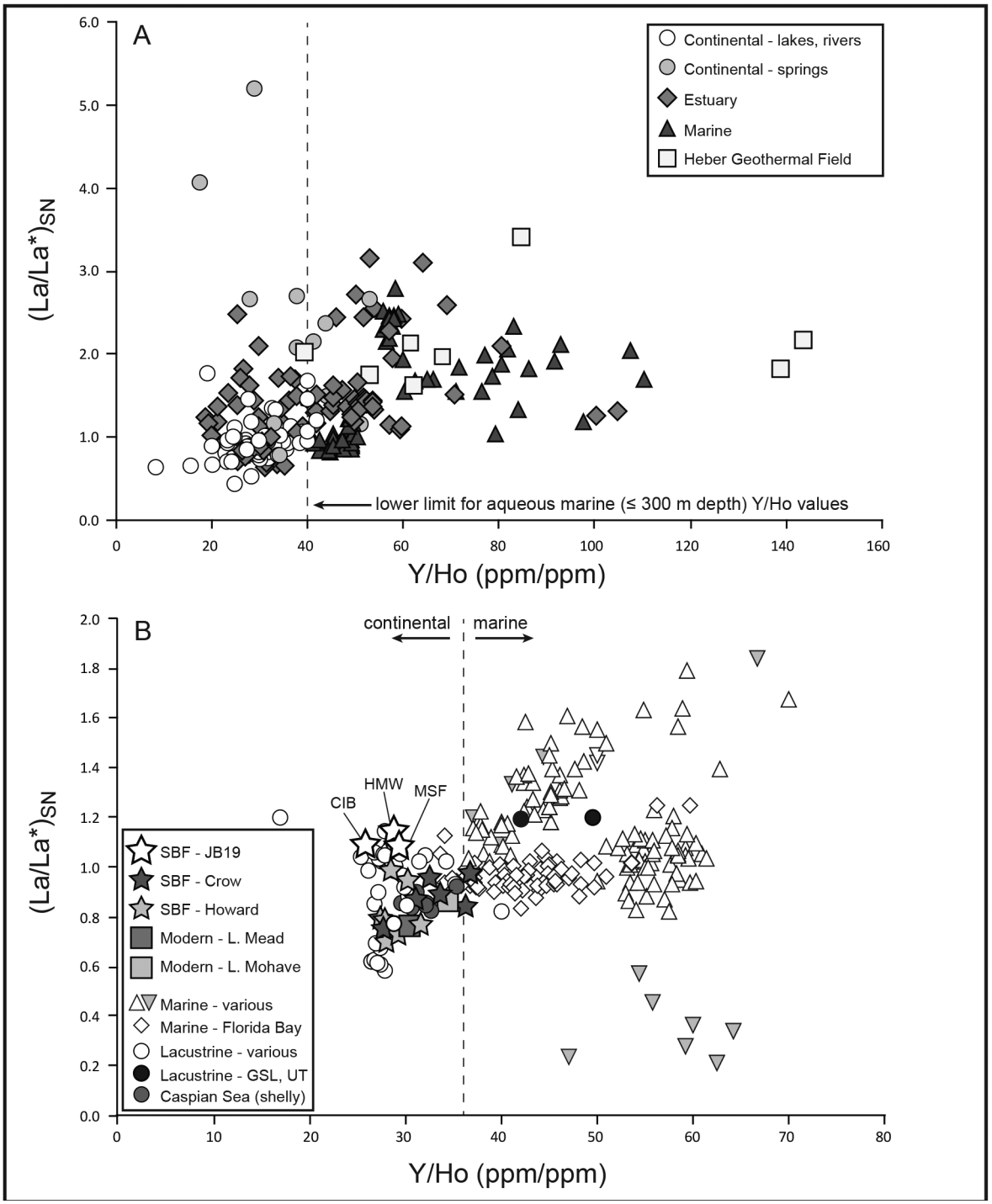

Figure 3. Non-exhaustive comparison of Y/Ho and $(La/La^*)_{SN}$ values from a variety of natural waters and depositional environments. See text for discussion. Sources used are highlighted by an (*) in the References. Additional details are available upon request. A. Open marine water (≤ 300 m depth), estuaries, continental rivers and lakes, continental springs, and fluids from the Heber Geothermal Field (see Fig. 1 for location). No aqueous marine Y/Ho values in this compilation fall below 40 (vertical dashed line). Compilation features filtered water when possible. B. Marine, nearshore marine (Florida Bay), and lacustrine sediments compared against sediments from along the lower Colorado River corridor (SBF, Lake Mead, Lake Mohave). Vertical dashed line approximates the boundary between marine and continental samples in this compilation (Y/Ho ≈ 37). Only data from OCD1 from Verdel et al. (2018) are shown. Dolomitized samples from Nothdurft et al. (2004) are excluded. Data are derived from partial digestions with the exception of the marine data from Mastandrea et al. (2010) and Madhavaraju et al. (2017) (inverted grey triangles), Crow's Lakes Mead and Mohave samples, and the Howard and Crow SBF samples, which used total digestions. The JB19 samples are partial digestions.

average [Eu] of 4.6 ± 9.0 parts per trillion (ppt) (Goldstein and Jacobson, 1988; Haraguchi et al., 1998; Johannesson et al., 2000; Möller, 2002; Takahashi et al., 2002; Zhu et al., 2005; Han and Liu, 2007; Leyborne and Johannesson, 2008; Jiang and Ji, 2012; Soyol-Erdene and Huh, 2013). In contrast, a compilation of 36 water samples from sea-floor spreading geothermal environments yield average [Eu] of 232 ± 234 ppt (Klinkhammer et al., 1994; Bau et al., 2010). Three analyses of geothermal fluids specifically from the Guaymas Basin, located in the central GoC (Fig. 1), yield [Eu] of 33, 40, and 228 ppt (Klinkhammer, 1994). Thus, Eu in GoC waters may be a particularly valuable seawater-leveraged indicator that could compliment continental-leveraged Sr-based water source interpretations in the upper GoC region, particularly with respect to the ongoing SBF debate (e.g., Spencer et al., 2013).

In a similar fashion, Y/Ho values effectively discriminate between continental and marine environments (Figs. 3A,B). Low Y/Ho ratios (<40) in continental waters (e.g., Haraguchi et al., 1998; Zhu et al., 2005; Han and Liu, 2007; Leybourne and Johannesson, 2008) reflect the low Y/Ho value of continental rocks (Webb and Kamber, 2006). Holmium is scavenged from seawater twice as fast as Y (Nozaki et al., 1997), leading to seawater Y/Ho values that are characteristically higher (> 40) than continental water values (Fig. 3A). There is debate over whether most Ho scavenging occurs in estuaries (Webb and Kamber, 2006) or in marine surface waters (Nozaki et al., 1997), but regardless, aqueous estuarine Y/Ho values span continental to marine values (Fig. 3A) and are often positively correlated with salinity (Fig. 4).

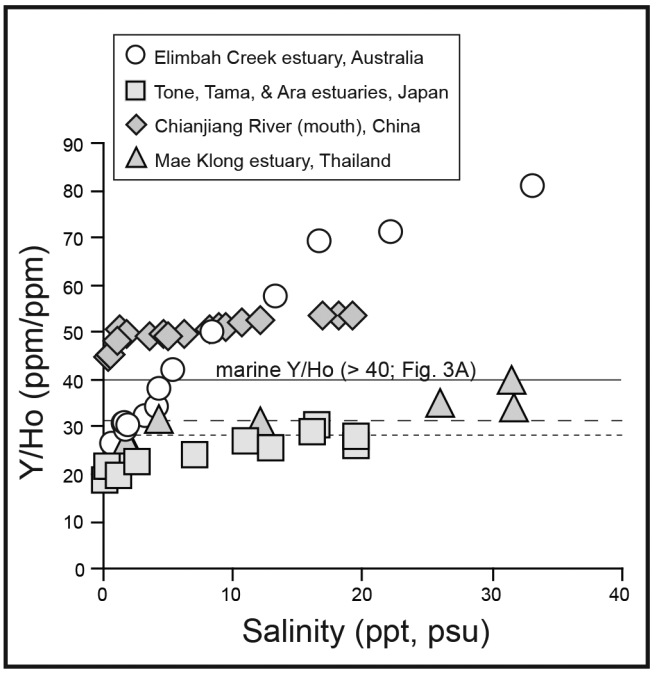

Figure 4. Plot showing the relationship between the salinity of several estuaries and their Y/Ho values. Data from Nozaki et al. (2000a), Wang and Liu (2000), Lawrence and Kamber (2006), and Censi et al. (2007). Not all compiled literature sources provided salinity units. When lacking, salinity is assumed to be in parts per thousand (ppt) or practical salinity units (psu) which, for the purposes of this paper, can be considered equivalent. Coarse dashed line - average Y/Ho value for the Howard and Crow total digestions. Fine dashed line – average Y/Ho value for JB19-HMW and –CIB partial digestions. If there was a marine influence on the SBF, then the Y/Ho values suggest the salinity was well below standard seawater.

The diagnostic differences in Y/Ho values are preserved in marine and continental sediments. Carbonates formed on open marine environments yield high Y/Ho ratios (> 40), reflecting their seawater origin (Fig. 3B). Nearshore marine sediments that are influenced by continental runoff (e.g., Florida Bay) may yield Y/Ho values between ~ 38 and 50 (Fig. 3B). In contrast, several studies have used Y/Ho values < 35 to infer continental or freshwater depositional environments (Fig. 3B). Modern ooids from the hypersaline Great Salt Lake, Utah, yield marine-like Y/Ho values, however (Fig. 3B). Thus, Y/Ho values may provide a second powerful geochemical tool for discriminating between continental and marine carbonates in the upper GoC region.

Collectively, positive Eu anomalies, Y/Ho values (as well as other REE ratios) (Fig. 3B), and REE profiles (Fig. 5A) have proven to be useful tools for discriminating between geothermal, marine, and lacustrine deposits in the geologic record (e.g., Webb and Kamber, 2000; Northdurft et al., 2004; Bolhar and Van Kranendonk, 2007; Li et al., 2019; Zeng et al., 2019). Within the GoC region, REEs and Y may be useful for identifying the onset of geothermal fluid development (e.g., a positive Eu anomaly) in relation to the timing of continental rupture (i.e., pre- or post-rupture). REEs and Y may be especially useful for distinguishing between marine (Y/Ho > 38) and continental (Y/Ho < 35) deposits in the Salton Trough (Ross et al., this volume) and the lower Colorado River corridor (Dorsey et al., 2018; Bright et al., 2018a,b).

This paper reports preliminary REE and Y data from two carbonate-rich SBF sediment samples from Cibola and Hart Mine Washes of southwestern Arizona (Fig. 1) and from one extra-local carbonate-rich sediment sample from near Las Vegas, Nevada (Fig. 1). The results will be used to assess whether SBF carbonate is more likely to have precipitated in an exclusively marine embayment that was simply an extension of the early GoC (Marine Only model) or in a Colorado-River-fed continental lake (Lacustrine Only or Marine-Influenced models). Additional unpublished REE data from the SBF and previously published REE data from a variety of water types and uncontested open marine, nearshore marine, lacustrine, and upper GoC sediments provide critical context.

Methods

The author collected carbonate-rich sediment from just above the contact of Miocene fan gravels and the overlying SBF carbonate (Marl 1 of Homan (2014)) exposed at the mouth of the informally named Cibola Wash (JB19-CIB)

(Fig. 1). A second sample of SBF was collected from a thick section of Marl 2 (Homan, 2014) exposed in Hart Mine Wash (JB19-HMW) (Fig. 1). Both samples are located at the southern end of Blythe basin (Fig.1), presumably in a location most proximal to a possible marine influence from the ancestral GoC. A third sample of carbonate-rich sediment was collected from an outcrop of Bouse-like sediments near Las Vegas, NV, (JB19-MSF) (Fig. 1). Sample JB19-MSF provides an uncontested continental sample for comparison against the potentially marine or lacustrine JB19-CIB and JB19-HMW samples.

Each sample was gently disaggregated at the Amino Acid Geochronology Laboratory at Northern Arizona University using a porcelain mortar and pestle before being passed over a 120 um sieve. The <120 um fractions were placed in plastic beakers and turned into slurries using 16.7 megohm cm^{-1} distilled deionized water. The slurries were sequentially centrifuged at different speeds and durations to target silt sized particles. The most rapidly settling material and the milky supernatants, presumed to be mostly clays, were separated and discarded. The targeted sediments were dried at 50° C overnight and then gently broken into a fine powder using a porcelain mortar and pestle before being stored in new 50 ml plastic centrifuge tubes.

A rough quantitative estimate of percent $CaCO_3$ in each sample was determined using a loss on ignition (LOI) method modified from Dean (1974). Aliquots of each powder were dried for 1 hr at 80° C, weighed into clean, oven-roasted ceramic crucibles, and then baked for 2 hr at 950° C. I bypassed the intermediate 550° C heating step because the powders do not contain measurable organic matter. I assumed that the difference in mass between the dry and baked powders was due primarily to the conversion of carbonate to carbon dioxide. Two samples (JB19-CIB and –MSF) were analyzed using x-ray diffraction (XRD) to check for the presence of silicates such as quartz and feldspar.

Approximately 55 gm of each powder was sent to ACZ Laboratories in Colorado Springs, CO, to be analyzed for their REE concentrations as well as calcium, magnesium, silicon, manganese, and iron concentrations. The analytical procedure at ACL Laboratories follows EPA 3050B protocol (U.S. EPA 1996), which uses concentrated nitric acid, concentrated hydrochloric acid, and 30% hydrogen peroxide to digest the samples. The EPA 3050B method is a partial rather than total digestion because it does not use hydrofluoric acid (HF) to digest silicates. All REE concentrations are normalized using the chondrite values of Taylor and McLennan (1988) or the North American Shale Composite (NASC) values of McLennan (1989).

Lanthanum (La) anomalies (Fig. 3B) were calculated geometrically by the equation:

$$(La/La^*)_{SN} = La_{SN}/(Pr_{SN} \times (Pr_{SN}/Nd_{SN})^2)$$

following Lawrence et al. (2006), where the subscript SN refers to shale-normalized values, in this case the NASC values of McClennan (1989). A $(La/La^*)_{SN}$ value of 1 represents no anomalous La behavior.

Results

The LOI analysis reveals that $CaCO_3$ comprises 83%, 84%, and 89% of the JB19-CIB, -HMW, and –MSF powders, respectively. The XRD analyses of JB19-CIB and –MSF show clean calcite peaks (Fig. 6). Quartz and feldspar peaks are present, but they are small (Fig. 6). The centrifuge process was modestly successful at separating carbonate from silicates, but it was not completely successful. Silicon concentrations ([Si]) in JB19-HMW, –MSF, and -CIB are 58, 43, and 32 mmol/kg, respectively (Fig. 7). The Y/Ho values for JB19-HMW, –MSF, and -CIB are 29, 29, and 26, respectively (Fig. 3B). The chondrite-normalized REE profiles (minus Y) from samples JB19-CIB, -HMW, and –MSF show a strong enrichment in the light REEs (La to Nd), a clear depletion of Eu, and a noticeable gradual depletion of middle and heavy REEs (Gd to Yb) (Fig. 5B).

Discussion

Southern Bouse Formation REE+ Y composition: preliminary interpretations

The three JB19 chondrite-normalized REE profiles are broadly similar to, but more dilute than, the NASC standard, although heavy REEs are more depleted (Fig. 5B) as might be expected from partial dissolution of the samples (Condie, 1991). The JB19 REE profiles (Fig. 5B) are also similar to the average acid soluble REE profile from lake sediments in Qaidam Basin, China, (Zhang et al., 2009) and, to a lesser extent, from ooids of the Great Salt Lake, Utah (Fig. 5A). Other Bouse workers (K. Howard and R. Crow) have produced total digestion REE data from additional silicate-rich but carbonate-bearing (Howard) and carbonate-rich (Crow) SBF sediments (Figs. 3B, 5B). The Howard and Crow samples are also similar to the NASC standard, although the Crow profiles are more dilute and are more similar to the JB19 profiles (Fig. 5B).

The similarity of the SBF REE profiles with NASC may suggest contamination by silicate REEs. The use of the centrifuge and partial digestion method reduced [Si] (an indicator of silicate contamination) in the JB19 samples by one and two orders of magnitude compared to the total digestions of Crow and Howard, respectively (Fig. 7), but Si was not completely eliminated. Nothdruft et al. (2004) suggests that as little as 2% contamination by clays is enough to compromise an REE analysis. Frimmel (2009) calculated that a digestion yielding a zirconium concentration ([Zr]) in excess of four ppm (≈ 2% shale) constituted a compromised sample. The JB19 samples were not analyzed for [Zr], but [Zr] was measured in Howard's and Crow's total digestion samples. There is a strong correlation between [Zr] and [Si] in Howard's and Crow's

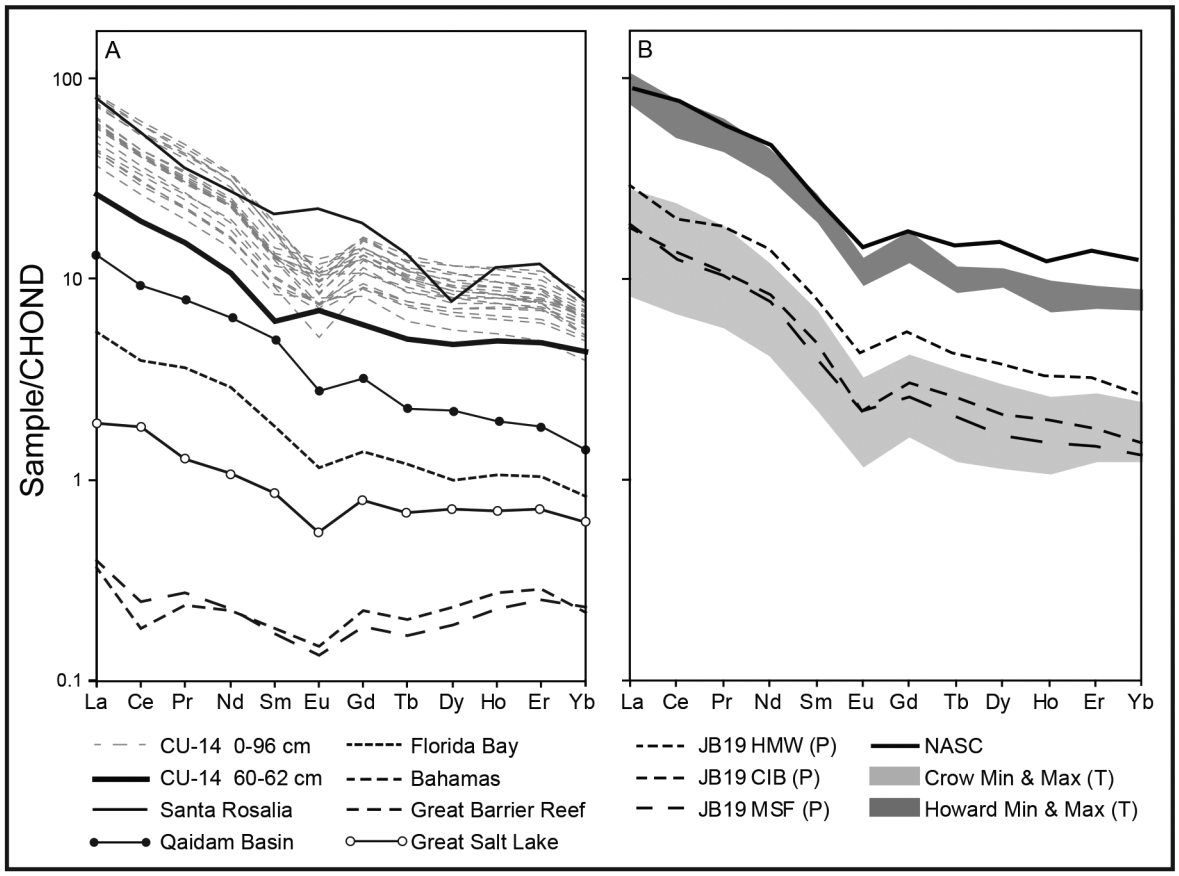

Figure 5. Comparison of chondrite-normalized REE profiles discussed in this paper. A. REE profiles from uncontested marine and near-shore marine environments, from uncontested lacustrine environments, and from the GoC. Data compiled from Shumilin et al. (2002, 2005), Zhang et al. (2009; estimated values), Li et al. (2019), Caccia and Millero (2007), Webb and Kamber (2000). B. SBF REE profiles. Howard's (n = 6) and Crow's (n = 8) data are total (T) digestions. JB19 data are from centrifuged and partially digested (P) samples. Solid black line – North American Shale Composite (NASC; McLennan, 1989).

total digestions (Fig. 7). When the JB19 [Si] are converted to their equivalent [Zr], and assuming that the partial digestion method did not alter the relationship between [Zr] and [Si] that was taken into solution, then all three JB19 samples yield [Zr] that are below Frimmel's (2009) four ppm threshold (Fig. 7). Thus, the JB19 digestions are not compromised by clays using this particular criterion, even though they yield REE and Y results that are broadly similar to the total digestions of Crow's samples (Figs. 3B, 5B) that do exceed this criterion (Fig. 7). The similarities between the JB19 REE profiles and Crow's profiles is surprising given the use of a method designed to avoid incorporating silicate REEs. The centrifuge and partial digestion method yields improved results over the total digestions of Howard and Crow (e.g., orders of magnitude lower [Si]), but additional work is needed to better understand the source of REE in the JB19 samples.

The primary goal of this study was to test whether or not any of the carbonate-rich SBF samples yield REE and Y data that could indicate deposition in a GoC marine environment. They do not (Figs. 3B, 5B). For example, modern seawater typically yields $(La/La^*)_{SN}$ values between 1.3 and 1.5 in combination with Y/Ho values > 40 (Allwood et al., 2010) (Fig. 3A), values that are typically recorded in marine carbonates (Fig. 3B). The low $(La/La^*)_{SN}$ values and Y/Ho values slightly less than 40 from partially digested Florida Bay sediments (Fig. 3B) are interesting in this context. Florida Bay may provide a passingly reasonable modern analog for older estuarine models for the SBF (e.g., Smith, 1970). Florida Bay is a shallow (< 4-m-deep) estuary in which $CaCO_3$ comprises 66-93% of the sediment (Caccia and Millero, 2007) and where variability in precipitation amounts and freshwater runoff from the Everglades leads to seasonal salinities < 20 ppt (well below normal seawater) in different parts of the bay (Nuttle et al., 2000; Kelble et al., 2007). Although the % $CaCO_3$ and REE profile for the Florida Bay sediments are broadly similar to the SBF (Fig. 5), the Florida Bay sediments are clearly distinguishable from the SBF by their lower $(La/La^*)_{SN}$ values and higher Y/Ho values (Fig. 3B). In contrast to the marine examples, the JB19-HMW and -CIB samples from the SBF yield $(La/La^*)_{SN}$ values near 1.1 and Y/Ho values near 29 (Fig. 3B). These values could indicate a strong freshwater influence, especially when considering the low [Zr] (~ 1 ppm) calculated for both samples (Fig. 7) (Frimmel, 2009). These values are

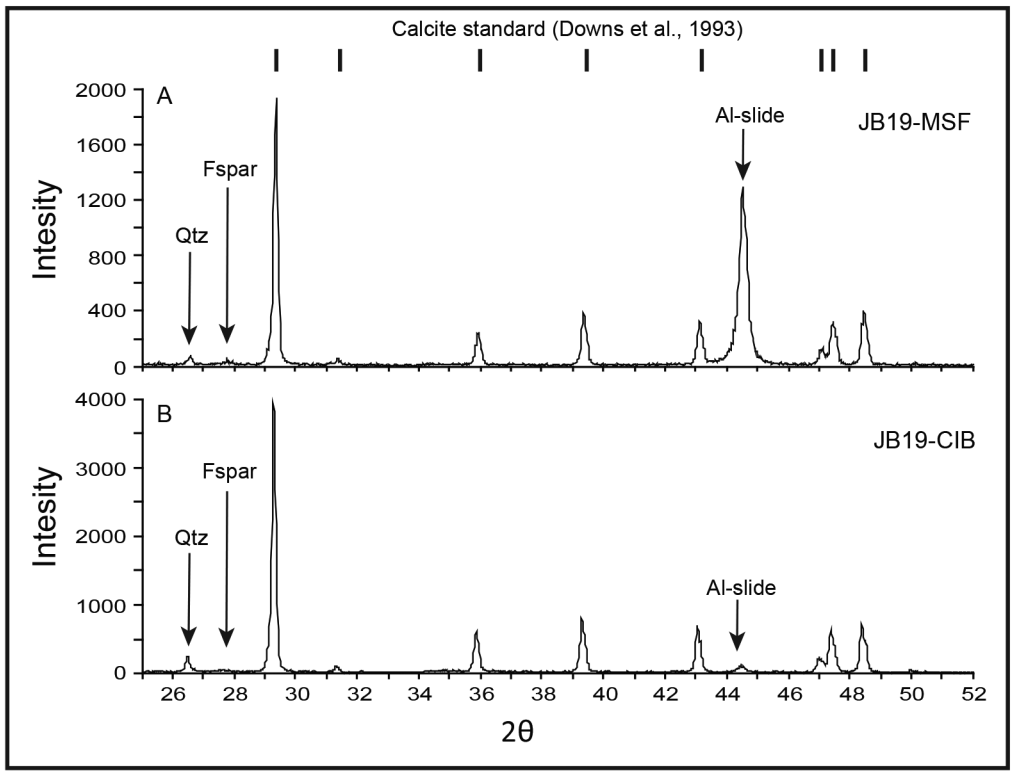

Figure 6. X-ray diffraction patterns for samples JB19-MSF and JB19-CIB. Vertical black bars at top represent key 2θ values for calcite. Response from the aluminum sample slide (Al-slide) is noted. Qtz – quartz. Fspar – feldspar.

not indicative of a significant marine influence, however (e.g., Florida Bay). The carbonate-rich, presumably lacustrine, JB19-MSF sample from near Las Vegas (Fig. 1) also yields similarly low [Zr] (Fig. 7) and similarly low $(La/La^*)_{SN}$ and Y/Ho values as the two SBF samples (Fig. 3B). Additionally, the REE profiles for all three JB19 samples are similar (Fig. 5B), suggesting that the two SBF samples and the presumably lacustrine sample from near Las Vegas (JB19-CIB; Fig. 1) share similar origins. Collectively, the REE and Y results for the three partially digested JB19 samples are more consistent with deposition in a continental environment than either an open or a nearshore/estuarine marine environment (Figs. 3 and 5B).

The lack of a positive Eu anomaly in SBF carbonate (Fig. 5B) is likely significant. Numerous studies have documented positive Eu anomalies in modern central and upper GoC sediments (Alekseev et al., 1998; Shumilin et al., 2005, 2005; Canet et al., 2005; Demina et al., 2009). Shumilin et al. (2002) cored the Colorado River delta in about 10 m of water slightly north of San Felipe, BCN (CU-14; Fig. 1). The REE profiles from that core consistently yield negative Eu anomalies (Fig. 5A). However, the core penetrated a carbonate-bearing horizon (10% calcium vs. ~ 3% for the rest of the core) at about 61 cm depth (Shumilin et al., 2002). This particular horizon yields a REE profile that is overall similar to the other silicate-rich core samples, but it also yields a conspicuous and positive Eu anomaly that is unique within the context of the core (Fig. 5A). Shumilin et al. (2002) attributed this Eu anomaly to biogenic carbonate that accumulated during a storm event or perhaps after a plankton bloom. Thus, this one core horizon contains a portion of carbonate uncontestably produced in the upper GoC environment. A similar but smaller positive Eu anomaly exists in marine surface sediments near Santa Rosalia, BCS (Figs. 1 and 5A) (Shumilin et al., 2005). Analysis of marine sediments along the western coast of the GoC near Loreto, BCS (Fig. 1), of submarine microbialites near Bahía Concepcíon, BCS (Fig. 1), and of biologic carbonates from geothermal fields in Guaymas basin (Fig. 1), reveal additional NASC-normalized positive Eu anomalies interpreted to reflect the influence of hydrothermal fluids (Alekseev et al., 1998; Canet et al., 2005; Demina et al., 2009). However, chondrite-normalized REE analyses of totally digested upper GoC surface sediments taken to the northwest of Isla Tiburón (Fig. 1) did not reveal any Eu anomalies, although none of the samples analyzed contained more than 6% calcium (Daesslé et al., 2004). Perhaps the $CaCO_3$ content in GoC sediment needs to exceed a certain threshold before a chondrite-normalized REE analysis can confidently detect an Eu anomaly. Unfortunately, none of the published studies on GoC sediments analyzed for Y, thus a comparison of GoC and SBF Y/Ho values is currently impossible. The lack of positive Eu anomalies (Fig. 5B) and marine Y/Ho values in SBF carbonate (Fig. 3B) is interesting and at face value does not support the Marine Only hypothesis for the origin of the SBF.

Several explanations are possible for the lack of marine GoC indicators in SBF carbonate. The low [Si] in the three partially digested JB19 samples (Fig. 7) suggests that adverse contamination by silicate REEs is unlikely (Frimmel, 2009). Perhaps post-depositional alteration somehow removed the original GoC signature (Lucchitta et al., 2001; Dorsey et al., 2018). This is unlikely for several reasons. Carbonate REE and Y concentrations are typically reported in parts per million (e.g., Webb and

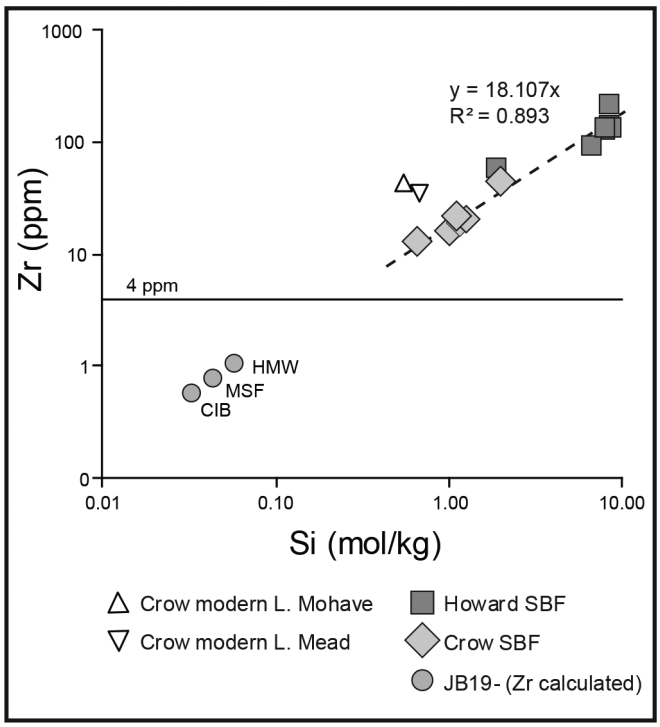

Figure 7. Cross-plot of silicon (Si) concentrations in moles per kilogram (mol/kg) versus zirconium (Zr) concentrations in parts per million (ppm). Solid black line represents the 4 ppm Zr threshold for compromised samples proposed by Frimmel (2009). Howard and Crow samples are total digestions. JB19 samples are partial digestions. See text for discussion.

Kamber, 2000). In contrast, REE and Y concentrations in surface and non-geothermal ground water are typically reported in parts per trillion (e.g., Goldstein and Jacobsen, 1998). Non-geothermal regional surface and groundwater sources (Crossey et al., 2015) would be ineffective at altering the original REE composition of SBF carbonate. If SBF carbonate was altered after deposition by geothermal groundwater, like that present in the Salton Trough (Figs. 1 and 2B), then presumably the result would be either undetectable, or at worst, the alteration would potentially impart its own positive Eu anomaly (Fig. 2B) or a marine-like Y/Ho value (Fig. 3A).

Another explanation might be that rapid and thorough scavenging of Eu at hydrothermal vents by hydrothermal minerals might have eliminated a positive Eu anomaly in early GoC water (e.g., Olivarez and Owen, 1991). The positive Eu anomaly in modern upper GoC sediments and biogenic carbonate suggests that this was probably not the case (Fig. 5B; Shumilin et al., 2002, 2005). Removal of Eu from the early GoC water column would not adversely affect Y or Ho, however, and could not account for the lack of marine Y/Ho values in SBF carbonate (Fig. 3B).

Finally, perhaps the SBF depositional environment predates the development of the geothermal Eu anomaly that is prevalent in modern upper GoC sediments. The most likely source of geothermal Eu in the early GoC would have been the continental rupture of Guaymas basin and the onset of seafloor development that occurred at ~ 6 Ma (Lizarralde et al., 2007). It is unclear if the development Eu-rich geothermal fluids could have predated the initiation of seafloor spreading in Guaymas Basin (or in basins farther north), however. This idea could be tested by analyzing well-preserved late Miocene marine bivalve shells from the more proximal Isla Tiburón (Gastil et al., 1999) that could slightly predate the ~ 6 Ma continental rupture of Guaymas basin (Lizarralde et al., 2007; Bennett et al., 2015). If the SBF is as old as the Marine Only model asserts (> 6 to 5.3 Ma; Dorsey et al., 2018) then it is temporally plausible that an early Eu anomaly from Guaymas basin could have infiltrated Blythe basin via mixing or transport by currents. The possibility of mixing increases if the SBF is younger than what that Marine Only model asserts. If the SBF marine flora and fauna represents a marine incursion that occurred closer to 4.9 Ma (age of the Lawlor Tuff in the SBF), then that incursion would post-date the rupture of Guaymas basin by nearly a million years. Continued faulting in the northern GoC basins, as another potential source of geothermal fluids to Blythe basin (e.g., Prol-Ledesma et al., 2013), would also have been a million years more developed. Regardless if an Eu anomaly was present in Blythe basin, at a minimum a marine Y/Ho value should have be present if the SBF was deposited in a fully marine embayment (McDougall and Miranda-Martinez, 2014; Miranda-Martinez et al., 2017; Dorsey et al., 2018), yet it is not (Fig. 3B).

The absence of a positive Eu anomaly and marine Y/Ho values in carbonate-rich SBF sediments (Figs. 3B, 5B) suggests the SBF depositional environment was unrelated to flooding of Blythe basin by the early GoC. It also suggests that geothermal groundwater typical of the Salton Trough (Figs. 2B, 3A) did not influence SBF carbonate during or after precipitation. Preliminary analysis of the REE composition of SBF carbonate does not support the Marine Only model. If GoC water was present during SBF carbonate precipitation, then it was undetectable in this study. If it was present, then the SBF Y/Ho values suggest that salinity in Blythe basin was likely well below standard seawater (Fig. 4) (Bright et al., 2018b). This interpretation could be consistent with the Marine-Influenced model where SBF carbonate was deposited in a lacustrine-dominated environment that perhaps experienced only weak or intermittent interactions with the early GoC (Crossey et al., 2015; Bright et al., 2018a,b). The preliminary interpretations presented here best support numerous other geochemical-based interpretations favoring a continental origin for SBF carbonate (Spencer and Patchett, 1997; Roskowski et al., 2010; Crossey et al., 2015; Bright et al., 2016, 2018a).

Future work

Using REE and Y data from the SBF to test for the influence of marine or continental geochemistry during SBF carbonate precipitation shows promise. The

methodology presented here could be expanded to test other presumably marine and lacustrine deposits in the upper GoC and Salton Trough region. Additional interpretive analysis of the currently available SBF REE and Y data is in progress. The largest obstacle to future studies will be obtaining cleaner carbonate samples. This study used a centrifuge and a partial digestion method that reduced [Si] by 1-2 orders of magnitude from other totally digested SBF samples and resulted in [Zr] values that are not indicative of compromised samples (Frimmel, 2009), but Si was not eliminated. Thus, some contribution by silicate REEs may also have been present. Future work should consider using weak acid for sample dissolution (e.g., Wang et al., 2014), perhaps in combination with multiple partial digestions per sample (e.g., Verdel et al., 2018) and steps to separate and concentrate REEs and Y, which could also potentially reduce sample size (e.g., Bau et al., 2010 and references therein) . The current study is the first of its kind for the lower Colorado River corridor and upper GoC region and is limited in both the number of samples and in its geographic range. This study warrants improvement given its potential usefulness. Future studies will benefit from analyzing other regional carbonates for broader context. Prime targets include the age-appropriate Hualapai and Nellis Limestones (Faulds et al., 2016) exposed near Grand Wash Trough and Las Vegas, respectively (Fig. 1), additional northern and southern Bouse Formation locations, and both modern and age-appropriate marine carbonates from around the GoC and the Salton Trough.

Conclusion

The use of REE and Y data in studies of the upper GoC and lower Colorado River corridor shows promise for differentiating between marine or continental water sources. Positive Eu anomalies and Y/Ho values > 40 could provide additional tools for detecting marine (i.e., GoC) influences on aquatic deposits in the Salton Trough and Blythe basin.

In this study, partial digestions of two centrifuged samples of carbonate-rich SBF sediments and one sample of centrifuged carbonate-rich Bouse-like sediments from near Las Vegas, NV, were analyzed for their REE and Y contents. None of the samples exceeded an established criterion for adverse silicate REE and Y contamination. All three samples yield broadly similar chondrite-normalized REE profiles that are also similar to lacustrine sediments from Qaidam basin (China) and the North American Shale Standard.

Southern Bouse Formation carbonate does not yield the positive Eu anomaly repeatedly documented in modern GoC sediments, nor does it yield marine Y/Ho values. Collectively this provides compelling evidence that SBF carbonate did not precipitate from early GoC water and thus, does not support the Marine Only model for the origin of SBF carbonate. Carbonate precipitation in a continental environment is more likely and is consistent with both the Lacustrine Only and perhaps the lacustrine but Marine-Influenced models for the origin of the SBF.

Acknowledgements

The author thanks Ryan Crow (USGS) and Keith Howard (USGS) for sharing their REE data, and R. Parnell at NAU for the two XRD analyses. Evgueni Shumilin (GoC core CU-14) and Scott Wood (geothermal springs of Oregon, Nevada, and California) graciously shared their REE data. Insightful comments on earlier versions of this manuscript by P. Pearthree, R. Crow, and A. Cohen are appreciated. Review comments by D. Miller improved the final manuscript.

References

Alekseev, A.V., Shumilin, E.N., Nava-Sanches, E., Sapozhnnikov, D.Yu., 1998. Anomalous Europium behavior in the coastal bottom sediments of the southwestern Gulf of California. Doklady Earth Sciences, v. 361A, p. 876-878 [Translated from Doklady Akademii Nauk, v. 361, p. 689-691].

*Alibo, D.S., and Nozaki, Y., 1999. Rare earth elements in seawater: Particle association, shale-normalization, and Ce oxidation. Geochimica et Cosmochimica Acta, v. 63, p. 363-372.

Allwood, A.C., Kamber, B.S., Walter, M.R., Burch, I.W., Kanik, I., 2010. Trace elements record depositional history of an Early Archean stromatolitic carbonate platform. Chemical Geology, v. 270, p. 148-163.

Bau, M., and Dulski, P., 1999. Comparing yttrium and rare earths in geothermal fluids from the Mid-Atlantic Ridge: implications for Y and REE behaviour during near-vent mixing and for the Y/Ho ratio of Proterozoic seawater. Chemical Geology, v. 155, p. 77-90.

Bau, M., Dulski, P., Möller, P., 1995. Yttrium and Holmium in South Pacific seawater: vertical distribution and possible fractionation mechanisms. Chemie der Erde, v. 55, p. 1-15.

*Bau, M., Balan, S., Schmidt, K., Koschinsky, A., 2010. Rare earth elements in mussel shells of the *Mytilidae* family as tracers for hidden and fossil high-temperature geothermal systems. Earth and Planetary Science Letters, v. 299, p. 310-316.

Bennett, S.E.K., Oskin, M.E., Dorsey, R.J., Iriondo, A., Kunk, M.J., 2015. Stratigraphy and structural development of the southwest Isla Tiburón marine basin: Implications for the latest Miocene tectonic opening and flooding of the northern Gulf of California. Geosphere, v. 11, p. 977-1007.

*Bolhar, R., and Van Kranendonk, M.J., 2007. A non-marine depositional setting for the northern Fortescue Group, Pilbara Craton, inferred from trace element geochemistry of stromatolitic carbonates. Precambrian Research, v. 155, p. 229-250.

Bright, J., Cohen, A.S., Dettman, D.L., Pearthree, P.A., Dorsey, R.J., and Homan, M.B., 2016. Did a catastrophic lake spillover integrate the late Miocene-early Pliocene Colorado River and the Gulf of California?: Microfossil and stable isotope evidence from Blythe basin, California-Arizona, USA: PALAIOS, v. 31, p. 81-91.

Bright, J., Cohen, A.S., Dettman, D.L., Pearthree, P.A., 2018a. Freshwater plumes and brackish lakes: Intergrated microfossil and O-C-Sr isotopic evidence from the late Miocene and early Pliocene Bouse Formation (California-Arizona) supports a lake overflow model for the integration of the lower Colorado River corridor. Geosphere, v. 14, p. 1875-1911.

Bright, J., Cohen, A.S., Starratt, S., 2018b. Distinguishing brackish lacustrine from brackish marine deposits in the stratigraphic record: A case study from the late Miocene and early Pliocene Bouse Formation, Arizona and California, USA. Earth-Science Reviews, v. 185, p. 974-1003.

*Caccia, V.C., and Millero, F.J., 2007. Distribution of yttrium and rare earths in Florida Bay sediments. Marine Chemistry, v. 104, p. 171-185.

Canet, C., Prol-Ledesma, R.M., Antonio Proenza, J., Rubio-Ramos, M.A., Forrest, M.J., Tores-Vera, M.A., Rodriguez-Diaz, A.A., 2005. Mn-Ba-Hg mineralization at shallow submarine hydrothermal vents in Bahía Concepcíon, Baja California Sur, Mexico. Chemical Geology, v. 224, p. 96-112.

*Censi, P., Sprovieri, M., Saiano, F., Di Geronimo, S.I., Larocca, D., Placenti, F., 2007. The behaviour of REEs in Thailand's Mae Klong estuary: Suggestions from the Y/Ho ratios and lanthanide tetrad effects. Estuarine, Coastal and Shelf Science, v. 71, p. 59-579.

*Chevis, D.A., Johannesson, K.H., Burdige, D.J., Tang, J., Moran, S.B., Kelly, R.P., 2015. Submarine groundwater discharge of rare earth elements to a tidally-mixed estuary in Southern Rhode Island. Chemical Geology, v. 397, p. 128-142.

Condie, K.C., 1991. Another look at rare earth elements in shales. Geochimica et Cosmochimica Acta, v. 55, p. 2527-2531.

Crossey, L.C., Karlstrom, K.E., Dorsey, R., Pearce, J., Wan, E., Beard, L.S., Asmerom, Y., Polyak, V., Crow, R.S., Cohen, A., Bright, J., Pecha, M.E., 2015. Importance of groundwater in propagating downward integration of the 6-5 Ma Colorado River system: geochemistry of springs, travertines, and lacustrine carbonates of the Grand Canyon region over the past 12 Ma: Geosphere, v. 11, p. 660-682.

Crow, R.S., Schwing, J., Karlstrom, K.E., Heizler, M., Pearthree, P.A., House, P.K., Dulin, S.A., Stelten, M.E., Crossey, L.J., 2019. Redefining the age of the Colorado River. Geological Society of America Annual Meeting, September 22-25, 2019, Phoenix, Arizona, USA, Paper 134-9.

Daesslé, L.W., Camacho-Ibar, V.F., Carriquiry, J.D., Ortiz-Hernández, 2004. The geochemistry and sources of metals and phosphorus in the recent sediments from the Northern Gulf of California. Continental Shelf Research, v.24, p. 2093-2106.

Dean, W.E., Jr., 1974. Determination of carbonate and organic matter in calcareous sediments and sedimentary rocks by loss on ignition: Comparison with other methods. Journal of Sedimentary Petrology, v. 44, p. 242-248.

Demina, L., Galkin, S., Shumilin, E., 2009. Lanthanides in some organisms from two hydrothermal fields of the Northeast Pacific Ocean: Guaymas Basin (Gulf of California) and 9°50'N on the East Pacific Rise. Frontiers in Trace Elements - Research and Education. 10th International Conference on the Biogeochemistry of Trace Elements. July 13-18, 2009. Chihuahua, Chih., Mexico.

Dorsey, R.J., O'Connell, B., McDougall, K., Homan, M., 2018. Punctuated sediment discharge during early Pliocene birth of the Colorado River: Evidence from regional stratigraphy, sedimentology, and paleontology. Sedimentary Geology, v. 363, p. 1-33.

Downs, R.T., Bartelmehs, K.L., Gibbs, G.V., Boisen, M.B., Jr., 1993. Interactive software for calculating and displaying X-ray or neutron powder diffractometer patterns of crystalline minerals. American Mineralogist, v. 78, p. 1104-1107.

U.S. EPA, 1996. Method 3050B: Acid digestion of Sediments, Sludges, and Soils. Revision 2. Washington D.C.

Faulds, J.E., Schreiber, C., Langenheim, V.E., Hinz, N.H., Shaw, T.H., Heizler, M.T., Perkins, M.E., El Tabakh, M., Kunk, M.J., 2016. Paleogeographic implications of the late Miocene lacustrine and nonmarine evaporate deposits in the Lake Mead region: Immediate precursor to the Colorado River. Geosphere, v. 12, p. 721-767.

Folger, D.W., 1972. Estuarine sediments of the United States. U.S. Geological Survey Professional Paper 742. U.S. Government Printing Office, Washington D.C., 94 pp.

Frimmel, H.E., 2009. Trace element distribution in Neoproterozoic carbonates as palaeoenvironmental indicator. Chemical Geology, v. 258, p. 338-353.

*Garcia-Solonsa, E., Jeandel, C., Labatut, M., Lacan, F., Vance, D., Chavagnac, V., Pradoux, C., 2014. Rare earth elements and Nd isotopes tracing water mass mixing and particle-seawater interactions in the SE Atlantic. Geochimica et Cosmochimica Acta, v. 215, p. 351-372.

Gastil, R.G., Neuhaus, J., Cassidy, M., Smith, J.T., Ingle, J.C., Jr., Krummenacher, D., 1999. Geology and paleontology of southwestern Ilsa Tiburón, Sonora, Mexico. Revista Mexicana de Ciencias Geológicas, v. 16, p. 1-34.

Goldstein, S.J., and Jacobson, S.B., 1988. Rare earth elements in river waters. Earth and Planetary Science Letters, v. 89, p. 35-47.

González-Fernández, A., Dañobeitia, J.J., Delgado-Argote, L.A., Michaud, F., Córdoba, D., Bartolomé, R., 2005. Mode of extension and rifting history of upper Tiburón and upper Delfín basins, northern Gulf of California. Journal of Geophysical Research, v. 110, B01313,doi:10.1029/2003JB002941.

*Grenier, M., Jeandel, C., Lacan, F., Vance, D., Venchiarutti, C., Cros, A., Cravatte, S., 2013. From the subtropics to the central equatorial Pacific Ocean: Neodymium isotopic composition and rare earth element concentrations variations. Journal of Geophysical Research, v. 118, p. 592-618.

Gootee, B., House, P.K., Pearthree, P.A., Crow, R., Bright, J., 2019. The Trigo sediments – an early Pliocene offlap sequence recording the demise of paleolake Blythe, lower Colorado River corridor, southwest USA. Geological Society of America Abstracts with Programs, v. 51, No. 5, Paper No. 134-12. Geological Society of America Annual Meeting, September 22-25, 2019, Phoenix, AZ.

Han, G., and Liu, C.-Q., 2007. Dissolved rare earth elements in river waters draining karst terrains in Guizhou Province, China. Aquatic Geochemistry, v. 13, p. 95-107.

*Haraguchi, H., Itoh, A., Kimata, C., Miwa, H., 1998. Speciation of yttrium and lanthanides in natural water by inductively coupled plasma mass spectrometry after preconcentration by ultrafiltration and with a chelating resin. Analyst, v. 123, p. 773-778.

*Hatje, V., Bruland, K., Flegal, A.R., 2014. Determination of rare earth elements after pre-concentration using NOBIAS-chelate PA-1® resin: Method development and application in the San Francisco Bay plume. Marine Chemistry, v. 160, p. 34-41.

*Hatje, V., Bruland, K.W., Flegal, A.R., 2016. Increases in anthropogenic Gadolinium anomalies and rare earth element concentrations in San Francisco Bay over a 20 year record. Environmental Science and Technology, v. 50, p. 4159-4168.

Homan, M.B., 2014. Sedimentology and stratigraphy of the Miocene-Pliocene Bouse Formation near Cibola, Arizona and Milpitas Wash, California: implications for the early evolution of the Colorado River. University of Oregon [MS Thesis], Eugene, Oregon, 128 pp.

Jiang, Y., and Ji, H., 2012. Rare earth geochemistry in the dissolved, suspended, and sedimentary loads in karstic rivers, Southwest China. Environmental Earth Sciences, v. 66, p. 2217-2234.

*Johannesson, K.H., Lyons, W.B., Bird, D.A., 1994. Rare earth element concentrations and speciation in alkaline lakes from the western U.S.A. Geophysical Research Letters, v. 21, 773-776.

*Johannesson, K.H., Zhou, X., Guo, C., Stetzenbach, K.J., Hodge, V.F., 2000. Origin of rare earth element signatures in groundwaters of circumneutral pH from southern Nevada and eastern California, USA. Chemical Geology, v. 164, 239-257.

Kelble, C.R., Johns, E.M., Nuttle, W.K., Lee, T.N., Smith, R.H., Ortner, P.B., 2007. Salinity patterns in Florida Bay. Estuarine, Coastal and Shelf Science, v. 71, p. 318-334.

*Klinkhammer, G.P., Elderfield, H., Edmond, J.M., Mitra, A., 1994. Geochemical implications of rare earth element patterns in geothermal fluids from mid-ocean ridges. Geochimica et Cosmochimica Acta, v. 58, p. 5105-5113.

*Lawrence, M.G., and Kamber, B.S., 2006. The behaviour of the rare earth elements during estuarine mixing – revisited. Marine Chemistry, v. 100, p. 147-161.

Lawrence, M.G., Greig, A., Collerson, K.D., Kamber, B.S., 2006. Rare earth element and yttrium variability in Southeast Queensland Waterways. Aquatic Geochemistry, v. 12, p. 39-72.

*Leyborne, M.I., and Johannesson, K.H., 2008. Rare earth elements (REE) and yttrium in stream waters, stream sediments, and Fe-Mn oxyhydroxides: Fractionation, speciation, and controls over REE + Y patterns in the surface environment. Geochimica et Cosmochimica Acta, v. 72, p. 5962-5983.

*Li, F., Webb, G.E., Algeo, T.J., Kershaw, S., Lu, C., Oehlert, A.M., Gong, Q., Pourmand, A., Tan, X., 2019. Modern carbonate ooids preserve ambient aqueous REE signatures. Chemical Geology, v. 509, p. 163-177.

Lonsdale, P., 1989. Geology and tectonic history of the Gulf of California. In: Winterer, E.L., et al., Eds., The eastern Pacific Ocean and Hawaii: Geology of North America, v. N. Boulder, Colorado, Geological Society of America, p. 499-521.

Lucchitta, I., McDougall, K., Getzger, D.G., Morgan, P., Smith, G.R., Chernoff, B., 2001. The Bouse Formation and post-Miocene uplift of the Colorado River. In: Young, R.A., Spamer, E.E., Eds., The Colorado River: Origin and evolution. Grand Canyon, Arizona, Grand Canyon Association Monograph 12, p. 173-179.

*Madhavaraju, J., Löser, H., Scott, R.W., Sandeep, S., Sial, A.N., Ramasamy, S., 2017. Petrography, geochemistry and stable isotopes of carbonate rocks, Lower Cretaceous Alistos Formation, Los Torotes section, Baja California, Mexico. Revista Mexicana de Ciencias Geológicas, v. 34, p. 63-77.

Martín-Barajas, A., González-Escobar, M., Fletcher, J.M., Pacheco, M., Oskin, M., Dorsey, R., 2013. Thick deltaic sedimentation and detachment faulting delay the onset of continental rupture in the Northern Gulf of California: analysis of seismic reflection profiles. Tectonics, v. 32, p. 1294-1311.

*Mastandrea, A., Barca, D., Guido, A., Tosti, F., Russo, F., 2010. Rare earth element signatures in the Messinian pre-evaporitic Calcare di Base formation (Northern Calabria, Italy): evidence of normal seawater deposition. Carbonates Evaporites, v. 25, p. 133-143.

McDougall, K., and Miranda Martínez, A.Y., 2014. Evidence for a marine incursion along the lower Colorado River corridor. Geosphere, v. 10, p. 842-869.

McLennan, S.M., 1989. Rare earth elements in sedimentary rocks: Influence of provenance and sedimentary processes. Reviews in Mineralogy and Geochemistry, v. 21, p. 169-200.

Metzger, D.G., 1968. The Bouse Formation (Pliocene) of the Parker-Blythe-Cibola area, Arizona and California: U.S. Geological Survey Professional Paper 600-D, p. 126-136.

*Michard, A., 1989. Rare earth systematics in geothermal fluids. Geochimica et Cosmochimica Acta, v. 53, p. 745-750.

Miller, D.M., Reynolds, R.E., Bright, J.E., Starratt, S.W., 2014. Bouse Formation in the Bristol basin near Amboy, California, USA. Geosphere, v. 10, p. 462-475.

Miranda-Martínez, A.Y., Carreno, A.L., McDougall, K., 2017. The Neogene genus *Streptochilus* (Brönniman and Resig, 1971) from the Gulf of California. Marine Micropaleontology, v. 132, p. 35-52.

Lizarralde, D., Axen, G.J., Brown, H.E., Fletcher, J.M., González-Fernández, A., Harding, A.J., Holbrook, W.S., Kent, G.M., Paramo, P., Sutherland, F., Umhoefer, P.J., 2007. Variations in styles of rifting in the Gulf of California. Nature, v. 488, p. 466-469.

*Maslov, A.V., Kozina, N.V., Klyuvitkin, A.A., Novigatsky, A.N., Filippov, A.S., Shevchenko, V.P., 2016. Distribution of some rare and trace elements in modern bottom sediments of the Caspian Sea. Oceanology, v. 56, p. 552-563.

Möller, P., 2000. Rare earth elements and yttrium as geochemical indicators of the source of mineral and thermal

waters. In: Stober, I., and Bucher, K., Eds., Hydrogeology of Crystalline Rocks. Water Science and Technology Library, Volume 34, Springer, Dordrecht, p. 227-246.

Möller, P., 2002. The distribution of rare earth elements and yttrium in water-rock interactions: field observations and experiments. In: Stober, I., and Bucher, K., Eds., Water-Rock Interactions. Kluwer Academic Publishers, Netherlands, p. 97-123.

Nuttle, W.K., Fourqurean, J.W., Cosby, B.J., Zieman, J.C., Robblee, M.B., 2000. Influence of net freshwater supply on salinity in Florida Bay. Water Resources Research, v. 36, p. 1805-1822.

*Nothdurft, L.D., Webb, G.E., Kamber, B.S., 2004. Rare earth element geochemistry of Late Devonian reefal carbonates, Canning Basin, Western Australia: confirmation of a seawater REE proxy in ancient limestones. Geochimica et Cosmochimica Acta, v. 68, p. 263-283.

*Nozaki, Y., and Alibo, D.S., 2003. Importance of vertical geochemical processes in controlling the oceanic profiles of dissolved rare earth elements in the northeastern Indian Ocean. Earth and Planetary Science Letters, v. 205, p. 155-172.

Nozaki, Y., Zhang, J., Amakawa, H., 1997. The fractionation between Y and Ho in the marine environment. Earth and Planetary Science Letters, v. 148, p. 329-340.

*Nozaki, Y., Lerche, D., Alibo, D.S., Tsutsumi, M., 2000a. Dissolved indium and rare earth elements in three Japanese rivers and Tokyo Bay: evidence for anthropogenic Gd and In. Geochimica et Cosmochimica Acta, v. 64, p. 3975-3982.

*Nozaki, Y., Lerche, D., Alibo, D.S., Snidvongs, A., 2000b. The estuarine geochemistry of rare earth elements and indium in the Chao Phraya River, Thailand. Geochimica et Cosmochimica Acta, v. 64, p. 3983-3994.

O'Connell, B., Dorsey, R.J., Humphreys, E.D., 2017. Tidal rhythmites in the southern Bouse Formation as evidence for post-Miocene uplift of the lower Colorado River corridor. Geology, v. 45, p. 99-102.

Olivarez, A.M., and Owen, R.M., 1991. The europium anomaly of seawater: implications for fluvial versus hydrothermal REE inputs to oceans. Chemical Geology, v. 92, p. 317-328.

*Osborne, A.H., Haley, B.A., Hathorne, E.C., Plancherel, Y., Frank, M., 2015. Rare earth element distribution in Caribbean seawater: Continental input versus lateral transport of distinct REE compositions in subsurface water masses. Marine Chemistry, v. 177, p. 172-183.

*Phanke, K., van de Flierdt, T., Jones, K.M., Lambelet, M., Hemming, S.R., Goldstein, S.L., 2012. GEOTRACES intercalibration of neodymium isotopes and rare earth element concentrations in seawater and suspended particles. Part 2: Systematic tests and baseline profiles. Limnology and Oceanography:Methods, v. 10, p. 252-269.

Pearthree, P.A., and House, P.K., 2014. Paleogeomorphology and evolution of the early Colorado River inferred from relationships in Mohave and Cottonwood valleys, Arizona, California, and Nevada: Geosphere, v. 10, p. 1139-1160.

*Ponnurangam, A., Bau, M., Brenner, M., Koschinsky, A., 2016. Mussel shells of *Mytilus edulis* as bioarchives of the distribution of rare earth elements and yttrium in seawater and the potential impact of pH and temperature on their partitioning behavior. Biogeosciences, v. 13, p. 751-760.

Poulson, S.R., and John, B.E., 2003. Stable isotope and trace element geochemistry of the basal Bouse Formation carbonate, southwestern United States: Implications for the Pliocene uplift history of the Colorado Plateau. Geological Society of America Bulletin, v. 115, p. 434-444.

Prol-Ledesma, R.M., Torres-Vera, M.-A., Rodolfo-Metapa, R., Ángeles, C., Deveze, C.H.L., Villanueva-Estrada, R.E., Shumilin, E., Robinson, C., 2013. High heat flow and ocean acidification at a nacent rift in the northern Gulf of California. Nature Communications, v. 4: 1388.

Roskowski, J.A., Patchett, P.J., Spencer, J.E., Pearthree, P.A., Dettman, D.L., Faulds, J.E., and Reynolds, A.C., 2010. A late Miocene-early Pliocene chain of lakes fed by the Colorado River: Evidence from Sr, C, and O isotopes of the Bouse Formation and related units between Grand Canyon and the Gulf of California: Geological Society of America Bulletin, v. 122, p. 1625-1636.

Ross, J.E., Kidwell, S.M., Dettman, D.L., Bright, J., McDougall-Reid, K., Dorsey, R.J., Jefferson, G.T., Miller, D.M., this volume. Evidence of late Pleistocene marine incursions into the Salton Basin. Desert Symposium, April 17-20, Desert Studies Center, Zzyzx, CA. Abstract.

Sarna-Wojcicki, A.M., Deino, A.L., Fleck, R.J., McLaughlin, R.J., Wagner, D., Wan, E., Wahl, D., Hillhouse, J.W., Perkins, M., 2011. Age, composition, and areal distribution of the Pliocene Lawlor Tuff, and three younger Pliocene tuffs, California and Nevada. Geosphere, v. 7, p. 599-628.

Shumilin, E., Rogriguez-Figueroa, G., Sapozhnikov, D., 2005. Lanthanide contamination and strong positive Europium anomalies in the surface sediments of the Santa Rosalia copper mining region, Baja California Peninsula, Mexico. Bulletin of Environmental Contamination and Toxicology, v. 75, p. 308-315.

Shumilin, E.N., Carriquiry, J.D., Comacho-Ibar, V.F., Sapozhnikov, D., Kalmykov, S., Sánchez, A., Aguíñiga-García, S., Sapozhnikov, Y.A., 2002. Spatial and vertical distributions of elements in sediments of the Colorado River delta and Upper Gulf of California. Marine Chemistry, v. 79, p. 113-131.

Smith, P.B., 1970. New evidence for a Pliocene marine embayment along the Lower Colorado River area, California and Arizona. Geological Society of America Bulletin, v. 81, p. 1411-1420.

Soyol-Erdene, T.-O., and Huh, Y., 2013. Rare earth element cycling in the porewaters of the Bering Sea Slope (IODP Exp. 323). Chemical Geology, v. 358, p. 75-89.

Spencer, J.E., Patchett, P.J., Pearthree, P.A., House, P.K., Sarna-Wojcicki, A.M., Wan, E., Roskowski, J.A., Faulds, J.E., 2013. Review and analysis of the age and origin of the Pliocene Bouse Formation, lower Colorado River Valley, southwestern USA: Geosphere, v. 9, p. 444-459.

Spencer, J.E., and Patchett, P.J., 1997. Sr isotope evidence for a lacustrine origin for the upper Miocene to Pliocene Bouse Formation, lower Colorado River trough, and implications for timing of Colorado Plateau uplift: Geological Society of America Bulletin, v. 109, p. 767-778.

Sutherland, F.H., Kent, G.M., Harding, A.J., Umhoefer, P.J., Driscoll, N.W., Lizarralde, D., Fletcher, J.M., Axen, G.J., Holbrook, W.S., González-Fernández, A., Lonsdale, P., 2012. Middle Miocene to early Pliocene oblique extension in the southern Gulf of California. Geosphere, v. 8, p. 752-770.

*Takahashi, Y., Yoshida, H., Sato, N., Hama, K., Yusa, Y., Shimizu, H., 2002. W- and M-type tetrad effects in REE patterns for water-rock systems in the Tono uranium deposit, central Japan. Chemical Geology, v. 184, p. 311-335.

Taylor, S.R., and McLennan, S.M., 1988. The significance of the rare earths in geochemistry and cosmochemistry. In: Gschneidner, K.A., Jr., and Eyring, L., Eds., Handbook on the Physics and Chemistry of Rare Earths. North-Holland, Amsterdam, p. 486-578.

*Verdel, C., Phelps, B., Welsh, K., 2018. Rare earth element and $^{87}Sr/^{86}Sr$ step-leaching geochemistry of central Australian Neoproterozoic carbonate. Precambrian Research, v. 310, p. 229-242.

Umhoefer, P.J., Darin, M.H., Bennett, S.E.K., Skinner, L.A., DoREE, R.J., Oskin, M.E., 2018. Breaching of strike-slip faults and successive flooding of pull-apart basins to form the Gulf of California seaway from ca. 8-6 Ma. Geology, v. 46, p. 695-698.

Wang, Q., Lin, Z., Chen, D., 2014. Geochemical constraints on the origin of Doushantuo cap carbonates in the Yangtze Gorges area, South China. Sedimentary Geology, v. 304, p. 59-70.

*Wang, Z., and Liu,C. 2000. Distributions of dissolved rare earth elements during estuarine mixing at the Changjiang River mouth. Chinese Science Bulletin, v. 45, p. 1795-1799.

*Webb, G.E., and Kamber, B.S., 2000. Rare earth elements in Holocene reefal carbonates: a new shallow seawater proxy. Geochimica et Cosmochimica Acta, v. 64, p. 1557-1565.

*Wood, S.A., and Shannon, W.M., 2003. Rare-earth elements in geothermal waters from Oregon, Nevada, and California. Journal of Solid State Chemistry, v. 171, p. 246-253.

Zeng, L.-Q., Yi, H.-S., Xia, G.-O., Simon, K., Heim, C., Arp, G., 2019. Palaeoenvironmental setting of lacustrine stromatolites in the Miocene Wudaolian Group, northern Tibetan Plateau. Journal of Palaeogeography 8,18, doi:10.1186/s42501-019-0033-7.

*Zhang, J., and Nozaki, Y., 1996. Rare earth elements and yttrium in seawater: ICP-MS determinations in the East Caroline, Coral Sea, and South Fiji basins of the South Pacific Ocean. Geochimica et Cosmochimica Acta, v. 60, p. 4631-4644.

Zhang, H.C., Zhang, W.X., Chang, F.Q., Yang, L.Q., Lei, G.L., Yang, M.S., Pu, Y., Lei, Y.B., 2009. Geochemical fractionation of rare earth elements in lacustrine deposits from Qaidam Basin. Science in China Series D: Earth Sciences, v. 52, p. 1703-1713.

*Zhao, Y.-Y., Zheng, Y.-F., Chen, F., 2009. Trace element and strontium isotope constraints on sedimentary environment of Ediacaran carbonates in southern Anhui, South China. Chemical Geology, v. 265, p. 345-362.

*Zheng, X.-Y., Plancherel. Y., Saito, M.A., Scott, P.M., Henderson, G.M., 2016. Rare earth elements (REEs) in the tropical South Atlantic and quantitative deconvolution of their non-conservative behavior. Geochimica et Cosmochimica Acta, v. 177, p. 217-237.

*Zhu, Y., Hattori, R., Rahmi, D., Okuda, S., Itoh, A., Fujimori, E., Umemura, T., Haraguchi, H., 2005. Fractional distributions of trace metals in surface water of Lake Biwa as studied by ultrafiltration and ICP-MS. Bulletin of the Chemical Society of Japan, v. 78, p. 1970-1976.

A new theropod dinosaur tracksite in the Aztec Sandstone, Valley of Fire State Park, Nevada

Drew Clark, Sarah E. Grove, and Stephen M. Rowland
Department of Geoscience, University of Nevada, Las Vegas Las Vegas, NV 89154-4010, dcrnlv@gmail.com

ABSTRACT—Here we describe and interpret a recently discovered theropod dinosaur tracksite in the Jurassic Aztec Sandstone of Valley of Fire State Park, Nevada. The site consists of multiple undertracks assignable to the ichnogenus *Grallator*. Several of the tracks define a distinct, northeastward-directed trackway preserved within a cross-bedded duneset. Tracks are seen in more than one of the centimeter-scale stratigraphic horizons, indicating that this tracksite lay in the toe of a dune where increased moisture content enhanced the potential for trackway preservation. Based on stride length and estimated hip height, we calculate that this animal was walking at a slow rate of 2.6 km/hr. This study underscores the presence and ecological importance of theropod predators in the Aztec Sandstone dune-field ecosystem.

Introduction

The Jurassic Aztec Sandstone is an eolian sandstone exposed in southeastern California and southern Nevada (Bohannon, 1977). It is correlative with the Navajo and Nugget sandstones of Utah and adjacent states (Porter, 1985, 1987). These three formations—Aztec, Navajo, and Nugget—are the erosional and tectonically dismembered remnants of an erg that occupied the western margin of Pangaea as this supercontinent was beginning to disintegrate. The Aztec Sandstone represents the southwestern margin of this erg system (Porter, 1987). These erg deposits contain a meager body-fossil record (Irmis, 2005), and no body fossils have been reported from the Aztec Sandstone. However, all three of these formations contain a diverse trace-fossil fauna, including the tracks of dinosaurs, synapsids (mammals and/or protomammals), and arthropods (Lockley and Hunt, 1995; Hamblin and Bilbey, 1999; Rowland and Mercadante, 2014; Rowland et al., 2014).

Dinosaur tracks were first reported from the Aztec Sandstone in exposures of the Mescal Range of southeastern California (Reynolds, 2002, 2006). Many of the Mescal Range tracks, including the only dinosaur tracks known to occur in California, were collected and reposited in the San Bernardino County Museum and the Natural History Museum of Los Angeles County, the latter of which placed many of these tracks on display (Springer et al., 2009).

Dinosaur tracks were first reported from Nevada exposures of the Aztec Sandstone by Rowland et al. (2012). The first reported tracks in Nevada were reported from within Red Rock Canyon National Conservation Area, west of Las Vegas (Fig. 1) (Rowland et al., 2012). Soon thereafter, dinosaur tracks (among tracks of other taxa) were published from observations made in Valley of Fire State Park (Fig. 1) and Gold Butte National Monument

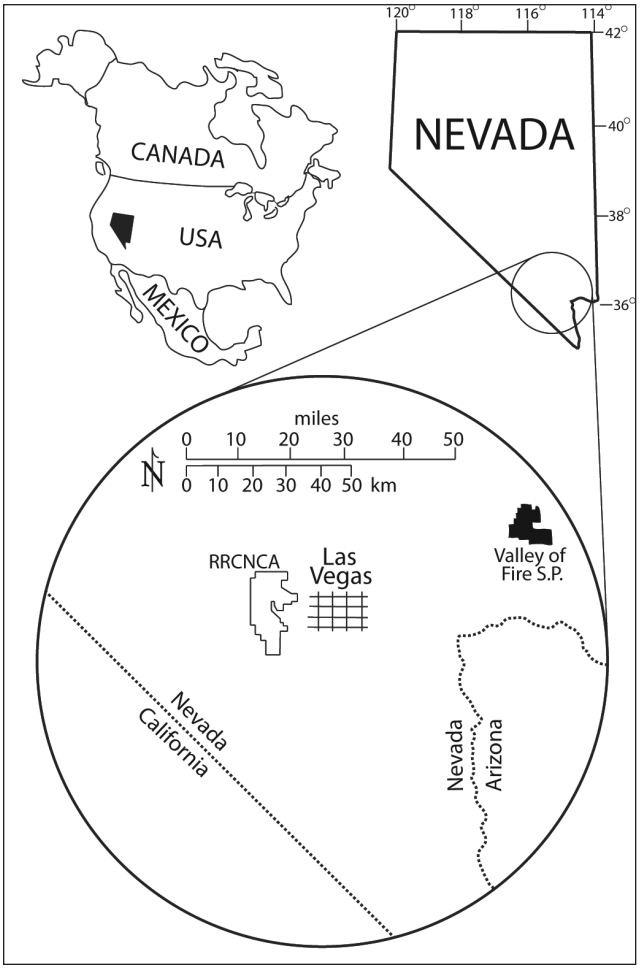

Figure 1. Location of Valley of Fire State Park and Red Rock Canyon National Conservation area, both of which contain extensive exposures of Aztec Sandstone.

(Stoller, 2013; Stoller et al., 2013; Rowland and Caputo, 2016). Here we describe a recently discovered theropod tracksite in Valley of Fire State Park. This site and others are part of ongoing research and consistent with Nevada State Parks policy the precise location of this tracksite is not disclosed to ensure its protection.

Tracksite UNLV-AZ-045 near Atlatl Rock

Atlatl Rock and nearby exposures of the Aztec Sandstone in Valley of Fire State Park have proven to be extraordinarily rich in trace fossils, including those of arthropods, synapsids, and dinosaurs (Stoller et al., 2013; Rowland and Mercadante, 2014; Rowland and Caputo, 2016). The site described here, UNLV-AZ-045, contributes to the richness of this area by providing an in-situ example of track preservation across multiple bedding planes and can provide insight into the environmental conditions at the time of deposition. The site was discovered in approximately 2015 by a student at College of Southern Nevada, and preliminary observations and measurements by a team of students were recorded at the site shortly thereafter.

Preserved traces reported here represent undertracks, impressions of footprints that were translated some distance below the surface on which the animal walked. As is typical of dinosaur tracksites in the Aztec Sandstone (Rowland and Caputo, 2016), the trackway surface lies near the bottom of a crossbed set (Fig. 4), which represents the toe portion of a dune. Due to the position in the duneset and what we are interpreting as increased moisture content, the fidelity of preservation of the trackmakers' feet is poor. When light conditions are not optimal, most of the tracks disappear into the irregularities of the sandstone surface, but through the use of three-dimensional modeling using photogrammetric reconstructions we have identified at least forty tracks, most of which were previously unrecognized (Fig. 2). An oblique view (Fig. 3A) and closer views of some of the more distinct tracks (Fig. 3B, C) display the absence of clearly defined margins preventing us from confidently characterizing size variation.

We assign all of the tracks with either a tridactyl morphology or tracks of a similar size accompanied by an expulsion rim to the ichnogenus *Grallator*. The *Grallator* trackmaker is commonly assumed to have been a small, bipedal, gracile, carnivorous, theropod dinosaur (Lockley,

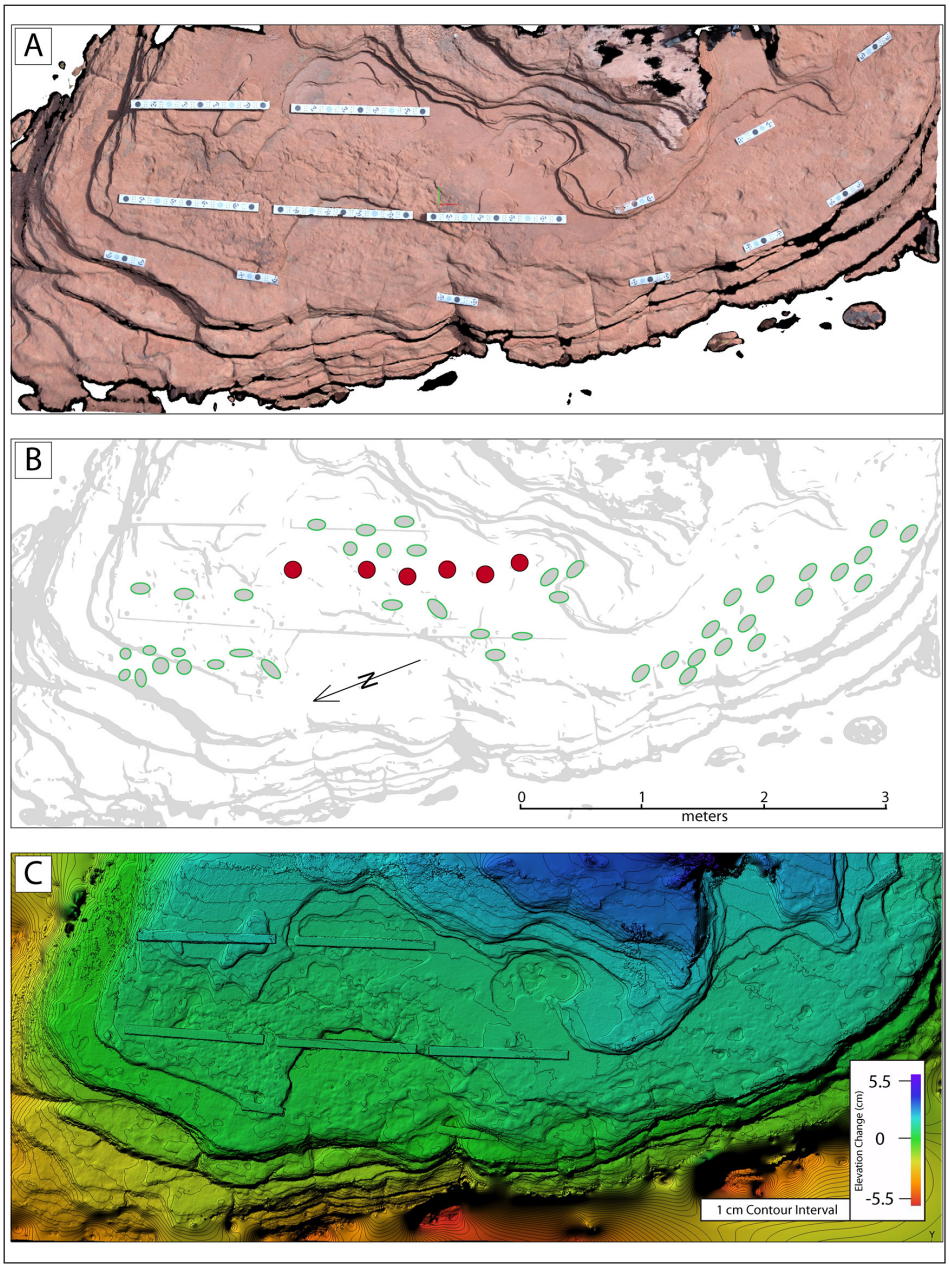

Figure 2. A. Three-dimensional model created in Agisoft Metashape Version 1.5.4.8885 of Tracksite UNLV-AZ-045, showing specialized targets alongside trackways used to identify and process overlapping photosets. B. Interpretation of the tracksite, with more than 40 individual tracks circled. Tracks in red define the trackway describe in detail in the text. C. Digital elevation model with a depth range of 11 cm and overlain by 1 cm contour intervals.

1991; Lockley and Hunt, 1995), similar to the Triassic dinosaur *Coelophysis*.

Photogrammetry methods and results

We began studying this tracksite with traditional field methods, including ground-based measurements, photography of individual tracks, and chalk outlines. As technology advanced and photogrammetric reconstructions became more accessible, the precision and quality of data vastly improved. The ability to preserve and easily share models of tracks and trackways has allowed enhanced interpretations.

Methods utilized for this study are adapted from the photogrammetric history and methodology described by Matthews et al. (2016). Photosets for this study were processed using Agisoft Metashape Version 1.5.4.8885, following the general workflow outlined in the accompanying user's manual (*Agisoft Metashape User Manual Professional Edition, Version 1.5*, 2019). The photoset consisted of 137 photos with 129,243 tie points used to align photos. Once aligned, we used the ultra high quality options to create 132 depth maps and a dense cloud consisting of 287,470,867 points. Digital elevation modelling, marker identification, and contouring of the surface were also completed to more precisely identify ichnological and sedimentological features.

The results are illustrated in Figure 2. The photogrammetric model produced for this and other studies increases the confidence of track identification by reducing the impact of shadows and the limits of daylight. The three-dimensional reconstruction (Fig. 2A) allows us to recognize more than 40 individual tracks in at least four separate trackways (Fig. 2B), most of which are extremely difficult to identify in the field. As identification of additional tracks has just been completed, for the remainder of this paper we focus our analysis on the most conspicuous trackway which has benefited from longer-term analysis. The tracks that compose this trackway are shown in red in Figure 2B and outlined in chalk in Figure 3. The pace angulation, stride, and trackway width of this trackway are illustrated in Figure 5. These tracks are preserved as concave impressions into the bedding plane; in some the central portion is slightly elevated (Fig. 3C), perhaps resulting from the rearward movement of sand as the toes pushed the animal forward. This trackway is oriented N25E in present coordinates with all of the other tracks at this tracksite for which a direction can be determined appear to also be headed northward and northeastward (Fig. 2).

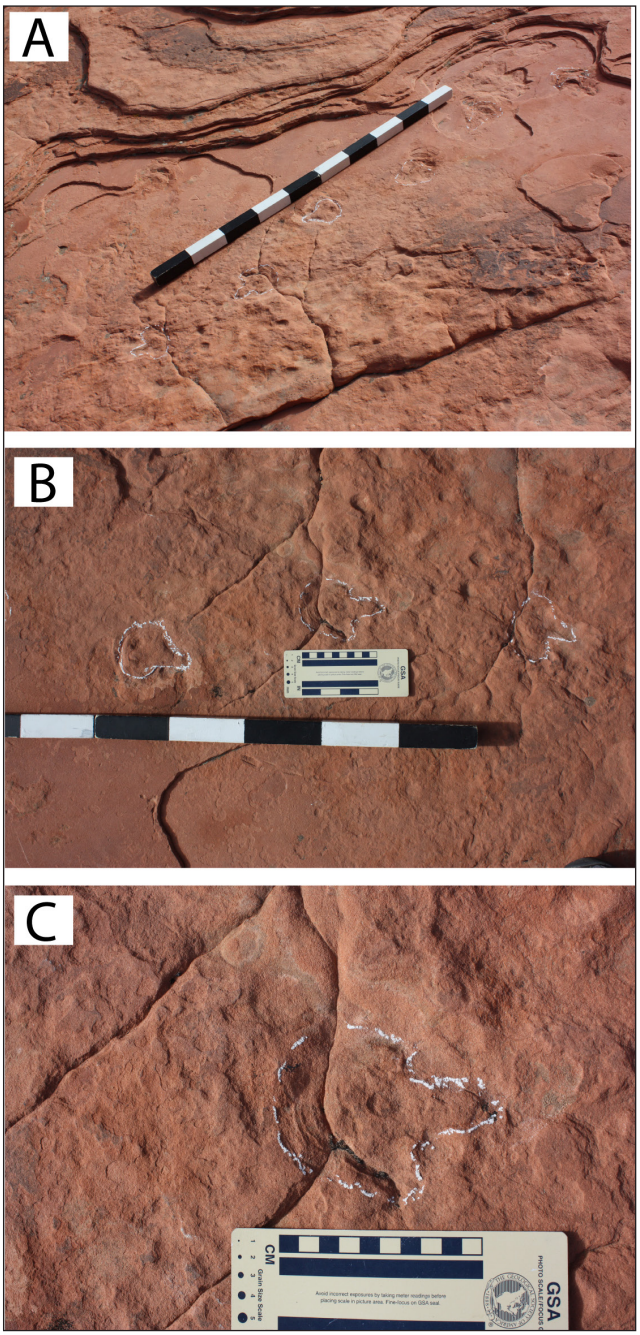

Figure 3. A. Oblique view of the most conspicuous *Grallator* trackway at this tracksite, with tracks outlined in white chalk. Scale is one m long, divided into decimeters. B. Three tracks in the same trackway. C. One of the *Grallator* tracks, outlined in chalk. The lack of distinct impressions of three digits in this and other tracks in this trackway indicates that they are undertracks.

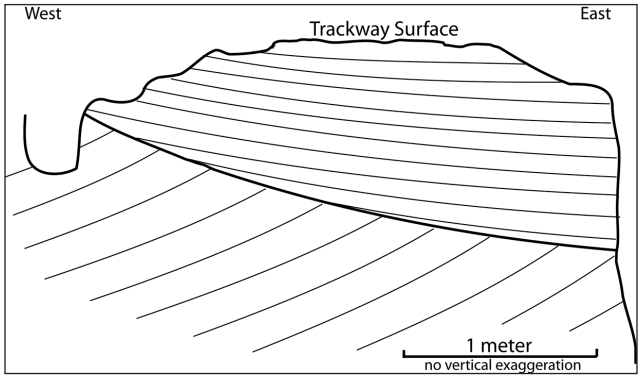

Figure 4. Cross-section sketch of the sedimentological setting of Tracksite UNLV-AZ-045, showing its position near the bottom of a crossbed set

How fast was this dinosaur moving?

Based on the work of Alexander (1976, 1989), Thulborn (1990), and Wright and Breithaupt (2002), we can determine whether this animal was walking or running, and its speed. In dinosaurs (including birds), the foot length is proportional to the hip height (*h*). For small theropods, such as the *Grallator* trackmaker, hip height is 4.5 times the foot length (Wright and Breithaupt, 2002). The foot length recorded in the most conspicuous trackway is 9.5 cm (Fig. 3C), so this animal's hip height is inferred to have been 43 cm. The stride is 53 cm (Fig. 5). Because this animal's foot length is considerably less than eight times the stride, we conclude that it was walking and not running (Wright and Breithaupt, 2002). For walking dinosaurs, the following formula is used to estimate the animal's velocity (Wright and Breithaupt, 2002):

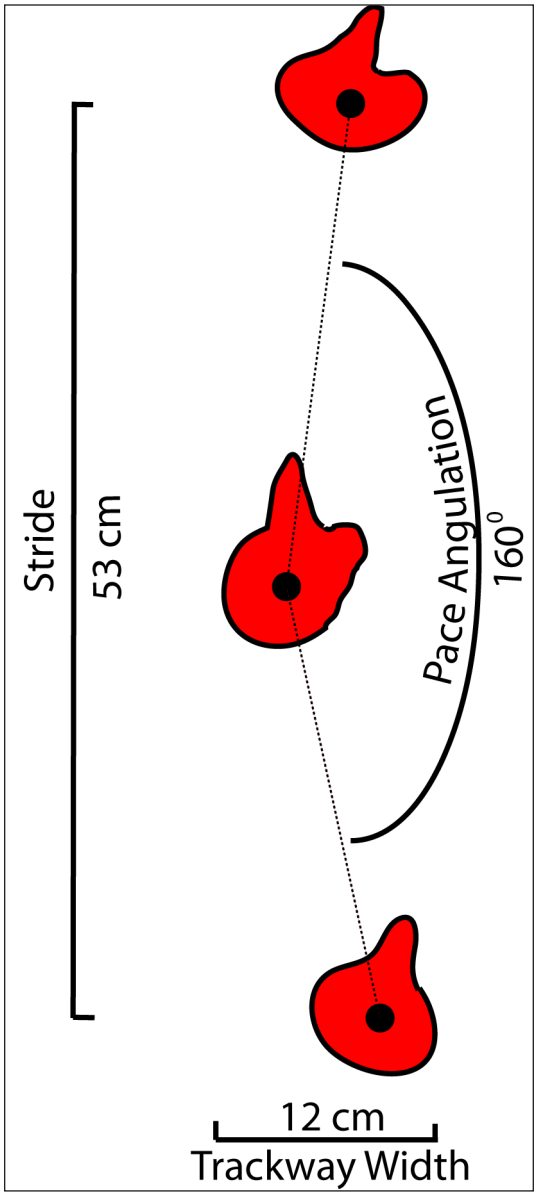

Figure 5. Measurements of the most conspicuous trackway at this tracksite..

$$V = 0.25g^{0.5}\ S^{1.67}\ h^{-1.17}$$

V = velocity in m/sec g = acceleration due to gravity (9.8 m/sec^2)
S = stride length h = hip height

Based on the measurements of this trackway, the results are as follows: V = 0.73 m/sec = 2.6 km/hr = 1.6 miles per hour. We conclude, therefore, that this dinosaur was walking very slowly, at a rate of 2.6 km/hr, as opposed to a faster pace which would indicate the trackmaker was chasing prey.

Discussion

The combination of sedimentological and ichnological features at this site suggests that this surface was a low point between adjacent dunes and that it was repeatedly traversed—perhaps over an interval of days, weeks, or months—by theropod dinosaurs heading north and northeast. We do not infer that this site records gregarious behavior in these dinosaurs, however it does suggest that small theropod dinosaurs were prevalent during at least some intervals of deposition of the Aztec Sandstone. At a more expansive Aztec Sandstone tracksite in Red Rock Canyon NCA, Rowland and Haight (2016) recorded five *Grallator* trackways, widely separated from one another, which record the passage of solitary animals, moving at different speeds in different directions over the same surface. In terms of the abundance of *Grallator* undertracks in sediments that were deposited in the toe of a dune, Tracksite UNLV-AZ-045 is similar to Tracksite UNLV-AZ-004 in Red Rock Canyon NCA (Rowland et al., 2014).

Conclusions

Along with previous work (Stoller et al., 2013; Rowland et al., 2014; Grove et al., 2019) this study supports the conclusion that theropods were an important component of the Jurassic ecosystem recorded in the Aztec Sandstone. Through the identification of *Grallator* tracks in multiple locations and their temporal and geographic relationship with *Brasilichnium* trackmakers, we can aid in the future identification of the paleoecological history of southern Nevada and southern California during the Jurassic Period (Grove et al., 2019). Tracksite UNLV-AZ-045 records the footsteps of many animals, at least one of which walked very slowly in a northeastward direction across the toe of a sand dune sometime between 200–170 Ma (Porter, 1985, 1987). Due to the presence of tracks on multiple bedding planes, other theropods may have preceded it by perhaps a few days or weeks, or perhaps the same animal repeatedly passed this way. This tracksite displays the type of preservation that is common in the Aztec Sandstone, and which can be expected to occur at other dinosaur tracksites within Valley of Fire State Park and elsewhere in Southern Nevada. Our study of tracks and trackways in the Aztec Sandstone is ongoing.

Acknowledgments

Thanks to Jennifer Lange for alerting DC about this tracksite and to CSN Professor Cindy Shroba for her key role in the early phase of this study. SEG gratefully acknowledges generous support from the Southern Nevada Conservancy. SMR thanks Park Manager Jim Hammonds for a permit to conduct research in Valley of Fire State Park. Special thanks to Josh Bonde for a helpful review.

References cited

Agisoft Metashape User Manual Professional Edition, Version 1.5, 2019,

Alexander, R.M., 1976, Estimates of speeds in dinosaurs. *Nature*, 261:129-130.

Alexander, R.M., 1989, *Dynamics of dinosaurs and other extinct giants*. New York: Columbia Univ. Press.

Bohannon, R.G., 1977, Geologic map and sections of the Valley of Fire region, North Muddy Mountains, Clark County, Nevada: U.S. Geological Survey Miscellaneous Field Studies Map MF-849, scale 1:25,000.

Grove, S.E., and Rowland, S.M., 2019, Dancing on the dunes: an ichnological examination of the Aztec Sandstone of the Southern Nevada region. Geol. Soc. Amer. Abstracts with Programs, v. 51, No. 5, ISSN 0016-7502.

Hamblin, A.H. and Bilbey, S.A., 1999, A dinosaur tracksite in the Navajo-Nugget Sandstone, Red Fleet Reservoir, Uintah County, Utah. *In* Gillette, D.D., ed., *Vertebrate Paleontology in Utah*, Utah Geological Suvey, Misc. Pub. 99-1, p. 51-57.

Irmis, R.B., 2005. A review of the vertebrate fauna of the Lower Jurassic Navajo Sandstone in Arizona. In: *Vertebrate Paleontology of Arizona*, R.D. Mc Cord, ed., Mesa Southwest Museum Bulletin No. 11, p. 55-71.

Lockley, M.G., 1991, *Tracking Dinosaurs: a new look at an ancient world*. Cambridge: Cambridge University Press, 238 p.

Lockley, M.G., and Hunt, A.P., 1995, Dinosaur tracks and other fossil footprints of the western United States. New York: Cambridge Univ. Press, 338 p.

Matthews, N.A., Noble, T., and Breithaupt, B.H., 2016, Close-range photogrammetry for 3-D ichnology: the basics of photogrammetric ichnology. *In* Falkingham, P.L., Marty, D., and Richter, A., eds., *Dinosaur Tracks: The Next Steps*. Bloomington & Indianapolis: Indiana University Press, p. 29-55.

Porter, M.L., 1987, Sedimentology of an ancient erg margin: the Lower Jurassic Aztec Sandstone, southern Nevada and southern California. *Sedimentology*, v. 34, p. 661-680.

Reynolds, R.E., 2002, California dinosaur tracks: inventory and management. *In* Reynolds, R.E., ed. *Between the Basins: Exploring the Western Mojave Desert and Southern Basin and Range Province*. Fullerton: California State Univ. Desert Studies Consortium, p. 15-18.

Reynolds, R.E., 2006, Jurassic tracks in California. *In* Reynolds R.E., ed. *Making Tracks Across the Southwest*. Fullerton: California State Univ. Desert Consortium, p. 19-24.

Rowland, S.M., and Caputo, M.V., 2016, *Trace Fossils in Relation to Eolian Stratification, Lower and Middle Jurassic Aztec Sandstone, Valley of Fire State Park, Southern Nevada*. SEPM (Society for Sedimentary Geology) Publication 119, 51 p.

Rowland, S.M., and Haight, G., 2016, An ichnotaxonomically diverse fossil tracksite with multiple *Grallator* trackways in the Aztec Sandstone (Jurassic) of Red Rock Canyon National Conservation Area, Las Vegas, Nevada. *In* Reynolds, R.E., ed. *Going LOCO: Investigations along the Lower Colorado River*. Fullerton: California State Univ. Desert Consortium, p. 303-308.

Rowland, S.M., and Mercadante, J.M., 2014, Trackways of a gregarious, dunefield-dwelling, Early Jurassic therapsid in the Aztec Sandstone of Southern Nevada. *Palaios*, v. 29, p. 539-552.

Rowland, S.M., Saines, M., and Stoller, H.M., 2012. Discovery of dinosaur tracks and arthropod tracks in the Aztec Sandstone (Lower Jurassic), Red Rock Canyon National Conservation Area, Las Vegas, Nevada. *In* Reynolds, R.E., ed., *Search for the Pliocene: the Southern Exposures*. Fullerton: California State Univ. Desert Studies Consortium, p. 182-183.

Rowland, S.M., Breithaupt, B.H., Stoller, H.M., Matthews, N.A., and Saines, M. 2014, First report of dinosaur, synapsid, and arthropod tracks in the Aztec Sandstone (Lower-Middle Jurassic) of Red Rock Canyon National Conservation Area, southern Nevada, *in* Lockley, M.G., and Lucas, S., eds., *Fossil Footprints of Western North America*. New Mexico Museum of Natural History and Science, Bulletin 62, p. 247-256.

Springer, K.B., Chiappe, L., Sagebiel, J.C., and Scott, E., 2009. Preserving California's only dinosaur trackways by collection—an unprecedented opportunity for public protection and interpretation of fossil specimens from federal land. *In* Foss, S.E. et al., eds., *Proceedings of the Eighth Conference on Fossil Resources,* St. George, Utah, p. 26-27.

Stoller, H.M., 2013, Ichnology and paleoecology of the Jurassic Aztec Sandstone. M.S. thesis, University of Nevada Las Vegas.

Stoller, H.M., Rowland, S.M., and Jackson, F.D., 2013, Dinosaur and arthropod tracks in the Aztec Sandstone of Valley of Fire State Park, Nevada. *In* Reynolds, R.E., ed., *Raising Questions in the Central Mojave Desert*. Fullerton: California State Univ. Desert Studies Consortium, p. 159-164.

Thulborn, T., 1990, *Dinosaur Tracks*. New York: Chapman and Hall.

Wright, J.L., and Breithaupt, B.H., 2002, Walking in their footsteps and what they left us: dinosaur tracks and traces. In *Dinosaurs: The science behind the stories*. Soc. Vert. Paleontol, p. 117-126.

Extension directions in the Colorado River Extensional Corridor compared to fragmentation of a structurally disrupted caldera in the Sacramento Mountains, southeastern California

Keith A. Howard[1] and Charles A. Ferguson[2]
[1]*U.S. Geological Survey, Moffett Field, CA 94035, khoward@usgs.gov*
[2]*Arizona Geological Survey, University of Arizona, Tucson, AZ 85701, caf@email.arizona.edu*

ABSTRACT—The northwest trend of the southern Colorado River extensional corridor in the southwestern USA veers northward between 34° and 35° north latitude. The tilt axes of early Miocene west-tilted volcanic strata in the west-central Sacramento Mountains mirror this bend. Steeply dipping early Miocene strata and volcanics north and south of the bend indicate the strong respectively westward to southwestward tilt of detached fault blocks and probably of the detachment fault on which they are superposed. These fault panels include fragments of the 18.8 Ma Peach Spring Tuff's (PST) source caldera. The PST occurs in two major detached fault domains in the Sacramento Mountains where outflow facies ignimbrite grades southward into intracaldera facies. The facies transitions, interpreted as part of the PST's source caldera's northeastern margin, lie on a northeast extensional azimuth that would restore them to continuity with the Silver Creek caldera in the Black Mountains, AZ, 50 km to the northeast. This extensional vector agrees with some but not other indicators of extension azimuth such as fault striae, ductile lineations, tilt axes, and elongated plutons. The new results imply spatial variability of extension direction and raise questions about the how this variability may relate to the bend in the Colorado River extensional corridor.

Introduction

The Colorado River extensional corridor south of Las Vegas, Nevada, forms one of several subregions within the Basin and Range that experienced a high degree of extension in Cenozoic time (Fig. 1). The extensional corridor exposes steeply tilted syntectonic volcanic and sedimentary deposits in shingled fault panels, structurally superposed on regional gently dipping extensional faults and metamorphic core complexes that were tectonically uplifted and unroofed from midcrustal levels during Miocene extension (Howard and John, 1987). Our mapping along the west side of the extensional corridor in and near the Sacramento Mountains provides new perspectives for evaluating the spatial variability in extension direction in an extensional corridor (Figs. 2, 3).

A revised stratigraphic and structural framework of detached extensional fault-bounded domains in the western Sacramento Mountains based on our new mapping improves an understanding of the synextensional Miocene stratigraphy including western fragments of the disrupted and extended source caldera for the Peach Spring Tuff (PST), one of the planet's most widely distributed

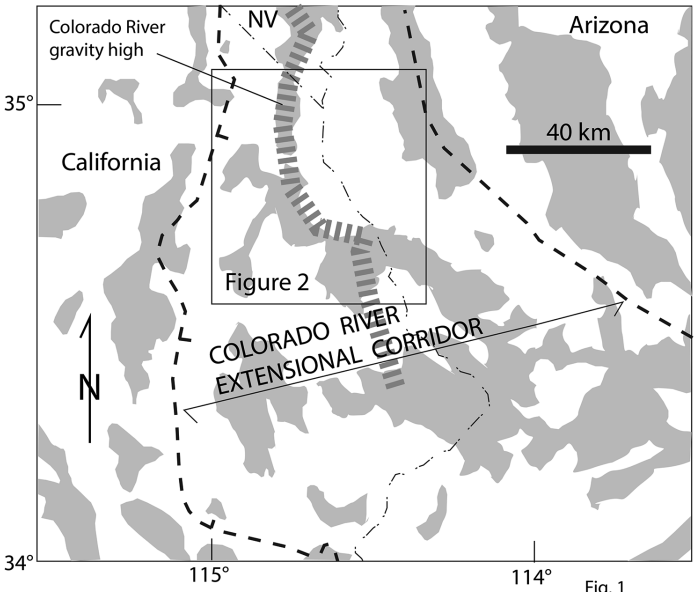

Fig. 1. Index map of the Colorado River extensional corridor in the southwestern USA. Mountain ranges are shaded and wide tracts of alluvial deposits shown white. Location of the Colorado River gravity high (Simpson et al., 1990) is derived from Mariano et al. (1986). Rectangle shows area of Figure 2. Metamorphic core complexes form a belt (wide dashed line) centered in the corridor.

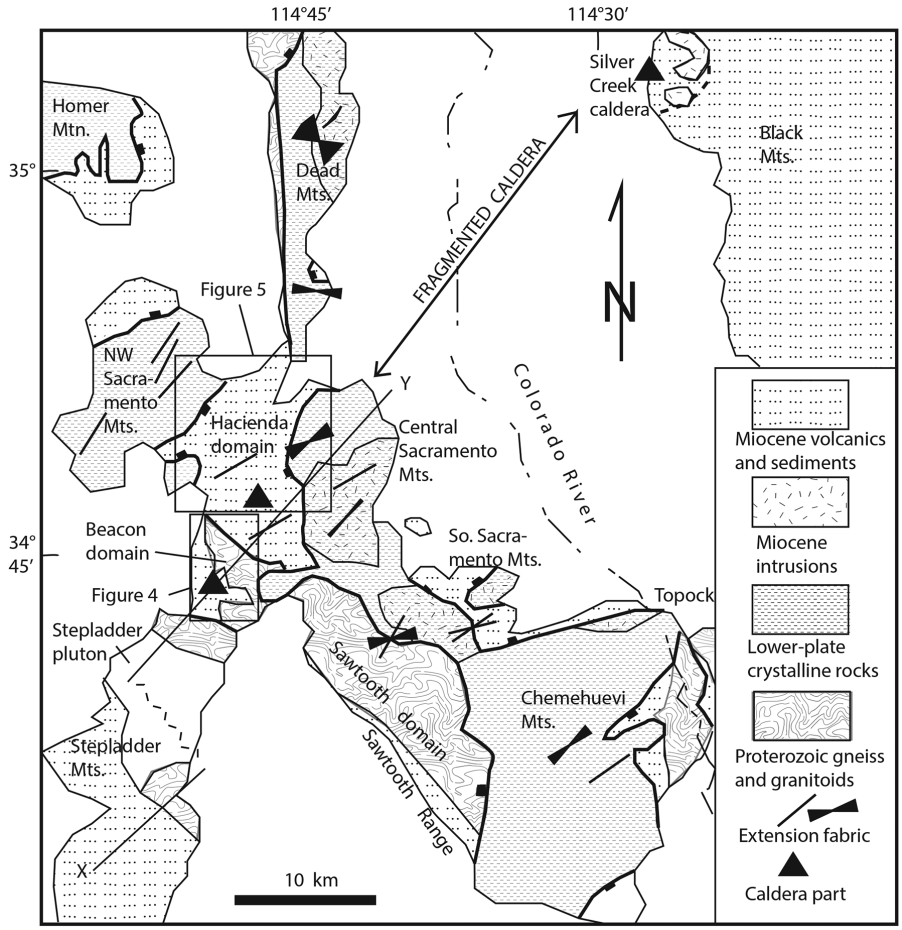

Fig. 2. A. Generalized geology of the Sacramento Mountains area in the west part of the Colorado River extensional corridor (in part after Campbell-Stone et al., 2000). Miocene intrusions that are within lower-plate crystalline rocks are shown patterned for both units. Quaternary to upper Miocene cover and some Cretaceous rocks are in white. The Silver Creek caldera is the recognized eruptive source of the Peach Spring Tuff (Ferguson et al. (2013). Major faults shown as heavy lines, with rectangular teeth on the upper plate of detachment faults. The orientation of extension fabrics (lines and bowtie fans, from Table 1) are for lineation and fault striae data highlighted (bold) in Table 1 as the most direct indicators of extension. X-Y approximates the (locally offset) line of the cross section sketched as Figure 6.

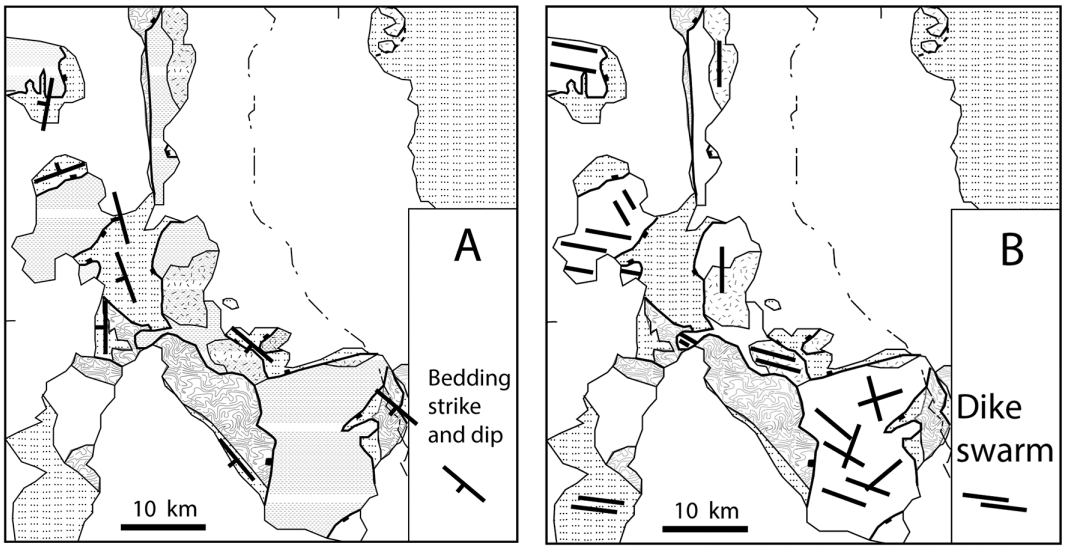

Fig. 3. Area of Figure 2, showing: Generalized strike and dip of Miocene bedding. Generalized orientations of Miocene dike swarms.

ignimbrites. Recognition of intracaldera and outflow facies of the tuff in two domains in the Sacramento Mountains allows reconstruction of fragments of the caldera, which confirms an NE–SW extension azimuth for the fragmented caldera (Ferguson et al., 2013). This azimuth of net extension for a geologic marker provides an independent check against which various previously determined fabric and other more localized structural indicators of extension direction can be compared.

Geologic framework

The eastern Mojave Desert in California and adjacent parts of Arizona and Nevada (Fig. 1) was part of the stable North American craton prior to Mesozoic time, the craton here consisting of a basement dominated by Paleoproterozoic gneisses and granitoids 1.8–1.6 billion years old (Anderson and Bender, 1989; Wooden and Miller, 1990; Wooden et al., 2012). Plutons 1.4 billion years old and diabase intrusive sheets 1.1 billion years old are

also present. The diabase sheets (Hammond, 1990) mostly had horizontal original orientations and provide a useful structural reference in these basement rocks to evaluate younger deformation (Howard, 1991).

After uplift and deep erosion, the Proterozoic rocks served as depositional basement for layers of Paleozoic shallow-marine continental platform strata (Stone et al., 1983). These strata were largely stripped from a region ~200 km across, centered along the lower Colorado River region, during post-Paleozoic orogeny and deep erosion. Active late Paleozoic and Mesozoic plate convergence along the western margin of southwestern North America led to a succession of Mesozoic magmatic and orogenic events that mobilized the crust as far eastward as the SW margin of the Colorado Plateau province. Granitoid plutons intruded the crust, with Late Cretaceous plutonism prominently affecting the eastern Mojave Desert region (Howard et al., 1987; Miller et al., 1990; John and Mukasa, 1990; Foster et al., 1991, 1992).

Paleogene erosion and Neogene setting

A post-orogenic Paleogene highland occupied the former Mesozoic orogenic and plutonic belt, forming a major drainage divide in the Mojave Desert region (Elston and Young, 1991; J. Howard, 1996; DeCelles, 2004; Shulaker et al., 2019). Evidence of 70–150°C of Paleogene cooling suggests 3–7 km of slow Paleogene denudation (Foster et al., 1991, 1992; Foster and John, 1999).

The margin of southwestern North America evolved in the early Miocene from a convergent margin to a transform margin (Dickinson and Snyder, 1979; Severinghaus and Atwater, 1990; Ward, 1991). A slab window is believed to have developed under southern California at the latitude of the Colorado River extensional corridor at 15–20 Ma (Atwater and Stock, 1998; Carter et al., 2006). This coincided with extension in the initially ~50-km-wide Colorado River extensional corridor. Extension and related magmatism migrated northward approximately coincident with the northward migration of the Mendocino triple junction and the slab window (Glazner and Supplee, 1982; Glazner and Bartley, 1984). As magmatism migrated northward in the Colorado River extensional corridor it peaked slightly earlier than the highest rates of extensional faulting (Gans et al., 1989; Gans and Bohrson, 1998; Gans and Gentry, 2016).

Colorado River extensional corridor

The 50–100 km wide Colorado River extensional corridor displays a common set of structural elements responsible for doubling its width (stretching factor beta = 2): a system of breakaway or headwall faults on the up-dip side of the fault system, numerous fault blocks tilted toward the breakaway, a central zone of updomed extensional faults and metamorphic core complexes, and a distal zone where the fault system roots downdip under less deformed blocks (Fig. 4). At depth a bulge in the middle crust approximately coincides with the updomed core complexes (McCarthy et al., 1991).

An excellent geologic framework of the Sacramento Mountains part of the extensional corridor was provided by McClelland (1982, 1984), Spencer and Turner (1982, 1983) and Spencer (1984, 1985), building on unpublished mapping by the Southern Pacific Land Company. Later detailed studies further enhanced this framework (Simpson et al., 1991; Fedo, 1993; Fedo and Miller, 1992; Campbell and John, 1996; Pease and Argent, 1999; Pease et al., 1999; Campbell-Stone et al., 2000; Campbell-Stone and John, 2002). Tilted lower Miocene volcanic and sedimentary rocks occupy upper-plate positions there, structurally superposed on a domed detachment fault system over metamorphic and plutonic rocks in the mountain cores (Fig. 4; McClelland, 1982, 1984; Spencer, 1985; Pease and Argent, 1999; Pease et al. 1999; Campbell-Stone et al., 2000).

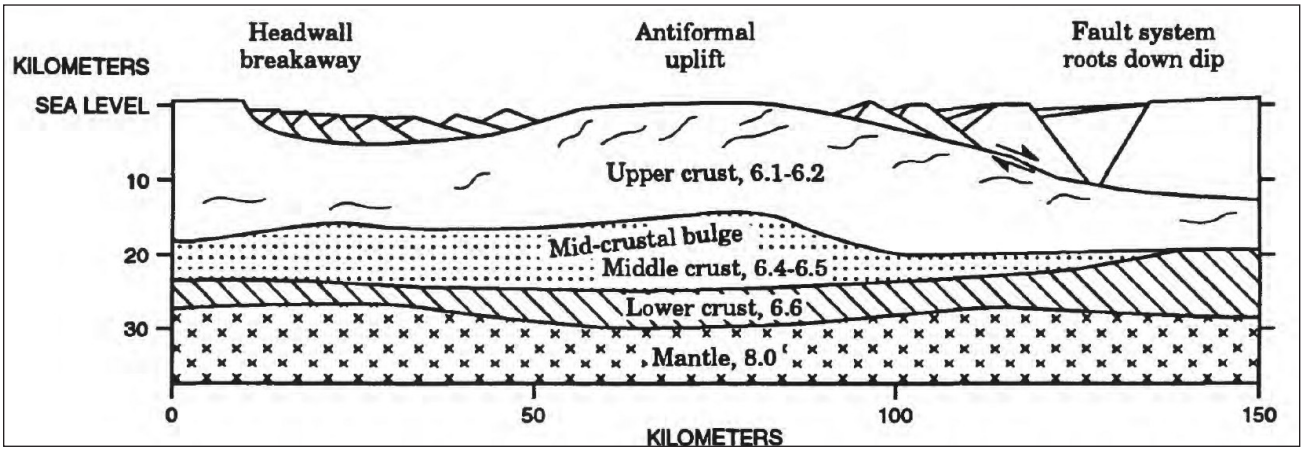

Figure 4. Schematic cross section of the Colorado River extensional corridor (Howard et al., 2019). Seismic velocities are in km/s for a velocity model across the Whipple Mountains area (McCarthy et al., 1991). Alternative models can include secondary breakaway faults and multiple rooted faults (Spencer, 1985; Gans and Gentry, 2016).

Miocene stratigraphy in the Sacramento Mountains

The early Miocene stratigraphy throughout the extensional corridor and adjacent regions (Sherrod and Nielson, 1993) commonly begins with a lower volcanic section of intermediate, mafic, and silicic rocks hundreds of meters thick (Carr, 1991; Nielson and Beratan, 1995; Howard et al., 1999, 2013, 2019). A widespread rhyolitic ignimbrite, the 18.8 Ma Peach Spring Tuff (PST), caps this lower volcanic section across much of the area of Figure 2. Emplacement of the PST coincided in this area with a marked slowing of magmatism and with the onset of major extensional faulting accompanied by thick sedimentary accumulations. Extensional faulting and tilting began ca. 20–23 Ma and ended by ca. 12 based on unconformities and fanning dips within dated Miocene stratigraphic sections. Farther north in the corridor younger compositional counterparts of the thick lower volcanic section mostly overlie the PST as the Patsy Mine Volcanics.

The 3-part Miocene succession in the Sacramento Mountains consists of the volcanic-dominated lower sequence, the overlying PST, and an upper sequence of tuff, basalt, and thick sedimentary rocks. The Miocene stratigraphy differs in some respects among fault-block domains into which we divide upper-plate rocks in the west-central and southwestern Sacramento Mountains: the Sawtooth, Beacon, and Hacienda domains (Figs. 2, 5).

Lower volcanic sequence —volcanic rocks of Snaggletooth

Volcanic flows, breccias, and tuffs of basaltic, intermediate, and rhyolitic composition and interbedded sedimentary rocks form the Miocene lower volcanic sequence (labeled Tvs in Fig. 6; >18.8 Ma in Fig. 7). We refer to the sequence informally as the volcanic rocks of Snaggletooth (shortened here for convenience to Snaggletooth volcanics) for outcrops at Snaggletooth pinnacle in the southern Sawtooth Range (Fig. 2). Sedimentary rocks up to 150 m thick interbedded with the volcanic rocks in the west-central Sacramento Mountains include shale, limestone (including dolomite and magnesite), and chert (Vitaliano, 1950; McClelland, 1982, 1984; Miller and Leach, 1993). Similar magnesite-bearing lacustrine and volcaniclastic rocks in the Black Mountains occur interbedded with pre-caldera dacitic lavas that are truncated along the southeastern margin of the Silver Creek caldera (Fig. 2; McCosby et al, 2015; Ferguson et al., 2017).

In the Beacon domain sedimentary rocks occur both at the base and near the top of the Snaggletooth volcanics (Fig. 6). Thin basal conglomerate locally rests directly on basement crystalline rocks there. Carbonates, chert, and shale imply lacustrine deposition and their limited distribution records deposition in small basins, perhaps isolated by volcanic flows. The interbedded volcanic rocks that dominate the Snaggletooth volcanics were dated in the Stepladder Mountains and southern Sawtooth domain as ranging from about 22 to 19 Ma (Fig. 1; Howard et al., 1993; Chapman et al. 2018). A welded biotite dacite tuff up to 100 m thick forms the upper unit of the Snaggletooth volcanics in the Hacienda domain and on the east flank of the NW Sacramento Mountains. We tentatively correlate this tuff to the Cook Canyon Tuff of Buesch and Valentine (1986), which directly underlies the PST at Kingman, Arizona.

The Snaggletooth volcanics reach about 700 m thickness in the Beacon and Sawtooth domains, where their nonconformable base on Proterozoic gneisses shows as much as 200 m of local relief. Thin basalt takes the place of the Snaggletooth volcanics on the north flank of the NW Sacramento Mountains. Some mapped faults in the Snaggletooth volcanics in the Beacon and Sawtooth domains terminate westward against the PST and may record faulting and an unconformity before the PST was emplaced.

Peach Spring Tuff

The PST ignimbrite forms an important stratigraphic and structural marker in the Colorado River extensional corridor and surrounding regions. Magnetic polarity measurements in the tuff documented vertical-axis rotations of various structural blocks in the region and

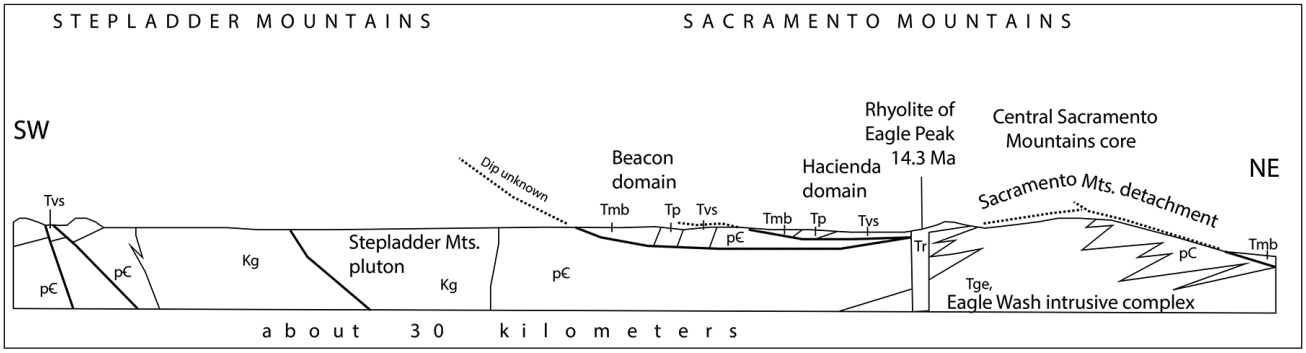

Fig. 5. Cross sectional sketch from the Stepladder Mountains across the Sacramento Mountains (located approximately along XY in Figure 2) showing relations between the fault domains. pC = Proterozoic rocks. Kg = Cretaceous granodiorite. Tge = early Miocene Eagle Wash intrusive complex. Tvs = Snaggletooth volcanics. Tp = Peach Spring Tuff (caldera facies). Tmb=upper sedimentary and volcanic sequence. Tr = rhyolite of Eagle Peak (post-detachment).

also identified flow fabrics that helped point toward its eruptive source area (Wells and Hillhouse, 1989; Hillhouse and Wells, 1991). Detailed studies of the tuff and related volcanic rocks established the igneous processes leading up to and following its eruption (Pamukcu et al., 2013; McDowell et al., 2014; Barry et al., 2015).

At its proxy type section at Kingman, Arizona (Young and Brennan, 1974), approximately 30 km northeast of the partial Silver Creek caldera in the Black Mountains from which it erupted (Fig. 2; Ferguson et al., 2013), the PST forms a classic outflow sheet of mostly densely welded ignimbrite up to 180 m thick. At the Kingman section, the PST overlies a biotite-rich dacitic, locally welded tuff known as the Cook Canyon Tuff (Buesch and Valentine, 1986; Ferguson and Cook, 2015a), and is overlain by a 17.6-Ma, high-silica, phenocryst-poor rhyolite tuff containing conspicuous, euhedral sanidine phenocrysts up to 6 mm across known as the tuff of Bonelli House (Regula et al. 2015; Ferguson and Cook, 2015a, 2015b).

At Kingman the PST is a single flow unit that can be divided into 4 lower zones or members (Ferguson and Cook, 2015a) defined by welding characteristics, and a localized 5th uppermost Warm Springs zone (member) defined by an abrupt upward, normal (more mafic upwards) zonation from rhyolite to trachyte accompanied by phenocryst content increasing from 15-35% (Ferguson et al., 2013, Ferguson and Cook, 2015b). The distinctive uppermost Warm Springs zone (member) provides a direct link between the main mass of the ignimbrite's moderately phenocryst-poor rhyolite outflow sheet and its trachytic, very phenocryst-rich intracaldera facies, which originally was described by Ransome (1923), and interpreted as an intracaldera ignimbrite by Thorson (1971). Despite the contrast in composition between the two facies, Thorson (1971, in his appendix) suggested that the two might be correlative, but this relationship was not confirmed until it became clear that the uppermost Warm Springs zone (member), which is limited to areas within 20 km of the caldera, was an integral part of the ignimbrite (Ferguson et al., 2013).

The PST crops out in the Sacramento Mountains as outflow facies in the northern part of

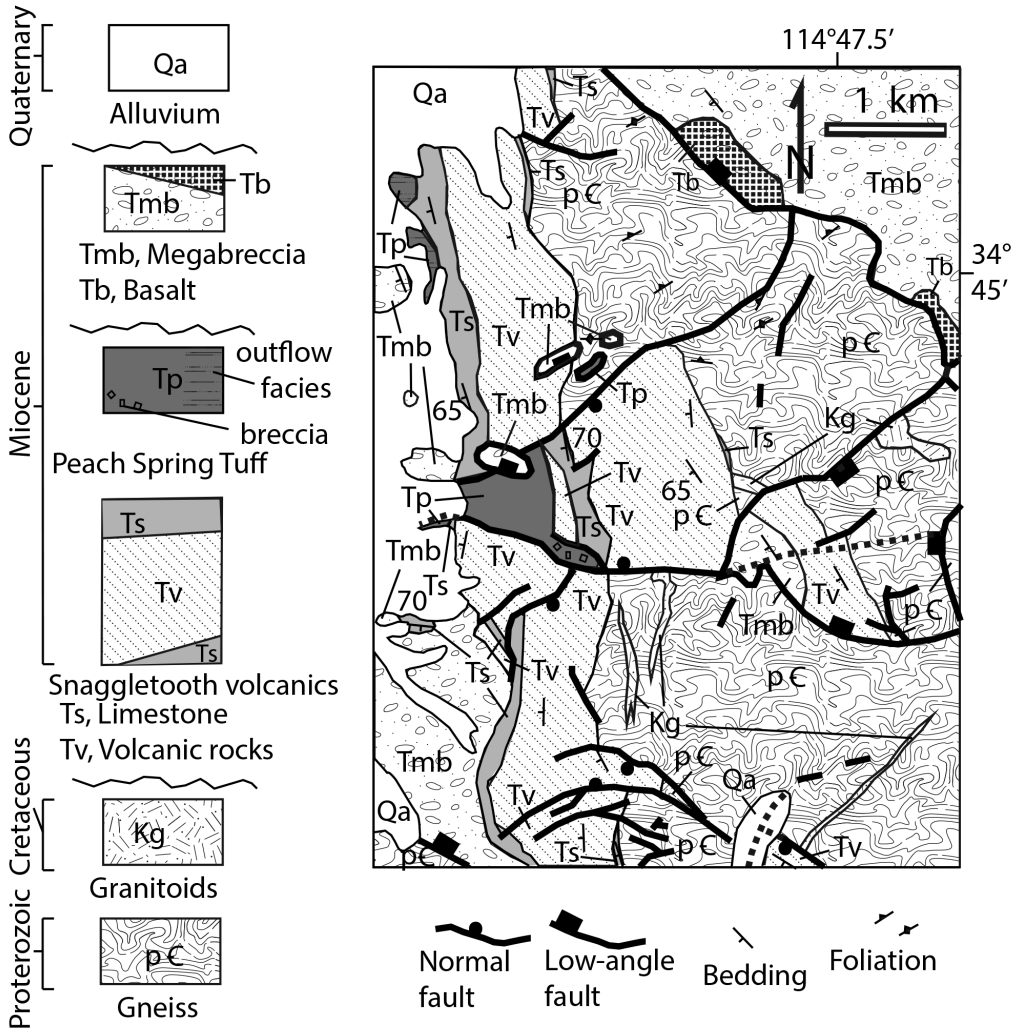

Fig. 6. Geologic map of part of the Beacon domain (see location in Fig. 2). Unconformities indicated by wiggly lines in legend. W-tilted fault panels include a fault-bounded remnant of 600-m-thick caldera-fill facies of the Peach Spring Tuff (Tp). If viewed down structure from the right using the method of Mackin (1950), the thick (caldera facies) Tp is bounded by two faults that diverge structurally downward (eastward) such that older rocks stratigraphically beneath the caldera facies of the tuff appear to define a block bounded by reverse faults, reminiscent of downward-widening sandbox models of collapse calderas (Roche et al., 2000; Howard, 2010). Megabreccia and basalt in the structurally higher Hacienda panel are in the upper right part of the map. The lower left corner of the map area exposes the fault on which the Beacon domain panels are superposed on Proterozoic rocks of the Stepladder Mountains. Not all faults are shown.

the Beacon and Hacienda domains and in the southern part of the Sawtooth domain, where it may reach 110 m thick (John, 1987b; Howard et al., 1993). The tuff thins to zero thickness north of our three domains on the north flank of the NW Sacramento Mountains, where basalt flows underlie and overlie it. Outflow facies ignimbrite in the Hacienda domain had been divided into a sequence of 3 distinct unidentified tuff units by Spencer and Turner (1982) with uncertain correlation with the PST (Spencer, 1985). These tuff units (their Tt2, Tt3, Tt4) are not separated by obvious flow-boundary or cooling unit boundary contacts and are herein interpreted to correlate with zones in the single cooling unit sequence of the Peach Spring Tuff recognized near Kingman. We correlate Tt2 with the lower two rhyolitic zones (members) of the Kingman sequence of

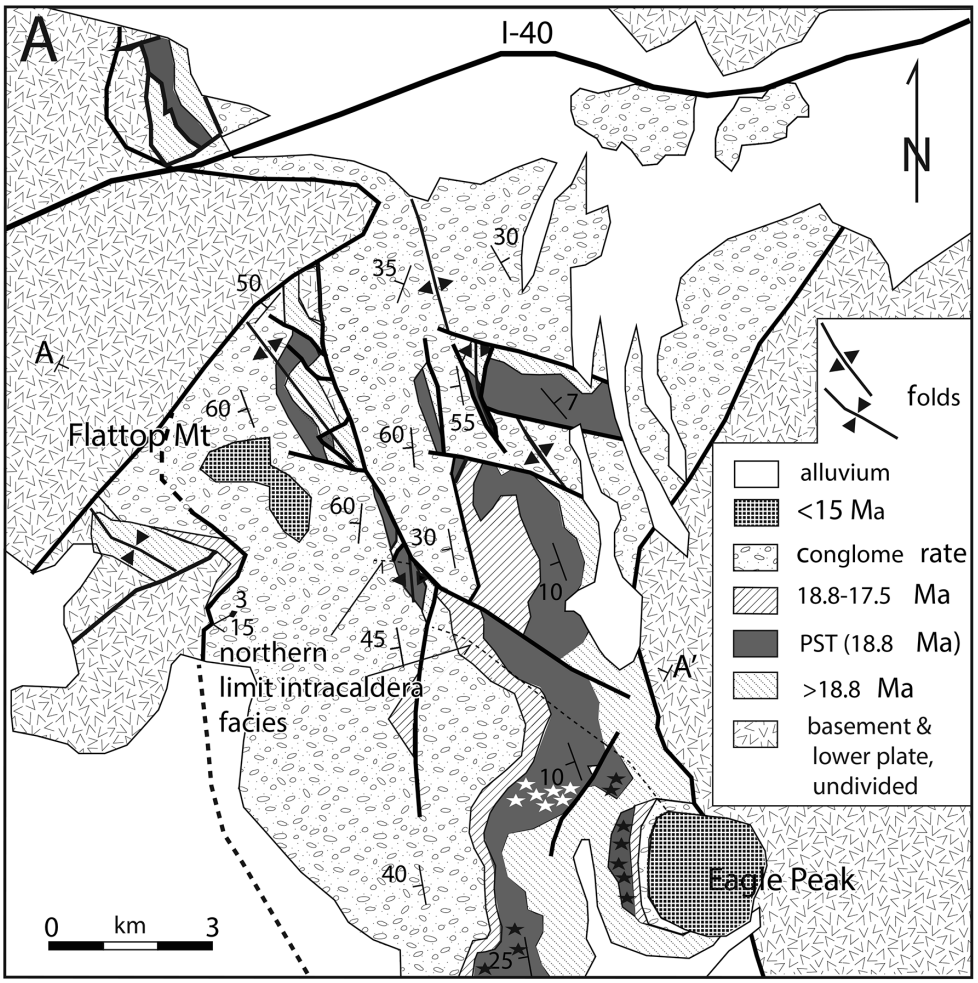

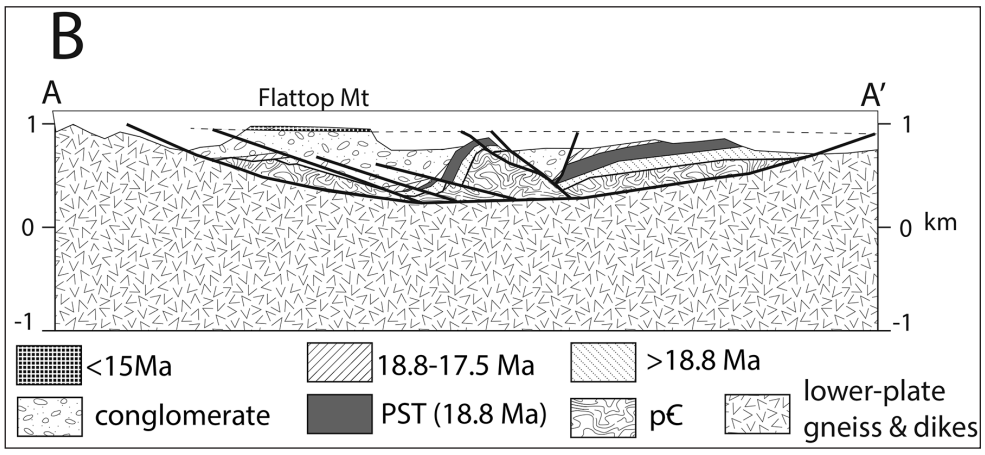

Fig. 7A. Simplified geologic map of part of the Hacienda domain, reinterpreted from mapping by Spencer and Turner (1983) and McClelland (1984) and including new mapping from this study. Units are divided by age into (1) alluvium (Quaternary), (2) <15 Ma (mafic flow of Flattop Mountain and rhyolite of Eagle Peak), (3) conglomerate (conglomerate, breccia, and sparse intervals of lacustrine limestone and fine-grained sedimentary rocks, all part of the upper sequence), (4) 18.8–17.5 Ma (correlated to the Patsy Mine Volcanics, here primarily two ash-flow tuff units correlated to the tuff of Bonelli House, the younger being a 17.6-Ma rhyolite ignimbrite), (5) PST 18.8 Ma (Peach Spring Tuff, consisting of caldera facies in the southern half of the map, and showing >30 m megablocks of older rocks as solid stars, and megablocks of older PST as white stars), (6) >18.8 Ma (Snaggletooth volcanics, here chiefly andesitic-dacitic volcanics with lesser volcaniclastic and locally lacustrine rocks), and (7) basement (gneisses and Miocene dikes). Some faults are not shown, including a down-to-the east normal fault that cuts the mafic flow of Flattop Mountain (Spencer and Turner, 1982) and postdates the detachment fault.

Fig. 7B. Simplified NW-SE cross section (AA' on Fig. 7A; units are as in Fig. 7A). A prominent roll-over anticline apparently relates to a prominent, low-angle, down-on-the east normal fault(s), that is cut by and structurally repeated by a younger down-on-the east normal fault. Faults on either end of the cross-section presumably connect at depth as parts of the Sacramento Mountains detachment fault system in a broad down-warp, against which upper-plate faults would truncate.

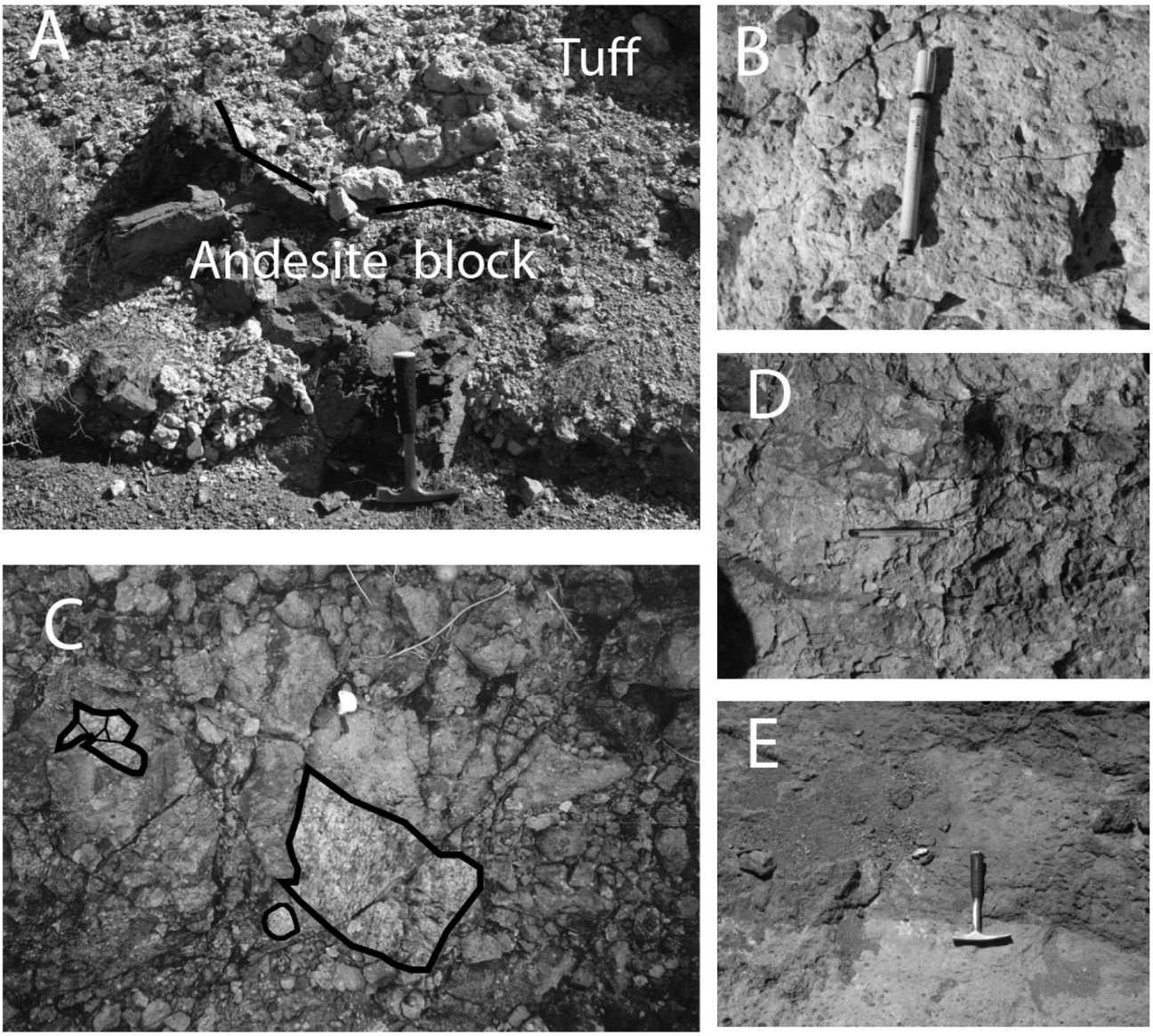

Fig. 8. Field photos of intracaldera-facies Peach Spring Tuff and related rocks (in the Beacon domain except where indicated).
A. Dark andesite block 0.6 m across in light-toned PST (hammer for scale) in a klippe (Hacienda domain) superposed on the Beacon domain in the area of Fig. 2.
B. Dark lithic clasts in light-toned PST. Pen is 14 cm long.
C. Granodiorite-clast breccia in PST matrix. Field of view is about 1 m wide. Some of the granodiorite clasts are outlined
D. Dark psuedotachylyte veins in the PST in the 600-m-thick caldera-facies section. Pen near center is 13 cm long. The veins imply faulting after relatively deep burial of the tuff.
E. Contact between dark welded tuff clast 5 m across against light-toned PST matrix in the Hacienda domain (hammer for scale). The dark tuff mineralogically and lithologically resembles the PST and may represent a facies of it.

Ferguson and Cook (2015b) and we correlate Tt3 with the middle two rhyolitic zones there. We correlate Tt4 directly with the uppermost Warm Springs trachyte zone (member). Intracaldera mesobreccia matrix in the Hacienda domain at the one locality where it has been analyzed is trachytic (Barry et al., 2015).

The Hacienda and Beacon domains also expose intracaldera (caldera-fill) facies of the PST. The intracaldera-facies In the Hacienda domain (Figs. 7, 8D) includes both mesobreccia (containing numerous small clasts visible within a single outcrop; Lipman, 1976) and large exotic blocks. At least a dozen megabreccia blocks up to 300 m across are composed of Snaggletooth volcanics, limestone, and granite (solid stars in Fig. 7A). The mesobreccia typically has poorly welded matrix. Locally, the ignimbrite adjacent to the megablocks is densely welded and vitric. The intracaldera ignimbrite is up to 400 m thick and thins and transitions abruptly northward into outflow facies. A dashed line (Fig. 7A) demarcates this transition as the NE limit of megabreccia lenses and(or) megabreccia blocks in the ignimbrite, NE of which the Kingman welding zonations abruptly appear within a

distance of <300 m. Additionally, just to the south of the transition, arrays of large (up to 200 m across) jigsaw-fit blocks of welded, outflow-facies rhyolite ignimbrite occur as megabreccia blocks (open stars in Fig. 7A) suspended within poorly welded mesobreccia in trachyte matrix. The proportion of mesobreccia matrix relative to megablocks increases to the south, and blocks of outflow facies become larger and more closely spaced to the NE, where the blocks merge gradually into intact, continuous outflow facies ignimbrite.

We interpret the caldera margin in the Hacienda domain as a southwest-tilted trap-door hinge-like margin where a pre-caldera rhyolitic outflow facies was flexed and broken into blocks surrounded by a culminating, super-eruptive, caldera-forming trachyitic (mostly mesobreccia) phase. The uppermost, Warm Springs trachyte zone (member) of the outflow sheet might therefore represent the only part of the super-eruption that escaped the caldera. Presumably, although not yet identified, rhyolitic composition PST might be expected to occur on the "floor" of the caldera. Consistent with this scenario, the northernmost occurrence of megabreccia (Fig. 7) is near the top of a normal section of outflow facies "rhyolite" that is capped and enveloped by phenocryst-rich ignimbrite that resembles the Warm Springs "trachyte" zone (member).

In the Beacon domain the tuff includes an intracaldera-facies thickness reaching at least 600 m (Fig. 6). There it locally includes a pod of granodiorite-clast-rich mesobreccia in tuff matrix (Fig. 8C). The granodiorite clasts match porphyritic biotite granodiorite of the Late Cretaceous Stepladder pluton to the west, from which the western panel is structurally detached. Discrete quartz 5–10 mm across characterizes that pluton and distinguishes it from otherwise similar Late Cretaceous biotite granitoids elsewhere in the eastern Mojave Desert. Small bodies of granodiorite porphyry that may be hypabyssal equivalents of that pluton intrude Proterozoic rocks underlying the Snaggletooth volcanics in the Beacon domain (Fig. 6).

Upper sedimentary and volcanic sequence

The upper sequence, above the PST, comprises tuff, basalt and many hundreds of meters of conglomerate and sedimentary breccia, exposed most extensively in the Hacienda domain (Fig. 7; Spencer and Turner, 1983; McClelland, 1982, 1984; Fedo and Miller, 1992; Miller and Leach, 1993; Fedo, 1993). Dips show an upward fanning geometry indicative of syndepositional tilting and faulting. Previous workers considered the dominantly sedimentary upper parts in the western Sacramento Mountains to constitute a structurally high plate detached from and faulted onto the volcanic rocks (Spencer and Turner, 1983; Spencer, 1985; McClelland, 1982, 1984; Simpson et al., 1991; Miller and Leach, 1993). We find evidence the upper sequence is structurally detached only locally from lower volcanic rocks; instead tuffs and bedded sedimentary rocks depositionally overlie the Peach Spring Tuff, and higher thick sedimentary rocks in the sequence fill paleovalleys cut into them. An unconformity at the top of the PST is indicated by steeper dips in the tuff than in the higher sedimentary rocks, and by faults that cut the PST and truncate upwards at the base of the sedimentary rocks. Two distinctive post-PST ignimbrites near the base of the upper sequence are correlated tentatively to the <17.6-Ma tuff of Bonelli House.

Clasts in the thick sedimentary rocks of the upper sequence, including abundant breccias, are largely dark orthogneiss and paragneiss, or light-toned porphyritic granodiorite some of which lithologically matches the Stepladder pluton (Miller and Leach, 1993). The upper sequence also includes an apparent landslide deposit 1 km long formed of nearly intact Snagglethooth volcanics and PST in the northeastern part of the Hacienda domain. On the north flank of the NW Sacramento Mountains the upper sequence consists of mafic and silicic lava flows of overlain by hundreds of meters of granite-clast and gneiss-clast conglomerate, diamictite, and breccia. In the Chemehuevi Mountains sedimentary rocks of the upper sequence unconformably overlie the PST and were shown to record rapid sedimentation into growing middle Miocene half-graben basins as the extending upper crust fragmented and the core complex was eventually unroofed (Miller and John, 1999).

Structure

The Colorado River extensional corridor and its chain of core complexes trend NW in the southern part of the area of Figure 1 but veer northward into Nevada in the northern part of the area of Figure 1. Tilt axes of tilted fault panels in and near the Sacramento Mountains reflect this change in trend (Fig. 3A). The structurally low Sawtooth domain (in and near the Sawtooth Range, Fig. 2) consists of steeply SW-tilted fault-bounded panels. Nearly on strike to the north, the Beacon domain occupies a similar structural position (included in plate A of McClelland, 1984) but is west-tilted. The structurally higher, more eastern Hacienda domain (plates B and C of McClelland, 1984) sits geographically between the Beacon domain and the subjacent central Sacramento Mountains core.

The Sawtooth domain forms a major steeply SW-tilted fault panel of Snaggletooth volcanics overlain by PST and their depositional Proterozoic basement. To the NW the tilt direction bends abruptly to W at the south end of the otherwise similar Beacon domain of Miocene volcanic and sedimentary rocks and their basement (in plate A of McClelland, 1984) (Fig. 6). The structurally higher Hacienda domain sits to the east geographically between the Beacon domain and the subjacent central Sacramento Mountains core (Fig. 7).

The Sawtooth domain's steep SW tilt is shown by dips of the Snaggletooth volcanics and by Proterozoic diabase sheets tilted to near vertical (Howard, 1991;

Campbell-Stone et al., 2000). Similarly steeply tilted diabase occurs in extensional fault blocks of basement rock in the Chemehuevi and Mohave Mountains to the southeast in the extensional corridor (Howard, 1991, 2011; Howard et al., 1999, 2013). A paleomagnetic site in the PST in the southern Sawtooth domain showed no apparent vertical-axis rotation after correcting for tilt, but approximately 29° anticlockwise rotation for another PST site there (Wells and Hillhouse, 1989).

The Beacon domain along strike to the NW is structurally superposed against Proterozoic basement gneiss in the Stepladder Mountains along one of the breakaway faults for the extensional corridor (Figs. 2, 5). Steeply west-tilted fault panels in the Beacon domain restore structurally westward over Proterozoic and Cretaceous basement exposed in the Stepladder Mountains. The southwestern part of that basement is tilted less in the southern Stepladder Mountains where it is nonconformably overlain by a faulted gently SW-dipping section of Snaggletooth volcanics (Fig. 5; Howard et al., 1993). Younger basalt dated 18.1±0.6 Ma overlies a western part of the Stepladder pluton (Howard et al., 1982).

Extensional fault klippen of the Hacienda domain are superposed onto the Beacon domain (Figs. 5, 6). Miocene rocks in the Hacienda domain are in part less steeply tilted than in the Sawtooth and Beacon domains (Fig. 5). Dominantly W to SW stratal dips in the Hacienda domain (Fig. 7) imply that it is displaced relatively eastward to northeastward over both the Beacon domain and the metamorphic core (McClelland, 1984). Clast provenance and sedimentology in alluvial deposits of the upper sedimentary sequence in the Hacienda domain were interpreted to indicate that they were structurally displaced eastward from proximal sources in the Stepladder pluton (Miller and Leach, 1993). The gently tilted eastern half of the Hacienda domain forms the eastern limb of a major anticline (Fig. 7B). It may have been east-tilted before being back rotated or experienced fault drag to decrease its apparent tilt.

The mountain-core footwalls below the Sacramento Mountains detachment fault system expose early Miocene (20–18 Ma) plutons and dike swarms intruded into Proterozoic gneisses (Pease et al., 1999; Campbell-Stone et al., 2000). Mylonitized 20–19 Ma granodiorite records emplacement at midcrustal levels (7–12 km) in the central Sacramento Mountains followed shortly by ductile extensional shearing at temperatures between 600° and 450°C, while antithetic ductile to brittle shears characterize originally shallower rocks in the NW Sacramento Mountains, and 18-19-Ma diorite and granite occupy the core of the southern Sacramento Mountains where they cut mylonitic fabrics (Pease and Argent, 1999; Pease et al., 1999; Campbell and John, 1996; Campbell-Stone et al., 2000; Campbell-Stone and John, 2002). Modeling of a gravity high over the post-mylonite diorite in the southern Sacramento Mountains led Campbell-Stone and John (2002) to conclude that steep early Miocene dike-like intrusions through much of the crustal thickness accommodated about 10 km (range 5–18 km) of northeast-southwest crustal extension there, separate from the extensional faulting at higher crustal levels. The rocks below the system of detachment faults rocks were tectonically unroofed in the middle Miocene (Spencer, 1985; Pease et al., 1999; Campbell-Stone et al., 2000), as in the adjacent Chemehuevi Mountains to the south (John, 1987a; Miller and John, 1999; John and Foster, 2003; Carter et al., 2006).

A flat-lying 14.6±0.2-Ma mafic lava flow capping Flattop Mountain stratigraphically overlies the upper sedimentary and volcanic sequence in the Hacienda domain and postdates extensional tilting at this latitude (Spencer, 1985). Additional evidence of the end of major detachment faulting on the west side of the central Sacramento Mountains comes from the nonconformable overlap of an exhumed part of the Sacramento Mountains detachment fault by the rhyolite of Eagle Peak (Figs. 5, 7A), dated by John Nakata at about 14.3 Ma (14.0±0.4 K/Ar sanidine, 14.6±0.4 Ma K/Ar biotite; Simpson et al., 1991).

Caldera correlation and subcaldera architecture

The following criteria robustly correlate the PST-filled caldera fragments in the Sacramento Mountains to the Silver Creek caldera in the Black Mountains (Fig. 2; Ferguson et al., 2013): (1) lithologic identification of the zoned PST, (2) stratigraphic position of the tuff, as at Kingman, between units lithologically correlated to underlying Cook Canyon Tuff and overlying tuff of Bonelli House, (3) presence of similar underlying magnesite-bearing Miocene sedimentary rocks as at the Silver Creek caldera, (4) exceptional local PST thickness in the Beacon (600 m) and Hacienda (400 m) domains, (5) thin-section petrologic identification of Peach Spring Tuff matrix, and precise dating of sanidine phenocrysts in the matrix (Ferguson et al., 2013) for breccias , (6) clasts in these breccias include older volcanics (Fig. 8A), limestone, granodiorite (Fig. 8C), and also welded PST (Fig. 8E).

Clasts in the tuff-matrix breccias are inferred to be derived from gravitational failure of caldera wall as the caldera floor collapsed during emplacement of the tuff. The local thickness as much as 600 m requires development of a syneruption depression. The correlation of the caldera facies to the PST seemingly records collapse into a caldera above a single magma chamber system eviscerated during eruption of the tuff. We confirm Ferguson et al. (2013)'s proposed correlation of the Sacramento Mountains caldera fragments to the Silver Creek caldera in the Black Mountains as parts of an original caldera.

Faults that bound the two sides of the thickest (600 m) tuff section diverge eastward, stratigraphically downward in the subcaldera basement (Fig. 6, Beacon domain). This fault pattern, if viewed downstructure from the east, resembles reverse faults that bound a central, upward-narrowing collapse plug in some sandbox and other

caldera-collapse analogs (Roche et al., 2000; Howard, 2010). These two faults may postdate caldera collapse, but if they date from the collapse, they may bound the downdrop shape of a narrow caldera segment such as a corner, the floor block widening downward and eastward.

The PST intracaldera facies crops out as much as 8 km along strike in the Hacienda domain (Fig. 7A). Identification there of a SW-facing trap-doorlike caldera margin for the Peach Spring Tuff implies that the caldera fragment in the Hacienda domain represents part of the NE margin of the caldera. The Black Mountains also expose a NE margin of the caldera (Fig. 2).

Other aspects of the caldera fragments in the Sacramento Mountains remain enigmatic. The recognized caldera fragment in the Beacon domain is exposed only 500 m along strike, with any more southern stratigraphic correlatives concealed by the upper sedimentary and volcanic sequence and by younger alluvium (Fig. 6). Basement exposed nonconformably underlying the caldera fragments lacks Miocene plutons that could represent a subcaldera magma chamber either in the western Sacramento Mountains or in areas farther west to which they could restore before faulting. At least 3 km thickness of tilted Proterozoic basement gneiss and granitoids nonconformably underlie the caldera fragment in the main panel of the Beacon domain (Fig. 6), and the Sawtooth domain exposes greater basement thickness. Any sub-caldera plutonic connections to the tuff would have to reside at deeper paleodepths. Further, the Beacon-domain caldera fragment restores, before extension, westward toward positions above Proterozoic and Cretaceous basement exposures in the Stepladder Mountains that also lack Miocene plutons (Fig. 2). Those exposures include granodiorite that sourced clasts in the granodiorite-clast breccia facies of tuff (Fig. 8C).

Candidates for subcaldera intrusives related to the tuff eruption are however widely exposed in the central Sacramento Mountains core complex, as gneissic granodiorite and quartz diorite collectively called the Eagle Wash intrusive complex, about the same age as the 18.8-Ma tuff (Figs. 2, 5; McClelland, 1984; Simpson et al., 1991; Pease et al., 1999; Ferguson et al., 2013). That intrusive complex crystallized at depths of 7–15 km and deformed ductiley during extension prior to intrusion of a ~19-Ma pluton in the southern Sacramento Mountains (Pease et al.,1999; Campbell-Stone et al., 2000). Similar gneissic quartz diorite occurs in the Dead Mountains. These intrusions may have expanded the crustal width during extension.

Structural reconstruction of the caldera compared to other Indicators of extension azimuth

The caldera fragments in the Beacon and Hacienda domains and the Silver Creek caldera lie on a NE trend, consistent with Ferguson et al.'s (2013) proposed net azimuth of NNE (002° to 045°[1]) for extensional fragmentation of the caldera (Fig. 2). If the caldera fragment in the Hacienda domain correctly correlates to the NE margin of the Silver Creek caldera in the Black Mountains, the net extension azimuth is about 040°. This orientation can be compared to other more local indicators of extension direction across this part of the Colorado River extensional corridor (Figs. 2, 3).

We synthesize published indicators of dominant extension direction and some of our own, and categorize these observations by the crustal level of formation, from shallow (brittle) to deep (ductile or magmatic)(Table 1[1]). Average or dominant orientations of fault striae and stretching lineations are highlighted in Table 1 (bold type) and portrayed on Figure 2, on the assumption that they, of all the indicators, most directly indicate the orientation of extensional faulting or shearing. Generalized orientations of Miocene bedding and dikes are shown separately (Fig. 3). Dip directions of faults and of tilted or folded markers (Fig. 3A) provide useful but indirect indications of the orientations of extension. Dikes (Fig. 3B), elongate plutons, and gravity-modeled dike-like bodies record an azimuth of *crustal expansion* (italicized in Table 1), which may be either normal to or oblique to extension, but they commonly form perpendicular to extensional stress direction (Anderson, 1951).

The listed features, except for dike orientations, indicate NE–SW extension for most crustal levels south from the Sacramento Mountains. More southeastern sites in the extensional corridor similarly show NE-SW extension (Singleton et al., 2019). Extension azimuth north of the Sacramento Mountains is more E–W but less well documented (Figs. 2, 3A). Miocene dike swarms (italicized in Table 1) represent as much as 5–10% inflation. Their most common orientation in the Sacramento and Stepladder Mountains and Homer Mountain (100°–105° strike) mismatches most other indicators of extension and remains poorly understood (Fig. 3B). Campbell-Stone et al. (2000) proposed that the strikes of progressively younger plutons and dikes in the southern Sacramento Mountains imply a progressive anticlockwise rotation of extensional stress azimuth (from 035°1 for a 19-Ma pluton to 015° for the ca. 17-16 Ma dike swarm). Whether that intrusive inflation was by normal or oblique extension is not documented. Explanations for the dike orientations could include intrusion into pre-existing fractures or other anisotropy (LaForge et al., 2017), or stress responses to crustal flexure from core-complex doming (Spencer, 1985) or to north-to-south crustal gravitational spreading (Gans et al., 2018). Campbell-Stone et al. (2000) used post-dike tilt axes and fault striae to infer that post-dike extension in the southern Sacramento Mountains rotated clockwise (to 055°-075° azimuth by 12 Ma).

The NE direction of fragmentation of the caldera contrasts with more E–W extensional indicators in

[1] Azimuths generally are here specified as clockwise from north without connoting polarity.

northern parts of the area of Figure 2: Homer Mountain and the Dead Mountains. Those E–W indicators are however consistent with the northward swing of the extensional corridor and the Colorado River gravity high (Fig. 1), and of the strike of tilted panels in the Sacramento Mountains (Fig. 3A). If the gravity high represents thick dike-like intrusions as modeled by Campbell and John (1996), then its trend northward from the southern Sacramento Mountains implies E-W crustal expansion. An ad hoc model of left-lateral transtensional spreading of the north-trending extensional corridor might be one way to explain both the NE-SW direction of caldera fragmentation and any E-W inflation by thick dike-like intrusions under the gravity high. This model however would contradict predicted late Neocene plate-margin right-lateral shear NW-SE as is documented in the SE part of the area of Figure 1 (Singleton et al., 2019). Moreover, mylonitic lineations oriented E-W to SE-NW in the Dead Mountains (Fig. 2) and the indirect E-W extensional indicators at Homer Mountains do not easily fit such a left-lateral model. Future work is needed to test the strain interpretation of the lineations, sequential changes in extension direction, and the possible E-W extension at Homer Mountain and

Table 1. Indicators and azimuths of extension, magmatic inflation, or least principal stress[1]. The most direct indicators are in **bold font** and shown in Fig. 2.

Area	Upper Crust	Upper Middle Crust	Middle Crust	Deep (Middle To Lower) Crust
Topock Area	040° (dip directions of tilted diabase sheets and strata) (1)			
Chemehuevi Mountains	**040°–060° (fault striae, drag folds, minor faults, stratal dip)**(2) 040°(dip directions of strata)(14)	*VARIOUS (variously oriented 19–21.5-Ma dikes)* (3, 15) **055° (lineations in dikes)**(15)	045° (penetrative lineations, some Miocene although mostly much older)(4)	
Southern Sacramento Mountains	040° (dip directions of tilted diabase sheets and strata)(5) **030° & 065°–090° (striae on western detachment fault)**(5) **055°, 075° (striae on ~14–12-Ma eastern detachment fault)** (5)	*015° (perpendicular to dike swarm)* (5)	035° (perpendicular to elongate 19-Ma 3±0.6-kb dioritic pluton)(5) 020°–030° later (perpendicular to elongated 18-Ma granite pluton) (5)	NE (perpendicular to dike-like intrusions ~10 km thick modeled from gravity high) (5, 6)
Central Sacramento Mountains	**060±15° (striae on Sacramento Mts. detachment fault)** (7) **060°(striae on lower-plate normal faults)**(7) 065°(dip directions of lower-plate normal faults)(7) 050°(dip directions of upper-plate normal faults(7) **060°(striae on upper-plate faults)**(7) NE (perpendicular to folds in sediments)(7) **NE(strike of strike-slip faults)**(7) 055°, 070, 090°(dip directions of tilted strata) (14, 9)	*090° and 060° (perpendicular to sparse 13-Ma dikes)*(7, 9)	**045°–040° (top-to-NE elongation lineation in 19-Ma 3.3±0.75-kb granodioritic Eagle Wash intrusive complex and other lower-plate rocks)**(7, 10, 11)	090° (perpendicular to Colorado River gravity high) (12)

Table 1 continues

Table 1 continued

NW Sacramento Mountains	**032° (striae on antithetic lower-plate faults)**(10)	**042° (lineated antithetic brittle - ductile shear zones)**(10)
	Possibly 065° (corrugated detachment fault)(13)	**027° (lineated antithetic ductile shear zones)**(10)
	060° (top-to-the-NE shear indicators along a major, low-angle normal fault just south of Flattop Mtn.)(9)	**034° (lineated antithetic sheared dikes)**(10)
		015° (perpendicular to dike swarm)(13)
Homer Mountain	East (stratal dip & offsets of dike and granodiorite)(13)	*015° (perpendicular to dike swarm)*(13)
S. Dead Mountains	(Note: stratal and fault dip directions and folded foliation indicate contraction after 12 Ma oriented 090°) (13, 9)	*090° (perpendicular to sparse dikes)*(9) **096±10°(elongation lineation, n=11)**(9) 090° (perpendicular to Colorado River gravity high) (12)
N. Dead Mountains		**132±35° (lineation, n=18)** 090° (perpendicular to Colorado River gravity high) (12)
Sacramento Mountains to Black Mountains	**NE (~040°, restored fragmented caldera)**(16, 9)	

[1]Italicized for dikes, which commonly indicate orientation of local stress (Anderson, 1951) but not necessarily much extension.

[2]REFERENCES: (1) Howard et al. (2019); (2) John (1987a); (3) John (1982); (4) John and Mukasa (1990); Howard et al. (2013); (5) Campbell-Stone et al. (2000); (6) Campbell and John (1996); (7) McClelland (1985); (8) McClelland (1982); (9) This report (± estimates are from *n* number of measurements); (10) Simpson et al. (1991), Schweitzer (1991); (11) Pease and Argent (1999); (12) Simpson et al. (1990); Mariano et al. (1996); (13) Spencer, 1985; (14) Howard and John (1987); (15) LaForge et al. (2017); (16) Ferguson et al., 2013

the Dead Mountains in relation to the proposed net NE extensional fragmentation of the source caldera for the Peach Spring Tuff.

Conclusions

New mapping in the west-central Sacramento Mountains of southeastern California recognizes fragments of the source caldera for the 18.8-Ma Peach Spring Tuff in fault panels of two major structural domains. Correlation of these caldera fragments to the Silver Creek caldera 50 km to the northeast in the Black Mountains requires that the reconstructed caldera was fragmented in NE-SW extension. This extension orientation of a geologic marker broadly agrees with a wide variety of other kinds of extensional indicators at several crustal levels in several nearby mountain ranges. Where the Colorado River extensional corridor veers northward at the Sacramento Mountains, more northern ranges yield apparent E-W extensional indicators not obviously consistent with the net extension of the fragmented caldera.

Acknowledgements

We are grateful to Scott Bennett and Ben Melosh for carefully reviewing and critiquing an early version of the manuscript and suggesting many valuable improvements.

References cited

Anderson, E.M., 1951, The Mechanics of Faulting and Dyke Formation with Applications to Britain: Edinburgh, Oliver and Boyd, 206 p.

Anderson, J.L., and Bender, E.E., 1989, Nature and origin of Proterozoic A-type granitic magmatism in the southwestern United States: Lithos, v. 23, p. 19–52, doi: 10.1016/0024-4937(89)90021-2.

Atwater, T., and Stock, J., 1998, Pacific–North America plate tectonics of the Neogene southwestern United States: An Update: International Geology Review, v. 40, no. 5, p. 375–402, https://doi.org/10.1080/00206819809465216.

Barry, E. E., Winslow, H. B., Miller, C. F., Caliborne, L. L., Ferguson, C. A., Gomez, C. D., Varga, R. J., and Lackey, J. D., 2015, Magma chamber zonations and eruptive inversion in the Peach Spring Tuff: Geochemical and paleomagnetic evidence (abs.): Geological Society of America, annual meeting, paper 210-57.

Buesch, D.A. and Valentine, G.A., 1986, Peach Springs Tuff and volcanic stratigraphy of the southern Cerbat Mountains, Kingman, Arizona, in Niellson, J.E. and Glazner, A.F., eds., Cenozoic stratigraphy, structure, and mineralization in the Mojave Desert: Los Angeles, California State University, Guidebook and Volume for Geological Society of America Cordilleran Section Meeting Field Trips, p. 7–14.

Campbell, E.A., and John, B.E., 1996, Constraints on extension-related plutonism from modeling of the Colorado River gravity high: Geological Society of America Bulletin, v. 108, p. 1242–1255, https://doi.org/10.1130/0016-7606(1996)108<1242:COERPF>2.3.CO;2.

Campbell-Stone, E., and John, B.E., 2002, Temporal changes in deformation mode: From failure to flow in the Colorado River extensional corridor: International Geology Review, v. 44, p. 512–527, https://doi.org/10.2747/0020-6814.44.6.512.

Campbell-Stone, E.A., John, B.E., Foster, D.A., Geissman, J.W., and Livaccari, R.F., 2000, Mechanisms for accommodation of Miocene extension—Low-angle normal faulting, magmatism, and secondary breakaway faulting in the southern Sacramento Mountains, southeastern California: Tectonics, v. 19, p. 566–587, https://doi.org/10.1029/1999TC001133.

Carr, W.J., 1991, A Contribution to the Structural History of the Vidal-Parker Region, California and Arizona: U.S. Geological Survey Professional Paper 1430, 40 p.

Carter, T.J., Kohn, B.P., Foster, D.A., Gleadow, A.J.W., and Woodhead, J.D., 2006, Late-stage evolution of the Chemehuevi and Sacramento detachment faults from apatite (U-Th)/He thermochronometry—Evidence for mid-Miocene accelerated slip: Geological Society of America Bulletin, v. 118, p. 689–709, doi: 10.1130/B25736.1

Chapman, J.B., Dafov, M.N., Gehrels, G., Ducea, M.N.,Valley, J.W., and Ishida, A., 2018, Lithospheric architecture and tectonic evolution of the southwestern U.S. Cordillera: Constraints from zircon Hf and O isotopic data: Geological Society of America Bulletin, v. 130, p. 2031–2046, doi: 10.1130/B31937.1

DeCelles, P.G., 2004, Late Jurassic to Eocene evolution of the Cordilleran thrust belt and foreland basin system, western U.S.A.: American Journal of Science, v. 304, p. 105–168, https://doi.org/10.2475/ajs.304.2.105.

Dickinson, W.R., and Snyder, W.S., 1979, Geometry of subducted slabs related to San Andreas transform: The Journal of Geology, v. 87, p. 609–627, https://doi.org/10.1086/628456.

Elston, D.P., and Young, R.A., 1991, Cretaceous-Eocene (Laramide) landscape development and Oligocene-Pliocene drainage reorganization of transition zone and Colorado Plateau, Arizona: Journal of Geophysical Research, v. 96, no. B7, p. 12,389–12,406, https://doi.org/10.1029/90JB01978.

Fedo, C.M., 1993, Geologic framework of middle Tertiary strata, northern Sacramento Mountains, southeastern California, in Sherrod, D.R. and Nielson, J.E., eds., Tertiary stratigraphy of highly extended terranes, California, Arizona, and Nevada: U.S. Geological Survey Bulletin 2053, p.111–113.

Fedo, C.M. and Miller, J.M.G., 1992, Evolution of a Miocene half-graben basin, Colorado River extensional corridor, southeastern California: Geological Society of America Bulletin, v. 104, p. 481–493.

Ferguson, C.A., and Cook, J. P., 2015a, Geologic map of the Kingman 7.5' quadrangle, Mohave County, Arizona: Arizona Geological Survey Digital Geologic Map DGM-113, 1 sheet, 24,000 scale.

Ferguson, C.A., and Cook, J. P., 2015b, Geologic map of the Kingman NW 7.5' quadrangle, Mohave County, Arizona: Arizona Geological Survey Digital Geologic Map DGM-114, 1 sheet, 24,000 scale.

Ferguson, C.A., Pearthree, P. A., Johnson, B. J., Guynn, J., and McCosbie, J.B., 2017, Geologic map of the Oatman 7.5' quadrangle, Mohave County, Arizona: Arizona Geological Survey Digital Geologic Map DGM-119, 1 sheet, 24,000 scale.

Ferguson, C.A., McIntosh, W.C., and Miller, C.F., 2013, Silver Creek caldera—The tectonically dismembered source of the Peach Spring Tuff: Geology, v. 41, p. 3–6, https://doi.org/10.1130/G33551.1.

Foster, D.A., Miller, D.S., and Miller, C.F., 1991, Tertiary extension in the Old Woman Mountains area, California: Evidence from apatite fission track analysis: Tectonics, v. 10, p. 875–886, https://doi.org/10.1029/91TC00865.

Foster, D.A., Miller, C.F., Harrison, T.M., and Hoisch, T.D., 1992, 40Ar/39Ar thermochronology and thermobarometry of metamorphism, plutonism, and tectonic denudation in the Old Woman Mountains area, California: Geological Society of America Bulletin, v. 104, p. 176–191, https://doi.org/10.1130/0016-7606(1992)104<0176:AATATO>2.3.CO;2.

Foster, D.A., and John, B.E., 1999, Quantifying tectonic exhumation in an extensional orogen with thermochronology: Examples from the southern Basin and Range Province, in Ring, U., Brandon, M., Lister, G.S., and Willett, S.D., eds., Exhumation Processes: Normal faulting, ductile flow, and erosion: Geological Society, London, Special Publication 154, p. 356–378, https://doi.org/10.1144/GSL.SP.1999.154.01.16.

Gans, P.B., and Bohrson, W.A., 1998, Suppression of volcanism during rapid extension in the Basin and Range Province, United States: Science, v. 279, no. 5347, p. 66–68, https://doi.org/10.1126/science.279.5347.66.

Gans, P.B., and Gentry, B.J., 2016, Dike emplacement, footwall rotation, and transition from magmatic to tectonic extension in the Whipple Mountains metamorphic core complex, southeastern California: Tectonics, v. 35, p. 2564–2608, https://doi.org/10.1002/2016TC004215.

Gans, P.B., Mahood, G.A., and Schermer, E., 1989, Synextensional Magmatism in the Basin and Range Province: A Case Study from the Eastern Great Basin: Geological Society of America Special Paper 233, 55 p., https://doi.org/10.1130/SPE233-p1.

Gans, P.B., Newmann, Justin, Monroe, Evan, and Kylander-Clark, Andrew, 2018, Orthogonal(N-S) extension at the leading edge or a propagating continental rift: A reassessment of Homer Mountain and environs, lower Colorado River extensional corridor (CREC): Geological Society of America, Cordilleran and Rocky Mountains Sections Meeting, Flagstaff, Abstracts with Programs, v. 50, no. 5, Paper No. 46-4, https://gsa.confex.com/gsa/2018RM/webprogram/Paper313804.html, doi: 10.1130/abs/2018RM-313804

Glazner, A.F., and Bartley, J.M., 1984, Timing and tectonic setting of Tertiary low-angle normal faulting and associated magmatism in the southwestern United States: Tectonics, v. 3, p. 385–396, https://doi.org/10.1029/TC003i003p00385.

Glazner, A.F., and Supplee, J.A., 1982, Migration of Tertiary volcanism in the southwestern United States and subduction of the Mendocino fracture zone: Earth and Planetary Science Letters, v. 60, p. 429–436, https://doi.org/10.1016/0012-821X(82)90078-4.

Hammond, J.G., 1990, Middle Proterozoic diabase intrusions in the southwestern U.S.A. as indicators of limited extensional

tectonism, in Gower, C.F., Rivers, T., and Ryan, B., eds., Mid-Proterozoic Laurentia-Baltica: Geological Association of Canada Special Paper 38, p. 517–531.

Hillhouse, J.W., and Wells, R.E., 1991, Magnetic fabric, flow directions, and source area of the lower Miocene Peach Springs Tuff in Arizona, California, and Nevada: Journal of Geophysical Research, v. 96, no. B7, p. 12,443–12,460, https://doi.org/10.1029/90JB02257.

Howard, J.L., 1996, Paleocene to Holocene paleodeltas of ancestral Colorado River offset by the San Andreas fault system, southern California: Geology, v. 24, p. 783–786, https://doi.org/10.1130/0091-7613(1996)024<0783:PTHPOA>2.3.CO;2.

Howard, K.A., 1991, Intrusion of horizontal dikes: Tectonic significance of Middle Proterozoic diabase sheets widespread in the upper crust of the southwestern United States: Journal of Geophysical Research, v. 96, p. 12,461–12,478.

Howard, K.A., 2010, Caldera collapse -- Perspectives from comparing Galápagos volcanoes, nuclear-test sinks, sandbox models, and volcanoes on Mars: GSA Today, v. 20, no. 10, p. 4–10. http://www.geosociety.org/gsatoday/archive/20/10/article/i1052-5173-20-10-4.htm.

Howard, K.A., 2011, The upper crust on its side—Steeply tilted slabs in the Basin and Range, in Steininger, R., and Pennell, B., eds., Great Basin Evolution and Metallogeny: Geological Society of Nevada 2010 Symposium: Reno, Geological Society of Nevada, v. 1, p. 289–298.

Howard, K.A., Christiansen, P.P., and John, B.E., 1993, Cenozoic stratigraphy of northern Chemehuevi Valley and flanking Stepladder Mountains and Sawtooth Range, southeastern Calif., in Sherrod, D.R. and Nielson, J.E., eds., Tertiary stratigraphy of highly extended terranes, California, Arizona, and Nevada: U.S. Geological Survey Bulletin 2053, p. 95-97.

Howard, K.A., House, P.K., John, B.E., Crow, R.S, and Pearthree, P.A., 2019, A river is born: Highlights of the geologic evolution of the Colorado River extensional corridor and its river: A field guide honoring the life and legacy of Warren Hamilton, in Pearthree, P.A., ed., Geologic Excursions in Southwestern North America: Geological Society of America Field Guide 55, p. 61–113, doi.org/10.1130/2019.0055(03).

Howard, K.A., and John, B.E., 1987, Crustal extension along a rooted system of imbricate low-angle faults: Colorado River extensional corridor, California and Arizona, in Coward, M.P., Dewey, J.F., and Hancock, P.L., eds., Continental Extensional Tectonics: Geological Society, London, Special Publication 28, p. 299–311, https://doi.org/10.1144/GSL.SP.1987.028.01.19.

Howard, K.A., John, B.E., and Miller, C.F., 1987, Metamorphic core complexes, Mesozoic ductile thrusts, and Cenozoic detachments: Old Woman Mountains–Chemehuevi Mountains transect, California and Arizona, in Davis, G.H., and Vandendolder, E.M., eds., Geologic Diversity of Arizona and Its Margins: Excursions to Choice Areas: Arizona Bureau of Geology and Mineral Technology Special Paper 5, p. 365–382.

Howard, K.A., John, B.E., Nielson, J.E., Miller, J.M.G., and Wooden, J.L., 2013, Geologic Map of the Topock 7.5-Minute Quadrangle, Arizona and California: U.S. Geological Survey Scientific Investigations Map 3236, scale 1:24,000 + 60-p. pamphlet.

Howard, K.A., Nielson, J.E., Wilshire, H.G., Nakata, J.K., Goodge, J.W., Reneau, S.L., John, B.E., and Hansen, V.L., 1999, Geologic Map of the Mohave Mountains area, Mohave County, Western Arizona: U.S. Geological Survey, Miscellaneous Investigations Map I-2308, scale 1:48,000.

Howard, K.A., Stone, Paul, Pernokas, M.A., and Marvin, R.F., 1982, Geologic and geochronologic reconnaissance of the Turtle Mountains area, California: West border of the Whipple Mountains detachment terrane, in Frost, E.G., and Martin, D.L., eds., Mesozoic-Cenozoic tectonic evolution of the Colorado River Region, California, Arizona, and Nevada (Anderson-Hamilton Volume): San Diego, Cordilleran Publishers, p. 341-355.

John, B.E., 1982, Geologic framework of the Chemehuevi Mountains, southeastern California, in Frost, E.G., and Martin, D.L., eds., Mesozoic-Cenozoic tectonic evolution of the Colorado River Region, California, Arizona, and Nevada (Anderson-Hamilton Volume): San Diego, Cordilleran Publishers, p. 317–325.

John, B.E., 1987a, Geometry and evolution of a mid-crustal extensional fault system: Chemehuevi Mountains southeastern California, in Coward, M.P., Dewey, J.F., and Hancock, P.L., eds., Continental Extensional Tectonics: Geological Society, London, Special Publication 28, p. 313–335, https://doi.org/10.1144/GSL.SP.1987.028.01.20.

John, B.E., 1987b, Geologic map of the Chemehuevi Mountains area, San Bernardino County, California and Mohave County, Arizona: U.S. Geological Survey Open-file Report 87-666, 1:24,000 scale.

John, B.E., and Foster, D.A., 1993, Structural and thermal constraints on the initiation angle of detachment faulting in the southern Basin and Range: The Chemehuevi Mountains case study: Geological Society of America Bulletin, v. 105, p. 1091–1108, https://doi.org/10.1130/0016-7606(1993)105<1091:SATCOT>2.3.CO;2.

John, B.E., and Mukasa, S.B., 1990, Footwall rocks to the mid-Tertiary Chemehuevi detachment fault: A window into the middle crust in the Southern Cordillera: Journal of Geophysical Research, v. 95, p. 463–485, https://doi.org/10.1029/JB095iB01p00463.

LaForge, J.S., John, B.E., and Grimes, C.B., 2017, Synextensional dike emplacement across the footwall of a continental core complex, Chemehuevi Mountains, southeastern California: Geosphere, v. 13, no. 6, p. 1867–1886, https://doi.org/10.1130/GES01402.1.

Lipman, 1976, Caldera-collapse breccias in the western San Juan Mountains, Colorado: Geological Society of America Bulletin, v. 87, p. 1397–1410, doi: 10.1130/0016-7606(1976)87<1397:CBITWS>2.0.CO;2

MacKin, J.H., 1950, The down-structure method of viewing geologic maps: The Journal of Geology, v. 58, p. 55–72, https://doi.org/10.1086/625695.

Mariano, John, Helferty, M.G., and Gage, T.B., 1986, Bouger and isostatic residual gravity maps of the Colorado River region, including the Kingman, Needles, Salton Sea, and El Centro quadrangles: U. S. Geological Survey Open-file report 86-347, 7 sheets.

McCarthy, J., Larkin, S.P., Fuis, G.S., Simpson, R.W., and Howard, K.A., 1991, Anatomy of a metamorphic core complex: Seismic refraction wide-angle reflection profiling in southeastern California and western Arizona: Journal Geophysical Research, v. 96, p. 12,259–12,291, https://doi.org/10.1029/91JB01004.

McClelland, W.C., 1982, Structural geology of the central Sacramento Mountains, San Bernardino County, California, in Frost, E.G., and Martin, D.L., eds., Mesozoic-Cenozoic tectonic evolution of the Colorado River Region, California, Arizona, and Nevada (Anderson-Hamilton Volume): San Diego, Cordilleran Publishers, p. 401–406.

McClelland, W.C., 1984, Low-angle Cenozoic faulting iun the central Sacramento Mountains, San Bernardino County, California: Los Angeles, University of Southern California, M.S. thesis, 94 p.

McDowell, S.M., Miller, C.F., Mundil, R., Ferguson, C.A., and Wooden, J.L., 2014, Zircon evidence for a ~200 k.y. supereruption-related thermal flare-up in the Miocene Black Mountains, western Arizona, USA: Contributions to Mineralogy and Petrology, v. 168, 1031, https://doi.org/10.1007/s00410-014-1031-5.

McCosby, J. B., Lang, N. P., Beard, E. M., Miller, C. F., and Ferguson, C. A., 2015, Stratigraphic relations between two volcanic units and the possible lacustrine sediments between them: implications for the paleoenvironment in Times Gulch, NW Arizona (abs.): Geological Society of America, annual meeting, paper 210-59.

Miller, C.F., Wooden, J.L., Bennet, V.C., Wright, J.E, 1990, Petrogenesis of the composite peraluminous-metaluminous Old Woman-Piute Range batholith, southeastern California: isotopic constraints, in Anderson, J.L., Editor, The nature and origin of Cordilleran magmatism: Geological Society of America Memoir 174, p. 99–110.

Miller, J.M.G. and John, B.E., 1999, Sedimentation patterns support seismogenic low-angle normal faulting, southeastern California and western Arizona: Geological Society of America Bulletin, v. 111, p. 1350–1370, https://doi.org/10.1130/0016-7606(1999)111<1350:SPSSLA>2.3.CO;2.

Miller, J.M.G. and Leach, B.R., 1993, Tertiary stratigraphy of the central Sacramento Mountains, southeastern California, in Sherrod, D.R. and Nielson, J.E., eds., Tertiary stratigraphy of highly extended terranes, California, Arizona, and Nevada: U.S. Geological Survey Bulletin 2053, p.115–117.

Nielson, J.E., and Beratan, K.K., 1995, Stratigraphic and structural synthesis of a Miocene extensional terrane, southeast California and west-central Arizona: Geological Society of America Bulletin, v. 107, p. 241–252, https://doi.org/10.1130/0016-7606(1995)107<0241:SASSOA>2.3.CO;2.

Pamukcu, A.S., Carley, T.L., Gualda, G.A.R., Miller, C.F., and Ferguson, C.A., 2013, The evolution of the Peach Spring giant magma body; Evidence from accessory mineral textures and compositions, bulk pumice and glass geochemistry, and rhyolite MELTS modeling: Journal of Petrology, v. 54, p. 1109–1148, https://doi.org/10.1093/petrology/egt007.

Pease, V. and Argent, J., 1999, The northern Sacramento Mountains, southwest United States. Part I. Structural profile through a crustal extensional detachment system, in Mac Niocaill, C., and Ryan, P.D., eds., Continental Tectonics: Geological Society of London, Special Publication 164, p. 179–198.

Pease, V., Foster, D., Wooden, J., O'Sullivan, P., Argent, J., and Fanning, C., 1999, The northern Sacramento Mountains, southwest United States. Part II: Exhumation history and detachment faulting, in Mac Niocaill, C., and Ryan, P.D., eds., Continental Tectonics: Geological Society of London, Special Publication 164, p. 199–238, https://doi.org/10.1144/GSL.SP.1999.164.01.11.

Ransome, F. L., 1923, Geology of the Oatman gold district, Arizona: U. S. Geological Survey Bulletin 743, 58 pp.

Regula, A. J., Ferguson, C. A., Miller, C. F., Claiborne, L. L., McDowell, S. M., Cribb, W. Flood, T. P. and Covey, A., 2015, Tuff of Bonelli House, Part 1: petrologic characterization in type area at Kingman, Regional correlation and constraints on extent (abs.): Geological Society of America, annual meeting, paper 210-30.

Roche, O., Druitt, T.H., and Merle, O., 2000, Experimental study of caldera formation: Journal of Geophysical Research, v. 105 (B1), p. 395–416.

Severinghaus, J., and Atwater, T., 1990, Cenozoic geometry and thermal state of the subducting slabs beneath western North America, in Wernicke, B.P., ed., Basin and Range Extensional Tectonics near the Latitude of Las Vegas, Nevada: Geological Society of America Memoir 176, p. 1–22, https://doi.org/10.1130/MEM176-p1.

Sherrod, D.R., and Nielson, J.E., eds., 1993, Tertiary Stratigraphy of Highly Extended Terranes, California, Arizona, and Nevada: U.S. Geological Survey Bulletin 2053, 250 p.

Shulaker, D.Z., Grove, M., Hourigan, J.K., Van Buer, N., Sharman, G., Howard, K., Miller, J., and Barth, A.P., 2019, Detrital K-feldspar Pb isotopic evaluation of extraregional sediment transported through an Eocene tectonic breach of southern California's Cretaceous batholith: Earth and Planetary Sciences Letters, v. 508, p. 4–17, https://doi.org/10.1016j.epsl.2018.11.040.

Simpson, Carol, Schweitzer, Janet, and Howard, K.A., 1991, A reinterpretation of the timing, position, and significance of part of the Sacramento Mountains detachment fault, southeastern California: Geological Society of America Bulletin, v. 101, p. 751–761.

Simpson, R.W., Howard, K.A., Jachens, R.C., and Mariano, J., 1990, A positive gravity anomaly along the Colorado River extensional corridor: Evidence for new crustal material?: Eos (Transactions, American Geophysical Union), v. 71, p. 1594.

Singleton, J.S., Seymour, JN.M, Reynolds, S.J., Vommmocil, Terrence, and Wong, M.S., 2019, Distributed Neogene faulting across the western to central Arizona metamorphic core complex belt: Synextensional constriction and superposition of the Pacific–North America plate boundary on the southern Basin and Range: Geosphere, v. 15, p. 1409–1435, doi: 10.1130/GES02036.1

Spencer, J.E., 1985, Miocene low-angle normal faulting and dike emplacement, Homer Mountain and surrounding areas, southeastern California and southernmost Nevada: Geological Society of America Bulletin, v. 96, p. 1140–1155, https://doi.org/10.1130/0016-7606(1985)96<1140:MLNFAD>2.0.CO;2.

Spencer, J.E., 1984, Role of tectonic denudation in uplift and warping of low-angle normal faults: Geology, v. 12, p. 95–98, https://doi.org/10.1130/0091-7613(1984)12<95:ROTDIW>2.0.CO;2.

Spencer, J.E., 1985, Miocene low-angle normal faulting and dike emplacement, Homer Mountain and surrounding areas, southeastern California and southernmost Nevada: Geological Society of America Bulletin, v. 96, p.1140–1155.

Spencer, J.E. and Turner, R.D., 1982, Dike swarms and low-angle faults, Homer Mountain and the northwestern Sacramento Mountains, southeastern California, in Frost. E.G. and Martin, D.L., Mesozoic-Cenozoic tectonic evolution of the Colorado River region, California, Arizona, and Nevada (Anderson-Hamilton volume): San Diego, California, Cordilleran Publishers, p. 97–107.

Spencer, J.E. and Turner, R.D., 1983, Geologic map of part of the northwestern Sacramento Mountains, southeastern California: U.S. Geological Survey Open-file Report 83-614, scale 1:24,000.

Stone, Paul, Howard, K.A., and Hamilton, Warren, 1983, Correlation of metamorphosed Paleozoic strata of the southern Mojave Desert region, California and Arizona: Geological Society of America Bulletin, v. 94, no. 10, p. 1135-1147.

Thorson, J. P., 1971, Igneous petrology of the Oatman district, Mohave County, Arizona (Ph.D. thesis): University of California–Santa Barbara, 189 pp., 2 plates 1:24,000 scale.

Vitaliano, C.J., 1950, Needles magnesite deposit, San Bernardino County, California: California Journal of Mines and Geology, v. 46, no. 3, p. 357–372.

Ward, P.L., 1991, On plate tectonics and the geologic evolution of southwestern North America: Journal of Geophysical Research, v. 96, no. B7, p. 12,479–12,496, https://doi.org/10.1029/91JB00606.

Wells, R.E., and Hillhouse, J.W., 1989, Paleomagnetism and tectonic rotation of the lower Miocene Peach Springs Tuff—Colorado Plateau to Barstow, California: Geological Society of America Bulletin, v. 101, p. 846–863, doi: 10.1130/0016-7606(1989)101<0846:PATROT>2.3.CO;2.

Wooden, J.L., Barth, A.P., and Mueller, P.A., 2012, Crustal growth and tectonic evolution of the Mojave crustal Province: Insights from hafnium isotope systematics in zircons: Lithosphere, v. 5, p. 17–28, doi:10.1130/L218.1.

Wooden, J.L., and Miller, D.M., 1990, Chronologic and isotopic framework for Early Proterozoic crustal evolution in the eastern Mojave Desert region, SE California: Journal of Geophysical Research, v. 95, no. B12, p. 20,133–20,146, https://doi.org/10.1029/JB095iB12p20133.

Young, R. A., and Brennan, W. J., 1974, The Peach Springs Tuff: Its bearing on structural evolution of the Colorado Plateau and development of Cenozoic drainage in Mohave County, Arizona: Geological Society of America Bulletin, v. 85, p. 83-90, doi: 1130/0016-7606(1974)85<83:PSTIBO>2.0.CO;2.

Insular avifauna and woodlands of the New York Mountains in Mojave National Preserve

Shane E. Jordan
shane.jordan.407@my.csun.edu

ABSTRACT—The formation of insular habitats due to long term climate change has allowed unique species assemblages to occur within the highest mountains of Mojave National Preserve. Woodland communities of the preserve appear to support plant and bird species uncommon in much of the Mojave Desert, yet common in other physiographic provinces. Here, indicator plant species were used to characterize three woodland communities along an elevational gradient from 1200–1800 meters in the New York Mountains. More than 75% of the plants recorded were restricted to specific assemblages, and 83% were completely absent beyond the woodland habitat. Seventy-five percent of the bird species observed were not found beyond the woodland environment, while 68% had been reported from there previously. Comparisons with the known distribution ranges of these species suggest that 10% of the observed bird species are possibly limited to using woodland habitats when they occur within Mojave National Preserve. Regionally uncommon avifauna such as the declining pinyon jay and gray vireo may be dependent upon these plant communities for survival. The potential effects of climate change, disturbance, and species invasion warrant continued monitoring of both plant and bird species richness within these insular woodlands so that any subsequent changes in local biodiversity are recognized.

Introduction

An insular habitat may be defined as a localized area where the associated biota differs significantly from that of the surrounding region, and where the constituent species may be separated from their nearest relatives by a considerable distance due to some geographic barrier such as a desert, scrubland or large body of water (MacArthur and Wilson 1963, 1967). High mountain ranges may often serve as insular habitats (i.e. sky islands) due to the large range in elevation which affects microclimate and the distribution of plant communities (Brown 1978; Thorne et al. 1981). In the desert southwest, relict plant populations may be limited to niches found atop mountains still influenced by a climate reflective of their ancestral past (i.e. via habitat tracking) (Wells and Berger 1967; Brown 1978; Holmgren et al. 2014). The New York Mountains are one of a set of high mountains in Mojave National Preserve which harbor disjunctive plant communities otherwise absent from the surrounding low desert basins. These communities provide an important habitat for avifauna that is not typically found in the creosote scrub communities occupying the majority of the California desert (Johnson 1978; Cardiff and Remsen 1981). As many bird species currently face marked decline in North America (Rosenberg et al. 2019), including some that occur in the California Desert (Iknayan and Beissinger 2018; Ridell et al. 2019), such ecological relationships may be critical for the distribution of bird populations within the Mojave region.

The crest of the New York Mountains divides the endoheric Ivanpah and Cadiz basins from the Colorado River watershed (Figure 1). The range generally rises from the upper bajada at 1200 m and reaches 2295 m at its summit. Rocks are primarily sedimentary or

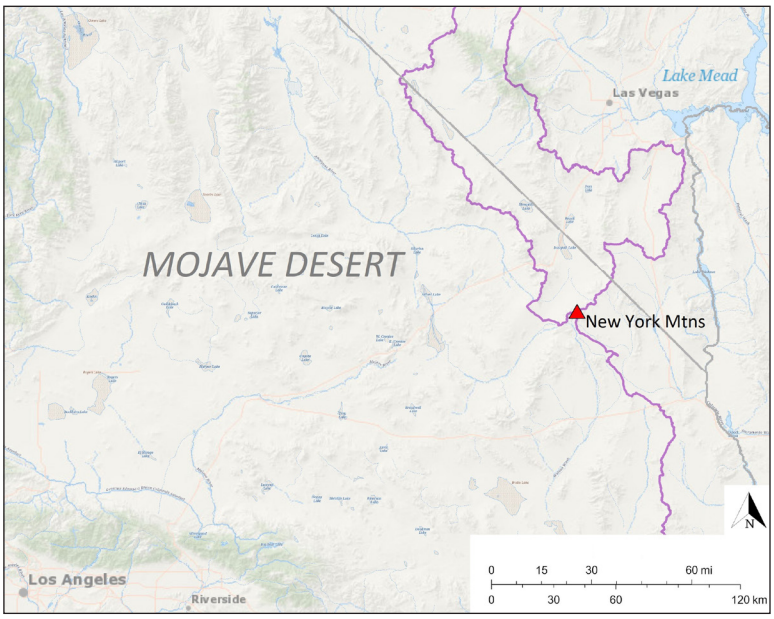

Fig 1. Map showing watershed boundaries divided at the New York Mountains within the Mojave Desert.

———
See Appendices, this volume, for additional data.

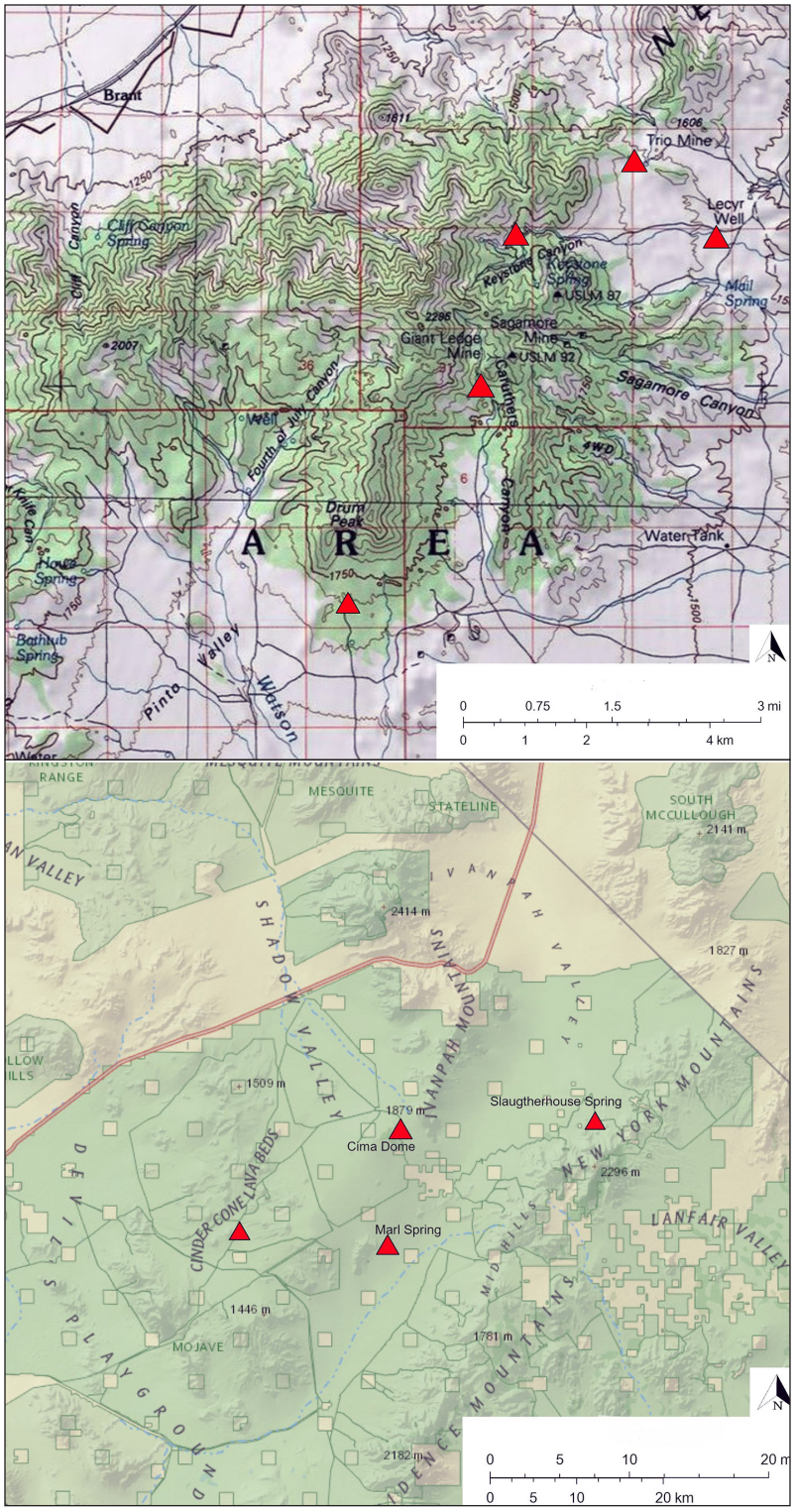

Fig 2. Maps indicating plant community and avifauna point survey locations within woodland habitats (above) and non-woodland habitats (below).

igneous in origin (Miller and Wooden 1993) and soils tend to be coarse grained on slopes and ridges. Many of the ridges are adorned with a complex array of large boulder outcroppings, and drainages are characterized by sandy alluvium. Precipitation in this region follows a bi-seasonal pattern, with 66% of rainfall coming from cool season Pacific storms and 29% from the warm season North American monsoon (Tubbs 1972; Hereford et al. 2006). In the mountains of the east Mojave there is increased precipitation and cooler temperatures at higher elevation (Thorne et al. 1981; Pavlik 2008). Near the New York Mountains at Mountain Pass (35.4706657 N, - 115.545561 W; elev. 1440 m), the annual mean precipitation is 21.8 cm, with annual temperatures ranging between -1.4° and 33.8°C (Western Regional Climate Center data). This contrasts the annual mean precipitation 43 km away in Baker (35.26330 N, -116.07165 W; elev. 280 m), where annual mean precipitation is less than 11 cm, and annual temperatures range between 1.4° and 43.4°C (Western Regional Climate Center data).

Three woodland plant communities generally characterize an elevational gradient in the New York Mountains (Figure 3). Joshua tree and juniper-woodland occurs at about 1200–1500 m. Pinyon pine and juniper woodland occurs at about 1500–1800 m, and pinyon pine and live oak-forest occurs in isolated groves above 1700 m. A fourth, especially disjunct community of Rocky Mountain white fir (Abies concolor var. concolor) with pinyon pine is found in a single isolated grove near the summit of the range, as well as in the nearby Clark and Kingston ranges (Cardiff and Remsen 1981; Thorne et al. 1981). While these communities are characterized by regionally common indicator species, they also contain numerous plants that are especially unusual to find in the Mojave Desert (Brown 1978; Andre 2006). Such disjunctive taxa are more commonly known from the California Floristic Province, Great Basin, or Colorado Plateau.

Although inventories of plant and bird species of the Mojave National Preserve exist, few publications specifically concern the ecology of plant communities in the New York Mountains (e.g. Trombulak and Cody 1980). Prigge (1979) and Thorne et al. (1981) published among the earliest studies that address the flora of the region; 231 plant species were documented by Prigge along an elevation gradient in Keystone Canyon on the northeast side of the range. Andre (2006) published an inventory of vascular plants in the region and reported 831 plant species within Mojave National Preserve, including sites around the

Fig 3. Three characteristic plant communities along an elevational gradient: Joshua tree–juniper woodland (top); pinyon–juniper woodland (middle); pine–oak forest (bottom).

New York Mountains. These reports indicate that the New York Mountains flora represents at least 28% of the plant species richness within the preserve, although this mountain range occupies less than 18% of the preserve's total area. Surveys of breeding avifauna conducted by Cardiff and Remsen in the 1970s provide the only documented inventory of birds known specifically in the New York Mountains; results indicated about 40 different species found in the insular woodland communities.

In my present study, insular plant communities of the New York Mountains were surveyed, and indicator species were identified for each. I predicted that the common plant and bird species within these insular woodland habitats would be absent at elevations below 1500 m. Because taxa from different physiographic provinces occur in this range, unusual associations among plant and bird populations found in these communities will be presented. Results here seek to improve an understanding of community assemblages within the insular woodlands of the New York Mountains and elucidate the importance of such habitats for the conservation of flora and fauna within Mojave National Preserve.

Methods

Various sites in the New York Mountains and vicinity were surveyed from May 23–27 2016. For this study, insular habitats were defined within the range occupied by conifers above 1500 m. Sites were selected based on community structure and reflected the similarities and differences in the area. Surveys of dominant plant species were conducted in the three communities described in order to characterize each assemblage and compare them to one another based on the presence or absence of species recorded.

Avifauna surveys consisted of area searches and point counts conducted at sites with rich observation potential, indicated in Figure 2. Area searches were also conducted at several sites outside the insular woodlands to differentiate species relationships that were restricted to the insular habitat from those of the lower basin habitat. A total of approximately 40 hours were spent surveying with these two methods at the different sites. Within the insular habitats, surveys were conducted between 1490–1890 m: near Drum Peak, Caruthers, and Keystone Canyons, and along the eastern ridge extending away from the summit block. Beyond the insular habitats comparative surveys were conducted below 1500 m: at the Cinder Cone Lava Beds, along portions of the Mojave Road, Marl Spring, Slaughterhouse Spring, and around Cima Dome.

The known distribution ranges of bird species were determined from the Cornell Lab of Ornithology database. For plants, the Consortium of California Herbaria was referenced using the Calflora database (Calflora.org), in addition to records of Great Basin and Colorado Plateau species (Van Buren et al. 2011). These distributions were compared with my field observations to evaluate the overlap of species ranges. Associations between flora and avifauna observed were then used to indicate which bird species seemed to be specific to the woodland communities. For both plant and bird species, a paired sign test was used to evaluate if a significant number of species were only found within an insular habitat (i.e. above 1500 m). When species were

Table 1. Dominant plant species of three characteristic communities along an elevational gradient Joshua tree-juniper woodland (1200 – 1500 m), abbr. Jsh-Junp; Pinyon-juniper woodland (1500 – 1800 m), abbr. Pin-Junp; Pine-oak forest (> 1700 m), abbr. Pin-oak.

Family	Taxon	Common name	Jsh-Junp	Pin-Junp	Pin-oak
Asparagaceae	*Yucca brevifolia*	Johsua tree	x		
Asteraceae	*Ambrosia eriocentra*	Wolly bursage	x		
Cactaceae	*Cylindropuntia acanthocarpa*	Buck horn cholla	x		
Rosaceae	*Prunus fasciculata*	Desert almond	x		
Asparagaceae	*Yucca baccata*	Banana yucca	x	x	
Cupressaceae	*Juniperus osteosperma*	Utah juniper	x	x	
Polygonacaeae	*Eriogonum fasciculatum*	East Mojave buckwheat	x	x	
Pinaceae	*Pinus monophylla*	Single-leaf pinyon pine	x	x	x
Asteraceae	*Artemisia tridentata*	Big sagebrush		x	
Asteraceae	*Brickellia californica*	Brickell brush		x	
Berberidaceae	*Berberis haematocarpa*	Mexican barberry		x	
Cactaceae	*Opuntia polyacantha ursina*	Grizzlybear prickly pear		x	
Rosaceae	*Fallugia paradoxa*	Apache plume		x	
Rosaceae	*Purshia mexicana*	Cliffrose		x	
Rosaceae	*Purshia tridentata*	Bitterbrush		x	
Fagaceae	*Quercus turbinella*	Turbinella oak		x	x
Anacardiaceae	*Rhus aromatica*	Skunkbush			x
Boraginaceae	*Eriodictyon angustifolium*	Narrowleaf yerba santa			x
Ericaceae	*Arctostaphylos pungens*	Mexican manzanita			x
Fagaceae	*Quercus chrysolepis*	Canyon live oak			x
Garryaceae	*Garrya flavescens*	Silk tassel			x
Pinaceae	*Pinus edulis*	Colorado pinyon pine			x
Pinaceae	*Pinus edulis x monophylla*	Pinyon pine hybrid			x
Rhanmnaceae	*Ceanothus pauciflorus*	Mojave ceanothus			x
Rhanmnaceae	*Frangula californica*	California coffeeberry			x
Rhanmnaceae	*Rhamnus ilicifolia*	Hollyleaf redberry			x
Rosaceae	*Amelanchier utahensis*	Utah serviceberry			x

consistently absent from surveys conducted outside the woodlands it was concluded that they were likely to favor the insular communities. My observations were also compared with those reported by Cardiff and Remsen (1981) to identify bird species that are probably residents or frequent visitors, and therefore dependent upon the isolated woodlands for habitat.

Results

The plant community assemblages appear to be well defined (Table 1). Joshua tree–juniper woodland shared only 25% of the dominant species with pinyon–juniper woodland, and 12.5% with the pine–oak forest. Pinyon–juniper woodland shared only 8.3% of the dominant species with the pine–oak forest, and 84.6% of dominant species found in the pine–oak forests were absent from the other two communities.

Bird species appeared to define each community less clearly (Table 2). The Joshua tree–juniper woodland shared 80% of the species found in common with the pinyon–juniper woodland, and 40% with the pine–oak forest. The pinyon–juniper woodland shared 61.9% of the species found with the pine–oak forest. Of the 23 species found in the pine–oak forest, 45.8% were found only in that community.

Results of the paired sign test for plants were significant ($n = 23$, $p = 0.0013$). Eighty-three percent of species found within the insular habitat were absent below 1500 m. Likewise, results of the paired sign test for birds were also highly significant ($n = 27$, $p = 0.000025$). Ninety percent of species found within the insular habitat were absent below 1500 m.

Discussion

The insular woodlands of the New York Mountains seem to be an ecological confluence where plant species of the California Floristic Province, Mojave Desert, Great Basin, and Colorado Plateau co-occur in unique assemblages. Both *Pinus monophylla* and *Pinus edulis* were found as well as what appeared to be individual hybrids. *P. monophylla* is one of the most characteristic tree species of the Great Basin while *P. edulis* is much more common on the Colorado Plateau. *P. edulis* populations in Mojave National Preserve may be the only in California and their presence supports the likelihood of a more widespread distribution of both species in the ancient past (Trombulak and Cody 1980). *Juniperus osteosperma, Amelanchier utahensis, Berberis haematocarpa, Fallugia paradoxa* and *Purshia mexicana* are similarly found here at the western limit of their distribution and are characteristic species of the Colorado Plateau. In contrast, *Quercus chrysolepis, Arctostaphylos pungens, Eriodictyon angustifolium, Brickellia californica, Garrya flavescens, Rhamnus ilicifolia* and *Frangula californica* are disjunctive in the New York Mountains, and are more characteristic of the California Floristic Province. *Quercus turbinella,*

Yucca brevifolia, and *Yucca baccata* are species typical of the high Mojave Desert, found here in combination with species ordinarily absent from more common Mojave plant communities. *Artemisia tridentata*, which is highly characteristic of the Great Basin, is also found in the area. The distribution of these species characterizes an isolated zone of associated plants that form unique islands of habitat within Mojave National Preserve. Some of these taxa are derived from the Madro-Tertiary Geoflora (Raven and Axelrod 1978) and have been described as relics of interior chaparral (Brown 1978).

The atypical combination of plant species described here probably reflects the environmental opportunism of species as well as the relictual effects of a changing environment. Long-term climate change which has impacted the distribution of montane species throughout the Great Basin (Johnson 1978) appears to have isolated these unique assemblages in the mountains of Mojave National Preserve, where adequate elevation and geographic orientation support plant species that are otherwise extirpated from lower areas of the Mojave Desert (Wells and Berger 1967). Unlike many other Mojave ranges, perhaps the New York Mountains are high enough and lie so far east that they receive greater precipitation despite the rain shadow of the Sierra Nevada and Transverse Ranges. Evidence of this can be seen in the Ord Mountains of the western Mojave Desert which rise over 1800 m. There, the woodland and chaparral plants found above 1500 m in the New York Mountains are completely absent (personal observation). Interestingly, some of these taxa have been reported at lower elevations within sky islands of the Sonoran Desert in Arizona (Brown 1978). It seems that the North American monsoon may have influence in the higher elevations of Mojave National Preserve that supports species typical of other physiographic provinces such as the Colorado Plateau and Sonoran Desert, where the monsoon is more prevalent (Tubbs 1972; Adams and Comrie 1997; Hereford et al. 2006). The potential for local katabatic air flow to influence the distribution of relatively mesic plant species in the higher elevations of the east Mojave may be important as well.

Many plant species found above 1700 meters in the New York Mountains may have occurred commonly at lower elevations in the region during the Pleistocene and have probably shifted their range upward as the climate of the Mojave Desert and Great Basin has become drier in the last 10,000 years (Wells and Berger 1967). Dendrochronology records taken from ancient timber stands in the desert southwest indicate a wetter climate in the past (Bruening et al. 2017), as do ancient plant materials recovered from pack rat middens (Wells and Berger 1967; Van Devender 1977; Holmgren et al. 2014), suggesting that the pinyon–juniper woodlands likely were more widespread at one time. Likewise, the oak and chaparral populations that are today found in only isolated stands may have been more common throughout the Mojave region when the climate was more favorable to them. Evidence from pack rat middens has shown that plant assemblages in the low elevation Colorado River watershed typically included Quercus turbinella, Pinus monophylla, Juniperus californica and several chaparral plant species during the Pleistocene (Van

Table 2. Avifauna inventory within insular plant communities
Joshua tree-juniper woodland (1200 – 1500 m), abbr. Jsh-Junp; Pinyon-juniper woodland (1500 – 1800 m), abbr. Pin-Junp; Pine-oak forest (> 1700 m), abbr. Pin-oak.

Taxon	Common name	Jsh-Junp	Pin-Junp	Pin-oak
Asio otus	Long eared owl	x		
Phalaenoptilus nuttallii	Common poorwill	x	x	x
Gymnorhinus cyanocephalus	Pinyon jay	x	x	
Amphispiza bilineata	Black throated sparrow	x	x	
Baeolophus ridgwayi	Juniper titmouse	x	x	x
Corvus corax	Common raven		x	
Campylorhynchus brunneicapillus	Cactus wren		x	
Catherpes mexicanus	Canyon wren		x	
Salpinctes obsoletus	Rock wren		x	
Polioptila caerulea	Blue-gray gnatcatcher		x	
Eremophilia alpestris	Horned lark		x	
Cathartes aura	Turkey vulture		x	x
Zenaida macroura	Mourning dove		x	x
Calypte costae	Costa's hummingbird		x	x
Empidonax oberholseri	Dusky flycatcher		x	x
Aphelocoma woodhouseii	Woodhouse's scrub jay		x	x
Cardellina pusilla	Wilson's warbler		x	x
Pheucticus melanocephalus	Black headed grosbeak		x	x
Pipilo maculatus	Spotted towhee		x	x
Piranga ludoviciana	Western tanager		x	x
Poecile gambeli	Mountain chickadee		x	x
Icterus parisorum	Scott's oriole		x	x
Buteo jamaicensis	Red Tail hawk			x
Accipiter cooperii	Cooper's hawk			x
Tyto alba	Barn owl			x
Picoides scalaris	Ladderback woodpecker			x
Spizella atrogularis	Black chinned sparrow			x
Tyrannus vociferans	Cassin's kingbird			x
Haemorphus mexicanus	House finch			x
Psaltriparus minimus	Bushtit			x
Thryomanes bewickii	Bewick's wren			x
Vireo vicinior	Gray vireo			x

Table 3. Avifauna that may be regionally limited to insular woodlands in Mojave National Preserve

Taxon	Common name	Common distribution range
Gymnorhinus cyanocephalus	Pinyon jay	Great Basin, Colorado Plateau, Rocky Mountains
Aphelocoma woodhouseii	Woodhouse's scrub jay	Great Basin, Colorado Plateau, Madrean Highlands
Cardellina pusilla	Wilsons warbler	Throughout North and Central America
Poecile gambeli	Mountain chickadee	Pacific Coast, Great Basin, Colorado Plateau, Rocky Mountains
Pipilo maculatus	Spotted towhee	Pacific Coast, Great Basin, Colorado Plateau, Rocky Mountains
Vireo vicinoir	Gray vireo	Pacific Coast, Colorado Plateau, Sonoran Desert
Baeolophus ridgwayi	Juniper titmouse	Great Basin, Colorado Plateau
Psaltriparus minimus	Bushtit	Pacific Coast, Great Basin, Colorado Plateau, Madrean Highlands
Thryomanes bewickii	Bewick's wren	Pacific Coast, Colorado Plateau, Gulf of Mexico Coast
Pheucticus melanocephalus	Black headed grosbeak	Western North America

Devender 1990; Holmgren et al. 2014). Perhaps past oak and chaparral populations in the Mojave Desert were connected during the early Holocene, via mid-elevation environments, to those currently found along the Pacific Coast. As extant populations of such plant species have been long disconnected, investigating the occurrence of local ecotypes within the isolated woodlands of Mojave National Preserve would be a subject worthy of future study.

These results also suggest which bird species are unique to the insular habitat, those which may be residents, and those which may be only seasonal visitors. Many bird species observed within the area have quite broad geographic ranges, but a distributional confluence similarly seen with plants appears to exist for some birds. Moreover, some of these species may not commonly co-occur. Forty-seven percent of the bird taxa observed were typical of other regions or environments: northern migrants, Pacific and Intermountain West residents, Colorado Plateau residents, or southern and desert migrants and residents. These species apparently ventured into the area and found suitable habitats that are absent in adjacent areas. The results also indicate that as many as 75% of birds found in the New York Mountains are not commonly found in the surrounding basins. This suggests that the isolated plant communities of the New York Mountains offer a special habitat for bird species atypical of the Mojave Desert. Many of these birds reach their limit of distribution around the New York Mountains or were found beyond their normal range. At least 68% of bird species observed by Cardiff and Remsen (1981) were also present within the communities surveyed.

Within Mojave National Preserve, 10 bird species identified here appeared to be limited to the insular woodlands of the region (Table 3), based on data showing their common natural range. These comprise about 32% of the total species surveyed in the study area. Such species probably depend upon these plant communities as a critical habitat that is scarcely found in the Mojave Desert. Habitat values such as microsite diversity, vegetation cover, food resources, and nesting sites are very different in these insular woodlands than in the surrounding desert basins (Johnson 1975). Environmental pressures imposed by climate change may cause physiological challenges for bird species facing decline in the Mojave Desert (Ridell et al. 2019), perhaps leading some populations to favor cooler high elevation woodlands where water is more abundant. These studies indicate that such insular plant communities are a critical natural resource that promotes local biodiversity and increases the regional species richness of Mojave National Preserve. In addition, the pinyon jay and gray vireo were both observed in the study area and are known to be declining in number (Boone et al 2017; Hargrove and Unitt 2017). Records of distribution indicate that pinyon–juniper woodlands are particularly favorable to the reproductive success of these sensitive bird species (Ligon 1978; Schlossberg 2006). Results here support the importance of such insular habitats for species that have likely been affected by fragmentation and long-term environmental change (Johnson 1978). The protection of woodland communities within Mojave National Preserve will likely contribute to the preservation of habitat for bird populations substantially affected by industrialization and urbanization elsewhere.

Exploring the ecology of the New York Mountains and similar neighboring ranges may provide deeper insight into the phenomena that cause an unusual array of species to occur just beyond an environment that is otherwise inhabited by organisms with very different survival strategies. As factors such as climate change, increased fire frequency, species invasion, and livestock grazing threaten ecosystems within the Mojave Desert, these communities warrant conservation and continued monitoring to protect their ecological value. Ultimately, insular woodland habitats contribute to biodiversity within Mojave National Preserve by supporting uncharacteristic flora and fauna. We should be concerned about the extirpation of these species in the future. Conservation of regional species richness will depend in part upon the persistence of these communities and the protection of their natural range.

Acknowledgements

I would like to thank Paula Schiffman, Naomi Fraga and Richard Rachman for their comments on the manuscript. Steve Pickering assisted during avifauna surveys, and Roy Huse helped with producing the maps.

Literature cited

Adams, D.K. and Comrie, A.C. 1997. The North American Monsoon. Bulletin of the American Meteorological Society 12: 2197-2214.

Andre, J.M. 2006. Inventory of Vascular Plants at Mojave National Preserve and Manzanar Historic Site. Technical report #Q2280201178, Inventory and Monitoring Program, U.S. Department of the Interior, National Park Service.

Boone, J. D., Ammon, E., and Johnson, K. 2018. Long-term declines in the Pinyon Jay and management implications for piñon–juniper woodlands, in Trends and traditions: Avifaunal change in western North America (W. D. Shuford, R. E. Gill Jr., and C. M. Handel, eds.), pp. 190–197. Studies of Western Birds 3. Western Field Ornithologists, Camarillo, CA; DOI: 10.21199/SWB3.10.

Brown, David E. 1978. The Vegetation and Occurrence of Chaparral and Woodland Flora on Isolated Mountains within the Sonoran and Mojave Deserts in Arizona. Journal of the Arizona-Nevada Academy of Sciences 13: 7-12.

Brown, James H. 1978. The theory of insular biogeography and the distribution of boreal birds and mammals. Great Basin Naturalist Memoirs 2: 209-227.

Bruening et al. 2017. Fine-scale modeling pine treeline position Great Basin, USA. Environmental Research Letters DOI: 10.1088/1748-9326/aa5432

Calflora: Information on California plants for education, research and conservation. [web application]. 2020. Berkeley, California: The Calflora Database [a non-profit organization]. Available: https://www.calflora.org/ [accessed 3 March 2020]

Cardiff, S.W. and Remsen, J.V. 1981. Breeding Avifaunas of the New York Mountains and Kingston Range: Islands of Conifers in the Mojave Desert of California. Western Birds 12: 73-86.

Hargrove, L. and Unitt P. 2017. Poor reproductive success of Gray Vireos in a declining California population. Journal of Field Ornithology 88: 16-29.

Hereford, R.; Webb, R.H.; Longpre, C.I. 2006. Precipitation history and ecosystem response to multidecadal precipitation variability in the Mojave Desert region, 1893–2001. Journal of Arid Environments 67: 13-34.

Holmgren, C.A. et al. 2014. Evidence against a Pleistocene desert refugium in the Lower Colorado River Basin. Journal of Biogeography 14: 1769-1780.

Iknayan, Kelly J. and Beissinger, Steven R. 2018. Collapse of a desert bird community over the pat century driven by climate change. PNAS 34: 8597- 8602.

Johnson, Ned K. 1975 Controls of number of bird Species on montane islands in the Great Basin. Evolution 29: 545-567.

Johnson, Ned K. 1978. Patterns of Avian Geography and Speciation in the Intermountain Region. Great Basin Naturalist Memoirs 2: 137-159.

Ligon, David J. 1978. Reproductive Interdependence of Pinon Jays and Pinon Pines. Ecological Monographs 48: 111-126.

Miller, D.M. and Wooden, J.L. 1993. Geologic Map of the New York Mountains, California and Nevada. USGS Open-File Report 93-198. DOI: 10.3133/ofr93198

Macarthur, R. H.; Wilson, E. O. 1963. An equilibrium theory of insular zoogeography. Evolution 17:373-387.

Macarthur, R. H.; Wilson, E. O. 1967. The theory of island biogeography. Princeton University Press, Princeton N.J.

Pavlik, Bruce M. 2008. The California Deserts: An Ecological Rediscovery. University of California Press, Berkley. Pp. 71-76.

Prigge, Barry A. 1979. A checklist of vascular plants, Keystone Canyon, New York Mountains, Mojave Desert. U.S. Bureau of Land Management Floristic Inventory of the Eastern Mojave Subdivision.

Raven, P. H and D. I. Axelrod. 1978. Origin and Relationships of the California Flora. University of California Press.

Riddel, E.A et al. 2019. Cooling requirements fueled the collapse of a desert bird community from climate change. PNAS 116: 21609-21615.

Rosenberg, K.V. et al. 2019. Decline of the North American Avifauna. Science 366: 120-124.

Schlossberg, Scott. 2006. Abundance and Habitat Preferences of Gray Vireos (Vireo vicinior) on the Colorado Plateau. The Auk 123: 33-44.

Tubbs, A.M. 1972. Summer Thunderstorms Over Southern California. Monthly Weather Review 100: 799-807.

Trombulak, S.C. and Cody M.L. 1980. Elevational Distributions of Pinus edulis and P. Monophylla (Pinaceae) in the New York Mountains, Eastern Mojave Desert. Madrono 27: 61-67.

Thorne, Robert P.; Prigge, Barry A.; and Henrickson, James. 1981. A Flora of the Higher Ranges and the Kelso Dunes of the Eastern Mojave Desert in California. Aliso: A Journal of Systematic and Evolutionary Botany 10: 71-186.

Van Buren, R. et al. 2011. Woody Plants of Utah. Utah State University Press, Logan UT.

Van Devender, T.R. 1977. Holocene Woodlands in the Southwestern Deserts. Science 198: 189-192.

Van Devender, T.R. 1990. Late quaternary vegetation and climate of the Sonoran Desert, United States and Mexico. *Packrat middens: the last 40,000 years of biotic change* (ed. By J.L. Betancourt, T.R. Van Devender and P.S. martin), pp. 134-165. University of Arizona Press, Tucson AZ.

Wells, Philip V. and Berger, R. 1967. Late Pleistocene History of Coniferous Woodland in the Mohave Desert. Science 155: 1640-1647.

Appendix 1. Avifauna inventory within insular plant communities

South of Drum Peak, Pinyon-juniper woodland (1700 m)

- Horned lark (*Eremophilia alpestris*). One male was seen lower at 1585 m in an open area of mostly juniper and sagebrush scrubland. They are considered in steep decline in California as of 2014.
- Woodhouse's scrub jay (*Aphelocoma woodhouseii).* At least two individuals were seen and heard.
- Rock wren* (*Salpinctes obsoletus*). Two individuals heard calling and one seen perched on top of a large boulder outcropping.
- Wilson's warbler (*Cardellina pusilla*). One female seen. Outside of its summer breeding range although isolated populations have been observed breeding elsewhere in the Great Basin mountains. Not commonly found in the Mojave Desert.
- Western tanager (*Piranga ludoviciana*). At least one seen. Near the extreme of an isolated part of its summer range.
- Dusky flycatcher* (*Empidonax oberholseri*). Two seen, possibly a mating pair. Near the extreme of its summer breeding range.
- Juniper titmouse (*Baeolophus ridgwayi*). At least two seen, likely a mating pair. Feeding around understory shrubs and on the ground. At the extreme of its southwestern range.
- Common raven (*Corvus corax*). Two seen, aerial.
- Turkey vulture (*Cathartes aura*). One seen, aerial.
- Costa's hummingbird* (*Calypte costae*). One seen, possibly exhibiting territorial behavior against juniper titmouse. Near the boundary of its summer breeding range.
- Common poorwill (*Phalaenoptilus nuttallii*). One heard in the evening. Near the boundary of its summer breeding range.
- Mourning dove (*Zenaida macroura*).

Caruthers Canyon, Pine-oak forest (1740 m)

- Cooper's hawk (*Accipiter cooperii*). At least one seen and heard. Near the southern boundary of its summer breeding range.
- Red tail hawk (*Buteo jamaicensis*). One seen, aerial.
- Common poorwill (*Phalaenoptilus nuttallii*). One heard in the evening. Near the boundary of its summer breeding range.
- Barn owl* (*Tyto alba*). One heard screaming in the evening.
- Mountain chickadee (*Poecile gambeli*). One pair observed nesting in a canyon live oak trunk. Near the boundary of its year-round range where normally found in mountain conifer forests. Not common in the Mojave Desert.
- Spotted towhee (*Pipilo maculatus*). Several seen and heard foraging understory shrub and perched. Near the boundary of its year-round range. Not common in the Mojave Desert.
- Wilson's warbler (*Cardellina pusilla*). One male seen.
- Bushtit (*Psaltriparus minimus*). Small group seen and heard foraging in understory shrubs. Near the southwestern boundary of its range and not commonly found in the Mojave Desert.
- Costa's hummingbird* (*Calypte costae*). At least one seen.
- Gray vireo* (*Vireo vicinoir*). At least one seen. Near the western limit of its range centered around the Colorado Plateau. Not common in the Mojave Desert or in California. Isolated summer populations have been observed in the peninsular range of northern Baja California. Species is listed on the 2014 California state bird watch list.
- Juniper titmouse (*Baeolophus ridgwayi*). One heard and seen.
- Woodhouse's scrub jay (*Aphelocoma woodhouseii).* Several heard and seen.
- Cassin's kingbird* (*Tyrannus vociferans*). One possibly seen.
- Dusky flycatcher*(*Empidonax oberholseri*). Several seen. Near the southern boundary of its summer breeding range.

Caruthers Canyon riparian zone (1740 m)

- Turkey vulture (*Cathartes aura*). One seen, aerial.
- Black chinned sparrow (*Spizella atrogularis*). One seen next to water. Near the boundary of its summer breeding range. Not commonly found in the Mojave Desert.
- Western tanager (*Piranga ludoviciana*). Several seen.
- Scott's oriole (*Icterus parisorum*). One male and at least one female seen. Near the boundary of its summer breeding range.
- House finch* (*Haemorphus mexicanus*). One female seen. Near the limit of its elevational range.
- Juniper titmouse (*Baeolophus ridgwayi*). One seen and heard.
- Mourning dove (*Zenaida macroura*).

Caruthers Canyon pinyon-juniper-chaparral woodland (1740 – 1890 m)

- Canyon wren (*Catherpes mexicanus*). At least two heard.
- Mountain chickadee (*Poecile gambeli*). One pair seen and heard amongst shrubs and large boulders.
- Spotted towhee (*Pipilo maculatus*). At least one seen and heard.
- Woodhouse's scrub jay (*Aphelocoma woodhouseii).* Several seen and heard amongst boulder outcrops above the canyon floor.
- Costa's hummingnird (*Calypte costae*). At least one seen.

Keystone Canyon, Pinyon-juniper- chaparral woodland (1580 – 1800 m)

- Pinyon jay (*Gymnorhinus cyanocephalus*). Several seen and heard. Near the western boundary of its range centered mainly on the Great Basin, Colorado Plateau and western Rocky Mountains. Species has an IUCN Conservation Status as vulnerable and at risk of becoming endangered due to habitat loss and fragmentation. Not commonly found in the Mojave Desert beyond mountains with pinyon forest.
- Woodhouse's scrub jay (*Aphelocoma woodhouseii).* Several seen and heard, and exhibiting territorial behavior against pinyon jays.

- Black headed grosbeak (*Pheucticus melanocephalus*). One seen and heard perched amongst shrubs. Just beyond its summer breeding range.
- Dusky flycatcher (*Empidonax oberholseri*). One seen within understory shrubs.
- Blue gray gnatcatcher (*Polioptila caerulea*). Several seen and heard while feeding amongst understory shrubs.
- Spotted towhee (*Pipilo maculatus*). One seen on the ground beneath chaparral shrubs.
- Scott's oriole (*Icterus parisorum*). One male and one female seen separately.

Keystone Canyon, Pine-oak forest (1700 – 1800 m)

- Costa's hummingbird (*Calypte costae*). At least two seen and heard.
- Black headed grosbeak (*Pheucticus melanocephalus*). One pair seen at Keystone spring (Fig 4).
- Bewick's wren (*Thryomanes bewickii*). Observed nesting in a canyon live oak trunk. Near an isolated part of its summer breeding range and not commonly found in the Mojave Desert.
- Turkey vulture (*Cathartes aura*). One seen, aerial.
- Ladder-backed woodpecker* (*Picoides scalaris*). One heard at Keystone spring. Near the northwest boundary of its year-round range where it is common in the Southern U.S. and Mexico.
- Western tanager (*Piranga ludoviciana*). One seen.
- Wilson's warbler (*Cardellina pusilla*). One male seen.

Lower Keystone Wash, Joshua tree-juniper woodland (1500 m)

- Pinyon jay (*Gymnorhinus cyanocephalus*). At least one seen and heard.
- Juniper titmouse (*Baeolophus ridgwayi*). Several seen and heard.
- Common poorwill (*Phalaenoptilus nuttallii*). At least two heard in the evening.
- Long eared owl (*Asio otus*). One heard in the evening. Near the limit of its year-round range.
- Black throated sparrow (*Amphispiza bilineata*). At least one seen perched on top of Joshua trees. Near the southern boundary of its summer breeding range.

Guzzler Ridge near Trio Mine, Pinyon-juniper woodland (1500 m)

- Pinyon jay (*Gymnorhinus cyanocephalus*). Several seen and heard in a group.
- Cactus wren (*Campylorhynchus brunneicapillus*). One seen. Near the northwest boundary of its year-round range. Some California populations have been displaced and locally extirpated due to intensive urban development and consequent habitat loss.
- Western tanager (*Piranga ludoviciana*). One pair seen in a pinyon pine.
- Black throated sparrow (*Amphispiza bilineata*). One pair seen.

*Brief observations that could be in error

Circular structures from the Precambrian Bass Formation in Grand Canyon National Park—biogenic or non-biogenic?

Chun Heng Chiu,[1] Ian Igleheart,[1] and Donald Lofgren[2]
[1]*The Webb Schools, Claremont, CA 91711*
[2]*Raymond M. Alf Museum of Paleontology, Claremont, CA 91711*

ABSTRACT—Raymond Alf found circular structures on bedding planes of the Bass Formation in Grand Canyon National Park in the 1950s that he interpreted as jellyfish impressions, which were later identified as sedimentary structures and largely forgotten. More recently, Paleoproterozoic Stirling Biota medusoids similar in morphology to the Bass structures were reported from Australia, which inspired a reanalysis of the Bass Formation impressions that consist of two morphotypes. The smaller morphotype has concentric inner and outer rings, with a hypo-relief central core and pitted concentric annuli on the outer margin of the inner ring. The larger morphotype is similar in most respects but has an asymmetrical outer ring. Bass impressions are not rain imprints because rain discs lack the morphological complexity of the Bass structures nor are they holdfasts of fossil organisms because cross sections indicate sediment laminae were not disrupted. Bass Formation structures are probably the result of gas or gaseous fluid erupting through substrate via a gas dome sand volcano as the morphology of Bass impressions is similar to features of recent and Proterozoic sand volcanos/gas domes. The inner ring of Bass impressions represents the breached dome and its margin of highly disturbed sediment, and the outer ring represents substrate disruption that diminished laterally. Smaller morphotype impressions that abut represent adjacent sand volcanos, clusters of structures with disrupted inner and outer rings represent closely spaced eruptions, and mound-like structures appear to be unerupted domes. The Bass impressions are most likely sedimentary structures that superficially resemble extant algal colonies and fossil medusae impressions.

Introduction

The Bass Formation crops out along the Kaibab Trail on the South Rim of the Grand Canyon and at other localities within the park. The Bass Formation is composed primarily of dolomite and arkose interbedded with shale deposited about 1255 Ma (Hendricks and Stevenson, 1990; Timmons et al., 2005; Timmons et al., 2019). Raymond Alf, a teacher at The Webb Schools (Southern California secondary school) hiked the Kaibab Trail with his students in 1955 when they found discoidal impressions in the Bass Formation (Figure 1) which Alf believed were traces of jellyfish (Lofgren et al., 2019). Alf's search for fossils in the Bass Formation was probably inspired by an earlier discovery of a disc-like structure with radiating lobes in the Nankoweap Formation that was thought to represent a jellyfish (Van Gundy, 1937, 1951). Alf (1959) identified his Bass imprints

Figure 1. Raymond Alf and Webb Schools students searching for rocks bearing what Alf thought were jellyfish impressions from the Bass Formation in the Inner Gorge of the Grand Canyon in 1957 (Alf second from right).

Earliest Animal Fossil Found By Claremont Science Teacher

Billion-Year-Old Trace Turned Up on Field Trip

By HARRISON STEPHENS

CLAREMONT, — A science field trip by a group of Claremont schoolboys and their teacher has turned up what may be the earliest traces of animal life ever found on earth.

Raymond Alf, Webb School instructor who led the trip, said today other scientists have concurred with him in terming his finds the billion-year-old fossils of worms and jellyfish. If they are, they will change present theories on how long animal life has existed in the world.

"There'll be disputes over it," Alf said. "At least I hope so. Anything of significance usually starts an argument."

He plans to publish the facts on his discovery soon in a scientific journal. Then he'll wait and see what paleontologists have to say about it.

Found in Grand Canyon

Alf and his party of 10 Webb students and another teacher found the fossilized prints of the animals on a steep shale slope near the bottom of the Grand Canyon during an Easter vacation trip. The excursion was part of Alf's "History of Life" course.

The group had hiked 5½ miles down the Kaibab Trail from the South Rim of the canyon to study fossils of algae in the deep sedimentary deposits. These are the pre-Cambrian deposits. They represent the Proterozoic Era of geologic history, known among paleontologists for their almost total lack of animal fossils.

Alf spotted a piece of quartzite that had broken off a ledge and split. One half had impressed in it what looked like

sell and Malcolm McKenna, went back to the canyon to gather evidence on the find.

"They found more pieces of the same rock with prints of another jellyfish and part of a third, and other rock fragments covered with fossilized worms. They located the ledge from which the fragments had broken 330 feet from the bottom of 12,000 feet of pre-Cambrian sediment. The minimum age of the sediment at this point is a billion years, Alf said.

"If jellyfish and worms occurred at the bottom of this series, we must figure back much further to allow for development of animal life to this point," Alf said. "These traces force us to realize that the origin of animal life on earth goes further back than many had dared think."

Alf theorized that the jellyfish made clear prints in what is now stone because of the chance location of their deaths. The soft bodied little creatures must have died in the shallow, quiet waters of a Proterozoic lagoon, he said. Their bodies sank into the ooze at the bottom. Before they could decay and disappear forever, they were covered with a thin layer of sediment from a river emptying into the lagoon. Their shapes were formed in the

May 12, 1955

Figure 2. Inland Valley Daily Bulletin article on impressions discovered by Ray Alf and Webb School students in 1955 from the Bass Formation that were reported as representing the earliest trace of animal life on Earth.

as jellyfish impressions, which if correct, would have extended the known record of metazoans by about 500 million years (Figure 2). Alf's bold hypothesis was rejected because the Bass impressions were considered inorganic in origin (Cloud, 1960, 1968; Nitecki, 1971). However, the genesis of the Bass structures did generate debate (Glaessner, 1962), and some Bass imprints did resemble extant algal colonies (Glaessner, 1969). Alf did not provide a detailed analysis of the circular Bass structures to rebut the sedimentary structure hypothesis and interest in the specimens waned, resulting in their omission from the Treatise on Invertebrate Paleontology focused on trace fossils and problematica (Hantzschel, 1975).

More recently, Precambrian cyclomedusoids were reported, particularly from Ediacaran strata (Liu et al., 2015). Also, circular structures first described as fossils, then identified as sedimentary structures (Cloud, 1968), were reinterpreted as fossil medusoids (Gehling et al., 2000). Moreover, the Stirling Range Formation in southwestern Australia yielded discoidal structures interpreted to represent impressions of holdfasts of Ediacaran age (Cruse et al., 1993; Cruse and Harris, 1994) in rocks previously considered Mesoproterozoic (Turek and Stephenson, 1966). These strata were later determined to be Paleoproterozoic (Rasmussen et al., 2002, 2004), and other records of Meso or Paleoproterozic metazoans were reported from India and China (Shixing and Huineng, 1995; Seilacher et al. 1998; Bengston et al., 2009). In light of these reports, we reevaluated the circular Bass structures to determine if they represent an early life form or a type of sedimentary structure.

Locality

Two distinct medusa-shaped morphotypes were recovered at RAM (Raymond Alf Museum of Paleontology) locality I94003 from interbedded quartzites and shales (about 60 ft thick) associated with an algal laminated limestone of the Bass Formation at an elevation of about 3,750 feet, adjacent to the Kaibab Trail in Grand Canyon National Park, Arizona (Alf, 1959). Note: both Alf (1959, fig. 2) and Cloud (1968 fig. 4C-D) provided images of the circular Bass structures that show recessed impressions, here referred to as negative hypo-relief impressions. Thus, we assume that the slab on which a negative impression was made represents the bedding plane on which the structure was first preserved. Sediment eventually filled the structure, creating a positive epi-relief impression as seen in slab pairs (Alf, 1959, fig. 1).

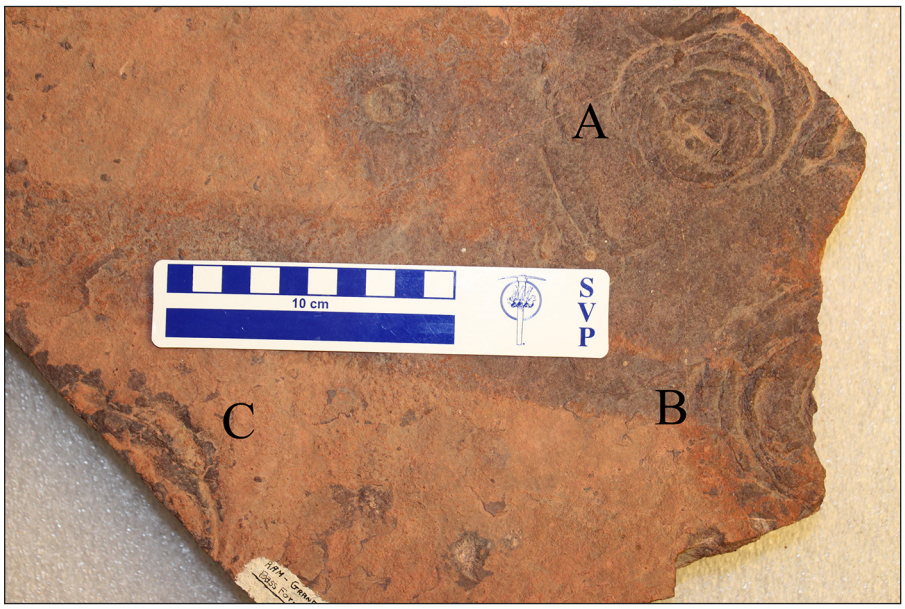

Figure 3. RAM 22007, negative impressions of larger Bass Formation morphotypes. A) most complete impression, B) about half of a complete impression, C) small fragment of impression.

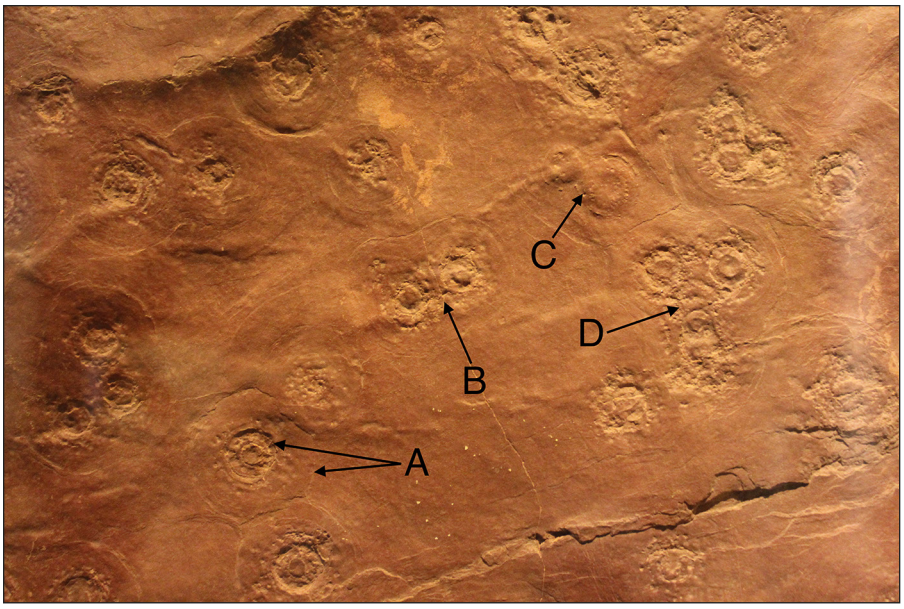

Figure 4. RAM 7140, negative impressions of smaller Bass Formation morphotypes. A) single impression with arrows pointing to outer margin of inner ring and outer margin of outer ring. B) pared impressions that abut but do not overlap, C) two dome shaped impressions that may represent unerupted gas dome sand volcanos, D) four or five closely spaced impressions whose inner and outer rings are highly to moderately disturbed; a chronologic order of impression formation is hard to discern in this cluster, but the upper right and left impressions are most intact and were probably last to form.

Larger morphotype

The larger morphotype is represented by imprints in two sets of paired slabs of quartzite (3.5 to 5 cm thick) which show negative and positive impressions of a partly asymmetrical medusa-like structure. An image of the most complete impression (now lost) shows a structure with a circular central area about 2.5 to 3 cm in diameter, with a partly distinct, asymmetrical outer margin that gives the impression a total diameter of about 7 cm (Alf, 1959, fig. 1, metric scale in photo). The slab margin appears to equal the outer edge of one side of the impression, and if so, the outer ring varies from 1.2 to 4 cm in width.

The second pair of slabs (RAM 22140 positive impression; RAM 22007 negative impression) has three incomplete impressions (Figure 3). The most prominent impression is about 80% complete (Figure 3A) and has a raised central boss 2.8 cm in diameter and a maximum outer edge diameter of 9.4 cm. The distinction between the central circular area and outer margin is not as evident compared to the lost slabs, but the central area was at least 4 cm in diameter and is ringed by one or two concentric annuli. The remainder of the outer part of the impression is less distinct, as outer annuli are faint and asymmetrical. The faint traces and the asymmetrical nature of the outer margin of the most complete impression (Figure 3A) were interpreted to represent successive imprints made by a jellyfish that impacted the substrate twice before making its final impression (Alf, 1959). Also, the central area appeared to exhibit a faint four- or five-fold radial symmetry (Alf, 1959). Although there is a faint four-fold division in the central area, the sections are unequal in area and therefore asymmetrical.

The other two impressions on RAM 22007 are much less complete (Figure 3B-C). Of the two, the more complete structure is truncated by breakage through its central area which is ringed by two apparently concentric annuli (Figure 3B), and there is no trace of the faint, asymmetrical outer annuli seen in the most complete impression (Figure 3A-B). The least complete impression preserves an arc of the outer part of the central area bordered by two partial outer annuli (Figure 3C).

Smaller morphotype

An image of the smaller Bass morphotype was provided by Alf (1959, fig. 2), and multiple examples are present on slabs in the RAM collections. Complete impressions (n=40) have a distinct inner and outer ring (Figure 4A), with the inner ring having a hypo-relief circular central core with raised

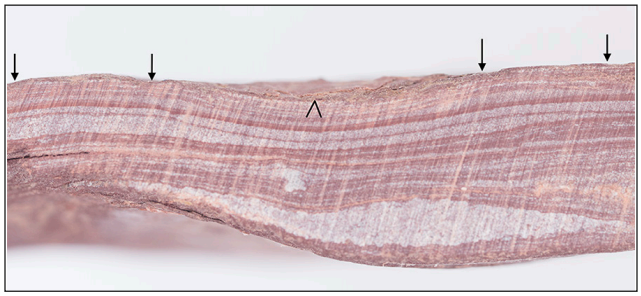

Figure 5. Cross section of negative impression of RAM 7140 that is 1 cm in thickness. Arrows denote central core and outside margins of both the inner and outer ring.

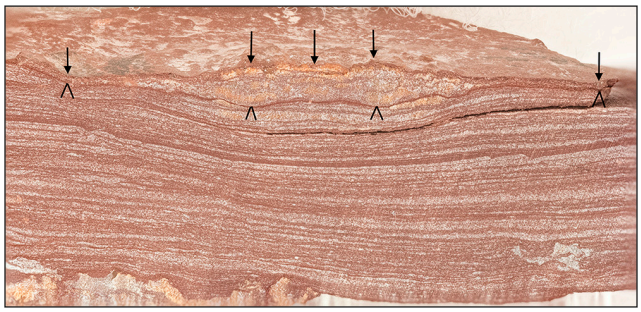

Figure 6. Slightly oblique cross section of positive impression of RAM 22078 that is 2 cm in thickness. Arrows denote the central core and outside margin of the inner and outer rings. Inverted V's denote the mud drape that capped the sediment lens filling the impression.

Table 1. Measurements in mm of the inner ring and total diameter of complete examples of the smaller morphotype from the Bass Formation.

Specimen Number	(Inner Ring and Total Diameters)
RAM 7140	(12.6, 28.7) (13.4, 31.2) (6.4, 25.7) (10.7, 27.3) (9.3, 28.0) (9.9, 26.2) (8.9, 28.8) (9.7, 31.4) (9.2, 30.0) (10.4, 34.7) (7.0, 28.0) (6.6, 24.6) (10.1, 28.0) (7.5, 27.9) (9.2, 29.3) (7.1, 26.1) (9.8, 33.6) (7.8, 34.3) (8.5, 37.3) (10.0, 34.5)
RAM 21995	(7.5, 28.7) (6.9, 25.1) (6.1, 27.4)
RAM 22678	(12.0, 30.4) (9.5, 25.6) (7.0, 22.5)
RAM 21926	(9.8, 27.4) (7.8, 22)
RAM 22080	(12.0, 26.0)
RAM 21989	(7.5, 24.8)
RAM 21971	(9.5, 32.7)
RAM 22065	(12.8, 26.2)
RAM 22034	(11.6, 40.2)
RAM 22023	(7.7, 30.6)
RAM 21935	(10.0, 32.0) (6.9, 22.0)
RAM 21951	(7.6, 23.4) (8.3, 29.7)
RAM 21928	(8.2, 23.0) (9.2, 23.4)

outer edges surrounded by a depressed concentric ring of undulating sediment exhibiting numerous pits. The depressed concentric inner ring rises at its outer margin which defines the boundary between the inner and outer ring; inner ring diameter is 6.1–13.4 mm (mean 8.9 mm). The outer ring is composed of a distinct horizontal band of faint concentric annuli whose outside edge defines its maximum extent; outer ring diameter is 22.0–40.2 mm (mean 27.2 mm) (Table 1).

There are many examples where outer rings of two adjacent impressions abut, each remaining intact, but their outer ring margins are deflected so they are no longer symmetrical (Figure 4B). A few impressions are concentric mounds with recessed central cores whose outside margin is defined by a low outer ring composed of faint annuli (Figure 4C). Clusters of multiple closely spaced impressions have highly deformed outer rings and moderately disrupted inner rings (Figure 4D).

The authors sectioned the negative hypo-relief (bedding plane impression) and positive epi-relief (cast of impression) parts of smaller morphotypes. A cross section of RAM 7140 (negative impression) shows a broad and shallow structure with distinct raised areas that define the outside edge of the inner ring. Faint raised areas also define the outside edge of the outer ring (Figure 5). A lens of thicker sediment corresponding to the inner ring is seen in a cross section of RAM 22078, a positive impression with depressions that conform to the outside edges of the inner ring (Figure 6). The lens thins throughout the extent of the outer ring before merging laterally with laminated sediment at the outside margins of the impression. Also, distinct mud drapes define the top and bottom of the lens (Figure 6).

Discussion

Bass Formation impressions have an intriguing morphology suggestive of a biogenic origin, but can this be convincingly demonstrated? Consider the case of *Brooksella canyonensis*, which was based on a single specimen found in the 1930s from the Nankoweap Formation and thought to represent a jellyfish (Van Gundy, 1937). Bassler (1941) described and named the specimen but was uncertain if it represented a jellyfish impression or some type of sedimentary structure. Probably in hopes of confirming its identification, Van Gundy (1951) searched for additional specimens, finding none, but still considered *Brooksella canyonensis* to represent a jellyfish impression. Later, *Brooksella canyonensis* was identified as a trace fossil (Seilacher, 1956), an inorganic sedimentary structure (Cloud 1960, 1968), and then was listed as Medusae Incertae Sedis by Hantzschel (1975). Similarly, in his only report on the Bass impressions, Alf (1959, p. 60) noted that "the purpose of the present paper is to call the attention of the scientific public to these specimens in the hope that professional comment may be forthcoming." However, the result was not as Alf expected because scientific scrutiny resulted in the Bass impressions being identified as inorganic structures (Cloud, 1968; Nitecki, 1971). However, Alf never accepted that the Bass impressions were nonbiogenic and considered them his greatest paleontological discovery (Lofgren et al., 2019). Whether the Bass structures represent rain drop imprints, holdfast scars, gas/fluid escape structures, or some type of fossil organism is discussed below.

Rain drop impressions

A drop of rain falling on unlithified sediment can leave a distinct circular impression. A specimen from the Permian Coconino Formation of Arizona in the RAM collection has simple circular impressions .5 to 1. cm in diameter on a bedding plane of fine sandstone. These impressions are smaller and lack the complexity of the inner and outer rings of the Bass structures. Also, the resulting impressions made experimentally by dropping water on soft plaster (Cloud, 1968, fig. 4A) do not resemble the Bass impressions, nor do rain drop impressions on red shale from Triassic strata in New Jersey (Lyell, 1851, fig. 2), which again are simple circles without multiple rings.

Holdfast scars

Aspidella terranovica, a Precambrian circular structure with radial lineations and a central cone thought to represent a type of metazoan from the late Neoproterozoic Fermeuse Formation in Newfoundland (Billings, 1872) was considered a sand volcano (Cloud 1968; Hoffman 1971, plate 5 figs. 3-4) or pseudo-fossil (Hantzschel, 1975), but was more recently reinterpreted as a body fossil based on restudy of the type locality (Gehling et al., 2000). Some morphs of *Aspidella* from the type locality in Newfoundland now interpreted as holdfasts of metazoans (Gehling et al., 2000, fig. 8, 15) closely resemble the smaller morphotype from the Bass Formation. Also, the smaller Bass morphotype and the Neoproterozoic specimens described by Gehling et al. (2000) exhibit mutually deformed boundaries where two or more abut, which is also a characteristic of other Ediacaran taxa (Wade, 1972, pl. 41, fig.1; Narbonne and Aitken, 1990, pl. 1, fig. 6). Some of these Neoproterozoic discoids, like these identified as *Aspidella*, were interpreted to represent holdfasts that had stem or frond-like extensions (Jenkins and Gehling, 1978; Gehling et al., 2000), and cross sections of these structures show disruption and/or truncation of sediment laminae (Gehling et al., 2000, fig. 10, 12).

The circular shape and morphology of the inner ring of the smaller Bass morphotype do resemble *Aspidella* and similar Ediacaran taxa. However, cross-sectioning of the smaller Bass morphotype shows undisturbed bedding (Figure 5), in contrast to *Aspidella* from the Neoproterozoic Fermeuse Formation where laminae are truncated (Gehling et al., 2000, fig. 12). Bass impressions also have a distinct outer ring with faint annuli (Figure 4A), features not seen in the Neoproterozoic discoids. Thus, the smaller Bass impressions are not consistent with holdfast scars.

Gas or fluid escape structures

Circular structures in sedimentary rocks that are the result of fluid/gas voiding through unlithified sediment are often referred to as "*Astropolithon*" or sand volcanos (Hantzschel, 1975; Dornbos et al., 2007). Originally, "*Astropolithon hindii*" was applied to circular structures with radial lines from Cambrian strata in Nova Scotia thought to be of biogenic origin (Dawson, 1878, 1890) and examples were reported elsewhere (Glaessner, 1966). However, Walter (1972) interpreted similar Precambrian structures as conical sand volcanoes, and Pickerill and Harris (1979) argued that "*Astropolithon hindii*" represented a type of sand volcano that left an imprint consisting of a low relief mound with a central apical depression surrounded by circular lineations. Sand volcanos can form on substrates with or without a biomat (Seilacher et al., 2002, figs. 7 and 8), and a substrate with a sediment biomat would crack radially as fluid erupted (Seilacher, 2007). Thus, circular impressions with radial lineations are referred to as "*Astropolithon*," and circular structures that lack radial lineations (made by sand volcanos erupting through substrates without biomats) are called "gas domes" (Dornbos et al., 2007). If such a distinction can be applied to the Bass Formation impressions, they would be gas dome sand volcanos.

Recent gas escape structures that are much larger than either Bass morphotype have a close similarity to the smaller morphotype as they have a recessed inner ring and an outer ring composed of a fairly horizontal band of sediment with distinct annuli (Maxson, 1940, fig. 4). Also, Cambrian structures that resemble the smaller Bass morphotype from the King Square Formation in New Brunswick, Canada, interpreted to represent sand volcanos, have a central depression with concentric rings and a broad trough surrounding the inner ring margin (Hagadorn and Miller 2011, fig. 2C-D). Additionally, where two of the Cambrian discoids abut, edges of their outer troughs always coalesce rather than overlap (Hagadorn and Miller, 2011, fig. 4G-K), similar to pairs of the smaller Bass morphotype (Figure 4B). Although these Cambrian structures have radial lineations ("*Astropolithon*") in some cases (Hagadorn and Miller 2011, fig. 4A-C), in most other respects, they closely resemble the smaller Bass impressions.

A schematic of sand volcano formation by Plummer (1980, fig. 2) shows that the result of the eruption is a shallow depression in the substrate which would correspond to the hypo-relief Bass impression (Figure 5), with subsequent infilling of sediment equivalent to the epi-relief Bass impression (Figure 6). Recent gas blisters in mud from a geyser field in New Zealand (Cloud, 1960, pl. 1, fig. 1) resemble the smaller Bass morphotype and were evidence cited to conclude that Bass Formation "jellyfish" impressions described by Alf (1959, fig. 2) were sedimentary structures caused by escaping gas (Cloud, 1960, 1968). The inner ring of Bass impressions would represent the breached dome and its margin of highly disturbed sediment, and the outer ring would represent a faint disruption of sediment that diminished laterally as the energy released from the eruption waned. Unerupted fluid or gas domes can also be associated with sand volcanos. RAM 7140 has two closely spaced dome-like structures (Figure 4C) on a bedding plane that also exhibits numerous structures that presumably represent erupted sand volcanos. The unerupted domes on RAM 7140 resemble experimentally developed silt domes with central depressions caused by trapped gas (Gill and Kuenen 1957, plate 36, 2-5) (Figure 4C).

Thus, multiple lines of observation suggest that the Bass Formation structures are consistent with gas dome sand volcanos where gas or gaseous fluid erupted through a muddy substrate lacking a biomat. However, a cross section of a Bass Formation structure (Figure 6) indicates sediment laminae immediately below the mud substrate interface are not disrupted, which might be expected as a result of the eruptive process; all other smaller Bass morphotype structure cross sections (n=8) also lack

disrupted laminae below the mud substrate interface. Kirkland et al. (2016) argued that no indication of vertical fluid escape structures in the center of similar discoidal structures from Silurian strata in Norway was evidence that the discoids were not the result of sand volcano development. However, no vertical oriented sediment or fluid shaft was developed below the substrate surface in impressions seen in cross section of the discoid structures (once described as fossil medusae) from the Cambrian site in New Brunswick interpreted to represent sand volcanos (Hagadorn and Miller, 2011, fig. 5). Perhaps the Bass structures were made by a less disruptive process where gas/gaseous fluid escaped through permeable sediment laminae before erupting through the more impermeable mud substrate interface (perhaps a weakly developed biomat was present, so when the mud substrate was breached, radial lineations did not form). Kirkland et al. (2016) argued that irregular disc formation would be the result when multiple sand volcanos abut/overlap within a confined area, a feature seen in RAM 7140 where densely packed individual impressions are highly disrupted (Figure 4D), suggesting sand volcano activity on the Bass Formation bedding plane. Thus, other than the lack of a vertical shaft in cross section providing visual evidence of upward fluid/gas movement, the Bass impressions appear to be the result of the eruption of numerous gas dome sand volcanos that released gas or gaseous fluids through substrates that had weakly developed or lacked biomats.

Algal colony or jellyfish

Alf (1959) interpreted the Bass structures as imprints of jellyfish, but most reports of Precambrian medusae represent trace fossils or inorganic features such as fluid/gas escape structures (Young and Hagadorn, 2010). Also, fossil medusae are almost never perfectly radially symmetrical nor oriented parallel on a bedding plane (Young and Hagadorn, 2010) like the Bass impressions. In addition, fossil medusae from mass stranding events in the Cambrian Mt. Simon/Wonewoc sandstones do not closely resemble the Bass structures, as they usually have a central convex mound of sediment surrounded by a convex sediment ring (Hagadorn et al., 2002). These Cambrian medusae were interpreted to have ingested sediment, which after decay, left a convex mound of sediment on the substrate that resulted in the raised central sediment mound (Hagadorn et al., 2002, appendix 2). The positive impression of Bass Formation structures in cross section is similar to Cambrian medusae impressions as there is a distinct thickening of sediment that forms the positive Bass impression. If Bass Formation fossil medusae had indeed left a raised mound of sediment, the top of the mound would correspond to the sediment level indicated by inverted V's in Figure 6. Thus, the lens of sediment seen in cross section would represent a medusa, but if so, one would expect that the strata would split at this sediment interface rather than below as it does in all Bass impressions (Figure 6). Also, every example of a Bass impression has a positive counterpart, and it seems unlikely that every fossil medusae would ingest that much sediment because only some medusae from the mass stranding event in the Cambrian Mt. Simon/Wonewoc sandstones ingested sediment (Hagadorn et al., 2002). Finally, the lensoidal thickening of sediment in positive Bass impressions thins and merges laterally with laminae outside the margin of the imprint, so the lens is part of a sedimentation event independent of the formation of the negative impression. In any case, Young and Hagadorn (2010) argued that there are no bona fide Proterozoic medusae, a statement that now also includes the Bass Formation impressions (Hagadorn, pers. comm. October 2019).

Extant diatomaceous algae colonies from Australia have circular gelatinous sheaths with concentric rings, and when two colonies are adjacent, in outline they resemble abutting pairs of the smaller Bass impressions (Glaessner, 1969, figs, 2-3). Whether the imprints of algal colonies on a substrate of soft sediment would leave such a distinctive and complex impression as the Bass Formation structures is unknown. Thus, although unlikely, the interpretation that the Bass Formation structures are the result of some type of biologic activity cannot be disproven.

Summary

Discoidal structures in outcrops of the Mesoproterozoic Bass Formation in Grand Canyon National Park were first thought to represent jellyfish impressions (Alf, 1959), but were later interpreted as sedimentary structures (Cloud, 1960, 1968; Nitecki, 1971) and largely forgotten. In the 1990s, Precambrian medusoids similar to the Bass Formation structures were reported from the Stirling Range Formation of Australia (Cruse et al. 1993; Cruse and Harris, 1994) and dating of these strata indicated a Paleoproterozoic age for the Stirling Biota (Rasmussen et al., 2002, 2004; Bengtson et al., 2007). These reports inspired re-evaluation of the Bass Formation impressions.

Bass Formation impressions are probably the result of gas or gaseous fluid erupting through the substrate because features of recent and Proterozoic structures identified as gas dome sand volcanos are very similar in morphology. Key similarities are concentric inner and outer rings, a depressed central core, abutment of paired impressions, disruption of adjacent inner and outer rings in clusters, and doming of some impressions. Bass impressions are not rain imprints or holdfasts because raindrop discs lack the morphological complexity of the Bass structures and cross sections show no disruption of sedimentary laminae associated with holdfasts of fossil organisms. The Bass structures superficially resemble extant algal colonies and fossil jellyfish impressions, but the gas dome sand volcano hypothesis is much more robust. Caution was recommended by Cloud (1973) when attempting to identify fossil medusae based on circular imprints in Precambrian strata. Raymond Alf hoped that his Bass "jellyfish" impressions would eventually be

recognized as fossil medusae (Lofgren et al., 2019), but we concur with Cloud (1960, 1968) and Nitecki (1971) that the Bass imprints are most likely sedimentary structures.

Acknowledgments

We thank the National Park Service for rock collecting permits issued to Raymond Alf in the 1950–60s; G. Santos, L. Gerken, F. Hu, and P. Fong for assistance with figures; J. M. Timmons for reviewing the manuscript; J. Hagadorn for informative discussion; and the David B. Jones Foundation and the Mary Stuart Rogers Foundation for financial support. This paper is dedicated to Raymond Alf and Webb Schools students who carried hundreds of Bass Formation specimens out of the Grand Canyon; approximate distance and elevation gain 10 km and 1,400 m, respectively (heaviest 25 kg!).

References cited

Alf, R. M. 1959. Possible fossils from the Early Proterozoic Bass Formation, Grand Canyon, Arizona. Plateau 31:60-63.

Bassler, R. S. 1941. A supposed jellyfish from the pre-Cambrian of the Grand Canyon. Proceedings of the United States National Museum 89:519-522.

Bengtson, S., V. Belivanova, B, Rasmussen, and M. Whitehouse. 2009. The controversial "Cambrian" fossils of the Vindhyan are real but more than a billion years older. Proceedings of the National Academy of Sciences 106:7729-7734.

Bengtson, S., B. Rasmussen, and B., Krapež. 2007. The Paleoproterozoic megascopic Stirling Biota. Paleobiology 33:351-381.

Billings, E. 1872. Fossils in Huronian rocks. Canadian Naturalist and Quarterly Journal of Science 6:478.

Cloud, P. 1960. Gas as a sedimentary and diagenetic agent. American Journal of Science 258-A:35-45.

Cloud, P. 1968. Pre-metazoan evolution and the origins of the Metazoa. Pp. 1-72 in E. T. Drake (editor), Evolution and Environment. Yale University Press, New Haven.

Cloud, P. 1973. Pseudofossils: a plea for caution. Geology 1:123-127.

Cruse, T., L.B. Harris, and B. Rasmussen. 1993. The discovery of Ediacaran trace fossils and body fossils in the Stirling Range Formation, Western Australia: implications for sedimentation and deformation during the "Pan-African" orogenic cycle. Australia Journal of Earth Sciences 40:293-296.

Cruse, T., and L. B. Harris. 1994. Ediacaran fossils from the Stirling Range Formation, Western Australia. Precambrian Research 67:1-10.

Dawson, J. W. 1878. Supplement to the second edition of Acadian Geology, the geological structure, organic remains, and mineral resources of Nova Scotia, New Brunswick and Prince Edward Island. MacMillan, London, 102 pp.

Dawson, J. W. 1890. On burrows and tracks of invertebrate animals in Palaeozoic rocks, and other markings. Quarterly Journal of the Geological Society 46:595-618.

Dornbos, S. Q., N. Noffke, and J. W. Hagadorn. 2007. Mat-decay features. Pp. 106-110 in J. Schieber, P.K. Bose, P.G. Eriksson, S. Banerjee, S. Sarkar, W. Altermann, and O. Catuneanu (eds.), Atlas of microbial mat features preserved within the siliciclastic rock record. Elsevier, Amsterdam, Netherlands.

Gehling, J. G., R. M. Narbonne, and M. M. Anderson. 2000. The first named Ediacaran body fossil, *Aspidella terranovica*. Palaeontology 43:427-456.

Glaessner, M. F. 1962. Pre-cambrian fossils. Biological Reviews 37:467-494.

Glaessner, M.F. 1969. Trace fossils from the Precambrian and basal Cambrian. Lethaia 2:369-393.

Glaessner, M. F., and M. Wade. 1966. The late Precambrian fossils from Ediacara, South Australia. Palaeontology 9:599-628.

Gill, W. D., and P. H. Kuenen. 1957. Sand volcanoes on slumps in the Carboniferous of County Clare, Ireland. Quarterly Journal of the Geological Society 113:441-460.

Hagadorn, J. W., R. H. Dott Jr, and D. Damrow. 2002. Stranded on a Late Cambrian shoreline: Medusae from central Wisconsin. Geology 30:147-150.

Hagadorn, J., and R. Miller. 2011. Hypothesized Cambrian medusae from Saint John, New Brunswick, reinterpreted as sedimentary structures. Atlantic Geology 47:66-80.

Häntzschel, W. 1975. Miscellanea, Supplement 1, Trace Fossils and Problematica. Treatise on Invertebrate Paleontology. Part W. Geological Society of America and University of Kansas Press, Lawrence, 269 pp.

Hendricks, J. D., and G. M. Stevenson. 1990. Grand Canyon Supergroup: Unkar Group. Pp. 49-70 in S.S. Beus and M. Morales (eds.), Grand Canyon Geology. Oxford University Press, New York.

Hofmann, H. J. 1971. Precambrian fossils, pseudofossils and problematica in Canada. Geological Survey of Canada Bulletin 189:1-146.

Jenkins, R. J., and J. G. Gehling. 1978. A review of the frond-like fossils of the Ediacara assemblage. Records of the South Australian Museum 17:347-359.

Kirkland, C. L., B. A. MacGabhann, B. L., Kirkland, and J. S. Daly. 2016. Cryptic Disc Structures Resembling Ediacaran Discoidal Fossils from the Lower Silurian Hellefjord Schist, Arctic Norway. PloS ONE 11:1-21.

Liu, A. G., C. G. Kenchington, and E. G. Mitchell. 2015. Remarkable insights into the paleoecology of the Avalonian Ediacaran macrobiota. Gondwana Research 27:1355-1380.

Lofgren, D., J. Liu., and E. Williams. 2019. Moment in Time: The Life of Raymond Alf and the History of the Peccary Society. The Webb Schools, Claremont, California, 340 pp.

Lyell, C. 1851. On fossil rain-marks of the recent, Triassic, and Carboniferous periods. Quarterly Journal of the Geological Society 7:238-247.

Maxson, J. H. 1940. Gas pits in non-marine sediments. Journal of Sedimentary Research 10:142-145.

Narbonne, G. M., and J. D. Aitken. 1990. Ediacaran fossils from the Sekwi Brook area, Mackenzie Mountains, northwestern Canada. Palaeontology 33:945-980.

Nitecki, M. H. 1971. Pseudo-organic Structures from the Precambrian Bass Limestone in Arizona. Fieldiana Geology 23:1-9.

Pickerill, R. K., and I. M. Harris. 1979. A reinterpretation of *Astropolithon hindii* Dawson 1878. Journal of Sedimentary Research 49:1029-1036.

Plummer, P. 1980. Circular structures in a late Precambrian sandstone: fossil medusoids or evidence of fluidization? Royal Society of South Australia Transactions 104:13-16.

Rasmussen, B., S. Bengtson, I. R. Fletcher, and N. J. McNaughton. 2002. Discoidal impressions and trace-like fossils more than 1200 million years old. Science 296:1112-1115.

Rasmussen, B., P. K. Bose, S. Sarkar, S. Banerjee, I. R. Fletcher and N. J. McNaughton. 2002. 1.6 Ga U-Pb zircon age for the Chorhat Sandstone, lower Vindhyan, India: Possible implications for early evolution of animals. Geology 30:103-106.

Rasmussen, B., I. R. Fletcher, S. Bengtson, and N. J. McNaughton. 2004. SHRIMP U–Pb dating of diagenetic xenotime in the Stirling Range Formation, Western Australia: 1.8 billion-year minimum age for the Stirling Biota. Precambrian Research 133:329-337.

Seilacher A. 1956. Der Beginn des Kambriums als biologische Wende. Neues Jahrb Geol P-A 103:155–180.

Seilacher, A. 2007. Trace Fossil Analysis. Springer-Verlag, New York, 226 pp.

Seilacher, A., P. K. Bose, and F. Pflüger. 1998. Triploblastic animals more than 1 billion years ago: trace fossil evidence from India. Science 282:80-83.

Seilacher, A., S. Lüning, M. A. Martin, E. Klitzsch, A. Khoja, and J. Craig. 2002. Ichnostratigraphic correlation of lower Palaeozoic clastics in the Kufra Basin (SE Libya). Lethaia 35:257-262.

Shixing, Z., and C. Huineng. 1995. Megascopic multicellular organisms from the 1700-million-year-old Tuanshanzi Formation in the Jixian area, North China. Science 270:620-622.

Timmons, J. M., K. E. Karlstrom, M. T. Heizler, S. A. Bowring, G. E. Gehrels, and L. J. Crossey. 2005, Tectonic inferences from the ca. 1254 -1100 Ma Unkar Group and Nankoweap Formation, Grand Canyon: Intracratonic deformation and basin formation during protracted Grenville orogenesis, Geological Society of America Bulletin 117:1573-1595.

Timmons, J. M., K. E. Karlstrom, E. C. Lathrop, M. T. Mohr, M. D. Schmitz, C. M. Dehler, J. C. Anderson, and L. J. Crossey. 2019. A glimpse within the great unconformity: parsing the Mesoproterozoic record of erosion, sedimentation and deformation preserved in the Grand Canyon Unkar Group. Geological Society of America Annual Meeting Abstracts 2019, #340738.

Turek, A., and N. C. N. Stephenson. 1966. The radiometric age of the Albany Granite and the Stirling Range Beds, southwest Australia. Journal of the Geological Society of Australia 13:449-456.

Van Gundy, C. E. 1937. Jellyfish from Grand Canyon Algonkian. Science 85:314.

Van Gundy, C. E. 1951. Nankoweap Group of the Grand Canyon Algonkian of Arizona. Geological Society of America Bulletin 62:953-959.

Wade, M. 1972. Hydrozoa and Scyphozoa and other medusoids from the Precambrian Ediacara fauna, South Australia. Palaeontology 15:197-225.

Walter, M. R. 1972. Tectonically deformed sand volcanoes in a Precambrian greywacke, Northern Territory of Australia. Journal of the Geological Society of Australia 18:395-399.

Young, G. A., and J. W. Hagadorn. 2010. The fossil record of cnidarian medusae. Palaeoworld 19:212-221.

On the origin and evolution of the Salton Sea

David K. Lynch[1] and Brian McNeece
[1]*dave@caltech.edu*

ABSTRACT—It is widely written and generally believed that the Salton Sea was created by an engineering accident. Many called it a blunder, gross negligence by Charles Rockwood. But we argue that the catastrophic inundation of 1905 was a natural event. Triggered by the Gila River's largest flood on record, Colorado River water would have reached into the Salton Trough whether or not Rockwood's California Development Company (CDC) had been there at all. Indeed, historical records show that the Colorado River flowed into the trough as early as 1840, long before the CDC. After the 1905-1907 flood subsided, the Salton Sea might have been expected to evaporate and percolate away in a few years. And it would have if the Alamo Canal had not continued to bring in river water, more in fact than was needed. For the past 115 years, the sea has been maintained by river water, not as the primary goal, but as the only practical way to dispose of irrigation runoff. The original Salton Sea may have been formed catastrophically, but the modern sea's existence is intentional, an inevitable result of Imperial Valley agriculture. Today's Salton Sea has little or nothing to do with the 1905 flood and should not be called an accident.

1. Introduction

The dramatic formation of the Salton Sea in 1905 has been much discussed and extensively studied[1-7]. The usual story is this: poor water management of the Colorado River and Alamo Canal near Yuma diverted the river water into the Salton Trough, creating the Salton Sea. Many narratives assign blame to Charles Rockwood, who allowed water from the river to flow into the Alamo Canal through open cuts without constructing head gates to control the flow. When the Colorado flooded as a result of floods on the tributary Gila River, it coursed unchecked through Rockwood's Lower Mexican Heading and into the Imperial Valley. This is the basis for the prevalent notion that the sea was Rockwood's fault. Yet the story is more complicated, and an examination of historical records leaves room for other interpretations.

We will not repeat the many fascinating accounts of the 1905 floods and subsequent return of the Colorado River to its natural bed in Mexico. Instead we will investigate two different though related topics: (1) The cause of the sea's 1905 inundation, and (2) some seldom-considered aspects of the sea's continued existence.

2. Origin of the Salton Sea

Water in the Salton Trough is nothing new. The geological record reveals that as a major body of water, Lake Cahuilla existed there episodically during the late Pleistocene and

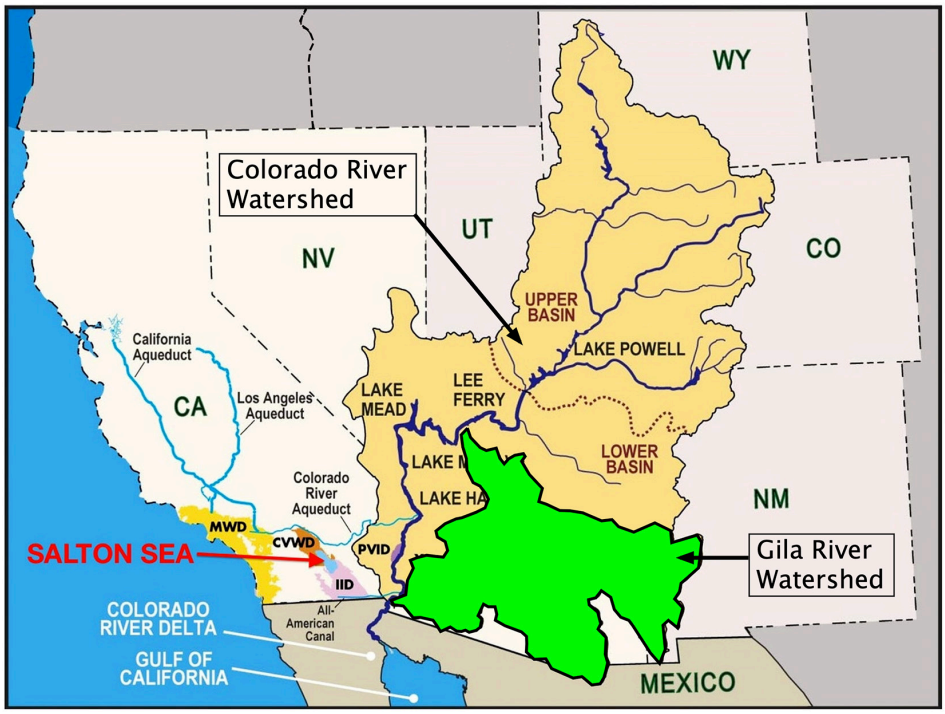

Figure 1. Drainage Basins of the Colorado and Gila rivers. Colorado River watershed includes the Gila's. Due to elevation, climate and latitude differences, the Gila River watershed is much warmer than the Colorado's. In winter, rain in the Gila's drainage basin runs off, but snow in the Colorado drainage basin stays on the ground. In summer, the Gila basin often experiences flash floods due to monsoons, less so in the upper Colorado basin because it is farther north and less likely to have monsoons. Figure adapted from the Central Basin Water District.

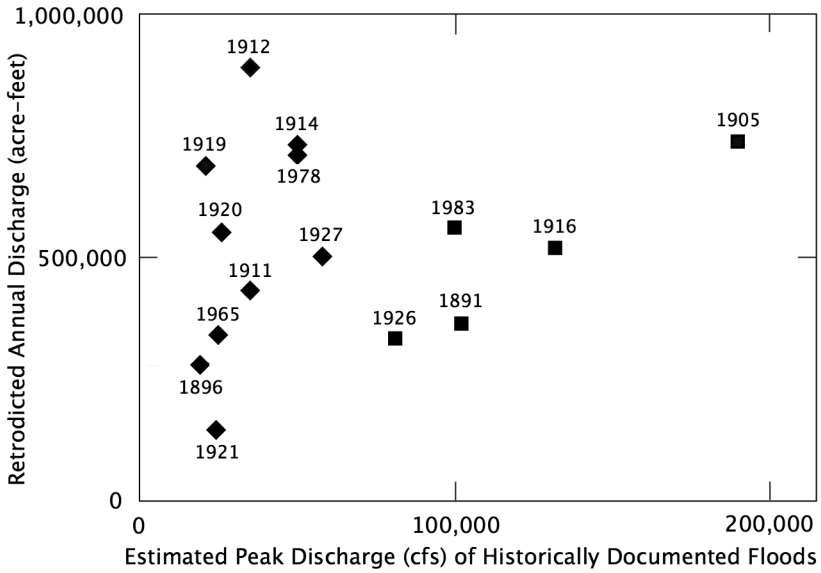

Figure 2. Historic Floods on the middle Gila River (adapted from Woodson, 2015)[18]. The earliest floods for which discharges and could be estimated ("retrodicted") were in 1891, 1896 and 1905. All three carried Colorado River Water into the Salton Trough. Given that the 1905 flood was much larger than the earlier ones, it seems certain that it produced a Lake Cahuilla, later called the Salton Sea. Squares are major floods.

Holocene at irregular intervals of between 500–1000 years[8]. Based on historical accounts[9], the last event was around 1540. Yet at least nine times in the 19th century (1840, 1842, 1852, 1859, 1867, 1862, 1884, 1891 and 1896)[10-13], there were reports of significant water in the trough, some with areas greater than the modern-day Salton Sea. In most cases, the water appeared after well-documented, natural floods on the Colorado River. The resulting short-lived lakes evaporated within a few years and had no enduring names, though some locals called them "inland seas". If we call natural occurrences "Lake Cahuilla" and manmade ones "Salton Sea", these 19th century bodies of water should have been called Lake Cahuilla. Thus, the lake's last highstand was 1896. If it can be established that the 1905 flood was a natural event, Lake Cahuilla's last highstand would be reckoned as February 1907.

As a manmade body of water, the Salton Sea formed in 1901, not 1905 as is usually cited[14-15]. In May 1901, water began flowing from the river along the newly constructed Alamo (Imperial) Canal and reached the Imperial Valley in June[1-7]. It seems that no one considered what to do with the water after it was used for irrigation, so it simply trickled down to the bottom of the sink. It was little more than a transitory wetland that didn't bother anyone. But it quietly marked a historic event for southern California's water saga: the birth of the Salton Sea.

The sea's catastrophic growth in 1905 is best understood by examining the source of the lower Colorado River's water before damming in the 20th century. Figure 1 shows its drainage basin, which includes that of the Gila River basin. Both watersheds reached their present configuration about 5 million years ago (early Pliocene). The Gila River's 58,000 sq mi drainage basin is mostly in Arizona, while the much larger Colorado drainage basin (246,000 sq mi, which includes the Gila's) extends as far north as Wyoming and as far east as Colorado and the Rocky Mountains. On average, the Gila watershed is at a lower elevation (2800 ft estimated) than the Colorado's (5500 ft), and is more southerly. Thus the Gila watershed is warmer than the Colorado's. Assuming a mean temperature drop off with elevation (adiabatic lapse rate[16]) of 18°F/mile, it is on average 9°F colder in the Colorado watershed than in the Gila's: When both climate and latitude are considered, another ~20°F is added. As an example, when it's 40°F and raining in Yuma, it's 11°F in Laramie and snowing.

The rivers have different seasonal variations. During winter, the Colorado River's discharge is low because precipitation in its upper drainage basin tends to be snow, which sticks to the ground and does not run off. Winter floods from the upper Colorado are rare but they occasionally occur on the lower, warmer Gila. Precipitation in the Gila watershed is mainly rain and it runs off to join the lower Colorado, but the discharge is normally small.

In the summer, weather patterns are different. Rain and snowmelt runoff from the Colorado swells the river from April to August and is fairly predictable. Monsoon[17] rains over the Gila watershed are unpredictable. They only occur in summer and affect relatively small areas, not the entire watershed. Monsoons can dump enormous amounts of water on the desert, enough to create flash floods.

Snowmelt and monsoons would seem to make summer the season for floods. But in 1905, the floods came in winter. And not from the Colorado River *per se*, but rather from its tributary, the Gila River[1-7]. What sparse data exists on Gila River floods is sufficient to gain some insight into its influence on the Colorado River.

Historic floods on the Gila[18] have been characterized by their *total discharge* and *peak discharge* (Figure 2). Prior to modern instrumentation, these values could only be estimated, but Figure 2 reveals that the 1891 and 1896 Gila floods, both being natural events, sent river water into the trough. Since the 1905 flood was much larger than the previous two, it seems certain this flood would have also overwhelmed the Colorado and created a Lake Cahuilla.

To see the actual timing, consider Figure 3, which shows the daily discharge of the Colorado and Gila Rivers in 1905, along with the typical daily discharge of

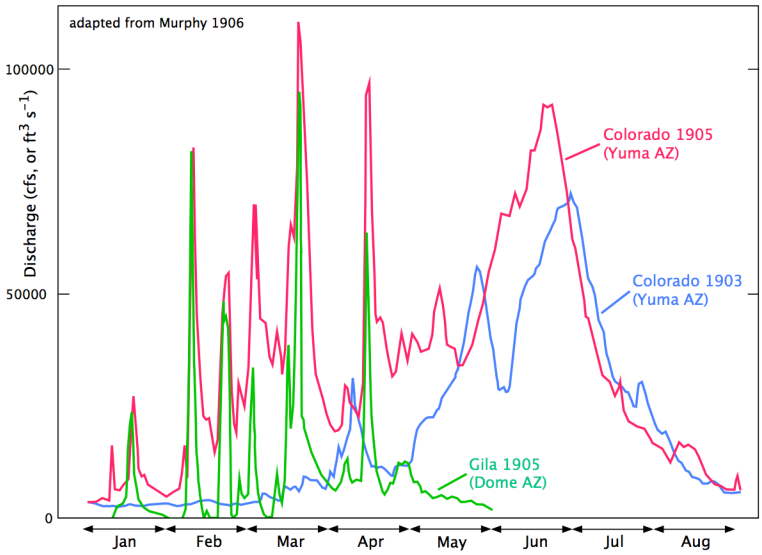

Figure 3. Colorado River discharges at Yuma, AZ and Gila River discharges at Dome, AZ. In normal years (1903), the Colorado River discharge peaks in summer. The Gila is usually very low or dry. In 1905, however, the Gila flooded at least 5 times, pushing the Colorado to record levels. Each flood on the Colorado was preceded (by a few hours) by floods on the Gila. Figure adapted from Murphy (1906).

the Colorado in 1903[19]. Normally the Colorado and Gila were low in the winter and early spring. While the Gila remained low all year, the Colorado discharge increased ~ten-fold from snowmelt in spring and summer. Since the Gila flows into the Colorado above Yuma, pulses of water on the Gila eventually reach the Colorado. Indeed, Figure 3 shows that in 1905, each flood on the Gila reached the Colorado a few hours later. Considering the total discharge in 1905—the area under the 1905 Colorado curve—it seems that the unusual but still natural floods on the Colorado were by themselves sufficient to inundate the trough.

If the 1905 floods were natural events, why hasn't the Colorado flowed into the trough again? After all, in 1909, the discharge was enormous[20], larger than any during 1905–1907, yet no water found its way to the trough. The answer is that Rockwood and Cory had learned their lesson and greatly enlarged the levees surrounding the Alamo Canal[21].

To summarize, the 1905–1907 Colorado River flood waters came through Rockwood's open cut in Mexico. This was the basis for believing the Salton Sea was the result of an engineering accident. But water reached the trough through the cut simply because it was the most efficient route at the time. Had this opening not been present, the 1905 Gila flood would have overflowed the Colorado, breached a levee somewhere else and made its way to the Salton Trough.

3. The enduring Salton Sea

What happened to the Salton Sea (not yet named) in 1905 is a matter of historical record[1-7]. By June a shallow body of water covering 150 sq mile (~12 x 12 miles) had collected at the bottom of the trough as 80,000 CFS flowed in. By October, the entire river reached the trough. The Salton Sea grew rapidly as the entire Colorado River flowed into the Salton Trough. Surging across the desert, the flood overran huge portions of the Mexicali Valley in a sheet of braided channels 8–10 miles wide (Figure 4). It reached Volcano Lake at the foot of Cerro Prieto and was channeled north to the New River, turning a shallow brush-filled depression into a torrent. Ultimately, Harry Thomas Cory, who made many courageous decisions concerning the flood and who probably convinced E. H. Harriman to fund the effort, took over. He closed the cut and finally put the Colorado River back where it belonged on February 10, 1907.

Figure 4. Published reports refer to a broad 8–10 mile wide shallow flood in 1905 as a sheet-like flow or shallow braided channels. No maps of the flood flow were produced because there were no surveyors in the areas during 1905-1907. This image is consistent with historic reports. Adapted from the Salton Sea Atlas, Redlands Institute (2002).

Once the Colorado River was returned to its former bed, the disaster was over but the Salton Sea remained. Left to itself, it would have vanished by about 1917 (Figure 5), losing about 6 ft per year to evaporation and percolation[22]. But with agriculture once again flourishing, the CDC kept the water flowing. After irrigating the fields, water was left to drain into the sink. While the flooding of 1905-1907 was a surprise, today's Salton Sea is not. It is there because farmers want it there. Not because they particularly like it, but because the sink was the natural sump for

their irrigation water. Indeed, President Coolidge formalized this in 1924 by an executive order setting aside land under the sea as a permanent drainage reservoir[23].

As Figure 5 shows, the Salton Sea grew steadily between 1924 and 1983. Part of its enlargement occurred because more and more water was needed to supply the growing acreage of farmland. But there was another reason. Farmers were taking more water than they needed to grow crops because they were trying to desalinate the soil and thereby improve crop yields. As an endorheic basin, sediments in the trough have accumulated salt and other evaporites from thousands of years of evaporation. Most evaporites are on or near the surface because the clay-like soil is poorly drained. To remove it, farmers began using an ancient desalination technique known to the Indus Valley Civilization[24], and this requires a lot of extra water; *deep drainage*.[25-27]. In 1920s, the Imperial Irrigation District (IID) began a massive program to desalinate the soil.

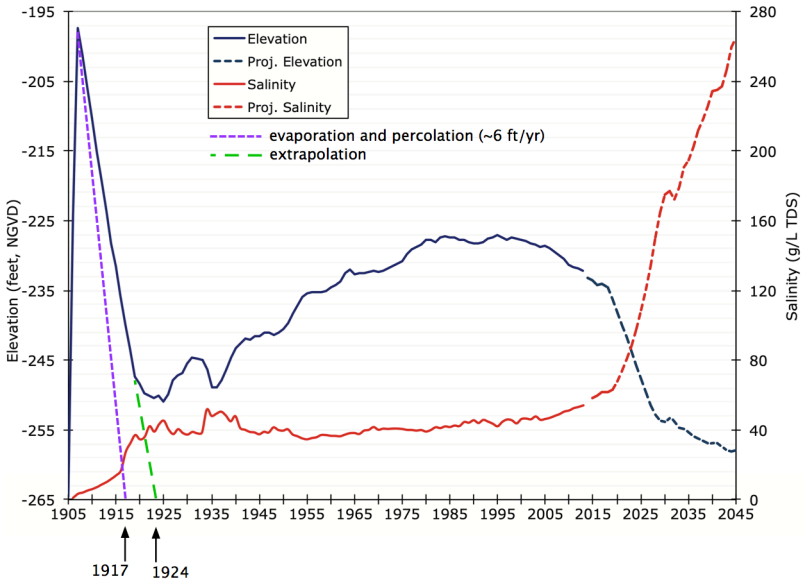

Figure 5. After the flood was stopped, the Sea level dropped sharply. This was due mostly to evaporation and percolation. Had the CDC not allowed Colorado River water to enter the trough through the Alamo Canal, the Salton Sea would have disappeared by about 1917. But the continuing growth in agriculture required more water than ever and the Sea level rose from 1925 until 1983.

In deep drainage (Figure 6), long lines (miles) of perforated or porous pipes are placed at a slight inclination a meter or so below ground, then covered. Though the soil is poorly drained, water eventually makes its way down to the pipes and is carried down to the sea by gravity, primarily through the Alamo and New rivers. This water carries salt and agricultural fertilizer from the topsoil and soil in the vadose zone to the drain pipes. For deep drainage to be efficient, however, farmers had to use more water than they had taken earlier. For every three acre-feet of water that a farmer applied to the ground, one acre-foot ended up in the Salton Sea[28]. This practice of using extra water caused the Salton Sea level to rise even faster.

Deep drainage in the Imperial Valley does three things: it lowers a high water table, removes surface salt, and also dumps salt into the Salton Sea. This is why the Sea is so salty, almost twice that of the ocean in 2019[29]. Drain water also contains large amounts of fertilizer including nitrogen and selenium[30] (selenium is also found

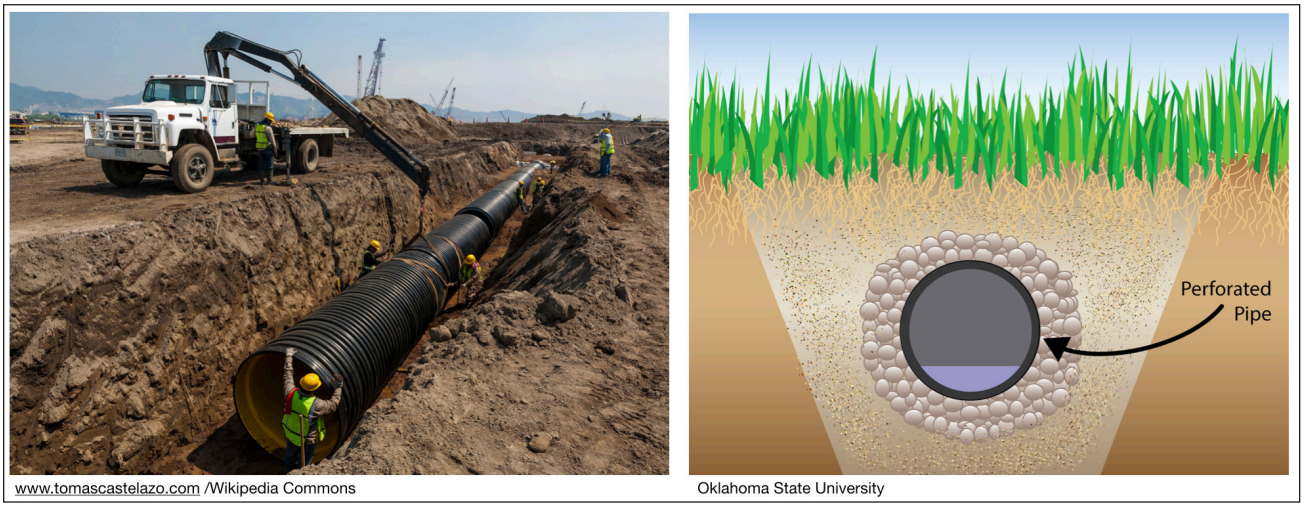

Figure 6. Deep drainage is a way to desalinate surface soils so that crops grow better. Perforated pipe inclined slightly downward toward the Sea are buried. Salt-laden water percolating down from the surface removes salt from the topsoil. This water and salt (and fertilizer), however, increase the salinity of the sea and raises its level. Deep drainage desalination requires more water than crops need.

in Colorado River water and sediments). Pollution from the Alamo and New rivers, the latter once called the most polluted river in the world, additionally adds to the sea's chemical soup.

Until the urban areas of Phoenix, Tucson, Los Angeles, and San Diego grew beyond water supplies, farmers in the Imperial Valley had no reason to limit their use of water. The IID receives its water from the Bureau of Reclamation for free; farmers are merely charged the cost to deliver the water. And since water is delivered by gravity, delivery is cheap. As a result, Imperial Valley farmers have paid some of the lowest rates in the nation. Today, they pay $20 for an acre-foot of water. In contrast San Diego area farmers pay above $900 for an acre-foot.[31]

Deep drainage, along with surface drainage known as *tailwater*, turned out to be a doubled-edged sword. Crops grew better, but in the late 1970s, agricultural drainage into the sea caused its level to rise enough to flood some productive agricultural land. The flooded farmers sued the IID. After years of litigation, the court ruled that the IID was wasting water and was ordered to begin conserving water in order to lower the elevation of the Salton Sea[32]. In 1984, Decision 1600 of the California State Water Resources Control Board forced the IID to limit water delivery to the Salton Sea and to accept funding from the Metropolitan Water District (MWD) of Los Angeles. MWD would pay for system improvements so the IID would use less water. In return, the MWD would receive 104,000 acre-feet of water annually. This was the first large agriculture-to-urban water transfer[33]. As of January of 2020, the IID now transfers nearly 500,000 acre-feet to Los Angeles, San Diego, Coachella, and Native American water districts. Because of these transfers, the Salton Sea, after decades of rising, is now falling.

Water will continue to flow into the Imperial Valley and maintain the Salton Sea for the foreseeable future because farmers need water. There are plans to shrink the sea but not to dry it up[34]. Eliminating the sea would mean eliminating Imperial Valley agriculture.

Summary and conclusions

The Salton Sea's origin and evolution have been a source of ridicule, uncertainty, misinformation, and speculation. While most people believe the initial formation took place in 1905 as the result of an engineering accident, it actually started in 1901 as man-made runoff from irrigation water brought from the Colorado River by the Alamo Canal. *We argue that the Salton Sea's 1905 "formation" was simply another natural inundation from a Colorado River flood, triggered by floods on the Gila.* The sea's beginning was inevitable, if not intentional. Nor is the sea's continued existence an accident. Rather it is a deliberate, even desirable, result of agriculture in the Imperial Valley and its farmers' efforts to desalinate the soil.

References

1. Kennan, George, *The Salton Sea; an account of Harriman's fight with the Colorado River*, New York, The Macmillan Company (1917). https://catalog.hathitrust.org/Record/006205158
2. Rockwood, Charles, Born of the Desert, Calexico Chronicle (1909) https://books.google.com/books?id=S-41AQAAMAAJ
3. https://en.wikipedia.org/wiki/Charles_Robinson_Rockwood Excellent account and many good references.
4. Cory, Harry T., *The Imperial Valley and Salton Sink,* San Francisco, John J. Newbegin (1915) https://www.google.com/url?sa=t&rct=j&q=&esrc=s&source=web&cd=17&ved=2ahUKEwjquum1wfnmAhUVrp4KHQBJBb4QFjAQegQICBAC&url=https%3A%2F%2Fnrm.dfg.ca.gov%2FFileHandler.ashx%3FDocumentID%3D9257&usg=AOvVaw3XgKu-thHpRTRIAVWdnIR4
5. Tout, Otis B., *The First Thirty Years, An Account of the Principal Events in the History of Imperial County, Southern California, USA*, Otis B. Tout. Publisher, 4612 Terrace Drive, San Diego, Calif., Produced by Arts & Crafts Press, San Diego, Calif. (1931) https://books.google.com/books?id=RskuAAAAIAAJ
6. Farr, Finnis, *The History of Imperial County California*, Berkley, CA, USA: Elms and Franks. pp. 311, 312. (1918)
7. McNeece, B., *The Early History of Water in the Imperial Valley*, Video script, Imperial Irrigation District (2015) https://www.iid.com/home/showdocument?id=13967, Video: https://www.youtube.com/watch?v=KAsntugo710 .
8. Waters, M. R., Late Holocene lacustrine chronology and archaeology of ancient Lake Cahuilla, California. Quaternary Research 19, 373-387 (1983)
9. Wilke, Phillip J., Late Prehistoric Human Ecology at Lake Cahuilla, Coachella Valley, California, University of California Archaeological Research Facility Contributions No. 38 (1978)
10. http://saltonseaauthority.org/get-informed/history/
11. Sykes, G. The Colorado Delta, Publication no. 460, Carnegie Institution, Washington D.C., (1937), https://babel.hathitrust.org/cgi/pt?id=uc1.31822010629376&view=1up&seq=6
12. Sykes, G., The delta and estuary of the Colorado River. Geog. Rev., vol. 16, p. 232–255. (1937)
13. Cecil-Stephens, B. A., The Colorado Desert and its recent flooding. Amer. Geog. Soc., Bull., vol. 23, p. 367–377 (1891)
14. https://water.ca.gov/LegacyFiles/pubs/conservation/salton_sea_history/history.pdf
15. https://www.parks.ca.gov/?page_id=639
16. https://en.wikipedia.org/wiki/Lapse_rate
17. https://en.wikipedia.org/wiki/North_American_Monsoon
18. Woodson, K., The Impact of Flooding on Hohokam Canal Irrigation Agriculture, in

Traditional Arid Lands Agriculture: Understanding the Past for the Future, Scott E. Ingram and Robert C. Hunter (eds), University of Arizona Press, 180-216 (2015)

19. Murphy, Edward C. (and others), Destructive Floods in the United States in 1905 with a Discussion of Flood Discharge and Frequency and an Index to Flood Literature, Water Supply and Irrigation Paper No. 162, Series M, General Hydrographic Investigations, 17, U.S. Government Printing Office (1906)

20. Fall, A. B. and Davis, A.P., Problems of Imperial Valley and Vicinity, US Bureau of Reclamation, Document No. 142, 87th Congress (Senate), Government Printing Office (1922)

21. Dowd, M. J., IID: THE FIRST 40 YEARS, IID (1956). https://www.iid.com/home/showdocument?id=6000

22. https://www.iid.com/home/showdocument?id=17297.

23. http://resources.ca.gov/docs/salton_sea/Salton_Sea_Chronology_(Prehistory-2015).pdf

24. https://en.wikipedia.org/wiki/Indus_Valley_Civilisation

25. https://www.agric.wa.gov.au/water-management/deep-drainage-salinity-management

26. https://en.wikipedia.org/wiki/Drainage#Early_history

27. Kovulek, Paul, Irrigation and Drainage Practices in the Colorado River Basin of California, paper prepared for the California Irrigation Institute, Fresno, California, (1964)

28. Author's personal conversation (McNeece) with Wally Leimgruber, Holtville farmer and former Imperial County Supervisor, January 28, 2020.

29. Cohen, Michael, Salton Sea +20, (2019) https://pacinst.org/salton-sea-20/

30. Selenium and the Salton Sea, https://www.google.com/url?sa=t&rct=j&q=&esrc=s&source=web&cd=2&ved=2ahUKEwiSzLfdvZPnAhWWlp4KHfPzB4AQFjABegQIAhAB&url=https%3A%2F%2Fnrm.dfg.ca.gov%2FFileHandler.ashx%3FDocumentID%3D9091&usg=AOvVaw2mXPvBQG0i7YMPPj1Sgtm1.

31. Author's personal conversation (McNeece) with Dennis Cushman, San Diego County Water Authority Assistant General Manager, March 7, 2019

32. Alleged waste and unreasonable use of water by Imperial Irrigation District. http://www.sci.sdsu.edu/salton/iidAllegedWasteofWater.html

33. This is the transfer of water rights from agricultural use to urban use, not the transfer of water that has reached farmland and then moving it to cities.

34. Salton Sea Hydrological Modeling and Results, Technical report by CH2M Hill, (2018) https://www.iid.com/home/showdocument?id=17299

Developments in the moving mud spring mystery

David K. Lynch,[1]* R. Travis Deane,[1] Carolina Zamora,[1] Andrea Donnellan,[2] Gregory A. Lyzenga,[2] and David S. P. Dearborn[3]
[1]*Shannon and Wilson, Inc.*
[2]*Jet Propulsion Laboratory, California Institute of Technology*
[3]*Lawrence Livermore National Laboratory;* *dave@caltech.edu

ABSTRACT—The mud spring discovered (or recognized) in 2016 is unique: an artesian and possibly CO_2-driven spring in Colorado River sediments that is moving across the California Desert in the Salton Trough near Niland, CA. Since June 2018 it has moved about 370 feet to the southwest. The spring has caused significant disruption to local infrastructure, especially the Union Pacific Railroad, which had to reroute their tracks several times. Kinder Morgan has diverted its underground pipeline and AT&T has raised its buried fiber optic cables to poles above ground. Caltrans has built a detour on CA SR111 in anticipation of the spring's continued movement toward the highway. Several UAV surveys have tracked the spring's surface path with a positional accuracy of about 3 feet. Its speed has slowed from about 7 feet/month in 2018 to less than 2 feet/month in late 2019. Initially an average of 40,000 gallons of water per day were pumped from the spring to maintain its subaerial level below grade but has since decreased to about 30,000 gal/day. Movement and pump rate are consistent with a model of sediment erosion in a near vertical soil pipe. The spring is predicted to stop its movement in the coming months or years when the soil pipe becomes near vertical. Being unprecedented, all predictions about the mud spring's future movement are uncertain, though it is probably following a fault whose existence and geometry have yet to be discovered.

1. First Year

The mud spring's dramatic developments between June 2018 and March 2019 have been previously described.[1-3] The spring began as a southwestern extension of a non-moving, pre-existing mound spring labeled W9.[4] The moving spring carved out a gently meandering, water-filled trough. After pumping out the trough, it was found to be flat-bottomed, 60 feet wide and ~20 feet deep (Figure 1). The mud spring continued its southwesterly movement. On October 4, 2018 the spring, now called W9a, suddenly jumped from about 30 feet northeast of a sheet pile wall to southwest of it, opening a sinkhole 60 feet across and 22 feet deep. The sheet piles had been placed across the spring's path to keep sediment supporting a Union Pacific Railroad (UPRR) track in place. When it was just east of the sheet piles, the spring spent about three months moving slowly northwestward. It continually eroded the trough walls until they were vertical and exposed more and more of the piles. While the spring appeared to linger just northeast of the sheet pile wall, it was actually moving underneath the wall and carving out a subterranean chamber southwest of the sheet piles. Then the roof collapsed. When it emerged within the sinkhole

Figure 1. UAV view of the mud spring looking west. This picture was taken before the spring breached the sheet piles and forced the abandonment of the original tracks. Approximate location of the three wells that were drilled to characterize the subsurface distribution of water and CO_2 are shown by stars. W9 is the location of a large, stationary mound spring[4] from where the moving mud spring emerged. The spring is moving toward the "wet" soil in the California Department of Fish and Wildlife's Wister Unit parking lot.

Figure 2. Oblique UAV view of the mud spring area, looking northwest. The original straight, originally active tracks were cut and taken out of service by UPRR, and replaced by two detour tracks (shooflies) that enclose them. Mud spring is near the earth-moving equipment between the detour tracks. Sheet piles have been cut off and are not visible. Photo taken 31 Oct 2018.

advanced. This was a hardship for the railroad. In addition to the construction costs, significant revenue was lost because freight trains had to slow down to safely pass the new curved tracks (Figure 2). As of this writing, UPRR has removed the original two tracks and built three shoofly tracks. The westernmost shoofly has now been completely abandoned and disassembled as the mud spring approached. The railroad's plan was to wait until the spring moved beyond their right-of-way, building tracks and sidestepping the spring as necessary to keep two tracks active, and then restore the tracks to their original straight configuration.

southwest of the sheet piles, there were two springs, a large one about 2 m in diameter and a tiny one to the west. Soon after, the railroad began filling in the gully with local sediments. For the next few months the large spring dwindled to nothing while the small one grew and became the main spring. It varied from a single source to several smaller ones adjacent to one another that slowly moved around at random, coming and going unpredictably on timescales of days to weeks. Sometimes the spring flow surged, other times it was steady. Pumping by the UPRR kept the surface of the spring about 22 ft below grade; otherwise it would have risen and overflowed. West of CA SR111 in the California Department of Fish and Wildlife's Wister Unit parking lot, there were a number of WSW trending dark soil lineaments ("wet") that first appeared in 2016, about the same time the spring appeared. To date, these have not changed discernibly.

As an imminent threat to the UPRR's two main lines, the railroad began constructing shoofly tracks (temporary detours) as the spring

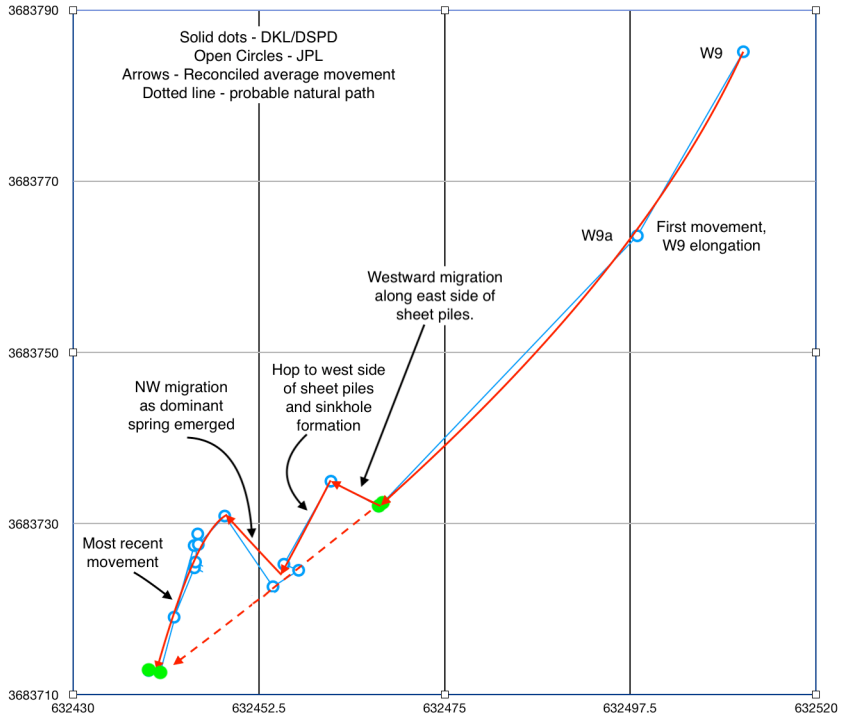

Figure 3. Measured locations and movement path of the mud spring. The spring appeared to move in a slightly curved line, with two diversion to the northwest before resuming its smooth course (dotted line). The spring began at the upper right and the latest positions are at the lower left, December 2019. Units are UTM northing and easting, zone 11, WGS84 datum.

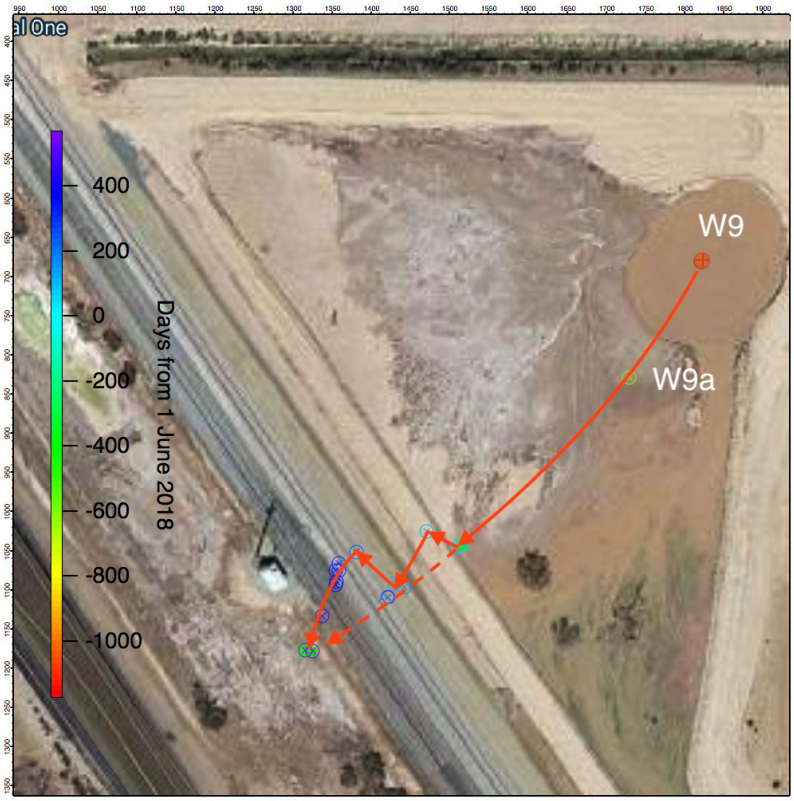

Figure 4. Trajectory from Figure 4 overplotted on Google Earth image from 3/20/15. Note that the spring has crossed and moved beyond the original railroad tracks, necessitating their relocation. Color scale refers to the day symbols (circle with x). See Figure 5 for dates.

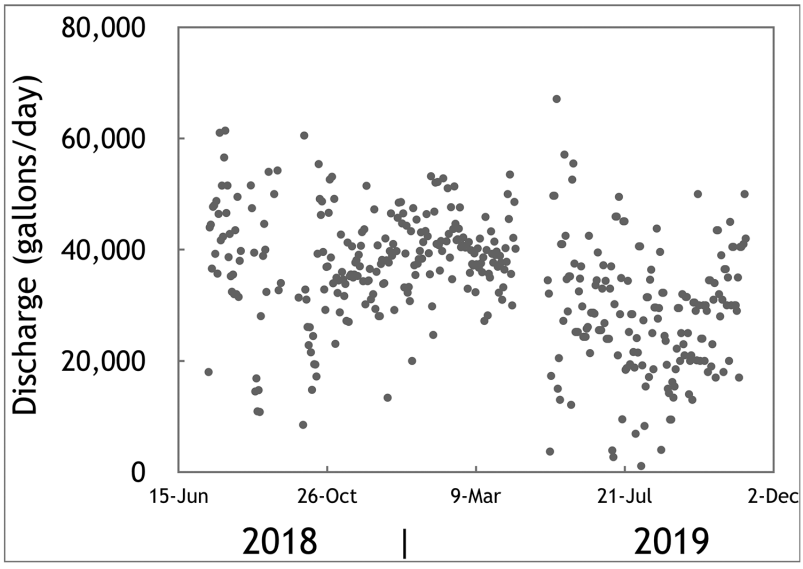

Figure 5. Mud spring discharge vs time. Initially the discharge was about 40,000 gallons/day but slowly decreased to about 30,000. Owing to the large scatter in the data, the discharge behavior is also consistent with two pumping regimes before and after April 2019 (see gap in the data) when the pumping contractor was changed: 40,000 gal/day before the change and 30,000 gal/day afterwards.

2. Recent Developments and Current Status.

The spring continued its southwesterly journey, but its precise location was hard to specify due to variations in the spring flow. To improve position accuracy, we began measuring the spring's location using unmanned aerial vehicles (UAVs, or "drones") in July 2018. In September 2018 scientists at the Jet Propulsion Laboratory (JPL) also started a UAV survey using a GPS base station, yielding positions to within a few cm. JPL's measurements revealed no ground movement or distortion between 2018 and 2020.

Figures 3 and 4 show the path of the spring between July 2018 and Dec 2019. Although the trend was mainly SW, there were at least two diversions, both to the NW. The first jog in the summer of 2018 was likely related to the sheet pile wall. The second occurred as the large spring in the sinkhole was taken over by the growing spring to the west.

Starting in October 2018, UPRR dumped riprap on the SW side of the sheet piles (NE side of the sinkhole.) The main spring grew smaller and the tiny spring grew larger until it become dominant. This was probably a response to the riprap blocking one spring and forcing it to surface at a slightly different location. This transition was also to the NW.

Workers who were on site every day said that dumping riprap was definitely altering the spring's behavior, creating multiples springs and moving them around. When UPRR began covering the NE side of the sinkhole so they could put their tracks back (Nov-Dec 2019), the mud spring moved again and became slightly more active, as though a smaller spring got plugged and had to get out through the main spring.

After it was first noticed (2016-2018), the spring was moving southwest by about 7 ft/month but by late December 2019 it was down to 2 ft/month. The direction remained the same and it was still within the railroad's right-of-way. In mid-2019 UPRR began dumping dirt and riprap into the NE side of the sinkhole to shrink it and prepare stable ground for new tracks. This caused the spring to become more active, probably because smaller water conduits to the surface were quenched, pushing the upwelling CO_2 into the main spring.

Water was pumped from the sinkhole every day to keep the spring level about 22 ft below grade. During 2018, the discharge remained steady at near 40,000 gallons/day. While we cannot be certain owing to the large day-to-day variations in pumping procedures due to worker schedules, pump repair, etc., it appears that the discharge gradually decreased until by November 2019 it was down to about 30,000 gal/day (Figure 5). A new diversion channel was built in November 2019 to eliminate the need for pumping, thereby passively draining away the water. This required the water in the sinkhole to be raised to about 6 ft below grade.

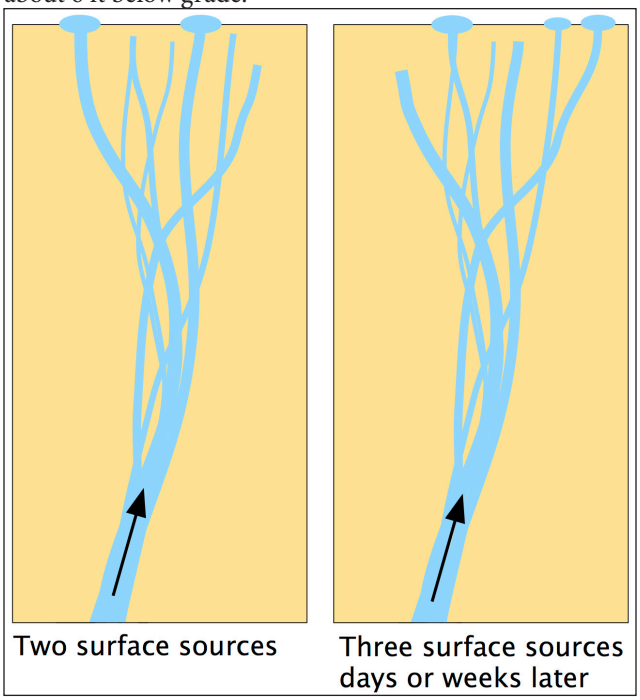

Figure 6. Hypothetical "flower structure" of the spring. As sediment collapses and blocks upward flow in one branch, excess pressure opens up another branch. Although the spring appears to "hop" around or migrate, the underlying source's position is not changing, except over periods of months or years.

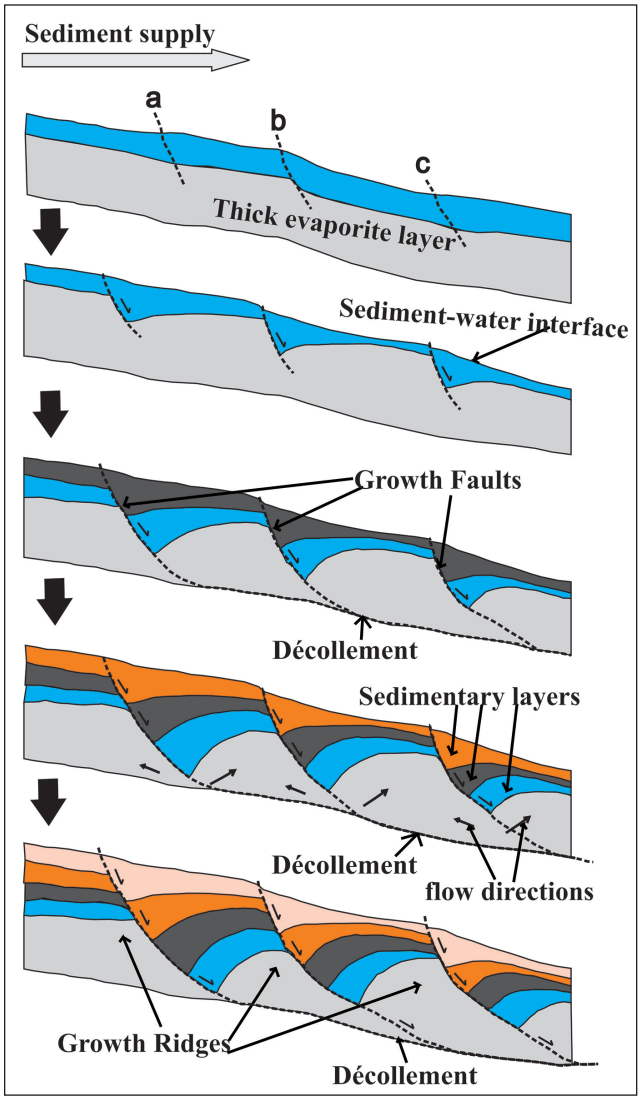

Figure 8. Growth Faults are normal, sometimes listric faults in aggrading sediment. Tectonically, they are commonly associated with extensional basins like the Salton Trough. (Figure by Emad Elfar, used under the fair use policy, see https://en.wikipedia.org/wiki/Growth_fault.)

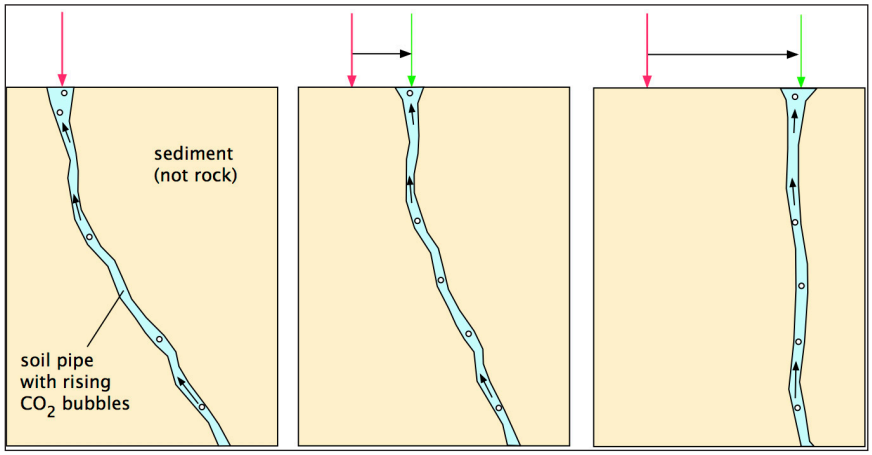

Figure 7. A tilted soil pipe with rising water and CO_2 would be expected to erode the walls of the pipe. This would remove sediment from the upper (right hand) part of the pipe and deposit it on the lower (left hand) part, leading to a gradual migration of the surface spring to the right, and toward the epicenter of the deep source.

3. Discussion

Since it was first detected, the spring has moved southwest by 370 feet, but at an ever-decreasing speed. During this time, water production has also decreased. Could these two functions be related?

Suppose that the CO_2 source originates in a pressurized cavity. Being finite, one might expect the pressure to decrease as the cavity degasses. Less pressure means less discharge, so spring production should decrease as well. With less discharge, erosion would be reduced.

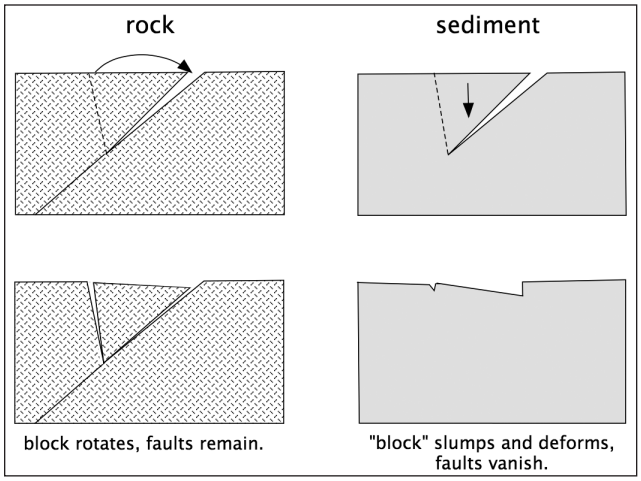

Figure 9. Rock and sediment deform differently. Faults in rock remain after the rock cracks and moves. Sediments, however, slumps when it deforms and cracks disappear because in some ways it can behave like a liquid and "flow".

If erosion in a tilted soil pipe is driving the horizontal motion of the spring as our model suggests, (Figures 6 and 7), we might expect the spring to slow down or stop moving altogether.

From a practical standpoint, UPRR wants the spring to move beyond its right-of-way so the original tracks can be restored. If the spring continues to behave the way our model predicts, it will eventually stop moving in the next few months or years. Will it stop? If it stops, when? Will it still be on the railroad's right-of-way? Caltrans is equally interested in the spring's future behavior. They have rebuilt a section of CA SR111 and constructed a detour. As of this writing the detour is not yet operational because the spring is presently 100 feet from the highway, too far to be an immediate threat.

Scientifically, there are many unanswered questions. What does the subsurface plumbing look like? Despite several seismic and microgravity studies, little was learned. Although the CO_2 is being generated by hydrothermal alteration of carbonates in the high geothermal gradient parts of the sediments, the gas and water sources are not spatially continuous but seem to be unevenly distributed both horizontally and with depth. We know this because three wells were drilled in the spring's vicinity (Figure 1): two had CO_2/water blow outs, and one was dry and produced no noticeable CO_2 despite being within a hundred feet of the spring. The usual concept of a planar water table does not seem to apply to this small region of desert. Whether this nonunifomity is characteristic of the larger area or is related in some way to the presence of the spring is not known. We don't know from what depth the water is coming.

We originally thought that the water was being entrained and brought to the surface by CO_2, as we have seen in nearby mudpots.[5-7] It is possible, however, that the spring is artesian and CO_2 is playing only a minor role in its dynamics.

Is the water source moving or is it the CO_2 source? Is there a fault controlling any aspect of the spring? Why did the spring suddenly appear in 2016? Perhaps there is a deep pocket of pressurized CO_2 that is rising along a fault where it encounters water and brings it to the surface. What fault? Seismicity reveals nothing, and agriculture and conservation have completely reworked the surface sediments so that scarps and cracks would have been erased.

We have no evidence that the spring lies on a fault but its roughly linear movement suggests it. We previously identified two fault geometries and associated spring dynamics that could reproduce the observed surface movement[1]. Some dip is required in both fault models but we cannot specify what type of fault is involved because transform, normal or reverse faults could produce the spring behavior that we have seen.

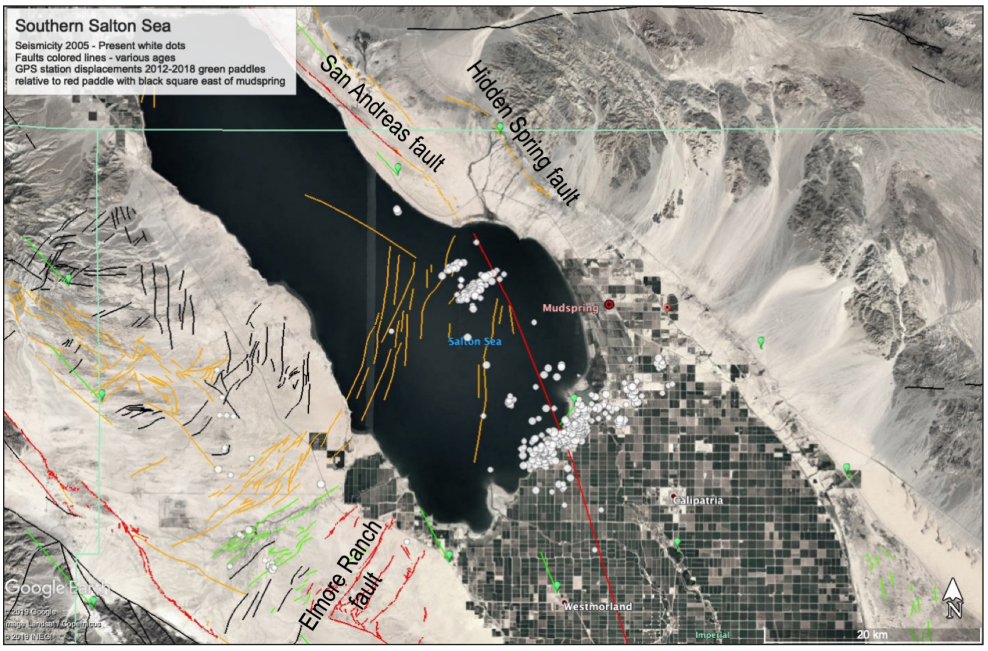

Figure 10. Tectonics of the mud spring area. Solid lines are faults. White dots are earthquakes with M > 3.5 and many fall along NE trending lines like cross faults. A northeastward extension of the Elmore Ranch Fault passes near the mud spring, as does a SE extension of the Hidden Spring Fault.

Another unknown involves the behavior of faults in actively aggrading sediment (Figure 8), some of which (normal faults) are called growth faults.[8-10] Unlike competent rock which can support and maintain faults by its own strength, faults in sediment can move and disappear as the poorly indurated material shifts and collapses (Figure 9). Sediment is friable and behaves like a viscous liquid in some ways. How does water from a discontinuous water table, possibly driven by CO_2, alter the sediment's dynamics?[11]

On a larger scale, how is the spring related to regional tectonic structure? Could it be a result of earthquakes or the earthquake swarms that frequently happen in the area? With so many cross faults in the area, the spring's path (heading 234°) suggests a fault that is perpendicular to the controlling San Andreas Fault and plate boundary.

We speculate that the mud spring may be related to transtensional tectonics. This region is known for a series of northeast striking left-lateral, and northwest striking right lateral faults, with possible tectonic subsidence near the spring as part of the Salton Trough (Figure 10). The spring lies on the northeastward extension of the Elmore Ranch Fault system as well as a southern projection of the Hidden Spring Fault and its presence may be related to one, both, or the intersection of these faults.

4. Summary

The mud spring remains a mystery. Although we have good observational information on its surface phenomenology, the spring's origin and dynamics are poorly understood. It is still moving and the UPRR is growing impatient with Mother Nature. Stay tuned! Nothing like a good geological puzzle!

5. Acknowledgements

Portions of this work were carried out at the Jet Propulsion Laboratory, California Institute of Technology under contract with NASA.

References

1. Lynch, David K., R. Travis Deane, Justin Rogers, Carolina Zamora, James S. Bailey, Dean Francuch, Christopher W. Allen, Cassandra Gouger, David Dearborn, Paul Adams, and Andrea Donnellan, **A mysterious moving mud spring near Niland, Imperial County, California**, In *Exploring Ends of Eras in the Eastern Mojave Desert*, proceedings of the 2019 Desert Symposium, David M. Miller (ed.), 168-175 (2019)

2. Lynch, David K. and R. Travis Deane, **A Moving Mystery**, Civil Engineering, July/August, 54-63 (2019)

3. Deane, R. Travis and David K. Lynch, **A Moving Mud Spring Threatening Critical Infrastructure, Imperial County, California**, Proceedings of the 2020 Geocongress, Feb 25-28, 2020 Minneapolis

4. Lynch, David K. and Kenneth W. Hudnut **"The Wister Mud Pot Lineament: Southeastward Extension or Abandoned Strand of the San Andreas Fault?"** Bull. Seismol. Soc. Amer. **98**, No. 4, 1720-1729 (2008)

5. Adams and Lynch, D. K., **A short-lived geothermal mud pot near Niland, Imperial County, California,** In Exploring Ends of Eras in the Eastern Mojave Desert, proceedings of the 2019 Desert Symposium, David M. Miller (ed.), 161-167 (2019)

6. Adams, Paul. M., David K. Lynch, Kerry N. Buckland, Patrick D. Johnson, David M. Tratt, **Sulfate mineralogy of fumaroles in the Salton Sea Geothermal Field, Imperial County, California**, Journal of Volcanology and Geothermal Research, 347, 15-43 (2017)

7. Lynch, David K., Kenneth W. Hudnut and Paul M. Adams, **Recently-Exposed Fumarole Fields near Mullet Island, Imperial Valley, California"**, Geomorphology 195, 27-44 (2013)

8. Gawthorpe, R. L. and M. R. Leeder, **Tectono-sedimentary evolution of active extensional basins**, *Basin Research*, **12,** 195–218 (2000)

9. Jones, Mervyn, **Mechanical principles of sediment deformation**, in The Geological Deformation of Sediments, A. Maltman (ed), Chapman and Hall (1994)

10. Reproduced here from **https://en.wikipedia.org/wiki/Growth_fault** under the *Fair Use* doctrine.

11. Sofie Gradmann and Christopher Beaumont, **Coupled fluid flow and sediment deformation in margin-scale salt-tectonic systems: 2. Layered sediment models and application to the northwestern Gulf of Mexico**, Tectonics **31**, Issue 4 (2012).

The history of fossil collecting in the Colorado Desert and Anza-Borrego Desert State Park®

B. Marrs, L. K. Murray, G. T. Jefferson, and L. Gilbert
Stout Research Center, California State Parks, Borrego Springs, CA 92004

ABSTRACT—The Colorado Desert of southeastern California, which includes Anza-Borrego Desert State Park (ABDSP), contains a geologic record of life that spans the late Miocene, Pliocene, and Pleistocene epochs, and the Hemphillian through Rancholabrean North American Land Mammal Ages (NALMA). The history of paleontologic discovery in the Colorado Desert and ABDSP dates back to the late 18th through the 19th centuries, with recorded observations of fossil oysters and other ancient marine and freshwater invertebrates by key members of various early military and geologic surveys and expeditions. These initial reports include observations on the desert's geologic history: the formation of the Salton Trough, the incursion of the Gulf of California, and the Colorado River's Imperial Valley Delta and eventual replacement of sea water with freshwater lakes (Lake Cahuilla). By the early 1900s, the Colorado Desert's invertebrates of the past were recognized as an unparalleled paleofauna, and today this exceptional invertebrate collection, housed in the Colorado Desert District (CDD) Stout Research Center (SRC) in Borrego Springs, includes the largest most complete stratigraphic assemblage of marine fossils from the ancestral Gulf of California. The discovery, recovery, and study of the Colorado Desert and ABDSP's vertebrate fossils began in the early 1900s, with expeditions from the American Museum of Natural History (AMNH), post-World War II expeditions conducted by the Natural History Museum of Los Angeles County (LACM), and later explorations that led to specimen collections in the Imperial Valley College Museum (IVCM). Altogether, over 13,000 fish, amphibian, mammal, bird, and reptile fossils were recovered and curated, and the LACM and IVCM collections now reside in the Stout Research Center. Studies of the desert's fossil sites' stratigraphy and lithology have provided gainful insight concerning the migration of terrestrial faunas to and from the Central and South Americas, and revealed thousands of feet of river-borne sediments laid down in a conformable biochronologic sequence in ABDSP's Vallecito Creek/Fish Creek (VCFC) badlands, which contained an impressive record of terrestrial vertebrate fossil fauna spanning a time of nearly four million years. The establishment of a CDD Resource Management Plan and a Collections Management Policy, the first California State Parks-sanctioned Certification Training Program in Paleontology, and the California State Parks's first (and only) District Archaeologist /Paleontologist position in the early 1990s secured ABDSP's paleontologic and geologic resources. Equipped with the new SRC Paleontology Laboratory, and using the latest field technology, laboratory methods, curation procedures, and database and cataloging innovations, the ABDSP Paleontology Program continued into the new millennium with a wave of desert discoveries: over 1,575 new fossil localities that produced more than 3,850 fossil specimens. Today, the Colorado Desert and ABDSP remain key locations for important research by visiting geologists, paleontologists, and other earth scientists and professionals from around the globe, as well as by paleontology and geology graduate students from universities throughout the U.S. Scientific publications on the region's internationally famous vertebrate and invertebrate paleofaunas and outstanding geologic features continue to prove the marked significance of this desert and its incredible scope of fossil resources.

The Colorado Desert of southeastern California, which includes Anza-Borrego Desert State Park (ABDSP) (Figure 1), contains a geologic record of life that spans the late Miocene, Pliocene, and Pleistocene epochs, and the Hemphillian through Rancholabrean North American Land Mammal Ages (NALMA). This desert region

> …lies in a unique geologic setting along the western margin of the Salton Trough…[that] forms the northern-most end of an active rift valley and makes a portion of the boundary between the North American and Pacific tectonic plates…Over the past seven million years, a relatively complete geologic record of more than 6,000 meters (19,000 ft.) of fossil-bearing sediment has been deposited within [this area] along the rift valley's western margin. Here, paleontologic remains are widespread and exceedingly diverse, and are found scattered over hundreds of square kilometers of eroded

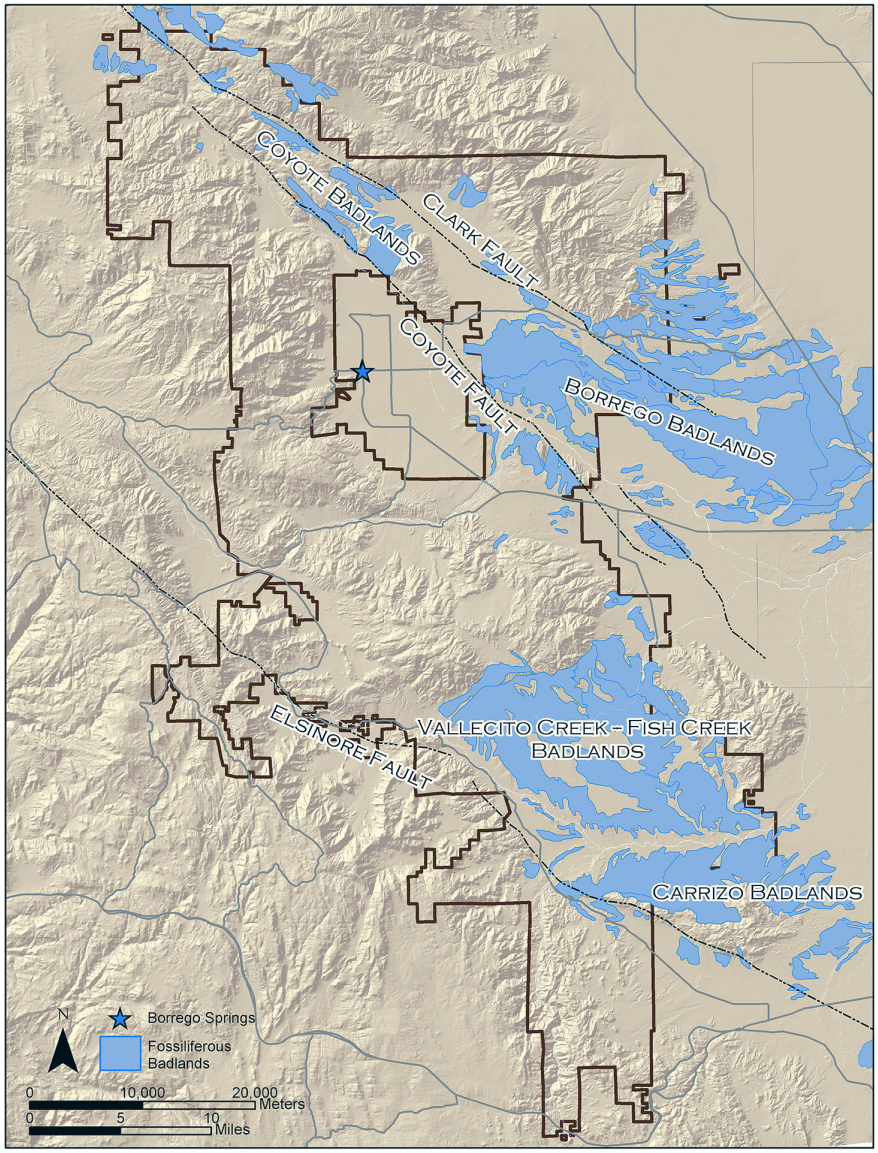

Figure 1. Fossiliferous Badlands of ABDSP. Major fossiliferous badlands are colored blue. The map is based on the outcrop patterns of sedimentary formations, which are often bounded by major faults. (Courtesy of the Colorado Desert District Stout Research Center, Borrego Springs, California).

> badlands terrain, extending south from the Santa Rosa Mountains into northern Baja California, Mexico (Jefferson and Lindsay 2006:xii).

Although some recorded marine fossils for ABDSP are over 450 million years old, and a few terrestrial vertebrate fossils from the Colorado Desert date a little beyond nine million years, most of the Colorado Desert and ABDSP fossil specimens date from six million to half million years ago, "comprising a continuous 5 ½ million-year record" (Jefferson and Lindsay 2006:xii).

Early Paleontologic and Geologic Explorations

The history of paleontologic discovery in the Colorado Desert and ABDSP dates back to the late eighteenth century, with observations written by Fray Pedro Font, official chaplain and recorder for Captain Juan Bautista de Anza, leader of the 1775 Spanish military expedition from Sonora, Mexico, that traveled across the Southern California desert, exploring a land route through the new territory for Spain. In his diary entry for December 9, 1775, Font wrote:

> On account of the unfruitfulness of these lands, so level, and of the aspect of the sand dunes, and especially of the abundance of shells of mussels [oyster deposits] and sea snails which I saw today in piles in some places, and which are so old and ancient that they easily crumble on pressing them with the fingers, I have come to surmise that in the olden times the sea spread over all this land, and that in some of the great recessions which the histories tell us about, it left these salty and sandy wastes uncovered" (Font 1775:123).

In 1853, William Phipps Blake (Figure 2) was the first to officially collect and describe these ancient shells, the earliest significant invertebrate fossil discoveries of the Colorado Desert, a title bestowed upon the region due to its desert origin, created by the Colorado River's deposition of sediment and displacement of its former marine waters. Blake was a geologist and mineralogist for the *U.S. Pacific*

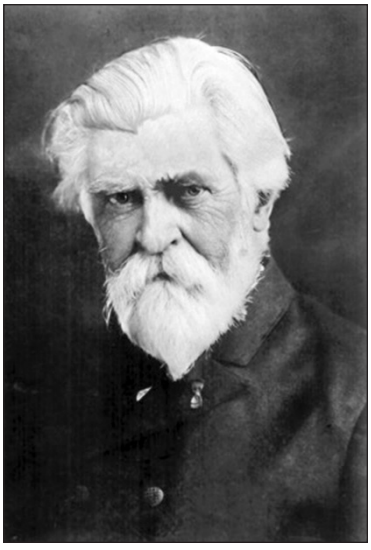

Figure 2. Portrait of William Phipps Blake, circa 1890s (Courtesy of the Arizona Historical Society, Tucson, Arizona).

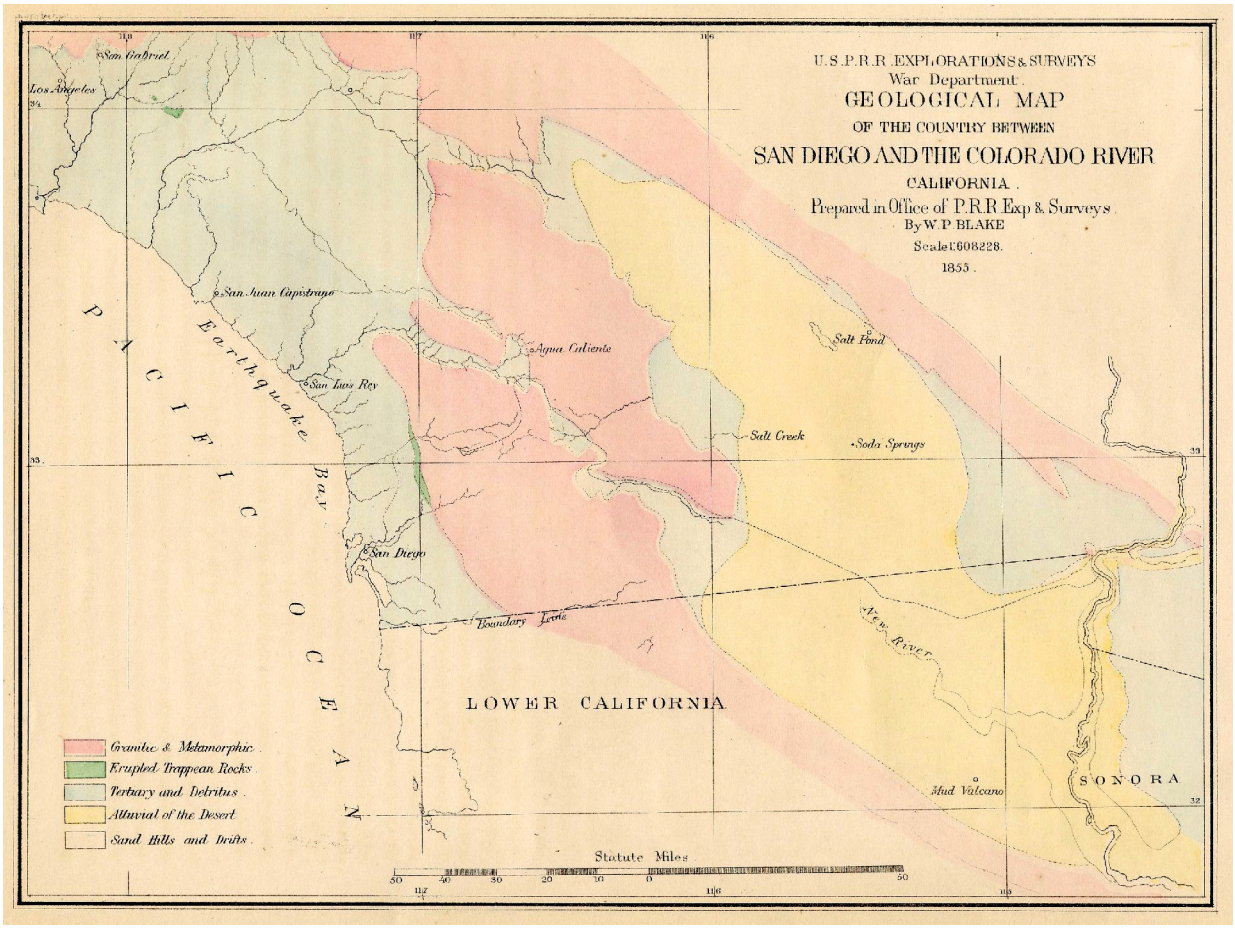

Figure 3. U.S. P.R.R. Explorations & Surveys War Department Geological Map of the Country between San Diego and the Colorado River California, prepared in Office of P.RR. Exp. & Surveys by W.P. Blake, 1858 (Courtesy of Jeffrey Patterson, San Diego Association of Geologists).

Railroad Survey, commissioned by Congress and President Pierce to assess and determine a practical railway route from Yuma, Arizona, to the Pacific Coast. By taking barometric elevation measurements as he traveled, Blake established that the region was an enclosed basin, the lowermost part of which was below sea level (the Salton Trough) (Figure 3).

The fossil shell specimens collected by Blake represented three major types: freshwater specimens (of which three were new species: *Amnicola protea*, *Physa humerosa*, and *Planorbis ammon*); a new brackish water genus; and Tertiary marine fossil shells. Blake concluded the valley was originally occupied by seawater from the Gulf of California [over six million years ago] as evidenced by the reefs of fossil oysters (Figure 4) and other marine shells (Blake 1853). He stated further that the influx of fresh water from the Colorado River eventually displaced the salt water, and the valley was soon completely occupied by fresh water [Lake Cahuilla] which then disappeared very slowly through evaporation and loss of water flow

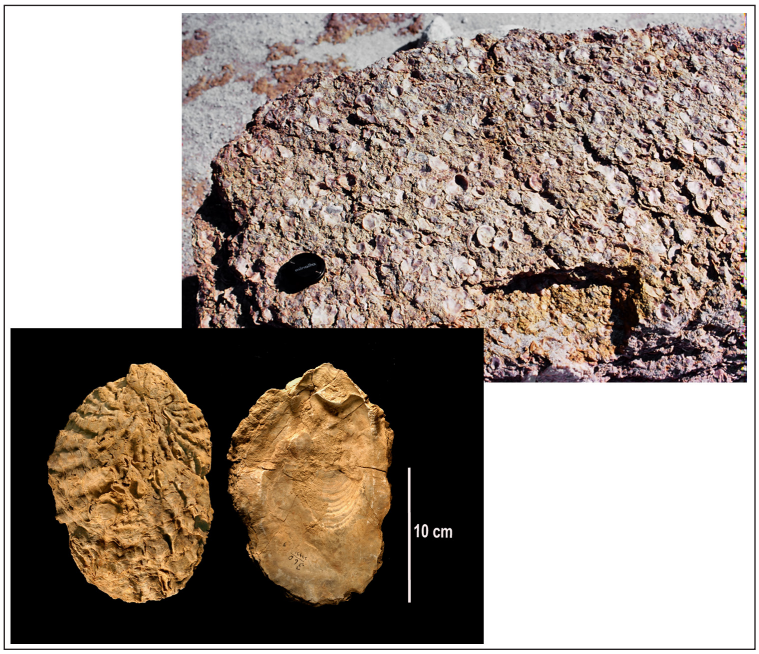

Figure 4. Upper right: Massive bed of oyster shells in the Deguynos Formation in Coyote Mountains ABDSP (Courtesy of the Colorado Desert District Stout Research Center, Borrego Spring, California.) Lower left: *Pycnodonte heermani*, the most common large fossil oyster in both the Deguynos and Latrania formations (Photograph by Barbara Marrs).

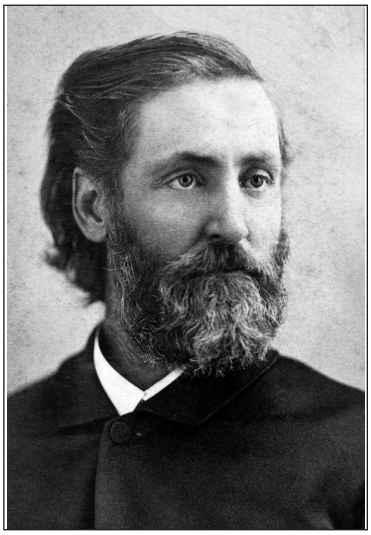

Figure 5. Portrait of Stephen Bowers, circa 1870s (Courtesy of the Ventura County Museum of History & Art, Ventura, California).

from the river (Blake 1858, 1914). Blake's in-depth geologic analyses of the region's rocks and sediments and of the basin's transition from marine waters to fresh water to desert (although flawed and much more complex than he could know) are major contributions to the scientific history of what is now the Colorado Desert and ABDSP.

The first official publication on the geology of the Colorado Desert to follow Blake's account was by Charles R. Orcutt in the California Journal of Mines and Geology (Orcutt 1890). Orcutt traveled extensively throughout the area, collecting large numbers of invertebrate fossils, primarily oysters, corals, and sea urchins, from the southern part of the Park. His data were prepared for the California State Mining Bureau, currently the California Geological Survey.

H. W. Fairbanks next collected in the Colorado Desert, circa 1892 (Fairbanks 1893). His invertebrate specimens were sent to the University of California Berkeley, where Dr. T. W. Vaughan described two new species and one new subspecies (Vaughan 1904).

In 1901, Stephen Bowers (Figure 5), a Methodist minister and an eminent geologist who became the State Mine Examiner of California, headed a Reconnaissance of the Colorado Desert Mining District for the California State Mining Bureau. Bowers divided the territory that he surveyed into four districts: Coyote Wells, Carrizo Creek, Fish Creek, and Seventeen Palms Springs (the latter three are part of ABDSP today). Throughout his survey, Bowers observed, as did Font, Blake, Orcutt, and Fairbanks before him, vast exposures of fossil oyster shell and coral reef deposits, and many other invertebrate deposits.

Bowers's final report to the California State Mining Bureau includes much information on his observations of the Colorado Desert's fossil invertebrates and their sediments, and of the former incursion of seawater into the region (Bowers 1901). However, Bowers's account also contains the first report of vertebrate fossils found in this desert: "Shark teeth and whale fossils…from the Coyote Mountains, and the remains of an extinct zebra-like horse from the eastern Borrego Badlands" (Jefferson and Lindsay 2006:xv).

Invertebrate Studies of the 1900s

In 1903, T. W. Vaughan studied Bowers's invertebrate collection and described five genera of corals that appeared in the fossil and recent fauna of the Antilles, West Indies, previously unknown on the Pacific Coast. This apparent anomaly prompted more detailed geologic research in the area. In 1904, W. C. Mendenhall (accompanied by Bowers) conducted physiographic and stratigraphic studies of the desert region, making a second extensive collection of its invertebrate specimens. From these data, Mendenhall published the most detailed account thus far of the geology of the Colorado Desert (Mendenhall 1910).

In 1919, G Dallas Hanna assumed the duties of curator for the paleontology department of the California Academy of Sciences that housed two large collections of fossil mollusks from the Colorado Desert. Hanna observed that these desert marine invertebrates, though closely related to the Atlantic West Indies fauna, were, beyond a doubt, most similar to the tropical fauna from the Gulf of California. This significant observation revealed a substantial clue to the mysterious history of the Colorado Desert's extinct animals of the sea. Hanna's extensive report described 80 species of gastropods, pelecypods, echinoderms, corals, and one shark. Some were new species identified by Hanna, and many more were new species previously described by earlier researchers (Hanna 1926). These added data corroborated the earlier reports of both Blake and Mendenhall: the Colorado Desert's invertebrates of the past were a truly unparalleled paleofauna.

Extensive collecting of the invertebrate fossils in the region tapered off in the 1930s with a simultaneous rise in the investigation, collection, and research of the Park's fossil vertebrates. But the value and far-reaching significance of these North American invertebrate fossil faunas and their strata did not diminish. Researchers in the 1930s through the 1960s continued to study the area's collections and regularly published their findings in hopes of unlocking more of the mysteries presented by this remarkable fossil evidence.

The introduction of the science of taphonomy in 1940, and the steady increase of taphonomic studies in the years thereafter, led to a resurgence of investigations and published works on the Colorado Desert's invertebrates from the 1970s to the present. Similarly, the later development of plate tectonics theory, well understood by the late 1960s, provided profound insights into the repositioning of continental boundaries and seaways that answered many of the questions posed by the early discoveries of ABDSP marine faunas. Direct connection of Caribbean waters through the Panama seaway to the southwestern coast of North America (prior to today's Central American land bridge) provided obvious routes for the dispersal of common marine species, information unavailable to earlier researchers.

These past 150 years of the desert's geologic and paleontologic investigations yielded " ... over 100 species of bivalves, 72 species of gastropods, 16 species of echinoids, and numerous ostracods, corals, barnacles, trace fossils, bryozoans, and foraminiferans" (Remeika 1998). Science professionals and graduate students from the University of California at Riverside, the University of Chicago, University of Oregon, California State University at San Diego, the United States Geological Survey, and other renowned institutions continued the comprehensive research, applying new techniques and theories to extract the answers to the region's extraordinary invertebrate fossil history.

Vertebrate Discoveries and Studies of the mid-1900s

Circa 1935, Guy Hazen began surveying for vertebrate fossils in the area later termed the Vallecito Creek-Fish Creek Badlands (VCFCB), in the southern part of ABDSP, and also in the Borrego Badlands, located in the northern part of the Park (Figure 1). The Colorado Desert revealed itself to be a virtual goldmine for late Tertiary fossil mammals, and over 360 fossil vertebrate specimens were recovered and shipped back to New York City (Murray 2008). Of more than twelve distinct taxa collected by Hazen, the only specimens published by Frick (1937) were some partial antlers, described as a new subspecies (*Odocoileus cascensis* var. 2b). Today, this collection still resides in the AMNH's Childs Frick Wing.

In 1941, nineteen-year-old Harley James Garbani (Figure 6) visited the Vallecito Creek-Fish Creek Badlands of ABDSP and found several significant vertebrate fossils. Garbani, a ranch hand/plumber by trade and a self-educated fossil enthusiast, had been discovering and recovering fossils in the San Jacinto Mt. Eden Fossil Beds since he was a child. He met Guy Hazen when both were collecting in the area and learned of ABDSP's fossils from the AMNH field paleontologist. Garbani continued to explore, survey, and collect fossils in the southern part of the Park until he enlisted in the U.S. Army in 1944. In the postwar years, Garbani eventually wanted to have his discoveries identified. After several California institutions showed little or no interest in his specimens, Garbani met with Dr. Hildegarde Howard, Chief Curator of Science at the Natural History Museum of Los Angeles County (LACM). Howard, in turn, directed him to Dr. Theodore Downs, recently appointed Curator of the museum's Vertebrate Paleontology Department. Downs was very interested in both the vertebrate finds, and in Garbani's description of the fossiliferous strata abounding in that section of the Park.

In January 1954, Garbani and Downs visited the former's ABDSP fossil localities in the Vallecito Badlands (Figure 1). Downs observed specimens that Garbani had left *in situ* and was decidedly intrigued by what he saw. The two commenced surveying and soon made several new vertebrate discoveries. In his field notes, Downs

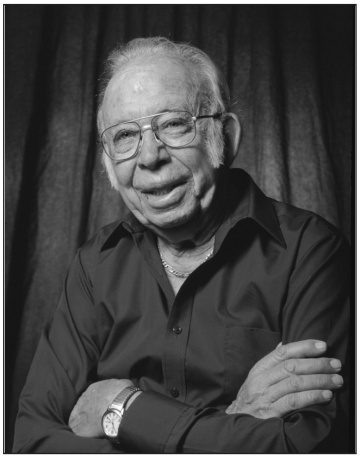

Figure 6. Portrait of Harley James Garbani, May 2002. (Courtesy of photographer, Barbara Marrs).

recorded findings of fossil horse, camel, antelope, pocket gopher, rabbit, and turtle—an amazing variety of prehistoric animals for one day's work! Downs also proceeded to number and re-record all of Garbani's previous finds, as well as note his own observations of the sediments and their lithology. Later that year, there were two more LACM expeditions, and thus began the most productive phase of paleontologic research in the region's history.

During the two decades that followed, Garbani recorded and recovered fossils under the aegis of Downs's State Park collecting permits during the many weeklong LACM expeditions or on his own. In addition to the amazing productivity and diversity of the vertebrate fossils found, Downs observed multiple puzzles inherent in the strata.

> This locality [Vallecito Badlands] adds a long chapter to the story of the history of ancient southern California. It may provide insight into the interchange of mammals from Mexico. It certainly suggests a different scene from what we know today (Downs, field notes, Dec. 17, 1954). "After walking the exposure out and taking several attributes, I am convinced there is a new sequence of events revealed here (Downs, field notes, Dec. 3, 1958).

In 1957, Dr. John A. White, a mammalogist and professor from California State College Long Beach, joined the LACM team. Because of the great numbers and varieties of microvertebrate fossils being recovered, Downs requested that White, a small mammal specialist, personally survey the new localities. White proceeded to discover and collect many new species of rodents and lagomorphs from the area's sites, among them an important new species of pocket gopher that he named after Garbani (*Geomys garbanii*), for which over 75 specimens of this significant rodent were recovered. In referring to the latter Downs states, "The 'paleo find' is *Geomys*, the pocket gopher, because of the quality and quantity of the remains for evolutionary study" (Figure 7) (Downs, field notes 1957).

The exceptionally high yield of many new microvertebrate fossil species coupled with the

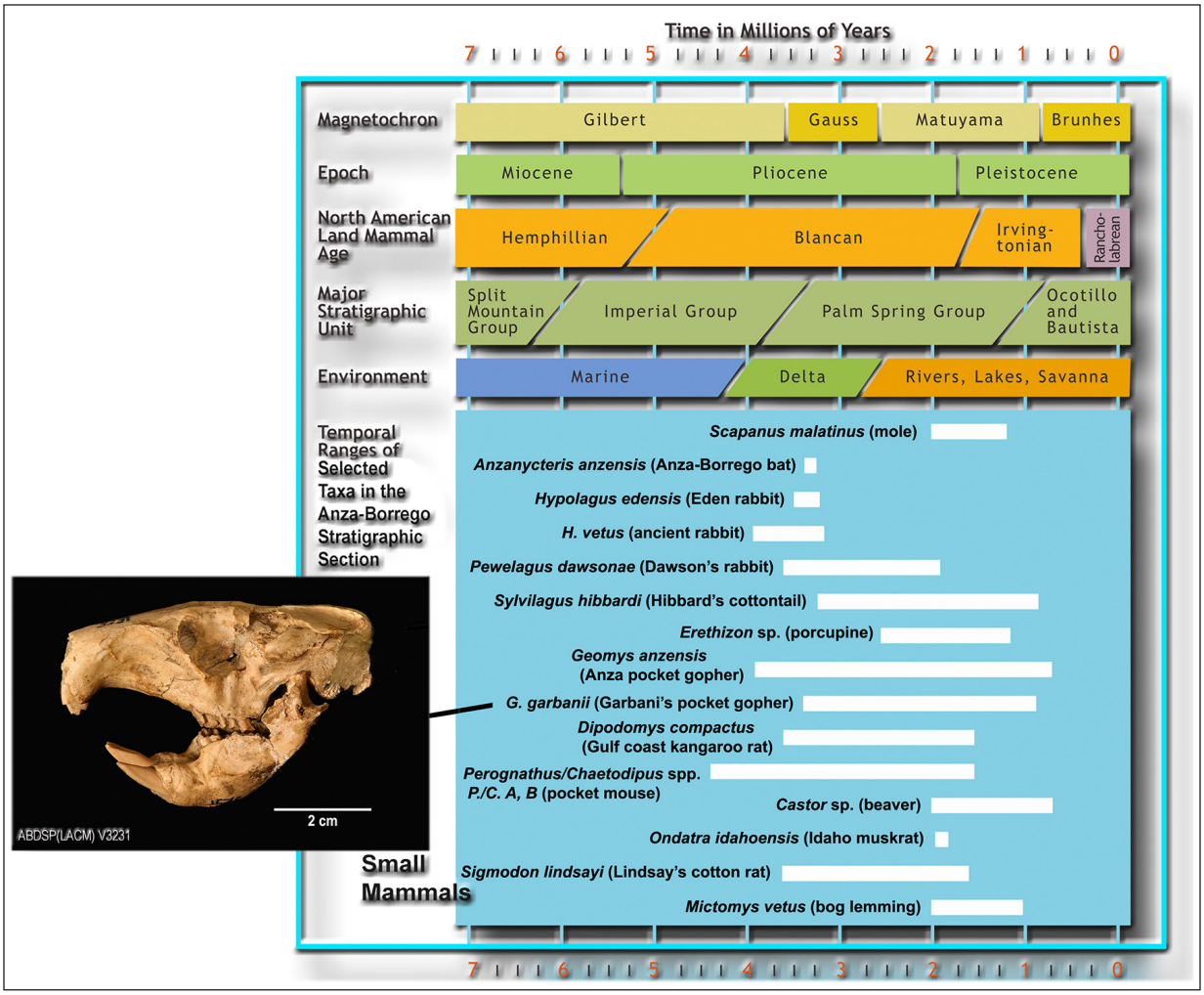

Figure 7. Timeline for fifteen small fossil mammals of ABDSP spanning about 4 million years, courtesy of George T. Jefferson and Lowell Lindsay 2006, Fossil Treasures of the Anza-Borrego Desert The Last Seven Million Years, Sunbelt Publications, Inc., and inset, the skull of *Geomys garbani*, Garbani's pocket gopher (Photograph by Barbara Marrs).

discovery of several significant fossil horizons in the Vallecito Badlands, convinced both Downs and White that the deposits from the south end of this geologic section to its north end were in fact a stratigraphic continuum of freshwater deposits. Both scientists realized that they were observing a true paleontological phenomenon, thus far unparalleled in North America: thousands of feet of thick layers of river-borne sediments that had been laid down in a conformable biochronologic sequence, which contained an impressive record of vertebrate fossil fauna spanning a time of no less than 2.5 million years.

The first few years of Downs and White's investigation were concentrated in the more accessible Vallecito Creek region of the Vallecito Badlands. This area consists of the uppermost stream-deposited strata of the complete stratigraphic section. At this point in time there were not many roads in ABDSP, and fewer still into the fossil areas. Most of these were dirt routes, and the terrain rough. Drinking water, food supplies, gasoline, etc., had to be brought in or obtained from local residents for the weeklong expeditions.

In the years that followed, LACM fossil excursions expanded to the lower marine and terrestrial deltaic parts of the section, accessed via Fish Creek Wash. Ultimately the entire section was referred to as Vallecito Creek/ Fish Creek, with multiple variations and abbreviations (VCFC, FCVC Basin) (Figure 1). White described the VCFC as similar to a deck of cards on its edge. He said you could walk about sixteen miles in a straight line and pass through layers of time on the ground. Both Garbani and White remembered when they first began collecting in this area, there were fossil bones littering the surface almost everywhere they looked, though not as much now (pers. comm. to LK Murray from White, 1992, and from Garbani, 1996).

In 1958, Downs invited G. Davidson Woodard, an Australian geologist working toward a Ph.D. at Berkeley, to evaluate the local stratigraphy. In order to understand the age of the fossils that appeared throughout the VCFC Badlands horizons, it was necessary for the region to be mapped geologically. Having a personal interest in the Plio-Pleistocene strata of southern California, Woodard

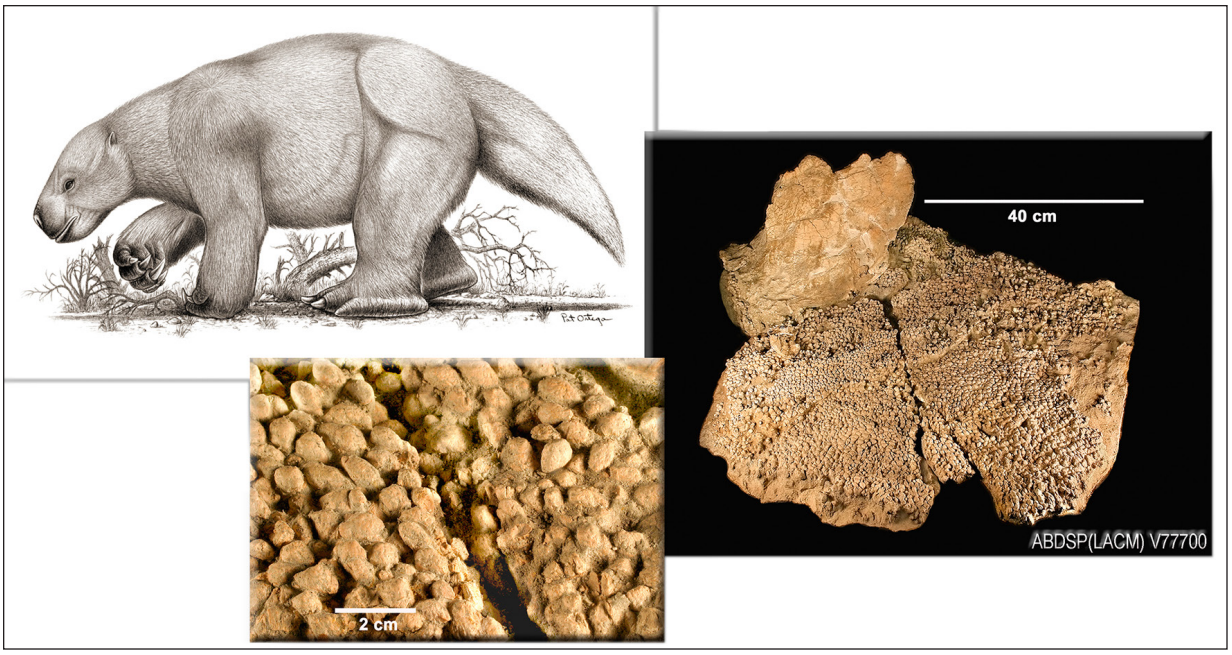

Figure 8. From left to right, *Paramylodon harlani*, Harlan's Ground Sloth (Drawing by Pat Ortega), detail of fossilized dermal ossicles from *Paramylodon harlani*, and dermal ossicle layer from *Paramylodon harlani* (photographs by Barbara Marrs).

joined LACM's Anza-Borrego team and worked to help complete Downs's lithologic and stratigraphic field notes.

Also in the late 1950s, Garbani was joined by his two sons, James and David, and the trio made many key fossil finds, among them the area's first porcupine and short-faced bear specimens, several large turtles and a giant tortoise, and two of Garbani's major vertebrate fossil discoveries—an aiolorn fossil (the largest flying bird to have ever lived in North America), and a rare specimen of a giant ground sloth hip attached to a square meter of dermal ossicles, distributed and oriented as they were in the living skin (Figure 8).

Promoted to LACM Chief Curator of Earth Sciences in 1961, the Colorado Desert's paleontologic and geologic history remained Downs's top priority until his retirement in 1980. He initiated the use of aerial photographs for plotting fossil sites; employed screen-washing methods for extracting microvertebrate fossils from sediments (Figure 9); had pollen analyses performed; and with White and Woodard, published the first reports of the paleontology and geology of the Vallecito Badlands and Borrego Badlands regions (Downs 1957, Downs and Woodard 1961; White and Downs 1965; Downs and White 1968). As LACM Chief Curator Emeritus, Earth Sciences, Downs continued working on the ABDSP fossils until the early 1990s. The 5,741 Anza-Borrego mammal, bird, and reptile fossils recovered by LACM between 1954 and 1970 were from 927 localities and numbered over 100 different species, over a dozen of which were new.

By 1970, the Colorado Desert and ABDSP had been acknowledged, beyond a doubt, as a region of tremendous paleontologic and geologic importance, featuring several significant fossil faunas and sedimentary depositional sequences unlike any other in North America. As stated by Downs,

> "The location of the region is particularly appropriate in terms of potential information concerning the migration of faunas to and from the Central and South Americas ... [There is] little evidence of immigrants from Eurasia to North America in Anza-Borrego. Seven or more taxa are from Central and South American sources. [We] hope to evaluate the possibility of in situ evolution relative to the concepts of gradualism and punctuated equilibrium" (Downs and White 1965:107).

Several professional paleontology papers were published on studies of ABDSP fossils recovered by Downs and his team including lizards, birds, bats, ground sloths, gophers, cotton rats, microtine rodents, rabbits, porcupines, coyotes, horses, and tapirs.

The Introduction of ABDSP's Paleontology Volunteers

In 1965, George J. Miller, a contractor/journeyman plumber who became a California State University Long Beach undergraduate studying geology and paleontology, joined Drs. Downs and White, and collected fossils for the LACM at ABDSP and elsewhere in southern California. In 1972, Miller was hired as a Professor of Geology and Paleontology at the Imperial Valley College in Imperial, California. With the help of Downs, he was able to obtain a permit to collect fossils in the State Park for the Imperial Valley College Museum (IVCM) in El Centro, for which they appointed him Curator of Paleontology in May of 1973. In 1974, Miller received a master's degree

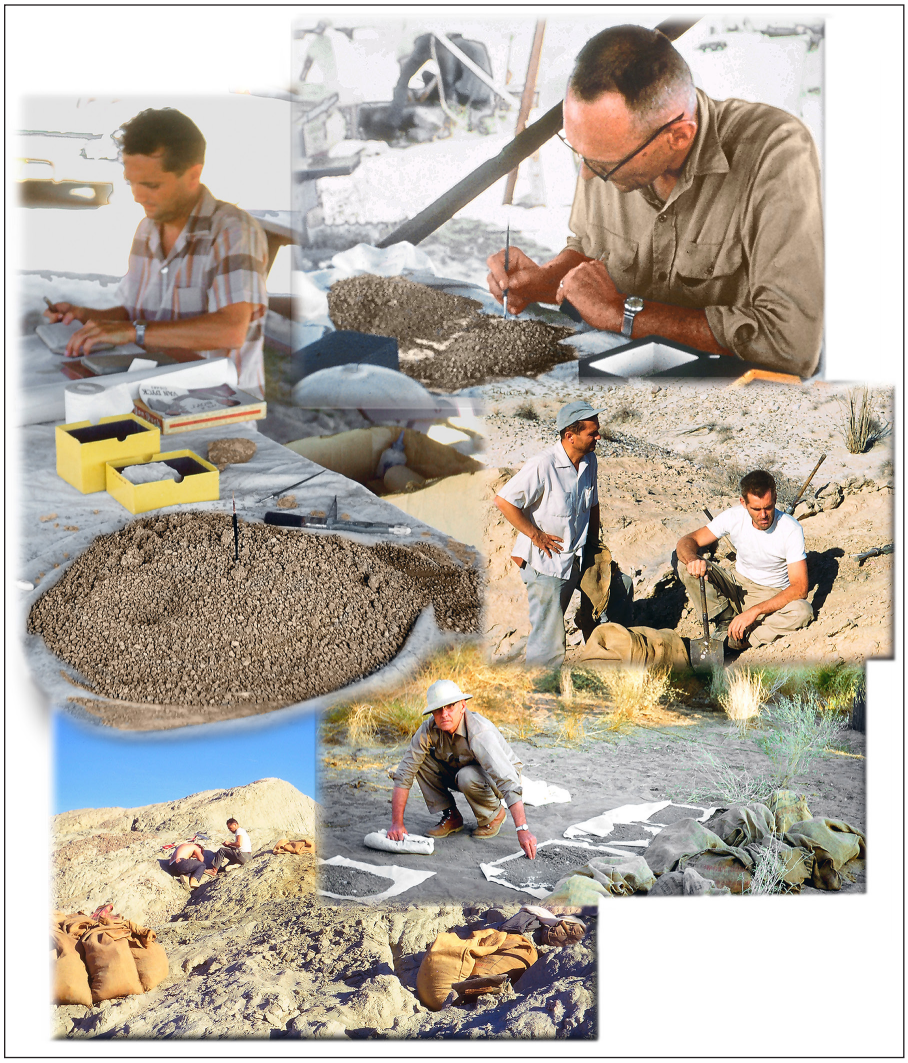

Figure 9. The "LACM Party" collects microvertebrate fossils from the Vallecito-Fish Creek Badlands, Anza-Borrego Desert State Park®, July, 1961; Clockwise from top: Dr. John A. White sorts through screenwashed sediments; Dr. Theodore Downs and preparator Leonard Bessom fill burlap bags with sediments from the Vallecito-Fish Creek Badlands; Dr. John A. White with screenwashed sediments; Burlap bags of Vallecito-Fish Creek Badlands sediments wait for their helicopter airlift to the screenwashing site at "Borrego Park" (sic); A large pile of screenwashed sediments awaits sorting, as Dr. Theodore Downs enters his notes (Photos courtesy of the Colorado Desert District Stout Research Center, Borrego Springs, California)

from Idaho State University Pocatello, and his advisor was Dr. White, who had become Curator of Vertebrate Paleontology at the Idaho Museum of Natural History. Miller continued to discover and recover vertebrate fossils from the Park, bringing his collections to IVCM for preparation and curation.

In 1969, through his ties with Anza-Borrego archaeology, Miller met Borrego Springs resident Betty Stout, a volunteer Park aide and naturalist, who often accompanied Anza-Borrego archaeologist, Bill Seidel, and Park rangers on various field trips and surveys. In September 1974, communications between Stout and Miller blossomed into the start of Anza-Borrego's first paleontology classes taught by Miller to a large group of volunteers (mostly retirees) at the Borrego Springs Youth Center. With his new group of paleontology students, Miller led the next big wave of productive paleontologic surveying and collecting in ABDSP, which continued through the 1980s. They surveyed and recovered vertebrate fossils from the southern part of the Park (VCFC) as well as the northern end in the Borrego Badlands and Coyote Canyon (Figure 1). Though previously "harvested" by both AMNH and LACM, these areas continued to yield fossil vertebrates, particularly horses, camels, cervids, and mammoths that were taken to IVCM for preparation and curation because the Park lacked proper facilities. However, with funds donated by the Stouts, and under Miller's guidance, the Stout Paleontology Laboratory was constructed and finally completed in May of 1982. This State Park facility did meet all the requirements for Miller's volunteer paleontology team, who were now recovering, preparing, and curating the majority of the fossils they collected in ABDSP.

Miller's premier discovery of a mammoth occurred in December 1986. In March1988, before an audience of paleontology volunteers, Park rangers, and newspaper and television crews, the massive jacketed skull and single complete tusk were separately airlifted by helicopter and flown to their new home at the Stout Laboratory (Figure 10). Five years later, after the excavation was completed and all the paleontologic and geologic evidence gathered, the "Miller mammoth" was determined to be the most complete skeleton of *Mammuthus meridionalis* (southern mammoth) found in North America (McDaniel and Jefferson 1997, 2003). Once again, Anza-Borrego's astonishing fossil treasures had placed the California State Park in the scientific world's national and international limelight.

Until his death in 1989, Miller continued to contribute to ABDSP's paleontologic history. He, along with volunteer Betty Stout, is credited with organizing the Park's first group of paleontology volunteers, and for actively recruiting these individuals from one of the area's most valuable resources—its senior citizens. It was the

Figure 10. Clockwise from top: George J. Miller points to the Miller Mammoth tusk ready to be jacketed, Jan. 1988; George Miller supervises as paleontology volunteers prepare the jacketed mammoth skull for airlift, March 1988; Helicopter prepares to airlift jacketed mammoth tusk, March 1988 (Photos courtesy of the Colorado Desert District Stout Research Center, Borrego Springs, California).

immense success of this volunteer program that enabled Miller to survey and collect as extensively as he did in the 1970s and 1980s. Said Miller, in a Los Angeles Times interview: "This group of senior citizens is unlike any other group anywhere. What they have done here has even amazed the national Society of Vertebrate Paleontologists" (Los Angeles Times, June 7, 1981). Between 1973 and 1989, Miller and the IVCM field crews recorded over 1,425 localities that yielded more than 7,250 catalogued specimens. The additional finds of Miller also produced new publications: bobcats, mole, woodrats, horses, and mammoths.

The Establishment of ABDSP Fossil Collection Policies

In 1989, David Van Cleve became the District Superintendent of the Colorado Desert District (CDD), which included seven parks, among them Anza-Borrego and two other fossil-producing areas within the Colorado Desert: Salton Sea State Recreation Area and Indio Hills Palms. Though he personally never met George Miller, Van Cleve soon became aware of the significance of ABDSP's paleontologic and geologic resources, and in 1991, he assembled a Paleontology Advisory Board comprised of paleontologists and museum professionals to advise him and the State of California on the management and conservation of these resources. The six-member board included Dr. John White, Betty Stout, and George T. Jefferson, Associate Curator for the Rancho La Brea George C. Page Museum in Los Angeles, California.

Following the board's recommendations, Van Cleve initiated and supervised the execution of both a Resource Management Plan and a Collections Management Policy that, for the first time, established formal goals, procedures, and policies for managing ABDSP's paleontologic collections by the California State Parks rather than by outside museums. Also instituted was the Park's first State-sanctioned Certification Training Program in Paleontology, taught by Park Ranger/paleontologist and geologist, Paul Remeika, who for many years had been studying and publishing papers on ABDSP's geology, and floral and faunal fossils. No longer to be left in "limbo," Miller's former students, as well as any interested parties, would now become official State Park Paleontology Volunteers and be recognized for their contributions.

One of Van Cleve's main concerns was to have the non-state agencies housing fossils excavated from the Park transfer those collections to the CCD's paleontologic facility. All research and collection was performed under State permit, with the stipulation that the fossils remained property of the California Department of Parks and Recreation, and curated by an approved repository. Thus, all of Downs's collections were curated at LACM, and about half of Miller's fossils were curated at IVCM, with the remainder housed at the ABDSP Visitor Center and Stout Laboratory.

Working with Paleontology Volunteer Collection Manager, Julie Parks, and Paul Remeika, and with financial assistance from the Anza-Borrego Desert Natural History Association (ABDNHA), the District

Supervisor executed the transfer of Miller's IVCM fossil collection to its rightful home at the Park's Stout Laboratory on March 31, 1992, only days before the approximately 6,000 fossil specimens were to be stored "… in 40-foot long Sealand cargo containers outside on the desert floor." (Remeika, Reacquisition of ABDSP Fossil Collection from IVCM, Oct. 7, 1991. Timeline on file at SRC).

In January 1993, George T. Jefferson, recently retired from LACM, was hired by Van Cleve as a Park Environmental Services Intern, and by the ABDNHA as a Park Paleontology Collections Manager, a temporary "joint" position so that the former LACM curator could oversee the Colorado Desert collections until a permanent post was available. At that time there was no classification of Paleontologist in the California State Parks system. In 1994, Jefferson became the CDD District Archaeologist in charge of paleontologic resources and the State's first (and only) District Archaeologist/Paleontologist. He was perfectly suited for the position for a variety of reasons, among them his graduate degree and many years experience in archaeology, geology, and paleontology.

But it was Jefferson's knowledge and expertise with the management of LACM's vertebrate fossil collections that ably guided him with the administration of ABDSP's paleontologic resources. Jefferson hired Lyndon Murray, an MS graduate in Quaternary Studies from Northern Arizona University, Flagstaff, and they established a collections management program. Jefferson revamped the Certification Training Program, taught the new lecture series, and succeeded in gathering what was once again a strong force of Paleontology Volunteers, comprised of both experienced and new members. Jefferson and Murray also tackled the colossal project of organizing ABDSP's botanic, invertebrate and vertebrate fossil collections into a professional working system, which included, among other standards, strict and accurate specimen curation, and the creation of official Specimen Recovery, Laboratory, and Collections Guidelines.

Another major project completed by the two ABDSP scientists was to convert all known fossil localities discovered by LACM and IVCM into digital data points for use in Geographic Information System (GIS) map production. Prior to 1994, localities were recorded by marking the position on an aerial photograph via poking a pin through the location of a find and labeling it with the field or locality number. In 1996, Murray transcribed all of the marks on these aerial "maps" to fresh photographs and sent them to the United States Geological Survey in Denver, Colorado, to be converted to digital format. Following this, the geographic positions of all new fossil localities have been recorded in the Universal Transverse Mercator coordinate system (UTM) and captured digitally via the Global Positioning System (GPS).

A key member of the ABDSP Paleontology Volunteer group at this time was George E. McDaniel Jr., a retired veterinarian who joined the program in 1986. A dedicated and avid Park Volunteer, McDaniel soon became the chief preparator, and eventually, the Paleontology Laboratory Director, a position he held full time for 15 years. Usually working eight hours a day, five days a week, McDaniel trained all new volunteers in field and laboratory preparation techniques and helped write the original curriculum for certification training. Because of his extensive work on the Miller mammoth, including its diagnosis as *Mammuthus meridionalis*, McDaniel began visiting museums around the country to measure and study other mammoth material. Over time, he became the Park's proboscidean expert, and published several abstracts and papers on ABDSP's gomphotheres and mammoths.

Late 1900s Discoveries, Studies, and Projects

A year before Jefferson left LACM to take his State Park position, plans had begun to transfer the L.A. museum's ABDSP fossil collection back to its Colorado Desert repository. Jefferson followed through with this major undertaking, and after three years of countless trips to Los Angeles, much lengthy correspondence, and numerous phone calls to LACM and Department of Parks and Recreation officials, his tenacity paid off. With the planning assistance of Murray, and hundreds of hours of recording, packing, and unpacking by Park Volunteers, LACM's Anza-Borrego collections, totaling over 7,000 items, were transferred to ABDSP in 1997, uniting all three of the Park's paleontologic collections (LACM, IVCM, and ABDSP) under one roof at the Stout Paleontology Laboratory in the Borrego Springs Park headquarters.

As a response to the Advisory Board's recommendation for the State to provide an onsite district collections facility and research center, and with funds provided by State appropriations and grants and the Stout Foundation, Jefferson, Van Cleve, and other ABDSP professionals worked together on plans for expanding the Stout Laboratory. The proposed structure had to meet the requirements not only of the State Park's paleontologic resources, but also those of Anza-Borrego's natural history and botanic collections as well. Construction of the new CDD Stout Research Center (built around the original Stout Laboratory) began in 1997, and the complex was completed in 1998. At the Center's dedication in 1999, it housed approximately 13,000 curated botanic, invertebrate, and vertebrate fossil specimens, and featured one of the most state-of-the-art laboratories for fossil preparation in the country. A second addition, doubling the size of the Stout Research Center Paleontology Laboratory, begun in 2009, was completed in 2011.

Equipped with the new State Park research facility, Jefferson, and a seasonal team of 30 to 40 Certified Paleontology Volunteers using the latest laboratory methods, curation procedures, and field technology, including the use of GPS, GIS map imagery, and linked computer data bases, ushered in the new millennium with

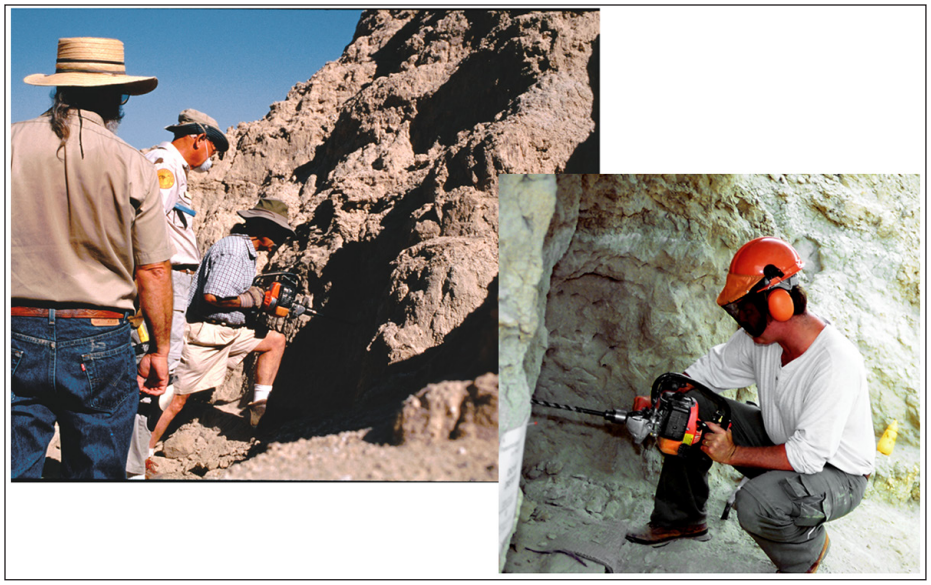

Figure 11. Left to right: George T. Jefferson supervises ABDSP Paleontology Volunteers as they use a gasoline-powered drill to break up and remove sediment surrounding mammoth fossil specimens. (Photographs courtesy of Barbara Marrs).

a continued wave of desert discoveries. As with Miller before him, these achievements were realized because of the Park's Paleontology Volunteer Program. Under Jefferson's supervision, trained Paleontology Volunteers carried out the rugged fieldwork, lab preparations, and curation duties. Some volunteers took on added managerial responsibilities, specifically in leading field surveys and excavations, managing the laboratory, teaching program protocols and techniques to new student volunteers, and tracking the fossils from the field through laboratory and curation. The construction of custom oversized cradles for the preservation of the Park's larger specimens developed into its own specialty undertaking headed by Park Volunteer Norbert Sanders.

Under Jefferson's direction and guidance, new cheetah-like cats, llamas, camels, and giant aiolorn bird specimens were "discovered" among the already collected and curated materials after the combined collections were reorganized and properly identified. Also during this time, fossil wood deposits and fossil animal tracks were mapped and documented by Paul Remeika. Based on these geologic maps and paleomagnetic studies of deposits in the Borrego Badlands, Remeika produced multiple publications on the geology, wood, and fossil ichnites of the Park (see Remeika and Sturz 1995).

Other "fossil firsts" included the discovery of *Gomphotherium* specimens, a possible new species of *Palaeolama* found by Harley J. Garbani, a fossil Gila monster, and important new discoveries in the VCFC: a diverse and unusual mix of both marine and terrestrial fossil vertebrates, including sharks, sea turtles, walruses, ground sloths, gomphothere, ancestral horses, camels, and llamas. The discovery of two tusk ends and skull fragments of a sub adult and a juvenile mammoth in the Borrego Badlands (Figure 1) in February 2002, prompted the use of gasoline-powered drills and pneumatic chisels connected to a gasoline-powered air compressor to break-up and remove layers of sediment, excavation methods unprecedented in Anza-Borrego's collection history (Figure 11).

During Jefferson's tenure as District Paleontologist over 1,575 new fossil localities were recorded, producing more than 3,850 fossil specimens (Table 1).

New Millennium Discoveries, Studies, and Projects

Another of Jefferson's major achievements was the 2006 publication of the science volume *Fossil Treasures of the Anza-Borrego Desert*. Edited by Jefferson and Lowell Lindsay of Sunbelt Publications, Inc., this landmark study is a comprehensive treatment of the geologic and paleontologic history of the Colorado Desert and Anza-Borrego Desert State Park. A project several years in the making, it features detailed chapters written by paleontologists and geologists from across the United States on the desert's stratigraphy, basin evolution, paleoclimates, biostratigraphy, and the complete fossil record: the marine and freshwater invertebrates, the petrified woods, the fossil plants, the lower vertebrates (fish, amphibians, and reptiles), the birds, the mammals, large and small, and the fossil animal tracks. Over one hundred color photographs, exquisite illustrations by anatomical artist, Pat Ortega, and stunning two-page full-color paleolandscapes by landscape artist, John Francis, help recreate the desert's former environments of seas, rivers, lakes, woodlands, and savannas, and bring the fossil creatures "back to life." In 2007, *Fossil Treasures of the Anza-Borrego Desert* won the Benjamin Franklin Award from the Independent Book Publishers Association—the gold medal in Science/Environment.

Between 1997 and 2011, Lyndon Murray continued research on the ABDSP fossil collection, completing a dissertation (2008) that examined serious data errors discovered when he began to compile catalogued and published taxonomic and locality records of the collection for a biochronology study. Primary causes of the errors were traced to long-term accumulation (50 years) of small-to-large-scale corruptions in the database and mis-transcription of field notes or inaccurate reporting of information (Murray et al., 2011). As a result of this work, dozens of invalid identifications were retired from the ABDSP faunal list, and all current listed taxa are anchored by catalogued voucher specimens. Since 2011, the database

catalogue has been restructured, standardized, and purged of known inaccuracies by the intense labor of Paleontology Volunteers James Landers and Linda Gilbert.

A critical technology developed in the past century that placed ABDSP fossils into historic geologic context is magnetostratigraphy (paleomag), the geophysical correlation technique used to date sedimentary and volcanic sequences. The first such ABDSP study was of the VCFC section, authored by Opdyke et al. (1977). A second study in 1983 (Johnson et al.) added a radiometric date on volcanic ash layers exposed in Arroyo Tapiado, calibrating the local sequence to the global polarity time scale. The VCFC section was re-sampled in the 2000s by Bernie Housen (Housen et al. 2005; Dorsey et al. 2011) (Figure 12). Several paleomag studies have also been published for other areas within the Park.

In 2009, Jefferson spearheaded another major project for the CDD fossil collections. From the mid-1980s through the early 1990s, Dr. Susan Kidwell and graduate students from the University of Arizona and the University of Chicago explored FCVC and collected marine invertebrate fossils from the shell beds in the Park's Latrania Formation. One of Kidwell's students, Charlie Winker, produced a geologic map of the FCVC still used as a primary research source. Over 5,000 fossil specimens were curated in Kidwell's laboratory, and arranged from the bottom to the top of the Latrania through Deguynos Formations of the Imperial Group. In October 2009, under Jefferson's direction, Paleontology Volunteers Jim and Judy Smith, Bob and Sandra Keeley, and Norbert Sanders, packed and prepared the Kidwell collection for shipment to a recent expansion room of the SRC. The project involved months of coordinating the transfer and over 200 hours of wrapping and packing the fossils. This exceptional invertebrate collection constitutes the largest most complete stratigraphic collection of marine fossils from the ancestral Gulf of California. In fall 2012, Dr. Astrid M. Boehringer, working on post-doctoral research at the Scripps Institution of Oceanography, San Diego, California, and N. Scott Rugh, from the San Diego Natural History Museum, collaborated to identify the Kidwell fossils, and the task was completed in spring, 2013. During the identification process, Paleontology Volunteers arranged the specimens in cabinetry, and prepared and entered the fossil data in the Park database, providing ready access to information by in-house and visiting researchers about this invaluable invertebrate collection.

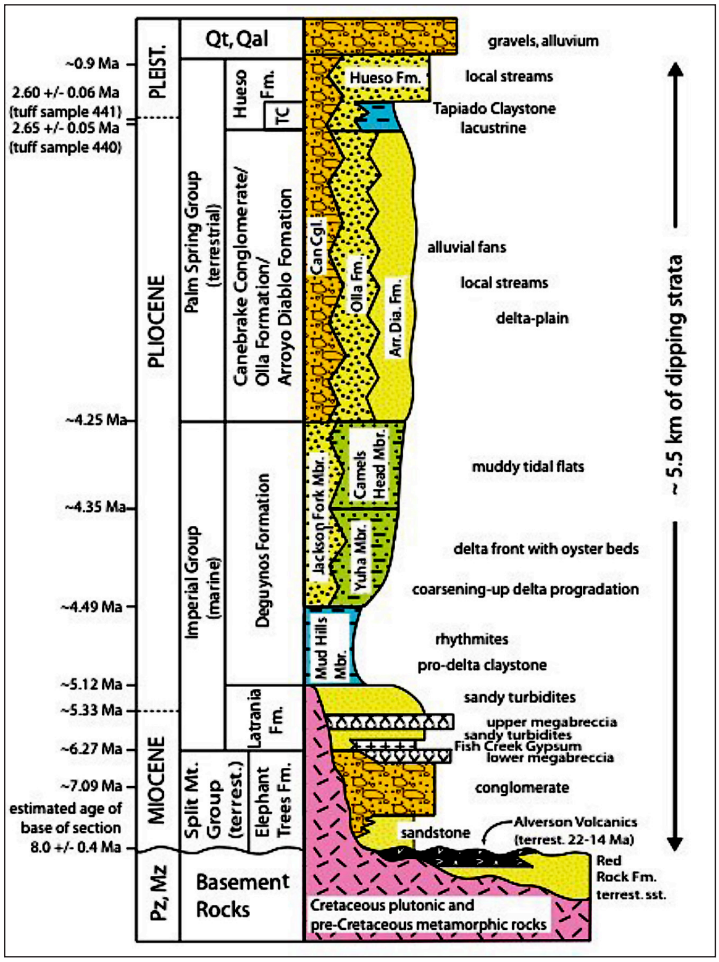

Figure 12. Modified by LK Murray from Dorsey 2006:fig 5.3 and Dorsey et al. 2011:fig 4, chronostratigraphic diagram of sedimentary rocks in the FCVC basin (does not include the Wind Caves member of the Latrania Formation). Stratigraphic nomenclature and interpretations are from Winker and Kidwell (1996), as modified slightly by Cassiliano (1999). The base of Elephant Trees Formation marks the earliest deposition related to onset of local deformation (extension or transtension) at ca. 8.0 ± 0.4 Ma (Dorsey et al. 2007).

Around the same time, a second, smaller collection of Colorado Desert invertebrate fossils was discovered at the University of Nevada Las Vegas, and also returned to the Park. These fossil specimens were collected from 1945 to 1965 by W. Morlin Childers, Curator of Paleo-Anthropology at the IVCM, and were originally curated at the college museum. Thus, nearly 75 years after their discovery, the various collections of the Colorado Desert's fossil mollusks, echinoderms, corals, and arthropods were formally housed back in their desert home, representing a rich and stellar slice of the region's past aquatic paleoenvironments (Table 2).

Recent Discoveries, Studies, and Projects

Jefferson officially retired from his State post in March, 2011, and the position of CDD District Paleontologist was filled by Dr. Lyndon K. Murray, who had worked with Jefferson at ABDSP from 1994 to 1997, and played a major role with the Park's key projects at that time. In addition to his former Park post, Murray's experiences as a Faunal Analyst, Field Archaeologist, and Museum Collections Manager (San Bernardino County Museum, Yale Peabody Museum, and The University of Texas Vertebrate Paleontology

Table 1: Systematic List of Fossil Vertebrates from Anza-Borrego Desert State Park, except where noted
Explanation: sp. = single indeterminate species in addition to named species; spp. = two or more indeterminate species in addition to named species. Taxonomic names have been revised to conform with current usage, and common names are provided in parentheses where applicable. Citations are of holotypes from ABDSP, parenthetical author of species nomen, bracketed author informal presentation of new or unnamed species

Class Actinopterygii (bony fish)
Order Cypriniformes
- Family Catostomidae (suckers)
  - *Xyrauchen texanus*
- Family Cyprinidae (minnow and carp)
  - *Cyprinodon*
  - *Gila elegans*
  - *Ptychocheilus lucius*

Order Cyprinodontiformes (small ray finned fish)
- Genus and Species indeterminate

Order Mugiliformes
- Family Mugilidae (mullet)
  - *Mugil* sp

Order Perciformes
- Family Istiophoridae (ray finned fish)
  - Genus and Species indeterminate

Order Salmoniformes
- Family Salmonidae (pacific salmon & trout)
  - Genus and Species indeterminate

Class Amphibia (amphibians)
Order Anura
- Family Bufonidae (toads)
  - *Bufo* sp.
- Family Ranidae (frogs)
  - Genus and Species indeterminate

Class Aves (birds)
Order Accipitriformes
- Family Accipitridae (hawks & eagles)
  - *Accipiter cooperii*
  - *Accipiter striatus*
  - *Aquila chrysaetos*
  - *Buteo jamaicensis*
  - *Buteo lineatus*
  - *Coragyps atratus*
  - *Neophrontops vallecitoensis*, n. sp. Howard 1963
- Family Cathartidae (condor)
  - *Cathartes aura*
  - *Gymnogyps*
- Family Teratornithidae (teratorns)
  - *Aiolornis incredibilis*, n. sp. (radius ABDSP (LACM) 1318/V3803 Howard 1963 –hypotype)
  - cf. *Teratornis merriami*

Order Anseriformes
- Family Anatidae (ducks, geese & swans)
  - *Anas acuta*
  - *Anas clypeata*
  - *Anas discors*
  - *Anser albifrons*
  - *Aythya affinis*
  - *Branta canadensis*
  - *Brantadorna downsi*, n. sp. Howard 1963
  - *Bucephala albeola*
  - *Bucephala fossilis*, n. sp. Howard 1963
  - *Chen rossii*
  - *Clangula hyemalis*
  - *Cygnus paloregonus*
  - *Melanitta persipicillata*
  - *Oxyura bessomi*, n. sp. Howard 1963
  - *Oxyura jamaicensis*
  - *Spatula cyanoptera*

Order Cariamiformes
- Family Phorusrhacidae (terror birds)
  - *Titanis* sp. (premaxilla ABDSP(LACM) 6747/V26697) Howard 1972a, 1972b as *Teratornis incredibilis* hypotype (tent.), Chandler et al. 2013) as *Titanis* sp.

Order Charadriiformes
- Family Charadriidae (plovers)
  - *Charadrius vociferus*
- Family Recurvirostridae (avocets)
  - *Recurvirostra americana*
- Family Scolopacidae (sandpipers)
  - *Calidris minutilla*
  - *Gallinago delicata*

Order Columbiformes
- Family Columbidae (passenger pigeon)
  - *Ecopistes migratorius*

Order Galliformes
- Family Odontophoridae (quail)
  - *Callipepla californica*
  - *Callipepla gambelii*
- Family Phasianidae (turkey)
  - *Meleagris anza*, , n. sp. (Howard 1963)

Order Gruiformes
- Family Gruidae (crane)
  - *Grus canadensis*
- Family Rallidae (rails)
  - *Fulica americana*
  - *Fulica hesterna*, n. sp. Howard 1963 [synonymized under *F. americana* by Olson 1974]
  - *Gallinula chloropus*
  - *Rallus prenticei*

Order Passeriformes
- Family Corvidae (crows & ravens)
  - *Corvus brachyrhynchos*
  - *Corvus cryptoleucus*
- Family Fringillidae (finch)
  - *Carduelis* sp.
- Family Icteridae (meadowlark & yellow headed blackbird)
  - *Sturnella neglecta*
  - *Xanthocephalus xanthocephalus*

Order Pelecaniformes
- Family Pelecanidae (pelicans)
  - *Pelecanus erythrorhynchos*

Order Phoenicopteriformes
- Family Phoenicopteridae (flamingos)
  - *Phoenicopterus copei*

Order Piciformes
- Family Picidae (woodpeckers)
  - *Colaptes auratus*
  - *Melanerpes uropygialis*
  - *Picoides scalaris*

Order Podicipediformes
- Family Podicipedidae (grebes)
  - *Aechmophorus occidentalis*
  - *Podiceps nigricollis*
  - *Podilymbus podiceps*

Order Strigiformes
- Family Strigidae (eared owls)
  - *Asio flammeus*
  - *Megascops kennicotii*
  - *Oraristrix brea*

Order Suliformes
- Family Phalacrocoracidae (cormorants)
  - *Phalacrocorax auritus*
  - *Phalacrocorax brasilianus*

Table 1-1

continues

Class Chondrichthyes (sharks, skates and rays)
Order Batoidea
Genus and Species indeterminate
Order Carcharhiniformes
Family Carcharhinidae (requiem sharks)
Carcharhinus sp.
Galeocerdo rosaliensis
Hemipristis serra
Order Lamniformes
Family Odontaspididae (sand sharks)
Odontaspis sp.
Order Myliobatiformes
Family Myliobatidae (eagle rays)
Myliobatus sp.
Order Squaliformes
Family Squalidae (dogfish sharks)
Genus and Species indeterminate

Class Mammalia (mammals)
Order Artiodactyla
Family Antilocapridae (pronghorn)
Antilocapra sp.
Capromeryx arizonensis
cf. *Stockoceros* sp.
? *Tetrameryx*
Family Bovidae (bison)
Ovibovini (cf. *Euceratherium*)
Bison sp.
Ovis canadensis
Family Camelidae (camels)
Blancocamelus meadei
Camelops spp. (? *C. hesternus, C. huerfanensis, C. minidokae*)
Gigantocamelus spatula
Hemiauchenia spp. (? *H. blancoensis, H. macrocephala, H. vera*)
Hemiauchenia gracilis
Paleolama sp.
Family Cervidae (deer)
Odocoileus spp. (phalanges larger than *O. hemionus* and size of *O. hemionus*)
Odocoileus cascensis (var. 2b), n. sp and ssp. (antler beam F:A.M. 31862) Frick 1937
Family Tayassuidae (peccary)
Platygonus sp. cf. *P. vetus*
Order Carnivora
Family Canidae (dogs)
Borophagus diversidens
Canis armbrusteri
Canis dirus
Canis edwardii
Canis latrans
Canis lepophagus
Urocyon sp. ? *U. progressus*
Family Felidae (cats)
Felis sp. (small ? *Herpailurus jaguarundi*)
Felis sp. cf. *F. rexroadensis*
Felis rufus
Miracinonyx inexpectatus
Panthera onca
Pseudaelurus sp.
Smilodon gracilis
Family Mustelidae (otters, weasels & skunks)
Satherium piscinarium
Spilogale sp.
Taxidea taxus
Trigonictis macrodon
Family Odobenidae (walrus)
Valenictus imperialensis
Family Otariidae (eared seal)
Genus and Species indeterminate
Family Procyonidae (raccoons & ringtails)
Bassariscus casei
Procyon sp. cf. *P. rexroadensis*
Family Ursidae (bears)
Arctodus simus
Tremarctos floridanus
Order Cetacea (baleen whales)
Family Balaenopteridae
Genus and Species indeterminate
Family Cetotheriidae
Genus and Species indeterminate
Order Chiroptera
Family Vespertilionidae (microbats)
Anzanycteris anzensis, n. gen. et sp. White 1969
Order Insectivora
Family Talpidae (shrews)
Scapanus malatinus, n. sp. Hutchison 1987
Order Lagomorpha
Family Leporidae (rabbits & hares)
Hypolagus edensis
Hypolagus vetus
Nekrolagus sp.
Pewelagus dawsonae, n. gen. et sp. White 1984
Sylvilagus hibbardi, n. sp. White 1984
Sylvilagus sp. cf. *S. floridanus*
Leporinae genus and species indeterminate
Order Perissodactyla
Family Equidae (horses)
cf. *Dinohippus* sp.
Equus enormis, n. sp. Downs and Miller 1994
Equus (Equus) sp. A [Downs and Miller 1994]
Equus scotti
Equus (Plesippus) sp. cf. *E. (P.) simplicidens*
Family Tapiridae (tapirs)
Tapirus merriami
Order Proboscidea
Family Elephantidae (mammoths)
Mammuthus columbi
Mammuthus meridionalis
Family Gomphotheriidae (gomphotheres)
Gomphotherium sp.
Stegomastodon sp.
Order Rodentia
Family Castoridae (beavers)
Castor sp.
Family Cricetidae (voles, rats & mice)
Arvicolinae
Baiomys sp.
Lasiopodomys morphotype sp.
Microtus (with 5 closed triangles on m1) sp.
Microtus meadensis
Mictomys vetus
Neotoma sp. a [Zakrzewski 1993]
Neotoma sp. b [Zakrzewski 1993]
Neotoma sp. c [Zakrzewski 1993]
Ondatra idahoensis
Onychomys sp.
Ophiomys parvus
Peromyscus sp.
Reithrodontomys sp.
Repomys sp.
Sigmodon minor
Sigmodon lindsayi, n. sp. Martin and Prince 1989
Family Erethizontidae (porcupine)
Erethizon sp.
Family Geomyidae (gophers)
Geomys anzensis, n. sp. Becker and White 1981
Geomys garbanii, n. sp. White and Downs 1961
Thomomys sp., cf. *T. gidleyi*
Family Heteromyidae (kangaroo rats)
Dipodomys sp. A, n. sp. [Cunningham 1984 unpublished MS thesis]
Dipodomys sp. B, n. sp. [Cunningham 1984 unpublished MS thesis]
Dipodomys compactus
Dipodomys hibbardi
Dipodomys sp. cf. *D. minor*

Table 1-2

continues

Perognathus/*Chaetodipus* sp. A [Gensler 2002 unpublished MS thesis]
Perognathus/*Chaetodipus* sp. B [Gensler 2002 unpublished MS thesis]
Family Sciuridae (squirrels)
Eutamias sp.
Spermophilus sp.
Order Sirenia
Family Dugongidae (dugongs)
Dugong sp.
Order Xenarthra (ground sloths)
Family Megalonychidae
Megalonyx jeffersonii (single specimen recovered from Coachella Canal outside ABDSP)
Megalonyx wheatleyi
Family Mylodontidae
Paramylodon harlani
Family Nothrotheriidae
Nothrotheriops texanus

Class Reptilia (reptiles)
Order Crocodilia
Family Crocodylidae (crocodiles)
Crocodylus sp.
Order Squamata
Family Anguidae (lizards)
Subfamily Gerrhonotinae
Genus and species undetermined
Family Colubridae (snakes)
Hypsiglena sp.
Lampropeltis getulus
Masticophis flagellum
Thamnophis sp.
Family Crotaphytidae (collared lizard)
Gambelia corona, n. sp. Norell 1989
Family Helodermatidae (beaded lizard)
Heloderma sp.
Family Iguanidae (iquanas)
Dipsosaurus dorsalis
Pumilia novaceki, new metaspecies Norell 1989
Family Phrynosomatidae (spiny lizards)
Sceloporine Type A [Norell 1989]
Sceloporine Type B [Norell 1989]
Phrynosoma anzaense, n. sp. Norell 1989
Family Scincidae (skink)
Eumeces sp.
Family Teiidae (whiptail lizards)
Ameiva and/or *Cnemidophorus* sp.
Family Viperidae (viper)
Subfamily Crotalinae
Crotalus sp.
Family Xantusiidae (night lizard)
Xantusia downsi, n. sp. Norell 1989
Order Testudines
Family Cheloniidae (marine turtles)
Genus and Species indeterminate
Family Emydidae (pond turtles)
Actinemys marmorata
Chrysemys picta
Pseudemys sp.
Trachemys scripta
Family Kinosternidae (mud turtle)
Kinosternon sp.
Family Testudinidae (tortoises)
Hesperotestudo sp.
Xerobates agassizii

Table 1-3

Laboratory) made him the most qualified successor to oversee the CDD collections and State Park Paleontology Program.

Under Murray's direction, the 2012 survey of a little known fossil area, designated Bow Willow beds, in the Carrizo Badlands (Figure 1), produced several Rancholabrean Land Mammal Age taxa previously unrecorded in the Park's seventy years of fossil collection activities (Murray et al. 2014). Prior to these finds, the youngest fossil-bearing beds in the Park were estimated to be about 500 ka. Of greatest interest from these new sites are late Pleistocene occurrences of mammoths, at least one of which shows impact evidence implying human bone processing, dated 18 to 25 ka. (Keeley et al. 2019).

Though officially retired from the State Park system, Jefferson continues to play a major role as the Paleontology Program's chief advisor, working with Murray and the volunteers on a variety of key projects. Collaborating with Dr. Robert M. Chandler, bird paleontologist at Georgia College, Milledgeville, Georgia, Jefferson assisted with the reclassification of one of the Park's key fossil specimens—the anterior-most part of a very large premaxilla (beak). Originally referred to *Teratornis incredibilis* (Howard 1972a, 1972b) and subsequently included among referred material supporting establishment of the new genus *Aiolornis* (Campbell et al. 1999), the specimen was re-examined using CT scanning technology, and reclassified as *Titanis sp.*, a phorusrhacid, commonly known as the fossil Terror Bird (Figure 13) (Chandler et al. 2013). This work emphasizes the potential wide-scale impact of re-identification of a single fossil specimen.

In addition to the ongoing tasks of reviewing and updating ABDSP's fossil collections, and planning, organizing, and overseeing fossil surveys in key areas of the Park, Murray and the Paleontology Volunteers have made significant revisions to the curation database and cataloging system. Taxonomic experts have reviewed and identified entire class categories of specimens, including

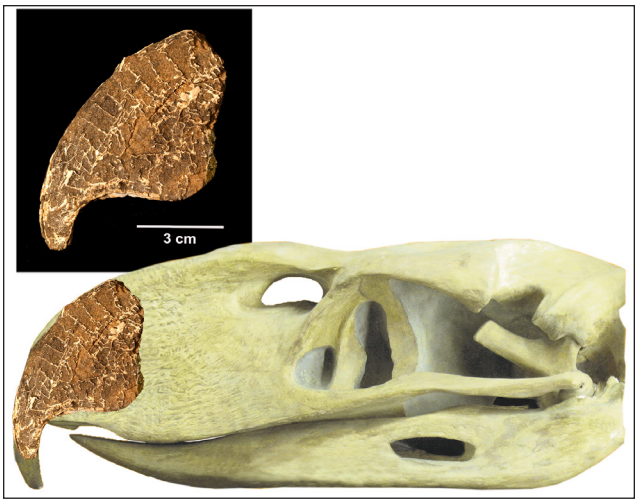

Figure 13. Top to bottom: Anterior-most part of a very large premaxilla beak of *Titanis sp.* (Photograph by Barbara Marrs). Bottom illustration of reclassified *Titanis sp.* (Courtesy of Robert M. Chandler).

Table 2. Systematic list of Fossil Invertebrates from Anza-Borrego Desert State Park® and the Salton Trough Region, San Diego, Imperial, & Riverside Counties.

Explanation: ★ = type specimens from the Salton Trough Region; † = extinct taxon; sp. = single indeterminate species in addition to named species present; spp. = two or more indeterminate species in addition to named species present; ** = missing taxonomic information, errors or spelling problems. Taxonomic names have been revised to conform to current usage. Higher taxonomic categories are included where known, and common names are provided where known. Subgenera are not listed. Authors and dates for species are included when known. Note that new names (nov.) of Stump (1972) and Powell (1986, 1988) remain informal. 'A' indicates specimens reported from ABDSP

Microfossils that comprise the Cretaceous age assemblage were eroded from the Colorado Plateau and redeposited within the Salton Trough during Plio-Pleistocene time.

Paleozoic Molluscs
(? Mississippian)

Phylum Mollusca (marine clams and snails)

Order indeterminate
- Family indeterminate
  - Genus and species indeterminate

Cretaceous Microfossils
(Plio-Pleistocene)

Subkingdom Protozoa
Phylum Sarcomastigophora
Subphylum Sarcodina (foraminifers)
Class Granuloreticulosea

Order Foraminifera
- Family Globotruncanidae
  - *Globotruncana globigerinoides* †
- Family Planomalinidae
  - *Globigerinelloides aspera* †
- Family Heterohelicidae
  - *Heterohelix globulosa* †
  - *Heterohelix reussi* †
  - *Heterohelix striata* †
- Family Turrilinidae
  - *Neobulimina canadensis* †
- Family Uvigerinidae
  - *Pseudouvigerina cretacea* †

Fish Creek Gypsum Assemblage
(Late Miocene)

Division Haptophyta
Class Prymnesiophyceae (Coccolithophyceae - calcareous nannoplankton)

Order Isochrysidales
- Family Gephrocapsaceae
  - *Dictyococcittes scrippsae* (?)
  - *Dictyococcittes minutes*
  - *Reticulofenestra pseudoumbilica*
  - *Crenalithus doronicoides* (?)

Order Discoasterales
- Family Sphenolithaceae
  - *Spenolithus abies*
  - *Spenolithus moriformis*
- Family Braarudosphaeracea
  - *Braarudosphaera bigelowii*

Order Eiffellithales
- Family Helicosphaeracea

Imperial Group Western Salton Troug
Coyote Mountains, and Vallecito/Fish Creek Basin
(late Miocene)

Subkingdom Protozoa
Phylum Sarcomastigophora
Subphylum Sarcodina (foraminifers)
Class Granuloreticulosa

Order Foraminifera
- Family Amphisteginidae
  - *Amphistegina gibbosa*
  - *Amphistegina lessoni*
- Family Miliolidae
  - *Quinqueloculina* sp.
- Family Buliminidae
  - *Bolivina interjuncta*
  - *Bolivina subaenariensis mexicana*
  - *Bolivina vaughani*
  - *Reussella pacifica*
  - *Uvigerina peregrina*
  - *Trifarina bella*
  - *Trifarina angulosa*
- Family Cassidulinidae
  - *Cassidulina delicata*
  - *Cassidulina laevigata*
  - *Cassidulina subglobssa*
  - *Cassidulina tortuosa*
- Family Anomalinidae
  - *Cibicides fletcheri*
  - *Hanzawaia nitidula*
  - *Hanzawaia basiloba*
  - *Planulina ornata*
- Family Discorbidae
  - *Epistominella subperuviana*
- Family Globigerinidae
  - *"Globigerina pachyderma"*
  - *Globigerina quinqueloba*
  - *Globigerinita uvula*
  - *Sphaeroidinella subdhiscens*
- Family Nonionidae
  - *Elphidium gunteri*
  - *Elphidium* sp.
  - *Nonion basispinata*
  - *Nonion miocenica stella*
  - *Nonion glabratalia californica*
- Family Planorbulinidae
  - *Planorbulina acervalis*
- Family Rotaliidae
  - *Ammonia beccarii*
  - *Ammonia* sp. cf. *A. parkinsonia*

continues

Phylum Cnidaria
Class Anthozoa
Subclass Zoantharia (corals)

Order Scleractinia
- Family Faviidae (star corals)
  - *Manicina* sp. (Ehrenberg, 1834)
  - *Plesiastrea californica* (Vaughan, 1917) †
  - *Solenastrea fairbanksi* (Vaughan, 1900) ★ †A
- Family Meandrinidae (starlet, brain, and flower corals)
  - *Meandrina bowersi* (Vaughan, 1917) ★ †A
  - *Dichocoenia merriami* (Vaughan, 1900) ★ †A
  - *Dichocoenia eminens* (Weisbord, 1974) A†
  - *Eusmilia carrizensis* (Vaughan, 1917)★ †A
- Family Poritidae (finger corals)
  - *Porites carrizensis* (Vaughan, 1917)★ †A
- Family Pocilloporidae
  - *Madracis* sp. (Milne Edwards & Haime, 1849) A
- Family Rhizangiidae (= Astrangiidae) (cup corals)
  - *Astrangia haimei* (Verrill, 1866) † A
- Family Siderastreidae (starlet corals)
  - *Siderastrea mendenhalli* (Vaughan, 1917)★ †A

Phylum Mollusca
Class Gastropoda (marine snails)

Order Cephalaspidea
- Family Bullidae (bubble snails)
  - *Bulla gouldiana* (Pilsbry, 1895) A
  - *Bulla punctulata* (A. Adams in Sowerby, 1850)
  - *Bulla striata* (Bruguière, 1792) A

Order Cycloneritida
- Family Neritidae (nerites)
  - *Nerita scabricosta* (Lamarck, 1822) A
  - *Nerita funiculata* (Menke, 1851) A
  - *Theodoxus luteofasciatus* (Miller, 1879)

Order Lepetellida
- Family Fissurellidae (keyhole limpets)
  - *Diodora alta* (C.B. Adams, 1852) A
  - *Diodora cayenesis* (Lamarck, 1822)
  - *Fissurella* sp. (Bruguiere, 1789)
  - *Hemitoma emarginata* (Blainville, 1825)
  - *Rimula cancellata* (Schremp, 1981)★ †
- Family Haliotidae (abalones)
  - *Haliotis pourtalesii* (Dall, 1881)

Order Littorinimorpha
- Family Bursidae (frog snails)
  - *Bursa calcipicta* (Dall, 1908) A
- Family Calyptraeidae (cup and saucer snails)
  - *Calyptraea* sp. (Lamarck, 1799) A
  - *Crepidula onyx* (Sowerby, 1824)
  - *Crepidula scutellatum* (Wood, 1828) A
  - *Crepidula spinosum* (Sowerby, 1824)
- Family Cassidae (helmet snails)
  - *Cassis subtuberosus* (Hanna, 1926)★ †A
  - *Semicassis centiquadrata* (Valenciennes, 1832) A
- Family Cypraeidae (cowries)
  - Cypraea *henekeni amandosi* A
  - *Macrocypraea* sp. (Schilder, 1930) A
  - *Macrocypraea cervinetta* (Kiener, 1843) A
  - *Muracypraea* sp. (Woodring, 195)7 A
  - *Zonaria* sp. (Jousseaume, 1884)
- Family Epitoniidae (wentletraps)
  - *Epitonium efferum* (Bramkamp *in* Durham, 1937)
- Family Ficidae (fig snails)
  - *Ficus* sp. (Röding, 1798) A
- Family Hipponicidae (horse-hoof limpets)
  - *Cheilea cepacea* (Broderip, 1834)
  - *Hipponix panamensis* (C.B. Adams, 1852) A
- Family Naticidae (moon snails)
  - *Natica chemnitzii* (Pfeiffer, 1840) A
  - *Natica unifasciata* (Lamarck, 1822)
  - *Polinices bifasciatus* (Griffith and Pidgeon, 1834)A
  - *Polinices uber* (Valenciennes, 1832) A
  - *Sinum debile* (Gould, 1853) A
- Family Personidae (distorsio snails)
  - *Distorsio constricta* (Broderip, 1833) A
- Family Strombidae (conchs)
  - *Strombus galeatus* (Swainson, 1823) A
  - *Strombus granulatus* (Swainson, 1822)
  - *Strombus gracilior* (Sowerby, 1825) A
  - *Strombus obliteratus* (Hanna, 1926) † A
- Family Tonnidae (tuns)
  - *Malea ringens* (Swainson, 1822) A
  - *Ficus ventricosa* (Sowerby, 1825) A
- Family Triviidae (trivids)
  - *Trivia sanguinea* (Sowerby, 1832) A
- Family Vermetidae (worm snails)
  - *Thylaeodus* sp. (Mörch, 1860) A
- Family Xenophoridae (carrier shells)
  - *Xenophora* sp. (Fischer von Waldheim, 1807) A

Order Neogastropoda
- Family Cancellariidae (nutmeg snails)
  - *Cancellaria cassidiformis* (Sowerby, 1832) A
  - *Cancellaria coronadoensis* (Durham, 1950) † A
  - *Cancellaria gemmulata* (Sowerby, 1832) A
  - *Cancellaria obesa* (Sowerby, 1832) A
  - *Cancellaria urceolata* (Hinds, 1843)
- Family Colubrariidae (dwarf tritons)
  - *Colubraria* sp. (Schumacher, 1817) A
- Family Columbellidae (dove shells)
  - *Anachis* sp. H. (Adams & A. Adams), 1853 A
  - *Mitrella* sp. (Risso, 1826) A
  - *Strombina solidula* (Reeve, 1859)
- Family Conidae (cone snails)
  - *Conus arcuatus* (Broderip and Sowerby), 1829 A
  - *Conus bramkampi* (Hanna and Strong), 1949★† A
  - *Conus californicus* (Reeve, 1844) A
  - *Conus durhami* (Hanna and Strong, 1949)★ †
  - *Conus gladiator* (Broderip, 1833) A
  - *Conus gradatus* (W. Wood, 1828) A
  - *Conus fergusoni* (Sowerby, 1873) A
  - *Conus patricius* (Hinds, 1843)
  - *Conus planiliratus* (G. B. Sowerby I, 1850) †A
  - *Conus regularis* (Sowerby, 1833) A
  - *Conus ximenes* (Gray, 1839)
- Family Drilliidae (sea snail)
  - *Clavus* sp. (Montfort, 1810) A
- Family Fasciolariidae (tulip snails and horse conchs)
  - *Fusinus dupetitthouarsii* (Kiener, 1840) A
  - *Pleuroploca princeps* (Sowerby, 1825) A
  - *Latirus concentricus* (Reeve, 1847) A
  - *Leucozonia cerata* (Wood, 1828) A
- Family Liotiidae (liotias)
  - *Arene stephensoni* (Schremp, 1981) ★ †
- Family Melongenidae (crown conchs)
  - *Melongena patula* (Broderip and Sowerby, 1829) A
  - *Triplofusus princeps* (G. B. Sowerby,1825) [F*asciolaria*] A
- Family Mitridae (miter snails)
  - *Mitra crenata* (Broderip, 1836)
  - *Subcancilla longa* (Gabb, 1873) † A
  - *Subcancilla sulcata* (Swainson *in* Sowerby,1825) A
- Family Muricidae (murex snails)
  - *Dermomurex cunninghamae* (Berry, 1964)[*Aspella*]A
  - *Ceratostoma sp.* (Herrmannsen, 1846) A
  - *Cymia* sp. (Mörch, 1860) A
  - *Eupleura muriciformis* (Broderip, 1833) A
  - *Hexaplex sp.* (Perry, 1810) A
  - *Hexaplex brassica* (Lamarck, 1822) A
  - *Murex* sp. (Linnaeus, 1758) A
  - *Thais* sp. (Röding, 1798) A
- Family Nassariidae (basket shells)
  - *Nassarius* sp. (Duméril, 1805) A
  - *Antillophos sp.* (Woodring, 1928) A
  - *Northia* sp. (Gray, 1847) A

Table 2-2

continues

Family Olividae (olive snails)
Agaronia sp. (Gray, 1839) A
Agaronia testacea (Lamarck, 1811) A
Oliva incrasatta [Lightfoot, 1786] A
Oliva porphyria (Linnaeus, 1758) A
Oliva spicata (Röding, 1798) A
Olivella gracilis (Broderip and Sowerby, 1829) A
Family Pisaniidae (false tritons)
Piso sp. Gray, 1833 [Calicantharus] A
Cantharus sp. (Röding, 1798) A
Gemophos ringens (Reeve, 1846) A
Solenosteira anomala (Reeve, 1847) A
Family Pseudolividae (false olives)
Macron sp. (H. Adams & A. Adams, 1853) A
Triumphis distorta (Wood, 1828) A
Nicema subrostrata (W. Wood, 1828) [*Triumphis*] A
Family Terebridae (auger snails)
Terebra dislocata (Say, 1822)
Terebra elata (Hinds, 1844)
Terebra gauspata A
Terebra robusta (Hinds, 1844) A
Family Trochidae (top snails)
Calliostoma bonita (Strong, Hanna, and Hertlein, 1933)
Calliostoma olssoni (Schremp, 1981)★ †
Tegula mariana (Dall, 1919)
Family Turbinellidae (vase snails)
Vasum pufferi (Emerson, 1964)★ † A
Family Turridae (turrid snails)
Knefastia olivacea (Sowerby, 1833)
Polystira oxytropis (Sowerby, 1834) A
Order Patellogastropoda
Family Patellidae (limpets)
"Patella" sp. **(**Linnaeus, 1758) †A
Order Trochida
Family Turbinidae (turban snails)
Mirachelus imperialis (Schremp, 1981) ★ †
Turbo magnificus (Jonas, 1844) A
Turbo mounti (Schremp, 1981)★ †
Homalopoma maiquetiana (Weisbord, 1962) †
Order [unassigned] Caenogastropoda
Family Cerithiidae (ceriths) A
*Cerithium incisum (*Sowerby, 1855) A
Liocerithium judithae (Keen, 1971)
Family Littorinidae (periwinkles)
Littorina varia (Sowerby, 1832)
Family Modulidae (button snails)
Modulus catenulatus (Philippi, 1849) A
Family Potamididae (horn snails)
Cerithidea mazatlanica (Carpenter, 1857)
Family Turritellidae (tower snails)
Turritella gonostoma (Valenciennes, 1832)
Turritella imperialis (Hanna, 1926)★ † A
Vermicularia pellucida (Broderip and Sowerby, 1829)
Order undesignated [Superfamily Architectonicoidea]
Family Architectonicidae (sundials)
Architectonica nobilis discus (Grant & Gale, 1931)† A
Order undesignated [Superfamily Ellobiidae]
Family Ellobiidae (marsh snails)
Melampus sp. (Montfort, 1810)

Class Scaphopoda (tusk shells)

Order Dentaliida (tusks)
Family Dentaliidae
Dentalium sp. **(**Linnaeus, 1758) A

Class Bivalvia (marine clams)

Order Arcida
Family Arcidae (ark clams)
Arca mutabilis (Sowerby, 1833)
Arca pacifica (Sowerby, 1833) A
Anadara carrizoensis (Reinhart, 1943)★ † A
Anadara adamsi (Olsson, 1961) A
Anadara concinna (Sowerby, 1833)
Anadara formosa (Sowerby, 1833) A
Anadara multicostata (Sowerby, 1833) A
Anadara reinharti (Lowe, 1935)
Barbatia reeveana (Orbigny, 1846) A
Barbatia gradata (Broderip & G. B. Sowerby I, 1829) A
Family Glycymerididae (bittersweet clams)
Glycymeris bicolor (Reeve, 1843)
Glycymeris delessertii (Reeve, 1843) A
Glycymeris gigantea (Reeve, 1843) A
Glycymeris maculata (Broderip, 1832)
Glycymeris multicostata (Sowerby, 1833) A
Family Limopsidae (deep sea bivalve)
Limopsis compressa (Nevill & Nevill, 1874) A
Order Cardiida
Family Cardiidae (cockles or heart clams)
Acrosterigma pristipleura (Dall, 1901) [*Trachycardium*]A
Americardia biangulata (Broderip & G. B. Sowerby I, 1829) A
Dinocardium sp. (Dall, 1900) A
Laevicardium sp. (Swainson, 1840) A
Lophocardium gurabicum (Maury, 1917)
Papyridea sp. (Swainson, 1840) A
Trachycardium consors (G. B. Sowerby I, 1833) A
Trigoniocardia sp. aff. *T. guanacastensis* (Hertlein and Strong, 1947)
Family Solecurtidae (tagelus clams)
Solecurus gatunensis (Toula, 1909)
Tagelus affinis (C. B. Adams, 1852) A
Tagelus californianus (Conrad, 1837)
Tagelus violascens (Carpenter, 1857)
Family Semelidae (semele clams)
Semele bicolor (C.B. Adams, 1852)
Semele rosea (G. B. Sowerby I, 1833) A
Semele sayi (Toula, 1909)
Family Tellinidae (tellens)
Eurytellina simulans (C. B. Adams, 1852) [*Tellina*] A
Florimetis dombei (Hanley, 1844)
Leporimetis cognata (Pilsbry & Vanatta, 1902) [*Psammotreta*] *A*
Macoma elytrum (Keen, 1958) A
Macoploma pura (Gould, 1853) [*Psammotreta viridotincta*] A
Macoploma siliqua (C.B. Aams, 1852)
Psammotreta dombei (Hanley, 1844) A
Psammotreta grandis (Hanley, 1844) [*Macoma*] *A*
Rexithaerus secta (Conrad, 1837) [*Macoma*] *A*
Tellina cumingii (Hanley, 1844) A
Tellina ochracea (Carpenter, 1864) A
Tellina pristiphora (Dall, 1900)
Tellina ulloana (Hertlein, 1968)
Order Carditida
Family Carditidae (carditas)
Cardites crassicostata (Sowerby, 1825) A
Cardites laticostatus (G. B. Sowerby I, 1833) A
Cardites megastropha (Gray, 1825) A
Cardites frederikseni (Stump, 1972 unpub.) A
Carditamera laticostata (Sowerby, 1833) A
*Carditamera affinis (*Sowerby, 1833) A
Family Crassatellidae (crassatellas)
Crassinella mexicana (Pilsbry and Lowe, 1932)A
Eucrassatella digueti (Lamy, 1917)
Eucrassatella subgibbosa (Hanna, 1926) ★ † A
Kalolophus antillarum (Reeve, 1842) [*Eucrassatella*] A
Order Limoidea
Family Limidae (file shells)
Ctenoides floridana (Olsson and Harbison, 1953)
Limaria sp. (Link, 1807) †
Lima sp. (Bruguière, 1797) † A
Order Lucinida
Family Lucinidae (lucine clams)
Calucina quincula (Olsson, 1961 ?)

Table 2-3

continues

Codakia distinguenda (Tryon, 1872) A
Divalinga eburnea (Reeve, 1850) A
Lucinisca fenestrata (Hinds, 1845) *A*
Miltha xantusi (Dall, 1905) A
Pegophysema edentuloides (Verrill, 1870) A
Parvilucina mazatlanica (Carpenter, 1857)
Pleurolucina undata [*Lucina undatoides*] (Carpenter, 1865**)** A
Pleurolucina leucocymoides (H. N. Lowe, 1935) A
Ctena sp. (Mörch, 1861) A

Order Myida
Family Myidae (softshell clams)
Crpytomya sp. (Conrad, 1849)
Family Corbulidae (corbulas)
Corbula allisoni (Stump 1972 unpub). A
Corbula mexicana (Perrilliat, 1984) †
Family Haitellidae (geoducks)
Panopea abrupta (Conrad, 1849)
Panopea generosa (A. A. Gould, 1850) A
Panopea globosa (Dall, 1898) A
Family Pholadidae (rock piddocks)
Cyrtopleura costata (Linnaeus, 1758) A

Order Mytilida
Family Mytilidae (mussels)
Lithophaga sp. aff. *L. plumula* (Hanley, 1844) A
Mytilus (Linnaeus, 1758) A★ †

Order Nuculida
Family Nuculidae (nut clams)
Nucula sp. (Lamark, 1799) A
Family Nuculanidae
Nuculana acuta (Conrad, 1831) A
Nuculana santarosaensis (Perrilliat, 1976) †

Order Ostreida
Family Ostreidae (true oysters)
Crassostrea columbiensis (Hanley, 1846)
Crassostrea. corteziensis (Hertlein, 1951) [*Ostrea corteziensis*] A
"Dendostrea" angermani (Hertlein and Jordan, 1927)
Dendostrea vespertina (Conrad, 1854) ★† A
Hyotissa fisheri (Dall, 1914) [*Ostrea fischeri*] *A*
Saccostrea palmula(Carpenter, 1857)[*Ostrea palmula*]A
Striostrea prismatica (Gray, 1825) [*Crassostrea iradescens*] A
Ostrea angelica (Rochebrune, 1895) [*Myrakeena angelica*] A
Ostrea megodon (Hanley, 1846*)* [*Undulostrea megadon*] *A*
Family Isognomonidae (Tree oysters)
Isognomon alatus (Gmelin, 1791) A
Isognomon janus (Carpenter, 1857) A
Family Gryphaeidae (oysters)
Pycnodonte heermanni (Conrad, 1855) ★ † A
Family Pinnidae (penshells)
Atrina stephensi (Hanna, 1926) A
Pinna latrania (Hanna, 1926)★ † A
Pinna mendenhalli (Hanna, 1926)★ † A

Order Pectinida
Family Anomiidae (jingles)
Anomia subcostata (Conrad, 1855)★ † A
Placunanomia hannibali (Jordan and Hertlein, 1926) †
Family Pectinidae (scallops)
Aequipecten antonitaensis (Durham, 1950) A
Aequipecten corteziana [*Lindapecten*] *A*
Antipecten? praevalidys (Jordan and Hertlein, 1926)
*Argopecten circularus (*Sowerby, 1835*) A*
*Argopecten abeitis (*Jordan & Hertlein, 1926) [*abeitis abeitis*] A
Argopecten deserti (Conrad, 1855) ★ † A
Argopecten circularis bramkampi (Durham, 1950) ★† A
Argopecten revellei (Durham, 1950) A
Argopecten mendenhalli (Arnold, 1906) † A
Argopecten sverdrupi (Durham, 1950) † A
Argopecten ventricosus (Sowerby, 1842) A
Chlamys corteziana (Durham, 1950) † A
Chlamys lowei (Hertlein, 1935)
Chlamys mediacostata (Hanna, 1926) ★ † A
Cyclopecten pernomus (Hertlein, 1935)
Euvola keepi (Arnold, 1906) † A
Flabellipecten carrizoensis (Arnold, 1906) ★ † A
Pecten (O. F. Müller, 1776) [*Flabellipecten*]
Leptopecten palmeri (Dall, 1897)
Leptopecten velero (Hertlein, 1935)
Lyropecten tiburonensis (Smith, 1991) † A
Lyropecten subnodosus (G. B. Sowerby I, 1835) A
Family Plicatulidae (kittenpaws)
Plicatula inezana (Durham, 1950)
Plicatula *penicillata* (Carpenter, 1857)
Family Spondylidae (thorny oysters)
Spondylus bostrychites (Guppy, 1867) † A
Spondylus calcifer (Carpenter, 1857)
Spondylus princeps (Broderip, 1833) A
Spondylus barkeri (Stump, 1972 unpub.) A

Order Venerida
Family Chamidae (jewelbox clams)
Arcinella arcinella (Linnaeus, 1767)
Arcinella californica (Dall, 1903) A
Chama frondosa (Broderip, 1835) A
Chama pellucida (Broderip, 1835) A
Pseudochama (Odhner, 1917) A
Family Cyrenidae (marshclams)
Corbicula fluminea (O. F. Müller, 1774) A
Polymesoda notabilis (Deshayes, 1855) A
Family Donacidae (bean or wedge clams)
Donax sp. cf. *D. gracilis* (Hanley, 1845)
Family Veneridae (Venus clams)
Callpita frizzelli (Hertlein & A. M. Strong, 1948) A
Chione hannai (Parker, 1949)
Chione subrugosa (Wood, 1828) A
Chione mariae (d'orbigny, 1846) A
Chione californiensis (W. J. Broderip, 1835) A
Cyclinella cyclica (Guppy, 187x)
Dosinia dunkeri (Philippi, 1844) A
Dosinia ponderosa (Gray, 1838) A
Dosinia semiobliterata (Deshayes, 1853) A
Globivenus isocardia (Verrill, 1870) A
Gouldia californica (Dall, 1917)
Humilaria (Grant & Gale, 1931)
Irus ellipticus (Sowerby, 1834) A
Leukoma grata (Say, 1831) [*Protothaca*] A
Megapitaria squalida (G. B. Sowerby I, 1835) A
Periglypta multicostata (Sowerby, 1835) A
Pitar catharius (Dall, 1902) A
Pitar pollicaris (P. P. Carpenter, 1864) A
Pitar mexicanus (Hertlein & A. M. Strong, 1948) A

SuperOrder Anomalodesmata
Family Pandoridae (pandoras)
Pandora sp. (Rafinesque, 1815) A
Family Thraciidae (thracias)
Cyathodonta undulate (Conrad, 1849) A

Phylum Echinodermata
Class Asteroidea (sea stars)

Order Paxillosida
Family Astropectinidae (sand stars) A
Astropecten armatus (Gray, 1840)

Class Ophiuroidea
Family,Genus and species indeterminate (brittle stars) A

Class Echinoidea (sea urchins and sand dollars)

Order Cidaroida
Family Cidaridae (club-spined urchins)
Cidaris sp. **(**Leske, 1778)
Eucidaris thouarsii (Valenciennes, 1846) A

Table 2-4

continues

Order Diadematoida
- Family Diadematidae (sea urchins)
  - *Centrostephanus* sp. (Peters, 1855)

Order Arbacioida
- Family Arbaciidae (regular sea urchins)
  - *Arbacia stellata* (Blainville, 1825; ?Gmelin, 1791) [*Arbacia incisa*] A

Order Camarodonta (sea urchins)
- Family Toxopneustidae (white urchins)
  - *Lytechinus pictus* (Verrill, 1867) [*Lytechinus* sp. cf. *L. anamesus*] A
  - *Tripneustes californicus* (Kew, 1914) † A
  - *Toxopneustes roseus* (Agassiz, 1863)
- Family Strongylocentrotidae (sea urchins)
  - *Strongylocentrotus purpuratus* (Stimpson, 1857)

Order Clypeasteroida
- Family Clypeasteridae (Sea biscuits)
  - *Clypeaster bowseri* (Weaver, 1908) ★ † A
  - *Clypeaster carrizoensis* (Kew, 1914)★ †
  - *Clypeaster deserti* (Kew, 1915) ★ † A
- Family Echinarachniidae (sand dollar)
  - *Vaquerosella* sp. (Durham, 1955) †
- Family Echinoneidae (regular heart urchins)
  - *Echinoneus burgeri* (Grant and Hertlein, 1938) †
- Family Mellitidae (Key-hole sand dollar)
  - *Encope arcensis* (Durham, 1950) †
  - *Encope sverdrupi* (Durham, 1950) † A
  - *Encope tenuis* (Kew, 1914) ★ † A

Order Spatangoida
- Family Brissidae (heart urchins)
  - *Brissus obesus* (Verrill, 1867)
  - *Metalia spatagus* (Linnaeus, 1758) A
  - *Meoma* (Gray, 1851) A
- Family Loveniidae (Porcupine heart urchins)
  - *Lovenia hemphilli* (Israelsky, 1923) †A
- Family Prenasteridae (puffball heart urchins)
  - *Agassizia* sp. (Valenciennes, 1846) A
  - *Agassizia scrobiculata* (Valenciennes, 1846) † A
- Family Schizasteridae
  - *Schizaster morlini* (Grant and Hertlein, 1956) † A
- Family Toxasteridae
  - *Macraster elegans* (Shumard, 1853) A

Phylum Bryozoa
Class Gymnolaemata (bryozoans)

Order Cheilostomata
- Family Membraniporidae
  - *Conopeum commensale* (Kirkpatrick and Metzelaar, 1922) A

Phylum Brachiopoda
Class Inarticulata

Order Artremata
- Family Lingulidae
  - *Glottidia?*sp.

Phylum Arthropoda
Subphylum Crustacea
Class Maxillopoda

Order Sessilia
- Family Balanidae (barnacles)
  - *Arossia* sp. (Newman, 1982) A
  - *Balanus Trigonus* (Darwin, 1854) A
  - *Megabalanus* sp. (Hoeck, 1913) A
  - *Megabalanus californicus* (Pilsbry, 1916) A
  - *Megabalanus tintinnabulum* (Linnaeus, 1758)

Class Malacostraca

Order Decapoda
- Family Goneplacidae
  - *Speocarcinus berglundi* (Tucker, Feldman, and Powell, 1994) (crab)
- Family Paguridae A

Class Ostracoda (marine water fleas)

Order Podocopida
- Family Trachyleberididae
  - *Puriana* sp.
  - *Hermanites* sp.
- Family Loxoconchidae
  - *Loxocorniculum* sp.
  - *Loxoconcha* sp.
- Family Xestoleberideidae
  - *Xestoleberis* sp.
- Family Cytheruridae
  - *Cytheura* sp.
  - *Anterocythere* sp.
- Family Hemicytheridae
  - *?Aurila* sp
  - *?Ambostracon* sp.
  - *Caudites* sp.
- Family Cytheridae
  - *Perissocytheridea* sp.
- Family Microcytheridae
  - *Microcytherua* sp.

Typanites Marine Ichnofauna (borings and tracks)
(late Miocene)

- *Entobia* (clionid sponge boring)
- cf. *Gastrochaenolites torpedo* (clam boring)
- *Maeandro polydora* (polychaete worm boring)
- *Typanites* (polychaete worm or barnacle boring)
- Echinoid (boring)

Fresh Water Lacustrine & Terrestrial Assemblages
(Plio-Pleistocene)

Phylum Mollusca
Class Bivalvia (fresh water clams)

Order Unionida
- Family Unionidae (freshwater mussels)
  - *Anodonta californiensis* (Lea, 1852) *A*

Order Sphaerida
- Family Sphaeriidae (pea clams)
  - *Pisidium compressum* (Prime, 1852) A

Order Venerida
- Family Mactridae (rangia clams)
  - *Raeta undulata* (Gould, 1851) A
  - *Rangia lecontei* (Conrad, 1853) ★ † A
  - *Simomactra dolabriformis* (Conrad, 1867) [*Spisula*] *A*

Class Gastropoda (fresh water & land snails)

Order Littinmorphamalea
- Family Hydrobiidae (various freshwater snails)
  - *Hydrobia* sp. (W. Hartmann, 1821) A
  - *Pyrgulopsis longinqua* (Gould, 1855) A
- Family Amnicolidae
  - *Amnicola* sp. (Gould & Haldeman, 1840)
  - *Tryonia* sp. (Stimpson, 1865) A
  - *Tryonia porrecta* (Mighels, 1845) [Amnicola protea] A
- Family Lithoglyphidae
  - *Fluminicola* sp. (Carpenter, 1864) A

Order Hygrophila
- Family Physidae (physa snails)
  - *Physa humerosa* (Gould, 1855) A
  - *Physa virgata* (Gould, 1855) A
- Family Lymnaeidae (lymnaea snails)
  - *Fossaria techella* (Haldeman, 1867)
- Family Planorbidae (rams-horn snails)
  - *Gyraulus parvus* (Say, 1817) A
  - *Planorbella tenuis* (Dunker, 1850) A

Order Stylommatophora
- Family Zonitidae (zonite land snails)
  - *Zonitoides arboreus* (Say, 1816)
- Family Agriomacidae(slugs)
  - *Deroceras* sp. (Rafinesque, 1820) A

Table 2-5

continues

Phylum Arthropoda
Subphylum Crustacea
Class Ostracoda

Order Podocopia (fresh water fleas)
- Family Candonidae
  - *Candona patzcuaro* var. *C. p. mexico*
  - *Candona sigmoides*
  - ? *Lineocypris* sp.
- Family Limnocytheridae
  - *Elkocythereis bramlettei*
  - *Limnocythere bradburyi*
  - *Limnocythere camera*
  - *Limnocythere herricki*
  - *Limnocythere inopinata*
  - *Limnocythere itasca*
  - *Limnocythere pseudoreticulata*
  - *Limnocythere staplini*
  - *Limnocythere verrucosa*
- Family Ilyocyprididae
  - *Ilyocypris* sp.

Order Decapoda
- Suborder Pleocyemata
  - Family, genus, and species indeterminate (crayfish)

Class Insecta (insects)

Order Coleoptera
- Family Bostrichidae
  - cf. *Lyctus* sp. (powder-post beetle)

Cnidaria (Andres Lopez-Perez), Mollusca (N. Scott Rugh and Astrid Montiel-Boehringer), Pisces (Mark A. Roeder), Testudines (Howard H. Hutchison), and Aves (Daniel A. Guthrie). The database now provides access to information about individual specimens, each specimen's specific locality, and stratigraphic data and listings of any other fossil specimens found in that same locality.

In 1998, Jefferson, McDaniel, and Murray began planning a reorganization of the entire paleontology collection strictly by stratigraphy, thus eliminating the collection's arbitrary divisions by taxon, prior institution collection, and geographic collecting area. Planning and execution of the reorganization was carried out between 2013 and 2018 by Paleontology Volunteers, led by Linda Gilbert, Judy Smith, and Marsha Boring.

In conjunction with the recent revisions to the Park's curation database and cataloging system, Jefferson spearheaded a massive project to standardize the Colorado Desert's geologic formation names via the scientifically accurate revision of both individual formations and groups of formations from ABDSP to the Salton Trough. The current 2020 stratigraphic report, edited and compiled by Jefferson, "provides genetic and descriptive information, photographs, map distributions, and typical localities for early Miocene through Holocene named…sedimentary formations within the region" (Jefferson and Gallagher 2020:4). This major document provides a *Stratigraphy Master Index* that is divided into sequential time periods based on the tectonic and sedimentary events that affected the region's depositional environments and thus the sedimentary formations that followed (Jefferson and Gallagher 2020). The document correlates with the CDD fossil collections organized by these same stratigraphic units. A related project is the digitizing of all the geologic maps of ABDSP, headed by Park Volunteer Environmental Services Intern, Ron Shugan. The new digital copies of the maps have their unit names aligned with the stratigraphic units presented in the report. These digital map overlays enable improved field survey planning and management.

The most recent additions of new technology, led by ABDSP Paleontology Volunteers Jon Gilbert and Gabriel Vogeli, are the use of 3D photogrammetry, laser scanning, 3D printing, and UAS (drone) cameras. These tools provide new ways to monitor fossil tracks and trackways, document site stratigraphy, and reproduce collected specimens.

At present, Anza-Borrego Desert State Park is still a location for important research by visiting geologists, paleontologists, and other earth scientists and professionals from around the globe, as well as by paleontology and geology graduate students from universities throughout the U.S. Scientific publications on the region's internationally famous vertebrate and invertebrate paleofaunas and outstanding geologic features continue to prove the marked significance of this desert, and its incredible scope of fossil resources. Regarding the future of the State Park's scientific status, Jefferson stated,

> …there's only one reason to do this whole business,…and that's because this [ABDSP] is an important place paleontologically…this is an actively researched area and currently under study, and even with all of the work that Miller and Downs and LACM and IVCM have done, there are still big questions that this place can answer in terms of paleontologic history and the last couple of million years. No question about it (Jefferson pers. comm. 2001).

References Cited

A comprehensive bibliography of Salton Trough Paleontology and Geology is maintained at SRC: contact lyndon.murray@parks.ca.gov for queries.

Abbreviations

CSUDSC – California State University Desert Studies Consortium

NHMLAC – Natural History Museum of Los Angeles County

LACM – Los Angeles County Museum of Natural History

Becker, J.J., and J.A. White 1981. Late Cenozoic geomyids (Mammalia: Rodentia) From the Anza-Borrego Desert, southern California. Journal of Vertebrate Paleontology 1:211-218.

Blake, W.P. 1853. (untitled personal diary). Unpublished Manuscript on File, Arizona Historical Society, Southern Arizona Division 26, book 12.

Blake, W.P. 1858. Report of a Geological Reconnaissance in California. Bailliere, New York, 310 p.

Blake, W.P. 1914. The Cahuilla Basin and Desert of the Colorado; pp. 1-12 in The Salton Sea, A Study of the Geography, the Geology, the Floristics, and the Ecology of a Desert Basin, Carnegie Institution of Washington Publication 193.

Bowers, S. 1901. Reconnaissance of the Colorado Desert Mining District. California State Mining Bureau Special Publication 11:1-19.

Campbell, K.E., E. Scott Jr., and K.B. Springer 1999. A new genus for the incredible teratorn (Aves: Teratornithidae); pp. 169-175 in S. Olson (ed.) Avian Paleontology at the Close of the 20th Century, Smithsonian Contributions to Paleobiology 89.

Cassiliano, M.L. 1999. Biostratigraphy of Blancan and Irvingtonian mammals in the Fish Creek-Vallecito Creek section, southern California, and a review of the Blancan-Irvingtonian boundary. Journal of Vertebrate Paleontology 19:169-186.

Chandler, R.M., G.T. Jefferson, Lowell Lindsay, and S.P. Vescera 2013. The terror bird, *Titanis* (Phorusrhacidae) from the Pliocene Olla Formation, Anza-Borrego Desert State Park, southern California; pp. 171-183 in R.E. Reynolds (ed.) Raising Questions in the Central Mojave. CSUDSC.

Cunningham, G. D. 1984. The Plio-Pleistocene Dipodomyinae and geology of the Palm Spring Formation, Anza-Borrego Desert, California. M.S. thesis, Idaho State University, Pocatello, Idaho, 115 pp.

Dorsey, R. 2006. Stratigraphy, tectonics, and basin evolution in the Anza-Borrego Desert region; pp. 89-106 in G. T. Jefferson and L. Lindsay (eds.), Fossil Treasures of the Anza-Borrego Desert. Sunbelt Publications, Inc., San Diego, California, 394 pp.

Dorsey, R. J., A. Fluette, K. McDougall, B. A. Housen, S. U. Janecke, G. J. Axen, and C. R. Shirvell. 2007. Chronology of Miocene-Pliocene deposits at Split Mountain Gorge, Southern California: A record of regional tectonics and Colorado River evolution. Geology 35:57-60.

Dorsey, R.J., B.A. Housen, S.U. Janecke, C.M. Fanning, and A.L.F. Spears 2011. Stratigraphic record of basin development within the San Andreas fault system: Late Cenozoic Fish Creek-Vallecito basin, southern California. Geological Society of America Bulletin 123(5, 6):771-793.

Downs, T. 1954-1960. Unpublished field notes: copies on file at Colorado Desert District Stout Research Center; originals at NHMLAC, Vertebrate Paleontology Section (unpaginated).

Downs, T. 1957. Late Cenozoic vertebrates from the Imperial Valley region, California. Geological Society of America Bulletin 68(12, 2):1822-1823.

Downs, T., and G.J. Miller 1994. Late Cenozoic equids from Anza-Borrego Desert, California. NHMLAC Contributions in Science 440:1-90.

Downs, T., and J.A. White 1965. Pleistocene vertebrates of the Colorado Desert, California. International Association for Quaternary Research, VII International Congress, General Session Program p. 107.

Downs, T., and J.A. White 1968. A vertebrate faunal succession in superposed sediments from late Pliocene to middle Pleistocene in California. In Tertiary/Quaternary Boundary, International Geological Congress 23, Prague 10:41-47.

Downs, T., and G.D. Woodard 1961. Stratigraphic succession of the western Colorado Desert, San Diego and Imperial Counties, California. GSA Special Paper 68:73-74.

Fairbanks, H.W. 1893. Geology of San Diego County, also portions of Orange and San Bernardino Counties, California. Annual Report of the California State Mineral Bureau 11:88-90.

Font, F.P. 1775 (1930). Diary of an Expedition to Monterey by way of the Colorado River; pp. 1-533 in H.E. Bolton (translator, ed.) Anza's California Expeditions Volume IV, Font's Complete Diary of the Second Anza Expedition. University of California Press, Berkeley.

Frick, C. 1937. Horned ruminants of North America. Bulletin of the American Museum of Natural History 69:1-669.

Gensler, P.A. 2003. The late Irvingtonian (mid-Pleistocene) vertebrate fauna from Ash Wash, Coyote Badlands, Anza-Borrego Desert State Park, California. MS Thesis, Northern Arizona University, Flagstaff 104 p.

Grant, U.S., IV, and L.G. Hertlein 1956. *Schizaster morlini*, a new species of echinoid from the Pliocene Imperial County, California. Southern California Academy of Sciences Bulletin 55:107-110.

Hanna, G D. 1926. Paleontology of Coyote Mountains, Imperial County, California. Proceedings of the California Academy of Sciences, 4th Series 26:247-322.

Housen, B. A., R. J. Dorsey, S. U. Janecke, and G. J. Axen 2005. Rotation of Plio-Pleistocene sedimentary rocks in the Fish Creek Vallecito Basin, western Salton Trough, CA. Eos Transactions of the American Geophysical Union, 86(52), Fall Meeting Supplement, Abstract GP13A-0039.

Howard, H.H. 1963. Fossil birds from the Anza-Borrego Desert. LACM Contributions in Science 73:1-33.

Howard, H. 1972a. Type specimens of avian fossils in the collections of the Natural History Museum of Los Angeles County. NHMLAC Contributions in Science 228:1-27.

Howard, H. 1972b. The incredible teratorn again. Condor 74(3):341-344.

Hutchison, J.H. 1987. Moles of the *Scapanus latimanus* group (Talpidae, Insectivora) from the Pliocene and Pleistocene of California. NHMLAC Contributions in Science 386:1-15.

Jefferson, G.T., and L. Lindsay (eds.) 2006. The Fossil Treasures of the Anza-Borrego Desert, Sunbelt Publications, San Diego, California, 394 p.

Jefferson G.T., and N. Gallagher (eds.) 2020. Summary of late Neogene and Quaternary stratigraphy of the Salton Trough, Colorado Desert District of California State Parks; Version 6. Manuscript on File, Stout Research Center, Colorado Desert District, California State Parks, Borrego Springs, California, 25 February 2020, 132 p.

Johnson, N. M., C.B. Officer, N.D. Opdyke, G.D. Woodard, P.K. Zeitler, and E.H. Lindsay 1983. Rates of Cenozoic tectonism in the Vallecito-Fish Creek basin, western Imperial Valley, California. Geology 11:664-667.

Keeley, S., R. Keeley, K. Holen, G.T. Jefferson, and L.K. Murray 2019. The Sand Mammoth, Anza-Borrego Desert State Park, California: an interim report. In Exploring Ends of Eras in the Eastern Mojave Desert, edited by D.M. Miller, 2019 Desert Symposium and Field Guide Apriel 2019, p. 199-200.

Martin, R.A., and R.H. Prince 1989, A new species of early Pleistocene cotton rat from the Anza-Borrego Desert of

southern California. Bulletin of the Southern California Academy of Sciences 88:80-87.

McDaniel, G.E., Jr., and G.T.Jefferson 1997. A nearly complete skeleton of *Mammuthus meridionalis* from the Borrego Badlands, Anza-Borrego Desert State Park, California. In Memories, Minerals, Fossils, and Dust, Abstracts from Proceedings of the 1997 Desert Research Symposium, San Bernardino County Museum Association Quarterly 44(1):35-36.

McDaniel, G.E. and G.T. Jefferson 2003. *Mammuthus meridionalis* (Proboscidea: Elephantidae) from the Borrego Badlands of Anza-Borrego Desert State Park, California: phylogenetic and biochronologic implications. DEINSEA 9:239-252.

Mendenhall, W.C. 1910. Notes on the geology of Carrizo Mountain and vicinity, San Diego County, California. Journal of Geology 18:336-355.

Murray, L.K. 2008. Effects of taxonomic and locality inaccuracies on biostratigraphy and biochronology of the Hueso and Tapiado formations in the Vallecito Creek-Fish Creek section, Anza-Borrego Desert, California. PhD Dissertation, The University of Texas at Austin 531 p.

Murray, L.K., D.R. Ruez, Jr., and C.J. Bell 2011. New perspectives on lagomorph and rodent biochronology in the Anza-Borrego Desert of southern California, USA. Palaeontologia Electronica 14(3):1-14

Murray, L.K., G.T. Jefferson, S. Keeley, and R. Keeley 2014. The first record of Rancholabrean age fossils from the Anza-Borrego Desert; pp. 126-129 in R.E. Reynolds (ed.) Not a Drop Left to Drink, CSUDSC.

Norell, M.A. 1989. Late Cenozoic lizards of the Anza-Borrego Desert, California. NHMLAC Contributions in Science 414:1-31.

Olson, S.L. 1974. The Pleistocene rails of North America. Condor 76(2):169-175.

Opdyke, N.D., E.H. Lindsay, N.M. Johnson, and T. Downs 1977. The paleomagnetism and magnetic polarity stratigraphy of the mammal-bearing section of Anza Borrego State Park, California. Quaternary Research 7:316-329.

Orcutt, C.R. 1890. The Colorado Desert. California State Mining Bureau State Mineralogist's Report 10:899-919.

Remeika, P. 1998. Marine invertebrate paleontology and stratigraphy of the Vallecito-Fish Creek Basin; pp. 59-92 in L. Lindsay and W.G. Hample (eds.) Geology and Geothermal Resources of the Imperial and Mexicali Valleys, San Diego Association of Geologists.

Remeika, P., and A. Sturz (eds.) 1995. Paleontology and geology of the western Salton Trough Detachment, Anza-Borrego Desert State Park, California, Volume 1. San Diego Association of Geologists, 136 pp.

Vaughan, T.W. [summary by A.H. Brooks] 1904. A California Tertiary coral reef and its bearing on American Recent coral faunas. Science 19(482):503.

White, J.A. 1969. Late Cenozoic bats (Subfamily Nyctophylinae) from the Anza-Borrego Desert of California. University of Kansas Museum of Natural History, Miscellaneous Publications 51:275-282.

White, J.A. 1984. Late Cenozoic Leporidae (Mammalia, Lagomorpha) from the Anza-Borrego Desert, southern California. Special Publication of the Carnegie Museum of Natural History 9:41-57.

White, J.A., and T. Downs 1961. A new *Geomys* from the Vallecito Creek Pleistocene of California. Los Angeles County Museum of Natural History Contributions in Science 42:1-34.

White, J.A., and T. Downs 1965. Vertebrate microfossils from the Canebrake Formation of the Imperial Valley region. California. Society of Economic Mineralogists and Paleontologists, Pacific Section, Abstracts p. 33.

Winker, C. D., and S. M. Kidwell. 1996. Stratigraphy of a marine rift basin: Neogene of the western Salton trough, California; pp. 295-336 in P. L. Abbott and J. D. Cooper (eds.), Field Conference Guidebook and Volume for the American Association of Petroleum Geologists, Fullerton, California, Book 80.

Zakrzewski, R. J. 1993. Morphological change in woodrat (Rodentia: Cricetidae) molars; pp. 392-409 in R. A. Martin and A. D. Barnosky (eds.), Morphological Change in Quaternary Mammals of North America. Cambridge University Press, New York.

Microscopic life forms beneath transparent/ translucent minerals of the Mojave Desert

Stephen P. Mulqueen
P.O Box 911538, St. George, UT 84791-1538 mulques1@yahoo.com

ABSTRACT—A large variety of minerals occur in the desert regions of the western North America. Some of them possess unusual transparent or translucent physical properties that allow sunlight to pass through their crystalline masses. These light-penetrating minerals can act as "miniature greenhouses", allowing for the growth and survival of microalgae with other microorganisms within the biological soil crust (BSC) exposed on and immediately beneath the surface. In some scientific articles, the term biological soil crust is referenced with the term cryptogamic, cryptobiotic, microbiotic, and microphytic soil crusts or the term microbiotic crust (Belnap et al, 2001).

Microalgae, with other microorganisms, have also been observed in fractures within translucent rocks such as milky quartz, in the absence of a soil horizon. Numerous studies have been made by scientists regarding the unique microenvironments found beneath light-penetrating minerals exposed within the BSC. The Mojave Desert is one of the best regions to observe and study the microorganisms that coexists beneath these transparent/translucent minerals. The purpose of this article is to make the reader who frequently explores the Mojave to be observant of these micro-environments that are exposed throughout this desert, especially on pediment surfaces.

Introduction

Common transparent or translucent minerals may include quartz and its many varieties such as clear-colorless crystalline quartz, milky quartz, rose quartz, agate, and chalcedony. Agate and chalcedony are cryptocrystalline varieties of the mineral quartz. Minerals such as muscovite, white marble, opal (a mineraloid), opalite, porcelanite, calcite, selenite gypsum, satin spar gypsum and many others can also allow for the penetration of sunlight.

Halite on salt flats within dry lake surfaces (in the absence of soil) can contain living red algae and bacteria that coexist below, on, and encased within the crystal. The dry salt flats of Searles Lake, located beyond the northern boundary of the Mojave Desert near Trona, have many examples of red, pink, and some green halite, exhibiting the hues of algae with bacteria. In general, desert regions contain an abundance of transparent/translucent minerals, many that originated from volcanic eruptions, the crystallization of minerals from hydrothermal fluids, crystalline rocks formed from magmatic intrusions, or their deposition and crystallization in sedimentary basins. The slow process of erosion and deposition allow for the distribution of a huge variety of rocks and minerals at the surface of the Mojave Desert.

Pediment surfaces, desert pavement and alluvium

Thousands of years of deposition, erosion, surface water runoff, clay expansion, microorganic activity, and soil movement have allowed for a wide distribution of transparent/translucent minerals to be exposed on the floor of the Mojave Desert. Some of the best examples that exhibit ideal occurrences of these light-penetrating minerals are found on *pediment* surfaces that contain semi-flat *desert pavement* (Wells et al, 1996). In this geomorphic setting, rocks and minerals are well distributed at the surface. On the desert pavement, the observer can easily see white and other light-colored minerals that invite further investigation for their occurrence of colonial microalgae within the biological soil crust (BSC), the primary indicator of microscopic life that is visible by the naked eye.

Penetration of sunlight

The intense sunlight in the desert can easily penetrate these non-opaque minerals. Some of them such as chalcedony and agate can efficiently disperse and scatter sunlight within the mineral due to their cryptocrystalline physical properties. Other crystalline masses, depending on their shapes, can act as lenses that concentrate the sun's energy. Some minerals that are half-buried in surface soil can absorb enough light that can easily reflect, refract and scatter sunlight throughout the crystal. A mass of transparent/translucent mineral that is almost completely buried, with a small portion exposed to the sunlight, can gather enough energy from the sun to benefit a colony of microalgae and associated microorganisms in contact with the mineral (Figure 1).

It doesn't take much surface area of exposure for sunlight to propagate throughout the light-penetrating mineral. The best examples are mineral masses or crystalline clusters that are less than several centimeters in overall length and a few centimeters thick. The thicker the mineral, the less light that will penetrate to where it contacts the soil.

Microalgae and associated soil microorganisms have also been observed living in fractures in a vein of milky quartz, in the absence of contact with soil

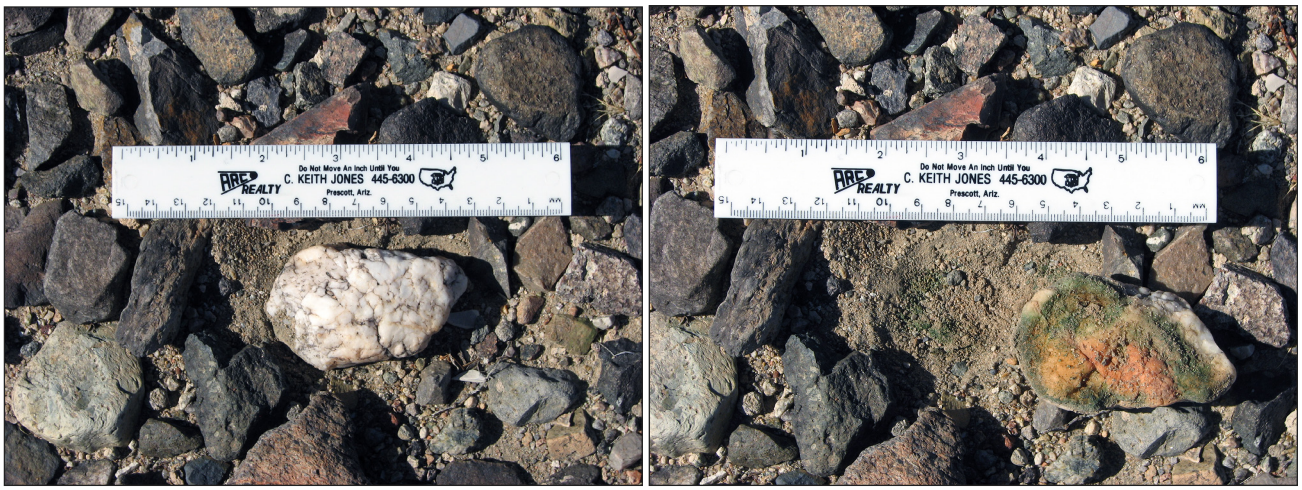

Figure 1. a. Translucent milky quartz on a desert pavement surface. This mineral specimen measures 7.3 cm x 4.6 cm and is as much as 2.5 cm thick. b. The underside of the same mineral, exhibiting a colony (or colonies) of microalgae with associated BSC microorganisms. Note that some of the colony of algae is attached to the mineral while a portion of it is well established on the BSC. The pattern of microorganisms on the milky quartz and soil may in part be related to the angle of the sun. The general direction of south is at the top of the photos. These photos were taken during mid-summer on August 10, 2019 on a remote desert pavement surface in the Mojave Desert, several miles south of Barstow, CA.

(Figure 2). Another example would include a pegmatite granite where algae is observed in association with translucent minerals muscovite and quartz, in contact with feldspar and other minerals within the rock. Minerals can also exhibit a combination of light-penetrating and opaque varieties in one specimen or crystalline mass.

Figure 2. a. Milky quartz slab that was once eroded from a quartz vein. The dime is included for relative scale. The rock exhibits surface fractures that contain dust, microalgae, and associated microorganisms. A fractured layer of the rock, with a general thickness of 10 mm, was removed between the surface and the first fracture that parallels the surface. Airborne dust has washed into the fractures with time, acting as an immature soil, providing a water retention medium and an ion exchange medium for the colony of microorganisms. b. Close-up of the milky quartz in Figure 2. a.

Algae and other soil microorganisms

The process of photosynthesis will allow for the growth of a colony of microalgae on a mineral's underside. However, the microalgae are not alone. They usually thrive within the moist environment in a symbiotic relationship with aerobic and anaerobic bacteria, micro fungi, mosses, and lichens (Belnap et al, 2001). Cyanobacteria are the common anerobic bacteria that may occur when soil chemistry is favorable. Cyanobacteria and microfungal filaments work together to provide soil binding agents that are very important to biological soil crusts (Belnap, et al, 2001). The wicking action caused by soil moisture tension, capillary forces, and permeability can move dissolved ions and concentrate soil nutrients beneath the mineral for the benefit of the microalgae and other microscopic life forms.

These microorganisms live together under the armored "roof" of the "greenhouse", on the mineral's bottom portion that is in contact with the soil. In this unique setting, the BSC is protected throughout the year from:

- the high rate of surface evaporation of moisture within the soil.
- the erosional effects of flowing surface water during intense rainstorms.

A colony of microalgae has a way of gathering and retaining dust and moisture for the availability and benefit

of the associated microorganisms living within or in proximity to the colony of microalgae.

Soils and the occurrence of sulfate-reducing bacteria

Soils contain an abundance of life in the form of microorganisms, plants, and animals including many varieties of insects. Soils are living/breathing mediums that provide nutrients, moisture-retention, and ion exchange. In soils that are rich in gypsum (hydrated calcium sulfate, $CaSO_4 \cdot 2H_2O$) or other highly soluble sulfate minerals, anaerobic sulfate-reducing bacteria (SRBs) can thrive below the surface and beneath the mineral with other microorganisms (Jeong, 2018).

The sulfate-reducing bacteria acquire their energy through the process of chemosynthesis. The best example is with the chemistry associated with the dissolution and availability of sulfate ions from the soluble mineral gypsum and from water that is rich in dissolved sulfate ions. SRBs will force the reduction of sulfate ions (SO_4^{-2}, and SO_3^{-2} if available) and the reduction of water molecules, releasing H_2S gas to the atmosphere. Sulfate ions are also beneficial as a soil nutrient to aerobic microorganisms. In agricultural applications, crushed gypsum is often applied as a soil amenity in order to condition adobe soils and to supply plant nutrients.

Clear-colorless (transparent) selenite gypsum and white translucent satin spar gypsum, exposed on the surface of soils, can provide four essential benefits to SRBs and other microorganisms:

1. Protection from the harsh desert elements,
2. Penetration of sunlight through the mineral,
3. Moisture retention beneath the mineral, and
4. Provide available sulfate ions within the soil for the propagation of the sulfate-reducing cyanobacteria with microalgae, micro fungi, mosses, lichens and aerobic bacteria in a symbiotic relationship.

Field observations

Visitors to the Mojave Desert should be observant of these *miniature greenhouses*. In the Mojave, they are well exposed in volcanic regions that may contain an abundance of transparent/translucent silicate minerals of the quartz mineral family such as agate and chalcedony. Pediment surfaces with desert pavement features are ideal settings for locating these white or light-colored minerals. The next time you are hiking in the Mojave Desert, begin by looking for white-colored translucent minerals. By picking up the mineral from the ground, one can observe the green color of colonial microalgae on its underside. After making your observations, be sure to carefully return the mineral in the same position from which it was found. Once it is returned to its original location, press lightly to reduce the air gap between the mineral and soil surface.

The green color is the primary physical indicator to the field observer of a suitable environment for microalgae that allows for photosynthesis in a protected microenvironment within the biological soil crust. These microenvironments are what can be referred to as *miniature greenhouses* of the Mojave Desert and can be common in other desert regions of North America and throughout the world.

Conclusion

Nature has a way of compensating for the general scarcity of water in arid environments. The retention of soil moisture below rocks and minerals and the unusual microenvironments that exist under transparent/translucent minerals are just a few examples of the ability of microorganisms to survive in hot, dry climates at or near the surface of the ground. Microalgae plays an important role in the gathering and retention of moisture, providing water for a variety of other microorganisms.

Soils, including biological soil crusts, are dynamic ion-exchange mediums that are hosts to an abundance of life. For the microbiologist, a wealth of opportunities exists in soil research, beginning with microbial life-forms and the microenvironments that exist beneath light-penetrating minerals that occur in abundance on the surface throughout the Mojave Desert and other arid regions of the world. Under the transparent/translucent mineral within the biological soil crust, it appears to be one happy family of microorganisms, all working together to survive.

References

Belnap, Jayne, et al, 2001, Biological Soil Crusts: Ecology & Management, Technical 1730-2, USDI, USGS, Published by BLM, Denver, CO.

Bonewitz, Ronald L., 2007, Rocks & Gems, Oklahoma Publishing, Inc., Oklahoma City.

Chesterman, C. & Lowe, K., 1985, The Audubon Society Field Guide to North American Rocks and Minerals, 4th edition, published by Alfred A. Knopf, Inc., New York.

Elias, Scott, editor, 2018, Reference Module in Earth Systems and Environmental Sciences, Elsevier Reference Modules.

Jeong, Ara., et al, 2018, Urban Geomorphology of an Arid City: Case Study of Phoenix, AZ, Chapter 10, Urban Geomorphology, Landforms and Processes in Cities, p. 177-204.

Mottana, A., et al, 1978, Simon & Schuster's Guide to Rocks & Minerals, The American Museum of Natural History.

Paul, Eldor, 2015, Soils Microbiology, Ecology and Biochemistry, 4th edition.

Pough, F., 1960, A Field Guide to Rocks and Minerals, third edition, Houghton Mifflin Company, Boston.

Wells, Stephen., et al, 1996, Cosmogenic ^{3}He Surface Exposure Dating of Stone Pavements: Implications for Landscape Evolution in Deserts, Geology, Vol. 23 #7, p. 613 – 616.

Formation of California's Salton Sea in 1905–07 was not "accidental"

Jenny E. Ross
Stout Research Center, Colorado Desert District, California State Parks, Borrego Springs, CA 92004; jenny@jennyross.com

ABSTRACT—It is widely thought that the Salton Sea was created accidentally in 1905–07 because of engineering negligence in the diversion of Colorado River water for agricultural use in California's Imperial Valley. This is a misconception. Scientific data and historical records establish that formation of the Salton Sea was not accidental. The lake formed during 1905–07 in the same manner that numerous other large Salton Basin lakes did for at least tens of thousands of years from the Late Pleistocene through the late 19th century: as a result of the lower Colorado River's natural hydrodynamic regime, floodplain morphodynamics, and established avulsion style in combination with changes in streamflow attributable to regional hydroclimate. A large body of scientific and historical evidence indicates the 1905–07 Colorado River flooding into the Salton Basin and the creation of a large lake there would have occurred regardless of man-made modifications to the river's natural levee and distributary channels. In fact, the flooding would likely have been even worse in the absence of human intervention.

Introduction—the creation flood

For over 100 years it has been widely accepted that the Salton Sea, California's largest lake, was created accidentally in 1905–07 within an otherwise desiccated desert basin (e.g., Nijhuis, 2000; Barringer, 2014) as the result of engineering negligence by the California Development Company (CDC) as it struggled to keep irrigation water flowing from the lower Colorado River into the fledgling agricultural community of the Imperial Valley within the Salton Basin (Figure 1). The first diversion point for moving Colorado River water into the Imperial Valley ("Heading No. 1" on Figure 2) was constructed beginning in 1900 about 500 m north of the US–Mexico border. The opening from the lower Colorado River into the company's diversion canal was cut out of the river's natural western levee at an oblique angle, and flow into the main course of the canal was controlled by a wooden headgate placed a few hundred feet from the river bank down the canal (Grunsky, 1907). Below the headgate the canal connected to one of the Colorado River's natural delta distributary channels, the Alamo River, which was then dry. Diversion of water began in June 1901, and soon the river's heavy load of silt began to repeatedly obstruct the headgate and canal. As a consequence, water shortages in the Imperial Valley agricultural area began occurring in 1902 and continued through 1903 and into 1904, putting tremendous pressure on the CDC to fix the problems.

Eventually, in the fall of 1904, the company resorted to making two unprotected cuts into the river's natural levee farther south in an attempt to achieve reliable diversion of river water into the canal and onward into the Imperial

Figure 1. Overview map. (1) Colorado River; (2) Gila River; (3) Yuma, AZ; (4) approximate path of the modern, controlled Colorado River's channel through the lower delta (where the channel is mostly dry today); (5) lower delta region below the crest; (6) Imperial Valley in the Salton Basin; (7) Salton Sea.

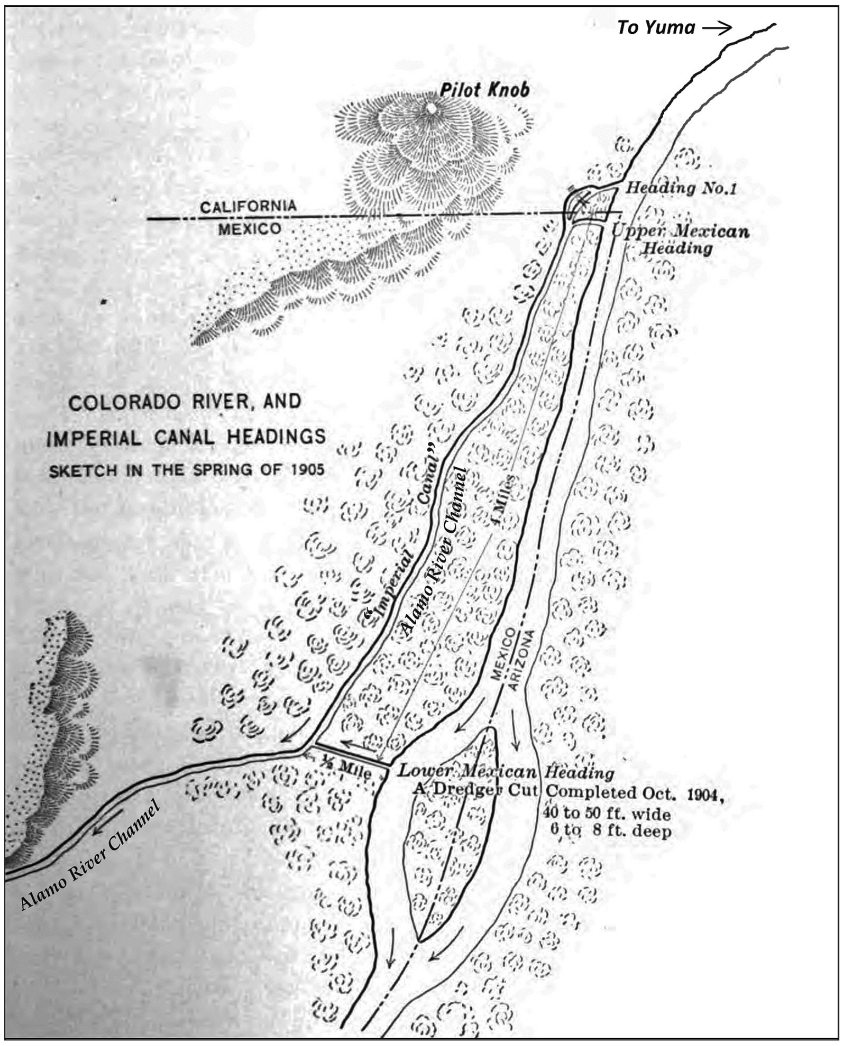

Figure 2. Sketch map of the lower Colorado River below Yuma, and the California Development Company's diversion headings below Pilot Knob. (Modified from Grunsky (1907), Fig. 2., to specify the location of Yuma and designate the Alamo River channel.)

Valley via the Alamo River (Grunsky, 1907; Cory, 1915; Kennan, 1917; Brown, 1923).

The first additional cut, known as the Upper Mexican Heading, was made just below the US–Mexico border. It quickly showed a pronounced tendency to silt up. The CDC eventually decided to close the first cut and try again slightly farther south. The second cut, known as the Lower Mexican Heading, was made about 4 miles (~6.4 km) below the international border. It was a simple cut with a dredger, made about 40 to 50 feet (~12-15 m) wide and 6 to 8 feet (~2-2.5 m) deep. It was connected to the CDC canal, which in turn connected to the Alamo River channel. There was no headgate. Through this cut there was sufficient fall from the river to the canal for the water to achieve scouring velocity, so silt did not accumulate. Instead, natural erosion of the unprotected cut began immediately. In the CDC's haste to reinitiate the flow of irrigation water into the valley, the company failed to add a control structure at the new diversion point, although they intended to do so eventually. The company's engineers perceived no urgency in adding that structure because the primary problem they had experienced up until that time was too little flow from the river into the valley rather than too much (Grunsky, 1907; Cory, 1915; Kennan, 1917; Brown, 1923).

Unanticipated high streamflow on the lower Colorado River arrived in early 1905, and floodwaters soon rapidly eroded the unreinforced cut and rushed through it. The river's high flows avulsed across the delta and streamed north primarily through the Alamo River channel and another previously dry but well-established natural distributary channel of the Colorado, the New River, that headed into the Salton Basin. Continuing to widen the breach in the Colorado River's natural levee and erode and overtop the river's distributary channels, the floodwaters coursed across the delta in sheetflow, rampaged through recently-developed farm fields in the Imperial Valley, poured into the central Salton Basin, flooded the Southern Pacific Company's railroad tracks, and began creating an enormous lake dubbed the "Salton Sea." The CDC, Southern Pacific, and hundreds of workers made many desperate attempts to block the breach in the river's levee. Each time the efforts ultimately failed as numerous large floods raced down the lower Colorado River below Yuma during 1905. By August 1905, the entire flow of the Colorado River was rushing through the breach, into the river's distributary channels, across the Imperial Valley, and into the growing Salton Sea. Extremely high streamflow continued on the lower Colorado River in 1906 and washed away every structure the CDC attempted to use to block the breach. In November 1906, the river finally appeared to be thwarted and human control achieved. But on December 5, 1906 another huge flood roared down the Colorado past Yuma. New breaks occurred in the repaired levee, and soon the river was once again flowing uncontrollably through the Imperial Valley and onward into the central Salton Basin. After many additional efforts, in January 1907 the Southern Pacific Company was finally able to block the floodwaters and turn the river toward the Gulf of California by using millions of tons of quarried rock dumped into the breach (Grunsky, 1907; Cory, 1915; Kennan, 1917; Brown, 1923).

The story of the epic two-year battle to stanch the raging flow of the wild Colorado River and redirect the

river toward the Gulf of California is a well-known tale of man against nature described fully in many historical accounts (e.g., Cory, 1915). The saga of this "Creation Flood" that formed the Salton Sea, crippled the nascent Imperial Valley, and led ultimately to the damming and complete control of the Colorado River for human purposes (e.g., LaRue 1916, 1925) is engaging and highly memorable. At the time the events unfolded, they "were so spectacular as to result in world-wide notoriety." (Cory, 1915.) For the pioneers of the region who toiled to create what they hoped would be an agricultural Eden in the desert, as well as for others who followed in developing the Imperial Valley into an extraordinarily productive agricultural region, the story served as an inspirational saga demonstrating the power of persistence and human ingenuity to succeed despite seemingly insurmountable odds. The tale vividly demonstrated the capacity of mankind to triumph over and control wild nature (e.g., Larkin, 1907; Howe & Hall, 1910; Farr, 1918; Sperry, 1975). But the memorable story and its appealing allegorical aspects led to the widespread adoption of a fundamental misconception that has colored opinions of the Salton Sea ever since: namely, the misimpression that the 1905–07 flooding into the Salton Basin would not have occurred, and the Salton Sea would not have been created, were it not for the infamous series of incautious decisions made by the California Development Company. The Creation Flood story has resulted in the ingrained but mistaken view that the Salton Sea is accidental and unnatural, a man-made lake in a parched desert where such an expanse of water should not be.

But historical records and scientific data of various types indicate that formation of the Salton Sea in 1905–07 was not an accident, and engineering negligence was not the cause. The lake formed in the same manner that lakes had been forming in the Salton Basin, sustained by Colorado River water, for at least tens of thousands of years from the Late Pleistocene through the late 19th century: as a result of the Colorado River's natural hydrodynamic regime, floodplain morphodynamics, and established avulsion style in combination with changes in streamflow attributable to regional hydroclimate. A large body of scientific and historical evidence indicates the 1905–07 Colorado River flooding into the Salton Basin and the creation of a large lake there would have occurred regardless of man-made modifications to the river's natural levee and distributary channels. In fact, the flooding would likely have been even worse in the absence of human intervention.

Geologic and geographic context

The Colorado River arrived at the proto-Gulf of California approximately 4.8 Ma (Crow *et al*., 2019; Dorsey, 2012), and began building a vast delta at the boundary of the Pacific and North American tectonic plates. The Salton Trough, the northwest landward extension of the Gulf of California Shear Zone, was originally part of the proto-Gulf and began accumulating Colorado River sediments during the early Pliocene (Dibblee, 1954; Muffler and Doe, 1968; Winker and Kidwell, 1996). The northern Salton Trough likely became cut off from marine waters of the Gulf by latest Pliocene time, as the result of aggradation of delta sediments and net plate movement to the northwest along the San Andreas fault (Winker and Kidwell, 1986; Winker, 1987; Winker and Kidwell, 1996; Dorsey, *et al*., 2011); but marine incursions northward may have occurred during periods of very elevated sea level (Ross *et al*., 2020, this volume). The Salton Basin is a below-sea-level, fault-bounded rift valley lying within the northern Salton Trough north of the U.S.-Mexico border and straddling the plate boundary (Figure 1). The lowest elevation in the central Salton Basin was determined by the Southern Pacific Company in 1891 to be 280.2 feet (85.4 m) below sea level (McGlashan and Dean, 1913); in 1903 it was found to be -286 feet (-87 m) (MacDougal, 1907); and in 1907 it was measured at -278 feet (-84.7 m) (Grunsky, 1907).

The Salton Basin was part of the Colorado River's delta and shifting floodplain, and received part or all of the river's flow at various times as a result of avulsion and channel switching that delivered water to the north. Affected by tectonic, sedimentary, hydrologic, and climatic factors, the Colorado River adjusted its flow sometimes into the Salton Basin, sometimes into the Gulf, and sometimes to both regions (Cecil-Stephens, 1891; Blake, 1914; MacDougal, 1915; Brown, 1923; Kniffen, 1932). When the Colorado River flowed into the Salton Basin, large lakes were often created and sometimes sustained for long periods (Blake 1854, 1858; LeConte 1855; Sykes 1914, 1937; Kniffen, 1932; Li *et al*., 2008a,b; Rockwell *et al*., 2018). Thick lacustrine and fluvial-deltaic sedimentary deposits with a Colorado River provenance that accumulated in the Salton Basin from the Pleistocene through the Holocene have a total thickness of several thousand meters and include the Borrego Formation (Tarbet, 1951), the Brawley Formation (Dibblee, 1954), and the Lake Cahuilla beds (Blake, 1907).

Throughout the Late Pleistocene and Holocene, the path of the lower Colorado River through its floodplain and delta was extremely variable. Until the river was dammed and controlled in the mid-20th century, the entire delta region was a maze of constantly shifting distributary channels transporting heavily silt-laden water. According to Ives (1861):

> "The channel is circuitous . . . Slues branch in every direction . . .The water is perfectly fresh, of a dark red color, and opaque from the quantity of mud held in suspension. The shifting of the channel, the banks, the islands, the bars is so continual and so rapid that a detailed description, derived from the experiences of one trip, would be found incorrect, not only during the subsequent year, but perhaps in the course of a week, or even a day. . ."

The Salton Basin is topographically separated from the Gulf of California by a region of aggraded deltaic sediments where today the city of Mexicali, Mexico and the Mexicali Valley agricultural area are located (Brown, 1923). The highest elevation portion of that region, the crest of the Colorado River delta, is a broad linear zone beginning east of the Sierra de Los Cucapah and Cerro Prieto at Volcano Lake, and trending northeast across the delta toward the mainstem of the Colorado River (Kniffen, 1932; Muffler and Doe, 1968). There is a pronounced asymmetry in the slopes directing drainage in opposite directions on either side of the delta crest—toward the Gulf of California in the south and toward the Salton Basin in the north (Grunsky, 1907; Brown, 1923; Kniffen, 1932). Kniffen (1932) explained, "South of the crest the slope is quite uniform to the gulf, with a gradient of less than two feet to the mile. North of the crest the slope to the Salton Sea is much greater." At its east end, the delta crest meets the course of the Colorado River's mainstem where, prior to damming and course modification, the river turned sharply south-southwest near Pilot Knob after flowing due west from its junction with the Gila River (Emory, 1848; Kniffen, 1932; Muffler and Doe, 1968). The low point of the delta crest in the west, where it reaches Volcano Lake, was approximately 13 m when measured in the mid-twentieth century, but is now lower as the result of tectonic and anthropogenic subsidence (Arnal, 1961; Sarychikhina *et al*., 2011).

The Imperial Valley agricultural region is located within the Salton Basin and extends north from the US–Mexico border to the southern and southeastern shores of the Salton Sea. The current elevation of the Imperial Valley along its southern border with Mexico ranges from approximately sea level in the west to approximately 13 m above sea level in the east, excluding the area farther east covered by the Algodones Dunes. The Salton Sea, which is currently receding from water-deprivation, is located in the central Salton Basin and presently has a surface elevation of approximately 72.4 m below sea level (USGS, 2020). The lake has been sustained primarily by irrigation drainwater from the Imperial Valley since the Colorado River was dammed and controlled in the mid-twentieth century and prevented from flowing into the Salton Basin.

Delta distributaries and floodplain morphodynamics

Just as it had for millions of years, in the 19th and early 20th centuries the lower Colorado River flowed at will through an extensive and complex network of distributary

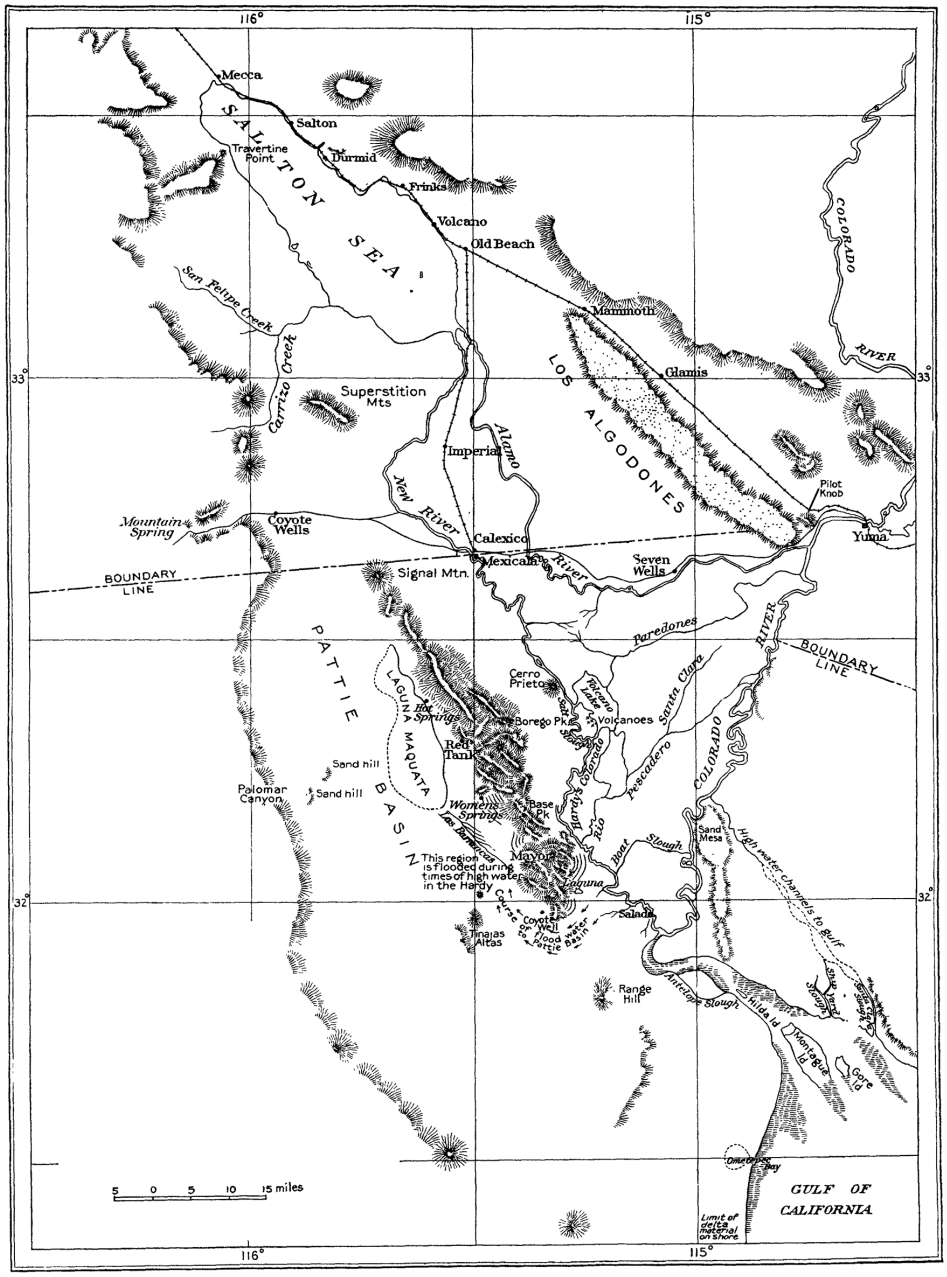

Figure 3. Sketch map of the Colorado River delta and Salton Basin showing distributary channels. (Modified from Fig. 1 in MacDougal (1907), drawn by Godfrey Sykes, to clarify the label for Pilot Knob.)

channels, sloughs, and lagoons in a delta and floodplain covering thousands of square kilometers, including the Salton Basin. Sykes (1937) estimated that the areal extent of the Colorado River delta was approximately 8600 km^2 in the early 20th century. The dynamic and capricious course of the river in its lower reaches was described by C.K. Clark in 1913: "The lower Colorado has no fixed channel, because of the character of the soil, which is a deposit of silt, easily eroded. The current swings back and forth, cutting the banks and changing the meander line…." (Cory, 1913).

The Alamo River and the New River are Holocene delta distributary channels of the Colorado River that were established sometime prior to the mid-1800s (Emory, 1848; LeConte, 1855; Blake 1854, 1858). They conveyed flow from the Colorado River into the Salton Basin during high-water periods (LeConte, 1855; Blake 1854, 1858; Kniffen, 1932) until damming and control of the Colorado River in the mid-20th century. Descriptions of the configurations of those streams during the 19th and early 20th centuries make clear their ongoing relationship with the mainstem of the lower Colorado River and with other delta distributary channels (Figure 3). The Alamo River branched off of the Colorado's western levee near where the mainstem turned sharply south-southwest after flowing "perfectly straight" west for approximately 3–4 miles (~4.8–6.4 km) from its junction with the Gila River (Emory, 1848). During periods of high water, the Alamo flowed southwest from the Colorado and then meandered west and north as it followed the topographic contours in the area north of the delta crest (Emory, 1848; Sykes, 1914). When filled, the Alamo flowed through a series of sloughs and lagoons in the northern delta region which sustained the wells of the Alamo Mocho Station, well-known to travelers through the desert (Grunsky, 1907; Jonas, 2009); then it curved northward and flowed into the Salton Basin if it contained sufficient streamflow (Grunsky, 1907; Sykes, 1914). The Rio Paradones, another delta distributary channel of the Colorado River, branched off the west levee of the mainstem south of the Alamo River. The beginning of the Rio Paradones bifurcation channel was situated at a place where the south-southwest flowing mainstem turned briefly toward the east before flowing generally south (Grunsky, 1907). The Paradones flowed west-southwest atop the delta crest and ended at the low point where Volcano Lake was perched adjacent to the beginning of the New River (Grunsky, 1907; Sykes, 1914; Jonas, 2009). During high-water periods, the New River collected Colorado River floodwater that was delivered to it via the Paradones and Volcano Lake. In addition, it received overbank discharge from the Alamo River, and also accumulated water from sheetflow across other portions of the delta (Grunsky, 1907). The New River flowed north from the delta crest and delivered its water into the Salton Basin (LeConte 1855; Sykes, 1914; Kniffen 1932). In 1848, U.S. Army Lieutenant Colonel W. H. Emory described additional arroyos north of the Alamo heading west and then north from the bend of the Colorado River where the mainstem turned sharply to the south-southwest after flowing due west from its junction with the Gila River (Emory, 1848).

Another distributary channel on the south slope of the delta crest, the Rio Hardy, flowed south from the divide at Volcano Lake and ended at the Gulf of California (Hardy 1829; Howe and Hall, 1910; Blake, 1914). During periods of normal flow, Volcano Lake emptied preferentially into the Rio Hardy, but during high flows its waters were distributed both into the Rio Hardy and the New River (MacDougal, 1915; Cory, 1915). When the Rio Hardy overflowed during high-water periods, sheetflow spread west through a gap below the Sierra de Los Cucapah and Sierra El Mayor to fill the shallow below-sea-level basin lying between those mountains and the Peninsular Ranges. The lake formed there, known as Laguna Salada or Laguna Maquata, sometimes achieved a maximum size of approximately 40 miles (~64 km) long by 20 miles (~32 km) wide, depending on available streamflow (Cory, 1915; MacDougal, 1915; Kniffen, 1932).

It was observed by Grunsky (1907) that the fall of the lower Colorado River's mainstem course southward to the Gulf of California along the east side of the delta region was significantly less than the fall of other courses through distributary channels that led into the Salton Basin:

> "The Colorado River flows southerly in a direction in which the general fall of the ground surface is only about 1.5 ft. per mile, which the river in its meanderings cuts down to an effective fall of about 1 ft. per mile. Toward Volcano Lake, southwest from the river, the general surface gradient is 2 ft. or more per mile; and westward, in the direction paralleling Alamo River, it is nearly 3 ft. per mile to a point near Calexico [at the southern edge of the Imperial Valley]. Thence northward into Salton Basin, on lines of greatest slope, the country falls away at the rate of from 4 to 5 ft. per mile."

In the 19th century it was recognized that flow through the Colorado River's distributary channels would bring water into the Salton Basin whenever high-water conditions existed in the mainstem (Blake 1854, 1858; LeConte, 1855; Cecil-Stephens, 1891; Grunsky, 1907; LaRue, 1916; Brown, 1923). LaRue (1916) noted that the geomorphology of the delta region was a crucial factor in this process: "As the slope of the delta is greatest toward the north and west, the river during flood periods is continually seeking a new channel to Salton Sea." It was observed that "overflows" of the river into the Salton Basin would occur at two times of year: in the spring and early summer, as a result of snowmelt in the headwaters of the Colorado River and its tributaries, and in the winter as a result of storms that brought heavy precipitation and caused flash flooding in the lower Colorado River basin,

particularly along the Gila River and its tributaries (Cecil-Stephens, 1891; Brown, 1923). During high-water periods the lower Colorado would overflow its banks at many points, particularly below Yuma beginning where the river curved abruptly toward the south-southwest after flowing due west. A relatively low natural levee on the west side of the curve below Pilot Knob was especially vulnerable to over-topping (Emory, 1848; LaRue, 1916). When the river's streamflow was high and overflows were of particularly significant volume, which happened numerous times during the 19th century as described below, large lakes were created in the Salton Basin via overflow and avulsion which shunted the mainstem's water into the Alamo and New Rivers (MacDougal, 1915; Brown, 1923; Kniffen 1932). In 1891, referring to the gage on the lower Colorado River at Yuma, Cecil-Stephens (1891) noted, "Hitherto, New River has always flowed when the Colorado marked 19 feet at Yuma." It was only during periods of drought that distributary channels did not bring Colorado River water into the Salton Basin (LeConte, 1855; Blake 1858; Cecil-Stephens, 1891). Even then, there was a residual vegetated salt marsh in the central basin stretching as much as 25 miles (~40 km) long and 5 miles (~8 km) wide holding Colorado River water that had become saline from evaporation (Farr, 1918).

As is true of all rivers, and particularly those that carry large loads of sediment and form fan deltas, the opening, shifting, blocking, and reopening of the lower Colorado River's distributary channels was affected by varying streamflow and fluctuating quantities of sediment the river carried, deposited, and eroded (Andrews, 1991). A characteristic of dryland rivers generally and the pre-dam Colorado River specifically is the transport of very large quantities of sediment, both as suspended load and as bedload (Andrews, 1991; Tooth, 2000). Kniffen (1932) noted, "As a carrier of silt the Colorado is probably without a peer among the greater streams of the world." He explained that in 1904, during a dry year preceding the 1905–07 flood, a researcher from "the Arizona Experiment Station made a careful study of the river silt. He found that an acre-foot of Colorado River water contained on an average 9.62 tons of silt, and that for the year the river's burden amounted to over 120,000,000 tons—this for a year when the total discharge was considerably under normal. The average annual load passing Yuma is probably around 160,000,000 tons, which translated into terms of volume of dry soil would be approximately 80,000 acre-feet."

During the portions of the 19th century for which historical records exist, the lake-creating floods from the Colorado River into the Salton Basin were all self-limiting due to silt deposition when streamflow slowed (LaRue, 1916). Extensive sedimentation occurring in the river's distributary channels as floodwaters slackened eventually caused cessation of flow northward into the Salton Basin (LaRue, 1916; Brown, 1923). During periods of drought and chronically slack flow on the lower Colorado River, openings from the mainstem to distributary channels became blocked by deposition of silt, and the courses of distributaries became clogged with sediments and blown sand, and were sometimes overgrown with vegetation (LaRue, 1916; Schyler, 1907). In addition, at those times the sedimentation in the mainstem raised the streambed considerably in relation to the river's floodplain below Yuma. Then, if flash flooding occurred, the elevated streambed of the mainstem could not hold the flow (Schyler, 1907; LaRue, 1916). The river would rapidly overtop its natural levees along the western edge below Yuma. When such flooding ensued, sediment dams in clogged distributary channels would quickly erode—especially if drought had riddled them with mud cracks through which floodwaters could penetrate—and avulsion and bifurcation of the mainstem flow would occur (MacDougal, 1915; LaRue 1916). When streamflow slowed following a period of high water, and sedimentation once again blocked distributaries where they branched off the mainstem, the closures left zones of weakness in the Colorado's natural levees at the former bifurcation points, which encouraged reopening of the distributary channels in the same spots during the next period of high water (LaRue 1916; Andrews, 1991). The portion of the lower Colorado River's mainstem from the curve at Pilot Knob to the Rio Paradones below the US–Mexico border was known to be a stretch particularly vulnerable to avulsion and bifurcation (Grunsky, 1907; Schyler, 1907; MacDougal, 1915; LaRue, 1916; Brown 1923). These early reports of the lower Colorado River's behavior are entirely consistent with the modern understanding of floodplain morphodynamics and processes initiating avulsion and bifurcation (Slingerland and Smith, 1998; Kleinhans *et al*., 2012; Hajek and Edmunds, 2014; Dean *et al*., 2016).

Pleistocene-to-Holocene Salton Basin lakes

Scientific data and historical records establish that many large lakes occurred in the Salton Basin from the Late Pleistocene through the Holocene, sustained by Colorado River water. The most generally well-known among them is Lake Cahuilla, an enormous Late Pleistocene-to-Holocene lake with a highstand overflow path south across the delta crest that filled the Salton Basin to an elevation of approximately 13 m above sea level beginning at least 20.5 kya and continuing intermittently through the 18th century (Blake 1854, 1858, 1907; Brown, 1923; Li *et al*., 2008a,b; Rockwell *et al*., 2018). At various times Lake Cahuilla was closed, through-flowing, or overflowing, depending on climate conditions and the amount of Colorado River streamflow available (Li *et al*., 2008a,b). At its southern end the giant lake was supported by the elevated zone trending northeast across the delta. When the lake's level reached about 13 m above sea level it overflowed at the lowest point of that delta crest, sending a stream to the Gulf of California.

Lake Cahuilla was first described by geologist William Phipps Blake in the mid-19th century, following his

participation in the initial survey of the West for possible railroad routes during which he visited the Salton Basin in 1853 (Blake 1854, 1858). He noticed thick layers of calcium carbonate encrusting the east face of the Santa Rosa Mountains and terminating in a line at a consistent elevation on the mountainside, and he realized that this tufa deposit had been formed by an immense lake. He later decided that 'Lake Cahuilla' was an appropriate name for the body of water (Blake 1907), to honor one of the Native American tribes that lived along its shores and exploited its rich natural resources for thousands of years. Blake was also the first scientist to note that the elevation of the Salton Basin extended far below sea level (Blake 1854, 1858). Research conducted a century later concluded there is evidence at various locations in the Salton Trough indicating that even larger lakes, including at least one that reached an elevation of about 46 m above sea level, existed during the late Pleistocene prior to Lake Cahuilla (Thomas, 1963).

Focused scientific studies of the timing of Lake Cahuilla were first conducted in the late 1970s and early 1980s (Wilke 1978; Waters 1983). That research concluded there were at least six lengthy episodes during the past 2000 years when the 13-m lake existed, and its last occurrence was either in the 15th (Wilke, 1978) or 16th (Waters, 1983) century. More recent studies (Li *et al*., 2008a,b) based on stable isotope analysis and serial radiocarbon dating of Lake Cahuilla's thick tufa deposits, determined that the giant lake began depositing tufa on the east face of the Santa Rosa Mountains about 20.5 kya, and there was no hiatus in that deposition through at least 1300 years BP. Li *et al.* (2008a,b) determined that the lake was sustained primarily by flow from the Colorado River, and was either a full closed lake or was overflowing at its delta sill intermittently or continuously as the result of the Colorado River's high streamflow during periods of very wet regional hydroclimate. An additional study by Rockwell *et al.* (2018) used radiocarbon dating, historical records, and modeling of lake filling and evaporation rates to place the timing of the penultimate occurrence of Lake Cahuilla during approximately the first half of the 17th century and the final incarnation of the 13-m lake during approximately the mid-18th century.

Tree-ring based reconstructions of Colorado River streamflow indicate that the last two incarnations of Lake Cahuilla as identified by Rockwell *et al.* (2018) correspond with periods when extremely wet hydroclimate existed in all or a portion of the Colorado River basin—in the upper basin as reflected in reconstructed streamflow for the river at Lees Ferry (Figure 4a; Woodhouse *et al*., 2006; Meko *et al*., 2007), and/or in the lower basin as reflected in reconstructed streamflow for tributaries of the Gila River (Figure 4b; Meko *et al*., 2008). It's important to note that these tree-ring based data may understate very high flow and flash-flooding (Woodhouse *et al*., 2006; Meko *et al*., 2008). Nonetheless, the data indicate: (a) the penultimate occurrence of Lake Cahuilla was during a long period of extremely wet hydroclimate in the 17th century that caused exceptionally high streamflow in both the upper and lower Colorado River basins; and (b) Lake Cahuilla's final occurrence was during a long period of very wet

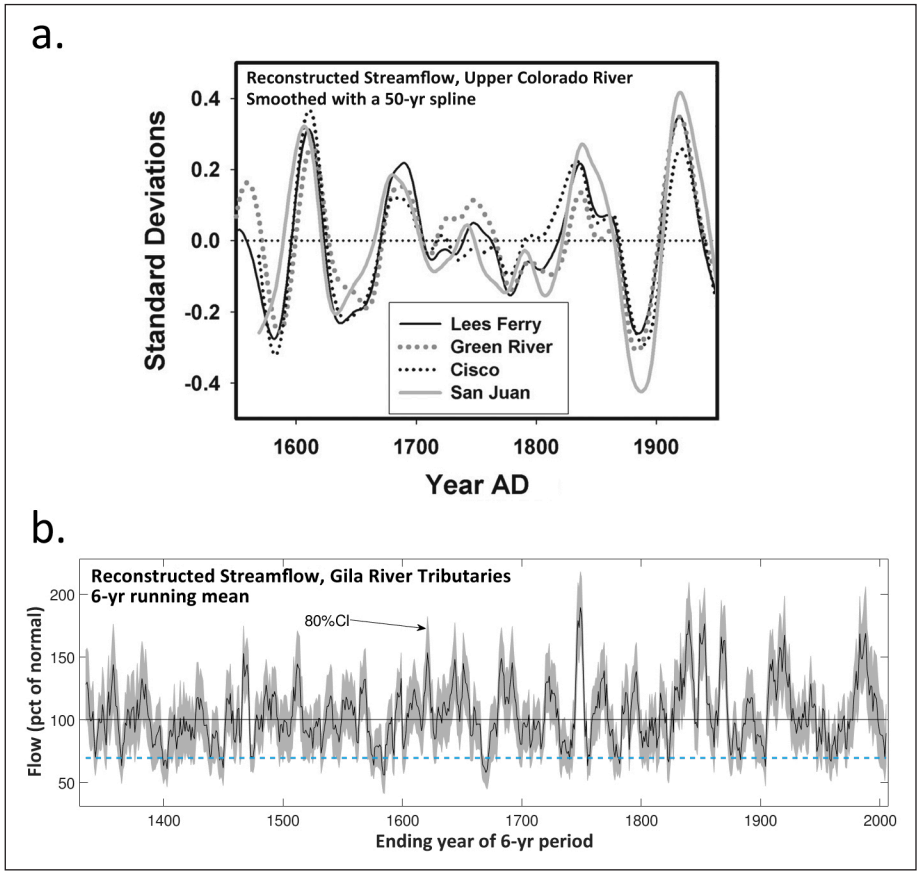

Figure 4. Tree-ring based streamflow reconstructions: (a) Reconstructed streamflow 1550-1950 for three major upper Colorado River tributaries and for the mainstem at Lees Ferry, smoothed with a 50-year spline to highlight low-frequency variability (modified from Woodhouse *et al*. (2006), Fig. 9). (b) Reconstructed streamflow for the Salt + Verde + Tonto Rivers (tributaries of the Gila that are important sources of flow for the lower Colorado River below Yuma), based on a 6-year running mean for 1330-2005. Solid black line represents averaged flows plotted as % of normal, where normal is the median of all 6-year running means. Dashed aqua line is reconstructed 6-year mean for 1999-2004, to serve as a baseline comparison for the entire record. Gray areas define the 80% confidence interval. (Modified from Meko *et al*. (2008), Fig. 13.)

hydroclimate in the 18th century that most affected the lower Colorado River basin and caused particularly high streamflow on the Gila River's tributaries. Notably, the reconstructions also confirm the occurrence of extremely wet hydroclimate in the entire Colorado River basin during the early 20th century, as discussed below.

Additional support for the conclusions of Rockwell *et al.* (2018) regarding the timing of Lake Cahuilla's final occurrence exists in the form of a large detailed map of North America by John Rocque, topographer to England's King George III, published in 1762 (Figure 5). The map shows the Colorado and Gila Rivers pouring their entire flow into a giant lake that is separated from the northern Gulf of California to its south by an expanse of land. According to text on the map within the cartouche, the details shown were "taken from Actual Surveys and Observations Made in the Army employ'd there, From the year 1754, to 1761."

Although for most of the 19th century the Salton Basin was only occasionally visited by people who kept records of what they saw, historical reports indicate that particularly heavy "overflows" from the Colorado River into the Salton Basin via the New and Alamo Rivers were observed to occur and form lakes in the central basin numerous times during the 1800s—in at least 1828, 1840, 1849, 1852, 1859, 1862, 1867, 1884, and 1891 (Grunsky, 1907; Cory 1913; MacDougal, 1914, 1915; Kniffen 1932). At other times there was flow from the Colorado River into the Salton Basin that filled large sloughs and lagoons along the distributary courses, but was insufficient to form a large lake in the central basin (Blake 1854, 1858; LeConte, 1855; Grunsky, 1907). For example, Grunsky (1907) explained:

> "In the mesquite and arrow-weed thicket at the original head of the Alamo, there was an occasional accumulation of so much water, and submersion of so much land, that the locality was called 'The Lagoons' (*Las Lagunas*). Although these lagoons received water at practically every high-water stage of the river, they did not always yield enough to the Alamo River to produce a flow throughout the river's entire length. In other words, there were many years in which the Alamo did not discharge any water into the lowest portion of the Salton Basin. The lagoons, in addition to feeding the Alamo, appear also to have been one of the sources of supply for the Rio Paradones."

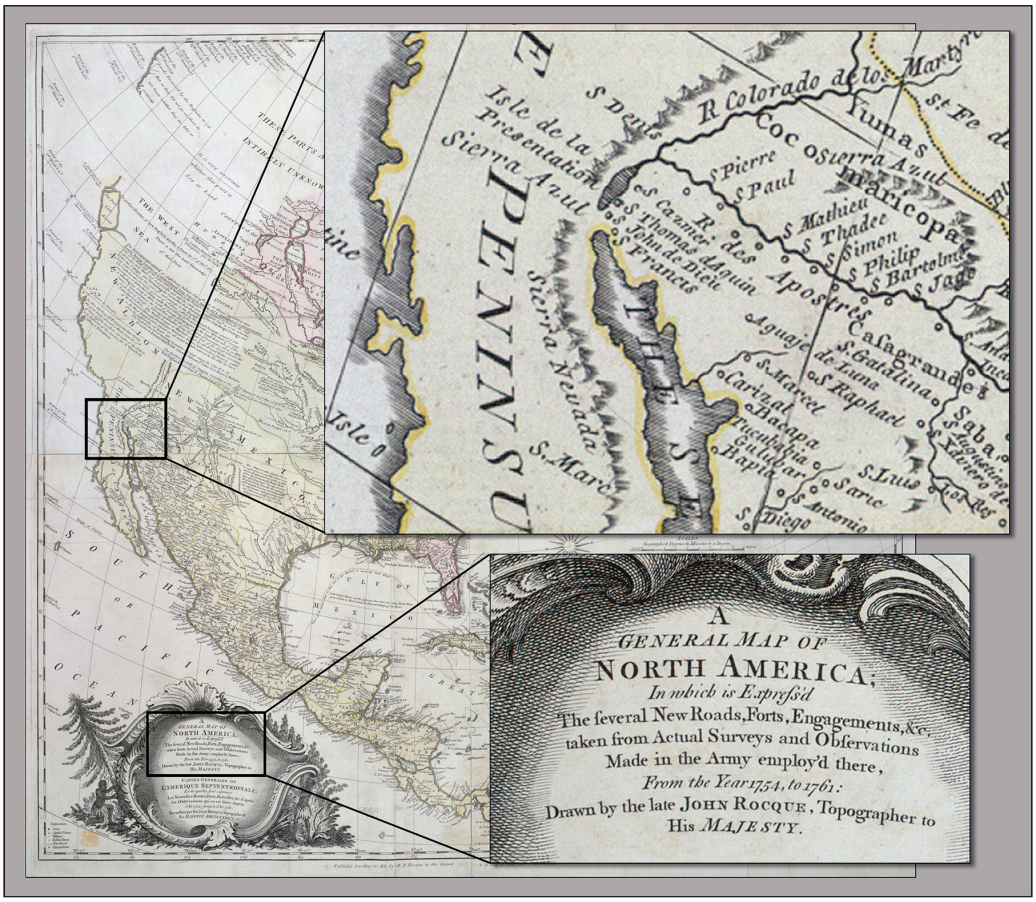

Figure 5. A General Map of North America by John Rocque, published in 1762, with superimposed enlargements showing (a) the Colorado and Gila Rivers emptying into a large lake that is separated from the northern end of the Gulf of California and appears to be Lake Cahuilla; and (b) the text in the map's cartouche.

For a long period in the late 19th century there was at least some flow of Colorado River water into the Salton Basin on an annual basis as the result of a recurring breach in the river's natural levee along the stretch below where the mainstem curved sharply toward the south-southwest near Pilot Knob (Brown, 1923; Kniffen, 1932). Kniffen (1932) stated:

"During the last decades of the nineteenth century there was a minor break in the Colorado near Algodones, occurring annually at the time of the summer flood. A portion of the diverted water went down to the Salton Basin

> in the channel of the Alamo. A greater portion passed through the Paredones to Volcano Lake and was there divided, the larger part passing south through the Hardy, the smaller northward through the New."

In 1850, Dr. J.L. LeConte and U.S. Army Major General S.P. Heintzelman traveled to the Salton Basin seeking mysterious "boiling springs" and volcanic features reported to be at the shore of a salt lake (LeConte 1852, 1855). Accompanied by an Indian guide, they went to the southeast portion of the central Salton Basin where they found several "volcanic mounds" about 100–150 feet (~30.5–45.7 m) high that were near the shore of a large salt lake and "arranged in the arc of a circle." The features LeConte (1855) described are the Salton Buttes, dormant rhyolite domes (Wright *et al*., 2015). When the surface elevation of the Salton Sea was approximately 227–231 feet (~69.2–70.4 m) below sea level from 2005 to 2014 before its more recent decline (Imperial Irrigation District, 2020), the southeast shore of the lake was close to the Salton Buttes (personal observations, 2005–2014). Thus, it is apparent that in 1850 there was a large lake in the Salton Basin that was the size of the modern Salton Sea, roughly 48 km (30 miles) long and 24 km (15 miles) wide.

From December 1861 to January 1862 an extraordinary period of extremely heavy precipitation lasting for approximately 43 days, likely caused by a series of major atmospheric river events (Dettinger and Ingram, 2013), caused a megaflood affecting vast expanses of the western and southwestern U.S., including Oregon, Washington, California, Nevada, Idaho, Utah, Arizona, and New Mexico. The Colorado River delta region was completely inundated, the Army's Fort Yuma at the junction of the Colorado and Gila Rivers was transformed into an island, entire settlements on the lower Gila River and lower Colorado River were washed away, and a large lake estimated to be 60 miles (96 km) long and 30 miles (48 km) wide formed in the Salton Basin (Rigg, E.A., 1862; Wheeler, G.M., 1876). In the vicinity of Lees Ferry, Arizona, between the upper and lower Colorado River basins, the 1862 flood had an extraordinary peak discharge that was estimated to be in excess of 400,000 cubic feet per second (second-feet) (Dickinson, 1944).

In February 1891, the lower Colorado River "rose to an unusually high stage, the water at that time being contributed mainly by the Gila and its tributaries. It overtopped its banks below Yuma, and submerged large areas along the Alamo and New Rivers." (Grunsky, 1907.) During a lengthy dry period preceding the February 1891 flood, those distributary channels became blocked with sediment and thick deposits of blown sand; so in February 1891 the floodwaters pooled rather than flowing onward (Grunsky, 1907; Schuyler 1907; MacDougall, 1915). But later when the usual spring high water caused the Colorado to breach its western levee in the stretch south of Pilot Knob below the U.S.-Mexico border, the already-swollen distributary channels received enough additional flow to fully erode the blockages along their courses, and floodwaters poured into the Salton Basin (Schuyler 1907). The flooding created a large lake in the central basin that was estimated to cover approximately 150-160 square miles (~388-414 km^2) (Schuyler, 1907).

Discussion

Analysis of lower Colorado River hydrodynamics and floodplain morphodynamics

By latest Pleistocene time, the lower Colorado River had developed characteristic hydrodynamics, floodplain morphodynamics, and avulsion style across its delta that were contingent on regional hydroclimate. The unique topography of the region played an important role. The well-established patterns of the river's fluvial-deltaic behavior continued through the Holocene until the river was dammed and controlled in the mid-twentieth century. There were three main patterns in the river's behavior based on different hydroclimate conditions:

(a) Average hydroclimate: During periods of typical spring high water, and sometimes as a result of large winter storms briefly yielding heavy precipitation and flash flooding in the lower Colorado River basin, the river overflowed or occasionally broke through its levee along the stretch below its junction with the Gila River, avulsed moderately, and sent a portion of its flow toward the Salton Basin. When streamflow naturally decreased, channel sedimentation increased, distributaries became blocked, and the river's flow was once again confined within the mainstem.

(b) Temporarily very wet hydroclimate: During periods of extremely high streamflow mediated by short-lived changes in the region's hydroclimate, the lower Colorado River overflowed, avulsed, bifurcated, and moved by sheetflow across its floodplain, reopening established distributary channels and creating new ones. Because of delta topography and exceedingly low base level on the north side of the delta crest, once floodwaters were streaming into the Salton Basin they became temporarily entrenched while wet climate conditions continued. When streamflow subsided significantly with a shift to a drier climate, sedimentation blocked distributaries, and the river's flow was once again limited to its mainstem channel.

(c) Prolonged periods of extremely wet hydroclimate: Lengthy periods of extraordinarily high streamflow lasting for decades, centuries, or millennia caused major, long-lived modifications to the river's floodplain geomorphology and delta. Cutbacks of distributary channels, extreme erosion at points of bifurcation, and long-term entrenchment of the river in courses delivering flow into the Salton Basin resulted in the creation and perpetuation of Lake Cahuilla. Once established, the huge lake was filled to a through-flowing condition (i.e., it was constantly overflowing

at its delta sill), or was regularly filled to the point of overflowing, or was simply sustained near its highstand level as a closed lake—depending on the amount of Colorado River streamflow available at any given time, which was in turn dictated by variations in the region's overall extremely wet hydroclimate. When the climate shifted to drier conditions, Lake Cahuilla shrank, became saline from evaporation, and may sometimes have disappeared entirely when very lengthy droughts occurred.

Although the position of the lower Colorado River's mainstem in the region below its current junction with the Gila is not known with precision for much earlier periods, historical documentation indicates that at least for the past several hundred years (until the damming and control of the river) there were four geomorphic factors crucial to the Colorado's floodplain morphodynamics in its lower reaches: (1) the sharp curve to the south-southwest near Pilot Knob made by the mainstem after briefly heading due west from its junction with the Gila; (2) the existence of an unusual elevated zone trending northeast across the central delta, and forming a pronounced drainage divide within that region; (3) the morphology and position of the delta crest in relation to the big curve near Pilot Knob; and (4) extraordinarily low regional base level north of the delta crest. In combination, these factors led with virtual inevitability to overflow, avulsion, and bifurcation of streamflow along the river's western levee at and below the curve, and to flooding into the central Salton Basin during periods of very high flow—such as occurred during 1905-07.

Other workers have suggested that base level and gradient fully determined the issue of whether the river flowed to the Gulf or to the Salton Basin throughout the Holocene. Howard and Lundstrom (2005) state, "In line with evidence that in the late Holocene the huge Salton basin filled several times to overflowing (ancestral Lake Cahuilla), an automatic delta-switching mechanism governed by changing base levels is here proposed. In this model, incised N-directed channels graded to below sea level would tend to capture the river's flow from other delta distributaries until Lake Cahuilla filled to above sea level. When the flow then switched back toward the Gulf, the lake would evaporate and the cycle would renew." Similarly, Howard *et al.* (2007) assert, "We infer that when Lake Cahuilla rose to its spillover level, the feeding distributaries silted in and lowered their grade enough to provide an impetus for the river to switch back to paths down the south side [sic] of the delta to the Sea of Cortez. Shut off from inflow, evaporation of 1.8 m/yr would dry Lake Cahuilla in a few decades, again lowering the base level below sea level and setting the stage for another cycle of northward diversion, downcutting, lake filling, and spillover."

However, this hypothesis is not consistent with the data on Lake Cahuilla developed by Li *et al.* (2008a,b), or with the historical record. Lake Cahuilla existed at its highstand level for millennia, and could not have done so if this cyclical switching model were correct. In addition, there were numerous occasions when lakes much smaller than Lake Cahuilla, with surface elevations very far below sea level, were formed by Colorado River flow into the Salton Basin; and then their filling was truncated when—notwithstanding significantly lower base level in the Salton Basin—the river's course switched back toward the Gulf of California. Thus, while base level and gradient have played important parts in the formation of Salton Basin lakes, those factors have not been fully determinative of the direction of the Colorado River's flow. Climate-related changes in streamflow, erosional capacity, sediment load and sedimentation, along with the unique geomorphology of the floodplain, have all played crucial roles.

Comparison of 1891 versus 1905

In order to understand whether the 1905 formation of the Salton Sea was truly "accidental" and caused by human negligence, or was the result of the lower Colorado River's well-established floodplain morphodynamics and avulsion style combined with regional hydroclimate, it is useful to compare what occurred in 1905 with what happened in 1891 prior to any man-made modification of the river's natural levee and distributary channels below Pilot Knob. The 1891 flood is the event selected for this comparative purpose because it is the only significant lake-creating flood that occurred prior to 1905 for which there is a gaged discharge record of the river at Yuma.

A comparison of the river discharge that resulted in the 1891 flood into the Salton Basin with the discharge that occurred during the 1905 flood shows that the conditions on the lower Colorado River during 1905 were far more hydrologically extreme than during the lake-forming flood of 1891. The extraordinarily wet conditions during 1905, in combination with the nature of the river's well-established floodplain morphodynamics and avulsion style, indicate that flooding into the Salton Basin and initiation of Salton Sea formation would have occurred that year even in the absence of man-made modifications to the river's natural levee and distributary channel.

- The location where the Colorado River bifurcated in 1905 as a result of the man-made cut in the river's levee was along the same stretch of the lower course below Pilot Knob, just below the US–Mexico border, where the river broke through its natural levee in 1891. In addition, prior to 1891 the river had previously overtopped, avulsed, and bifurcated along that same vulnerable stretch of its levee many times in the absence of any human intervention. Thus, it's reasonable to conclude that the same underlying hydrodynamic forces and characteristic floodplain dynamics were operational in 1905 as in 1891 (and in earlier floods).

- There was a delay between the river overtopping its natural levee during flash flooding in the winter of 1891 and flooding into the central Salton Basin the following spring because the river's distributary channels had previously become clogged with silt and huge deposits of blown sand during a lengthy period of drought preceding the February 1891 high water (Schuyler, 1907). For several months the winter floodwaters soaked into those accumulated sediments and ponded extensively. Then, during the spring high water and levee break, the obstructions in the distributary channels were eroded and the accumulated floodwaters were released into the central Salton Basin. In contrast, in 1905 the river had a clear course through its distributary channels into the central basin because the major blockages in those channels had already been scoured away by previous flooding (Schuyler, 1907). Thus, it's reasonable to conclude that the unblocked conditions of the distributary channels in 1905 made it even more likely that year than in 1891 that floodwaters would make their way into the central Salton Basin.
- In the winter of 1891, there was a seven-day period of extreme high water on the lower Colorado River below Yuma, as the result of major flash flooding on the Gila and its tributaries that occurred from February 23 through March 1 (Murphy, 1906; Schuyler, 1907; McGlashan and Dean, 1913). Later, the spring high water that occurred during two periods in May and June was not in itself remarkable, but it was able to break through the already-weakened western levee below Pilot Knob (Schuyler, 1907; McGlashan and Dean, 1913). In contrast, in 1905, an extraordinary series of seven major back-to-back floods occurred on the Gila River and its tributaries from January 15 to April 30 that pushed the lower Colorado River's discharge below Yuma to extreme levels for prolonged periods (Murphy, 1906; USGS, 1906; McGlashan and Dean, 1913). Following the January–April floods, very high streamflow (over 19,000 second-feet; details in the next paragraph) continued during May and July, and extreme discharge (over 50,000 second-feet; details in the next paragraph) occurred again throughout June and from the end of November to early December (Murphy, 1906; USGS, 1906; McGlashan and Dean, 1913).
- According to Schuyler (1907), as a general matter the stage of the river during which overflow began below Yuma was 22.0 feet above sea level, and at that high-water stage the lower Colorado's discharge was typically about 19,000 second-feet. Using those numbers as a low-threshold indicator for what constitutes 'very high' streamflow, and 50,000 second-feet as a low-threshold indicator for what constitutes 'extreme' streamflow, a comparison of the circumstances in 1891 and 1905 yields the conclusion that stage and discharge of the lower Colorado River below Yuma in 1905 were exceedingly high for much longer than they were in 1891. During the flood from February 23 to March 1, 1891 when gage height ranged from 23.9 to 33.2 feet, discharge significantly exceeded 19,000 second-feet for a total of seven days (McGlashan and Dean, 1913). Discharge above an extreme level of 50,000 second-feet occurred on five of the seven days. During that seven-day period the highest daily discharge achieved was 101,000 second-feet on one day (Schuyler, 1907). In May and June 1891, the gage height slightly exceeded 22.0 feet for a total of 45 days, ranging mostly from 22 to 23 feet on those days but reaching 24 to 25 feet on a total of five days (McGlashan and Dean, 1913). No measurements of the associated discharge are available for that spring high-water period. In contrast, during 1905 the gage height was above 22.0 feet on 151 days, and on 79 of those days it exceeded 25 feet. During the entire month of June it was above 27 feet, and in November it reached a maximum of 31.3 feet (USGS, 1906). Of the 148 days in 1905 for which discharge measurements are available, the river's discharge significantly exceeded 19,000 second-feet during a total of 76 days (USGS, 1906; McGlashan and Dean, 1913). Discharge higher than an extreme level of 50,000 second-feet occurred during a total of 26 days, and extraordinarily high discharge greater than 70,000 second-feet occurred on 15 of those extreme-flow days. During January-April the highest daily discharge achieved was 111,000 second-feet, and two other days had discharges well above 90,000 second-feet (Dickinson, 1944). In addition, another period of extreme streamflow occurred throughout June 1905, with discharge above 50,000 second-feet every day for which measurements are available that month (USGS 1906; McGlashan and Dean, 1913). During June 1905 the highest daily discharges achieved were 94,300 and 92,400 second-feet (Dickinson, 1944). From November 30 to December 5, 1905 another period of flash flooding with very high streamflow occurred with discharge above 19,000 second-feet on each of those days (USGS, 1906; McGlashan and Dean, 1913), and two days had extreme discharges of 103,000 and 77,360 second-feet (Dickinson, 1944).

Inevitability of Salton Basin flooding during high flows

It is important to note that even after the lower Colorado River had been forced to flow toward the Gulf of California in January 1907 by construction of an enormous rock dam across the site of the breach in the western levee, there was ongoing concern about the possibility, and even likelihood, of additional flooding into the Imperial Valley and central Salton Basin. This concern demonstrates an understanding that flooding into the Salton Basin during very high discharge conditions was a characteristic and inevitable feature of the lower Colorado River's hydrodynamic regime and floodplain morphodynamics in the event of sufficiently

wet hydroclimate. In fact, this recognition and the desire to prevent the river from flooding into the Imperial Valley and central Salton Basin formed the primary motivation for the construction of Hoover Dam and other control structures built on the upper and lower Colorado River in succeeding decades. LaRue (1925) stated:

> "To protect these lands from floods extensive levee systems have been built and must be maintained… Although millions of dollars have been spent in constructing the levees, these works alone, however well maintained, cannot assure protection from the flood menace. There is grave danger that during periods of high run-off the levees will be breached and the entire flow of the Colorado will find its way into Imperial Valley and the Salton Sea. If these valuable properties on the lower river are to be protected, dangerous stages must be prevented by holding back a part of the flood-making waters. The need for flood control is therefore urgent."

Conclusion

Formation of the Salton Sea in 1905-07 was the result of wet regional hydroclimate and the river's characteristic hydrodynamic regime, floodplain morphodynamics, and avulsion style across its delta. As a result of extremely high flows on the lower Colorado River during that period, the river behaved in exactly the same manner it had since at least the latest Pleistocene when streamflow was high: by overflowing, avulsing, bifurcating, and flooding into the Salton Basin. Formation of the Salton Sea was only "accidental" from the standpoint of the people who were trying very hard to prevent the river from flowing into the basin in the same manner it had for millennia. Were it not for their strenuous and persistent efforts to block the river's flow, the flooding would likely have been far worse.

Acknowledgements

I thank George T. Jefferson for many constructive conversations over the course of years about the Salton Basin and Lake Cahuilla, David M. Meko for assistance with Figure 4b, Christian Schoneman for logistical support, and David M. Miller and George T. Jefferson for helpful reviews of this manuscript.

References cited

Andrews, E.D., 1991. Sediment Transport in the Colorado River Basin. In Colorado River Ecology and Dam Management: Proceedings of a Symposium May 24-25, 1990, Santa Fe, New Mexico. Washington: National Academies Press. pp.54-74.

Arnal, R.E., 1961. Limnology, sedimentation, and microorganisms of the Salton Sea, California. Geological Society of America Bulletin 72:427-478.

Barringer, F., 2014. Preserving an Accident, the Salton Sea in California, for the Good of Nature. New York Times, November 10, 2014. Retrieved from: https://www.nytimes.com/2014/11/11/us/-salton-sea-migrating-birds-preserving-a-mistake-made-by-our-meddling-with-nature-.html.

Berg, N., 2013. The Salton Sea: An accidental oasis turned environmental tragedy. Retrieved from: https://medium.com/changing-city/the-salton-sea-an-accidental-oasis-turned-environmental-tragedy-4a92a650c94.

Blake, W. P., 1854. Ancient Lake in the Colorado Desert. The American Journal of Science and Arts, Second Series, 17:435-438.

Blake, W.P., 1858. Report of a Geological Reconnaissance in California. New York: H. Ballèrre, 367 pp.

Blake, W.P., 1907. Lake Cahuilla, the ancient lake of the Colorado Desert. National Geographic Magazine 18:830.

Blake, W.P., 1914. The Cahuilla Basin and Desert of the Colorado. In MacDougal, D. T. and collaborators, The Salton Sea: A Study of the Geography, the Geology, the Floristics, and the Ecology of a Desert Basin. Washington, D.C.: The Carnegie Institution of Washington. pp. 1-12.

Brown, J.S., 1923. The Salton Sea Region, California - A Geographic, Geologic, and Hydrologic Reconnaissance with a Guide to Desert Watering Places. U. S. Geol. Survey Water-Supply Paper 497, 292 pp.

Cecil-Stephens, B.A., 1891. The Colorado Desert and Its Recent Flooding. Journal of the American Geographical Society of New York, 23:367-377.

Cory, H. T., 1915. The Imperial Valley and the Salton Sink. San Francisco: John J. Newbegin. 457 pp.

Crow, R., Schwing, J.E., Karlstrom, K.E., Heizler, M.T., Pearthree, P.A., House, P.K., Dulin, S.A., Stelten, M.E., Crossey, L.J., 2019. Redefining the Age of the Colorado River: Geological Society of America Abstracts with Programs, 51:(5), Paper No. 134-9.

Dean, D.J., Topping, D.J., Schmidt, J.C., Griffiths, R.E., Sabol, T.A., 2016. Sediment supply versus local hydraulic controls on sediment transport and storage in a river with large sediment loads. J. Geophys. Res. – Earth Surf. 121 (1):82–110.

Dettinger, M. D.; Ingram, B. L., 2013. The Coming Megafloods. Scientific American, 169: 64–71.

Dibblee, T.W., Jr. 1954. Geology of the Imperial Valley region, California. In Geology of Southern California, edited by R.H. Jahns, California Division of Mines and Geology Bulletin, 170(2, 2):21-81.

Dickinson, W. E. (1944), Summary of records of surface waters at base stations in Colorado River Basin 1891–1938, U.S. Geol. Surv. Water Supply Pap. 918. Washington: Government Printing Office. 272 pp.

Dorsey, R.J. 2012. Earliest delivery of sediment from the Colorado River to the Salton Trough at 5.3 Ma: evidence from Split Mountain Gorge. In Search for the Pliocene: the southern exposures, edited by R.E. Reynolds, California State University Desert Studies Consortium, The 2012 Desert Research Symposium, pp. 88-93.

Dorsey, R.J., Housen, B.A., Janecke, S.U., Fanning, C.M., and Spears, A.L.F., 2011. Stratigraphic record of basin development within the San Andreas fault system: late Cenozoic Fish Creek-Vallecito basin, southern California. Geological Society of America Bulletin, 123:771–793.

Emory, W.H., 1848. Notes of a Military Reconnaissance from Fort Leavenworth, in Missouri, to San Diego, in California. Washington: Wendell and Van Benthuysen. 614 pp.

Farr, F.C., 1918. History of Imperial County, California. Berkeley: Elms and Franks. 516 pp.

Grunsky, C.E., 1907. The Lower Colorado River and the Salton Basin. Transactions of the American Society of Civil Engineers, LIX:1-62.

Hajek, E.A. and Edmonds, D.A., 2014. Is river avulsion style controlled by floodplain morphodynamics? Geology, 42(3):199-202.

Hardy, R.W.H., 1829. Travels in the Interior of Mexico. London: Henry Colburn and Richard Bentley. 540 pp.

Howard, K.A., and Lundstrom, S.C., 2005. The Changing Paths of the Lower Colorado River. In Geologic and Biotic Perspectives on Late Cenozoic Drainage History of the Southwestern Great Basin and Lower Colorado River Region: Conference Abstracts, edited by M.C. Reheis, U.S. Geol. Survey Open-File Report 2005–1404, pp.12-13.

Howard, K.A., Stock, G.M., Rockwell, T.K., Schafer, J., and Webb, R.H., 2007. Holocene Cyclical Switching of Colorado River Water Alternatively to the Sea of Cortez or to the Salton Sink. American Geophysical Union, Spring Meeting 2007, abstract id. H44A-05.

Howe, E.F., and Hall, W.J., 1910. The Story of the First Decade in Imperial Valley, California. Imperial: Edgar F. Howe & Sons. 291 pp.

Imperial Irrigation District Water Department, 2020. Historical Monthly Elevations of Salton Sea at Fig Tree John, 1904-2020. Obtained via personal correspondence with M. Kidwell, IID Water Master.

Ives, J.C., 1861. Report upon the Colorado River of the West: Explored in 1857 and1858. Washington: US Government Printing Office. 368 pp.

Kennan, G. 1917. The Salton Sea: An Account of Harriman's Fight With The Colorado River. New York: The MacMillan Company. Retrieved from: https://books.google.com/books?id=uw64AAAAIAAJ.

Kleinhans, M.G., Ferguson, R.I., Lane, S.N., and Hardy, R.J., 2012. Splitting rivers at their seams: bifurcation and avulsion. Earth Surface Processes and Landforms, 38(12):47-61.

Kniffen, F.B., 1932. The Natural Landscape of the Colorado Delta. University of California Publications in Geography, 5:149-244.

Larkin, E.L., 1907. A Thousand Men Against A River: The Engineering Victory Over The Colorado River And The Salton Sea". The World's Work: A History of Our Time. XIII: 8606–10. Retrieved from: https://books.google.com/books?id=3IfNAAAAMAAJ&pg=PA8606#v=onepage&q&f=false

LaRue, E. C., 1916. Colorado River and Its Utilization. U.S. Geol. Survey Water-Supply Paper 395, 257 pp.

LaRue, E.C., 1925. Water Power and Flood Control of Colorado River Below Green River, Utah. Washington: Government Printing Office. 171 pp.

LeConte, J.L., 1852. On some fossils from California. Proceedings of the Academy of Natural Sciences of Philadelphia, Vol. V, 1850 & 1851, p. 264.

LeConte, J.L., 1855. Account of Some Volcanic Springs in the Desert of the Colorado, in Southern California. The American Journal of Science and Arts, Second Series, XIX(55):1-6.

Li, H.C., Xu, X.M., Ku, T.L., You, C.F., Buchheim, H.P., Peters, R., 2008a. Isotopic and geochemical evidence of palaeoclimate changes in Salton Basin, California, during the past 20 kyr: 1. $\delta^{18}O$ and $\delta^{13}C$ records in lake tufa deposits. Palaeogeography, Palaeoclimatology, Palaeoecology, 259:182–197.

Li, H.C., You, C.F., Ku, T.L., Xu, X.M., Buchheim, H.P., Wan, N.J., Wang, R.M., Shen, M.L. 2008b. Isotopic and geochemical evidence of palaeoclimate changes in Salton Basin, California, during the past 20 kyr: 2. $^{87}Sr/^{86}Sr$ ratio in lake tufa as an indicator of connection between Colorado River and Salton Basin. Palaeogeography, Palaeoclimatology, Palaeoecology, 259:198–212.

MacDougal, D.T., 1907. The Desert Basins of the Colorado River. Bulletin of the American Geographical Society, 39(12):705-729.

MacDougal, D. T., 1914. The Salton Sea: A Study of the Geography, the Geology, the Floristics, and the Ecology of a Desert Basin. Washington, D.C.: The Carnegie Institution of Washington. 182 pp.

MacDougal, D.T., 1915. The Salton Sea. The American Journal of Science, Fourth Series, XXXIX(231):231-250.

McGlashan, H.D., and Dean, H.J., 1913. Water Resources of California, Part III, Stream Measurements in the Great Basin and Pacific Coast River Basins. Washington: Government Printing Office. 922 pp.

Meko, D.M., Woodhouse, C.A., Baisan, C.A., Knight, T., Lukas, J.J., Hughes, M.K., and Salzer, M.W., 2007. Medieval Drought in the Upper Colorado River Basin. Geophysical Research Letters, Vol. 34, L10705, doi:10.1029/2007GL029988.

Meko, D. M., and Hirschboeck, K.K., 2008. The current drought in context: A tree-ring based evaluation of water supply variability for the Salt–Verde River basin, Final Report. Available at http://www.treeflow.info/sites/default/files/SRP-II-Final-Final-Report-08-08-08.pdf (last accessed January 2020).

Muffler, L.P.J., and Doe, B.R., 1968. Composition and mean age of detritus of the Colorado River delta in the Salton Trough, southeastern California. Journal of Sedimentary Petrology 38:384-399.

Murphy, E.C. and others, 1906. Destructive Floods in the United States in 1905. Washington: Government Printing Office. 87 pp.

Nijhuis, M., 2000. Accidental Refuge: Should We Save the Salton Sea? High Country News, June 19, 2000. Retrieved from: https://www.hcn.org/issues/181/5865.

Rigg, E.A., 1862. Correspondence between Maj. E.A. Rigg and Col. J.H. Carleton, January 23, 1862. U.S. Department of War, Official Records of the Union and Confederate Armies, Ser. I, 50(P. I, Ch. LXII):815–818.

Rockwell, T.K., Meltzner, A.J., and Haaker, E.C., 2018. Dates of the Two Most Recent Surface Ruptures on the Southernmost San Andreas Fault Recalculated by Precise Dating of Lake

Cahuilla Dry Periods. Bulletin of the Seismological Society of America, 108(5A):2634–2649.

Rocque, J., 1762. A General Map of North America. London: M. A. Rocque in the Strand & A. Dury in Dukes Court St. Martins Lane. British Museum, Catalogue of Maps, Prints, and Drawings, forming the geographical and topographical collection attached to the Library of his late Majesty King George III, London, 1829.

Ross, J.E., Kidwell, S.M., Dettman, D.L., Bright, J., Dorsey, R.J., and Jefferson, G.T., 2020. Evidence of Pleistocene Marine Incursions into the Salton Basin. In Changing Facies, edited by D.M. Miller, The 2020 Desert Research Symposium, this volume.

Sarychikhina, O., Glowacka, E., Mellors, R., Suárez-Vidal, F., 2011. Land subsidence in the Cerro Prieto Geothermal Field, Baja California, Mexico, from 1994 to 2005—An integrated analysis of DInSAR, leveling and geological data. Journal of Volcanology and Geothermal Research 204:76–90.

Schuyler, J.D., 1907. The Overflow of the Colorado River into Salton Basin. Report of J.D. Schuyler, Consulting Hydraulic Engineer, dated March 20, 1907. James D. Schuyler Papers, University of California at Riverside, Water Resources Collections and Archives, Collection Number WRCA 063.

Slingerland, R., and Smith, N.D., 1998. Necessary conditions for a meandering river avulsion. Geology 26(5):435–438.

Sperry, R.L., 1975. When the Imperial Valley Fought for its Life. The Journal of San Diego History, San Diego Historical Society Quarterly, Vol. 21, No. 1. Retrieved from: https://www.sandiegohistory.org/journal/1975/january/imperial-2/.

Sykes, G., 1914. Geographical Features of the Cahuilla Basin. In MacDougal, D. T. and collaborators, The Salton Sea: A Study of the Geography, the Geology, the Floristics, and the Ecology of a Desert Basin. Washington, D.C.: The Carnegie Institution of Washington. pp.13-20.

Sykes, G., 1937. The Colorado Delta. American Geographical Society Special Publication No. 19. Washington: Carnegie Institution. 193 pp.

Tarbet, L.A. 1951. Imperial Valley. American Association of Petroleum Geologists Bulletin 35:260-263.

Thomas, R.G., 1963. The Late Pleistocene 150 Foot Fresh Water Beach Line of the Salton Sea Area. Bulletin of the Southern California Academy of Sciences, 62(1):9-17.

Tooth, S. 2000. Process, form and change in dryland rivers: a review of recent research. Earth-Science Reviews 51:67-107.

USGS, 2020. National Water Information System, USGS 10254005 Salton Sea NR Westmorland CA, water surface elevation above NGVD 1929 on 24 January 2020. Retrieved from: https://waterdata.usgs.gov/ca/nwis/uv?site_no=10254005.

Waters, M.R., 1983. Late Holocene lacustrine chronology and archaeology of ancient Lake Cahuilla, California. Quat. Res. 19(3):373–387.

Wheeler, G.M., 1876. Annual report on the geographical surveys West of the one-hundredth meridian, in California, Nevada, Utah, Colorado, Wyoming, New Mexico, Arizona, and Montana, Appendix JJ. In Annual Report of the Chief of Engineers for 1876. Washington, D.C.: Government Printing Office. 355 pp.

Wilke, P.J., 1978. Late Prehistoric Human Ecology at Lake Cahuilla, Coachella Valley, California. Berkeley: University of California Archaeological Research Facility Contributions No. 38. 168 pp.

Winker, C.D., and Kidwell, S.M., 1986. Paleocurrent evidence for lateral displacement of the Pliocene Colorado River delta by the San Andreas fault system, southeastern California. Geology, 14:788-791.

Winker, C.D., 1987. Neogene stratigraphy of the Fish Creek – Vallecito section, southern California: implications for early history of the northern Gulf of California and Colorado delta. Ph.D. dissertation, University of Arizona, Tucson, 494 p.

Winker, C.D. and Kidwell, S.M., 1996. Stratigraphy of a marine rift basin: Neogene of the western Salton Trough, California. In Field Conference Guide, edited by P.L. Abbott and J.D. Cooper, Pacific Section of American Association of Petroleum Geologists, GB 73, Pacific Section Society of Economic Paleontologists and Mineralogists, Book 80, pp. 295-336.

Woodhouse, C. A., Gray, S.T., and Meko, D.M., 2006. Updated streamflow reconstructions for the Upper Colorado River Basin. Water Resour. Res. 42, W05415, 16 pp. doi:10.1029/2005WR004455.

Wright, H. M., Vazquez, J.A., Champion, D.E., Calvert, A.T., Mangan, M.T., Stelten, M.E., Cooper, K.M., Herzig, C., and Schriener, A.Jr., 2015. Episodic Holocene Eruption of the Salton Buttes Rhyolites, California, from Paleomagnetic, U-Th, and Ar/Ar Dating. Geochemistry, Geophysics, Geosystems, 16:1198–1210.

Abstracts from proceedings: the 2020 Desert Symposium

David M. Miller, compiler
USGS retired

Freshwater turtles in the Mojave Desert: what could go wrong?

*Kristy Cummings,[1] Jeffrey E. Lovich,[1] Shellie R. Puffer,[1] and Sara Greely[2]
*[1]U. S. Geological Survey, Southwest Biological Science Center, 2255 North Gemini Dr., Flagstaff, AZ 86001, USA; [2] The Living Desert Zoo, 47900 Portola Avenue, Palm Desert, CA 92260, USA; *Email: kcummings@usgs.gov*

The southwestern pond turtle (*Emys [Actinemys] pallida*) has occupied the Mojave River drainage basin in California since at least the Pleistocene. It is mostly aquatic, with the exception of basking, egg laying, and occasional terrestrial movements and over-wintering. Using terrestrial habitat exposes aquatic turtles to increased risk of injury or mortality from predation and other environmental hazards (i.e. human activities, road mortality, etc.). Predation is a threat to the southwestern pond turtle (both terrestrially and aquatically) and the list of predators is extensive. We collected injury data from turtles at three study sites along the length of the Mojave River in San Bernardino County, California: one site in the upper reaches and two sites in the lower reaches of the river. The studies were conducted during the turtle active season between May 1998–October 1999 and again from April 2016–September 2019. A total of 84 *Emys [Actinemys] pallida* were captured between all sites and all years. Male and female turtles were visually examined for shell damage and abnormalities on the plastron and carapace and shell measurements were taken for turtle size. Injuries included tooth marks, abrasions, missing shell along the marginal scutes. and missing or damaged appendages. Abnormalities were noted when we observed variations in the normal scute patterns covering the bony shell in this species (only recorded for the upper river population). We hypothesized that, 1) female turtles would have a higher incidence of shell injuries than male turtles since the former sex are exposed to terrestrial hazards when nesting, and 2) larger (presumably older) turtles would have more injuries than smaller (younger) turtles because scars from injuries might be expected to accumulate over time. Seventeen percent (n = 8) of the turtles captured at the upper Mojave River site exhibited shell abnormalities. Sixty-eight percent (n=26) of captured turtles at both of the lower Mojave sites combined had shell damage and 78 percent (n=36) of turtles captured at the upper Mojave river site alone also displayed shell damage. A total of 74 percent (n = 62) turtles had shell damage at all sites combined. Unexpectedly, our first hypothesis was rejected. There was no statistical significance between sex and shell damage for all sites combined or between the sexes for individual sites. Larger turtles had more shell damage than smaller turtles only when all sites were considered, a possible result of increased sample size. This suggests that older turtles have more accumulated shell damage than younger turtles. However, there was no obvious relationship between shell damage and carapace length when the sites were considered individually. Turtle shell damage may be an indicator of the extent of threats facing turtles but is a poor indicator of predator efficiency.

The Paleontological Resources Preservation Act and your enjoyment of federal lands

Chris Dalu
BLM Needles, 1303 S. Highway 95, Needles, CA 92363

This presentation provides information about the Paleontological Resources Preservation Act. It covers topics regarding 1) the circumstances that led to the need for the Act, 2) the federal mandate and various parties associated with the development of the Act, 3) the foundation on which the Act is based, 4) comparisons between agency implementation and applicability of the regulations, and 5) the status of promulgating the regulations.

The Paleontological Resources Preservation Act (PRPA, the Act) became federal law (codified as 16 U.S.C. 470aaa-aaa-11e) when the Omnibus Public Land Management Act of 2009 (Public Law 111-11—Mar 30, 2009) was signed by President Obama on March 30, 2009. The PRPA was enacted to "manage and protect paleontological resources on Federal land using scientific principals and expertise" for current and future generations because "paleontological resources are a non-renewable and irreplaceable part of America's heritage". The PRPA requires that the secretaries of the Interior and Agriculture coordinate with the land-managing agencies under their jurisdiction to establish regulations by which to implement the law. Those agencies include the U.S. Forest Service (FS) under the jurisdiction of the U.S. Department of Agriculture (USDA) and the Bureau of Land Management (BLM), Bureau of Reclamation (BOR), National Park Service (NPS) and U.S. Fish and Wildlife Service (FWS) under the jurisdiction of the Department of the Interior (DOI).

On May 23, 2013, the USDA promulgated a proposed rule for the FS to implement the PRPA on National Forest

Service lands (78 FR 30810 (/citation/78-FR-30810)). On April 17, 2015, the FS published their final regulations (80 FR 21588 (/citation/80-FR-21588)). The DOI promulgated their proposed rule with respect to the Office of the Secretary of the Interior, BLM, BOR, FWS and NPS on December 12, 2017 (81 FR 88173). It is anticipated that the DOI will publish the final regulations in spring or summer of 2020. The content of this document is consistent with the draft final rule, dated 03/02/2020.

The preservation and management of paleontological resources on public land administered by federal agencies has historically been constrained by a lack of authority, and laws specifically designed to protect and classify them as a unique class of non-renewable natural resources that provide various information on past life and conditions on earth. Misclassifications are thought to have been derived by English and Scottish mining laws that defined a mineral as a "fossil, or what is dug out of the earth, and which is of a predominantly metalliferous character". Paleontology throughout most of American history was conducted by professional and amateur paleontologists and museum curators who were motivated by the prospect of making new discoveries that would be displayed in museums and studied. As America expanded west in the latter part of the 19th century, so too did paleontological expeditions to excavate the numerous fossil localities in the western states, which were hauled to museums in the eastern states. This movement was epitomized by the "great dinosaur rush" or "bone wars", which included Othniel Marsh and Edward Drinker competing to find new fossils. The competition was heavily covered by radio and newspapers, which in turn inspired many Americans to look for fossils as a recreational activity.

In 1915, the first landmark decision for the protection of paleontological resources occurred when Earl Douglass, a paleontologist working for Carnegie Museum, located a placer claim in 1913 that consisted of dinosaur bones. The General Land Office cancelled the mineral entry. Douglass appealed the decision, but the Department of Interior ruled that "fossil remains of dinosaurs and other prehistoric animals are not mineral within the meaning of the United States mining laws and lands containing such remains are not subject to entry under such laws." The decision served to directly differentiate vertebrate fossils from minerals, while also indirectly recognizing the scientific value of vertebrate fossils. However, it left the whole class of invertebrate fossils as minerals, some of which are still considered minerals. For instance, coral and amber are locatable minerals. Diatomite, coal, oil, tar and some phosphates are leasable minerals. Petrified wood, coquina, some limestone, fossil-bearing flagstone and other building stone or decorative rock are considered saleable mineral material.

The lack of laws specifically designed to protect paleontological resources led to the Antiquities Act of 1906 or the NPS Organic Act of 1916 being used as the authorities to protect paleontological resources, in which case they were classified as antiquities or natural and historic objects. Between 1956 and 1974, variable decisions issued by DOI solicitors indicated use of the Antiquities Act to protect paleontological resources was questionable. In 1974, the 9th Circuit Court's U.S. v. Diaz decision ruled the term "object of Antiquity" to be unconstitutionally vague, which clearly shifted the balance away from reliance on the Antiquities Act to protect fossils. The U.S. v. Diaz case led to the Archaeological Resources Protection Act of 1979 (ARPA), which provided for the protection of only those paleontological resources that are in context and part of an archaeological site. A 1978 Federal Register notice of proposed rulemaking for the Preservation of American Antiquities included an end note that suggested the DOI was considering alternatives for paleontological specimens as "objects of scientific interest" aside from "objects of antiquity", and vertebrate specimens would continue to receive full protection under the act. The end notes also included a provision that if invertebrate and paleobotanical specimens were determined to be rare and endangered, such localities would also receive protection. However, no final rule/regulation followed. Other laws that provided some protection for vertebrate fossils included the 1960 Archaeological and Paleontological Salvage for Federal Highway Project, the National Environmental Policy Act of 1970 and the Federal Cave Resources Protection Act of 1988. The most effective modern law to provide the means to protect or mitigate impacts to paleontological resources was the Federal Land Policy and Management Act of 1976 (FLPMA), because paleontological resources could be considered in the environmental review associated with authorizations issued pursuant to FLPMA, such as mineral leasing rights-of-way (ROW), land management plans, renewable energy ROW, among others.

The management of paleontological resources on federal-administered land has always been highly dependent on the mission of each agency, the amount of land they manage and the availability of staff and funding. Although by the mid-1980s, laws, policies and precedence afforded some level of protection to paleontological resources because of their scientific values, there was a complete lack of any proactive activities and funding to develop a program. Other constraints in managing paleontological resources included: 1) the lack of staff paleontologists, 2) the lobbying strength of the mining industry as they challenged revisions to the Mining Law of 1872 that were proposed in FLPMA) 3) the BLM's paleontology program being managed by the BLM's Division of Geology and Mineral Resources, and, 4) the tendency for agency staff to place a higher priority on the mineral and recreational values of paleontological resources.

Over the past 35 years, there have been two periods of significant shifts towards effectively changing the paradigm of paleontological resources management on federal land, which led to the PRPA. The first came in 1984

when the USDA and DOI secretaries delegated to agency offices the authority to issue paleontological permits. That same year, a BLM reorganization transferred to the Division of Recreation, Cultural and Wilderness Resources the paleontological program, and assigned Carl Barna as the program lead. This fostered more of a focus on the proactive survey and management of resources, which in subsequent years under strong program leads provided paleontological resources management training to field office archaeologists and geologists, assigned regional paleontologists, created procedural manuals and handbooks, produced outreach materials and most recently developed the Potential Fossil Yield Classification (PFYC) system. Between 1984 and 1996, there were earnest attempts from the FS and BLM to generate laws and regulations to protect paleontological resources. The second important shift occurred in 1999, when the Senate Interior Appropriations Subcommittee requested that the DOI, the USDA and the Smithsonian Institution prepare a report on fossil resource management on federal lands. The request directed these entities to analyze: (1) the need for a unified federal policy for the collection, storage, and preservation of fossils, (2) the need for standards that would maximize the availability of fossils for scientific study, and, (3) the effectiveness of current methods for storing and preserving fossils collected from federal lands. The resultant DOI report to Congress, "Assessment of Fossil Management of Federal and Indian Lands," included significant public input from professional and amateur paleontologists, organizations such as the Society for Vertebrate Paleontology, as well as the Bureau of Indian Affairs, the BLM, BOR, FWS, FS, the US Geological Survey, and the Smithsonian. This report indicated that there is already in place a fundamental level of uniformity with regards to the need for a unified policy toward collection, storage and preservation of fossils, and the accessibility of fossils for scientific study and education. The report specified that administrative and congressional actions pertaining to fossils should be governed by the following seven basic principles:

1. Fossils on federal lands are a part of America's heritage.
2. Most vertebrate fossils are rare.
3. Some invertebrate and plant fossils are rare.
4. Penalties for fossil theft should be strengthened.
5. Effective stewardship requires accurate information.
6. Federal fossil collections should be preserved and available for research and public education.
7. Federal fossil management should emphasize opportunities for public involvement.

Much of the fundamental framework of the PRPA was derived from the content of this DOI report. In less than two years, lawmakers of the 107th Congress pulled information from this report and drafted H.R. 2974, the 2001 version of the PRPA. However, it was not until the 111th Congress in 2009 that the PRPA was finally approved by the House and Senate as part of a large Omnibus Bill. The PRPA directly addresses many paleontological resources management issues that in the past had been based on legal opinions, court precedence and federal laws that govern the management of other resources. The PRPA consists of 12 sections: Sec. 6301) Definitions, 6302) Management, 6303) Public awareness and education program, 6304) Collection of paleontological resources, 6305) Curation of resources, 6306) Prohibited acts and criminal penalties, 6307) Civil penalties, 6308) Rewards and forfeiture, 6309) Confidentiality, 6310) Regulations, 6311) Savings provision, and, 6312) Authorization of appropriations. The PRPA is structured very much like ARPA in form and intent. Each law consists of six pages, and each is broken up into 12 sections of content, of which seven sections are identically named and two others have similar names that address the same subject matter.

The PRPA defines paleontological resources as "any fossilized remains, traces, or imprints of organisms, preserved in or on the earth's crust, that are of paleontological interest and that provide information about the history of life on earth, except that the term does not include any materials associated with an archaeological resource (as defined in section 3(1) of ARPA, or any cultural item (as defined in section 2 of the Native American Graves Protection and Repatriation Act (25 U.S.C. 3001))". The PRPA specifies that "paleontological resources on Federal land are to be managed and protected using scientific principals and expertise". The PRPA establishes 1) felony level criminal penalties, 2) civil penalties for non-criminal violations, 3) hearing procedures and, 4) the means to assess a penalty based on paleontological and commercial value. The PRPA also authorizes rewards to any members of the public that provide information leading to a criminal conviction or a finding of a civil violation.

One aspect of the PRPA that stands out as unique among various federal environmental laws and policies, is that it allows the authorized officer to follow a process that includes consulting with regional or lead paleontologists, private sector paleontologists, office staff or others with specific expertise to conclude that specimens that are found to be redundant, lack adequate associated data, or otherwise are determined not to further or no longer further paleontological knowledge, public education, or management of paleontological resources may be removed from museum collections and placed into working collections.

It is worth noting what the PRPA does not do. The PRPA and its implementing regulations does not impose additional requirements on activities permitted under general mining or mineral laws, and it does not apply to land other than those lands administered by the BLM, BOR, FS, FWS and NPS. This means that the bureaus will not add requirements under PRPA and the proposed rule

Table 1: Variability in approach to "Casual Collecting"

	BLM	BOR	FWS	NPS	USDA	National Monuments
Is casual collecting allowed?	Yes, unless area is closed and if collected in a certain manner (see definition below)	Yes, but only in specific areas designated for casual collecting	No	No	Yes, unless area is closed and consistent with the commonplace meaning of casual (see definition below)	Not allowed in FS Monuments. Could be allowed in BLM Monuments if included in Monument management plan.
What is negligible disturbance?	Little or no change to the surface of the land (see definition below)	Same as BLM	NA	NA	The Authorized Officer has discretion to determine what constitutes negligible disturbance	Specific to Agency definition.
What are Reasonable Amounts?	25 pounds per day per collector, not to exceed 100 pounds per year per collector. Pooling not allowed.	Same as BLM, unless specified otherwise in designated area information	NA	NA	Same as BLM	FS – NA BLM – dependent on whether Monument management plan would set a limit.
Petrified wood-locatable mineral, or saleable mineral, or free-use mineral, or paleo resource or gemstone	Managed as mineral resource subject to commercial sale and free-use regulations but under PRPA, could be a paleontological resource – (see definitions)	Managed as paleo resource	Managed as paleo resource	Managed as paleo resource	Managed as a mineral in accordance with the FS petrified wood regulation, but Officer can determine an occurrence is a paleo resource (see definition)	Dependent on Monument management plan.

to mining- and mineral-related permits. For example, the PRPA cannot be the justification to require mitigation measures for a mining operation. However, because PRPA does not limit the applicability of other legal authorities such as the Mining in the Parks Act and FLPMA, the bureaus may continue to cite those other authorities as protection for paleontological resources when authorizing land or resource uses under those authorities.

The PRPA directs the Secretary to allow casual collecting of common invertebrate and plant paleontological resources without a permit on land administered by the BLM, BOR and FS. The PRPA is relatively specific and explicit, with one exception. The definition of "casual collecting" and its descriptive terminology is inexplicit, which requires the regulations to clarify the meaning of the ambiguous terms. It appears this vagueness was intentional, as it allows for flexibility in agency policies and requirements to accommodate the different mandates of each agency.

The PRPA states the following:

> the term "casual collecting" means the collecting of a reasonable amount of common invertebrate and plant paleontological resources for non-commercial personal use, either by surface collection or the use of nonpowered hand tools resulting in only negligible disturbance to the Earth's surface and other resources. As used in this paragraph, the terms "reasonable amount", "common invertebrate and plant paleontological resources" and "negligible disturbance" shall be determined by the Secretary.

Matters relating to "casual collecting" clearly represent the greatest amount of variation in approach between the bureaus/departments, and those differences are summarized in Table 1, and described more fully in the definitions that follow Table 1.

Definitions

1. Casual Collecting on BLM, BOR and FS land (five underlined phrases represent the five conditions that must be met to be considered casual collecting): the collecting without a permit of a reasonable amount of common invertebrate or plant paleontological resources for non-commercial personal use, either by surface collection or the use of non-powered hand tools, resulting in only negligible disturbance to the Earth's surface or paleontological or other resources.

> a. Specific to FS: as stated in the final rule discussion: "The Department considers that in establishing the term "casual collection" rather than "amateur collection" or "hobby collection" or "recreational collection", the Act intended that casual collection reflect the commonplace meaning of "casual," which includes the elements "happening by chance; not planned or expected",

"done without much thought, effort, or concern", and "occurring without regularity".

b. Specific to FS: Casual collecting is not allowed in national monuments or other specially designated lands managed by the FS, or on any lands that the authorized officer has closed to casual collecting.

c. Specific to BLM: Casual collecting is not allowed in BLM-administered national monuments, BLM-administered national conservation areas, outstanding natural areas, forest reserves, or cooperative management and protection areas, except where the bureau has specifically determined that casual collection would not impair the intent of the preservation designation, or where allowed by other statutes, executive orders, regulations, or land use plans.

d. Specific to BLM and BOR: The DOI PRPA regulations at 43 CFR 49.805(c) would clearly place full responsibility on persons interested in casual collecting to ascertain which bureau manages the land where those persons would like to collect paleontological resources, whether the land is open to casual collecting, and what may be collected in an area, and to obtain information about the managing bureau's casual collecting procedures.

2. **Negligible Disturbance** on BLM and BOR land: Little or no change to the surface of the land and minimal or no effect to natural and cultural resources, specifically,

a. Specific to BLM and BOR: Surface disturbance cannot exceed one square yard per individual collector

b. Specific to BLM and BOR: For multiple collectors, each square yard of surface disturbance must be separated by at least 10 feet.

c. Specific to BLM and BOR: All areas of surface disturbance must be backfilled with the material that was removed so as to render the disturbance substantially unnoticeable to the casual observer.

3. Petrified Wood on BLM: The management of petrified wood on public land administered by the BLM is somewhat complex because it has been managed as a locatable mineral, saleable mineral, free-use mineral, a plant paleontological resource, as well as it was historically managed as a locatable mineral resource under the 1872 Mining Law.

a. As a locatable mineral, the removal was causing extreme damage to public land, and any claimed material was not available to the public.

b. In the 1960s petrified wood was determined to be a saleable and free-use mineral under the Mineral Materials Act. As a saleable mineral, commercial sale can be competitive or non-competitive. As a free-use mineral, collection must be for personal use, cannot be bartered or sold and collection was limited to 25 pounds per day plus one piece per person, and annual limit is 250 pounds.

i. Free use permits are available to nonprofit organizations with limits up to 5,000 cubic yards or weight equivalent in any 12 consecutive months, and permitee must show it will not be used for commercial or industrial purposes.

c. Petrified wood cannot be casually collected under 43 CFR 8365.1-5) Visitor Services, Rules of Conduct) because 1) the authority for disposal is the Mineral Materials Act of 1947, and 2) casual collection is a recreational activity conducted under the authority of FLPMA.

d. After the DOI publishes the final rule for the PRPA, petrified wood could be considered a paleontological resource if a professional paleontologist can show that a petrified wood locality is a significant paleontological resource, in which case the collection must be conducted under a permit and the material submitted to a museum. Whether this will be tested when the final regulation is published in unknown.

Preliminary results of geologic mapping in and around the Blackwater Well 7.5-minute quadrangle, central Mojave Desert, CA

Tracey J. Felger
U. S. Geological Survey, 2255 N. Gemini Dr, Flagstaff, AZ 86001, tfelger@usgs.gov

The Blackwater Well 7.5-minute quadrangle is in the central Mojave Desert and within the Eastern California Shear Zone (ECSZ). The map area is ~20 km south of the Garlock Fault and includes a 25 km-long portion of the Blackwater Fault, the trace of which has an average northwest-trend of ~320°. Previous work has proposed that the Blackwater Fault is a right-lateral fault with Quaternary offset that accommodates "a significant proportion of active right slip across the ECSZ". On the southwest side of the Blackwater Fault, rhyolite outcrops form a northwest-trending string of hills. These outcrops, mapped by previous workers as Tertiary-age hypabyssal intrusions, appear to be structurally controlled and therefore may be important for understanding the evolution of the Blackwater Fault and the ECSZ. Detailed mapping of the area is being conducted in part to characterize these outcrops and their relation to the

Blackwater Fault. Following is a summary of preliminary results from this mapping effort, combined with important information from previous investigations.

The main geologic units within the map area are: 1) Mesozoic plutonic rocks; 2) Miocene volcanic rocks of mafic, intermediate, and felsic compositions, and associated volcaniclastic rocks; 3) Miocene sedimentary rocks, and; 4) Quaternary surficial deposits.

Mesozoic plutonic rocks of granitic to dioritic composition are widespread throughout the map area. K-Ar analyses of biotite and hornblende by previous workers from multiple samples in and immediately adjacent to the map area produced late Cretaceous ages of ~70 to 80 Ma. Dikes of aplite and lesser pegmatite are prevalent, as are xenoliths and/or mafic magmatic enclaves. Most of the observed dikes are one to several meters thick, can be traced for 10s to 100s of meters, and have a consistent average southeast strike and southwest dip of ~130°/40° (± 10° for both strike and dip); however, at some locations aplite-pegmatite forms large, irregularly-shaped bodies that may represent dike swarms, or smaller intrusions within the larger plutonic bodies. These outcrops are more resistant and typically form higher-relief topography relative to the coarser-grained, grussy-weathering country rock. The Blackwater Fault cuts the plutonic rocks, and at several locations is well-expressed as a northeast-facing scarp that is one to several meters high and several kilometers in length. In the central part of the map area, ~2.5 km west of and parallel to the current trace of the Blackwater Fault, is a southwest-facing scarp ~ 2 m high. The scarp separates Mesozoic plutonic rocks to the east from Quaternary surficial deposits that overlie plutonic rocks to the west and may represent an old strand of the Blackwater Fault, or may simply reflect a lithologic difference in the plutonic rocks.

Miocene volcanic rocks intrude and overlie the Mesozoic plutonic rocks, and include basalt, rhyolite and associated volcaniclastic rocks, and dacite. In the Black Hills in the northern part of the map area, basalt flows are exposed east of the Blackwater Fault. The flows, which are undated but inferred to be early Miocene in age (~20 to 22 Ma), nonconformably overlie decomposed granitic rocks. The basalt has sparse phenocrysts of plagioclase and pyroxene, and possible xenocrysts of quartz. The flows are tabular, with a total thickness of ~100 m. The basalt is not cut by the Blackwater Fault but is deformed by small normal faults.

Rhyolite occurs as intrusions, domes, and flows, with associated volcaniclastic units present locally. Outcrops are well-foliated and generally have < 10% total phenocrysts of sanidine, quartz, and plagioclase 2 mm or less in size. Biotite is present locally. None of the outcrops in the map area have radiometric ages, but they are inferred to be correlative to similar units south of the map area, which are early Miocene in age. Previous workers analyzed a sample from the Gravel Hills that yielded a whole rock K-Ar age of 18.9 ± 1.3 Ma. The rhyolite generally intrudes or directly overlies the Mesozoic plutonic rocks, which show little to no weathering or decomposition at the contact. Black vitrophyre is present locally at the contact and is generally less than 1 m thick. Columnar joints are also present locally at the contact, and are typically ~10 cm in diameter, < 1 m in length, and oriented perpendicular to the contact. Cogenetic volcaniclastic units have only been observed at two locations thus far – at the rhyolite dome north of Blackwater Well and under the rhyolite flow in the southwest part of the map area, southeast of the Cuddeback Lake landing strip. At both locations the volcaniclastic units are mainly grayish tuff and tuffaceous sandstone with abundant pumice. Outcrops vary from well-bedded to massive, and probably represent airfall and possibly small pyroclastic flow deposits. Most of the rhyolite outcrops form long, narrow ridges and dome-shaped buttes that rise up to 250 m above the surrounding alluvial surface, forming the most prominent topographic features in the map area. They are strongly aligned along a northwest trend, suggestive of structural control. The dominant trend is ~300°, with subordinate trends of ~320° (parallel to the Blackwater Fault), and ~65°. The rhyolite outcrops are not cut by the Blackwater Fault and are found only to the west of the fault. The alignment of the outcrops, coupled with their spatial relation to the Blackwater Fault, could indicate that they were emplaced along an older, inactive splay of the Blackwater Fault, or (based on their inferred age) they may reflect the tectonic regime of the Mojave Extensional Belt that existed prior to inception of the ECSZ.

Dacite forms a prominent mesa in the Black Hills that is ~5 km long and up to ~2.5 km wide. The dacite has small lath-shaped phenocrysts of hornblende in a fine-grained matrix that varies from devitrified to glassy. Glass from the flow was analyzed by previous investigators and produced a late Miocene 40Ar/39Ar age of 7.23 ± 1.07 Ma. The dacite is ~100 m thick and generally well-foliated. Low-relief, arcuate ridges on the surface of the mesa suggest that the dacite erupted from a vent near the south end of the mesa and flowed north across Mesozoic plutonic rocks. A conglomerate composed primarily of rhyolite boulders up to 4 m in diameter, and lesser, smaller boulders and cobbles of fine- and coarse-grained plutonic rocks is locally exposed under the west side of the flow. Pumice tuff and vitric lapilli tuff are also exposed under the west side of the flow. The relation between the conglomerate and tuff units is currently unclear, as is the spatial extent of those units. Furthermore, it is unclear if the tuff units are rhyolitic or dacitic in composition. If they are dacitic, it would indicate that the eruption that produced the dacite flows had an explosive component as well as an effusive one. Some dacite boulders observed in old Quaternary alluvial deposits west of the mesa are interpreted to be breadcrust bombs of an explosive eruption. The Blackwater Fault cuts the dacite flows along the southwest edge of the mesa and is expressed as a

series of linear topographic features (mostly notches and valleys). Mapping to date is insufficient to characterize the style and amount of offset; however, previous investigators have used features in the dacite as markers to infer up 1.8 km of right-lateral offset.

Sedimentary rocks that are not genetically related to the volcanic units described above have thus far only been observed at two locations in the map area, and include: 1) poorly sorted conglomerate of granitic clasts and thin-bedded tuffaceous limestone underlying the rhyolite flow in the southwest part of the map area, and; 2) boulder conglomerate (described above) that locally underlies the dacite flows in the Black Hills. The overall lack of these types of deposits, coupled with the volcanic units being deposited directly on the Mesozoic plutonic rocks in most cases, suggests that the landscape that existed during Miocene time was probably dominated by pediments of Mesozoic plutonic rocks similar to the modern landscape.

Surficial deposits and features of Quaternary age are widespread throughout the map area and include alluvial fans of several generations (some possibly as old as Pliocene), pediments, talus and colluvium, and groundwater discharge deposits. The alluvial units are composed dominantly of grussy material derived from the plutonic rocks. Talus and colluvial deposits are concentrated around the high-relief terrain formed by the volcanic rocks. A large area of groundwater discharge deposits is present in the southeast corner of the map area, along the trace of the Blackwater Fault. In the northern part of the map area, west of the Black Hills, alluvial fans tentatively designated as old- (middle to early Pleistocene) and intermediate-age (late to middle Pleistocene) have northeast-facing scarps associated with the Blackwater Fault.

Initial fieldwork has focused on developing a framework of map units that can be systematically applied across the map area and can inform on the evolution of the ECSZ. Future efforts will focus on developing a comprehensive large-scale geologic map of the area that will include geochronology and geochemistry data for the volcanic units, and improved characterization of the geometry and kinematic history of Blackwater Fault.

A case study of photogrammetry: how technological developments are providing better insight into the recovery of life after the end-Triassic extinction

Sarah E. Grove, Drew Clark, and Stephen M. Rowland
Department of Geoscience, University of Nevada, Las Vegas
4505 S. Maryland Pkwy Las Vegas, NV 89154-4010

We have used recently developed methods to examine the paleoecology, sedimentology, and ichnology of the fluvial and eolian sediments that immediately postdate the extinction event at the end of the Triassic Period (201.3 Ma). Documentation of significant physical features has been an integral part of the scientific process for as long as people have participated in organized data collection. Earth scientists encounter unique challenges related to scope, complexity, and preservation of the features of their interest. As our questions become more complex the advances in technology have generally kept pace.

Today, the use of digital imaging, processing, and modelling have opened a new realm of possibility as it relates to data accessibility, interpretive potential, and preservation. Photogrammetry has become the newest tool utilized by those interested in three-dimensional modelling, large-scale off-site analyses, or preservation in general.

The use of photogrammetry is particularly useful in the fields of anthropology and paleontology where in-situ documentation to preserve context is of the utmost importance. In addition to the traditional utility of photographs, this developing technology is allowing precise measurements even after weathering, removal, or vandalism have altered a site. Preservation and shareability of three-dimensional models can dramatically increase the accessibility of field-based analyses to those unable to directly access the area or features in question.

Photogrammetry has been particularly useful in this study by improving the accuracy and speed of documentation and preservation of ichnological features around the Las Vegas Valley. The improvement in data quality and collection has allowed much more rapid and accurate interpretation of sites within the Jurassic Aztec Sandstone. Preservation of these trace fossils and the adjacent sedimentary textures are providing insights into the faunal assemblage, paleoecology, and climatic variation of the Early to Middle Jurassic Period of present-day southern Nevada.

Standing on the edge of the erg: how the Jurassic Aztec Sandstone fits into the development of the western margin of Pangea

Sarah E. Grove and Stephen M. Rowland
Department of Geoscience, University of Nevada, Las Vegas
4505 S. Maryland Pkwy Las Vegas, NV 89154-4010

The Jurassic Aztec Sandstone is relatively correlative to the well-studied Navajo and Nugget Sandstones and is exposed in southern Nevada and adjacent southeastern California, but is often neglected in reconstructions of the erg system to which it belongs. The fossiliferous Nugget and Navajo Sandstones were deposited approximately 200-170 Ma and are exposed, mainly in cross-bedded dunesets, across Idaho, Wyoming, Colorado, Utah, and Arizona. Despite being the southwestern-most edge of one continuous erg system, the Aztec Sandstone has yet to provide any indication of body fossil preservation. Through boots-on-the-ground citizen science, technological advancement, and collaboration with local researchers the 21st century has brought ichnofossils (trace fossils) in Jurassic-age outcrops of Southern Nevada to the forefront of paleontological research efforts.

Over 60 tracksites have been reported in Red Rock Canyon National Conservation Area, Valley of Fire State Park, and Gold Butte National Monument. Examination and documentation of suitable trackways and their host rock provide insight into the depositional environment and the potential that the Aztec Sandstone records multiple pluvial intervals immediately following the end-Triassic extinction. Three-dimensional reconstructions and field-collected data allow us a unique perspective of behavioral patterns of the taxonomically diverse faunal assemblage present as well as the paleoecological setting in which life begins to recover and thrive.

The exact mechanisms and timing of deposition of the erg system are still enigmatic, but are increasingly more accessible through the use of modernized, interdisciplinary techniques. Use of geochronologic analyses of inter-dune carbonates, photogrammetric reconstructions of ichnological features, and geospatial referencing enable us to take a deeper look at the stratigraphic successions of the Aztec. This allows us to continue to demystify the development of the western margin of Pangea.

Flying squirrels and the Mojave, old and new questions

Peggy Eby-Howe and Tom Howe
Lake Arrowhead, CA 92352. peby2thowe@cs.com

The flying squirrels of the San Bernardino Mountains (*Glaucomys oregonensis californicus*) in many ways owe their existence to the development of the Mojave Desert. They are perched on their "sky island" at the headwaters of the Mojave River, after becoming isolated from their nearest related subspecies at the end of the Pleistocene. Fortunately, the sky island of the San Bernardino Mountains provided an ideal niche with many of the features the squirrels needed to survive and flourish. The Big Bear and Lake Arrowhead watershed provides plenty of water, good forest duff to provide the fungi they love, and a relatively dense canopy of conifer/deciduous growth. Add to that the modern addition of bird seed from the human residents, and this extremely adaptable little animal has endured.

Most researchers agree, and molecular studies have shown, that the flying squirrel originated from tree squirrels near the Oligocene/Miocene transition about 22 million years ago (mya). Molecular studies have also indicated a "sister" relationship to North American tree squirrels. The New World *Glaucomys* group split from the Asian flying squirrels 4 to 6 million years after splitting from tree squirrels, approximately 16 mya, leading to a probable Beringian dispersal into North America.

Older flying squirrels appeared in the Mojave about 18 mya in the mid-Hemingfordian LMA of the Cajon Valley and Crowder formations. By the Barstovian LMA (16–13 mya) they appeared in Barstow's Mud Hills as two examples of Petauristinae: one squirrel (*Sciuropterus jamesi*) possibly larger than today's *Glaucomys*, and a much smaller squirrel (*Sciuropterus minimus*). In Cuayama Valley, the Petauristinae record continues through the Clarendonian LMA.

Because identifications are based on cheek teeth and not postcranial fossils, questions can be raised about the accurate determination of true flying squirrels versus a different species of arboreal squirrel. Although the confusing variability of extinct and extant flying squirrel teeth makes it difficult to know for sure, the fossils do indicate the squirrels are from an arboreal environment, which in turn helps define the ecosystem for that locality.

Many of our early questions have been answered with recent research, but still leave us with a series of questions:

- Why do the flying squirrels glide while their "sister" tree squirrels don't? Both experienced the same environmental pressures of the Miocene climatic optimum.
- After their Miocene split, *Glaucomys* disappears in the fossil record until the Pleistocene. What happened in regard to their development during that period of time?
- Why do North American *Glaucomys* now fluoresce pink under ultraviolet light? Is this a possible development during that pre-Pleistocene time?

Camel tracks and stromatolites in a Miocene–Pliocene ephemeral lake deposit, Muddy Creek Formation near Mesquite, Nevada

AnnMarie Jones and Stephen M. Rowland
Department of Geoscience, University of Nevada Las Vegas, 4505 S Maryland Pkwy, Las Vegas, NV, 89154-4010, jonesa27@ unlv.nevada.com

A recently discovered camel tracksite near Mesquite, Nevada occurs in the Miocene–Pliocene Muddy Creek Formation. Seventeen variously oriented Lamaichnum tracks are exposed. Additional tracks are probably concealed by a soil crust that partially covers the track-bearing surface. The tracks are preserved as impressions into a 4-cm-thick, gray, silty limestone which is cracked and rapidly eroding away. On the basis of size and orientation of the tracks, we infer that at least three individuals are represented, and possibly as many as five. We are using photogrammetry to study this tracksite, as well as to digitally capture and preserve its evanescent features.

Sixty-five meters from the camel tracks, the same gray, silty limestone is exposed as a much thicker (~90 cm) interval packed with unusual, cm-scale stromatolites. Individual stromatolites are separated from one another, and they are floating in the limey matrix. Bands of silt are interbedded with some of the stromatolitic laminae, presumably recording dust storms that deposited silt in the lake.

We interpret this camel-track-and-stromatolite-bearing interval to record an ephemeral lake that developed during a rare, high-water-table episode within the

fluvial-and-eolian-dominated Muddy Creek Formation in the Mesquite region. No other carbonate beds have been reported in this region. Because stromatolites are slow-growing microbial structures, their presence in this deposit implies that the deeper portions of this lake existed continuously for decades, and possibly for a century or longer.

Understanding a century of vegetation change on the Colorado Plateau using repeat photography

Anne E. Kelly,* Evelyn Chang, Robert H. Webb, Michael Miller, Jayne Belnap, and Michael C. Duniway
**CSU Desert Studies Center, PO Box 490, Baker CA 92309; ankelly@fullerton.edu*

Vegetation in dryland ecosystems is highly sensitive to changes in precipitation amount and timing. Globally, forecasted increases in climate aridity and variability in these regions are likely to alter vegetation dramatically. The Colorado Plateau (CP) is an important dryland ecoregion in the southwest United States for which drier and more variable conditions are forecast. Vegetation across much of the CP has already undergone significant changes during the past century that have been largely attributed to grazing intensity and multidecadal shifts in precipitation regime. Long-lived native tree and shrub species (*Populus fremontii* and *Salix exigua*) as well as non-natives (*Tamarix chinensis* and *Eleaegnus angustifolia*) have filled previously barren streambeds, shifted plant functional type dominance, and remote areas have been colonized by invasive annual plant species. These large shifts in plant functional type have changed leaf area, phenology, and net primary productivity in many habitats, consequently altering the magnitude and timing of evapotranspiration and soil drying. We combine 100 years of historic repeat photography with remote sensing and field observations from across southeastern Utah, USA, to build a model of local water balance with respect to state changes in vegetation, climate, and land use. This model will aid in understanding how vegetation changes influence water cycling, and how climatic and edaphic factors limit the scope of vegetation change.

Geomagnetic polarity recalibration, upper unit of continental Hector Formation, northeastern Cady Mountains, San Bernardino County, southern California—implications regarding refined correlations and North American land mammal subage assignments for Hemingfordian Upper Cady Mountains Local Faunas and correlative assemblages containing earlier records of *Parapliohippus carrizoensis* (Mammalia, Perissodactyla, Equidae)

E. Bruce Lander
Paleo Environmental Associates, Inc., 2248 Winrock Avenue, Altadena, CA 91001-3205, paleo@earthlink.net, and Research Associate, Natural History Museum of Los Angeles County Vertebrate Paleontology Department, 900 Exposition Boulevard, Los Angeles, CA 90007-4057, USA, paleo@earthlink.net

The Hector Fm. underlies parts of the northeastern (NE) Cady Mountains (CadyMtns.) in the central Mojave Desert Province (MDProv.) of southern California (SoCal). It contains land mammal local faunas (LFs) of Hemingfordian (He) age. The upper part of its middle unit (MU) and the overlying Peach Springs Tuff (PST) occur in magnetozone (MZ) N6, previously correlated by successive authors with Chrons C5Dr.1n, C5En, and C6n. Later elements of the earliest He upper Lower CadyMtns. LF occur in the MU's lower part. Fault C separates the PST from the Hector Fm.'s overlying upper unit (UU). The UU comprises three MZs (R7–R8) correspondingly referred by the same authors to Chrons C5Dr.1r–C5Cr, C5Dr.2r–C5Cr, and C5Er–C5Dr.1r, respectively. Chronal assignments relied primarily on K-Ar and $^{40}Ar/^{39}Ar$ (Ar/Ar) dates then accepted for the PST. A new weighted regional mean Ar/Ar age of 18.814 ± 0.065 Ma is entirely consistent with MZ N6's assignment to Chron C6n, which spans the period 18.748–19.722 Ma ago. The new date is a compilation of 189 previously published ages generated by single-crystal laser-fusion analyses of sanidine phenocrysts. As necessary and to conform with the 2012 (but not forthcoming 2020) Geologic Time Scale, those ages were recalculated using "*ArArReCalc*" to account for (1) the more recent, total ^{40}K decay constant of 0.5463 ± 0.0107 Ga^{-1} and (2) the currently accepted Ar/Ar date of 28.201 ± 0.046 Ma for the Fish Canyon Tuff sanidine fluence monitor or calibration standard.

MZs N7–R8 in the Hector Fm.'s UU yielded the Upper CadyMtns. LFs (UCadyMLFs). Lowest and highest local stratigraphic occurrences (LLSOs and HLSOs, respectively) of the equid *Parapliohippus carrizoensis* and the camelid *Paramiolabis tenuis* bracket the fossil-bearing interval and local records of the camelid cf. "*Aepycamelus*" (= "*A.*" cf. "*A.*" *priscus*). *Parapliohippus carrizoensis*, which includes "*Merychippus*" *tehachapiensis*, is the type species for its monotypic genus, whereas *P. tenuis* and "*A.*" cf. "*A.*" *priscus* are their respective genera's type and earliest species. The UCadyMLFs have been regarded by some authors as coeval with the Box Butte Fauna's middle He Red Valley LF (RedVLF, new) from the Box Butte Fm.'s Red Valley Mbr. in the central Great Plains Province of northwestern (NW) Nebraska. That correlation was based on shared occurrences of *P. tenuis* and "*A.*" cf. "*A.*" *priscus*, but not the palaeomerycid *Aletomeryx*, which was mistakenly cited instead of "*Aepycamelus*." However, *P. tenuis* and "*A.*" *priscus* also belong to the Sheep Creek Fauna's latest (type) He Middle Sheep Creek LF (SheepCLF) from that part of the Sheep Creek Fm.'s MU at Thomson and Hilltop Quarries in NW Nebraska underlying Sheep Creek Ash No. 3. The ash is 16.36 ± 0.7–16.64 ± 0.7 Ma old (mean = 16.50 ± 0.7 Ma), relying on two uncorrected Ar/Ar dates. The last two taxa represent their respective species' regional last appearance datums.

On the other hand, the RedVLF shares the middle middle He oreodontid index species *Brachycrus vaughani* with the Split Rock Fauna's middle Split Rock LF (SplitRLF) from the Split Rock Fm.'s upper porous sandstone sequence in the southern Central Rocky Mountains Province of central Wyoming, whereas the overlying, upper SplitRLF includes the larger-bodied and facially and basicranially more-derived, early late middle He index taxon *B. sweetwaterensis* n. subsp. (smaller bodied subsp.). In contrast, the Lower and Middle SheepCLFs contain medium- and large-bodied subspecies, respectively, of *B. laticeps*, which is facially and basicranially more derived than *B. sweetwaterensis*. Consequently, *P. tenuis* and "*A*." cf. "*A*." *priscus* of the RedVLF represent generic regional first appearance datums (RFADs), while the early late He index taxon *B. laticeps wilsoni* in the Lower SheepCLF from the Sheep Creek Fm.'s lower unit at Long and Greenside Quarries is the species' RFAD. Unfortunately, the UCadyMLFs cannot be correlated confidently with any other middle or late He LF on the basis of shared age-diagnostic species alone.

Contrary to faunal data, recent assignment of MZs R7–R8 in the Hector Fm.'s UU to Chrons C5Er–C5Dr.1r suggests they are largely correlative with of the Runningwater Fm.'s composite MZs R6–R7 (= later Chron C5Er–earlier Chron C5Dr.2r; MZ R7 unbounded at top) in NW Nebraska. Accordingly, the UCadyMLFs from MZs N7–R8 should be (1) assignable to Chrons C5En–C5Dr.1r, (2) 17.533–18.524 Ma old, and (3) largely coeval with the middle early–late early He lower and upper Runningwater LFs (RunningWLFs), respectively, from composite MZs N6–R7. However, such correlations are incompatible faunally. Instead, shared occurrences of the late early He oreodontid index species *Mediochoerus johnsoni* suggest the late early He upper RunningWLF from upper composite MZ N6–composite MZ R7 is a contemporary of the lower Logan Mine LF (LoganMLF) from the Hector Fm.'s middle part (unit Tho) in the southwestern (SW) CadyMtns. Neither the LoganMLFs nor the RunningWLFs share any age-diagnostic species with the UCadyMLFs.

Rather than being referable to Chron C5En, integrated faunal, radiometric, and magnetostratigraphic data indicate the oldest *Parapliohippus carrizoensis*-bearing LFs of SoCal are from normal MZs assignable to Chron C5Dn, as previously concluded by some authors, and, therefore, 17.235–17.533 Ma in age. Thus, correlatives of the lower UCadyMLF from MZ N7 include (1) the lower Lower Cajon Valley LF (LCajonVLF) from the top of the Cajon Valley Fm.'s unit 2 in Cajon Valley at the western end of the Eastern Transverse Ranges Province (TRProv.) and (2) probably the lower Hidden Treasure Spring LF (HiddenTSLF) from the Caliente Fm.'s lowermost part in the Cuyama Valley Badlands of the west-central portion of the Western TRProv. The last LF, which occurs in an interval of undetermined polarity underlying a thin normal MZ assigned to Chron C5Dn, also contains "*Aepycamelus*" cf. "*A*." *priscus* and, like the lower LCajonVLF, lies below the early late He–earliest Barstovian LLSOs of *Brachycrus* (= medium-bodied *B. laticeps*) in higher normal MZs referred to Chron C5Cn. Based on magnetostratigraphic data, the lower UCadyMLF and its correlatives are contemporaries of the middle middle He, *B. vaughani*-bearing middle SplitRLF, which occurs at the top of the Second Bench and the base of the higher Third Bench, whereas the last LF, in turn, is coeval with the RedVLF, relying strictly on faunal data. The middle SplitRLF overlies the lower SplitRLF, which (1) contains the smaller-bodied and facially and basicranially more-primitive, late early middle He index species *B. rusticus*, (2) occurs at the top of the First Bench and the base of the higher Second Bench in a basally unbounded MZ assignable to later Chron C5Dr.1r, and (3) brackets the Split Rock Tuff (SplitRT). Chron C5Dr.1r. spans the period 17.533–17.717 Ma ago and the SplitRT is concordantly Ar/Ar dated at 17.65 ± 0.08 Ma (uncorrected). Consequently, oldest records of *P. carrizoensis, Paramiolabis tenuis*, and "*A*." cf. "*A*." *priscus* in the lower UCadyMLF and its correlatives represent their respective genera and species' RFADs, whereas the early-middle He North American Land Mammal Age (NALMA) boundary probably occurs near the middle of Chron C5Dr.1r.

If MZ N7 in the Hector Fm.'s UU in the NE CadyMtns. were assignable to Chron C5Dn based on faunal data, then underlying MZ R7, which overlay Fault C, would be referable to Chron C5Dr.1r. If so and MZ N6, which underlay the fault, belonged to Chron C6n, then Fault C removed four MZs equivalent to Chrons C5Er–C5Dr.1n and spanning the period 17.717–18.748 Ma ago. Middle early–late early He LFs representing that period include (1) the RunningWLFs, (2) the lower and upper LoganMLFs from the Hector Fm.'s PST clast-bearing unit Tho and overlying unit Thu, respectively, in the SW CadyMtns., and (3) the Hackberry LF (HLF) from southern Lanfair Valley in the eastern MDProv. of SoCal. The HLF occurs in an unnamed lacustrine unit lying above the PST and below the Wild Horse Mesa Tuff, the MU of which is Ar/Ar dated at 17.75 ± 0.19 Ma (uncorrected). It contains the camelid cf. *Hesperocamelus*, not "*Aepycamelus*."

Based on additional faunal, radiometric, and magnetostratigraphic data, slightly younger *Parapliohippus carrizoensis*-bearing LFs of SoCal are from reversed MZs referable to Chron C5Cr, as determined by some previous workers, and, thus, are 16.721–17.235 Ma old. Therefore, the upper UCadyMLF from MZ R8, which is unbounded at its top, is a contemporary of (1) the upper HiddenTSLF from the Caliente Fm.'s lower (but not lowermost) part, (2) the lower middle LCajonVLF from the middle middle part of the Cajon Valley Fm.'s unit 3, (3) the lower Wye LF (WyeLF) from beds 1–4 of the Crowder Fm.'s unit 1 in Cajon Valley, and (4) the Red Division (RedD) LF (RedDLF) from MZ R2 and ca. 30 m below the top of the Barstow Fm.'s RedD or Owl Conglomerate Mbr. at RedD Quarry in the Mud Hills of

the central MDProv. The RedDLF and the lower WyeLF also share the HLSOs for *Paramiolabis tenuis* with the upper UCadyMLF, while the last LF and the lower WyeLF share "*Aepycamelus*" cf. "*A.*" *priscus* HLSOs, as well. Magnetostratigraphic data indicate the upper UCadyMLF and its correlatives are at least partly coeval with the early late middle He, *Brachycrus sweetwaterensis*-bearing upper SplitRLF, which occurs at the top of the Third Bench in a reversed MZ unbounded at its top and equivalent to earlier Chron C5Cr.

Another *Parapliohippus carrizoensis*-bearing assemblage of comparable age is the Sunrise Canyon LF (SunriseCLF) from the southeastern Calico Mountains of the central MDProv. It occurs in the Barstow Fm.'s Calico (or Odessa) Mbr., which is intruded by dacitic domes Ar/Ar dated at 16.80 ± 0.2–17.11 ± 0.06 Ma (uncorrected) and overlain by dacitic breccia sheets Ar/Ar dated at 16.85 ± 0.15–17.0 ± 0.5 Ma (uncorrected). Those dates suggest the SunriseCLF is also assignable to Chron C5Cr and coeval with the Hector Fm.'s upper UCadyMLF and its correlatives, including the early late middle He upper SplitRLF from earlier Chron C5Cr.

Unfortunately, the age of the middle-late He NALMA boundary is poorly constrained chronologically and magnetostratigraphic data allowing calibration of the early late–latest He Lower and Middle SheepCLFs or correlative *Brachycrus laticeps*-bearing assemblages have not been compiled. Consequently, it cannot be concluded with certainty that younger elements of the upper UCadyMLF and correlative assemblages are not late instead of middle He in age.

The southwestern pond turtle *(Emys [Actinemys] pallida)* in the Mojave River of California: past, present and future

Jeffrey E. Lovich,[1] George Jefferson,[2] Robert Reynolds,[3] Peter A. Scott,[4] H. Bradley Shaffer,[4] Shellie Puffer,[1] Sarah Greely,[5] Kristy Cummings,[1] Robert N. Fisher,[6] Kathie Meyer-Wilkins,[7] and Morgan Ford[1]

[1]U.S. Geological Survey, Southwest Biological Science Center, 2255 North Gemini Drive, MS-9394, Flagstaff, AZ 86005; [2]Colorado Desert District Stout Research Center, California State Parks, Borrego Springs, California 92004; [3]220 S. Buena Vista St., Redlands, CA, 92373; [4]Department of Ecology and Evolutionary Biology, and La Kretz Center for California Conservation Science, Institute of the Environment and Sustainability, University of California, Los Angeles, CA 90095; [5]The Living Desert, 47900 Portola Avenue, Palm Desert, California 92260; [6]U.S. Geological Survey, Western Ecological Research Center, 4165 Spruance Road, Suite 200, San Diego CA 92101-0812; [7]249 Maple Ridge Drive, Big Bear City, CA 92314

The southwestern pond turtle (*Emys [Actinemys] pallida*) ranges from central California to northern Baja California, Mexico primarily in streams that drain into the Pacific Ocean. Scattered records exist for isolated populations in endorheic drainages of the Great Basin and Mojave deserts. Populations in the Mojave Desert were long thought to be restricted to the Mojave River, but recently another population was documented in the Piute Ponds, a terminal wetland complex associated with Amargosa Creek on Edwards Air Force Base. Pond turtle fossils, tentatively referable to this turtle, exist from the Miocene to the Pleistocene, especially in Pleistocene Irvingtonian and Rancholabrean North American Land Mammal Age deposits associated with former Lake Manix just upstream from Afton Canyon.

Recently, Pleistocene fossils have been found as far into the desert as Salt Springs south of Death Valley. The fossils lie in wetland deposits and imply that during pluvial periods in the Pleistocene, more wetlands in the area may have provided habitat for turtles. Later, Lake Mojave (a combination of today's Soda and Silver dry lakes) spilled over into Salt Springs and eventually into the Amargosa River, on its way to Lake Manly in the Death Valley sink, illustrating one potential way to connect wetlands. The older fossil record suggests that this species was present in Mojave Block wetlands and drainages prior to the uplift of the Sierra Nevada Range about 8 Ma and prior to the ~ 3 Ma uplift of the Transverse Ranges. They were widely distributed in the Pliocene, but as the climate became dryer their range contracted and shifted toward the Pacific coast, isolating the relictual Mojave River population.

Archaeological records document use of turtles by Native Americans for food and cultural purposes 1,000 or more years ago at the Cronese Lakes on the lower Mojave River and Oro Grande on the upper river. The first modern observation documenting their presence in the Mojave River was 1861. Museum specimens were collected as early as 1937. These fossil and early literature records support the indigenous status of pond turtles to the Mojave River. However, genetic evidence suggests that Mojave River turtles share the same haplotype as turtles on the coast in San Mateo Creek. Possible explanations for that similarity will be discussed. The species is currently under review by the U.S. Fish and Wildlife Service for possible listing under the Endangered Species Act. Overdraft of the river for municipal and agricultural uses, and invasion of tamarisk are threats to the continued survival of pond turtles in the Mojave River.

Tracing the fingerprint of climate change: 40 years of vegetation response across a dryland elevation gradient

Tesa Madsen-McQueen[1] and Marko Spasojevic[1]

[1]Department of Evolution, Ecology, and Organismal Biology, University of California Riverside, Riverside, California 92521 USA

Anthropogenic climate change is causing the rapid redistribution of vegetation as plant species move to track their climatic optima under accelerated warming. Despite a global trend of upward movement in latitude and elevation (predominantly found in alpine systems

in northern temperate latitudes), there is increasing evidence of idiosyncratic responses including downward shifts in both elevation and latitude. Understanding the drivers of these variable responses is critical for predicting how biodiversity patterns will change in the future. To understand how recent changes in climate are influencing the distribution of plants, we resampled a long-term vegetation dataset which was originally established in 1977. The Deep Canyon Transect is a steep elevational gradient rising from the Coachella Valley to the Santa Rosa Mountains in southern California, gaining 2,438 meters over a distance of 16 kilometers, and encompassing desert scrub, pinyon–juniper woodland, chaparral, and conifer forest plant communities. In 2019, we resampled 20 400-m long vegetation transects along this gradient and compared our findings to surveys completed in 1977 and 2008. We report general findings, but focus our comparative analysis to the dominant perennial species for which abundance data were collected in the previous surveys.

We recorded over 370 species along the transect, including trees, shrubs, forbs, and grasses from 61 plant families. While we found that the dominant species exhibited wide variability in the extent of changes in elevation and abundance, there was a general trend since 1977 of increasing total perennial plant cover at lower elevations and decreasing cover at higher elevations. We found that the most drastic changes occurred primarily at major ecotones along the gradient, with significant declines in cover and richness of perennials at the desert scrub–pinyon woodland transition, and large increases in species richness at the transition to conifer forest, primarily driven by a decrease in conifers and an increase in forbs. Species' leading-edge range margins along the gradient tended to shift upward in the 2008 survey, and we find continuation of this trend with some species. However, we also find that most of these upward-shifting species have now shifted downward in their leading-edge range margin since the 2008 survey. While some species have increased in their lower elevation range limits, we find that more species have shifted downward at these trailing edge margins, and this pattern is similar for species from all habitats across the gradient. Changes in abundance-weighted optimum elevation show extensive variability, with no clear trend among the different habitats. Our results are among the first to assess long-term climate change effects on dryland vegetation and highlight the extensive variability among species despite the general warming and drying trends within the region. Our results also support recent suggestions that water-limited ecosystems are likely to exhibit markedly different responses than temperature-limited ecosystems to anthropogenic climate change.

Kinematics of NW-striking right-separation faults in mountain ranges northwest of Blythe, California

S. P. Mavor,*[1,2] R. S. Crow,[1] S. E. K. Bennett,[1] S. Beard,[1] and J. S. Singleton[2]
*[1]U. S. Geological Survey; [2]Colorado State University; *skylermavor@gmail.com*

Numerous NW-striking right-separation faults, some with trace lengths >20 km, cut Mezozoic bedrock in the Big Maria, Little Maria, McCoy, and Palen ranges in southeastern California. Variably mapped as dextral or normal faults, the geometry and kinematics of these structures have not been described, and deformation timing is poorly constrained. We present kinematic data from these faults, and compile literature estimates of dextral separation markers across these mountain ranges.

Newly conducted mapping in the Big Maria range revises previous interpretations of the Quien Sabe fault as a single curviplanar fault. Instead, we map a throughgoing NW-striking oblique dextral-normal fault that crosscuts a NE-striking oblique sinistral-normal fault, and fault kinematic measurements may suggest the two faults are incompatible. At Palen Pass, the NE-dipping Packard Well fault places Mesozoic plutonic rocks above an undated Neogene fanglomerate. Slickenlines indicate dextral reverse-oblique slip, likely as part of a restraining bend that connects concealed NW-striking dextral faults. Bedding in the fanglomerate is asymmetrically folded against the bounding faults, and fold geometry is compatible with a NNE–SSW horizontal component of shortening, slightly oblique to the N–S shortening direction predicted by the Packard Well fault slickenline orientations, but consistent with regional shortening direction orientations in this sector of the Pacific-North America plate boundary. A ca. 6 Ma basalt near Palen Pass is undeformed at map scale, but an incipient conjugate fault fabric within the basalt is likewise compatible with NNE–SSW shortening and may record late stages of fault slip.

Overall, fault surface measurements indicate that NW-striking faults in the Big and Little Maria ranges and Palen Pass are steeply NE-dipping, and slickenlines span from normal, oblique normal-dextral, dextral, to shallowly oblique dextral-reverse. From the range of slickenline rakes and calculated strain axes, we postulate that the system of faults in these ranges records progressive deformation in an evolving strain field from middle-Miocene NE–SW extension to later E–W extension as part of a NW-directed dextral shear regime rather than a single deformational event. In order to test this hypothesis, $^{40}Ar/^{39}Ar$ geochronology is in progress for samples from the Palen Pass basalt and of an ash interbedded in the Palen Pass fanglomerate to constrain the timing of faulting in the study area. We estimate cumulative post-Mesozoic right separation across exposed and concealed faults to be on the order of ~15 km. Our data demonstrate that these faults have accommodated

significant cumulative offset and will help understand the evolution of the Neogene strain field of the diffuse Pacific-North America plate boundary.

Middle Miocene temperature and paleoenvironmental changes recorded in paleosol carbonates (Barstow Formation, Mud Hills, CA)

Katharina Methner,*[1,2] Katharine Loughney,[3] Lydia Jork,[4] Jens Fiebig,[4] Catherine Badgley,[3] and Andreas Mulch[2,4]

*[1]Stanford University, USA, *kmethner@stanford.edu; [2]Senckenberg Biodiversity and Climate Research Centre Frankfurt, Germany; [3]University of Michigan, USA; [4]Goethe University Frankfurt, Germany*

Spatial and temporal pattern of temperature and rainfall determine the evolution of biomes and ecosystems, and so reconstructing these parameters in the geologic past is crucial for paleo-environmental and paleo-ecological studies. Here we combine carbonate stable isotope ($\delta^{18}O_{carbonate}$, $\delta^{13}C_{carbonate}$) and clumped isotope temperature ($T(\Delta_{47})$) data obtained from pedogenic and palustrine carbonates of the middle Miocene Barstow Formation (Mud Hills, CA). The well-dated and thoroughly described sediments of the Barstow Formation in the Mud Hills provide a high-resolution (ca. 100 ka) terrestrial sediment record (Loughney and Badgley, 2017). This makes these sediments an excellent target to study local climate and paleoenvironmental changes during the global warmth of the middle Miocene Climate Optimum (MMCO, ~17.0-14.5 Ma) and the subsequent cooling during middle Miocene Climate Transition (MMCT, ~14.5-12.5 Ma). We sampled multiple sections of the Mud Hills, covering paleosols with an age of ca. 17.5 to 12.9 million years. Preliminary soil carbonate Δ_{47}-temperature results show temperatures between 12°C and 29°C. The lowest soil temperatures are recorded before and after the MMCO time interval ($T(\Delta_{47})$ = 17°C at 17.2 Ma and $T(\Delta_{47})$ = 12°C at 13.6 Ma), whereas samples from the MMCO-interval yield generally warmer temperatures of 24–29°C, yet with intervals of high temperature variability. $\delta^{18}O_{carbonate}$ values (in VSMOW) decrease from an average of 23.6‰ (~17.2-17.5 Ma) to ~21‰ throughout the younger sections. Combining pairs of $\delta^{18}O_{carbonate}$ and $T(\Delta_{47})$ values yields soil water $\delta^{18}O$ values, reflecting local rainfall $\delta^{18}O$ values, of -3 to -9‰ (in VSMOW) with ~ -7‰ during the MMCO and -9‰ thereafter. $\delta^{13}C_{carbonate}$ values range between 0 to -9‰ (in PDB) and show decreasing $\delta^{13}C_{carbonate}$ values through time. This likely indicates higher soil respiration rates associated with the overall more variable moisture conditions reported for the youngest time interval of the Barstow Formation (facies 5 and 6; Loughney et al., 2019). Overall, our preliminary soil carbonate $T(\Delta_{47})$ and $\delta^{18}O_{soil\ water}$ values are elevated during the MMCO interval and decrease thereafter, suggesting the Mud Hill sections record global patterns of Miocene climate change.

Loughney, K.M., Badgley, C., 2017. Facies, environments, and fossil preservation in the Barstow Formation, Mojave Desert, California. PALAIOS 32, 396–412.

Loughney, K.M., Hren, M.T., Smith, S.Y., Pappas, J.L., 2019. Vegetation and habitat change in southern California through the Middle Miocene Climatic Optimum: Paleoenvironmental records from the Barstow Formation, Mojave Desert, USA. Geol. Soc. Am. Bull.

A vascular flora of the Nopah Range, Inyo County, California

Carolyn Mills[1,2]

[1]Department of Botany, Claremont Graduate University, 150 East 10th Street, Claremont, CA 91711; [2]Rancho Santa Ana Botanic Garden, 1500 North College Avenue, Claremont, CA 91711.

The Nopah Range in southeastern Inyo County, California is a botanically diverse mid-elevation mountain range located in the northern Mojave Desert just west of the California–Nevada border. Like many mid-elevation ranges in the region, the Nopah Range has seen little botanical documentation, particularly at high elevations, where only 21 collections have ever been vouchered. This specimen-based study will assess vascular plant diversity throughout the range, where an abundance of calcareous substrates has the potential to yield exciting discoveries including rare and endemic species, range extensions, and new species records for California. The study area is approximately 510 km^2 (197 mi^2) and is located at the intersection of two major floristic provinces, the Mojave and Great Basin deserts. Nine hundred and eighty-six specimens have been collected as of February 2020, thus far yielding seven rare plant species new to the range and many new locations of rare plants previously known from the range. This presentation will present preliminary findings including new records for rare plant taxa in the range, including *Allium nevadense* (wild Nevada onion), *Cymopterus gilmanii* (Gilman's springparsley), and *Muilla coronata* (crowned muilla), and new populations of species at the edge of their range.

Paleoecology of Columbian mammoths (*Mammuthus columbi*) in southern Nevada and California: how Terminal Pleistocene ecosystems shaped mammoths at the population level

Lauren E. Parry[1,2] and Stephen M. Rowland[1]

Department of Geoscience, University of Nevada Las Vegas, 4505 South Maryland Parkway, Las Vegas, NV 89154 ; Las Vegas Natural History Museum, 900 Las Vegas Boulevard North, Las Vegas, NV 89109

We use this study to examine the population dynamics of the Columbian mammoth (*Mammuthus columbi*) in southern Nevada and southern California by testing a novel hypothesis developed by Ripple and Van Valkenburgh (2010). This hypothesis is supported by multiple datasets from the fossil record, which

suggests that North American Pleistocene carnivores kept megafaunal herbivore populations below carrying capacity, and a trophic cascade could have caused ecological collapse mediated by prey-switching. The more conventional hypotheses for megafaunal extinction include human over-kill and climate-change, however they both rely on the assumption that population sizes of megafaunal herbivores were resource dependent.

We constructed age profiles to evaluate time-averaged assemblages of fossil Columbian mammoth molar teeth from the Las Vegas Formation in southern Nevada and Rancho La Brea (RLB) in southern California for population dynamics and mortality patterns. These fossils are part of collections housed at the Las Vegas Natural History Museum and La Brea Tar Pits and Museum, respectively. Tooth age assignments were determined by measuring their length, width, and height, and counting tooth plates, referencing an extensive literature review of proboscidean dental progression and wear. The age profiles generated from the Gilcrease Cauldron Spring paleontological site suggest that the time-averaged population of mammoths that lived in the Las Vegas Valley during 15,830–22,516 cal BP experienced age and potentially sex-selective mortality. By far, juveniles and young adults are the most highly represented age cohorts, and the >40 African Elephant Year age cohorts are the most depleted. The shapes of our age profiles suggest that drought-related stress was not a significant factor in juvenile mortality during the Terminal Pleistocene in Las Vegas Valley. This mortality pattern suggests that juveniles were preferentially killed by predators due to their small body size and vulnerability, and then were subsequently underrepresented in older age cohorts due to time averaging. This suggests that mammoth population sizes in the Las Vegas Valley during the Terminal Pleistocene were controlled from the top of the food pyramid down and were likely below carrying capacity. The age profiles generated from Rancho La Brea show selective mortality within the mature adult age class, with a background "Type A" pattern in other age classes. This mortality pattern could be reflective of carnivore activity and mortality during the warmest months of the year and warmer overall years between 40,000–14,000 cal BP. In particular, this mortality was likely additive, considering presumably healthy, mature adults became mired within the asphalt, but not likely contributing to population instability. Our data, corroborated by other studies, do not suggest mammoth population instability or decline at RLB due to resource stress during the interval of 40,000–14,000 cal BP, allowing us to refute our alternative hypothesis of bottom-up control. Although we cannot support the top-down trophic control hypothesis directly with our dataset, data from numerous studies of large carnivores at RLB paint a picture of a diverse and competitive predator guild during the late Pleistocene. Age profiles cannot be used alone to determine trophic controls on Pleistocene mammoth populations, but they add important regional data to a much larger context.

Taking the road less traveled: a comparison of desert tortoise road crossing at two study sites in the Sonoran Desert of California

Shellie R. Puffer,[1,] Jeffrey E. Lovich,[1] Terence R. Arundel,[1] Kirsten Ironside,[1] Laura A. Tennant,[1] Amanda L. Smith,[2] Kathleen Brundige,[3] and Michael Vamstad[4]

*[1]U.S. Geological Survey, Southwest Biological Science Center, 2255 North Gemini Drive, MS-9394, Flagstaff, AZ 86001, USA; [2]The Sonoran Institute, 100 North Stone Avenue, Suite 400, Tucson, AZ 85701, USA; [3]Coachella Valley Association of Governments, 73-710 Fred Waring Drive, Suite 200, Palm Desert, CA 92260, USA; [4]National Park Service, Joshua Tree National Park, 74485 National Park Drive, Twentynine Palms, CA 92277, USA' *Corresponding author: mpuffer@usgs.gov*

The impacts of roads on wildlife are various, with both direct (e.g., road mortality, population isolation, decreased habitat quality) and indirect (e.g., inhibition of gene flow, altered population structure) effects possible. Growing human population and development have led to an increase in the amount of traffic and number of roads associated with infrastructure worldwide. In California, there are greater than 270,000 km of public roadways and more than 27 million cars registered in the state. Where the federally protected Agassiz's desert tortoise (*Gopherus agassizii*) resides in southern California, over 3,000 km of roads impact nearly 11,000 km^2 of designated critical tortoise habitat on lands managed by the Bureau of Land Management. Populations of desert tortoises near the eastern end of the Coachella Valley are managed under a Multiple Species Habitat Conservation Plan, and populations existing within the boundaries of Joshua Tree National Park are afforded an extra layer of protection. However, even within the park there is still annual tortoise road mortality from visitor traffic. From 2015–2018, we studied two populations of desert tortoises located approximately 5 km apart and separated by Interstate 10. One population was located just inside of the southern boundary of Joshua Tree National Park near the entrance to Cottonwood Canyon (Cottonwood study site). This site is bisected from north to south by the paved Cottonwood Springs Road that serves as the only entry/exit to the park from its south side. The other desert tortoise population was located on checkerboarded lands on the northern versant of the Orocopia Mountains (Orocopia study site). These land parcels are owned either privately, including by companies that do mitigation and conservation banking, or by Bureau of Land Management. The site has a network of unpaved roads, including a powerline service road that bisects the site from east to west and numerous well-known trails for off-highway vehicles. At both study sites, a subset of desert tortoises was outfitted with radiotransmitters and tracked biweekly to monthly for approximately 17 months (includes two tortoise activity

seasons). Only at the Orocopia study site were tortoises observed (both directly and indirectly) crossing the road. Here we compare road crossing potential between the two populations. We also investigate the effects of buffer zones on tortoise locations and densities in 500 m increments on either side of the major roads transecting the study sites. The percent of tortoise locations and the tortoise densities within 500 m of the paved road at the Cottonwood study site were lower than those surrounding the dirt roads at the Orocopia site, indicating that Cottonwood Springs Road acts as a stronger barrier to movement within that population.

Quantifying niche dynamics of Sahara mustard (*Brassica tournefortii)* to improve spatial predictions of areas at risk of invasion

Clarissa Rodriguez,[1]* Loralee Larios,[1] and Janet Franklin[1]

*[1] Department of Botany and Plant Sciences, University of California Riverside; *Crodr087@ucr.edu*

Drylands have traditionally been considered to be resistant to invasion, but in the past few decades we have seen an increase in introduced species being able to establish in these systems and altering native plant communities. Identifying areas at risk for the potential spread of invasive species is required in order to target management and prevention efforts to reduce costs associated with ecological damage. However, with the combination of the ruderal life history strategies of invasive species and a changing climate, predicting suitable habitat for invasive species under dynamic conditions is challenging. *Brassica tournefortii*, also known as Sahara mustard, is an herbaceous winter annual native to North Africa and parts of the Middle East. It has recently become a common plant invader of drylands in the southwestern United States. Species distribution modelling can be used to create spatial predictions for suitable habitat of invasive species by using occurrence data for the native and introduced ranges to assess the breadth of climatic tolerances. Here, we are modeling the climatic habitat suitability of Sahara mustard in its home range and introduced range, and quantifying the realized climatic niche (the climate characteristics of where the species grows) of Sahara mustard in order to address the following questions: (1) Are there differences in the realized climatic niche between the native and the North American introduced range of Sahara mustard? (2) What climatic factors are most important in explaining the distribution of the species, and how do these species–climate relationships differ in native and introduced ranges? Preliminary analysis suggests that this species is not restricted to climates analogous to its native range in its introduced range, as we detected niche expansion in the introduced range into drier and warmer climates. We also found precipitation in the coldest quarter and temperature seasonality to be strong predictors of Sahara mustard's distribution. This research could provide valuable insight as to why Sahara mustard has been able to continuously invade drylands and provide an improved spatial prediction model of invasion risk to be used for management purposes.

Evidence of Pleistocene marine incursions into the Salton Basin

Jenny E. Ross,[1] Susan M. Kidwell,[2] David L. Dettman,[3] Jordon Bright,[4] Rebecca J. Dorsey,[5] and George T. Jefferson[6]

[1]Stout Research Center, Colorado Desert District, California State Parks, Borrego Springs, CA 92004; jenny@jennyross.com; [2]Department of Geophysical Sciences, University of Chicago, Chicago, IL 60637; [3]Department of Geosciences, University of Arizona, Tucson, AZ 85721; [4]School of Earth and Sustainability, Northern Arizona University, Flagstaff, AZ 86011; [5]Department of Earth Sciences, University of Oregon, Eugene, OR 97403; [6]Stout Research Center, Colorado Desert District, California State Parks, Borrego Springs, CA 92004

The geologic record of the Pleistocene Epoch in the northern Salton Trough—the portion of the northwest landward extension of the Gulf of California Shear Zone that is north of the US–Mexico border—has long been interpreted as entirely non-marine and largely lacustrine. It has been thought that by Pleistocene time the Colorado River had deposited such an enormous quantity of sediments at its delta in the Gulf of California that the northern Salton Trough became cut off from the rest of the gulf and was fully isolated from marine waters. However, we have evidence that indicates marine incursions entered the northern Salton Trough in periods of high sea level during the Middle-to-Late Pleistocene. Within highly deformed and extensively faulted sediments of the Pleistocene Brawley Formation on both sides of the Salton Basin in the northern Salton Trough—in the Superstition Hills on the west side of the basin and in the Durmid Hill region on the east side—we have identified more than 70 outcrops of autochthonous, parautochthonous, and allochthonous shell deposits of three species of bivalves: *Rangia lecontei* (an extinct clam thought to have been estuarine based on the environmental requirements of extant species in the genus), *Chionista fluctifraga* (marine), and *Tagelus affinis* (marine). All shell beds in the Durmid Hill region are upsection from a previously-identified extensive bed of the Bishop Ash (~759 ka). Based on stratigraphic context, sedimentary characteristics, species composition and environmental requirements, taphonomy, initial stable isotope results ($\delta^{18}O$ and $\delta^{13}C$), preliminary microfossil analysis, and initial amino acid geochronology, we suggest that these features represent marine incursions into the Salton Basin during the Middle-to-Late Pleistocene, most likely during sea-level highstands in Marine Isotope Stages 11c and 5e, the periods of highest sea level during the past one million years. Autochthonous and parautochthonous shell beds contain articulated valves of

various sizes in life position or nearly so. We interpret the allochthonous deposits as shell pavements, beach ridges, shell cheniers, and possible tidal channels and storm deposits that we suggest are analogous to a characteristic suite of Holocene allochthonous shell deposits occurring along the northwest shore of the Gulf of California north of San Felipe, Mexico. Future work will focus on additional stable isotope and microfossil analyses, further amino acid geochronology, tephrochronology, and consideration of other possible dating techniques.

Trace element scavenging at the sediment-poor water interface in surficial sediments of an arid region of southern Nevada, USA

Douglas B. Sims,[1] Amanda C. Hudson,[1] John E. Keller,[1] Michael Strange,[2] David Ferrari,[2] Giavanna M. Fernandez,[1] Juan Garcia-Hernandez,[1] and Bailey D. Kesl[1]
[1]College of Southern Nevada, Dept. of Physical Sciences, North Las Vegas, Nevada 89030, USA; [2]University of Nevada, Las Vegas Dept. of Geological Sciences, Las Vegas, NV 89154

This study investigated trace metal scavenging by rock varnish coatings on ephemeral sediment particles in desert washes. Sediments were collected from dry ephemeral washes up gradient from the Techatticup Mine and Mill, a metal mining operation that operated between 1850 and 1960. Samples were used to evaluate movement and behavior of certain metals (i.e. Al, Ba, Cd, Cu, Fe, Mn, V) and metalloids (i.e. As, Pb). Sediment samples were sieved to retain >4.76 mm, >2.00 mm, >0.074 mm, and <0.074 mm, cleaned with deionized (DI) water, mixed with metal laden tailings and DI, and gently agitated for 20 minutes to simulate a flooding event and rinsed with DI water before being analyzed by ICP-OES. Fractions with the greatest increase were 2 mm and 0.074 mm while the >4.74 mm and <0.074 mm showed marginal increases in trace metals. Data show an increase in As, Ba, Pb, Ti, and V on sediment particles while there was a decrease in Al, Fe, and Zn, constituents of rock varnish (as oxides and oxyhydroxide). Copper and Ni showed no increase or decrease in concentrations across all fractions. Additionally, a field emission scanning electron microscope (FESEM) was used to evaluate trace metal scavenging. FESEM shows similar results of the ICP–OES with an increase in As, Ba, Pb, Ti, and V; no change with Cu and Ni; and a decrease in Al-, Fe-, and Zn-oxides and oxyhydroxides on sediment particles.

Lacustrine beds in the Chuckwalla Valley, southeastern California, and their likely facies relationship to the Chemehuevi Formation

W. Geoffrey Spaulding
Terra Antiqua, 2320 Cordelia Street, Henderson, NV 89044

In the southeastern lee of the Coxcomb Mountains, about 20 km north of the I-10 corridor near the mouth of the Palen Valley in the desert of southeastern California, there lies an expanse of subhorizontally bedded, salt- and gypsum-rich lacustrine sediments. They are capped by a half-meter thick evaporite (not carbonate) layer consisting of gypsum and salts, marking what appears to have been this paleolake's desiccation. In the past these sediments had been related to a possible "Pluvial Lake Palen," but Palen Dry Lake does not occupy a closed basin and hence cannot support a paleolake. In order for these evaporite-rich muds to have been deposited up to ca 156 m (ca. 512 ft) elevation, the entire Chuckwalla Valley would have to have been occupied by a water body on the scale of the Salton Sea. Except for the evaporite cap, these sediments are poorly consolidated, and neither deformed nor evidently faulted. They appear to be younger than Late Pliocene Bouse Formation sediments, visible nearby at higher elevations. Indeed, their altitude, evaporite content, and appearance all suggest that they are related to the Late Pleistocene (MIS-4) Chemehuevi Formation described by Malmon and colleagues. Elevational profiles of an aggraded Colorado River during MIS-4 time clearly imply overflow into the Chuckwalla Valley. The sill immediately west of Blythe separating the Chuckwalla Valley from the Colorado River trough is >15 m *lower* than the maximum elevation of these paleolake sediments. Therefore, connection with an aggraded Colorado River during Chemehuevi Formation-time seems evident. Presence of a spill-over lake in the Chuckwalla Valley, rather than an endorheic lake dependent on meager runoff from the surrounding low mountain ranges, is a paleohydrologically more realistic scenario, as well as fitting with models of Colorado River aggradation early in the last Glacial Age.

What? There's water in the desert?

Carole Ziegler
geologycarole@gmail.com

In 2014, California passed the Sustainable Groundwater Management Act and listed Borrego Spring's sole-source aquifer to be in "critical overdraft". With that in mind, this talk was developed for the general audience that visits the Imperial Valley Desert Museum, located near Highway 8 in Ocotillo, California. The talk looks at the sources of water in the Borrego Valley Ground Water Basin including rain storms, lakes, springs and aquifers. Of particular interest is the Borrego Springs Aquifer which occurs as 2 sub-basins, one near the town of Borrego Springs and the other in the area of Ocotillo Wells. Besides being divided into sub-basins, the aquifer's waters exhibit 3 distinct layers associated with age. Due to natural geologic barriers, waters from one sub-basin cannot be pumped to the other sub-basin. Secondly, there is not enough rainfall available for recharge of these sub-basins. Borrego Springs is currently developing a plan to reduce water consumption by almost 75% by 2040 as required by the state of California. If they don't, the state will take over and manage the water reduction themselves.

Founders Circle of the Desert Symposium Inc.

The Desert Symposium Inc., incorporated as a nonprofit 501c3 institution February 2018, is dedicated to supporting and encouraging original research related to deserts, through publications, hosting the Desert Symposium meetings, and related scientific and educational endeavors. Desert Symposium Inc. evolved directly from the Desert Symposium and its predecessor, the Mojave Desert Quaternary Research Center. Without the hard work and vision of the original founders, the current organization would not exist.

The Board of Directors initiated a Founders Circle in 2018 to help set the new organization on firm financial footing. Gifts will impact our shared scientific community for decades to come by expanding our academic services and publications to more readily available platforms and broadening our focus from the Mojave Desert to other deserts. The individuals described below are "Founding Fellows" of the Desert Symposium Inc. Founders Circle. Donations to the Circle closed at the end of 2019. A hearty thanks goes to these donors.

5-YEAR FELLOW
Bruce Hamilton
Tanya Henderson
Steve Finney
Pat Flanagan
Keith Howard
Sherry Keesey
Ed LaRue
Jane E. Rodgers
Steve Rowland
Cheryl Schweich

10-YEAR FELLOW
Ernie and Vera Rose Anderson
Hal Beesley
James Bishop
Bruce Bridenbecker
Anna Garcia
Gregor Losson
David Lynch
David Miller
Thomas Schweich
Joann Stock

25-YEAR FELLOW
Catherine Badgley
Victoria Langenheim
Kevin Schmidt
Gerald Smith
Geoffrey Spaulding
Gregg Wilkerson

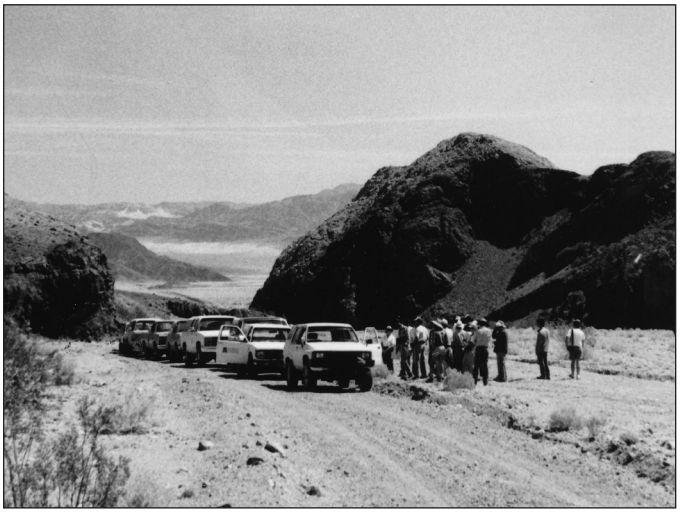

30 Years Ago: the 1990 Desert Symposium field trip

20 Years Ago: the 2000 Desert Symposium field trip